UNIVERSITY OF OKLAHOMA

GRADUATE COLLEGE

GEOCHEMISTRY OF THE STACK AND SCOOP OIL PLAYS, ANADARKO BASIN, OKLAHOMA

A DISSERTATION

SUBMITTED TO THE GRADUATE FACULTY

in partial fulfillment of the requirements for the

Degree of

DOCTOR OF PHILOSOPHY

By

CARL SYMCOX
Norman, Oklahoma
2021

Downloaded from SHAREOK. Persistent Handle URL: https://hdl.handle.net/11244/331232

GEOCHEMISTRY OF THE STACK AND SCOOP OIL PLAYS,
ANADARKO BASIN, OKLAHOMA

A THESIS APPROVED FOR THE
SCHOOL OF GEOSCIENCES

BY THE COMMITTEE CONSISTING OF

Dr. Mike Engel, Chair

Dr. R. Paul Philp

Dr. Richard Elmore

Dr. Matt Pranter

Dr. Deepak Devegowda

© Copyright by CARL SYMCOX 2021
All Rights Reserved.

Acknowledgements

This research was made possible because of the excellent facilities, staff, support, and mentorship of the Organic Geochemistry Group at the University of Oklahoma headed by Dr. Philp. A special thanks to Alta Mesa Resources, Casillas Petroleum Company, Continental Resources, Devon Energy, Echo Energy, Gastar Exploration, Marathon Oil, Newfield Exploration, Tapstone Energy, Vitruvian Exploration, and Warwick Energy Group for generously donating samples, support, and permission to present this work. Additional core data were provided from the Oklahoma Petroleum Information Center.

Table of Contents

Acknowledgements iv
Table of Contents v
List of Figures vi
List of Tables xvi
Abstract xix
List of Acronyms xviii
I. Introduction 1
    The STACK and SCOOP Plays 1
    Organic Geochemistry in Hydrocarbon Exploration and Development 4
II. Geologic Background 9
    The Anadarko Basin 9
    STACK and SCOOP Petroleum Systems 12
III. Dataset and Methods 23
    Oil Samples 23
    Core Samples 31
    Internal Standards and Calculating Absolute Concentrations 34
    Production Data 37
    Principal Component Analysis 38
    Mapping Software 38
IV. Thermal Maturity Model 39
    Bulk Composition Maturity Parameters 42
    Biomarker Maturity Parameters 54
    Light Hydrocarbon Maturity Parameters 68
    Aromatic Maturity Parameters 77
    Principal Component Model 84
    Thermal Maturity Maps 86
    Maturity and Oil Composition 92
    Summary of Findings 100
V. Organic Facies Determination 102
    Previous Geochemical Studies of Source Rocks in STACK and SCOOP 102
    Outline for Determining Organic Facies 106
    Characteristics of the STACK Petroleum System 109
    Characteristics of the SCOOP Petroleum System 176
    This Study in Relation to Previous Geochemical Findings 193
    Summary of Findings 201
VI. Secondary Processes 203
    Elevated Sulfur Trend in STACK West 203
    Predicting Overpressure 226
    Spatial Heterogeneity in Oil Charge and Accumulation 230
    Summary of Findings 238
VII. Conclusions 240
References 241
Appendix: Compound Structures 260

List of Figures

Figure 1. Map of the three Play Regions examined in this study and their producing counties. 3

Figure 2. Outline of the Anadarko Basin and its major structural boundaries. The STACK/SCOOP study area is highlighted. Modified from Pranter et al. (2016). 9

Figure 3. Cross section of the Anadarko Basin from southwest to northeast. From Johnson (2008). 12

Figure 4. Generalized stratigraphic column with major source rocks and reservoirs are shown in red and green, respectively. Height of formation boxes is not related to thickness of unit. Constructed based on the works of Harris (1975), Johnson (1989), Johnson and Cardott (1992), Henry and Hester (1995), Higley (2013), and Cardott (2017). 13

Figure 5. Approximate regional distribution of Upper Devonian and Lower Mississippian black shales in the United States, shown in blue. From Conant and Swanson (1961). 14

Figure 6. Thickness of the three Woodford Shale members as well as total Woodford isopach based on well logs; contour interval 25 ft. Areas where Woodford Shale is absent is hachured. Dots show well locations. The syndepositional structural axis is depicted as bold arrow. The Woodford Shale thins substantially towards STACK West, and the Upper and Lower members are absent in some cases. Modified from Hester et al. (1990). 16

Figure 7. Histogram of Osage facies in STACK measured from cores of four complete Mississippian intervals located in Blaine, Kingfisher, and Canadian counties. At least 37% of the Osage has been bioturbated by benthic organisms suggesting well-oxygenated bottom waters. From Bynum and Wethington (2020). 17

Figure 8. Histogram of Meramec facies in STACK. There is a notable increase in siltstone facies concurrent with a decrease in chert facies making the Meramec a preferred drilling target. From Bynum and Wethington (2020). 18

Figure 9. Isopach of the Meramec Fm. in STACK with subsea structure depths. From Price et al. (2020). 19

Figure 10. Histogram of Chester facies in STACK. Note the substantial increase in siliciclastic relative to carbonate facies as well as the absence of spicular chert facies. From Bynum and Wethington (2020). ... 20

Figure 11. Block diagram depositional model for the Mississippian Group showing the transition from a carbonate-dominated system to a siliciclastic-dominated system. The carbonate system ranges from grainstone dominated inner-ramp deposits to calcareous siltstone dominated outer- ramp deposits. The siliciclastic system ranges from arkosic sandstone dominated upper shoreface deposits to siltstone dominated offshore deposits. FWWB=fair weather wave base; SWB=storm wave base. From Bynum and Wethington (2020). 21

Figure 12. A gamma-ray cross section of STACK East along depositional trend and flattened on the Woodford Shale. The Meramec clinoform sets A-I can be seen prograding over the top of the Osage Fm and capped by the shaley Chester Fm. Gamma-ray scale 0-100 API. FSST=Falling Stage Systems Tract; LST=Lowstand Systems Tract; TST=Transgressive Systems Tract; HST=Highstand Systems Tract; SB=Sequence Boundary. Modified from Price et al. (2020) 22

Figure 13. Wellhead locations of the 172 study oil samples by producing formation and organized into separate panels corresponding to the STACK West, STACK East, and SCOOP Play Regions. Sample labels correspond to the sample key in Table 1. The square grid corresponds to township lines which are 6 miles on a side. 24

Figure 14. Map of oil samples in this study (upper) colored by producing formation as indicated by the adjoining cross section cartoon (lower). Woodford vitrinite isoreflectance contours (Ro%) provided (Cardott, 2012). 28

Figure 15. Map of cored wells incorporated into this study. 32

Figure 16. Examples of core sampling locations by stratigraphic interval and lithofacies for the ABCDS 1-6H core. The Chester facies are dominated by laminated siltstones, bioturbated siltstones, and calcareous sandstones and contain a slightly organic base in this core. The Meramec ranges from clean silt, silty shales, to shaley interbeds. The Osage ranges from crinoidal carbonate packstones and wackestones to cherty carbonates with stylolite dissolution features. The dark Kinderhook Shale is generally organic lean, while the Woodford Shale is organic rich. Not Shown: Hunton Fm or Springer Group. 33

Figure 17. An example relative response factor between the internal standard used in this study (5α-cholestane-2,2,3,3,4,4-D6) and adamantane. Adamantane has a larger machine response by nearly a factor of four. 36

Figure 18. Initially producing gas-oil ratio (IP GOR) is chosen from the first month after the well has finished cleaning up. The IP GOR for the well shown is 12,655 scf/STB. 37

Figure 19. Map of the 172 studied oil samples by producing reservoir and colored by total vertical depth (TVD) as shown in Table 1. Oklahoma Geological Society recognized faults are shown in light grey. Two notable north-south trending faults in Dewey and Woodward counties are highlighted which are referenced in the text. 40

Figure 20. a) Contour map of Woodford oil API gravity. A "flower-shaped zone" in a heavily faulted portion of eastern Dewey County bends the contours indicating an updip incursion of higher maturity oils. b) Map of the flower-shaped zone with study oils (labeled by 1002A API gravity) showing major shift in API gravity across notable N-S trending faults, marked red. Faulted lithology may contribute to updip migration of higher maturities from deeper in the basin. 46

Figure 21. Initial production API Gravity values for study wells (from OCC form 1002A). STACK oils generally increase with depth while SCOOP oils show little correlation with depth. A broad range of STACK West values around ~11,000 ft correspond to a flower-shaped zone of higher API gravity in Dewey County (see Figure 20). 47

Figure 22. Cross-plot of whole oil $\delta^{13}C$ isotope values versus TVD. A cluster of STACK East oils is circled as possible evidence of updip migration and are not included in regression trendline (see text). The STACK West oils at ~11,000- ft mirror the variable maturities observed in Woodward and Dewey counties which include the flower-shaped zone. 48

Figure 23. Map of STACK indicating the circled samples marked "Updip Migration" in Figure 22. These samples are produced from Mississippian reservoirs above immature Woodford, and plot approximately 1,000-2,000 ft TVD above the TVD-$\delta^{13}C$ trendline indicating that may be the extend of updip migration. 49

Figure 24. The IP GOR in this dataset generally increases with TVD but exhibits a very weak correlation. 50

Figure 25. The sum of SARA values for oils in this study plotted by depth and Play Region. Volatiles lost during sample preparation and fractionation account for the remaining weight up to 100%. Oils become more volatile with increased depth, but also show an increase in the relative abundance of saturates compared to aromatics, NSOs, and asphaltenes. Asphaltenes are only observed in meaningful quantities in shallow STACK West oils. 52

Figure 26. Colloidal Instability Index (CII) versus TVD for study oils. There is a strong relationship in STACK than in SCOOP which again plots below the main STACK trend. The flower shaped zone in STACK West is also present. 53

Figure 27. Kinetic precursor-product relationship of C_{29} sterane (**I**) stereoisomers common in mature geologic samples. Each structure has an implied 5α(H) configuration. Recreated from Seifert and Moldowan (1981).....55

Figure 28. Two GC-MS fragmentograms showing peak distribution of C_{27-30} regular steranes (**I**) and C_{27-30} diasteranes (**II**). Diasteranes can be measured using m/z 259 which are more specific for diasteranes than m/z 217. An example carbon skeleton of a regular sterane and diasterane show rearrangement of the methyl groups C-18 and C-19.....59

Figure 29. Two maturity parameters based on the isomerization of the C_{29} regular sterane (**I**). Upper: the ratio of C_{29} 5α(H),14α(H),17α(H) 20S/(S+R) sterane versus TVD. By 8,000 ft, the ratio 20S/(S+R) has reached equilibrium and shows no correlation with depth. Lower: the ratio C_{29} sterane ββ/(ββ+αα) using both 20S and 20R epimers shows a good correlation with TVD in STACK East and weak correlation in STACK West and SCOOP.....61

Figure 30. The ratio of diasteranes/steranes generally increases with TVD in STACK until 10,000-11,000 ft beyond which the ratio reaches unity. No correlation with depth is observed in SCOOP. 62

Figure 31. Detailed m/z 231 fragmentogram showing C_{20}-C_{28} triaromatic steroids and their common groupings TA[I] (**III**) and TA[II] (**IV**). Peak identification based on Mackenzie et al. (1981).....63

Figure 32. The triaromatic sterane maturity ratio TA[I]/TA[I+II] increases with TVD until ~0.85 beyond which no additional information is gained.....64

Figure 33. Detailed m/z 191 fragmentogram of a black oil B/C fraction. Labeled peaks are identified in Table 6. 65

Figure 34. Ratio of all C_{19}-C_{39} tricyclic terpanes (3R) over C_{19}-C_{39} tricyclic terpanes plus C_{27}-C_{35} hopanes (5R) versus TVD. In STACK, the ratio increases with depth until it reaches equilibrium around 9,000 ft. In SCOOP, the ratio increases with depth until reaching equilibrium around 12,000 ft. 67

Figure 35. Light hydrocarbon peaks labeled based on comparison to Walters and Hellyer (1998). 68

Figure 36. Maturity parameters for the isoheptane ratio, heptane ratio, normality, and paraffinicity versus depth based on Thompson (1979 and 1983). The isoheptane ratio plotted in semi-log displays the best correlation with depth, while the heptane ratio and paraffinicity show little correlation. The previously identified flower-shaped zone in STACK West of variable oil maturities at ~11,000 ft can also be observed, especially in the isoheptane ratio. HC=hydrocarbons.....74

Figure 37. Maturity parameters for Mango parameters 2-/3-methylhexane (upper) and expulsion temperature (lower) versus depth based on Mango (1997). Good correlations are observed in STACK East and SCOOP, but STACK West shows significant scatter especially in the previously identified flower-shaped zone at ~11,000 ft. 76

Figure 38. Peak identification for phenanthrene (P) and the methylphenanthrene isomers (x-MP) from the m/z 178+192 fragmentogram. Peak identification based on Radke et al. (1982). 77

Figure 39. Vitrinite reflectance equivalent (Rc%) values from the methylphenanthrene index (MPI-1) versus TVD. 81

Figure 40. Peak identification for dibenzothiophene (DBT) and the four methyldibenzothiophenes isomers (x-MDBT). Peak identification based on Radke et al. (1982) and Fang et al. (2016). 82

Figure 41. a) The MDR maturity parameter for this dataset whereby only STACK West shows a good correlation versus TVD. b) STACK West oils are enriched in 4- and 1-methyldibenzothiophene compared to STACK East and SCOOP and may contribute the higher signal-to-noise and less scatter of the MDR thermal maturity parameter.....83

Figure 42. Principal component analysis (PCA) model for each Play Region correlating maturity parameters to TVD where good correlations are circled and bold. All Play Regions are then aggregated into a single

PCA model (bottom right) to determine consensus between the most successful maturity parameters without consideration of TVD. The most successful maturity parameters in this dataset were colloidal instability, expulsion temperature, and Rc% (from MPI-1). 85

Figure 43. Map of Rc% (from MPI-1) which was found to be the most successful maturity parameter in this dataset and is the principal maturity parameter used in the remainder of this study. 87

Figure 44. The Expulsion Temperature (°C) maturity parameter makes apparent the effects of high maturity fluids invading the flower-shaped zone in eastern Dewey County compared to similar TVD reservoirs in Woodward and western Dewey counties. 88

Figure 45. Maps of the colloidal instability index (CII) and tricyclic terpanes/tricyclic terpanes plus hopanes, or 3R/(3R+5R) terpanes, maturity parameters which exhibit good correlation with TVD and other maturity parameters in PCA. The thermal maturity anomaly in eastern Dewey County is not readily apparent in these maturity parameters. 89

Figure 46. Maps of the isoheptane ratio and 2-MH/3-MH light hydrocarbon maturity parameters which exhibit good correlation with TVD and with other maturity parameters in PCA. Both the Isoheptane Ratio and 2-MH/3-MH maturity parameters highlight the flower-shaped zone thermal maturity anomaly previously identified in eastern Dewey County. 90

Figure 47. Maps of TA[I]/TA[I+II] and 4-/(4-+1-MDBT), also known as MDR, which have limited correlation with depth and other parameters in PCA. 91

Figure 48. A transect of wells in Kingfisher Country showing changes in the m/z 191 terpane fingerprint with increasing Rc%. Oils produced from wells labeled A-D also have the associated numerical key in parenthesis and which corresponds to concentration data in Table 10. Hopanes are generated at lower maturities and almost completely absent by Rc=0.94%, while tricyclic terpanes are generated at higher maturities and are present until Rc=1.05%. The absolute concentration of hopanes and tricyclic terpanes in ppm of whole oil is provided in the adjoining bar graph (bottom right). 93

Figure 49. Rate decline exponent calculations for bicyclic sesquiterpanes, tricyclic terpanes, steranes, and hopanes. 98

Figure 50. Rate decline exponent calculations for triaromatic steranes TA[I+II], phenanthrene, and dibenzothiophene. The dibenzothiophene in STACK West strongly deviates from the aggregate trend observed for STACK East and SCOOP and expresses a rate decline exponent approximately half. 99

Figure 51. Map of oil samples by Play Region and producing reservoir which will serve as preliminary guides for determining organic facies. 108

Figure 52. Typical light hydrocarbon fingerprint of oils from Springer (green), Mississippian (blue), and Woodford (red) reservoirs. Peaks for *n*-C_7 (*n*-heptane), MCH (methylcyclohexane), and Tol (Toluene) are highlighted. 109

Figure 53. Ternary diagram showing the percent abundances of *n*-C_7, MCH, Tol as a percentage of the sum of the three. STACK West oils are comparably enriched in Tol while SCOOP has two distinct clusters separating Springer production from Mississippian/Woodford production based on the relative abundances of *n*-C_7 and MCH. 115

Figure 54. Map of aromaticity values across STACK and SCOOP. STACK West oils contain elevated aromaticity compared to the other Play Regions with the approximate transition occurring in central Blaine and northwest Kingfisher counties. Aromaticity=Tol/(*n*-C_7+MCH) which is modified from B-Aromaticity (Thompson, 1983). 116

Figure 55. A schematic representation of the light hydrocarbon kinetic model at C_7 by the number of carbon ring in the intermediate structure. The connecting lines represent two-way reactions controlled by steady state catalysis rather than thermolysis. At steady state, the abundance of each grouping is controlled by temperature, pressure, and catalyzing agents. Groups “P” indicate parent compounds or are formed by

opening three-ring closure. Group "N" are cyclic compounds where the superscript gives the believed number of carbons in ring closure of the intermediary product. Recreated and modified from Mango, 1994. 118

Figure 56. Mango K_1 crossplot showing general invariance in isoheptanes. STACK West generally plots above the line K_1=1 and STACK East generally plot below. The term K_1 may be effective for oil-oil correlation in this dataset. 119

Figure 57. Crossplot derivation of the kinetic constant K_2 shows two clusters of STACK oils primarily along the X-axis representing N_2^5+P_2 as a percentage of light hydrocarbon peak area. The theorized invariance of K_2 is not observed. P_3=2,3-DMP+2,4-DMP+3,3-DMP+3-EP; N_2^5=1,1-DMCP+1*c*3-DMCP+1*t*3-DMCP; P_2=2-MH+3-MH. 120

Figure 58. Parent-daughter selectivity for 2-MH and 3-MH (P_2) based on kinetic scheme in Figure 55. STACK West shows a preference for branched isoalkanes in P_3, while STACK East exhibits a preference for cyclopentanes in N_2^5. P_2=2-MH+3-MH; P_3=2,3-DMP+2,4-DMP+3,3-DMP+3-EP; N_2^5=1,1-DMCP+1*c*3-DMCP+1*t*3-DMCP 121

Figure 59. Ternary diagram showing the fractional abundance of ring preference (RP) products for all STACK oils. Oils in STACK West generally exhibit higher Six RP compared to STACK East oils, likely driven by higher abundances of Tol. Six RP=MCH+Tol; Five RP=ECP+1*t*2-DMCP+1*c*2-DMCP+1,1-DMCP+1*c*3-DMCP+1*t*3-DMCP; Three RP=2-MH+3-MH+2,3-DMP+2,4-DMP+2,2-DMP+3,3-DMP+3-EP. 122

Figure 60. Generalized carbon skeleton of a C_{29} sterol. Additional methyl groups can be found at positions C-4, C-14, and C-23. Methyl, ethyl, or propyl groups occur at position C24 (denoted by R). Double bonds may be found at C-5, C-7, C-8, C-8(14), C-22, C-24, C-24(28), and C-25(27). From Volkman (2003). 124

Figure 61. Ternary diagram showing the relative abundance of C_{27}-C_{29} 5α(H),14α(H),17α(H) 20R steranes in STACK oils as a fraction of their sum. STACK West samples are characterized by slightly higher amounts of the C_{29} sterane. 129

Figure 62. Upper: absolute concentration of regular steranes versus Rc%. The solid black line shows the rate decline exponent of -4.34. Lower: Relative abundance of C_{27}-C_{29} 5α(H),14α(H),17α(H),20R steranes by Play Region. 130

Figure 63. The C_{30} Sterane Index (C_{30}/$C_{27\text{-}30}$ 5α(H),14α(H),17α(H),20R steranes) for all STACK oils. STACK West samples have consistently lower values at maturities and could indicate a restricted marine depositional environment. 131

Figure 64. Plot of the ratio diasteranes/steranes, defined as m/z 259 over m/z 217 over the range $C_{27\text{-}30}$ steranes. 132

Figure 65. Example m/z 217 mass chromatograms taken from six Woodford Shale core extracts from across STACK. The Woodford Shale in STACK West contain higher amounts of C_{29} regular sterane compared to C_{27} and C_{28} regular steranes. The Woodford Shale in STACK West also contains fewer diasteranes and slightly higher C_{30} sterane index. There is significant co-elution between regular steranes and some diasteranes (see Figure 28). 134

Figure 66. Simplified scheme of terpane structures. a) carbon skeleton of basic isoprene subunit; b) monoterpane skeleton showing head-to-tail linkage; c) carbon skeleton of hopane, a common polycyclic terpane, and its isoprene subunits. 135

Figure 67. Crossplot of pristane/*n*-C_{17} against phytane/*n*-C_{18} for all oils in this study showing a predominantly marine or transitional marine depositional environment. STACK East oils have slightly higher values for both axes compared to STACK West. SCOOP oils form two clusters discussed in the next section. Plot adapted from Shanmugam (1985). 136

Figure 68. Crossplot of DBT/P and Pr/Ph used to determine depositional environments (Hughes et al. 1995). A small number of STACK West samples are elevated in DBT/P despite originating from a marine shale. 137

Figure 69. Typical bicyclic sesquiterpane (BS) signature for STACK and SCOOP oils by producing formation. Peaks BS-1 through BS-8 and structures were identified from literature review (Philp et al., 1981; Alexander et al., 1983, 1984; Noble et al., 1987; Weston et al., 1989; Oung and Philp, 1994; Wang et al., 2005; Yang et al., 2009). 139

Figure 70. Ternary diagram of three closely eluting C_{15} sesquiterpanes include a rearranged drimane (BS-4), drimane (BS-5), and a third sesquiterpane (BS-6) as a fraction of the sum of the three. STACK East samples have higher relative abundances of rearranged drimane BS-4 compared to STACK West. This mirrors the higher abundances of rearranged diasteranes (**II**) also observed in STACK East and could indicate a higher abundance of acid clay sites. 140

Figure 71. Individual axes of the ternary diagram shown in Figure 70 and normalized to maturity. Lines of best fit are provided as a visual aid to guide interpretation and not meant to suggest a strong relationship with maturity. 141

Figure 72. Bicyclic sesquiterpane (BS) signature for six Woodford Shale extracts from STACK. Peaks BS-1 through BS-8 correspond to the peaks and structures identified in Figure 69. The Woodford Shale in STACK West has a higher relative abundance of BS-4 relative to BS-5 and BS-6 compared to the Woodford Shale in STACK East. 144

Figure 73. Identification of the tricyclic and tetracyclic terpane series between C_{19}-C_{39}. Chiral centers at C-22, C-27, and every five carbons thereafter form S and R couplets in C_{25}TT and higher homologues. Pentacyclic terpanes (hopanes) also share a dominant m/z 191 fraction in low maturity oils (Rc<0.9%). 146

Figure 74. Abundance of the C_{19} through C_{31} tricyclic terpanes for all STACK oils relative to total tricyclic terpanes as determined from peak areas. 147

Figure 75. Crossplot of the C_{22}/C_{21} TT versus C_{24}/C_{23} TT showing all STACK oils plot in the zone attributed to siliciclastic source material. Original plot from Zumberge et al., (2007). 152

Figure 76. Upper: Example rate decline exponent calculation for the C_{19} tricyclic terpane (STACK West=-0.79; STACK East=-2.61). Lower: Combination plot showing rate decline exponents for the tricyclic terpane series in STACK Play Regions (lines) as well as the difference in values between STACK East and STACK West (bars). 154

Figure 77. Two semi-log cross plots showing both enrichment of C_{24}TET in STACK West samples both in terms of absolute concentrate (upper) and relative to a nearby eluting tricyclic terpane (lower). 156

Figure 78. Examples of m/z 191 mass chromatograms from two oils in STACK West and STACK East of similar maturity. Peaks for C_{29} 17α(H),21β(H)-30-norhopane (C_{29}H), C_{30} 17α(H),21β(H)-hopane (C_{30}H), and the C_{31} through C_{35} 17α(H),21β(H)-homohopanes (C_{31}H through C_{35}H, respectively) are shown. STACK West oils have more C_{29}H and C_{31}-C_{35}H relative to C_{30}H which may indicate a more carbonate-style or reducing depositional environment. 157

Figure 79. Crossplot of the ratios $C_{29}H/C_{30}H$ versus $C_{31\text{-}35}H/C_{30}H$. Higher values in both ratios have been linked to depositional environment. Oils from the STACK West Play Region have higher values indicating a restricted marine or carbonate-style conditions when the source rock was deposited. Data in Table 17. 158

Figure 80. Map of the ratio of homohopanes ($C_{31\text{-}35}H/C_{30}H$) as expressed in Table 17. The transition between low values observed in STACK East and SCOOP mirrors the transition observed in aromaticity (Tol/MCH+*n*-C_7) values as shown in Figure 54. The STACK West side of the transition zone has higher values indicative of more reducing (low Eh) marine conditions during deposition and early diagenesis. 162

Figure 81. Homohopane distributions for each of the three Play Regions from data in Table 17. In general, STACK West exhibits a higher abundance of C_{35}/C_{34} homohopanes indicative of more reducing environments. STACK East shows a wide range of values indicative of the previously indicated transition zone which appears to occur in northern Kingfisher and central Blaine counties. Some SCOOP samples contain anomalous C_{33} homohopanes abundances..... 163

Figure 82. Example m/z 191 mass chromatograms taken from Woodford Shale core extracts from three cores in STACK. The Woodford Shale in STACK West contains higher $C_{24}TET/C_{26}TT(S)$ values than STACK East, but also higher values in the Upper Woodford than in the Lower/Middle Woodford. Large Ts and $C_{30}DH$ peaks observed in the Woodford core extracts were not observed in any STACK oils, but are more pronounced in the Upper Woodford than the Lower/Middle Woodford. 165

Figure 83. Maps showing the values for Mango's K_1 and $N_2^5+P_2$ (denominator in K_2) for all STACK oils showing slightly different transition zones across northern Kingfisher and central Blaine counties. 167

Figure 84. Maps showing values of $\%C_{29}$ Sterane ($C_{29}/C_{27\text{-}29}$ Sterane) and the C_{30} Sterane Index ($C_{30}/C_{27\text{-}30}$ Sterane) for all STACK oils showing mirroring transition zones across northern Kingfisher and central Blaine counties..... 168

Figure 85. Maps showing values of %Extended Tricyclic Terpanes ($C_{28\text{-}39}TT/C_{19\text{-}39}TT$) and $C_{20}TT/C_{23}TT$ for all STACK oils showing mirroring transition zones across northern Kingfisher and central Blaine counties. 169

Figure 86. Upper: Delineation of two organic facies based on Figure 54, Figure 80, Figure 82, Figure 83, and Figure 84. Lower: The transition corresponds with the thinning edge of Osage Platform and clinoformal deposition of the Meramec. Isopach from (Price, 2020)..... 171

Figure 87. Box and whisker plots detailing the geochemical parameters for two organic facies identified in Figure 85 and organized by Maturity/Isotopes, Redox/Lithology, Light Hydrocarbons, and Biomarkers. The West Facies (red) has 58 oil samples primarily in the STACK West Play Region while the East Facies (blue) has 61 oil samples. By comparison, the West Facies samples have a wider range of thermal maturities containing both the highest- and lowest-maturity oils. The West Facies have lower % Diasteranes, higher $C_{24}TET/C_{26}TT$, and higher $C_{29}H/C_{30}H$ indicative of a restricted marine environment with limited access to nutrient rich upwelling currents and low input of terrestrial sediments. Light hydrocarbons ratios based on kinetic equilibrium show differences in catalytic activity between the source rocks containing the two organic facies. The West Facies also contains a different tricyclic terpane fingerprint with lower % extended TT and higher amounts of $C_{20}TT/C_{23}TT$. Finally, the West Facies has higher $\%C_{29}$ sterane and lower C_{30} Sterane Index, indicating a more restricted marine and coastal waters with abundant green algae. 173

Figure 88. Stratigraphic type well log from SCOOP. This study includes oils produced from the Springer Group, Mississippian Group, and Woodford Shale denoted in green, blue, and red , respectively. Modified from Abrams and Thomas (2020). 176

Figure 89. Map of SCOOP oil samples in this dataset by producing formation. The SCOOP dataset includes a total of 53 oils from Woodford (26), Mississippian (8), and Springer (19) reservoirs. 177

Figure 90. Characteristic whole oil GC fingerprint for the three SCOOP reservoirs. Springer-produced oils have a distinct and different character than Woodford- and Mississippian-produced oils at the same level of thermal maturity. 178

Figure 91. The heptane ratio versus maturity forms separate trends for Woodford/Mississippian- and Springer-produced oils. Samples in map view and colored by heptane ratio values. Heptane ratio=100*n-C_7/(CC_6+2-MH+2,3-DMP+1,1-DMCP+3-MH+1c3-DMCP+3-EP+1t3-DMCP+1$t2$-DMCP+n-C_7+1c2-DMCP+MCH). 179

Figure 92. The isoheptane ratio shows separation betweenWoodford/Mississippian and Springer oils. Samples in map view and colored by isoheptane ratio values. Isoheptane ratio= (2-MH+3-MH)/(1*c*3-DMCP+1*t*3-DMCP+1*t*2-DMCP) 180

Figure 93. Ternary diagram showing the fractional abundance of three-, five, and six-ring preference (RP) compounds based on Mango's kinetic model. Six RP=MCH+Tol; Five RP=ECP+1*t*2-DMCP+1*c*2-DMCP+1,1-DMCP+1*c*3-DMCP+1*t*3-DMCP; Three RP=2-MH+3-MH+2,3-DMP+2,4-DMP+2,2-DMP+3,3-DMP+3-EP. 181

Figure 94. Ternary diagram of the C_{27}-C_{29} 5α(H),14α(H),17α(H) 20R steranes in SCOOP oils as a fraction of their sum. STACK data clusters are outlined. 182

Figure 95. Two plots generated from the distribution of steranes in SCOOP oils. The C_{30} Sterane Index=C_{30}/(C_{27}-C_{30}) steranes each of the 5α,14α,17α(H),20R isomers; diasteranes/total steranes=[m/z 259]/[m/z 217] over the range of C_{27}-C_{30} steranes 183

Figure 96. Ratio of Pr/*n*-C_{17} normalized to maturity show separate clusters for Woodford/Mississippian- and Springer-produced oils. Samples are plotted in map view and colored by Pr/*n*-C_{17} values. 184

Figure 97. Concentration of sesquiterpanes, tricyclic terpanes, and hopanes in ppm (whole oil) for all SCOOP oils. Springer oils have higher concentrations than Woodford and Mississippian oils when normalized to maturity. 185

Figure 98. Ternary diagram of three closely eluting C_{15} sesquiterpanes include a rearranged drimane (BS-4), drimane (BS-5), and a third sesquiterpane (BS-6) as a fraction of the sum of the three. Springer-produced oils plot separately from Woodford- and Mississippian-produced oils which cluster together. 186

Figure 99. Crossplot of the C_{22}/C_{21} TT as a function of C_{24}/C_{23} TT showing all STACK oils plot in the zone attributed to siliciclastic source material. Original plot from Zumberge et al., (2007). 187

Figure 100. Terpane fingerprints taken from the m/z 191 chromatogram from six oils produced from SCOOP reservoirs—three from Springer Group, two from the Woodford Shale, and one from the Mississippian Group. All oils are between 0.80-0.87% Rc and were produced from between 10,555-12,753 ft TVD. Oils from all three reservoirs show a dominance of tricyclic terpanes over hopanes, but Springer Group oils show dominant extended tricyclic terpanes between C_{28}TT up through C_{39}TT compared to Woodford and Mississippian oils. Springer Group oils also contain near equal abundances of C_{23}TT and C_{24}TT where the C_{23}TT is dominant in Woodford and Mississippian oils in both STACK and SCOOP. The C_{24}TET peak is small in all oil SCOOP oils, suggesting a more open marine depositional environment. Finally, a C_{30}DH is observed in Springer Group oils which is not readily observed in Mississippian and Woodford oils. 188

Figure 101. Abundance of the C_{19} through C_{31} tricyclic terpanes for all SCOOP oils relative to total tricyclic terpanes as determined from peak areas. 189

Figure 102. Combination plot showing rate decline exponents for the tricyclic terpane series in SCOOP (lines) as well as the difference in values between Woodford/Mississippian and Springer Group oils (bars). 190

Figure 103. Ratio of C_{24}TET/C_{26}TT(S) normalized to maturity show slightly higher values for Woodford/ Mississippian-produced oils than Springer-produced oils. Mapped sample are colored by C_{24}TET/C_{26}TT(S) values. 191

Figure 104. Map of STACK and SCOOP showing oils generated from each of the four identified organic facies. 194

Figure 105. LECO TOC measurements taken from 110 core depths across six Mississippian Group cores in STACK based on data in Table 20. Mississippian strata average a TOC of only 0.29% by weight in STACK. 196

Figure 106. Concentration of 28,30-bisnorhopane (BNH) by organic facies and producing reservoir. The highest concentration in this study is 11 ppm. 199

Figure 107. Tricyclic terpane fingerprints of Woodford Shale rock extract (upper) and Woodford-producing oil (lower) showing that extended tricyclic terpanes above C_{31}TT are present in both samples. 200

Figure 108. Box and whisker plots of aromaticity and DBT showing notable increases in oils generated from the STACK 1 (West) organic facies. DBT concentration includes both DBT and its methyl isomers (MDBT). 203

Figure 109. Crossplot of weight percent sulfur (from LECO) and Fe_2O_3 oxide (from XRF) of the ABCDS 1-6 core in Major County (map on Figure 109). The Ideal Pyrite Trend is a theoretical ratio whereby all iron and sulfur were sequestered in pyrite with none remaining. The Middle Woodford contains more sulfur than can be accounted for by pyrite mineralization based on the amount of iron in the sample. Data generated by Weatherford Labs (Table 21). 205

Figure 110. Map of STACK showing townships with reported incidents of H_2S gas. Most incidences occurred in deep wells producing from the volatile oil and wet gas window (1.0-1.3 Ro%) in the Woodward, Dewey, Ellis tricounty region with the shallowest instance occurring at 9,242 ft. 209

Figure 111. Kerogen generation products with increasing maturation. Small amounts of H_2S gas can be formed by BSR at low maturities (<0.5 Ro%). Most H_2S is formed by TSR between 1.0 and 2.0 Ro%. From (Machel, 2001). 210

Figure 112. Mango K_1 plot for oils sourced from each Woodford organofacies (after Figure 56). STACK 1 (West) oils consistently plot above unity which is characteristic in TSR-affected oils (ten Haven, 1996; Peters and Fowler, 2002). 212

Figure 113. Log-log plot of DBT and phenanthrene concentration (see Table 10). Most samples follow the main trend corresponding to changing DBT/P values with maturity. Samples which deviate from this trend are highlighted red. 213

Figure 114. Partial fragmentograms monitoring the C_{29} 5α(H),14α(H),17α(H),20R sterane in m/z 217 and the 4-, 1-, and 3-methyldiamantanes (x-MDA) in m/z 187 which are abundant in oils in mutually exclusive maturity ranges. In unmixed oils (blue), the low-maturity oil (Ward 21-1H) contains abundant steranes but low methyldiamantanes, and the high-maturity cracked oil (Mcalary 25-19-20 1H) contains abundant methyldiamantanes and no steranes. The mixed oil (Shaw Trust 30-22-19 1H) contains abundant steranes and methyldiamantanes indicating a likely mixture of low- and high-maturity oils. Methyldiamantane picks based off comparison to Grice et al. (2000). 214

Figure 115. Crossplot of the concentration of C_{29} 5α(H),14α(H),17α(H),20R sterane versus the sum of 4- and 3-methyldiamantane to determine mixing of low- and high-maturity oils. Based on Dahl et al. (1999). 217

Figure 116. Composite maps showing oils which indicate oil mixing between low- and high-maturity oils using MDA (see Figure 114), and oils which contain elevated DBT above which can be accounted for by changes in thermal maturity (see Figure 112). Both the mixed oils and the high DBT oils occur near the flower-shaped zone and where H_2S is observed in STACK West. There is not exact agreement between these two trends, but they both occur in similar portions of STACK West. 218

Figure 117. Map of DBT/P values in this study. Elevated DBT/P in shallow reservoirs likely the result of elevated organosulfur in organic source. Elevated DBT/P in deep wells possibly the result of TSR reactions. 220

Figure 118. A map of oil samples where CSIA $\delta^{13}C$ analysis was performed in this study. 222

Figure 119. (Upper) CSIA of gasoline and diesel range *n*-alkanes. STACK West samples show significant isotope excursion in the gasoline range *n*-alkanes and branched compounds. (Lower) CSIA of all gasoline range light hydrocarbons (C_4-C_8). Little or no isotope excursion is observed in the cyclic and monoaromatic

compounds over the same range. Samples marked * have GC traces shown in Figure 119. Hydrocarbon abbreviations provided in Table 7 with the addition of i-C_4 (isobutane), i-C_5 (isopentane), 2-MP (2-methylpentane), 3-MP (3-methylpentane), and MCP (methylcyclopentane). 224

Figure 120. Whole oil GC trace for eight oils depicted in Figure 118. STACK West oils with elevated CSIA $\delta^{13}C$ show a corresponding depletion in *n*-alkanes below *n*-C_{15}. Peaks corresponding to *n*-C_7 and *n*-C_{18} are marked with a star and circle, respectively. 225

Figure 121. Upper: Crossplot of IP GOR and Rc% showing two distinct production trends. Lower: Map of STACK colored by production trends overlain with STACK pressure gradients (black arrows) in psi/ft. The production-maturity trends mirror reservoir overpressure (>0.45psi/ft). Pressure gradient zones from Cullen (2017). Data found in Table 3 and Table 9. "East Wells" and "West Wells" refer to wellhead gas isotope samples (see text; Figure 121). 227

Figure 122. Two gas maturity plots for four STACK West wells showing possibly more mature (isotopically heavier) methane compared to ethane and propane. Well locations shown in Figure 120. Data generated by GeoMark Research..... 229

Figure 123. A comparison of the permeabilities between conventional and unconventional reservoir (marked by *). Note that tight sands and shales reservoirs are more similar to seals than they are to conventional sand and carbonate reservoirs. From Dembick (2016). 231

Figure 124. The heterogeneity in a conventional oil field shows a positive relationship between porosity and extracted oil maturity in core. High porosity intervals closely resemble DST produced oils. Modified from Leythaeuser and Rückheim (1989). 232

Figure 125. Terpane fingerprint of three core depths of the Caffey 32-16N-9W 1H core in STACK East with accompanying EOM (μg/g) and percent hopanes (hopanes/hopanes+tricyclic terpanes) values. There is an inverse relationship between EOM and percent hopanes over a cored interval of 246 ft. 234

Figure 126. a) Map showing location of the Caffey 32-16N-9W 1H core (black star). Offsetting wells in a nine-township region around the cored well are labeled by percent hopanes (hopanes/hopanes+tricyclic terpanes); b) Calculated percent hopanes of the three Caffey core depths in addition to the values for offsetting oils. The terpane signature of Caffey depth 9,669' has the highest producibility, as measured by EOM, and most resembles nearby produced oils. 235

Figure 127. Notable geochemical heterogeneity is observed in STACK solvent extracts. Three cores exhibit positive relationship between porosity and maturity proxies in core depths. In this model, percent hopanes is used to approximate the thermal maturity of the extracted oil at depth and EOM is used to approximate porosity. Porous beds (high EOM) correspond to higher maturity oils (low percent hopanes) and closely resemble offset oil production. 236

Figure 128. While all analyzed cores show significant spatial geochemical heterogeneity, the positive relationship between porosity and maturity proxies (EOM and % hopanes) was only observed in areas of reservoir overpressure. No relationship between EOM and % hopanes was observed in under- or normally pressured reservoirs. 237

List of Tables

Table 1. List of study oils by its 10-digit API number, well name, latitude, longitude, county, Play Region, total vertical depth (TVD) and producing formation. Each sample is given a unique numerical key between 1-172 which correspond to marker labels in Figure 13. 27

Table 2. Core samples by formation in this study. Capps Unit 1 and Ivan Ward 3-4 are legacy cores. 32

Table 3. Bulk composition parameter metrics utilized in determining thermal maturity in this chapter. The key refers to oil samples defined in Table 1. Missing API gravity values were not reported to OCC. %Volatile, %Sat, %Aro, %NSO, and %Asph correspond to percent volatile, saturate, aromatic, NSO, and asphaltene components measured during fractionation. Coll. Inst. Index=Colloidal Instability Index defined as (%Sat+%Asph)/(%Aro+%NSO). 45

Table 4. Values for sterane and terpane maturity parameters. (1) C_{29} sterane 5α(H),14α(H),17α(H) 20S/(S+R); (2) C_{29} sterane 14β(H),17β(H)/(14β,17β(H)+14α(H),17α(H)) using both 20S and 20R epimers; (3) m/z 259/m/z 217 over the range of C_{27}-C_{30} steranes; (4) $C_{20\text{-}21}$ triaromatic steroids/$C_{20\text{-}28}$ triaromatic steroids; (5) $C_{19\text{-}39}$ tricyclic terpanes/($C_{19\text{-}39}$ tricyclic terpanes + $C_{27\text{-}35}$ hopanes). 58

Table 5. Identification of numbered sterane peaks as illustrated in Figure 28. Peak identification based on comparison to Lillis et al. (1999). 60

Table 6. Identification of numbered terpane peaks as illustrated in Figure 33. Peak identification based on comparison to Lillis et al. (1999). 66

Table 7. Identification of numbered light hydrocarbon peaks as illustrated in Figure 35. Peak identification based on comparison to Walters and Hellyer (1998). 69

Table 8. Light hydrocarbon ratios tested as maturity parameters in this study. (1) (2-MH+3-MH)/(1*c*3-DMCP+1*t*3-DMCP+1*t*2-DMCP); (2) 100**n*-C_7/(CC_6+2-MH+2,3-DMP+1,1-DMCP+3-MH+1*c*3-DMCP+3-EP+1*t*3-DMCP+1*t2*-DMCP+*n*-C_7+1*c*2-DMCP+MCH); (3) *n*-C_7/2-MH; (4) *n*-C_7/MCH; (5) 2-MH/3-MH; (6) 140+15(ln[2,4-DMP/2,3-DMP]). 72

Table 9. Aromatic ratios tested as maturity parameters in this study. (1) 0.825 x (2-+3-methylphenanthrene)/(1-+9-methylphenanthrene+phenanthrene) + 0.44; (2) 4-methyldibenzothiophene/(4-+1-methyldibenzothiophene); (3) 4-+1-methyldibenzothiophene in ppm of whole oil without a relative response factor. 80

Table 10. Concentration of several biomarker classes by maturity as defined by Rc%. (1) ∑(BS-1 through BS-8) as defined in Figure 69; (2) ∑($C_{19\text{-}39}$ tricyclic terpanes); (3) ∑(m/z 217) over range of $C_{27\text{-}30}$ steranes; (4) ∑($C_{27\text{-}35}$ hopanes); (5) ∑($C_{20\text{-}28}$ triaromatic steroids); (6) phenanthrene; (7) dibenzothiophene. 97

Table 11. Light hydrocarbon isomers of heptane used in this chapter as a percentage of their sum. Compound identification shown previously in Figure 35 and Table 7. Groupings with labels “P” and “N” at top of table refer to light hydrocarbons which share a common parent or formation mechanism within the hydrocarbon kinetic scheme as described in Figure 55 and in the adjoining text. 114

Table 12. Sterane parameters used in this section for STACK and SCOOP oils. (1) C_{27}/$C_{27\text{-}29}$ steranes each of 5α(H),14α(H),17α(H),20R isomers; (2) C_{28}/$C_{27\text{-}29}$ steranes each of 5α(H),14α(H),17α(H),20R isomers; (3) C_{29}/$C_{27\text{-}29}$ sterane each of 5α(H),14α(H),17α(H),20R isomers; (4) C_{30}/$C_{27\text{-}30}$ steranes each of 5α(H),14α(H),17α(H),20R isomers; (5) [m/z 259]/[m/z 217] over the range of C_{27}-C_{30} steranes. 128

Table 13. Sterane parameters used for Woodford Shale Extracts in STACK. (1) C_{27}/$C_{27\text{-}29}$ sterane each of 5α,14α,17α(H),20R stereoisomerization; (2) C_{28}/$C_{27\text{-}29}$ sterane each of 5α,14α,17α(H),20R stereoisomerization; (3) C_{29}/$C_{27\text{-}29}$ sterane each of 5α,14α,17α(H),20R stereoisomerization; (4) C_{30}/$C_{27\text{-}30}$ sterane each of 5α,14α,17α(H),20R stereoisomerization; (5) [m/z 259]/[m/z 217] over the range of C_{27}-C_{30} steranes. 133

Table 14. Relative abundance of three sesquiterpanes from STACK oils labeled BS-4 (rearranged drimane), BS-5 (drimane), and BS-6 as a percentage of the peak area sum of the three (see Figure 69). Several high maturity oils had no discernible sesquiterpane peaks and have values marked NA (not available). 143

Table 15. Relative abundance of three sesquiterpanes from Woodford Shale core extracts in STACK labeled BS-4 (rearranged drimane), BS-5 (drimane), and BS-6 as a percentage of the peak area sum of the three (see Figure 69). 144

Table 16. The concentration in ppm of each member of the tricyclic terpane homologue series ranging from C_{19}TT through C_{39}TT and the C_{24} tetracyclic terpane (C_{24}TET). The extended tricyclic terpanes C_{33}TT through C_{39}TT are grouped into a single column C_{33}TT+. 151

Table 17. Select hopane values for oils in this study. (1) concentration of all hopanes in ppm of the whole oil; (2) (17α(H),21β(H)-homohopane (22S+22R) + 17α(H),21β(H)-bishomohopane (22S+22R) + 17α(H),21β(H)-trishomohopane (22S+22R) + 17α(H),21β(H)-tetrakishomohopane (22S+22R) + 17α(H),21β(H)-pentakishomohopane (22S+22R))/17α(H),21β(H)-hopane; (3) 17α(H),21β(H)-30-norhopane/17α(H), 21β(H)-hopane. Samples marked NA indicate where one or both ratios were not available due to insufficient signal to noise. (3) Abundance of each C_{31}-C_{35} homohopane (S+R) as a percentage of the sum of all homohopanes (C_{31}-C_{35})..... 161

Table 18. Selected ratios from the m/z 191 chromatograms of Woodford Shale extracts taken from three cores in STACK. (1) C_{24} tricyclic terpane/C_{23} tricyclic terpane; (2) C_{24} tetracyclic terpane/C_{26} tricyclic terpane (S); (3) 18α(H)-22,29,30-trisnorhopane/17α(H),21β(H)-hopane; (4) 5α(H)-methyl-17α(H)-27-norhopane/17α(H),21β(H)-hopane; (5) (17α(H),21β(H)-homohopane(22S+22R) + 17α(H),21β(H)-bishomohopane (22S+22R) + 17α(H),21β(H)-trishomohopane (22S+22R) + 17α(H),21β(H)-tetrakishomohopane (22S+22R) + 17α(H),21β(H)-pentakishomohopane (22S+22R))/17α(H),21β(H)-hopane. 164

Table 19. Summary of the four identified organic facies indicating the producing reservoirs, source formation, source lithology, interpreted depositional environment, and some notable geochemical characteristics described in this chapter. Geochemical parameters are given as a range between first- and third-quartile values, meaning at least half of the oils sourced from that organic facies fall within the presented range. 195

Table 20. TOC measurements by depth across the six Mississippian cores analyzed in this study. 197

Table 21. Elemental data from the ABCDS 1-6 core in Major County by core depth and formation. Data was generated by Weatherford Labs. (1) Weight percent of Fe_2O_3 as measured by x-ray fluorescence. (2) Weight percent elemental sulfur as measured by LECO analysis. (3) Estimated Gamma Ray (EGR) measured from elemental composition of uranium, thorium, and potassium in the sample. 208

Table 22. Total organic carbon (TOC) data from the ABCDS 1-6 core in Major County by core depth and formation. TOC data was generated from LECO by Weatherford Labs. 208

Table 23. Concentration in ppm of the C_{29} 5α(H),14α(H),17α(H),20R sterane and the sum of 4- and 3-methyldiamantae (MDA) isomers in all sample oils. Relative response factor of 0.27 was used to calculate absolute concentration methyldiamantanes from the deuterated sterane internal standard (see Figure 17). 216

Table 24. Compound specific $\delta^{13}C$ of branched and cyclic compounds taken from the gasoline fraction of 14 oils in this study. 223

Table 25. Compound specific $\delta^{13}C$ of *n*-alkane compounds taken from 14 oils in this study. The ratio DBT/P is also provided. 223

Table 26. Reservoir fluid defined by production and geochemistry. Scf/STB=standard cubic ft per stock tank barrel. 226

List of Acronyms

BO	Barrels of Oil
BOEPD	Barrels of Oil Equivalent Per Day
BSR	Bacterial Sulfate Reduction
BW	Barrels of Water
CFG	Cubic Feet of Gas
CII	Colloidal Instability Index
CSIA	Compound Specific Isotope Analysis
DCM	Dichloromethane
DFIT	Diagnostic Fracture Injection Test
EOM	Extractable Organic Matter
GC	Gas Chromatography
GC-MS	Gas Chromatography Mass Spectrometry
GOR	Gas Oil Ratio (Cubic Feet per Barrel)
IP GOR	Initially Producing Gas Oil Ratio
ISTD	Internal Standard
M- (Prefix)	Thousand
MM- (Prefix)	Million
MPI-1	Methylphenanthrene Index-1 (Radke, 1988)
NSO	Nitrogen, Sulfur, and Oxygen Containing Compounds
OCC	Oklahoma Corporation Commission
PCA	Principal Component Analysis
PPM	Parts Per Million
Rc%	Vitrinite Reflectance Equivalent (Calculated)
RF	Response Factor
Ro%	Vitrinite Reflectance Percent
RP	Ring Preference (Mango's Kinetic Model)
RRF	Relative Response Factor
SARA	Saturate, Aromatic, Resin [NSO], and Asphaltene
SCOOP	South Central Oklahoma Oil Province
STACK	Sooner Trend Anadarko (Basin) Canadian Kingfisher (Counties)
Sw_{irr}	Irreducible Water Saturation
TOC	Total Organic Carbon (often as weight percent)
TSR	Thermochemical Sulfate Reduction
TT	Tricyclic Terpanes (Cheilanthanes)
TET	Tetracyclic Terpane
TVD	Total Vertical Depth
W/W	Weight/Weight

Abstract

This project documents a large dataset of 172 produced oils and 59 core plugs from the across thirteen counties of the STACK and SCOOP petroleum systems with respect to their maturity, composition, distribution, source rocks, and producibility. Studied intervals include the Woodford Shale, the Mississippian Group, and the Springer Group of the Anadarko Basin, Oklahoma.

A principal component analysis (PCA) thermal maturity model was developed from sixteen maturity parameter inputs. The methylphenanthrene index was the best measure of thermal maturity across all plays and showed a strong covariance with depth with calculated vitrinite reflectance equivalent (Rc%) ranged from 0.74-1.43%. With increasing Rc%, the absolute concentration of biomarkers in the oils samples were observed to decline exponentially, and the rate of exponential decline was related to the biomarker complexity and stability.

Geochemical variations in produced oils were found to correspond to four organic facies which were mapped across STACK and SCOOP. Oils produced from Woodford and Mississippian Group reservoirs were generated from three organic facies across the large-scale Woodford depositional system ranging from sediment starved restricted marine in the Northwest Extension of STACK (STACK West), shallow open marine in the core of STACK (STACK East), and clay-rich open marine in SCOOP. In contrast, SCOOP oils produced from Springer Group reservoirs were generated from a single organic facies deposited in a clay-rich open marine depositional environment, probably the Caney or Goddard shales.

Three additional novel findings were made regarding the secondary subsurface mechanics and processes. First, a narrow zone of deep, volatile oil production in STACK West associated with H2S production contained high concentrations of thiophenic sulfur characteristic of thermochemical sulfate reduction (TSR) reactions. The same oils also contain high concentrations of methyldiamantanes only observed in high maturity condensates suggesting that deep TSR-affected fluids have migrated updip and mixed with lower maturity oils. Second, two separate trends were identified between Rc% and initial producing gas-oil ratios (IP GOR) for overpressured and normally pressured wells. Normally pressured wells exhibited IP GOR upwards of an order of magnitude higher than overpressured wells at any given Rc%, possibly due to mixing with methane sourced from deeper in the basin. Third, residual oil extracted from the Meramec and Osage core within the overpressured portion of the basin show that the oil is heterogeneous and not well-mixed within a vertical profile. The maturity of the fluid was found to be inversely proportional to the amount of extractable organic matter (EOM) per gram of rock, believed to be an approximation for porosity in an oil saturated reservoir. This new and exciting finding may provide a quick an effective way to predict reservoir quality and gain new insight into its charge history.

I. Introduction

The Devonian-Mississippian age reservoirs in the STACK/SCOOP resource plays of the Anadarko Basin in Oklahoma are a complex succession of very low permeability shale, mixed carbonate, and siliciclastic strata. In the last decade, prolific horizontal drilling and unconventional completion practices have demonstrated significant heterogeneity in the composition of oils produced from STACK/SCOOP reservoirs. This study explores some aspects of this heterogeneity and offers geoscientific explanations of these observations. While the analytical methods are well-documented in the peer reviewed literature, this study aims to characterize the STACK and SCOOP petroleum system not from the source rock perspective, but from a detailed geochemical analysis of the generated petroleum. This study will also explore new applications to well-established geochemical workflows to determine how source, maturity, and migration affect the composition and producibility of petroleum liquids across the basin.

The STACK and SCOOP Plays

In August of 1940, Champlin Oil & Refining successfully drilled the Kunkle #1 to its bottom hole depth of 6,939 ft in Sec. 23, T23N, R6W in what would later become the Enid field of Garfield County. Although the Missourian-aged Cottage Grove was the primary target at 5,015 ft, the operator drilled an additional 1,100 ft to explore deeper pay in the Mississippian strata below. An initial production test of the Mississippian flowed 25 BO and 2 BW over the following 24 hours, but the reservoir was considered uneconomic and not pursued. Although the well was unsuccessful, the Kunkle #1 would be among the first oils reported in the Meramec-Osage of the

Anadarko Basin. Two decades later, more discoveries near the towns of Dover and Hennessey in the Meramec-Osage triggered a surge of new drilling between 1960-1965. Development slowed when operators realized that most of the oil was produced from fractures which caused high initial production rates but rapid declines to uneconomic levels. The numerous Meramec-Osage fracture "pools" were eventually connected by later drilling and consolidated into what is now the Sooner Trend field—an area nearly 20 miles wide and extending northwest approximately 60 miles. By 1971, the cumulative production in the Sooner Trend field from Meramec-Osage production alone was 47 MMBO oil and 270 BCF of gas. With continued exploration came further understanding of its petroleum system elements, and Harris (1975) published an exhaustive review of the Meramec-Osage fracture play in the Sooner Trend field.

Thirty-six years after Harris published his landmark study in the AAPG Bulletin, a Newfield Exploration wildcat rig discovered an unconventional prospect in the Meramec formation offsetting old conventional production in the Sooner Trend field. The play was publicly announced two years later in 2013 and named the Sooner Trend Anadarko Basin, Canadian and Kingfisher Counties (STACK). In 2017, Devon completed the Privott 17-1HX, a 2-mile lateral in the Meramec offsetting the 1 Privott "8," drilled by The Rodman Corp in Sec.8, T16N, R9W of Kingfisher County. The 1 Privott "8" completion report filed in 1973 (OCC Form 1002A) reported "Mississippi Lime, shaly to silty, slightly oil stained" with an initial flow rate of 117 BOEPD (40° API gravity). Over its 16-year life, the 1 Privott "8" produced a cumulative 19.6 MBO and 176MMCFG. Forty-four years after the 1 Privott "8" was drilled, the Privott 17-1HX reported a world-class initial flow rate of 6,000 BOEPD and has produced a cumulative 595 MBO and 3.8 BCFG as of July, 2020 (Eucker and Ashby, 2020). Despite the recent downturn, drilling of the STACK has continued with development focused in Kingfisher, Canadian, Garfield, and Blaine

counties, but new operators have expanded a drilling corridor to the northwest towards Woodward, Dewey, and Major counties. Drilling and completion costs have steadily declined over the life of the play. The cost of a one-mile lateral in 2014 was $7MM with a breakeven cost of $76/bbl, and a similar well in 2016 cost $5MM with a breakeven cost of $43/bbl (Yee et al., 2017).

In 2012, Continental Resources announced a separate unconventional Mississippian-aged play in Grady and Stephens counties which would later become named the South-Central Oklahoma Oil Province (SCOOP) with the core of drilling focused in Carter, Garvin, Grady, and Stephens counties. In addition to the Meramec-Osage equivalent targets, drilling in the SCOOP also has focused on oily over-pressured sandstones within the Chesterian-aged Springer Group. Furthermore, the Mississippian-aged Caney Shale in SCOOP contains up to 9.79 wt.% TOC and serves as a substantial secondary source to the Woodford Shale (Cardott, 2017). This study differentiates production from three Play Regions based on broad regional changes in geology, operational development, and geochemical character: 1) STACK West, 2) STACK East, and 3) SCOOP. The counties that represent each of these Play Regions are shown in Figure 1.

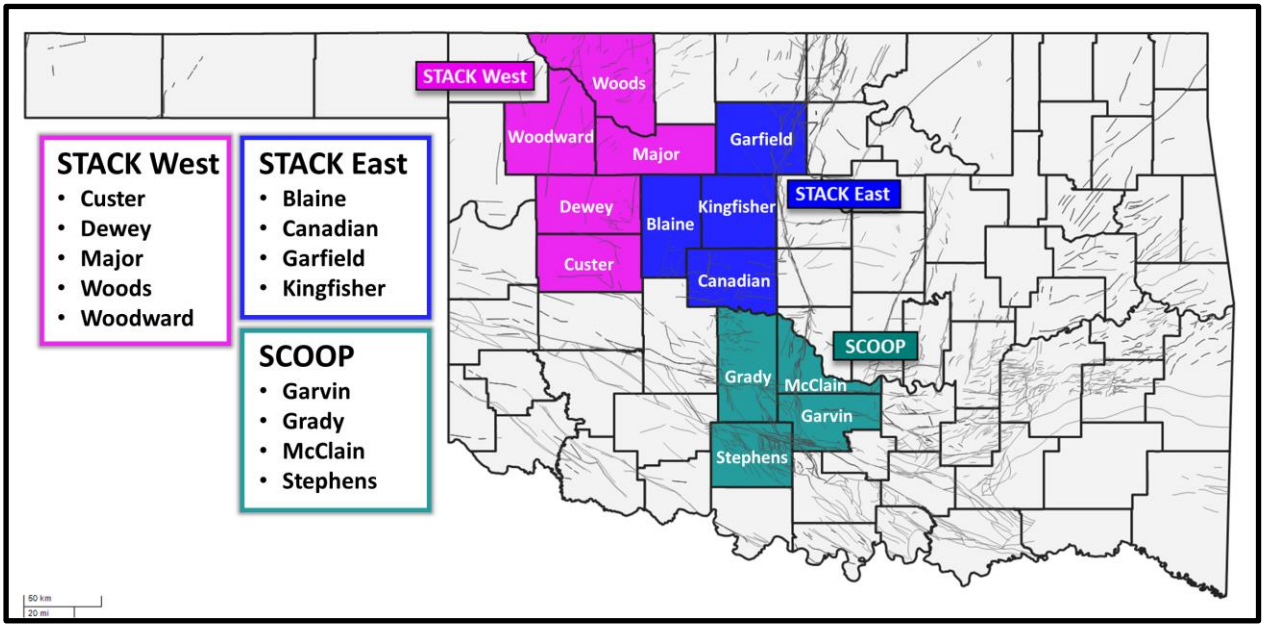

Figure 1. Map of the three Play Regions examined in this study and their producing counties.

Tight oil Mississippian reservoirs in STACK and SCOOP can be broadly characterized as "pervasive tight," a subset of tight oil reservoirs characterized by their lateral continuity and contact against a major source rock. Pervasive tight oil petroleum systems are distinguished by several specific criteria: 1) a close proximity to mature source rocks; 2) low porosity generally between 6-9% and permeability between 0.001-0.1 millidarcies (conventional porosity range 10-25% and permeability 10-1,000 millidarcies); 3) an inverted oil column with no down-dip water contact; and 4) near irreducible water saturation (Sw_{irr}) due to super-charging and dewatering by the nearby over-pressured source rock (Meckel and Thomasson, 2005). This type of tight oil reservoir is not charged by the traditional forces of buoyancy but instead from the expulsion forces and over-pressuring created by hydrocarbon generation in a nearby source rock. To maintain an inverted oil column, capillary action and surface tension must be stronger than the forces of buoyancy that drives conventional trapping mechanisms. Other examples of pervasive tight unconventional plays include the Austin Chalk (Gulf Coast), Middle Bakken/Three Forks (Williston Basin), Spraberry trend (Midland Basin), Altamont field (Uinta Basin), Cardium Pembina trend (Alberta Basin), and Chicontepec Field (Mexico) (Meckel and Thomasson, 2005).

Organic Geochemistry in Hydrocarbon Exploration and Development

Organic geochemistry has been integrated into the workflows of successful petroleum exploration and development programs for almost a century. For clarity, the following overview is divided into two subsections to discuss the separate advances made in non-biomarker and biomarker analyses. In this study, biomarkers refer specifically to organic compounds in a geologic sample that are structurally related to their precursor molecules occurring as a natural product in plants, animals, bacteria, fungi, or other living organisms (Philp and Lewis, 1987). Many of the analyses described below are incorporated into this work in later chapters.

Advances in Non-Biomarker Geochemistry

The first successful source rock-oil correlation was performed in the Uinta Basin of Utah in 1954 by integrating chromatography, infrared spectra, refractive indices, elemental analysis, and physical properties to identify four major source rocks and correlate them with liquid hydrocarbons in the basin (Hunt et al., 1954). The specific mechanisms of petroleum formation remained unknown at the time, but over the next decade it was demonstrated that hydrocarbons could not be spontaneously generated from sedimentary organic matter during burial (Forsman and Hunt, 1958; Bray and Evans, 1961), but instead must undergo a diagenetic transformation into kerogen prior to hydrocarbon generation (Abelson, 1963; McIver, 1967).

To better understand coal deposits, van Krevelen (1961) developed the van Krevelen diagram for rapidly determining the quality of coals by crossplotting the ratios of atomic H/C versus O/C as well as mapping maturation processes as the ratios change with coalification. The van Krevelen diagram was later expanded from coal research to petroleum exploration by cataloging sedimentary systems of different ages and depositional environments resulting in the popular distinction of organic matter into types I-IV (Tissot et al., 1974). Despite its success, the widespread use of the van Krevelen diagram was challenged because it required isolating organic matter and running an assay for hydrogen, carbon, and oxygen, so a more accessible "modified" van Krevelen diagram was developed following the development of the Rock-Eval pyrolyzer (Espitalié et al., 1977). Within a decade, the "modified" van Krevelen diagram had become a standardized best practice in source rock characterization by offering quick and cheap measurement of the quantity, quality, maturity, and producibility of sedimentary organic matter.

Several other breakthroughs in petroleum systems analysis were also occurring in parallel at this time. The first efforts to catalog the carbon isotopic composition of crude oils and other

source-related sedimentary organic matter was published (Silverman and Epstein, 1958) paving the way for landmark work linking carbon isotopes to thermal maturity (Fuex, 1977; Stahl, 1977), source-oil correlations (Stahl, 1978), depositional environments (Sofer, 1984), geologic age (Andrusevich et al., 1998), and even depositional paleolatitude (Andrusevich et al., 2000). Meanwhile, significant advances in capillary column technology opened a new field of study of the volatile gasoline range components of crude oil without prior distillation. Presenting at the 6th World Petroleum Congress, Martin et al. (1963) demonstrated a striking regularity in the ratios between certain isomeric groups of light hydrocarbons from unrelated oils and provided the first evidence that the composition of some light hydrocarbons is primarily controlled by thermodynamics. Over two decades later, Mango (1987) confirmed Martin's findings by deriving the equation for steady state kinetics between branched isomers of heptane and later showed that many heptane isomers are daughter products of *n*-heptane in steady state (Mango, 1990a). Thompson (1979) derived ratios of light hydrocarbons to describe the paraffinicity, aromaticity, and paraffin branching of oils and demonstrated their viability for describing both thermal maturity and source. Thompson's work was later expanded to include oil-source rock correlation (Thompson, 1983) and reservoir seal leakage (Thompson, 1987 and 1988). Through detailed measurements of light hydrocarbon ratios within an alternating organic shale-siltstone sequence, Leythaeuser et al. (1982 and 1983) first recognized and quantified the role of diffusion and expulsion efficiency during primary migration. His work would later lay the groundwork for modeling the diffusion of methane and ethane-rich gas caps through reservoir cap rock seals (Krooss and Leythaeuser, 1997).

Advances in Biomarker Geochemistry

The study of biological fossils made its first major impact on the earth sciences in 1936 when German chemist Alfred Treibs showed the link between chlorophyll-a in living photosynthetic organisms and metal-containing porphyrins from numerous crude oils and shales (Treibs, 1936). Treibs deduced that the oils were of biologic origin, thus providing the first strong evidence for an organic origin of petroleum. Despite Treibs insight, the widespread study of biological fossils would not begin until the 1960s after major breakthroughs interfacing gas chromatographs and mass spectrometer systems and the development of capillary gas chromatography columns. In the 1964, a team led by Geoffrey Eglinton from University of Glasgow published a paper in *Science* describing biological markers, or biomarkers, as classes of organic compounds that are stable for long periods of time under geologic conditions (Eglinton et al., 1964). In their search for Precambrian life, Eglinton and his team found certain molecular families (i.e. alkanes, long-chain fatty acids, and porphyrins) to be promising biomarker candidates if it could be demonstrated they were not synthesized by abiogenic means in significant quantities.

Early paleobiogeochemists continued to find notable biochemical similarities between modern and ancient sediments. Although organisms do synthesize unique compounds, different organisms may also produce many of the same compounds just in different proportions. This discovery paved the way for the new discipline of chemotaxonomic classification of ancient organisms (Eglinton and Calvin, 1967). Perhaps taking inspiration from James Hutton's Uniformitarianism (Hutton, 1788), paleobiogeochemists soon began comparing biomarkers in modern and ancient sediments to draw inferences about ancient organisms, depositional environments, and diagenetic history (Whitehead, 1973; Philp et al., 1976; Brassell et al., 1978).

A biomarker can be described as an organic compound in a geological sample that can be structurally related to its precursor molecule which occurs as a natural product in a plant, animal, bacteria, spore, fungi, or any other potential source material (Philp and Lewis, 1987). Biomarkers are distinguished from other organic compounds in several ways. First, biomarker structures are often composed of repeating subunits which indicates their precursors were components of a living organism; second, biomarker precursors are common in certain organisms which can be abundant or widespread; and third, biomarkers are stable during sedimentation and early burial (Peters et al., 2005a). In hydrocarbon exploration and development, biomarker studies have been successfully implemented to correlate oils with each other or suspected source rocks, quantify thermal maturity and/or biodegradation, detect regional variations in depositional environment and organic input, and derive petroleum generation kinetics in a basin history (Tissot and Welte, 1984; Hunt et al., 2002; Peters and Fowler, 2002; Peters et al., 2005a; Philp, 2014; Curiale and Curtis, 2016; Dembick, 2016).

II. Geologic Background

The Anadarko Basin

The following section attempts to summarize the history of the Anadarko Basin and relies heavily on the works of Huffman (1959), Ham et al. (1964), Ham and Wilson (1967), Rascoe and Adler (1983), Johnson et al. (1988), Johnson (1989), and Johnson and Cardott, (1992).

The Anadarko Basin is strongly asymmetric basin elongated west-northwest with the deepest sediments adjacent to the Amarillo-Wichita Uplift to the southwest. The basin is bounded to the southwest by the Amarillo-Wichita Uplift, to the southeast by the Arbuckle uplift and Marietta-Ardmore Basin, to the east by the Nemaha Ridge, and the north by the Anadarko shelf, and the west by the Cimarron Arch (Figure 2). The Anadarko Basin of western Oklahoma is the

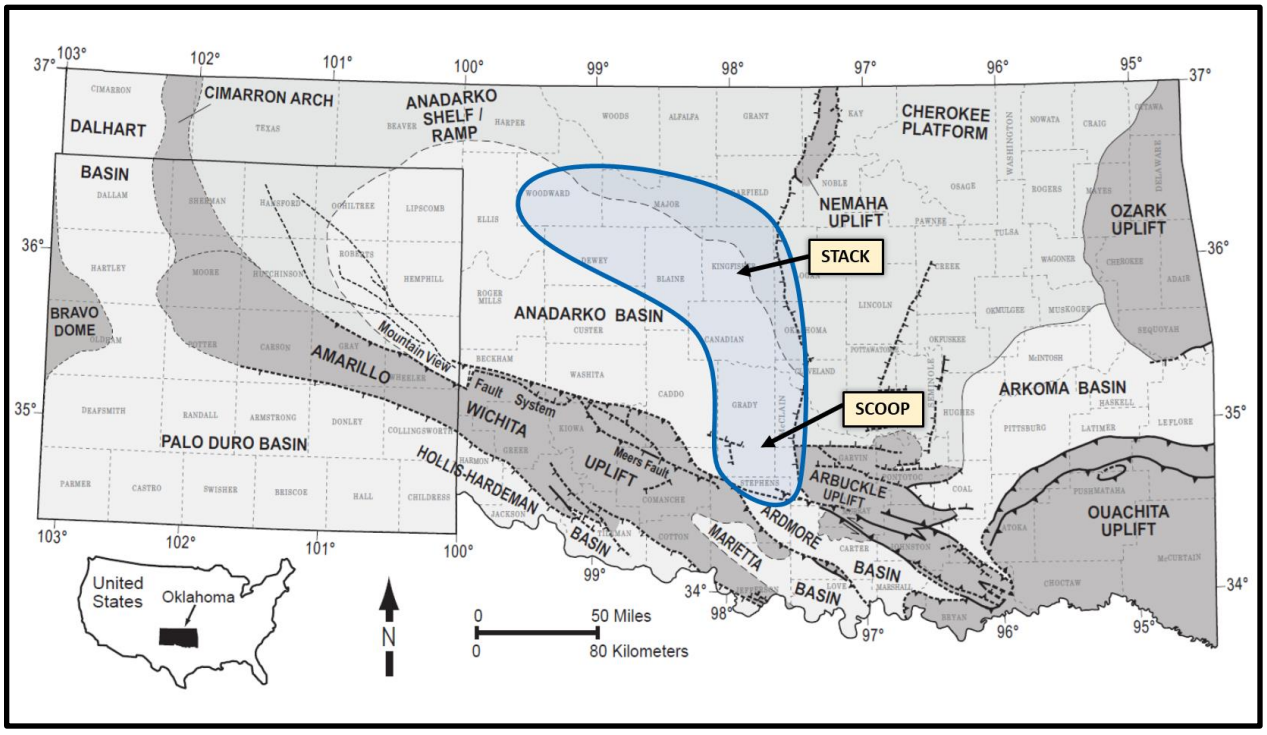

Figure 2. Outline of the Anadarko Basin and its major structural boundaries. The STACK/SCOOP study area is highlighted. Modified from Pranter et al. (2016).

deepest sedimentary basin in the cratonic interior of North America with as much as 40,000 feet of Paleozoic sediments. The history and formation of the Anadarko Basin can be divided into four distinct phases, described below.

The first stage of the development of the Anadarko Basin began during the Precambrian-aged Midcontinental Rifting when a triple junction rifting event failed during the separation of Rodinia and the opening of the Iapetus Ocean. The northwest extending limb of the failed triple junction created an isostatic depression of the crust, decompression melting, and formation of a large igneous province known as the Southern Oklahoma Aulacogen. The regional depression became the Oklahoma Basin and precursor to the modern-day Anadarko Basin (Johnson, 1989).

The second stage occurred from the Late Cambrian through Mississippian time as the newly formed Oklahoma Basin was covered in an epeiric sea which deposited thick sequences of sandstone, shale, and carbonates. Two major epeirogenic uplifts and unconformities occurred during the Early Devonian and pre-Woodford Late Devonian as the result of regional upwarpings. Despite regionally correlative unconformities, the epeirogenic uplifts during the Devonian created very little faulting and folding except near the edges of the basin, notably the faulting and uplift of the Nemaha Ridge. During the Late Devonian and Early Mississippian, the shallow marine environment over the Oklahoma Basin became highly productive with euxinic bottom water conditions, depositing of the organic-rich, black Woodford Shale source rock which covers much of Oklahoma. By the Osagean series, the euxinic inland sea was replaced by a shallow, well-oxygenated marine environment warmed by subtropical latitude (Curtis and Champlin, 1959) and allowing the formation of a wide carbonate ramp/shelf complex along the northern edge of the basin due to low clastic input. Mississippian deposits are mostly fossiliferous (often crinoidal) limestones with interbedded shales and carbonate cemented siltstones. As much as 15,000 ft of

sediments were deposited into the Oklahoma Basin between the Cambrian and Mississippian time (Johnson, 1989).

The third stage began in the Early Pennsylvanian when dormant extensional faults from the failed Precambrian rifting were reactivated in a new compressional system. The Wichita-Amarillo block was uplifted along a series of west-northwest trending reverse faults up to 40,000 ft at a steep angle creating a deep asymmetric foreland basin and forming the modern Anadarko Basin (McConnell, 1989). Proximal deposits to the Amarillo-Wichita uplift are coarse alluvial clastics known as "granite wash," while the rest of the basin was filled with mostly marine shales, sandstones, and limestones. The syndepositional wedge of sediment thickens southwards towards the modern-day Wichita Mountains and accounts for as much as 18,000 ft of Pennsylvanian sediment in the foredeep. Despite major tectonic activity, no major igneous or metamorphic activity occurred in or near the Anadarko Basin during this stage. Beginning in the Desmoinesian, the Anadarko Basin experienced three other orogenic events which affected regional stresses and sedimentation, including the Apishapa Uplift in southeastern Colorado, the Arbuckle Uplift in south-central Oklahoma, and the Ouachita Uplift in southeastern Oklahoma (Johnson, 1989).

The fourth and final stage began in the Permian when the major tectonism of the Pennsylvanian was replaced with epeirogenic subsidence and basin filling. The sediments of this period are characterized by Permian carbonates, red beds, evaporites, and thin post-Permian strata. Through Permian to the Jurassic, the Wichita-Amarillo block had ceased uplift and began to subside and become buried under its own clastic debris losing upwards of 7,000 ft in relief. Subsidence in the Anadarko Basin continued until the Cretaceous when the Farallon Plate began subducting under the North American Craton creating a major east-west compressional regime resulting in the Sevier and Laramide orogenies and the formation of the North American

Cordillera. The Laramide Orogeny uplifted the entire Anadarko Basin as well as tilting it east-southeast and causing the Cretaceous Inland Seaway to retreat from the basin (Johnson, 1989). A structural cross section of the Anadarko Basin is shown in Figure 3.

STACK and SCOOP Petroleum Systems

The Devonian-Mississippian STACK/SCOOP plays have the components in place for a prolific petroleum system, including porous facies and natural fractures, stratigraphic proximity to a mature and world class source rock, low water saturations, a competent and regionally extensive top seal, varying degrees of over-pressure, and a range of fluids spanning the entire oil and gas maturity window. The most common drilling targets include the Early Mississippian limestones and siltstones and Chesterian-age Springer Group sandstones (SCOOP only) but can also include the Woodford Shale source itself. Porous reservoir facies in the Mississippian generally have 5-10% porosity and approximately 40% water saturation of entirely bound water (Jefferies, 2016). Most drilling operations target the volatile oil window where reservoirs are solution gas drive, below bubble point pressure, and where produced oil averages 40-50° API. Conventional field analysis of the Sooner Trend suggests that oil was emplaced before the deposition of the Cherokee

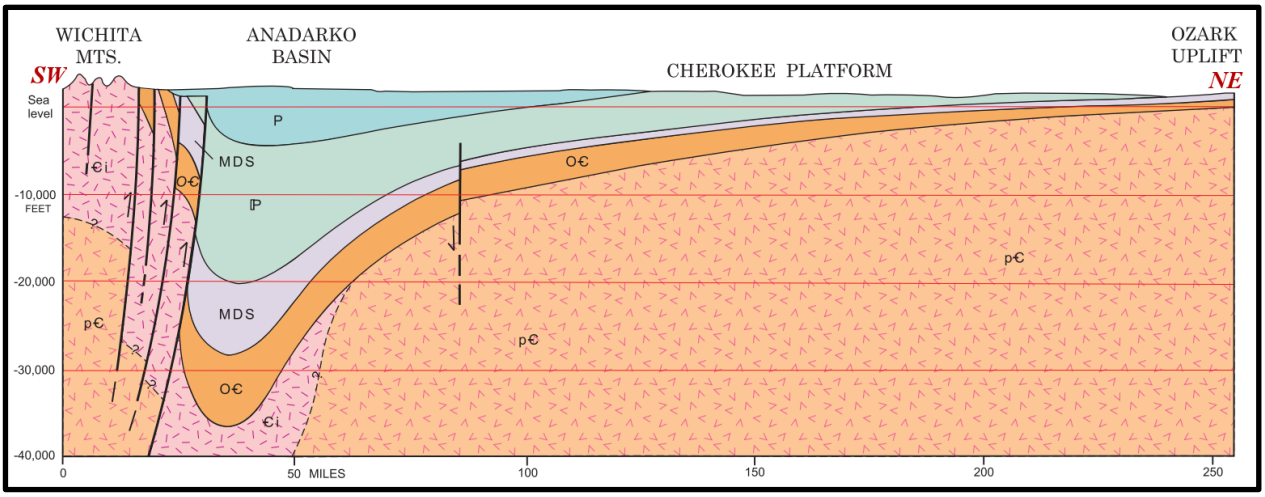

Figure 3. Cross section of the Anadarko Basin from southwest to northeast. From Johnson (2008).

Group on the pre-Pennsylvanian regional unconformity (Harris, 1975). The Devonian-aged Woodford Shale is believed to be the lower seal as well as the primary hydrocarbon source for Mississippian-aged reservoirs in the Anadarko Basin (Engel et al., 1988; Burruss and Hatch, 1989; Wavrek, 1992; Rahman et al., 2017; Symcox and Philp, 2019a). The Chesterian-aged Springer Group shales are believed to act as an upper seal in STACK East and SCOOP, however there is significant thinning of the sealing shales towards STACK West due to post-Chesterian subaerial exposure and erosion (Harris, 1975). In fact, the truncated erosional edge of the Springer Group coincides with the updip limit of conventional fractured Meramec-Osage production in the Sooner Trend field beyond which water production increases significantly. A generalized stratigraphic column for the STACK and SCOOP play regions discussed in this study is provided in Figure 4.

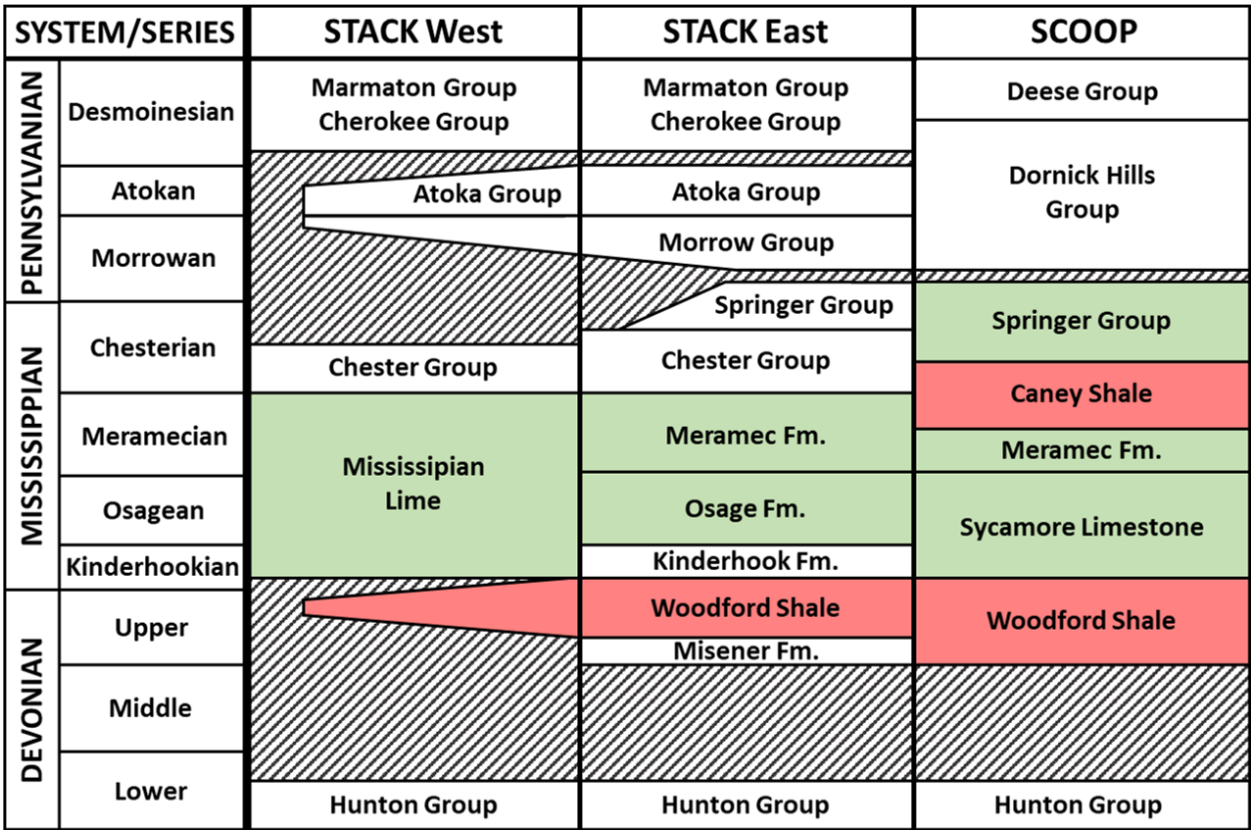

Figure 4. Generalized stratigraphic column with major source rocks and reservoirs are shown in red and green, respectively. Height of formation boxes is not related to thickness of unit. Constructed based on the works of Harris (1975), Johnson (1989), Johnson and Cardott (1992), Henry and Hester (1995), Higley (2013), and Cardott (2017).

The Late Devonian/Early Mississippian Woodford Shale is unquestionably the most prolific and well-studied oil and gas source rock in Oklahoma (e.g. Burruss and Hatch, 1989; Higley et al., 2014). The Woodford Shale occurs in Oklahoma, Texas, Arkansas, and New Mexico and is laterally equivalent to several other North American black shales including the Chattanooga, New Albany, Bakken, Antrim, and Ohio shales as shown in Figure 5 (Conant and Swanson, 1961; Ettensohn and Barron, 1981). The unconformable base of the Woodford Shale marks the bottom of the Kaskaskia sequence in the Midcontinent (Sloss, 1963). The Woodford is primarily a dark-grey to black fissile shale that also contains chert, siliceous and dolomitic mudstone, and siliceous shale (Portilla, 2017). Anaerobic sea floor conditions during Woodford deposition prohibited most benthic life but in turn facilitated excellent preservation of pelagic organic matter, commonly observed between 1-14% TOC by weight of primarily Type II kerogen (Burruss and Hatch, 1989;

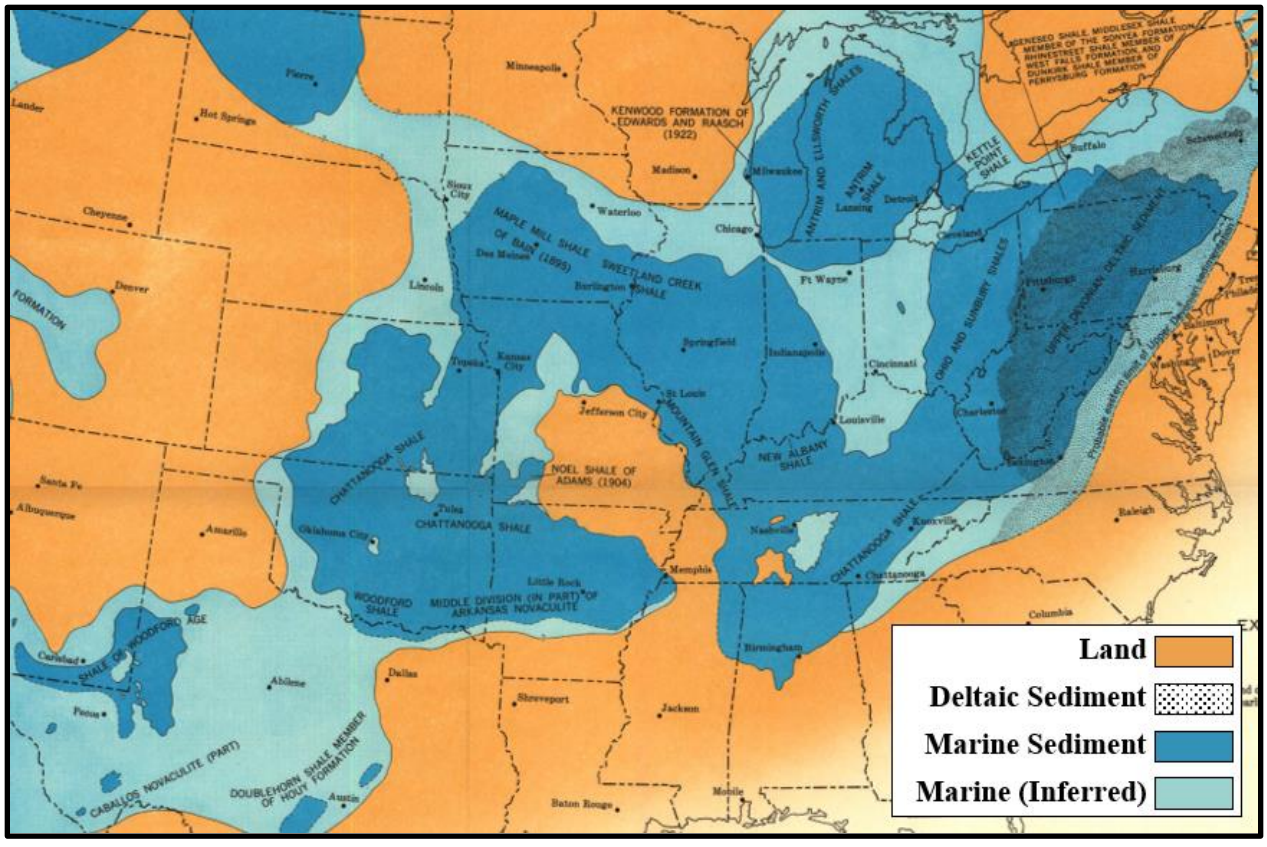

Figure 5. Approximate regional distribution of Upper Devonian and Lower Mississippian black shales in the United States, shown in blue. From Conant and Swanson (1961).

Cardott, 2012). The Woodford is present throughout most of the Oklahoma Basin (precursor to the modern Anadarko Basin) and ranges from 200-900 ft thick in the Southern Oklahoma Aulacogen but is 50-100 ft thick on the shelf areas which comprise the STACK and SCOOP (Johnson et al., 1988; Johnson and Cardott, 1992; Higley et al., 2014).

Excluding the basal Misener Sandstone, the Woodford Shale is divided into Upper, Middle, and Lower members based on well-log signatures, palynomorphs, geochemical proxies, and lithofacies associations (Sullivan, 1985; Hester et al., 1990; Lambert, 1993; Miceli Romero and Philp, 2012). Three maps provided in Figure 6 show a total Woodford isopach as well as the regional extent and thickness of its Upper, Middle, Lower, members across STACK. A period of regional subaerial exposure and erosion prior to the deposition of the Woodford resulted in the incision of stream channels in the underlying Hunton Group which were first flooded during the marine transgression advancing onto the craton from the south (Bunker et al., 1988; Zhang and Slatt, 2019). As a result, the thickness of the Lower Woodford is often inversely proportional to the thickness of the Hunton as eroded valleys and karsts provide isolated paleo-lows that provide accommodation space for thicker accumulations (Torres-Parada, 2020). The Woodford Shale thins considerably towards STACK West, especially the Upper and Lower members, due to reduced accommodation space approaching the basin margin. The pyritic Middle Woodford generally has the highest gamma ray and total organic carbon (TOC) values, likely the result of the Late Devonian oceanic anoxic event (OAE) which coincided with maximum flooding event, as is evident in map view of Figure 6 (Lambert, 1993). The Upper Woodford member contains cherty beds interbedded with fissile shale beds which contain abundant clays and carbonate minerals (Portilla, 2017), as well as numerous phosphate nodules indicative of deep marine conditions close to the oxygen minimum zone (Miceli Romero and Philp, 2012).

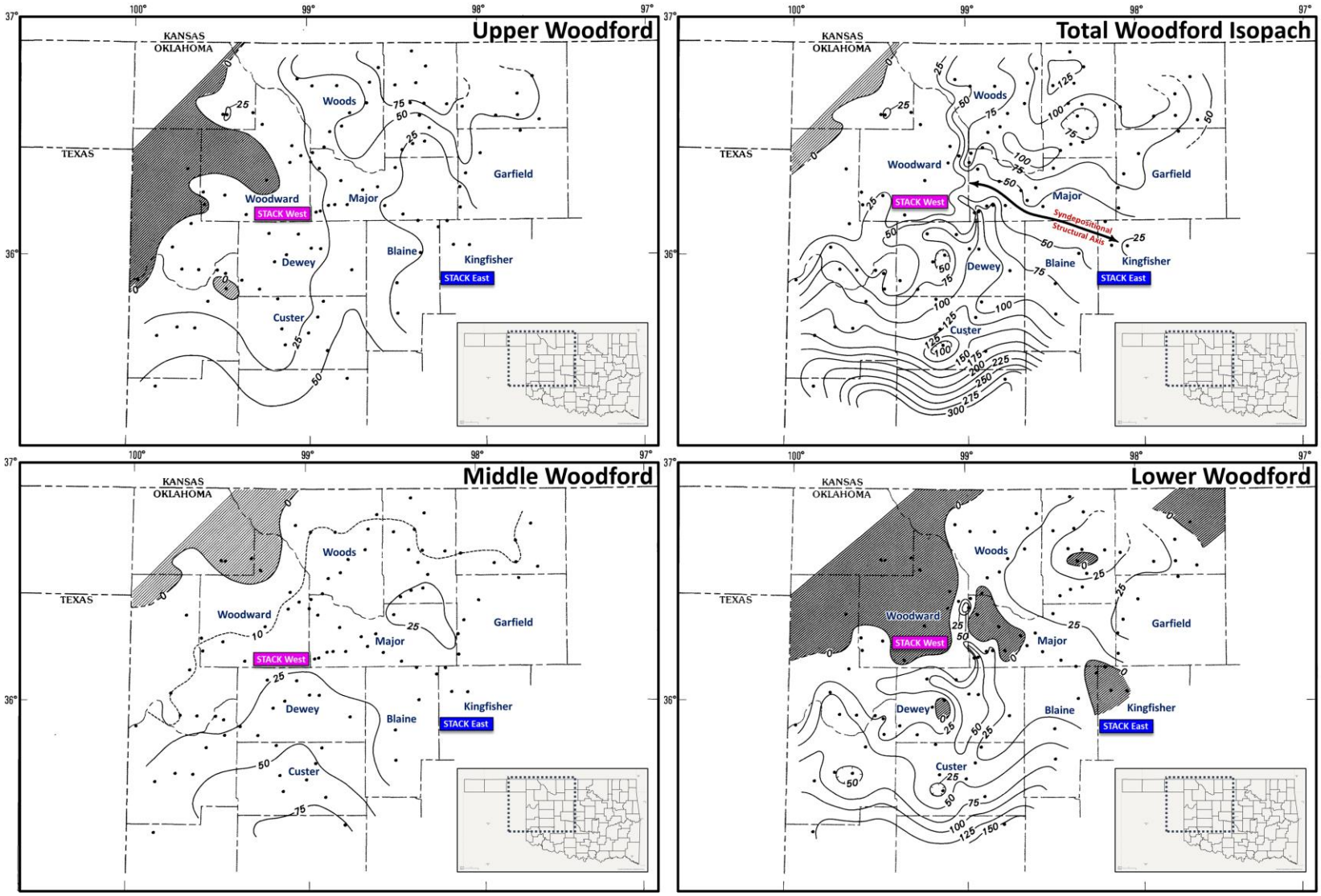

Figure 6. Thickness of the three Woodford Shale members as well as total Woodford isopach based on well logs; contour interval 25 ft. Areas where Woodford Shale is absent is hachured. Dots show well locations. The syndepositional structural axis is depicted as bold arrow. The Woodford Shale thins substantially towards STACK West, and the Upper and Lower members are absent in some cases. Modified from Hester et al. (1990).

The Mississippian system is a series of shallow-marine limestones, cherty limestones, silty mudrocks, and carbonate cemented siltstones deposited in shallow, well-oxygenated marine waters. During the Osagean, a widespread carbonate and sponge bank formed and began to aggrade along the shallow marine rim of the basin depositing predominantly bioturbated siltstones, bioturbated wackestones, grainstones, and spicular chert (Figure 7). The Osagean section is not typically a drilling target due to low intergranular porosity and abundant cherts which can damage drilling equipment, however the Osagean limestones likely contributed to the overlying reservoirs by providing migration pathways from the underlying Woodford through a fractured carbonate network (Bynum and Wethington, 2020). Drilling in the Osage is most common in STACK West where thicker accumulations of carbonate are deposited, however there is some production along the northeastern margins of STACK East. To the south in SCOOP, the Osage-equivalent Sycamore Limestone is primarily silty peloidal packstones to peloidal siltstones and shale and is believed to

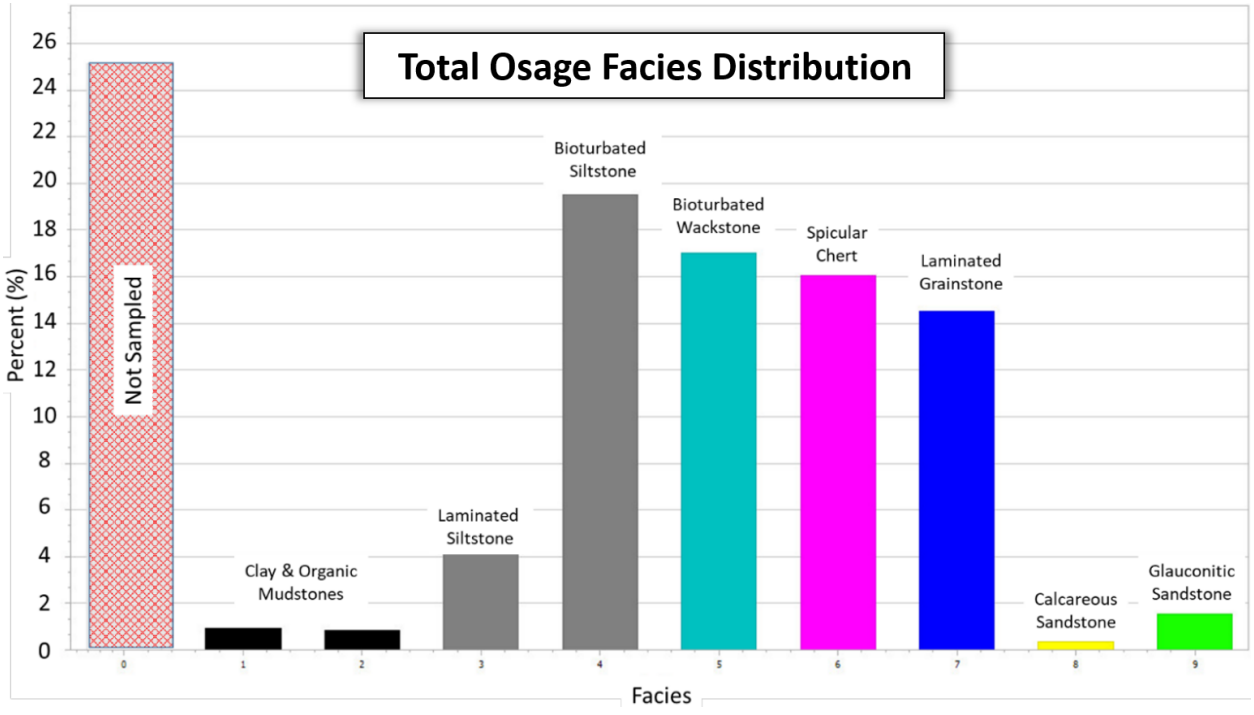

Figure 7. Histogram of Osage facies in STACK measured from cores of four complete Mississippian intervals located in Blaine, Kingfisher, and Canadian counties. At least 37% of the Osage has been bioturbated by benthic organisms suggesting well-oxygenated bottom waters. From Bynum and Wethington (2020).

represent deposits of transported terrigenous clastic rocks and reworked carbonate material, possibly as a result of strong marine storms (Cole, 1989).

Depositional facies changed dramatically during the Meramecian in response to the onset of the Acadian Orogeny along the eastern edge of Laurentia. The Meramec represents a transition period between the carbonate-dominated Osage section and siliciclastic-dominated Chester section and contains the most facies variability in the Mississippian System (Figure 8). The Meramec Fm. represents a period of progradation of the carbonate shelf in response to the first observable influx of siliciclastic mixing (Bynum and Wethington, 2020). The significant increase in siltstone facies and decrease in chert makes the Meramec a superior drilling target with higher intergranular porosity and lower drilling hazards. The Meramec parasequences comprise a stacked lenticular geometry associated with a progradational system ranging from 0 to 600 ft with an average thickness of 360 ft. over the play interval and thickening toward the basin-depocenter to the

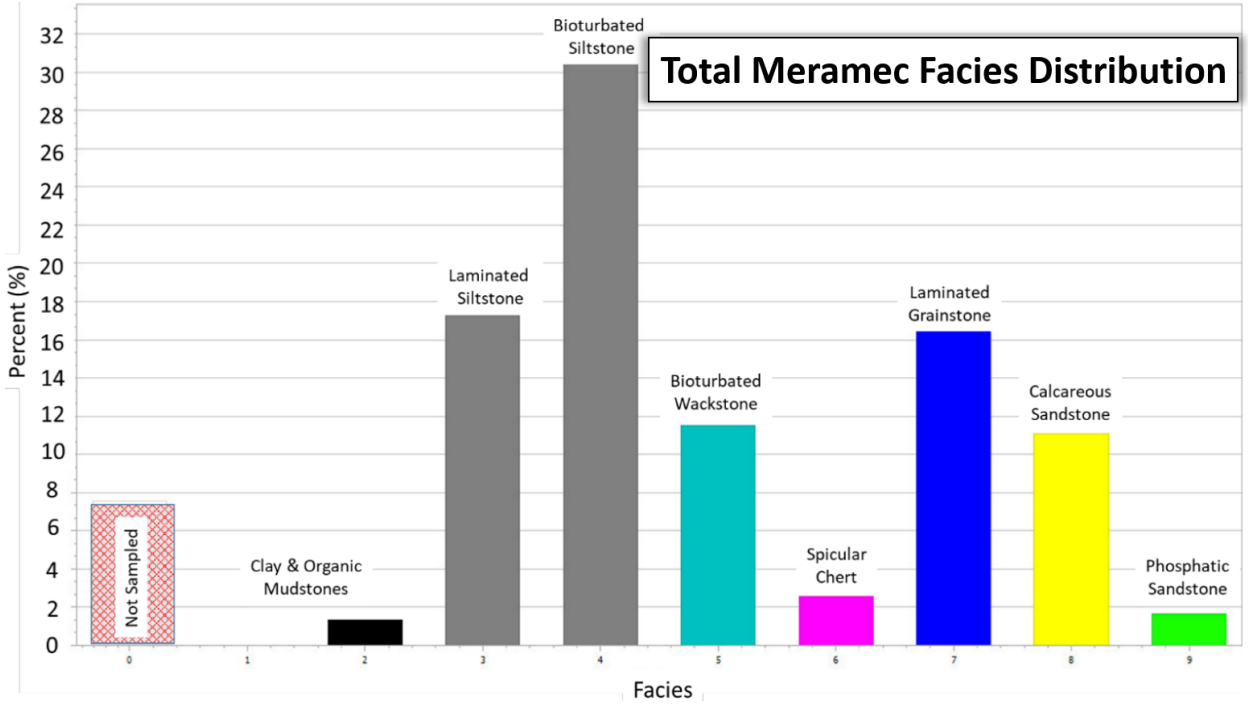

Figure 8. Histogram of Meramec facies in STACK. There is a notable increase in siltstone facies concurrent with a decrease in chert facies making the Meramec a preferred drilling target. From Bynum and Wethington (2020).

southwest, shown in Figure 9 (Price, 2020). The Meramec thins considerably towards SCOOP where it is comprised of the fine-grained distal toe deposits of the STACK progradational system.

After the carbonate-siliciclastic transitional period observed in the Meramecian, the Chesterian represents the transition to a siliciclastic-dominated system that choked out the carbonate biocommunities living along the shelf margins. In STACK, Chester facies are dominated by laminated siltstones, bioturbated siltstones, and calcareous sandstones while containing less than half the volume of carbonate facies observed in the underlying Meramec and Osage sections

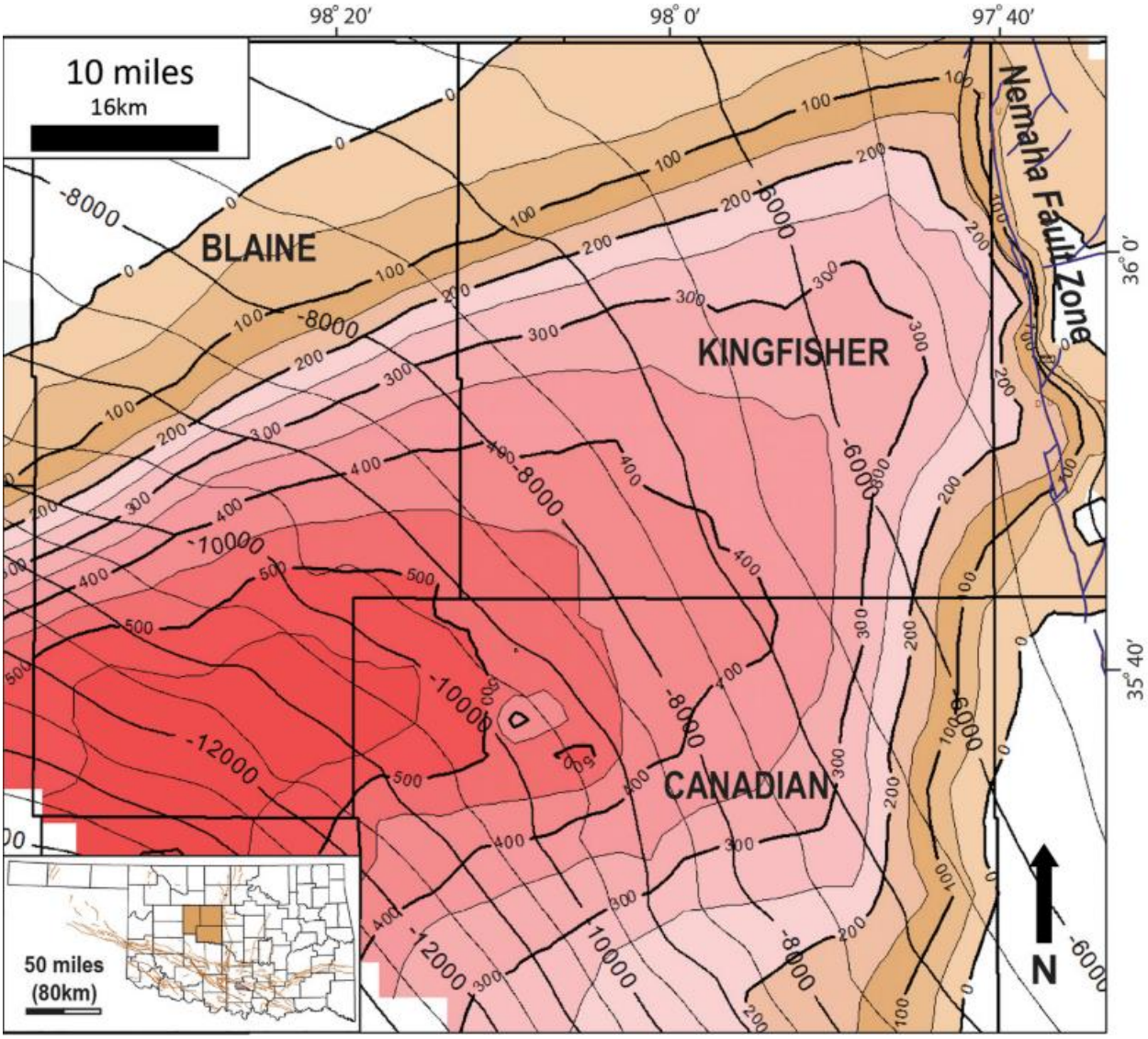

Figure 9. Isopach of the Meramec Fm. in STACK with subsea structure depths. From Price et al. (2020).

(Figure 10). The increase in siliciclastic facies and lower facies variability likely contribute to higher reservoir quality (Bynum and Wethington, 2020); however, the Chester is rarely targeted for drilling because of the risk of lower pressure and oil saturation due to its stratigraphic distance from the Woodford source. Further exploration of the Chester may prove successful south towards the SCOOP areas but at the expense of increased shale content deposited in deeper water.

Chesterian-aged Caney Shale found in SCOOP represents the deep-water organic-rich facies deposited distal to the dominant sedimentary inputs to the north. The Caney Shale is a series of mudrocks, limestones, and siltstones, as well as bituminous shales containing between 1-9% TOC of dominantly Type II kerogen (Cardott, 2017) and age equivalent to the Barnett Shale of Texas and the Fayetteville Shale of Arkansas. The Caney interval shows strong development of organic-rich mudrocks towards the south into the Ardmore basin (Miller and Cullen, 2018), but

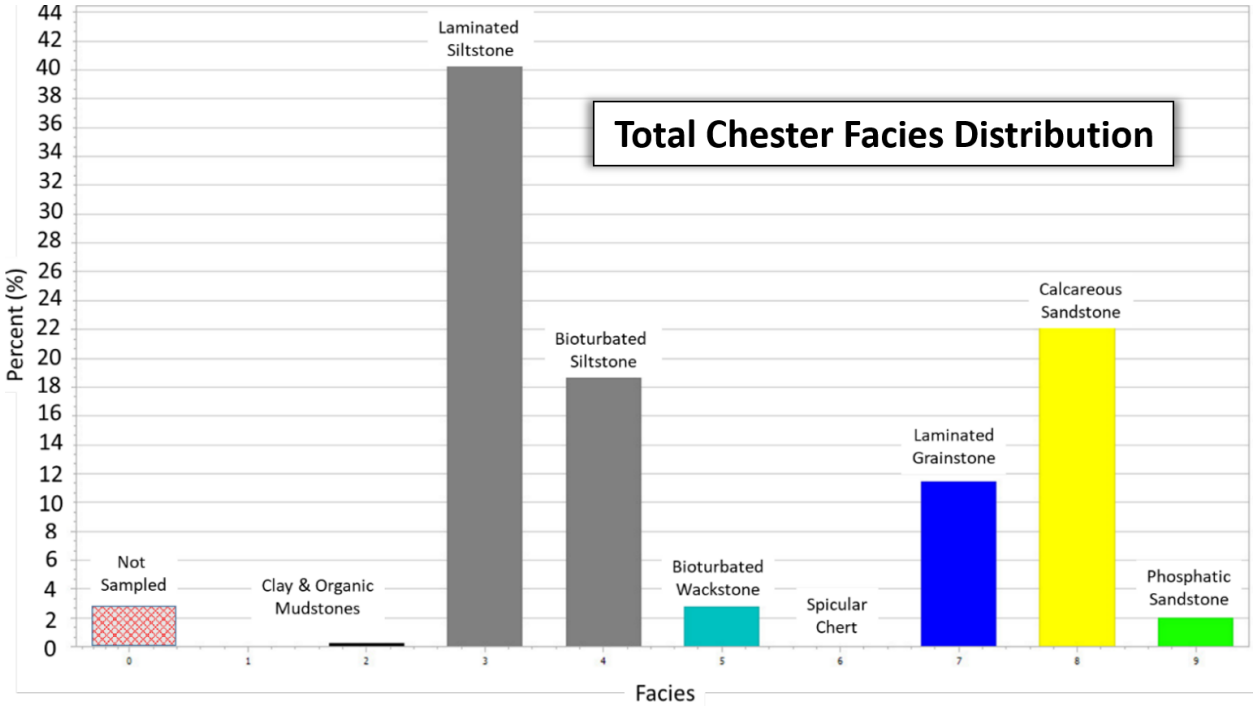

Figure 10. Histogram of Chester facies in STACK. Note the substantial increase in siliciclastic relative to carbonate facies as well as the absence of spicular chert facies. From Bynum and Wethington (2020).

due to high levels of clay and more ductile framework, commercial production from the Caney in the Anadarko is challenged.

The Mississippian system over STACK and SCOOP illustrates the transition from a carbonate-dominated shelf system to a siliciclastic-dominated system. The facies stacking patterns in conjunction with depositional geometries have facilitated stratigraphers in developing a robust depositional model for the Mississippian in the Anadarko Basin (Figure 11). A well-log gamma-ray cross section (Figure 12) shows the silty Meramec clinoforms which form a progradational wedge over the top of the Osage shelf. After the Meramec was deposited, the oceans transgressed depositing the siliciclastic Chester across the top of the entire system.

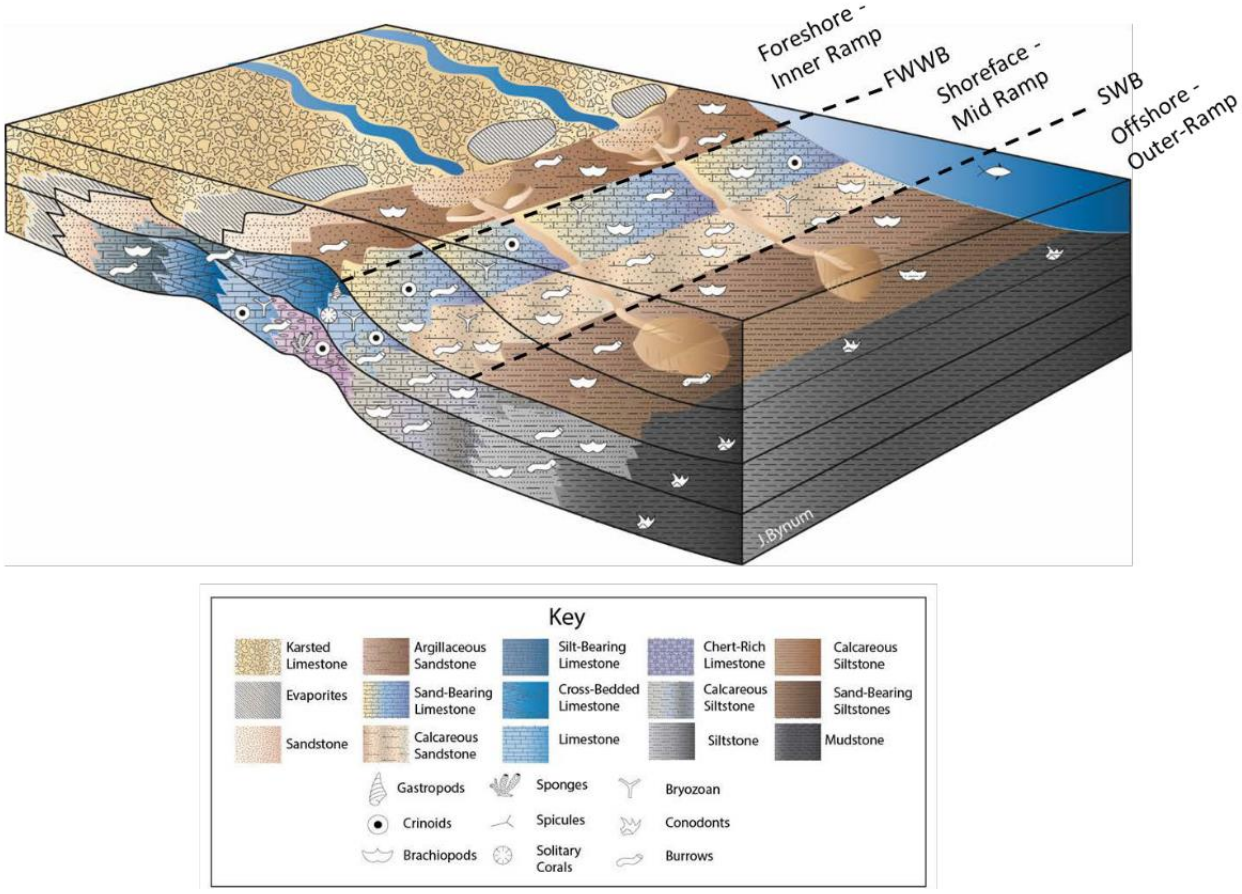

Figure 11. Block diagram depositional model for the Mississippian Group showing the transition from a carbonate-dominated system to a siliciclastic-dominated system. The carbonate system ranges from grainstone dominated inner-ramp deposits to calcareous siltstone dominated outer- ramp deposits. The siliciclastic system ranges from arkosic sandstone dominated upper shoreface deposits to siltstone dominated offshore deposits. FWWB=fair weather wave base; SWB=storm wave base. From Bynum and Wethington (2020).

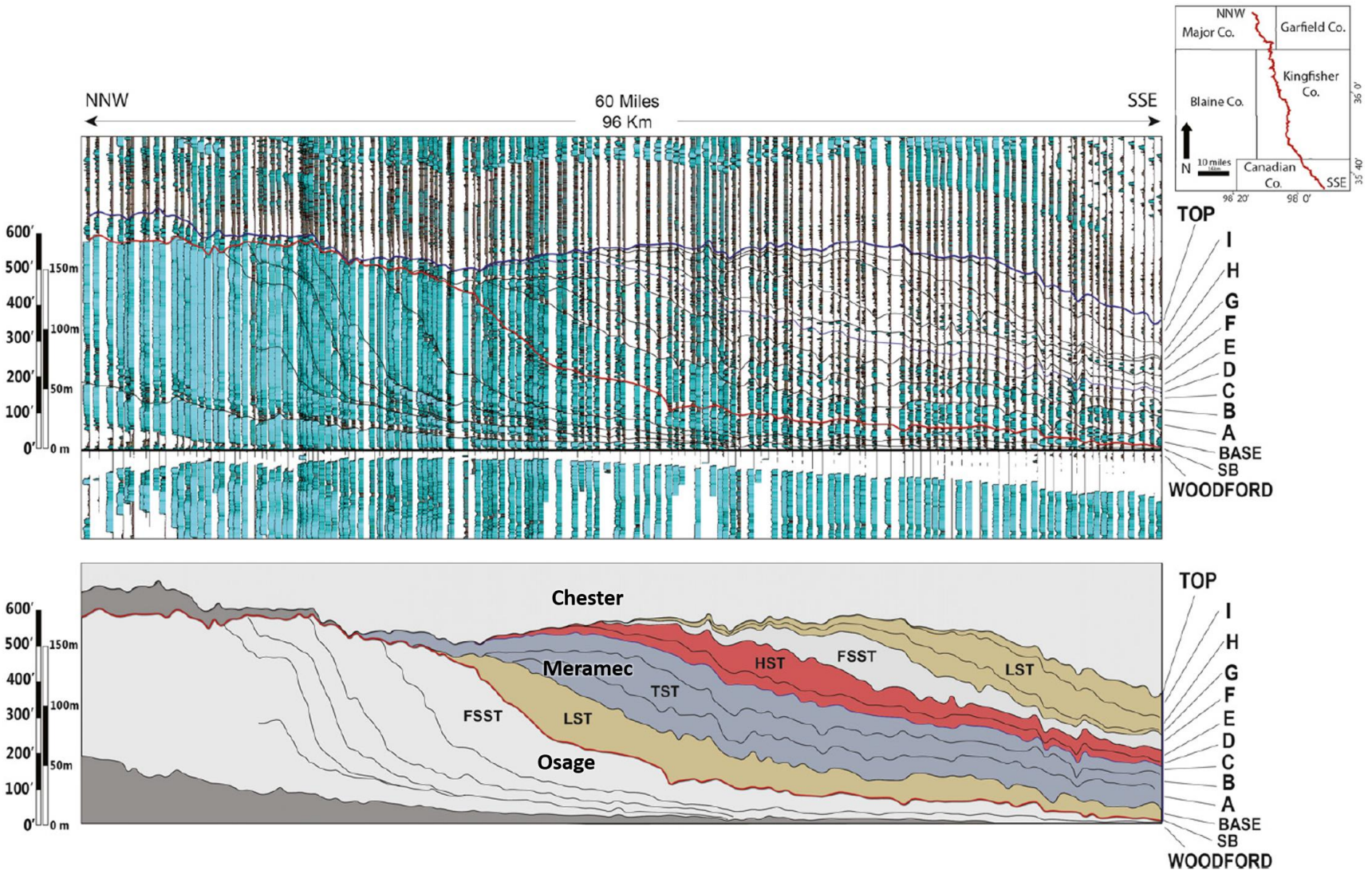

Figure 12. A gamma-ray cross section of STACK East along depositional trend and flattened on the Woodford Shale. The Meramec clinoform sets A-I can be seen prograding over the top of the Osage Fm and capped by the shaley Chester Fm. Gamma-ray scale 0-100 API. FSST=Falling Stage Systems Tract; LST=Lowstand Systems Tract; TST=Transgressive Systems Tract; HST=Highstand Systems Tract; SB=Sequence Boundary. Modified from Price et al. (2020)

III. Dataset and Methods

This study is based on a combined dataset of oils and core extracts from the Hunton Limestone, Woodford Shale, Mississippian Group, and Springer Group from 13 counties across the Anadarko Basin. Samples were separated into three geographically distinct Play Regions: 1) STACK West, 2) STACK East, and 3) SCOOP.

Oil Samples

Oils from 172 producing oil wells were collected from the separators of producing wellheads in 250mL or 500mL amber glass bottles with Teflon lids and immediately transferred to a refrigerated space for preservation of volatile components. For each oil, the well identification, wellhead location, producing formation, and total vertical depth (TVD) is summarized in Table 1, and wellhead locations are mapped by Play Region in Figure 13. All oil samples are mapped in Figure 14 accompanied by a north-south cross section spanning from STACK to SCOOP.

Whole Oil GC Analysis

Whole oil samples were analyzed by gas chromatography (GC) by using an Agilent Technologies 6890 gas chromatograph equipped with a split/splitless injector, a J&W Scientific DB-Petro 122-10A6 fused silica capillary column (100m length, 0.25mm inner diameter, and 0.50µm film thickness), helium as the carrier gas, and a flame ionization detector. Approximately 0.1µL of whole oil was injected using split injector mode and a carrier gas flow rate of 1.4mL/min. The GC program initialized at 40°C and was held for 1.5 minutes, increased by 2°C/min until 130°C, and increased by 4°C/min until a final temperature of 300°C and held for 26 minutes.

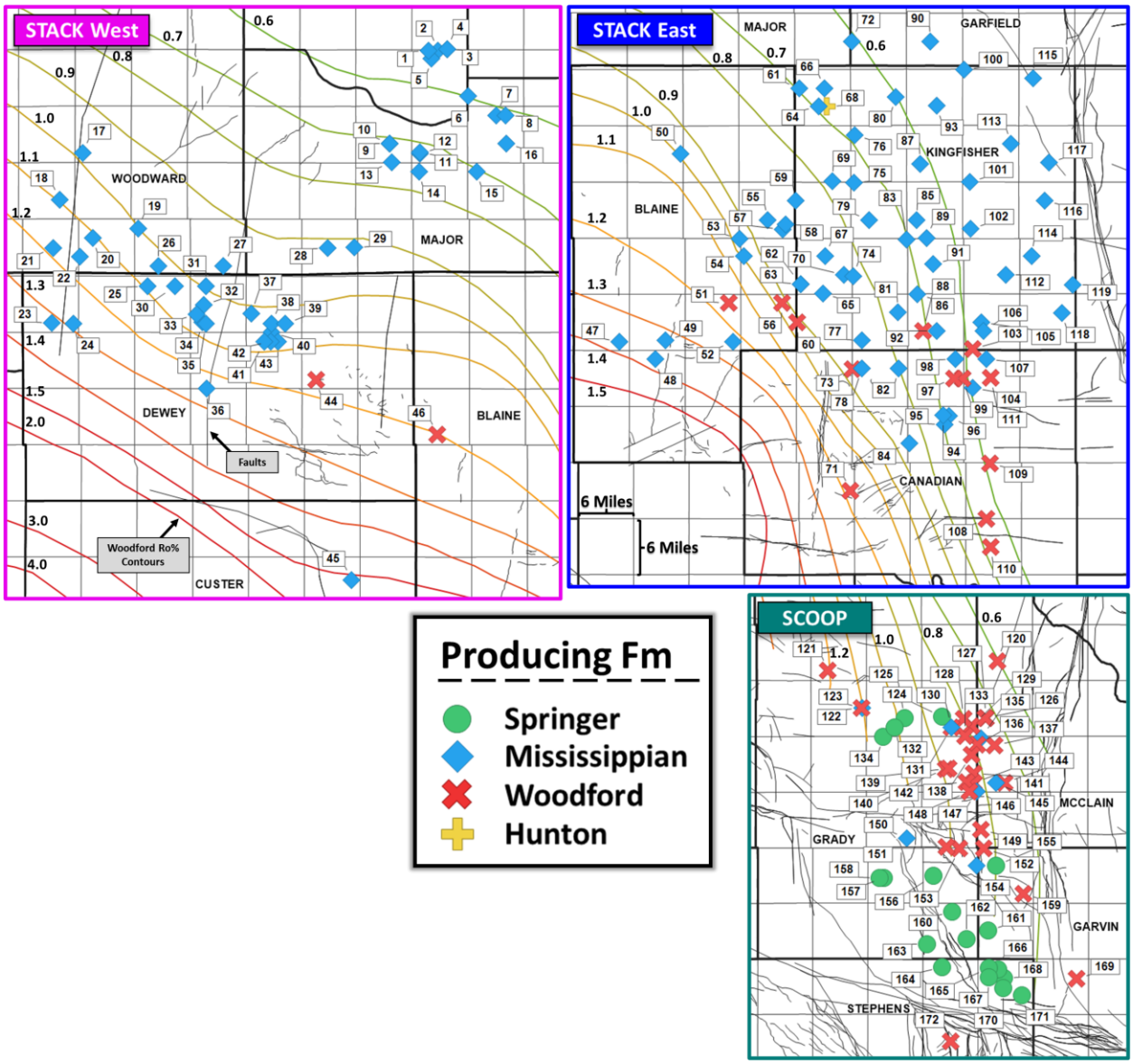

Figure 13. Wellhead locations of the 172 study oil samples by producing formation and organized into separate panels corresponding to the STACK West, STACK East, and SCOOP Play Regions. Sample labels correspond to the sample key in Table 1. The square grid corresponds to township lines which are 6 miles on a side.

Key	API Number	Well Name	Latitude	Longitude	County	Play Region	TVD	Producing Formation
1	3515124530	Rich 4-32H	36.5054	-98.6082	Woods	STACK West	7,130	Mississippian
2	3515124512	Burson 1-33H	36.5055	-98.5897	Woods	STACK West	6,791	Mississippian
3	3515124062	Shawna 3-34HL	36.5072	-98.5715	Woods	STACK West	7,179	Mississippian
4	3515124064	Dietz 4-3H	36.5072	-98.5716	Woods	STACK West	6,917	Mississippian
5	3515124523	Reihm 3-9H	36.4928	-98.6030	Woods	STACK West	6,980	Mississippian
6	3509325107	Newton 1-31H	36.4358	-98.5327	Major	STACK West	7,132	Mississippian
7	3509325158	Cornelson 2-3H	36.4056	-98.4788	Major	STACK West	6,934	Mississippian
8	3509324990	Regier 6-2HL	36.4061	-98.4610	Major	STACK West	7,444	Mississippian
9	3509324996	Phillips 3-27H	36.3626	-98.6821	Major	STACK West	7,690	Mississippian
10	3509324995	Phillips 4-27HL	36.3626	-98.6820	Major	STACK West	8,068	Mississippian
11	3509325130	Byfield 1-31H	36.3487	-98.6243	Major	STACK West	7,563	Mississippian
12	3509325139	Sutter 3-30H	36.3467	-98.6243	Major	STACK West	7,443	Mississippian
13	3509325069	Jordan 1-3H	36.3339	-98.6779	Major	STACK West	7,887	Mississippian
14	3509325114	Sunderman 1-7H	36.3196	-98.6258	Major	STACK West	7,792	Mississippian
15	3509325022	ABCDS 1H-6	36.3192	-98.5164	Major	STACK West	7,412	Mississippian
16	3509325121	Nickel 1-26H	36.3625	-98.4595	Major	STACK West	7,172	Mississippian
17	3515323569	Shaw Trust 30-22-19 1H	36.3477	-99.2676	Woodward	STACK West	9,068	Mississippian
18	3515323578	Story 23-21-20 1H	36.2764	-99.3111	Woodward	STACK West	11,096	Mississippian
19	3515323571	Young 6-20-18 1H	36.2319	-99.1617	Woodward	STACK West	10,024	Mississippian
20	3515323572	White 8-20-19 1H	36.2176	-99.2473	Woodward	STACK West	11,173	Mississippian
21	3515323574	Randall 15-20-20 1H	36.2024	-99.3229	Woodward	STACK West	11,729	Mississippian
22	3515323582	Linda 19-20-19 1H	36.1889	-99.2729	Woodward	STACK West	11,799	Mississippian
23	3504323457	Salisbury 27-19-20 1H	36.0869	-99.3266	Dewey	STACK West	13,107	Mississippian
24	3504323470	Mcalary 25-19-20 1H	36.0861	-99.2856	Dewey	STACK West	13,047	Mississippian
25	3504323452	Seidel 5-19-18 1H	36.1435	-99.1432	Dewey	STACK West	11,303	Mississippian
26	3515323573	Cara 28-20-18 1H	36.1740	-99.1227	Woodward	STACK West	10,909	Mississippian
27	3515323586	Breckenridge 27-20N-17W 1H	36.1739	-98.9994	Woodward	STACK West	9,687	Mississippian
28	3509325015	Ward 21-1H	36.2015	-98.7996	Major	STACK West	9,171	Mississippian
29	3509325035	Walters 13-1H	36.2029	-98.7487	Major	STACK West	8,883	Mississippian
30	3504323426	Branstetter 2-19-18 1H	36.1435	-99.0908	Dewey	STACK West	11,344	Mississippian
31	3504323431	Howard 5-19-17 1H	36.1433	-99.0328	Dewey	STACK West	11,440	Mississippian
32	3504323477	Russell 17-19-17 1H	36.1142	-99.0365	Dewey	STACK West	10,743	Mississippian
33	3504323480	Krows 19-19-17 1H	36.0998	-99.0506	Dewey	STACK West	11,583	Mississippian
34	3504323489	Merle 32-19-17 1H	36.0874	-99.0393	Dewey	STACK West	11,162	Mississippian
35	3504323437	Carter 29-19-17 1H	36.0855	-99.0319	Dewey	STACK West	11,609	Mississippian
36	3504323459	Drinnon 32-18-17 1H	35.9861	-99.0306	Dewey	STACK West	12,693	Mississippian
37	3504323441	Irving 19-19-16 1H	36.1015	-98.9452	Dewey	STACK West	11,311	Mississippian
38	3504323405	Dennis 28-19-16 1H	36.0852	-98.9074	Dewey	STACK West	11,229	Mississippian
39	3504323406	Wilson 35-19-16 1H	36.0858	-98.8807	Dewey	STACK West	11,353	Mississippian
40	3504323413	Bozarth 33-19-16 1H	36.0727	-98.9079	Dewey	STACK West	10,655	Mississippian
41	3504323447	Randy 9-18-16 1H	36.0583	-98.9207	Dewey	STACK West	11,693	Mississippian
42	3504323432	Seifried Trust 4-18-16 1H	36.0584	-98.9092	Dewey	STACK West	11,435	Mississippian
43	3504323464	Sportsman 3-18-16 1H	36.0583	-98.8954	Dewey	STACK West	11,065	Mississippian
44	3504323157	Wion 1-29H	35.9994	-98.8222	Dewey	STACK West	11,487	Woodford
45	3503922510	Yoder 1-13-12XH	35.6897	-98.7548	Custer	STACK West	14,085	Mississippian
46	3501123458	Crystal 1-28H	35.9140	-98.5912	Blaine	STACK West	11,227	Woodford
47	3501123747	Tres C FIU 1-35-2XH	35.7390	-98.5446	Blaine	STACK East	12,523	Mississippian
48	3501123570	Angus Trust 1-4-33XH	35.7122	-98.4758	Blaine	STACK East	12,208	Mississippian
49	3501123784	Holstein 2-27H	35.7407	-98.4562	Blaine	STACK East	12,298	Mississippian
50	3501123431	Boeckman 1-13H	36.0288	-98.4276	Canadian	STACK East	8,968	Mississippian
51	3501123467	Shortys Place 1-2XH	35.7983	-98.3354	Blaine	STACK East	11,605	Woodford
52	3501123669	Mowery 1-36H	35.7389	-98.3271	Blaine	STACK East	11,439	Mississippian
53	3501123551	Three Sisters 31 1H	35.8975	-98.3159	Blaine	STACK East	10,045	Mississippian
54	3501123528	Blurton 1-7-6XH	35.8707	-98.3075	Blaine	STACK East	9,892	Mississippian
55	3501123564	Olive June 1-27XH	35.9265	-98.2621	Blaine	STACK East	9,112	Mississippian
56	3501123459	York 1-2H	35.7984	-98.2345	Blaine	STACK East	10,573	Woodford
57	3501123547	Sonoyta 2623 3AH	35.9124	-98.2333	Blaine	STACK East	9,135	Mississippian
58	3501123568	Lloyd 1-25XH	35.9205	-98.2271	Blaine	STACK East	9,267	Mississippian
59	3507325117	Winters 1H-6X	35.9572	-98.2086	Kingfisher	STACK East	8,652	Mississippian

Key	API Number	Well Name	Latitude	Longitude	County	Play Region	TVD	Producing Formation
60	3507324806	Edra 1H	35.7692	-98.2058	Kingfisher	STACK East	10,677	Woodford
61	3507325922	Biggio 1909 7-1LOH	36.1299	-98.2009	Kingfisher	STACK East	8,207	Mississippian
62	3507325139	Born Free 30 2AH	35.8273	-98.1990	Kingfisher	STACK East	9,489	Mississippian
63	3507325141	Born Free 30 2H	35.8273	-98.1990	Kingfisher	STACK East	9,642	Mississippian
64	3507326156	Luke 1909 21-1LOH	36.1019	-98.1643	Kingfisher	STACK East	8,213	Mississippian
65	3507324923	Murray 1-33H	35.8130	-98.1567	Kingfisher	STACK East	9,343	Mississippian
66	3507325509	Pedlik 10-1H	36.1305	-98.1540	Kingfisher	STACK East	8,120	Mississippian
67	3507325121	Showboat 1003 1AH	35.8710	-98.1522	Kingfisher	STACK East	8,787	Mississippian
68	3507324989	The River 1-22H	36.1018	-98.1494	Kingfisher	STACK East	7,783	Hunton
69	3507325221	Pope 1H-26X	35.9862	-98.1381	Kingfisher	STACK East	8,297	Mississippian
70	3507325071	Alan 1H-13X	35.8420	-98.1159	Kingfisher	STACK East	8,813	Mississippian
71	3501724271	Lingo 1-13H	35.5070	-98.1040	Canadian	STACK East	11,932	Woodford
72	3504725112	Gary Hajek 2008 180LOH	36.2017	-98.1012	Garfield	STACK East	7,814	Mississippian
73	3501724302	Dougherty Bros 1-18H	35.6957	-98.0994	Canadian	STACK East	10,785	Woodford
74	3507324854	Yost 1H-18X	35.8404	-98.0982	Kingfisher	STACK East	9,915	Mississippian
75	3507325363	Geis 31-1H	35.9847	-98.0974	Kingfisher	STACK East	8,282	Mississippian
76	3507325784	Dr J 1808 7-1UOH	36.0584	-98.0953	Kingfisher	STACK East	8,307	Mississippian
77	3507325541	Richard 1H-32	35.7405	-98.0822	Kingfisher	STACK East	9,626	Mississippian
78	3501724659	Rother 1H-5X	35.6972	-98.0813	Canadian	STACK East	10,842	Mississippian
79	3507325219	Mike 1H-17X	35.9270	-98.0686	Kingfisher	STACK East	8,275	Mississippian
80	3507325513	Bennie Racer 14 1H	36.1170	-98.0180	Kingfisher	STACK East	7,897	Mississippian
81	3507325119	James 1H-2X	35.7839	-98.0137	Kingfisher	STACK East	8,540	Mississippian
82	3501724889	Simba 12-14N-8W 1H	35.6974	-98.0117	Canadian	STACK East	9,217	Mississippian
83	3507324895	Mueggenborg 1H-25X	35.8969	-97.9974	Kingfisher	STACK East	8,161	Mississippian
84	3501724901	Wehmuller 1307 2-19MH	35.5807	-97.9910	Canadian	STACK East	9,960	Mississippian
85	3507325270	Russell 1H-17X	35.9270	-97.9781	Kingfisher	STACK East	7,984	Mississippian
86	3507325196	Cow's Face 0805 1H	35.8120	-97.9756	Kingfisher	STACK East	8,402	Mississippian
87	3507325453	Best 20-1H	36.0135	-97.9710	Kingfisher	STACK East	7,552	Mississippian
88	3507325013	Laura 1H-17X	35.7556	-97.9658	Kingfisher	STACK East	8,857	Woodford
89	3507325480	Jolee 1H-5	35.8990	-97.9577	Kingfisher	STACK East	7,945	Mississippian
90	3504725097	Pribil 2007 27 21-1H	36.2023	-97.9516	Garfield	STACK East	7,630	Mississippian
91	3507325322	Firestone 1-16MH	35.8593	-97.9466	Kingfisher	STACK East	7,862	Mississippian
92	3507325034	Ralph 1H-15X	35.7557	-97.9397	Kingfisher	STACK East	7,970	Mississippian
93	3507325950	Cakes 1907 22-1LOH	36.1028	-97.9391	Kingfisher	STACK East	7,500	Mississippian
94	3501724671	Bohlman 1H-34X	35.6247	-97.9273	Canadian	STACK East	9,291	Mississippian
95	3501724793	Whistle Pig 10 3H	35.6101	-97.9243	Canadian	STACK East	9,033	Mississippian
96	3501724921	HRDY 1-11MH	35.6235	-97.9152	Canadian	STACK East	8,991	Mississippian
97	3501724916	Scott 1H-23	35.6813	-97.9066	Canadian	STACK East	8,848	Woodford
98	3501725190	Okarche 1407 6H-12X	35.7118	-97.9036	Canadian	STACK East	8,334	Mississippian
99	3501724564	Okarche 1H-12X	35.6813	-97.8895	Canadian	STACK East	8,586	Woodford
100	3507325266	Shimanek 1906 2-6MH	36.1592	-97.8875	Kingfisher	STACK East	7,452	Mississippian
101	3507325728	Towne 1806 1-31MH	35.9852	-97.8765	Kingfisher	STACK East	7,601	Mississippian
102	3507325243	Post 1706 1-30MH	35.9133	-97.8741	Kingfisher	STACK East	7,325	Mississippian
103	3507325124	McCarthy 1H-30X	35.7279	-97.8705	Kingfisher	STACK East	8,258	Woodford
104	3501724906	Wittrock 1406 1-30MH	35.6671	-97.8699	Canadian	STACK East	8,484	Mississippian
105	3507325170	Eve 1506 1-20MH	35.7691	-97.8535	Kingfisher	STACK East	7,887	Mississippian
106	3507325197	Alphons 1H-29X	35.7558	-97.8500	Kingfisher	STACK East	8,861	Mississippian
107	3501724834	Meyer 1406 2-4MH	35.7117	-97.8442	Canadian	STACK East	7,965	Mississippian
108	3501724768	Anderson 1206 1-33WH	35.4639	-97.8437	Canadian	STACK East	9,249	Woodford
109	3501724678	Wilds 1206 1-4H	35.5505	-97.8379	Canadian	STACK East	9,017	Woodford
110	3501724708	Meyer 1106 1-21WH	35.4201	-97.8362	Canadian	STACK East	9,532	Woodford
111	3501724836	VOGT 1H-9X	35.6831	-97.8357	Canadian	STACK East	8,392	Woodford
112	3507325441	Peat 1606 1-26MH	35.8425	-97.8067	Kingfisher	STACK East	7,533	Mississippian
113	3507325608	Meritt 12-1H	36.0440	-97.7972	Kingfisher	STACK East	7,292	Mississippian
114	3507325707	Jacob 1605 1-8MH	35.8713	-97.7581	Kingfisher	STACK East	7,162	Mississippian
115	3507325566	Buttercup 1905 1-5MH	36.1454	-97.7550	Kingfisher	STACK East	6,714	Mississippian
116	3507325148	Power 1705 2-16MH	35.9566	-97.7328	Kingfisher	STACK East	7,048	Mississippian
117	3507325316	Edwin 1805 4-22MH	36.0154	-97.7248	Kingfisher	STACK East	6,779	Mississippian
118	3507325252	Cronkite 1505 4-14MH	35.7832	-97.7003	Kingfisher	STACK East	7,004	Mississippian

Key	API Number	Well Name	Latitude	Longitude	County	Play Region	TVD	Producing Formation
119	3507325299	Garrett 1605 6A-36MH	35.8270	-97.6794	Kingfisher	STACK East	6,921	Mississippian
120	3508722065	Curry 21X 1VH	35.1472	-97.6320	McClain	SCOOP	10,105	Woodford
121	3505123703	Meadors 1-28H	35.1318	-97.9562	Grady	SCOOP	14,171	Woodford
122	3505124235	Kashmir 2-13WH	35.0735	-97.8904	Grady	SCOOP	14,504	Woodford
123	3505124236	Kashmir 1-13H	35.0735	-97.8902	Grady	SCOOP	14,150	Mississippian
124	3505124059	Strassle 1-28-33XH	35.0603	-97.7378	Grady	SCOOP	11,387	Springer
125	3505123947	Sawyer 1-23H	35.0585	-97.8080	Grady	SCOOP	11,901	Springer
126	3508722043	Allen 1H-29X	35.0577	-97.6542	McClain	SCOOP	10,950	Woodford
127	3508722045	McCorn 1H-18X	35.0577	-97.6541	McClain	SCOOP	10,555	Woodford
128	3505124226	Lillian 1-23-14XH	35.0574	-97.6957	Grady	SCOOP	10,844	Woodford
129	3505124076	Romanoff 1-25-24-13XH	35.0451	-97.6816	Grady	SCOOP	10,762	Woodford
130	3505123782	Ratliff 1H-22X	35.0432	-97.7194	Grady	SCOOP	11,363	Woodford
131	3505124152	Bridwell 1H-22X	35.0432	-97.7193	Grady	SCOOP	11,591	Mississippian
132	3504925028	Omer 1-17H	35.0430	-97.8284	Grady	SCOOP	12,989	Springer
133	3505123741	Triple Rimer 1-35-26XH	35.0303	-97.6936	Grady	SCOOP	11,179	Woodford
134	3505123937	Chester 1-32H	35.0288	-97.8492	Grady	SCOOP	12,939	Springer
135	3508722060	Wendling 1H-30XR	35.0260	-97.6627	McClain	SCOOP	10,671	Mississippian
136	3508722032	Harmon 1H-31XR	35.0160	-97.6695	McClain	SCOOP	10,922	Woodford
137	3508721847	Hayhurst 1H	35.0155	-97.6376	McClain	SCOOP	10,881	Woodford
138	3505123912	Shaw 1-12H	35.0010	-97.6813	Grady	SCOOP	11,421	Woodford
139	3505123902	May 7-21-16XH	34.9794	-97.7248	Grady	SCOOP	12,317	Woodford
140	3505123929	May 6-21-16XN	34.9778	-97.7299	Grady	SCOOP	12,303	Woodford
141	3505123931	Cooley 1-24H	34.9708	-97.6768	Grady	SCOOP	11,698	Woodford
142	3505123869	McBryde 1-26-23XH	34.9573	-97.6902	Grady	SCOOP	11,777	Woodford
143	3505123737	Bridwell 1-25H	34.9573	-97.6766	Grady	SCOOP	11,706	Woodford
144	3508722098	Tecate 1-34-3WXH	34.9565	-97.6172	McClain	SCOOP	11,004	Woodford
145	3508722073	Indultado 1-28-21-MXH	34.9565	-97.6345	McClain	SCOOP	11,104	Mississippian
146	3505124221	Dogfish 1-31-30MXHR	34.9437	-97.6715	Grady	SCOOP	11,522	Mississippian
147	3505124185	Dogfish 1-31-30MXH	34.9436	-97.6715	Grady	SCOOP	11,755	Mississippian
148	3505123780	Copeland 1-36H	34.9430	-97.6854	Grady	SCOOP	12,112	Woodford
149	3508722070	Maximus 1-19-18WXH	34.8835	-97.6628	McClain	SCOOP	9,642	Woodford
150	3505124073	Lynda 26-23-1XH	34.8701	-97.8045	Grady	SCOOP	14,766	Mississippian
151	3505123772	Leda Spark 1-33H	34.8561	-97.7285	Grady	SCOOP	12,832	Woodford
152	3504925065	Lori Ann 1-6-7XH	34.8543	-97.6570	Garvin	SCOOP	11,100	Woodford
153	3505124096	Cuadrilla 1-3-10 WXH	34.8538	-97.7041	Grady	SCOOP	12,053	Woodford
154	3504925102	Castle 1-8SH	34.8276	-97.6715	Garvin	SCOOP	9,812	Mississippian
155	3504925103	Muleta 1-16GH	34.8276	-97.6341	Garvin	SCOOP	9,460	Springer
156	3505123934	Prince 1-17X8H	34.8112	-97.7531	Grady	SCOOP	12,753	Springer
157	3505122860	Nix 1-20	34.8080	-97.8484	Grady	SCOOP	13,412	Springer
158	3505123131	Williamson 1-20	34.8076	-97.8568	Grady	SCOOP	14,125	Springer
159	3504925058	Wertz Trust 1-26-23XH	34.7834	-97.5817	Garvin	SCOOP	9,920	Woodford
160	3505123894	Auld 1H-3	34.7548	-97.7179	Grady	SCOOP	13,284	Springer
161	3505123808	Nancy J 1-28H	34.7257	-97.6495	Garvin	SCOOP	12,359	Springer
162	3505123941	Tannenbaum 1-23H	34.7122	-97.6904	Grady	SCOOP	13,398	Springer
163	3505124050	Murdock 4-30X31H	34.7040	-97.7659	Grady	SCOOP	15,760	Springer
164	3513727476	Orin 2-9H	34.6677	-97.7377	Stephens	SCOOP	14,235	Springer
165	3513727383	Celesta 1-5-32XH	34.6672	-97.6486	Stephens	SCOOP	13,521	Springer
166	3513727413	Hatchett 1H-33XR	34.6651	-97.6298	Stephens	SCOOP	13,130	Springer
167	3513727191	Robert Jo 1-8H	34.6525	-97.6482	Stephens	SCOOP	13,860	Springer
168	3513727414	Virginia 1H-4X	34.6516	-97.6197	Stephens	SCOOP	12,874	Springer
169	3504925038	Kessinger 1-11-2XH	34.6504	-97.4798	Garvin	SCOOP	8,507	Woodford
170	3513727241	Jarred 1H-9X	34.6350	-97.6205	Stephens	SCOOP	13,274	Springer
171	3513727409	Clarence 1H-14X	34.6239	-97.5854	Stephens	SCOOP	12,517	Springer
172	3513727276	Wilbern 1-15H	34.5515	-97.7204	Stephens	SCOOP	14,183	Woodford

Table 1. List of study oils by its 10-digit API number, well name, latitude, longitude, county, Play Region, total vertical depth (TVD) and producing formation. Each sample is given a unique numerical key between 1-172 which correspond to marker labels in Figure 13.

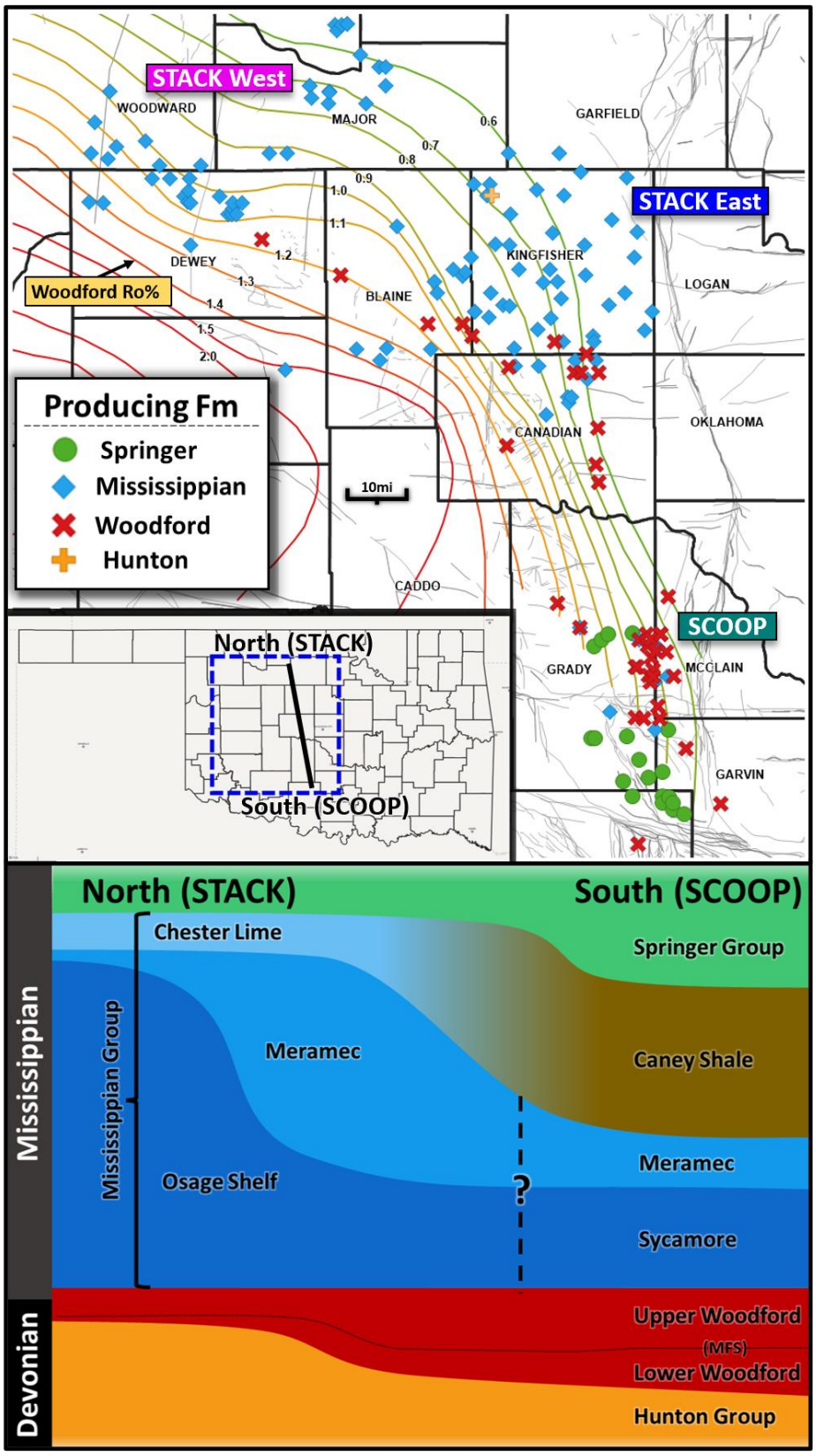

Figure 14. Map of oil samples in this study (upper) colored by producing formation as indicated by the adjoining cross section cartoon (lower). Woodford vitrinite isoreflectance contours (Ro%) provided (Cardott, 2012).

Oil Fractionation

Whole oil samples were separated according to their polarity and polarizability into their SARA fractions, an acronym representing the saturate, aromatic, resin (i.e. nitrogen, sulfur, and oxygen [NSO] compounds), and asphaltene components. Because many of the oils in this study are light or condensate oils, approximately 500mg of whole oil was added to a 4mL glass vial and placed under a stream of nitrogen for 2-3 hours to volatilize lighter compounds and concentrate heavier compounds, and the volatile weight lost was recorded. The remaining liquid was added to a 50mL centrifuge tube and filled with excess pentane and stored in a freezer (-2°C) overnight to precipitate the asphaltene fraction. The sample was centrifuged and the supernatant fluid containing the maltene fraction was removed and dried under a stream of nitrogen. The residual asphaltene fraction was collected and weighed.

The dried maltenes were collected and weighed, and a known amount of 5α-cholestane-2,2,3,3,4,4-D6 dissolved in hexane was added as an internal standard. Between 30-35mg of prepared maltenes was fractionated on an activated alumina column into saturate, aromatic, and NSO components using 15mL of *n*-hexane, and 25mL of a mixture of *n*-hexane:dichloromethane (DCM) (v/v=7:3), and 25mL of a mixture of DCM:methanol (v/v=1:1), respectively. Each fraction was dried and weighed. A pipette was packed with pre-extracted glass wool and approximately 2g of activated UOP brand S-115 powdered molecular sieve using pentane and water-free air to tightly pack the column. Approximately 10mg of saturate fraction was dissolved in 1mL of pentane and applied to the column and pushed through the molecular sieve with 2mL of *n*-pentane to isolate the branched and cyclic (B/C) fraction after the method described by West et al., (1990). Because the internal standard partitions into the saturate fraction, another aliquot of internal standard was added to the dried aromatic fraction.

GC-MS Analysis

The B/C and aromatic fractions were diluted in DCM to 4mg/mL and 2mg/mL, respectively, and analyzed by gas chromatography-mass spectrometry (GC-MS) using an Agilent Technologies 7890A gas chromatograph equipped with a split/splitless injector, a J&W Scientific DB-5MS 122-5562 fused silica capillary column (60m length, 0.25mm inner diameter, and 0.25µm film thickness), helium as the carrier gas, and interfaced with an Agilent Technologies 5975 XL Mass Selective Detector. Approximately 1.0µL of diluted B/C or aromatic fraction was injected using splitless injector mode and a carrier gas flow rate of 1.4mL/min. The GC temperature program initialized at 40°C and held for 1.5 minutes followed by a 4°C/min temperature ramp to 300°C which was held for 34 minutes. The GC-MS data were analyzed and integrated on MassHunter Qualitative Navigator by Agilent Technologies.

Stable Carbon Isotope Analysis

Stable carbon isotopes were measured on 69 whole oils. Approximately 200-300µg of sample was loaded into tin capsules, crimped, and analyzed by flash combustion in a Costech 4010 elemental analyzer connected by a Thermo Conflo III interfaced to a Thermo Delta V Plus isotope ratio mass spectrometer. The quartz combustion column was set to 1,000°C, the copper reduction column was set to 650°C, and the GC column oven was set to 55°C. The helium flow rate remained constant at 100ml/min. The $\delta^{13}C$ was calculated using the VPDB scale using Equation 1:

$$\delta^{13}\mathrm{C} = \left(\frac{\left(\frac{^{13}\mathrm{C}}{^{12}\mathrm{C}}\right)_{\mathrm{sample}}}{\left(\frac{^{13}\mathrm{C}}{^{12}\mathrm{C}}\right)_{\mathrm{standard}}} - 1 \right) \times 1000 \qquad \text{Equation 1}$$

The raw $\delta^{13}C$ values were corrected for ^{17}O contribution (Craig, 1957) and normalized by single-point linear normalization (Paul et al., 2007) with NBS22 oil standard ($\delta^{13}C$ = -30.03 per mil).

Gas Chromatography Isotope-Ratio Mass Spectrometry (GC-IRMS)

Individual compounds of the saturate fractions were analyzed for compound specific isotopes using an Agilent 7890 gas chromatograph with a Isolink and Carbon combustion reactor interfaced to an Conflo IV and a Thermo MAT 253 isotope-ratio mass spectrometer. The GC used a 60m x 0.25mm x 0.25µm film Agilent/J&W Scientific DB-1MS capillary column. The injection volume of sample was 1uL. The temperature program was initially set at 40ºC and held isothermal for 1.5 minutes. Then it was increased at a rate of 4ºC per minute to 300ºC and held constant for 24 minutes for a total run time of 90 minutes. Samples were analyzed in splitless mode injection using helium as the carrier gas. The method pulsed a CO_2 gas standard according to the time events. The samples were run with deuterated *n*-nonane (C_9D_{20}), *n*-decane ($C_{10}D_{22}$), *n*-hexadecane ($C_{16}D_{34}$), *n*-nonadecane ($C_{19}D_{40}$), *n*-tetracosane ($C_{24}D_{50}$), and *n*-dotriacontane ($C_{32}D_{66}$) as external standards.

Core Samples

The study also includes 59 core plug depths from 9 cores (seven new cores and two legacy cores) predominantly in STACK (Figure 15). Core plugs from the Hunton, Woodford, Meramec, Osage, and Chester formations are represented in this study (Table 2) with examples of each formation taken from the ABCDS 1-6 core are shown in Figure 16. Core plugs were crushed in a tungsten ball mill to 40 mesh and added to a Soxhlet extraction system and run overnight with a solvent mixture of DCM:methanol (v/v=1:1). The rock extract was deasphaltened, fractionated, and analyzed by GC-MS as described previously. Total extractable organic matter was calculated per gram of rock added to the Soxhlet extraction (EOM/g). Extra care was made to ensure all residual water was removed from the organic extract before calculating EOM/g.

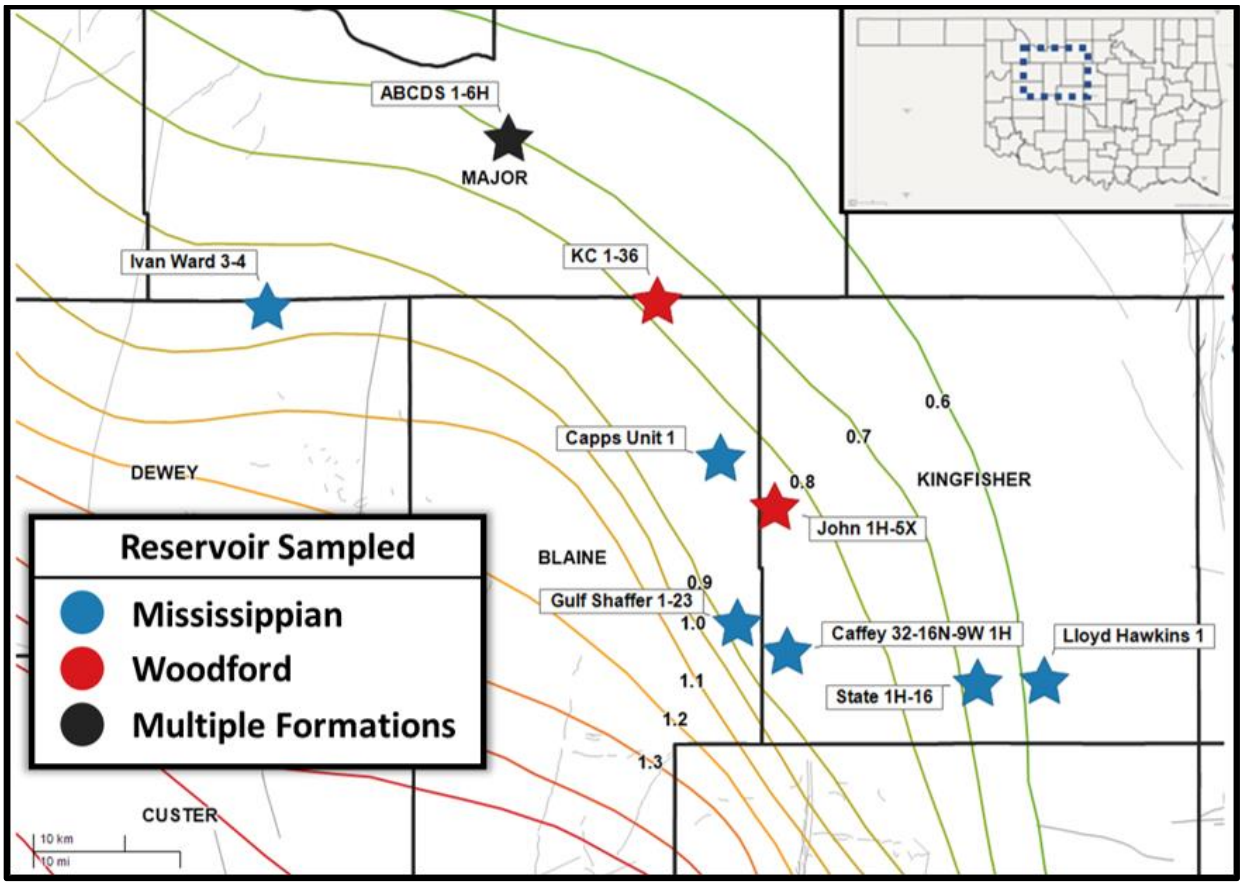

Figure 15. Map of cored wells incorporated into this study.

Cored Well	Latitude	Longitude	Hunton	Woodford	Osage	Meramec	Chester	Total Depths
ABCDS 1-6H	36.3193	-98.5164	1	4	5	3	1	14
Caffey 32-16N-9W 1H	35.8148	-98.1768				3		3
Capps Unit 1	36.0055	-98.2574			13			13
Gulf Shaffer 1-23	35.8429	-98.2363				5		5
Ivan Ward 3-4	36.1545	-98.8110					8	8
John 1H-5X	35.9573	-98.1916		3				3
KC 1-36	36.1597	-98.3339		4				4
Lloyd Hawkins 1	35.7858	-97.8630				6		6
State 1H-16	35.7835	-97.9443				3		3
Total			**1**	**11**	**18**	**20**	**9**	**59**

Table 2. Core samples by formation in this study. Capps Unit 1 and Ivan Ward 3-4 are legacy cores.

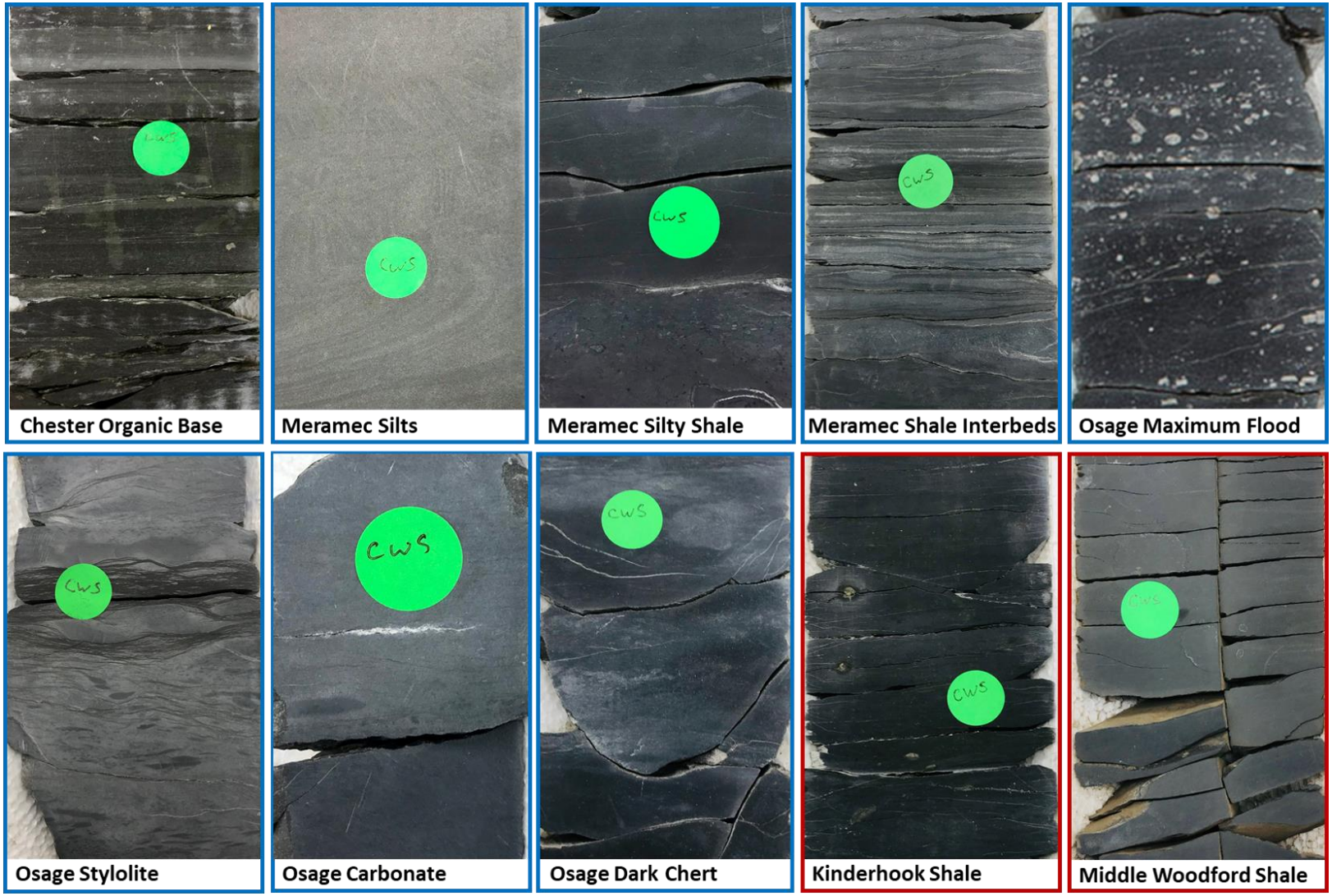

Figure 16. Examples of core sampling locations by stratigraphic interval and lithofacies for the ABCDS 1-6H core. The Chester facies are dominated by laminated siltstones, bioturbated siltstones, and calcareous sandstones and contain a slightly organic base in this core. The Meramec ranges from clean silt, silty shales, to shaley interbeds. The Osage ranges from crinoidal carbonate packstones and wackestones to cherty carbonates with stylolite dissolution features. The dark Kinderhook Shale is generally organic lean, while the Woodford Shale is organic rich. Not Shown: Hunton Fm or Springer Group.

Internal Standards and Calculating Absolute Concentrations

Absolute concentrations of compounds can provide critical insight into thermal maturity, organic facies, biodegradation, and oil mixing. To quantify biomarker concentrations, a known amount of 5α-cholestane-2,2,3,3,4,4-D6 was selected to be added to each sample as an internal standard because it does not occur naturally and does not coelute with any monitored compounds. The concentration of the internal standard is calculated using the mass of the standard divided by the mass of the sample (Equation 2):

$$[C_{ISTD}] = \frac{[C_{STD}] \times V_{STD}}{M_{Sample}} \quad \text{Equation 2}$$

Where $[C_{ISTD}]$ = Concentration of internal standard in whole oil in ppm (w/w)
$[C_{STD}]$ = Concentration of internal standard solution in ppm (w/v)
V_{STD} = Volume of internal standard added to whole oil in µL
M_{Sample} = Mass of whole oil aliquot before fractionation in mg

The ratio between the machine response produced by an analyte and the quantity of that analyte is called the response factor (RF) and can vary by instrumentation and run parameters. When sample dilution or injection volumes are not tightly controlled, it is more appropriate to use a relative response factor (RRF) between an internal standard and an analyte, defined as the ratio of their RF (Equation 3):

$$RRF = \frac{RF_X}{RF_{ISTD}} \quad \text{Equation 3}$$

Where RRF = Relative response factor between internal standard and analyte of interest
RF_X = Response factor of analyte of interest
RF_{ISTD} = Response factor of internal standard

Simply, the RRF defines the difference in machine response between an internal standard and an unknown analyte. Therefore, the concentration of an analyte compound is the concentration of the internal standard multiplied by the ratio of areas between the analyte and the internal standard and multiplied by their RRF (Equation 4):

$$[\mathbf{C_X}] = [\mathbf{C_{ISTD}}] \times \left[\frac{\mathbf{A_X}}{\mathbf{A_{ISTD}}}\right] \times \mathrm{RRF} \qquad \text{Equation 4}$$

Where $[C_X]$ = Concentration of unknown compound in ppm (w/w)
$[C_{ISTD}]$ = Concentration internal standard in ppm (w/w)
A_X = Area of analyte of interest peak
A_{ISTD} = Area of internal standard peak
RRF = Relative response factor between internal standard and analyte of interest

Deriving the RRF between an analyte and internal standard requires a series of controlled experiments of known concentrations for both the internal standard and the analyte of interest to measure their respective RFs. In chromatography, however, the area of a peak is proportional to the number moles injected into the GC, but the number of moles is the product of two variables—molarity and volume—making it difficult to rigorously control for (Equation 5):

$$A = \mathrm{RF} \times [C] \times V \qquad \text{Equation 5}$$

Where A = Area of analyte peak
RF = Response factor of analyte
[C] = Concentration of analyte mixture
V = Volume of mixture injected onto GC-MS

By injecting a mixture of both the analyte and the internal standard together, the volume terms cancel out when the equations are divided. The remaining equation is in slope-intercept form where the Y-axis is the ratio of peak areas, the slope of the line is given by RRF, and the X-axis is the ratio of concentrations in the mixture (Equation 6).

$$\frac{A_X}{A_{ISTD}} = \mathrm{RRF} \times \frac{[C_X]}{[C_{ISTD}]} \qquad \text{Equation 6}$$

Where A_X = Area of analyte of interest
A_{ISTD} = Area of internal standard
RRF = Relative response factor between internal standard and analyte of interest
$[C_X]$ = Concentration of analyte of interest
$[C_{ISTD}]$ = Concentration of internal standard

The RRF can be derived from the slope of the line when the experiment has been repeated a sufficient number of times to calculate a slope of the line by linear regression. An example RRF

derivation between adamantane and the internal standard 5α-cholestane-2,2,3,3,4,4-D6 is shown in Figure 17. In this example, the machine response for the internal standard is only 27% of the response measured for adamantane. Without this correction, the absolute concentration of adamantane may be over-estimated by nearly a factor of four.

Except where indicated in subsequent chapters, the relative response factor between 5α-cholestane-2,2,3,3,4,4-D6 and other biomarkers is assumed to be 1. Although this is certainly not correct, the error introduced does not influence any conclusions drawn from the comparison of quantitative biomarker data of separate samples when compared to each other. It is unreasonable to derive RRF for each class of biomarker, and because RRF is a constant, any enrichment or depletion between samples will be proportional across all samples (Rullkötter et al., 1984). All compound concentrations reported in this study are given in terms of ppm weight/weight (w/w) relative to its pristine whole oil as it was received or collected. Confidence intervals, marked using the ± symbol, are calculated using a "Z" factor of 1.960 which achieves a 95% confidence level.

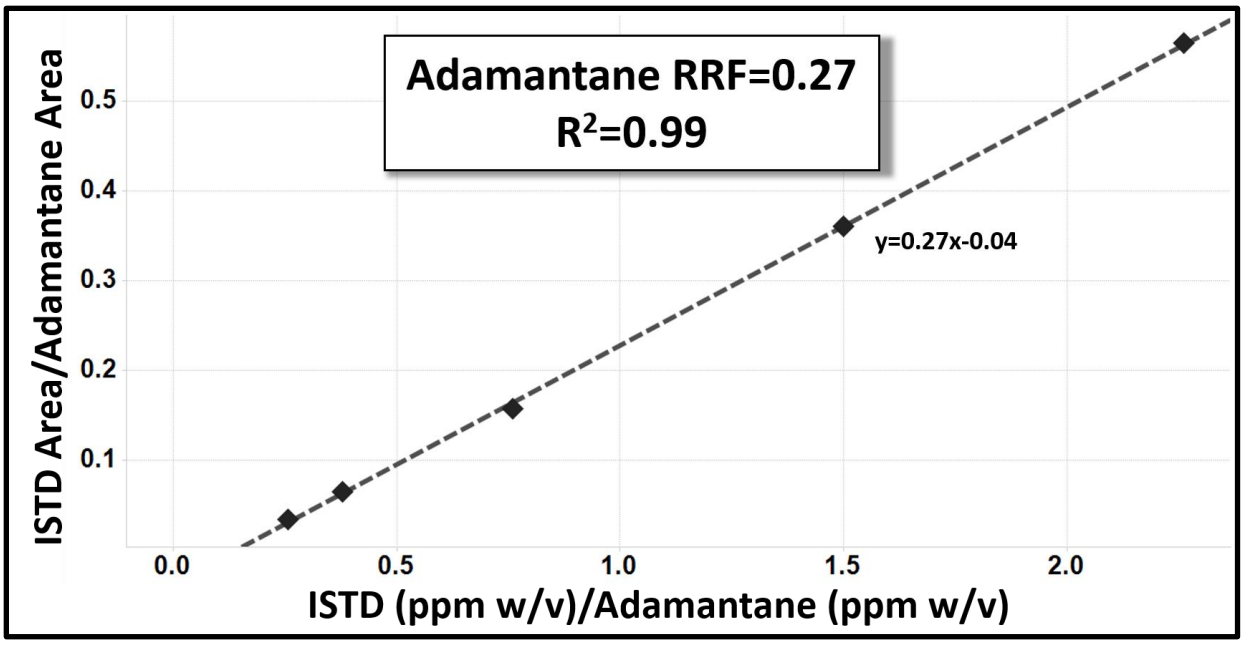

Figure 17. An example relative response factor between the internal standard used in this study (5α-cholestane-2,2,3,3,4,4-D6) and adamantane. Adamantane has a larger machine response by nearly a factor of four.

Production Data

The initial producing gas to oil ratio (IP GOR) for all 172 producing oil wells, measured in standard cubic feet per stock tank barrel (scf/STB), was determined from production data collected from the DrillingInfo web application by Enverus which collects monthly oil and gas volumes reported to the Oklahoma Corporation Commission. The GOR of a producing well often increases naturally over its lifetime even when the reservoir pressure remains above the oil bubble point pressure, and other operating factors like production interference from offset wells ("well bashing"), shut ins, and recompletions can affect the GOR over the life of a well. Consequently, the IP GOR was selected to most closely reflect the oil in the pristine reservoir. An example IP GOR selection is shown in Figure 18. In all cases, IP GOR values were selected at peak monthly oil and gas volumes within the first six months to account for a "clean up" period where flowback water used during completion is recaptured.

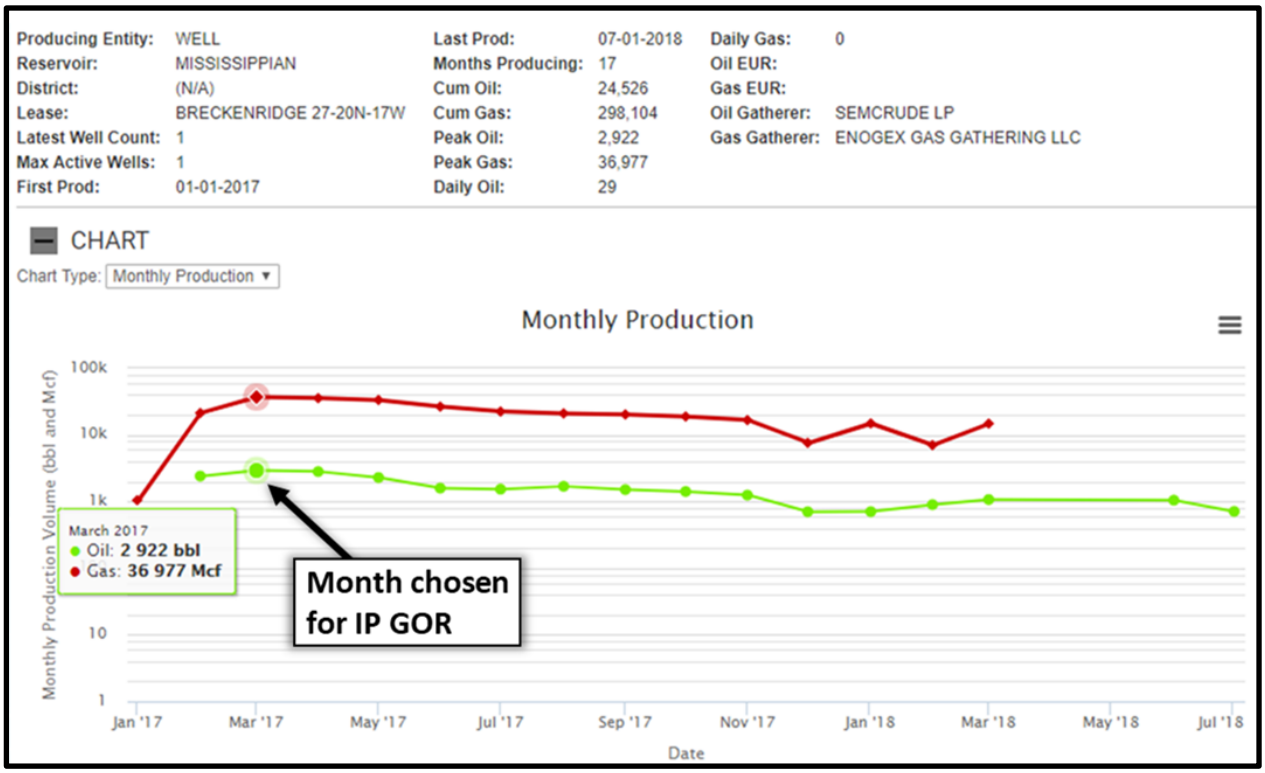

Figure 18. Initially producing gas-oil ratio (IP GOR) is chosen from the first month after the well has finished cleaning up. The IP GOR for the well shown is 12,655 scf/STB.

The specific gravity of an oil sample provides insight into the overall composition of a petroleum fluid. The American Petroleum Institute gravity, or API gravity, is an inverse measure of petroleum liquid's density compared to water (Equation 7):

$$\text{API gravity} = \frac{141.5}{\gamma} - 131.5 \qquad \text{Equation 7}$$

Where γ = specific gravity of the oil sample at 60°F

The specific gravity of water is 1 which corresponds to an API gravity of 10, so oils with API gravity values above 10 will float on water and those less than 10 will sink. The API gravity of produced oils are regularly measured directly from the stock tanks during collection but also during initial flowback tests which are reported to the Oklahoma Corporation Commission. The initial flowback API gravity values for all 172 wells study wells were taken from their respective completion reports (Oklahoma Corporation Commission form 1002A).

Principal Component Analysis

The variations between maturity parameters were summarized using principal component analysis (PCA). Broken stick models were used to assess the number of informative principal component axes (Legendre and Legendre, 2012). All ordination analyses were conducted using the R package Vegan in program R ver. 3.6.0 (Oksanen et al., 2015).

Mapping Software

Maps were generated using TIBCO Spotfire version 7.8.0. Shape files for Woodford vitrinite reflectance contours were made available by Brian Cardott of the Oklahoma Geological Survey, and the shape files for faults were taken from the Oklahoma Geological Survey Fault Database.

IV. Thermal Maturity Model

It is well understood that nearly all petroleum originates from the decomposition of organic matter in marine and lacustrine sediments of the earth's crust (McNab et al., 1952; Forsman and Hunt, 1958; Bray and Evans, 1961; Abelson, 1963; Eglinton and Calvin, 1967; McIver, 1967; Whitehead, 1973). Diagenetic processes during early burial convert preserved biomass into kerogen (insoluble, particulate organic matter) and bitumen (soluble organic matter), and continued burial and heating in turn converts part of this organic matter into petroleum and natural gas. In petroleum chemistry, thermal maturity describes the extent to which mostly heat-driven reactions have converted sedimentary organic matter or metastable petroleum compounds into other products with greater thermodynamic stability (Philippi, 1965; Dow, 1977). The systematic changes that occur to petroleum during thermal maturation can in turn be used to interpret the thermal history of sedimentary rocks. In hydrocarbon exploration and production, thermal maturity directly affects oil phase behavior, pressure, specific gravity, viscosity, and gas-oil ratio and often establishes the economic viability of a drilling prospect.

This study was presented with the challenge of modeling thermal maturity across a large unconventional petroleum system spanning 13 counties where fluid maturities range from black oils to retrograde condensate produced from reservoirs with total vertical depths (TVD) between 6,714–15,760 ft (Figure 19). Changes in oil chemistry from thermal maturity are primarily first-order thermodynamic reactions which are time/temperature dependent, but over geologic time, maximum temperature is the only determinant variable (Philippi, 1965; Connan, 1974; Pepper and Corvi, 1995; Pepper and Dodd, 1995).

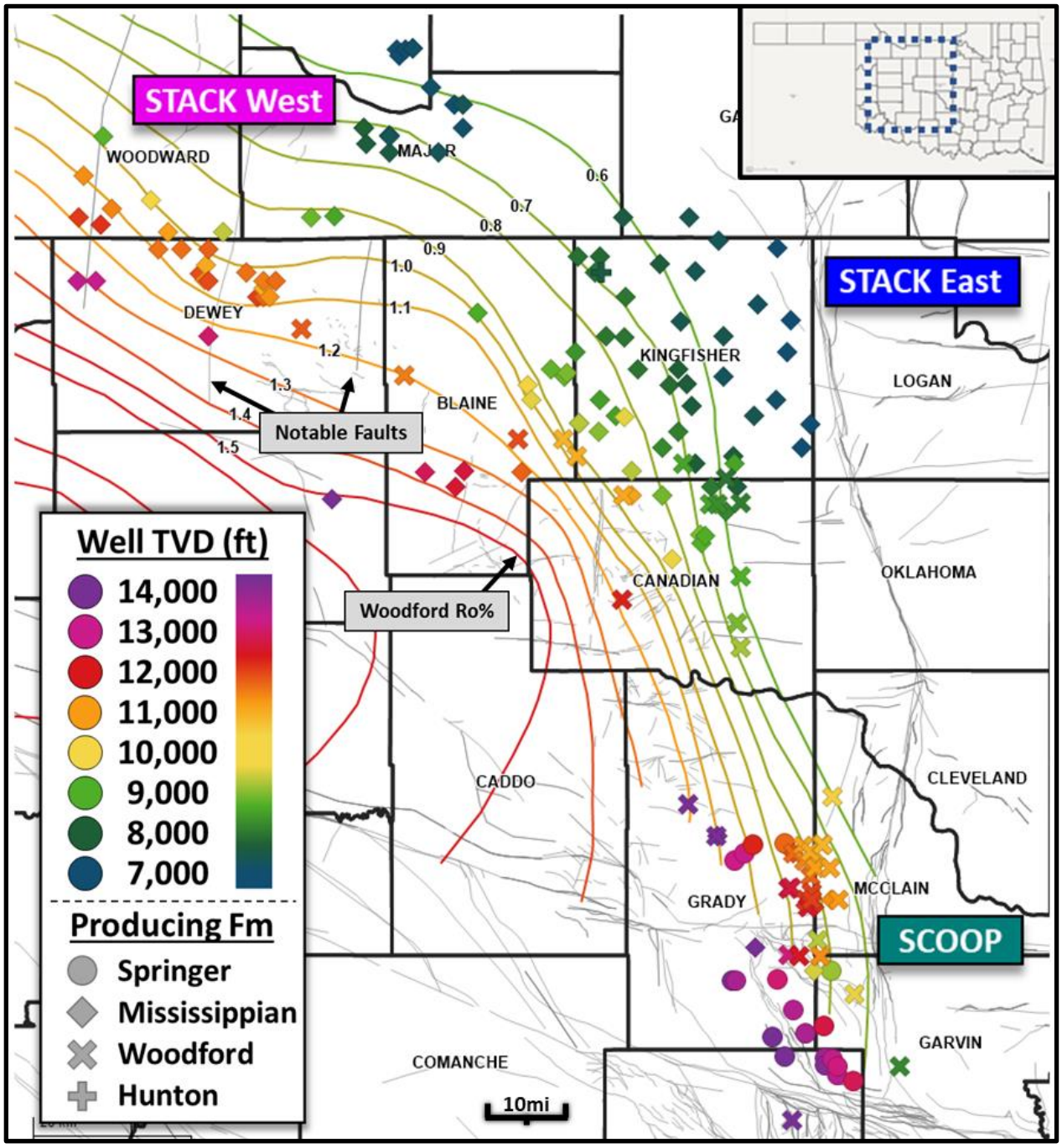

Figure 19. Map of the 172 studied oil samples by producing reservoir and colored by total vertical depth (TVD) as shown in Table 1. Oklahoma Geological Society recognized faults are shown in light grey. Two notable north-south trending faults in Dewey and Woodward counties are highlighted which are referenced in the text.

The thermal stress on an oil is expected to relate both to its maximum burial depth and the local geothermal gradient. In modeling thermal maturity, tight unconventional reservoirs benefit in that oils are captured near their organic source with limited updip migration (Meckel and Thomasson, 2005). In theory, the relative changes in maturity of unconventional reservoirs with depth should then mirror the geothermal gradient at the time of maximum burial. Moreover, the STACK/SCOOP provinces in the Anadarko Basin also benefit from a regular geothermal gradient common in foreland basins (Harrison et al., 1983; Carter et al., 1998). Compared to extensional basins, foreland basins form by flexure of thermally mature lithosphere and experience no significant change in basement heat flux because the lithosphere remains thermally stable except for the effect thermal blanketing by sediments (Beaumont, 1981; Jordan, 1981).

It is proposed here that for tight unconventional reservoirs with regular geothermal gradients, the efficacy of a geochemical maturity parameter can be approximated by its positive correlation with reservoir depth. Although the shallow dipping limb of the Anadarko Basin is mostly structurally inactive, some differences in the structural and burial history are expected between disparate portions of the basin which comprise the large STACK/SCOOP province. To account for this, the dataset is divided into three geographically coherent Play Regions which are modelled separately: STACK West, STACK East, and SCOOP.

The first portion of this chapter will catalogue several thermal maturity parameters based on bulk composition, biomarkers, light hydrocarbons, and aromatic compounds which will serve as inputs into a PCA model along with reservoir TVD. No attempt will be made to interpret the efficacy of individual maturity parameters based on its own merits, but rather by consensus between maturity parameters quantified by PCA. Finally, the results of each Play Region are aggregated into a single model predictive of oil maturity independent of organic facies or TVD.

Bulk Composition Maturity Parameters

The bulk composition of an oil systematically changes with maturity. This section discusses physical parameters of the oil that change with maturity including API gravity, whole oil $\delta^{13}C$, initially producing gas oil ratio (IP GOR), and oil SARA fraction (Table 3).

API Gravity

The API gravity measures the inverse of specific gravity of oil and describes the overall composition of a petroleum fluid. A contour map of Woodford-produced oil API gravity is shown in Figure 20 made by Warwick Energy using data from IHS Markit. In STACK East, Figure 20a depicts a broad plateau of 40-50° API gravity oils in Blaine, Kingfisher, and Canadian counties increases rapidly to 60° near the tricounty border. In STACK West, a heavily faulted portion of eastern Dewey County correspond to higher API gravity contours bending to the north creating a "flower-shaped zone." A map of just STACK West overlain with study oils in Figure 20b shows the flower-shaped zone is associated with several notable faults which are highlighted in red. In some cases, there are major shifts in API gravity values in oils across or along the faults, indicating that these faults may serve as migration pathways for higher maturity fluids into shallower reservoirs. Critically, the API gravity contours are not expected to exactly match the oil API gravity values collected from completion reports because they sample from different reservoirs at possibly different stages of the life of the well. However, the trends observed in the contour map mirrors those observed in the study oils. The API gravity for all study oils generally increases with TVD across all Play Regions, but there is a stronger correlation in STACK than in SCOOP (Figure 21). In STACK West, the flower-shaped zone corresponds to a wide range of API gravities (38-60°) at ~11,000 ft which could result from the mixing of higher maturity fluids. The flower-shaped zone oils will be tracked through other maturity parameters in this chapter to test this hypothesis.

Key	Play Region	TVD	API Gravity	Oil $\delta^{13}C$	IP GOR	% Volatile	% Sat	% Aro	% NSO	% Asph	Coll. Inst. Index
1	STACK West	7,130	35		1,710	20.7%	52.5%	18.1%	5.4%	3.3%	2.37
2	STACK West	6,791	32		2,066	24.0%	47.9%	18.0%	7.1%	3.0%	2.03
3	STACK West	7,179	34		1,121	24.6%	46.1%	19.3%	6.9%	3.1%	1.88
4	STACK West	6,917	33		1,563	26.7%	47.8%	16.9%	6.0%	2.6%	2.20
5	STACK West	6,980	29		4,005	27.6%	45.7%	16.3%	6.6%	3.8%	2.16
6	STACK West	7,132	37		2,842	34.0%	50.9%	11.1%	3.4%	0.7%	3.56
7	STACK West	6,934	34		870	28.2%	47.5%	16.3%	5.7%	2.4%	2.28
8	STACK West	7,444	36		4,272	27.6%	51.1%	14.4%	4.4%	2.4%	2.85
9	STACK West	7,690	36		3,662	25.9%	56.5%	12.9%	3.7%	1.0%	3.48
10	STACK West	8,068	40		9,528	23.7%	58.3%	13.3%	3.3%	1.4%	3.61
11	STACK West	7,563	30		2,885	27.6%	49.0%	16.0%	5.2%	2.1%	2.41
12	STACK West	7,443	37		4,718	32.3%	48.4%	13.2%	4.2%	1.9%	2.89
13	STACK West	7,887	31		2,556	27.2%	51.5%	15.3%	4.5%	1.4%	2.68
14	STACK West	7,792	32		2,943	33.7%	52.3%	10.1%	2.8%	1.1%	4.14
15	STACK West	7,412	37		3,742	38.5%	44.6%	11.2%	3.9%	1.8%	3.08
16	STACK West	7,172	35		2,985	32.1%	47.3%	14.5%	4.1%	2.0%	2.65
17	STACK West	9,068	38	-29.84	4,545	35.7%	59.7%	3.7%	0.6%	0.3%	13.85
18	STACK West	11,096		-29.93	26,543	59.0%	39.2%	0.9%	0.7%	0.2%	24.69
19	STACK West	10,024		-29.73	217,628	53.1%	42.9%	3.3%	0.6%	0.1%	11.05
20	STACK West	11,173	51	-30.16	20,130	47.2%	46.8%	4.8%	0.9%	0.3%	8.28
21	STACK West	11,729	50	-30.02	9,393	75.0%	23.8%	1.0%	0.1%	0.1%	21.15
22	STACK West	11,799	50	-30.16	26,078	63.5%	34.8%	0.7%	0.7%	0.3%	25.28
23	STACK West	13,107		-28.81	64,563	74.0%	25.1%	0.6%	0.4%	0.0%	25.81
24	STACK West	13,047	49	-29.33	78,210	60.8%	38.4%	0.3%	0.5%	0.0%	48.52
25	STACK West	11,303		-29.71	23,480	63.3%	34.9%	1.4%	0.3%	0.1%	20.60
26	STACK West	10,909	42	-30.16	12,052	51.7%	44.2%	3.4%	0.6%	0.1%	11.09
27	STACK West	9,687	39	-29.81	12,645	28.3%	57.4%	9.5%	2.0%	2.8%	5.21
28	STACK West	9,171	39	-30.12	1,798	24.5%	54.2%	13.9%	3.9%	3.5%	3.24
29	STACK West	8,883	35	-29.81	3,311	27.6%	53.3%	13.3%	3.2%	2.7%	3.41
30	STACK West	11,344	45	-30.23	9,817	54.0%	41.5%	3.7%	0.6%	0.1%	9.51
31	STACK West	11,440	38	-30.2	3,604	56.7%	39.2%	3.2%	0.7%	0.1%	9.90
32	STACK West	10,743	42	-30.23	5,763	43.9%	49.8%	5.5%	0.6%	0.3%	8.32
33	STACK West	11,583	47	-29.94	12,092	62.4%	35.0%	2.4%	0.2%	0.1%	13.92
34	STACK West	11,162	44	-29.59	6,840	44.0%	51.7%	3.5%	0.6%	0.2%	12.62
35	STACK West	11,609	53	-29.91	17,317	70.6%	27.9%	1.0%	0.4%	0.0%	19.25
36	STACK West	12,693	60	-27.44	627,107	62.4%	37.3%	0.2%	0.0%	0.1%	173.50
37	STACK West	11,311	48	-29.61	16,191	74.0%	23.1%	1.9%	0.9%	0.1%	8.29
38	STACK West	11,229	57	-29.03	34,472	81.5%	16.7%	1.3%	0.5%	0.1%	9.62
39	STACK West	11,353	46	-29.48	24,489	61.3%	35.8%	2.2%	0.5%	0.2%	13.50
40	STACK West	10,655	50	-29.48	25,738	63.6%	33.5%	2.0%	0.7%	0.2%	12.21
41	STACK West	11,693	54	-28.96	26,963	78.2%	21.1%	0.5%	0.1%	0.1%	36.87
42	STACK West	11,435	54	-29.12	36,585	74.8%	24.2%	0.5%	0.5%	0.0%	25.58
43	STACK West	11,065	49	-29.45	19,568	58.1%	38.6%	2.8%	0.4%	0.1%	12.12
44	STACK West	11,487	55	-28.34	80,617	89.4%	9.6%	0.4%	0.5%	0.0%	10.66
45	STACK West	14,085			477,929	62.8%	36.4%	0.4%	0.4%	0.0%	45.91
46	STACK West	11,227	49	-29.31	27,500	70.5%	25.4%	3.1%	1.0%	0.1%	6.25
47	STACK East	12,523	54		32,755	69.4%	29.6%	0.3%	0.6%	0.0%	32.36
48	STACK East	12,208	55		7,753	54.1%	45.5%	0.3%	0.1%	0.0%	101.73
49	STACK East	12,298	49		8,657	53.4%	45.6%	0.7%	0.3%	0.0%	47.48
50	STACK East	8,968		-29.98	15,889	59.8%	35.5%	4.0%	0.5%	0.2%	7.85
51	STACK East	11,605	46		4,762	58.5%	38.5%	2.2%	0.8%	0.0%	12.92
52	STACK East	11,439	49		5,542	52.8%	45.7%	0.9%	0.5%	0.0%	32.32
53	STACK East	10,045	41	-30.48	2,116	43.4%	50.8%	2.7%	3.1%	0.0%	8.75
54	STACK East	9,892	46	-30.66	1,613	44.4%	49.5%	5.0%	1.0%	0.2%	8.34
55	STACK East	9,112		-30.85	1,288	44.8%	48.8%	5.5%	0.8%	0.1%	7.79
56	STACK East	10,573	43	-29.86	4,867	47.5%	46.8%	3.8%	1.9%	0.1%	8.22
57	STACK East	9,135	41	-30.95	2,399	44.3%	48.3%	6.2%	1.2%	0.0%	6.54
58	STACK East	9,267		-30.67	1,531	44.5%	49.6%	4.0%	1.8%	0.1%	8.58
59	STACK East	8,652	43		3,652	32.4%	59.8%	6.2%	1.1%	0.5%	8.27

Key	Play Region	TVD	API Gravity	Oil $\delta^{13}C$	IP GOR	% Volatile	% Sat	% Aro	% NSO	% Asph	Coll. Inst. Index
60	STACK East	10,677	52	-29.48	11,783	46.0%	50.1%	3.1%	0.8%	0.0%	12.77
61	STACK East	8,207	46		13,238	45.2%	44.0%	8.1%	2.4%	0.3%	4.22
62	STACK East	9,489	48	-30.87	3,298	51.7%	44.1%	3.4%	0.7%	0.0%	10.56
63	STACK East	9,642	48	-31.02	5,996	52.7%	43.6%	2.6%	1.1%	0.0%	11.76
64	STACK East	8,213	44		3,506	39.8%	49.3%	8.5%	2.2%	0.1%	4.60
65	STACK East	9,343		-31.73	2,129	47.5%	45.6%	5.8%	1.1%	0.1%	6.69
66	STACK East	8,120	40	-30.38	7,390	43.5%	43.1%	9.0%	3.9%	0.5%	3.39
67	STACK East	8,787	42	-31.14	1,352	42.3%	51.2%	5.0%	1.5%	0.0%	7.88
68	STACK East	7,783			9,480	56.6%	35.4%	6.1%	1.8%	0.2%	4.54
69	STACK East	8,297	42		2,959	40.7%	49.3%	8.0%	1.7%	0.3%	5.09
70	STACK East	8,813	42		2,256	31.3%	58.1%	8.3%	2.0%	0.4%	5.72
71	STACK East	11,932	58	-27.64	12,221	73.0%	26.6%	0.2%	0.2%	0.0%	74.02
72	STACK East	7,814	40		4,245	32.1%	51.2%	12.8%	2.7%	1.1%	3.36
73	STACK East	10,785	53	-29.72	15,996	58.6%	36.8%	3.0%	1.6%	0.0%	8.11
74	STACK East	9,915	43		1,764	42.7%	50.3%	5.8%	0.8%	0.5%	7.73
75	STACK East	8,282	41		2,164	33.0%	51.9%	10.9%	3.8%	0.5%	3.57
76	STACK East	8,307	40		3,423	41.0%	46.3%	9.0%	3.5%	0.2%	3.73
77	STACK East	9,626	40		4,536	41.1%	52.0%	4.8%	1.9%	0.2%	7.74
78	STACK East	10,842	48		2,799	48.5%	47.9%	3.1%	0.5%	0.0%	13.30
79	STACK East	8,275	44		4,756	32.1%	54.6%	11.5%	1.6%	0.2%	4.19
80	STACK East	7,897	40	-30.77	1,281	51.4%	38.8%	8.7%	0.4%	0.6%	4.31
81	STACK East	8,540	45		4,068	37.7%	51.8%	8.1%	2.1%	0.3%	5.11
82	STACK East	9,217	44	-31.4	1,852	44.5%	48.6%	5.4%	1.5%	0.0%	7.07
83	STACK East	8,161	41		3,786	43.9%	46.5%	7.7%	1.7%	0.2%	4.99
84	STACK East	9,960		-30.32	7,717	41.3%	55.6%	2.3%	0.8%	0.1%	17.93
85	STACK East	7,984	40		3,579	36.0%	53.7%	8.5%	1.6%	0.2%	5.33
86	STACK East	8,402	43	-31.49	2,359	38.9%	46.7%	10.5%	3.9%	0.0%	3.25
87	STACK East	7,552	41		2,160	35.7%	45.3%	10.0%	4.7%	4.4%	3.38
88	STACK East	8,857	44		5,288	36.4%	52.8%	9.4%	1.2%	0.3%	5.03
89	STACK East	7,945	40		3,080	43.1%	47.6%	7.5%	1.6%	0.2%	5.24
90	STACK East	7,630	40	-30.35	1,581	41.0%	44.2%	11.3%	3.0%	0.5%	3.11
91	STACK East	7,862		-30.99	9,777	44.5%	45.6%	8.0%	1.6%	0.2%	4.75
92	STACK East	7,970	42		2,890	37.6%	49.4%	10.4%	2.5%	0.2%	3.87
93	STACK East	7,500	42		4,480	29.1%	51.2%	14.2%	4.7%	0.9%	2.76
94	STACK East	9,291	45		1,954	39.2%	50.3%	8.0%	2.3%	0.2%	4.89
95	STACK East	9,033	42	-31.02	8,238	52.5%	40.8%	4.3%	2.4%	0.0%	6.07
96	STACK East	8,991		-30.85	9,218	49.7%	42.1%	6.9%	1.2%	0.1%	5.21
97	STACK East	8,848	43		3,894	37.3%	51.1%	9.3%	2.1%	0.2%	4.51
98	STACK East	8,334	40		4,106	30.4%	53.5%	10.1%	5.7%	0.3%	3.41
99	STACK East	8,586	43		2,983	35.8%	50.9%	10.5%	2.6%	0.2%	3.92
100	STACK East	7,452	39	-30.90	497	29.7%	48.8%	16.3%	4.0%	1.2%	2.46
101	STACK East	7,601	39	-31.16	2,484	31.1%	52.9%	12.2%	2.9%	0.8%	3.56
102	STACK East	7,325	42	-31.22	10,609	33.3%	52.8%	10.9%	2.8%	0.2%	3.89
103	STACK East	8,258	39		2,425	42.7%	44.7%	10.1%	2.3%	0.2%	3.62
104	STACK East	8,484		-31.62	7,649	41.0%	49.0%	8.2%	1.7%	0.1%	4.93
105	STACK East	7,887	44	-31.94	3,441	38.5%	48.6%	10.6%	2.1%	0.2%	3.87
106	STACK East	8,861	43		1,111	32.4%	52.5%	11.9%	2.9%	0.3%	3.56
107	STACK East	7,965	41	-31.8	1,708	34.3%	48.1%	12.4%	5.0%	0.1%	2.76
108	STACK East	9,249	45	-30.39	3,068	44.7%	45.4%	8.3%	1.6%	0.1%	4.61
109	STACK East	9,017	45	-30.96	10,940	46.9%	44.1%	7.1%	1.7%	0.1%	5.00
110	STACK East	9,532	45	-30.24	12,775	54.8%	38.6%	5.6%	0.9%	0.1%	5.97
111	STACK East	8,392	40		2,279	40.6%	46.4%	9.6%	3.0%	0.3%	3.70
112	STACK East	7,533	39	-31.33	3,892	33.3%	51.8%	12.1%	2.6%	0.2%	3.53
113	STACK East	7,292	40	-31.12	1,132	33.2%	49.5%	13.7%	2.7%	0.9%	3.08
114	STACK East	7,162	39	-31.00	2,279	36.1%	50.3%	10.2%	3.1%	0.4%	3.81
115	STACK East	6,714	39	-30.87	674	32.0%	50.5%	13.9%	3.4%	0.3%	2.94
116	STACK East	7,048	39	-31.31	6,642	35.0%	49.4%	11.8%	3.5%	0.3%	3.25
117	STACK East	6,779	39	-31.24	2,761	31.9%	51.1%	14.4%	2.2%	0.4%	3.10
118	STACK East	7,004	39	-31.15	3,491	28.2%	53.5%	14.1%	3.4%	0.8%	3.09

Key	Play Region	TVD	API Gravity	Oil $\delta^{13}C$	IP GOR	% Volatile	% Sat	% Aro	% NSO	% Asph	Coll. Inst. Index
119	STACK East	6,921	39	-31.12	5,953	34.5%	51.4%	10.7%	3.1%	0.3%	3.76
120	SCOOP	10,105	39		379	38.0%	45.8%	12.4%	3.6%	0.3%	2.88
121	SCOOP	14,171	57		83,170	82.9%	16.1%	0.8%	0.2%	0.0%	16.26
122	SCOOP	14,504	49		32,689	74.2%	25.1%	0.7%	0.0%	0.0%	36.22
123	SCOOP	14,150	49		17,294	65.2%	33.2%	0.6%	1.0%	0.0%	20.24
124	SCOOP	11,387	44		730	43.8%	50.5%	4.9%	0.9%	0.0%	8.78
125	SCOOP	11,901	45		1,208	38.2%	48.5%	9.7%	3.7%	0.0%	3.62
126	SCOOP	10,950	47		1,226	37.4%	52.9%	8.6%	1.1%	0.0%	5.45
127	SCOOP	10,555	48		2,025	31.7%	59.7%	6.1%	2.5%	0.0%	6.93
128	SCOOP	10,844	46		2,086	36.9%	53.4%	6.8%	2.9%	0.0%	5.48
129	SCOOP	10,762	44		1,955	39.4%	43.8%	15.3%	1.6%	0.0%	2.60
130	SCOOP	11,363	47		1,171	42.0%	45.7%	11.2%	1.1%	0.0%	3.72
131	SCOOP	11,591	40		723	39.9%	48.9%	7.9%	3.2%	0.0%	4.39
132	SCOOP	12,989	46		1,235	41.4%	53.9%	3.7%	1.0%	0.0%	11.59
133	SCOOP	11,179	46		1,501	43.9%	44.1%	10.7%	1.3%	0.0%	3.67
134	SCOOP	12,939	47		2,421	48.6%	49.1%	2.3%	0.1%	0.0%	21.18
135	SCOOP	10,671	44		865	38.1%	49.5%	9.3%	3.1%	0.0%	3.99
136	SCOOP	10,922	45		992	39.2%	50.7%	9.1%	1.0%	0.0%	5.01
137	SCOOP	10,881	45		4,371	36.9%	54.8%	7.3%	0.9%	0.0%	6.62
138	SCOOP	11,421	43		1,767	32.4%	54.1%	8.3%	5.1%	0.1%	4.04
139	SCOOP	12,317	49		1,710	38.4%	48.6%	11.7%	1.4%	0.0%	3.73
140	SCOOP	12,303	43		1,845	37.8%	48.8%	11.8%	1.5%	0.0%	3.65
141	SCOOP	11,698	46		1,665	38.1%	54.4%	6.1%	1.4%	0.0%	7.27
142	SCOOP	11,777	44		3,156	38.8%	57.4%	2.8%	1.0%	0.0%	15.08
143	SCOOP	11,706	45		2,578	42.4%	48.5%	7.1%	2.0%	0.0%	5.34
144	SCOOP	11,004	45		4,801	41.8%	46.9%	9.9%	1.5%	0.0%	4.12
145	SCOOP	11,104	46		1,617	38.0%	45.8%	10.1%	6.2%	0.0%	2.81
146	SCOOP	11,522	44		993	46.0%	45.7%	6.7%	1.6%	0.0%	5.50
147	SCOOP	11,755	47		993	40.5%	52.8%	6.1%	0.6%	0.0%	7.86
148	SCOOP	12,112	46		4,921	44.3%	49.6%	5.4%	0.6%	0.0%	8.22
149	SCOOP	9,642	48		123,839	59.3%	34.4%	6.0%	0.3%	0.0%	5.43
150	SCOOP	14,766	53		20,060	73.8%	25.7%	0.5%	0.0%	0.0%	49.05
151	SCOOP	12,832	58		52,347	78.8%	20.2%	0.8%	0.2%	0.0%	21.10
152	SCOOP	11,100			22,185	54.2%	41.2%	4.0%	0.6%	0.0%	8.81
153	SCOOP	12,053	60		31,782	75.0%	24.3%	0.7%	0.1%	0.0%	33.82
154	SCOOP	9,812	46		8,405	42.5%	51.3%	6.1%	0.1%	0.0%	8.18
155	SCOOP	9,460			2,028	47.2%	44.9%	7.3%	0.6%	0.0%	5.65
156	SCOOP	12,753	45		1,210	35.0%	50.2%	9.8%	4.9%	0.1%	3.42
157	SCOOP	13,412	40		82,110	55.8%	41.1%	1.9%	1.3%	0.0%	13.07
158	SCOOP	14,125	50		212,505	45.0%	52.9%	2.0%	0.2%	0.0%	24.50
159	SCOOP	9,920			22,720	37.5%	51.2%	9.1%	2.2%	0.0%	4.53
160	SCOOP	13,284	45		910	40.0%	54.5%	4.6%	0.9%	0.0%	9.89
161	SCOOP	12,359	46		2,309	45.7%	50.5%	3.4%	0.4%	0.0%	13.43
162	SCOOP	13,398	47		2,140	48.2%	49.8%	1.8%	0.2%	0.0%	25.39
163	SCOOP	15,760	51		1,255,433	60.5%	35.6%	2.1%	1.8%	0.0%	9.34
164	SCOOP	14,235	51		15,120	62.6%	34.4%	1.7%	1.2%	0.0%	11.70
165	SCOOP	13,521	47		54	41.9%	54.2%	2.5%	1.4%	0.0%	14.02
166	SCOOP	13,130	45		999	37.1%	58.2%	2.0%	2.7%	0.0%	12.52
167	SCOOP	13,860	46		2,152	43.3%	53.6%	2.1%	1.0%	0.0%	17.64
168	SCOOP	12,874	43		819	34.7%	59.4%	3.5%	2.5%	0.0%	10.03
169	SCOOP	8,507	43		863	28.0%	52.3%	14.4%	5.2%	0.1%	2.68
170	SCOOP	13,274	43		962	40.3%	56.3%	2.9%	0.5%	0.0%	16.63
171	SCOOP	12,517	45		531	34.3%	60.1%	3.9%	1.6%	0.2%	10.97
172	SCOOP	14,183	52		172,826	76.4%	22.4%	0.7%	0.5%	0.0%	17.89

Table 3. Bulk composition parameter metrics utilized in determining thermal maturity in this chapter. The key refers to oil samples defined in Table 1. Missing API gravity values were not reported to OCC. %Volatile, %Sat, %Aro, %NSO, and %Asph correspond to percent volatile, saturate, aromatic, NSO, and asphaltene components measured during fractionation. Coll. Inst. Index=Colloidal Instability Index defined as (%Sat+%Asph)/(%Aro+%NSO).

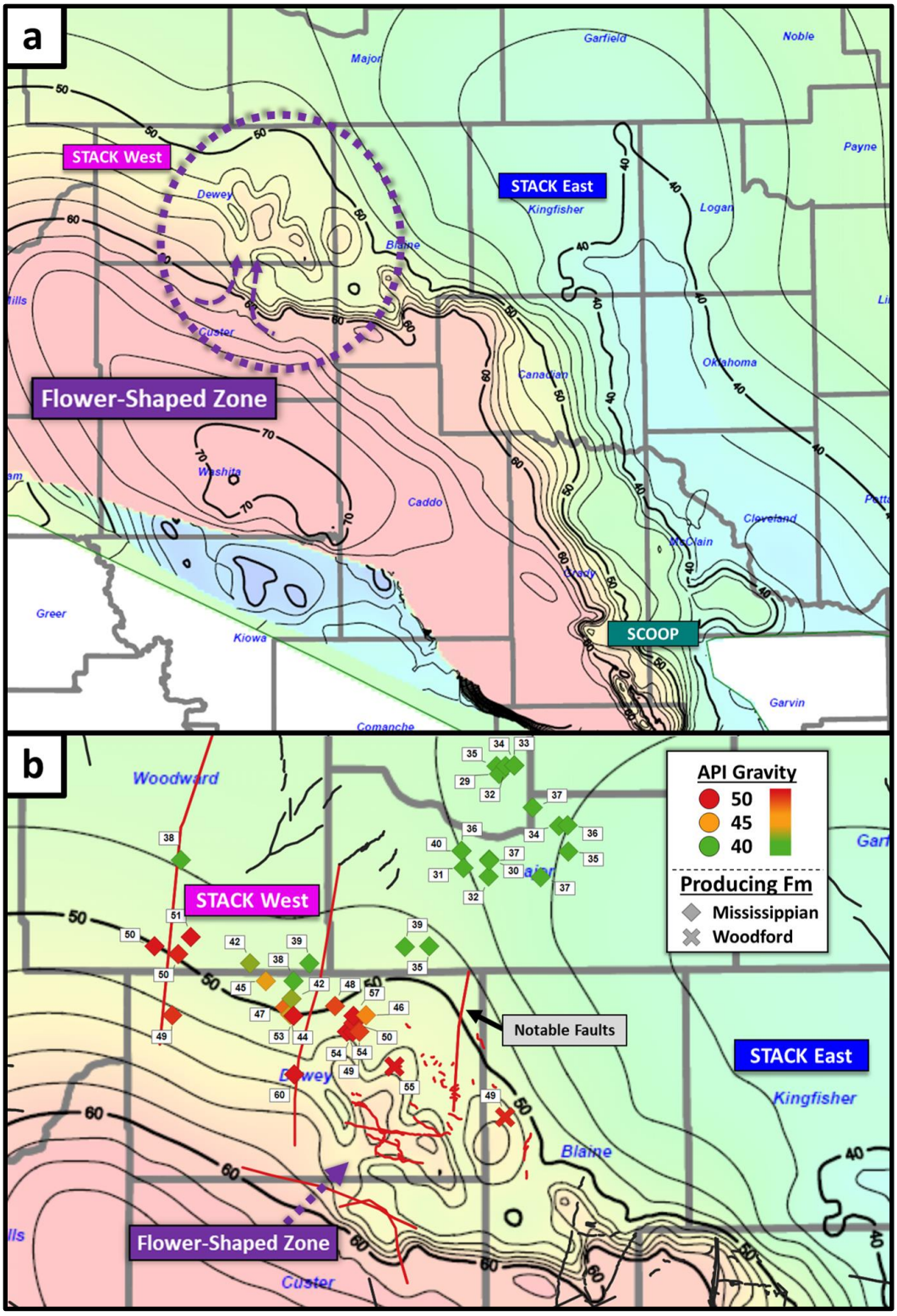

Figure 20. a) Contour map of Woodford oil API gravity. A "flower-shaped zone" in a heavily faulted portion of eastern Dewey County bends the contours indicating an updip incursion of higher maturity oils. b) Map of the flower-shaped zone with study oils (labeled by 1002A API gravity) showing major shift in API gravity across notable N-S trending faults, marked red. Faulted lithology may contribute to updip migration of higher maturities from deeper in the basin.

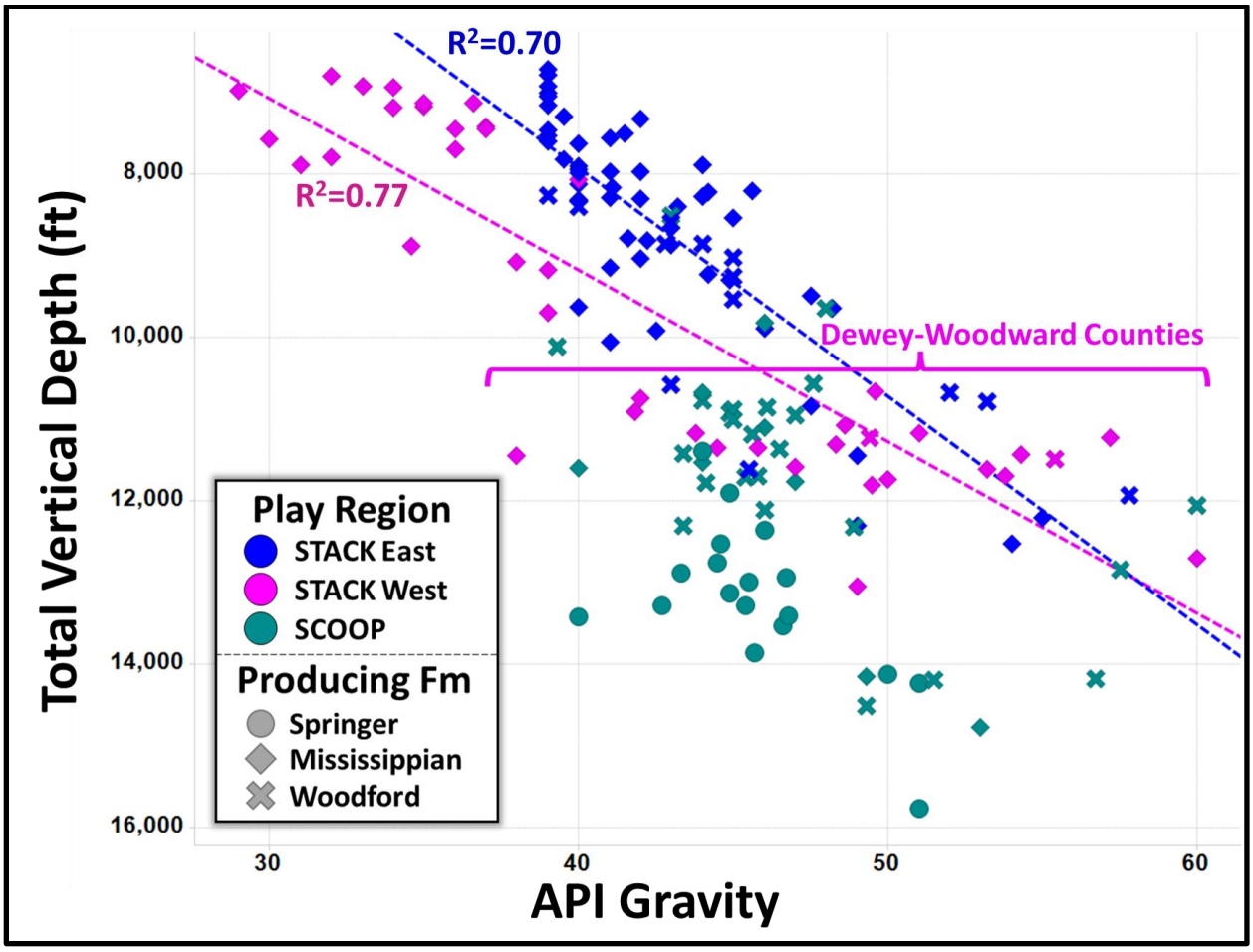

Figure 21. Initial production API Gravity values for study wells (from OCC form 1002A). STACK oils generally increase with depth while SCOOP oils show little correlation with depth. A broad range of STACK West values around ~11,000 ft correspond to a flower-shaped zone of higher API gravity in Dewey County (see Figure 20).

Stable Carbon Isotopes

Isotopes are atoms whose nuclei contain the same number of protons but different numbers of neutrons. Carbon has two isotopes which are stable over geologic time—a light isotope carbon-12 (^{12}C) which has six neutrons and a heavy isotope carbon-13 (^{13}C) which has seven. Covalent bonds containing isotopically heavy carbon (i.e. ^{13}C-^{12}C bonds) are slightly more stable than bonds which only contain isotopically light carbon (^{12}C-^{12}C bonds) (Urey, 1947). During maturation, hydrocarbons bound to kerogen by ^{12}C-^{12}C bonds are more readily broken which in turn generates isotopically lighter hydrocarbons than the remaining hydrocarbons (Fuex, 1977).

The $\delta^{13}C$ notation is a measure of the isotopic ratio $^{13}C/^{12}C$ relative to a reference standard and given in parts per thousand, or per mil (‰). More positive $\delta^{13}C$ values indicate a higher abundance of isotopically heavy ^{13}C in the sample material. The $\delta^{13}C$ for the 69 whole oil samples monitored in this study demonstrate an increase in isotopically heavy carbon with increased TVD (Figure 22). It has been argued that isotopic deviations greater than 2-3‰ are usually associated with different sources (Stahl, 1977, 1978; Sofer, 1984); however, other publications have documented broader ranges of isotopic carbon associated with changes in maturity and biodegradation (e.g. Chung et al., 1981). In this dataset, $\delta^{13}C$ values span over approximately a ~4‰ range between the shallowest and deepest samples, and the systematic increase in $\delta^{13}C$ with increased TVD suggestive of strong correlation with thermal maturity.

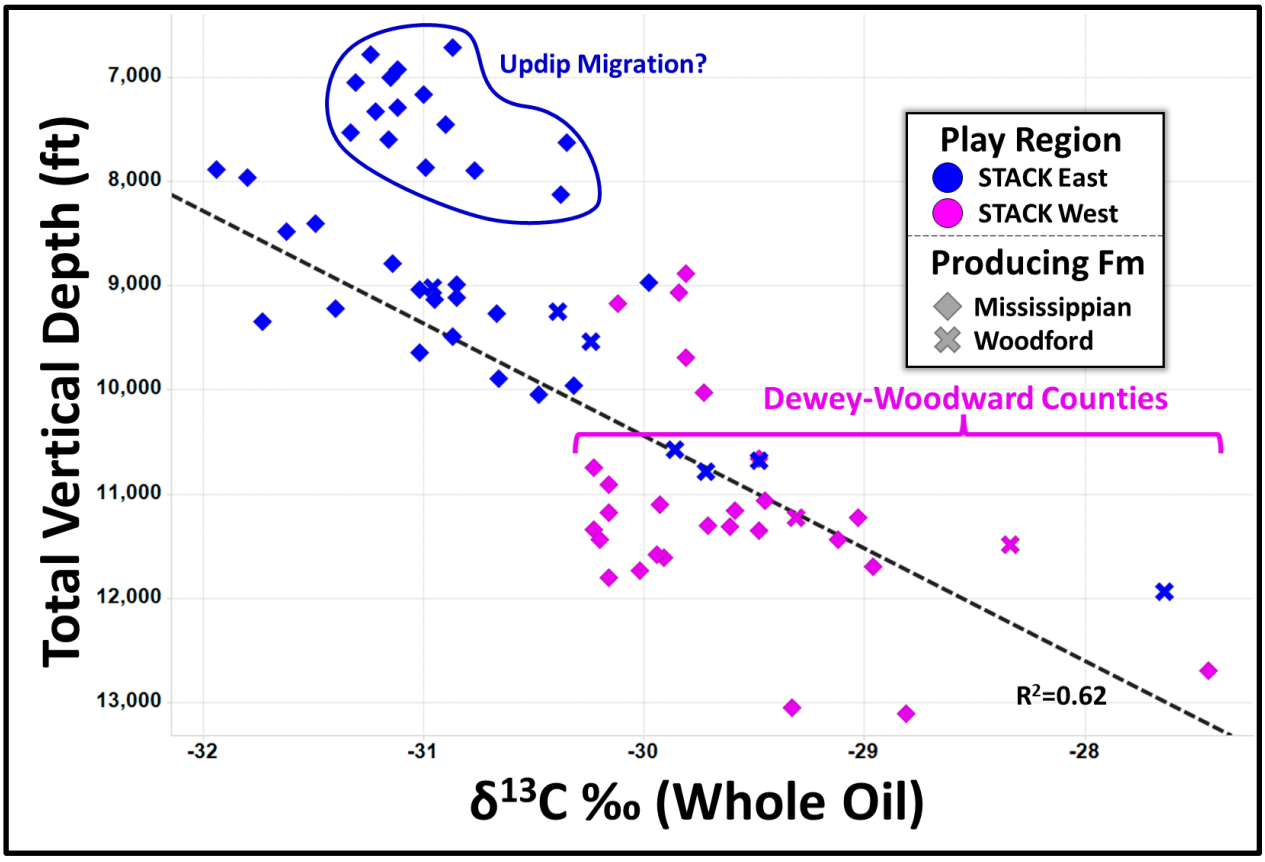

Figure 22. Cross-plot of whole oil $\delta^{13}C$ isotope values versus TVD. A cluster of STACK East oils is circled as possible evidence of updip migration and are not included in regression trendline (see text). The STACK West oils at ~11,000 ft mirror the variable maturities observed in Woodward and Dewey counties which include the flower-shaped zone.

The highly variable maturity oils in Woodward and Dewey counties in STACK West which include the higher maturity "flower-shaped zone" is also observed and spans a $\delta^{13}C$ range of ~2‰, but the high degree of variability is less apparent compared to other maturity parameters. One explanation is that if oil mixing is occurring the flower-shaped zone, the isotopically enriched mature fluid will be more abundant in lighter, more volatile hydrocarbons that may be lost during oil-water separation and routine handling. Furthermore, several oils—marked "Updip Migration" and circled in Figure 22—plot approximately 1,000-2,000 ft above the main trend. When plotted in map view, these oils were produced from shallow Mississippian reservoirs in STACK East above immature Woodford (Ro<0.6%), shown in Figure 23. Based on the trendline correlating $\delta^{13}C$ with TVD in STACK, these oils might have retained a pre-migration isotopic signature consistent with generation from a source rock at depths between 8,500-10,000 ft before migrating approximately 1,000-2,000 ft up section into its current, shallower Mississippian reservoir.

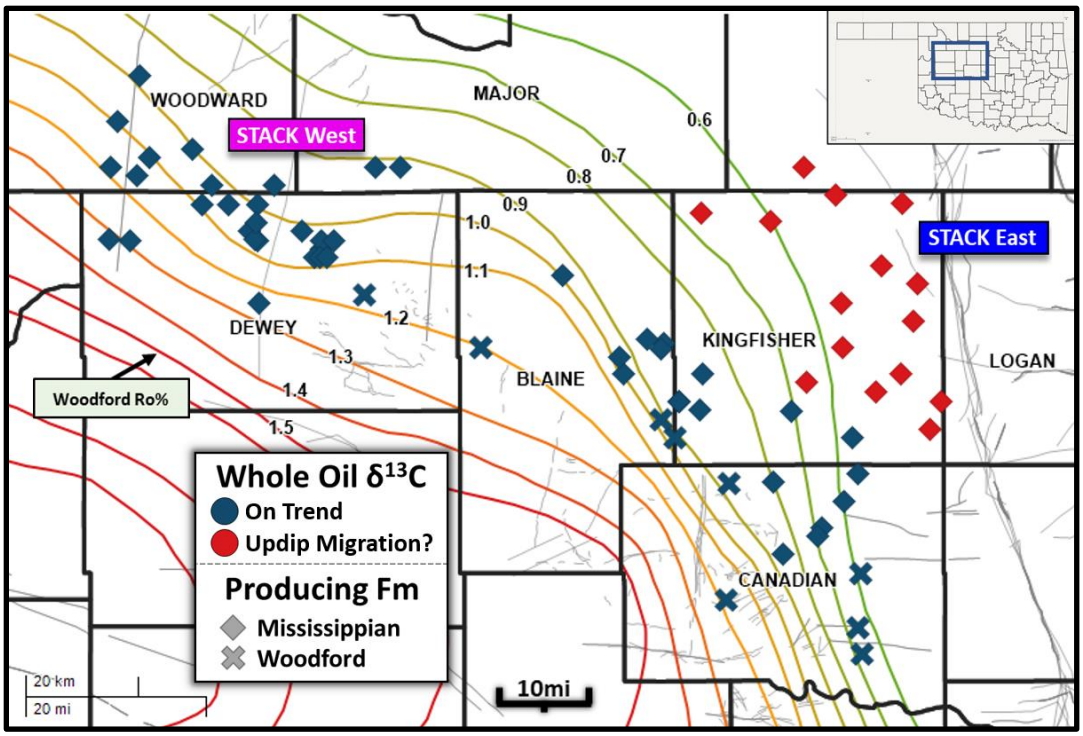

Figure 23. Map of STACK indicating the circled samples marked "Updip Migration" in Figure 22. These samples are produced from Mississippian reservoirs above immature Woodford, and plot approximately 1,000-2,000 ft TVD above the TVD-$\delta^{13}C$ trendline indicating that may be the extend of updip migration.

Gas-Oil Ratio

With increasing maturity, kerogen generates lower molecular weight and more volatile hydrocarbons which in turn increases the gas-oil ratio (GOR) of its generated oil (Tissot and Welte, 1984; Moses, 1986; McCain, 1990). Over the life of a well, the GOR generally increases as reservoir pressure drops approaching the oil bubble point pressure; therefore, the initially producing GOR (IP GOR) most closely represents an oil composition in a pristine reservoir. The IP GOR for all wells in this study is provided in Figure 24, showing general increases with depth in STACK, but the relationship is weak and has substantial scatter. Oils from SCOOP show no meaningful correlation between IP GOR and depth but, similar to API gravity, plot below the STACK Play Regions by several thousand feet which continue to suggest that SCOOP is either a cooler portion of the basin or has experienced less regional uplift since entering the oil window.

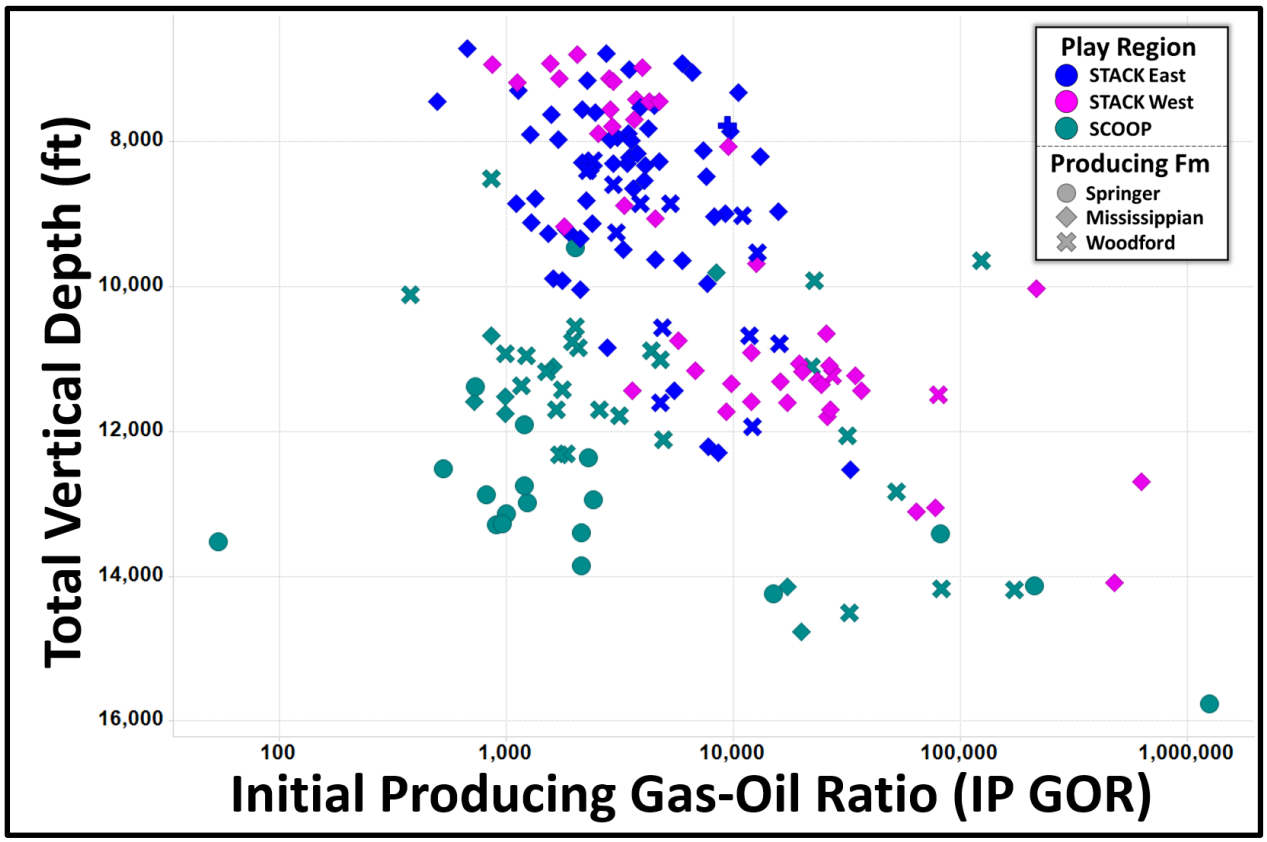

Figure 24. The IP GOR in this dataset generally increases with TVD but exhibits a very weak correlation.

Bulk Composition (SARA)

Mature oil samples can be subdivided into its SARA chemical classes, where the first letter refers to saturate, aromatic, resin (NSO), and asphaltene fractions. The saturate fraction consists of nonpolar compounds with only single bonds and includes linear, branched, and cyclic compounds. The aromatic fraction consists of slightly polar compounds containing one or more aromatic ring as well as some non-polar sulfur-containing compounds (e.g. benzothiophenes) and non-basic nitrogen compounds (e.g. benzocarbazoles). The NSO fraction consists of polar constituents often containing nitrogen, sulfur, or oxygen bearing non-hydrocarbons (Peters et al., 2005a). The asphaltene fraction is defined as the portion of crude oil precipitated by dilution in *n*-pentane and is comprised high molecular weight condensed aromatic macromolecules colloidally dispersed in oil (Pfeiffer and Saal, 1940). Asphaltenes are stabilized and remain in solution by adsorbing to aromatic and resin components which serve as peptizers forming the outer layer of a micelle with lower surface tension (Pfeiffer and Saal, 1940; Dickie and Yen, 1967; Mullins, 2011).

The weight percent of oil SARA fractions in this study are provided in Figure 25 whereby weight lost to volatilization during sample preparation accounts for the remaining percent up to 100%. Oils become more volatile with increased depth, but also show an increase in the relative abundance of saturates compared to aromatics, NSOs, and asphaltenes. Two modes of oils can be observed in STACK West oils. Oils produced at TVD shallower than 9,687 ft have relatively low volatile loss (~30% loss) and contain the only consistently measurable amounts of asphaltenes in the dataset. Deeper oils in STACK West are collectively the most volatile with samples losing up to 89% weight during processing. These deep samples are also dominated by saturates with almost no other fractions present. The relationship between depth, increased volatility, and saturate enrichment is stronger in STACK than SCOOP.

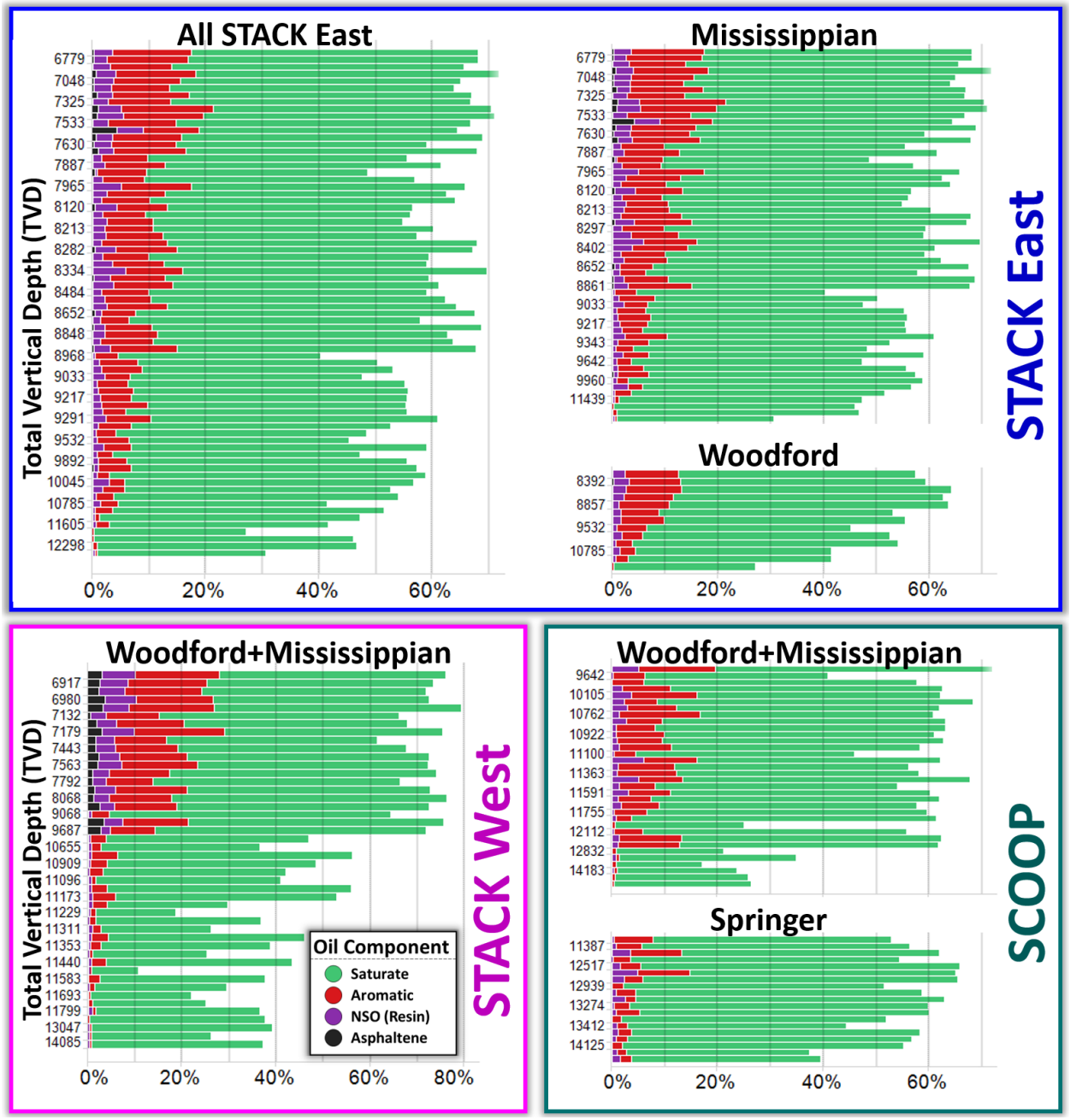

Figure 25. The sum of SARA values for oils in this study plotted by depth and Play Region. Volatiles lost during sample preparation and fractionation account for the remaining weight up to 100%. Oils become more volatile with increased depth, but also show an increase in the relative abundance of saturates compared to aromatics, NSOs, and asphaltenes. Asphaltenes are only observed in meaningful quantities in shallow STACK West oils.

The systematic decrease in aromatic and resin components relative to saturates with depth may provide a novel measure of maturity. Since resins and aromatics both contribute to asphaltene stability, it may be possible to quantify maturity as a mass ratio of the sum of asphaltenes and its flocculants (saturates) to the sum of its peptizers (resins and aromatics), also known as the colloidal instability index (CII) as defined in Equation 8 (Asomaning and Watkinson, 2000).

$$\text{Colloidal Instability Index (CII)} = \frac{\%\text{Saturates} + \%\text{Asphaltenes}}{\%\text{Aromatics} + \%\text{Resins}} \qquad \text{Equation 8}$$

Values for CII are plotted in Figure 26 and do show a strong correlation with TVD in STACK (R^2=0.80, 0.81); however, the study oils generally have low asphaltene concentrations therefore CII as a maturity parameter primarily reflects changes in saturates abundances relative to aromatics and resins. The oils comprising the flower-shaped zone in STACK West also show a wider range of CII values. SCOOP samples show a modest correlation with TVD and again plot below the STACK trends either as a cooler portion of the basin or having undergone less regional uplift.

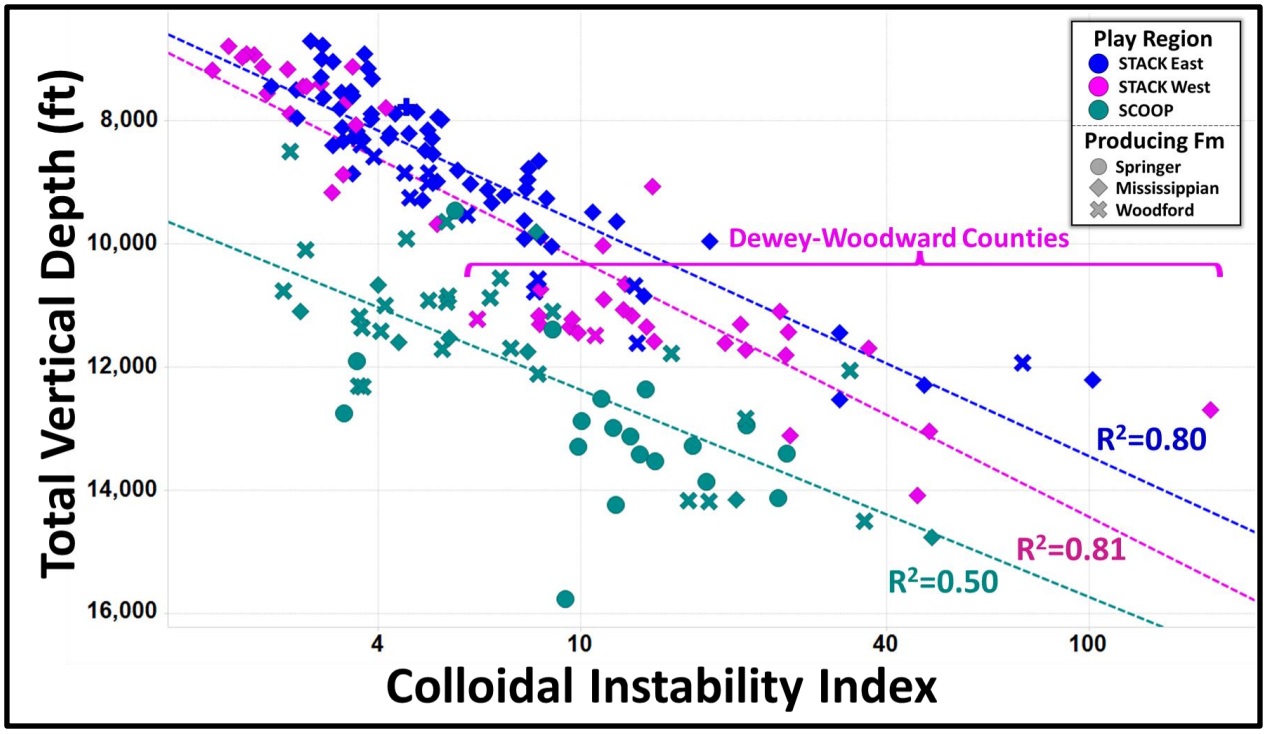

Figure 26. Colloidal Instability Index (CII) versus TVD for study oils. There is a strong relationship in STACK than in SCOOP which again plots below the main STACK trend. The flower shaped zone in STACK West is also present.

In summary, the bulk composition of oil samples STACK and SCOOP systematically change with increased depth and thermal stress. The SARA fractions show that most samples in this dataset have little or no asphaltene fraction, and oils contain a larger volatile and saturate fraction with increased burial. The CII ratio shows the best correlation with TVD in any given Play Region and is a promising maturity parameter, while IP GOR and API gravity show little correlation with TVD. Stable carbon isotope data from a limited number of whole oil samples show a promising correlation with depth in this dataset, but more testing is required to confirm the trend. Finally, a contour map of Woodford Shale API gravity across the Anadarko Basin in conjunction with known fault lines provided key insight into a flower-shaped zone of highly variable oil composition in eastern Dewey County that may be mixing with higher maturity oils migrating up from deeper in the basin.

Biomarker Maturity Parameters

The ratios of select biomarkers have been found to systematically change with oil maturity. Compound structures which are denoted by bold Roman numerals are shown in the Appendix. This section discusses several of these ratios related to the stereoisomerization of regular steranes (**I**), the relative abundance of rearranged steranes (**II**), the relative thermal stability of two groups of triaromatic steroids (**III** and **IV**), and the relative generation of tricyclic terpanes (**V**) and hopanes (**VI**). The data used in this section are summarized in Table 4.

Regular Steranes

Most steranes (**I**) in petroleum originate from sterols in the lipid membranes of eukaryotic organisms (Huang and Meinschein, 1979; Volkman, 1986, 2003). In general, living organisms will synthesize only one stereoisomer, but the configuration at asymmetric centers in sterols are

imposed by enzymes and are not necessarily the most thermodynamically stable orientation (Mackenzie et al., 1982). A kinetic precursor-product relationship is shown in Figure 27 illustrating how an example C_{29} sterol in a living organism is converted during diagenesis into C_{29} sterane and can undergo additional stereoisomerization during continued burial, heating, and catalysis. The isomerization at C-20 proceeds from all 20R to a near-equal mixture 20S and 20R until a kinetic equilibrium is reached whereby the ratio of C_{29} 5α(H),14α(H),17α(H) 20S/(S+R) is approximately 0.55 (Seifert and Moldowan, 1981). The asymmetric centers at C-14 and C-17 isomerize during burial and heating from the biologic α-configuration to the more stable β-configuration due to steric forces imposed by the rigid cyclic structure and reach equilibrium at approximately 0.7.

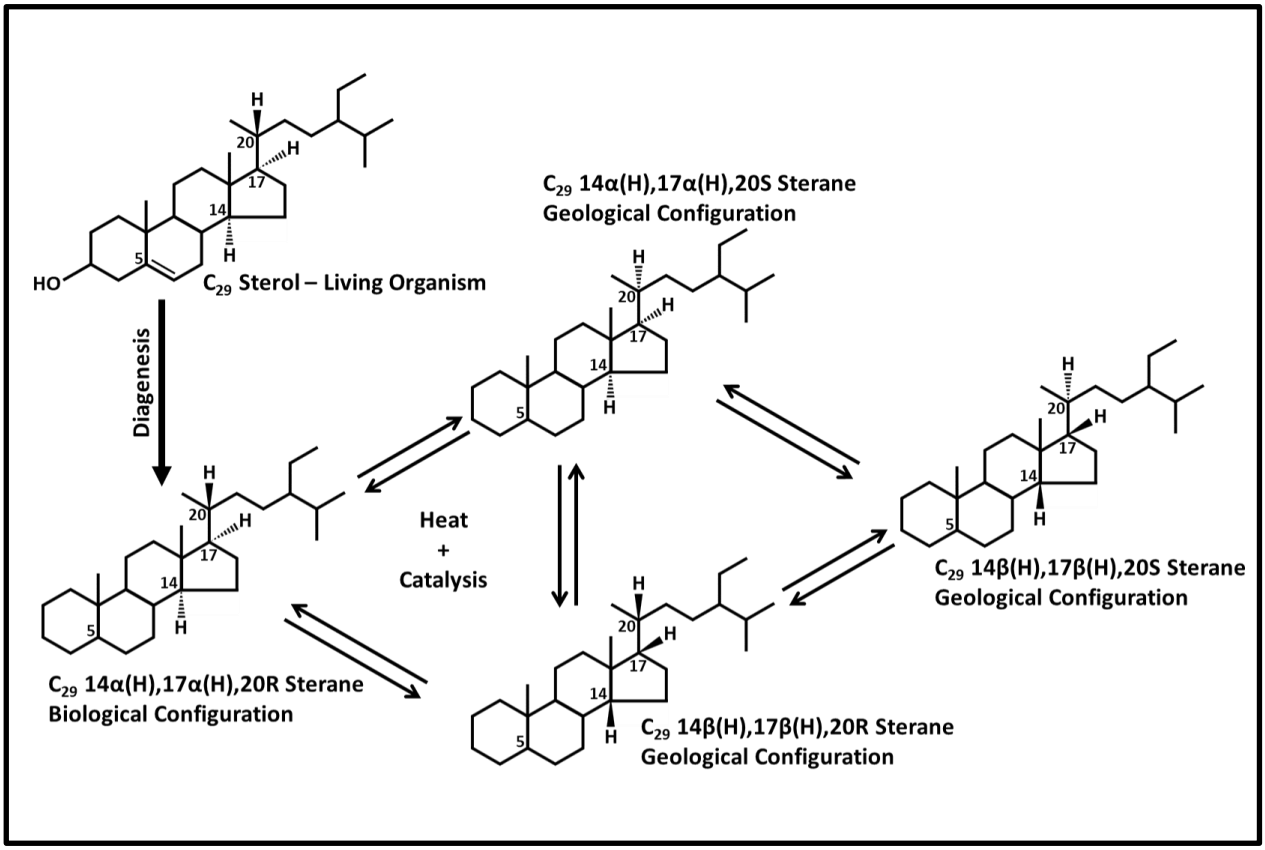

Figure 27. Kinetic precursor-product relationship of C_{29} sterane (**I**) stereoisomers common in mature geologic samples. Each structure has an implied 5α(H) configuration. Recreated from Seifert and Moldowan (1981).

Key	Play Region	TVD	C_{29} S/(S+R)[1]	C_{29} ββ/(αα+ββ)[2]	Diasteranes/Total Steranes[3]	TA[I]/(TA[I]+TA[II])[4]	3R/(3R+5R) Terpanes[5]
1	STACK West	7,130	0.41	0.60	0.41	0.22	0.47
2	STACK West	6,791	0.42	0.61	0.40	0.21	0.46
3	STACK West	7,179	0.41	0.60	0.49	0.33	0.44
4	STACK West	6,917	0.43	0.60	0.44	0.22	0.47
5	STACK West	6,980	0.41	0.61	0.43	0.21	0.46
6	STACK West	7,132	0.42	0.62	0.49	0.42	0.58
7	STACK West	6,934	0.43	0.62	0.37	0.28	0.49
8	STACK West	7,444	0.42	0.62	0.46	0.31	0.49
9	STACK West	7,690	0.40	0.61	0.45	0.39	0.59
10	STACK West	8,068	0.43	0.63	0.39	0.39	0.57
11	STACK West	7,563	0.41	0.62	0.39	0.31	0.51
12	STACK West	7,443	0.44	0.62	0.42	0.31	0.51
13	STACK West	7,887	0.41	0.61	0.40	0.42	0.60
14	STACK West	7,792	0.43	0.62	0.42	0.41	0.54
15	STACK West	7,412	0.42	0.64	0.45	0.49	0.60
16	STACK West	7,172	0.42	0.62	0.35	0.33	0.52
17	STACK West	9,068	0.39	0.63	0.50	0.87	0.91
18	STACK West	11,096	0.40	0.63	0.63	0.92	0.97
19	STACK West	10,024	0.42	0.63	0.47	0.81	0.88
20	STACK West	11,173	0.42	0.66	1.00	0.86	0.95
21	STACK West	11,729	0.37	0.61	0.87	0.90	NA
22	STACK West	11,799	0.40	0.63	0.99	0.88	0.97
23	STACK West	13,107	NA	NA	NA	0.91	NA
24	STACK West	13,047	NA	NA	0.99	0.91	NA
25	STACK West	11,303	0.42	0.64	0.88	0.85	0.95
26	STACK West	10,909	0.47	0.67	0.95	0.87	0.94
27	STACK West	9,687	0.42	0.61	0.50	0.74	0.80
28	STACK West	9,171	0.42	0.63	0.46	0.71	0.70
29	STACK West	8,883	0.43	0.63	0.41	0.69	0.78
30	STACK West	11,344	0.43	0.64	0.79	0.83	0.96
31	STACK West	11,440	0.40	0.64	0.84	0.81	0.97
32	STACK West	10,743	0.55	0.70	0.62	0.86	0.96
33	STACK West	11,583	0.41	0.66	0.94	0.87	0.96
34	STACK West	11,162	0.43	0.67	0.99	0.83	0.97
35	STACK West	11,609	0.21	0.54	0.99	0.87	0.87
36	STACK West	12,693	NA	NA	NA	0.65	NA
37	STACK West	11,311	0.42	0.64	0.62	0.80	0.96
38	STACK West	11,229	0.40	0.63	0.74	0.78	0.97
39	STACK West	11,353	0.41	0.66	0.86	0.81	0.98
40	STACK West	10,655	0.47	0.68	0.78	0.82	0.96
41	STACK West	11,693	0.31	0.61	0.55	0.84	NA
42	STACK West	11,435	0.29	0.59	0.99	0.85	0.96
43	STACK West	11,065	0.39	0.66	0.77	0.78	0.97
44	STACK West	11,487	0.30	0.42	0.63	0.77	NA
45	STACK West	14,085	NA	NA	NA	0.89	NA
46	STACK West	11,227	0.35	0.58	0.83	0.76	NA
47	STACK East	12,523	NA	NA	NA	0.85	NA
48	STACK East	12,208	NA	NA	NA	0.86	NA
49	STACK East	12,298	NA	NA	NA	0.87	NA
50	STACK East	8,968	0.41	0.62	0.66	0.72	0.94
51	STACK East	11,605	0.39	0.70	0.98	0.88	0.92
52	STACK East	11,439	NA	NA	NA	0.86	NA
53	STACK East	10,045	0.43	0.71	0.99	0.81	0.97
54	STACK East	9,892	0.44	0.71	0.99	0.82	0.96
55	STACK East	9,112	0.44	0.71	0.99	0.81	0.96
56	STACK East	10,573	0.80	0.85	0.89	0.80	NA
57	STACK East	9,135	0.37	0.68	0.99	0.85	0.96
58	STACK East	9,267	0.44	0.68	0.99	0.79	0.96
59	STACK East	8,652	0.44	0.69	0.86	0.66	0.95

Key	Play Region	TVD	C_{29} S/(S+R)[1]	C_{29} ββ/(αα+ββ)[2]	Diasteranes/Total Steranes[3]	TA[I]/(TA[I]+TA[II])[4]	3R/(3R+5R) Terpanes[5]
60	STACK East	10,677	NA	NA	0.99	0.89	0.86
61	STACK East	8,207	0.42	0.63	0.62	0.69	0.81
62	STACK East	9,489	0.44	0.73	0.99	0.82	0.96
63	STACK East	9,642	0.40	0.71	0.99	0.82	0.96
64	STACK East	8,213	0.41	0.63	0.71	0.71	0.82
65	STACK East	9,343	0.44	0.73	0.99	0.78	0.95
66	STACK East	8,120	0.42	0.63	0.53	0.72	0.72
67	STACK East	8,787	0.40	0.69	0.99	0.73	0.95
68	STACK East	7,783	0.40	0.63	0.74	0.71	0.83
69	STACK East	8,297	0.41	0.66	0.68	0.55	0.82
70	STACK East	8,813	0.43	0.67	0.99	0.68	0.95
71	STACK East	11,932	NA	NA	NA	0.90	NA
72	STACK East	7,814	0.41	0.64	0.63	0.57	0.77
73	STACK East	10,785	NA	NA	0.86	0.84	NA
74	STACK East	9,915	0.47	0.71	0.79	0.66	0.95
75	STACK East	8,282	0.45	0.67	0.68	0.53	0.85
76	STACK East	8,307	0.42	0.64	0.66	0.61	0.77
77	STACK East	9,626	0.38	0.72	0.91	0.79	0.94
78	STACK East	10,842	0.54	0.75	0.84	0.80	0.95
79	STACK East	8,275	0.41	0.67	0.57	0.53	0.83
80	STACK East	7,897	0.43	0.65	0.58	0.83	0.72
81	STACK East	8,540	0.47	0.69	0.74	0.59	0.87
82	STACK East	9,217	0.46	0.68	0.92	0.76	0.94
83	STACK East	8,161	0.45	0.67	0.60	0.56	0.85
84	STACK East	9,960	0.39	0.65	0.94	0.88	0.94
85	STACK East	7,984	0.38	0.66	0.89	0.50	0.84
86	STACK East	8,402	0.43	0.69	0.78	0.57	0.82
87	STACK East	7,552	0.42	0.66	0.69	0.45	0.78
88	STACK East	8,857	0.42	0.65	0.75	0.58	0.81
89	STACK East	7,945	0.46	0.66	0.62	0.59	0.85
90	STACK East	7,630	0.46	0.65	0.39	0.56	0.63
91	STACK East	7,862	0.43	0.66	0.66	0.54	0.82
92	STACK East	7,970	0.49	0.71	0.71	0.53	0.80
93	STACK East	7,500	0.44	0.64	0.53	0.47	0.66
94	STACK East	9,291	0.41	0.69	0.99	0.63	0.81
95	STACK East	9,033	0.41	0.67	0.90	0.69	0.90
96	STACK East	8,991	0.43	0.67	0.80	0.61	0.83
97	STACK East	8,848	0.38	0.68	0.71	0.55	0.76
98	STACK East	8,334	0.41	0.69	0.74	0.50	0.76
99	STACK East	8,586	0.42	0.66	0.74	0.50	0.73
100	STACK East	7,452	0.45	0.64	0.35	0.40	0.61
101	STACK East	7,601	0.45	0.64	0.44	0.38	0.73
102	STACK East	7,325	0.43	0.65	0.65	0.44	0.76
103	STACK East	8,258	0.43	0.66	0.68	0.37	0.71
104	STACK East	8,484	0.44	0.71	0.72	0.47	0.72
105	STACK East	7,887	0.44	0.65	0.63	0.33	0.72
106	STACK East	8,861	0.43	0.65	0.69	0.35	0.71
107	STACK East	7,965	0.44	0.66	0.58	0.34	0.71
108	STACK East	9,249	0.43	0.63	0.79	0.70	0.88
109	STACK East	9,017	0.50	0.72	0.87	0.60	0.80
110	STACK East	9,532	0.41	0.64	0.76	0.74	0.91
111	STACK East	8,392	0.44	0.66	0.61	0.34	0.69
112	STACK East	7,533	0.44	0.62	0.55	0.29	0.73
113	STACK East	7,292	0.44	0.64	0.47	0.31	0.67
114	STACK East	7,162	0.44	0.60	0.43	0.24	0.71
115	STACK East	6,714	0.41	0.62	0.54	0.39	0.67
116	STACK East	7,048	0.44	0.63	0.56	0.30	0.74
117	STACK East	6,779	0.41	0.65	0.51	0.31	0.70
118	STACK East	7,004	0.44	0.60	0.55	0.21	0.65

Key	Play Region	TVD	C_{29} S/(S+R)[1]	C_{29} ββ/(αα+ββ)[2]	Diasteranes/Total Steranes[3]	TA[I]/(TA[I]+TA[II])[4]	3R/(3R+5R) Terpanes[5]
119	STACK East	6,921	0.45	0.60	0.45	0.21	0.67
120	SCOOP	10,105	0.43	0.63	0.57	0.54	0.75
121	SCOOP	14,171	NA	NA	NA	0.85	NA
122	SCOOP	14,504	NA	NA	NA	0.93	NA
123	SCOOP	14,150	NA	NA	NA	0.97	NA
124	SCOOP	11,387	0.43	0.70	0.69	0.63	0.94
125	SCOOP	11,901	0.42	0.70	0.81	0.64	0.96
126	SCOOP	10,950	0.36	0.67	0.92	0.62	0.92
127	SCOOP	10,555	0.38	0.66	0.70	0.62	0.88
128	SCOOP	10,844	0.28	0.66	0.98	0.66	0.90
129	SCOOP	10,762	0.43	0.68	0.81	0.62	0.90
130	SCOOP	11,363	0.45	0.66	0.72	0.72	0.92
131	SCOOP	11,591	0.37	0.70	0.87	0.69	0.93
132	SCOOP	12,989	0.49	0.73	0.83	0.68	0.96
133	SCOOP	11,179	0.43	0.67	0.75	0.71	0.92
134	SCOOP	12,939	0.59	0.72	0.99	0.80	0.96
135	SCOOP	10,671	0.42	0.71	0.74	0.63	0.91
136	SCOOP	10,922	0.43	0.66	0.81	0.68	0.91
137	SCOOP	10,881	0.40	0.69	0.77	0.72	0.85
138	SCOOP	11,421	0.47	0.74	0.67	0.72	0.90
139	SCOOP	12,317	0.51	0.68	0.66	0.82	0.84
140	SCOOP	12,303	0.44	0.65	0.68	0.84	0.84
141	SCOOP	11,698	0.48	0.66	0.71	0.71	0.89
142	SCOOP	11,777	0.52	0.72	0.82	0.90	0.90
143	SCOOP	11,706	0.31	0.75	0.83	0.72	0.88
144	SCOOP	11,004	0.47	0.70	0.73	0.61	0.91
145	SCOOP	11,104	0.40	0.69	0.73	0.66	0.93
146	SCOOP	11,522	0.43	0.65	0.99	0.72	0.94
147	SCOOP	11,755	0.52	0.74	0.99	0.73	0.94
148	SCOOP	12,112	0.52	0.63	0.65	0.74	0.88
149	SCOOP	9,642	0.37	0.65	0.66	0.49	0.73
150	SCOOP	14,766	NA	NA	1.00	0.94	1.00
151	SCOOP	12,832	0.42	0.68	0.82	0.64	0.75
152	SCOOP	11,100	0.36	0.65	0.79	0.58	0.80
153	SCOOP	12,053	0.51	0.64	0.82	0.83	0.92
154	SCOOP	9,812	0.39	0.66	0.86	0.54	0.75
155	SCOOP	9,460	0.46	0.62	0.59	0.17	0.60
156	SCOOP	12,753	0.42	0.75	0.99	0.61	0.94
157	SCOOP	13,412	0.40	0.58	0.78	0.89	0.93
158	SCOOP	14,125	NA	NA	0.90	0.91	0.94
159	SCOOP	9,920	0.40	0.65	0.48	0.52	0.72
160	SCOOP	13,284	0.41	0.63	0.93	0.72	0.97
161	SCOOP	12,359	0.43	0.67	0.82	0.74	0.97
162	SCOOP	13,398	0.44	0.68	0.82	0.79	0.96
163	SCOOP	15,760	NA	NA	NA	0.90	NA
164	SCOOP	14,235	NA	NA	0.64	0.84	0.94
165	SCOOP	13,521	0.41	0.70	0.99	0.72	0.97
166	SCOOP	13,130	0.38	0.71	0.99	0.77	0.97
167	SCOOP	13,860	NA	NA	0.83	0.79	0.97
168	SCOOP	12,874	0.41	0.73	0.94	0.65	0.96
169	SCOOP	8,507	0.44	0.58	0.46	0.13	0.47
170	SCOOP	13,274	0.59	0.78	0.99	0.77	0.96
171	SCOOP	12,517	0.48	0.70	0.88	0.55	0.90
172	SCOOP	14,183	0.35	0.68	0.35	0.71	0.82

Table 4. Values for sterane and terpane maturity parameters. (1) C_{29} sterane 5α(H),14α(H),17α(H) 20S/(S+R); (2) C_{29} sterane 14β(H),17β(H)/(14β,17β(H)+14α(H),17α(H)) using both 20S and 20R epimers; (3) m/z 259/m/z 217 over the range of C_{27}-C_{30} steranes; (4) $C_{20\text{-}21}$ triaromatic steroids/$C_{20\text{-}28}$ triaromatic steroids; (5) $C_{19\text{-}39}$ tricyclic terpanes/($C_{19\text{-}39}$ tricyclic terpanes + $C_{27\text{-}35}$ hopanes).

The identification of C_{27}-C_{30} regular steranes (**I**) and diasteranes (**II**) are shown in Figure 28 and labeled peaks are color coded by compound family and defined in Table 5. Two maturity parameters shown in Figure 29 are based on the ratio of C_{29} sterane stereoisomers (Seifert and Moldowan, 1981). The first is defined as the peak area ratio of epimers at C-20 and defined as C_{29} 5α(H),14α(H),17α(H) 20S/(S+R). The second is the peak area ratio of epimers at C-14 and C-17 and defined as C_{29} sterane ββ/(ββ+αα) using both the 20S and 20R configuration. No correlation was observed between C_{29} ααα sterane 20S/(S+R) and TVD, and a weak correlation can be observed in the C_{29} sterane ββ/(ββ+αα) with TVD. In both cases, the ratios may have reached equilibrium because sterane isomerization occurs at low maturation levels (Mackenzie and Maxwell, 1981). In fact, the significant data scatter may result from the rapidly decreasing concentrations of most biomarkers with maturity (Rullkötter et al., 1984; van Graas, 1990).

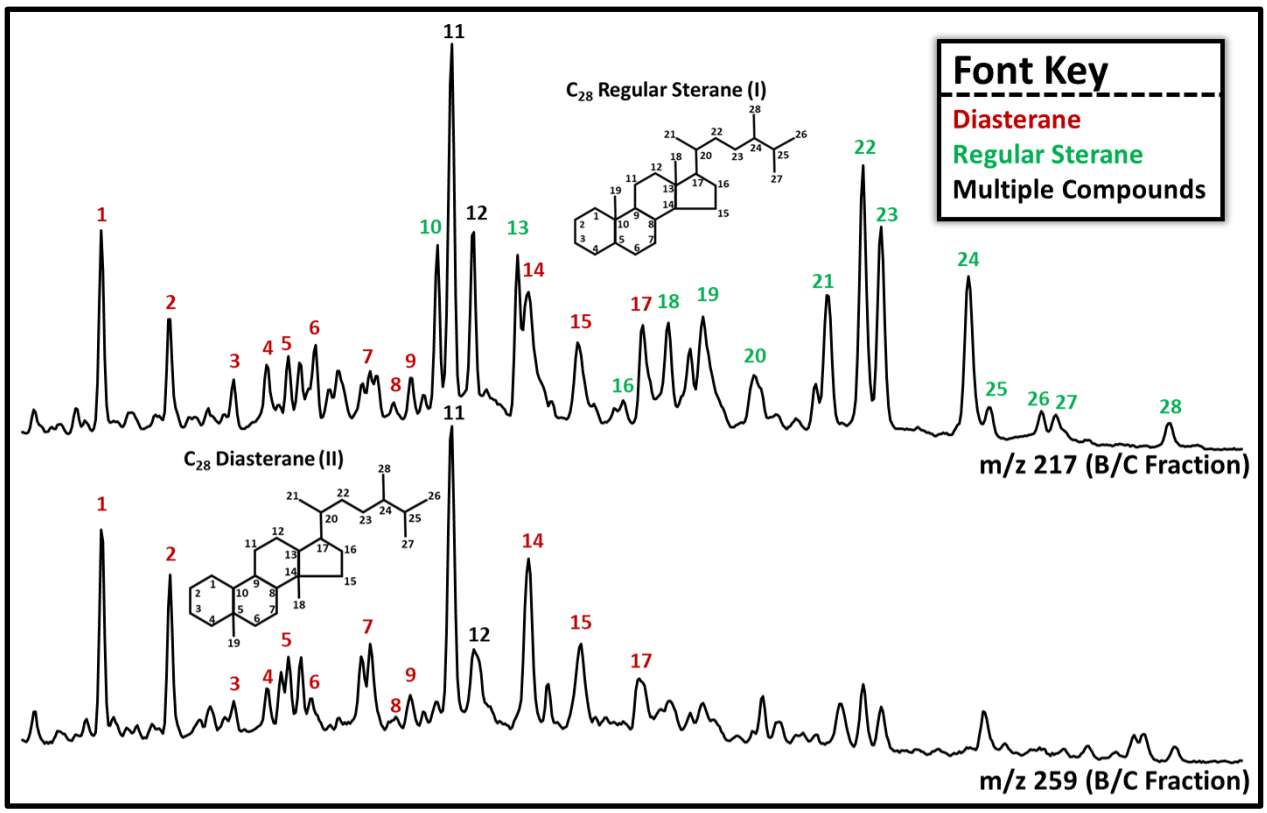

Figure 28. Two GC-MS fragmentograms showing peak distribution of $C_{27\text{-}30}$ regular steranes (**I**) and $C_{27\text{-}30}$ diasteranes (**II**). Diasteranes can be measured using m/z 259 which are more specific for diasteranes than m/z 217. An example carbon skeleton of a regular sterane and diasterane show rearrangement of the methyl groups C-18 and C-19.

N°	Compound Identification
1	13β(H),17α(H),20(S) Diacholestane
2	13β(H),17α(H),20(R) Diacholestane
3	13α(H),17β(H),20(S) Diacholestane
4	13α(H),17β(H),20(R) Diacholestane
5	24-Methyl-13β(H),17α(H),20(S) diacholestane 24(S)
6	24-Methyl-13β(H),17α(H),20(S) diacholestane 24(R)
7	24-Methyl-13β(H),17α(H),20(R) diacholestane 24(S)
8	24-Methyl-13β(H),17α(H),20(R) diacholestane 24(R)
9	24-Methyl-13α(H),17β(H),20(S)-diacholestane
10	14α(H),17α(H),20(S)-Cholestane
11	24-Ethyl-13β(H),17α(H),20(S)-diacholestane / 14β(H),17β(H),20(R)-Cholestane
12	14β(H),17β(H),20(S)-Cholestane / 24-Methyl-13α(H),17β(H),20(R)-diacholestane
13	14α(H),17α(H),20(R)-Cholestane
14	24-Ethyl-13β(H),17α(H),20(R)-diacholestane
15	24-Ethyl-13α(H),17ß(H),20(R)-diacholestane
16	24-Methyl-14α(H),17α(H),20(S)-cholestane
17	24-Ethyl-13α(H),17β(H),20(S)-diacholestane
18	24-Methyl-14β(H),17β(H),20(R)-cholestane
19	24-Methyl-14β(H),17β(H),20(S)-cholestane
20	24-Methyl-14α(H),17α(H),20(R)-cholestane
21	24-Ethyl-14α(H),17α(H),20(S)-cholestane
22	24-Ethyl-14β(H),17β(H),20(R)-cholestane
23	24-Ethyl-14β(H),17β(H),20(S)-cholestane
24	24-Ethyl-14α(H),17α(H),20(R)-cholestane
25	24-Propyl-14α(H),17α(H),20(S)-cholestane
26	24-Propyl-14β(H),17β(H),20(R)-cholestane
27	24-Propyl-14β(H),17β(H),20(S)-cholestane
28	24-Propyl-14α(H),17α(H),20(R)-cholestane

Table 5. Identification of numbered sterane peaks as illustrated in Figure 28. Peak identification based on comparison to Lillis et al. (1999).

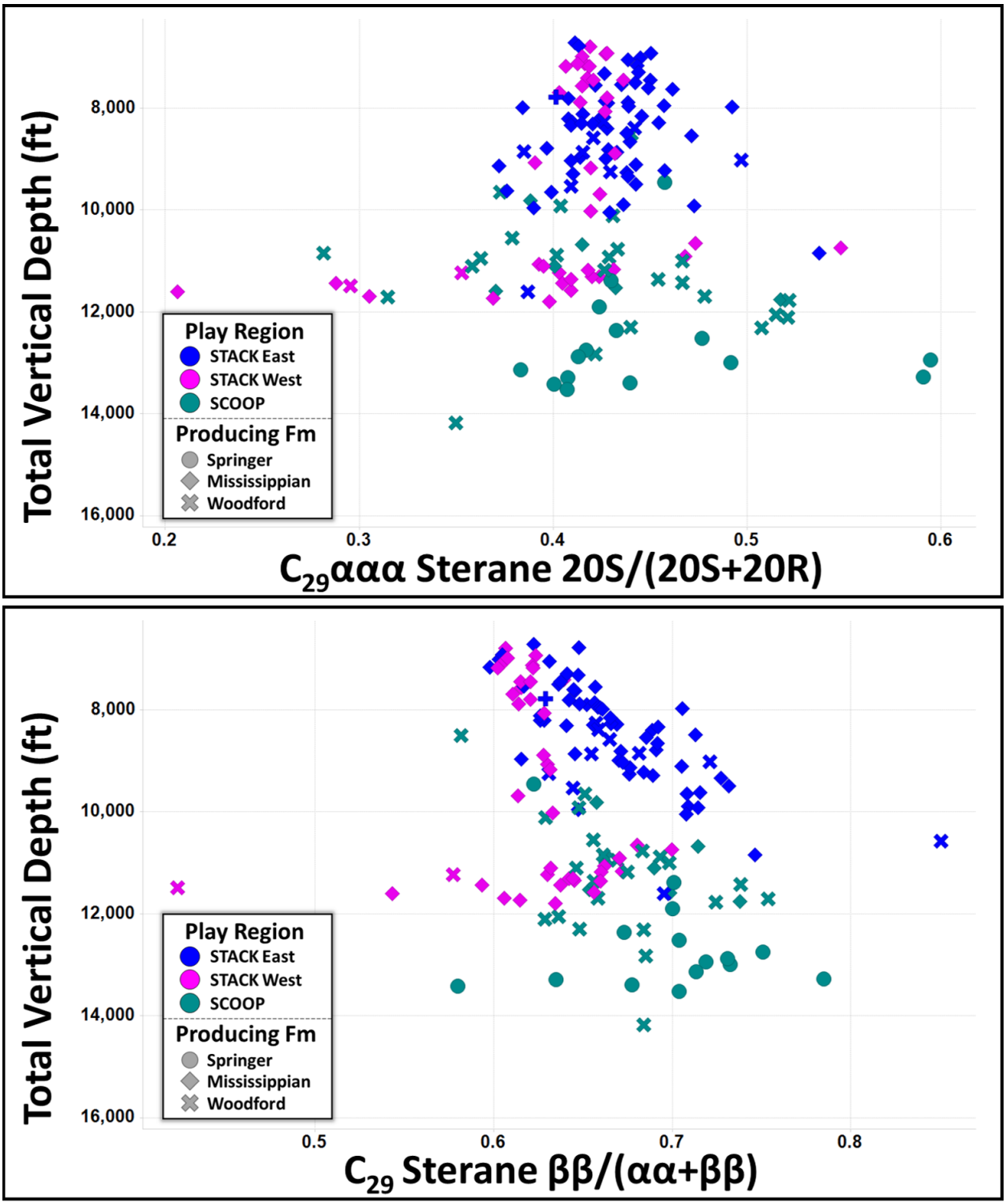

Figure 29. Two maturity parameters based on the isomerization of the C_{29} regular sterane (**I**). Upper: the ratio of C_{29} 5α(H),14α(H),17α(H) 20S/(S+R) sterane versus TVD. By 8,000 ft, the ratio 20S/(S+R) has reached equilibrium and shows no correlation with depth. Lower: the ratio C_{29} sterane ββ/(ββ+αα) using both 20S and 20R epimers shows a good correlation with TVD in STACK East and weak correlation in STACK West and SCOOP.

Diasteranes/Steranes

Diasteranes (**II**) are formed as the result of catalytic rearrangement of sterenes in the presence of active acid sites found on some clays during diagenesis (Rubinstein et al., 1975; Sieskind et al., 1979). Once formed, diasteranes are more stable than regular steranes (**I**), and hydrous pyrolysis experiments have shown that the ratio of diasteranes/steranes increases with maturity (Lewan et al., 1986; Peters et al., 1990). The ratio of diasteranes/total steranes shows a general increase with TVD in STACK until approximately ~10,000 ft after which the ratio reaches unity (Figure 30). The flower-shaped zone observable in STACK West oils around ~11,000 ft can also be observed. No correlation is observed in SCOOP although values range mostly between 0.5-1.0. The formation of diasteranes is strongly influenced by the presence of acidic clays so the diasterane/sterane ratio may be heavily affected by lithologic differences of the source rocks.

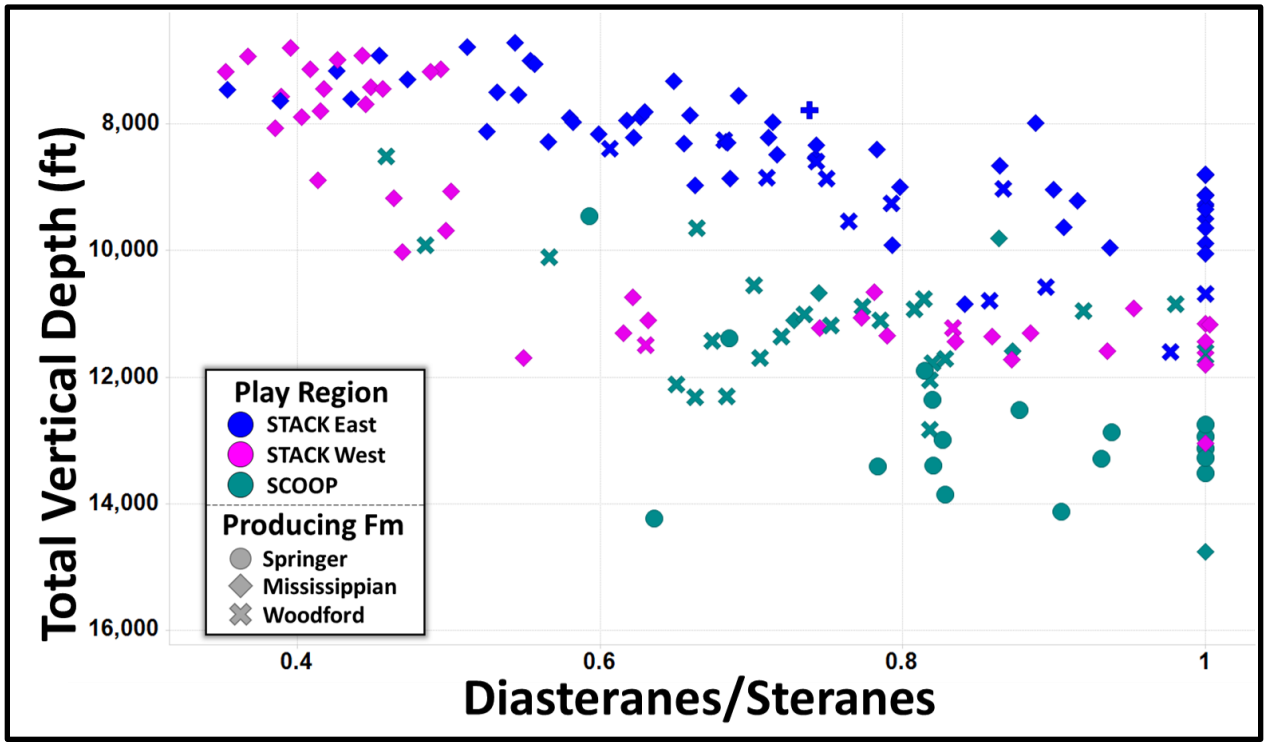

Figure 30. The ratio of diasteranes/steranes generally increases with TVD in STACK until 10,000-11,000 ft beyond which the ratio reaches unity. No correlation with depth is observed in SCOOP.

Triaromatic Steroid Hydrocarbons

Triaromatic steroid hydrocarbons are formed from the further aromatization of C-ring monoaromatic steroid hydrocarbons through the loss of a methyl group at the A/B ring junction and aromatization of the A and B rings (Mackenzie et al., 1981). Triaromatic steroid hydrocarbons can be divided into two groups, TA[I] (**III**) and TA[II] (**IV**), based on the length of the side chain (Figure 31). The group TA[I] includes the short-chained C_{20}-C_{21} members while TA[II] includes the long-chained C_{26}-C_{28} (S+R) members. The peak area ratio of TA[I]/TA[I+II] increases with thermal stress and has been used for several decades as a maturity parameter (e.g. Mackenzie et al., 1981; Riolo et al., 1986; Abbott and Maxwell, 1988; Clark and Philp, 1989; Lillis and Selby, 2013). Interestingly, artificial heating experiments of triaromatic steroid hydrocarbon standards indicate that TA[I]/TA[I+II] increases due to preferential degradation of the long-chained homologues rather than the conversion of long- to short-chained homologues (Beach et al., 1989).

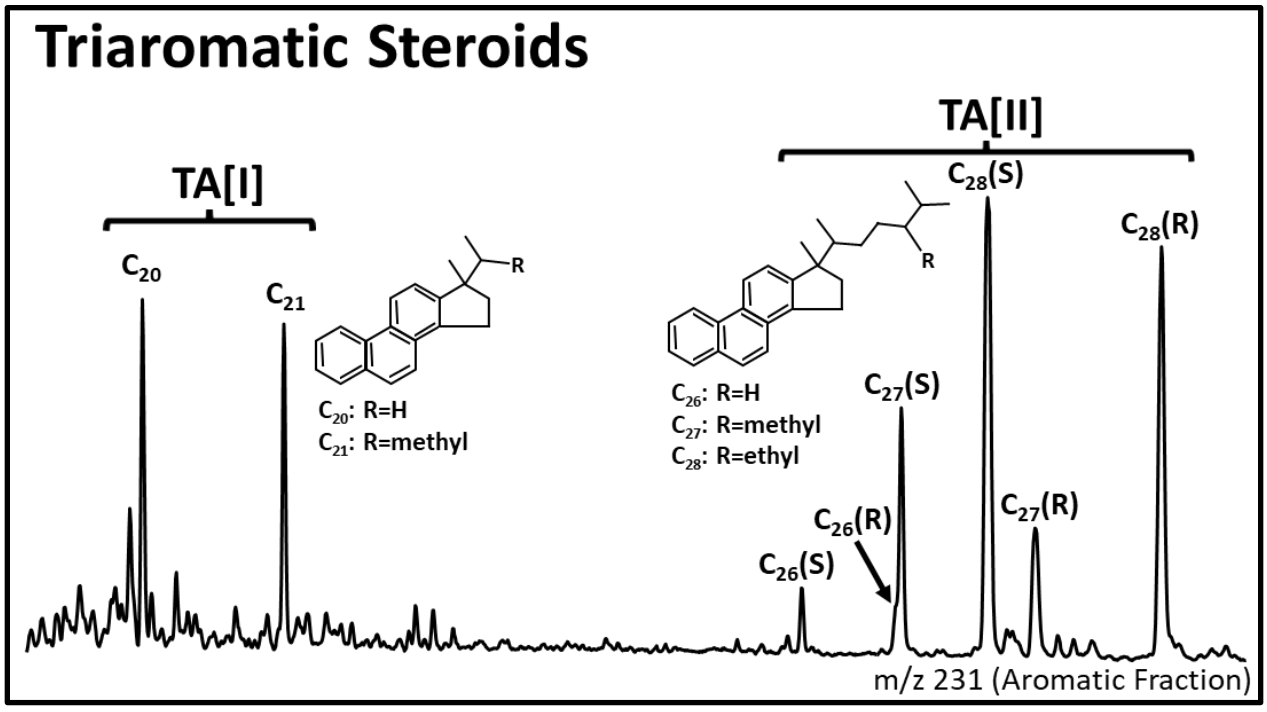

Figure 31. Detailed m/z 231 fragmentogram showing C_{20}-C_{28} triaromatic steroids and their common groupings TA[I] (**III**) and TA[II] (**IV**). Peak identification based on Mackenzie et al. (1981).

The TA[I]/TA[I+II] maturity parameter is plotted in Figure 32 and shows a modest correlation with TVD across all Play Regions. The ratio TA[I]/TA[I+II] appears to reach the end of its dynamic range at an equilibrium value (~0.85) beyond which no additional information is gained. The STACK West flower-shaped zone oils at ~11,000 ft do not exhibit a wide range of maturities, possibly because they have already reached equilibrium. The SCOOP oils plot below STACK oils by between 2,000-4,000 ft depending on producing reservoir. This suggests either that SCOOP is a cooler portion of the basin or that STACK has been uplifted and the maturity of its oils reflect a period of maximum thermal stress when the reservoir was buried deeper.

In summary, maturity parameters for regular steranes, diasteranes, and triaromatic steroid hydrocarbons generally show weak correlations with TVD or only have dynamic range over a limited portion of the dataset. The most successful sterane parameters, the TA[I]/TA[I+II] and diasterane/sterane ratios, are based on preferential thermal degradation rather than isomerization.

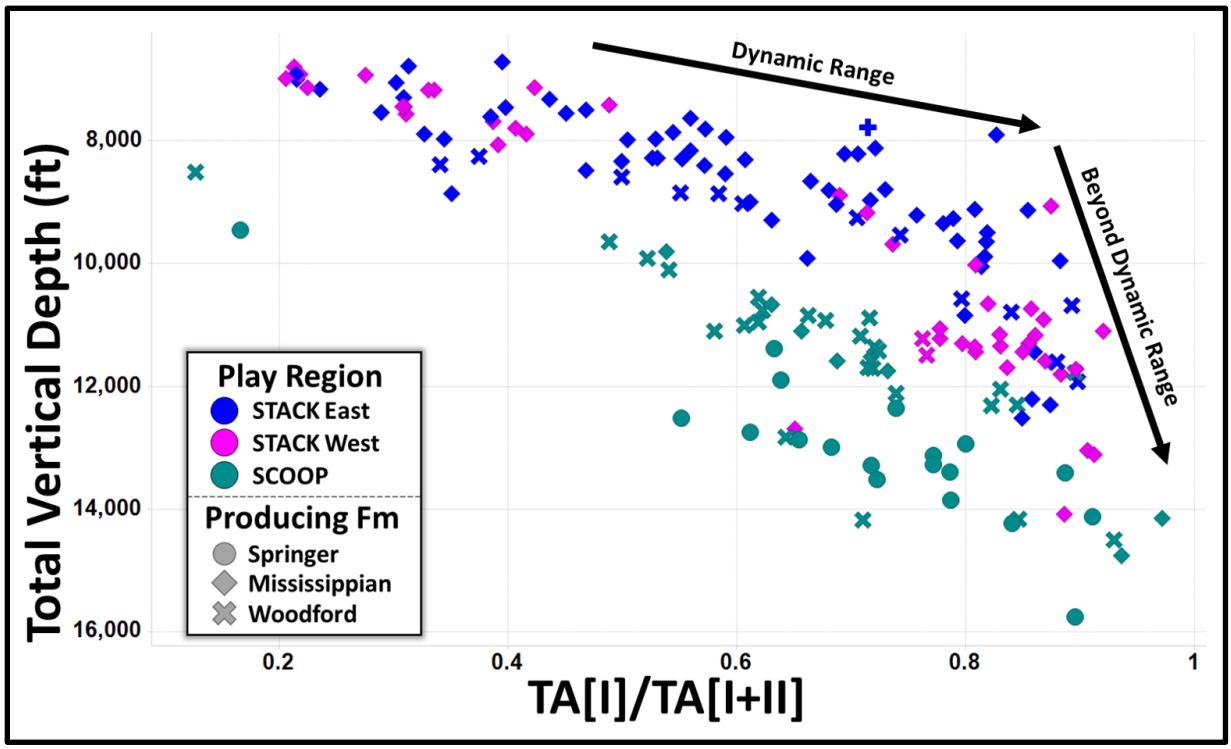

Figure 32. The triaromatic sterane maturity ratio TA[I]/TA[I+II] increases with TVD until ~0.85 beyond which no additional information is gained.

Terpanes (m/z 191)

Two major families of terpane biomarkers are the tricyclic (**V**; cheilanthanes) and pentacyclic (**VI**; hopanes) terpanes which share a dominant m/z 191 fragment (Budzikiewicz et al., 1963; Anders and Robinson, 1971). A m/z 191 fingerprint from the B/C fraction of a black oil sample is shown in Figure 33 with peaks colored red and blue as tricyclic terpanes and pentacyclic hopanes, respectively. With increasing maturity, the absolute concentration of both tricyclic terpanes and hopanes decrease, but the relative amount of tricyclic terpanes increases compared to hopanes (Seifert and Moldowan, 1978; van Graas, 1990). The abundance of tricyclic terpanes relative to hopanes increases because proportionally more tricyclic terpanes are released from the kerogen at higher levels of maturity (Aquino Neto et al., 1983; Kruge et al., 1990; Peters et al., 1990; Philp et al., 2021). Tricyclic terpanes and hopanes originate from different biological precursors (Ourisson et al., 1982, 1984), so care should be taken when comparing the abundances of tricyclic terpanes and hopanes from different organic facies.

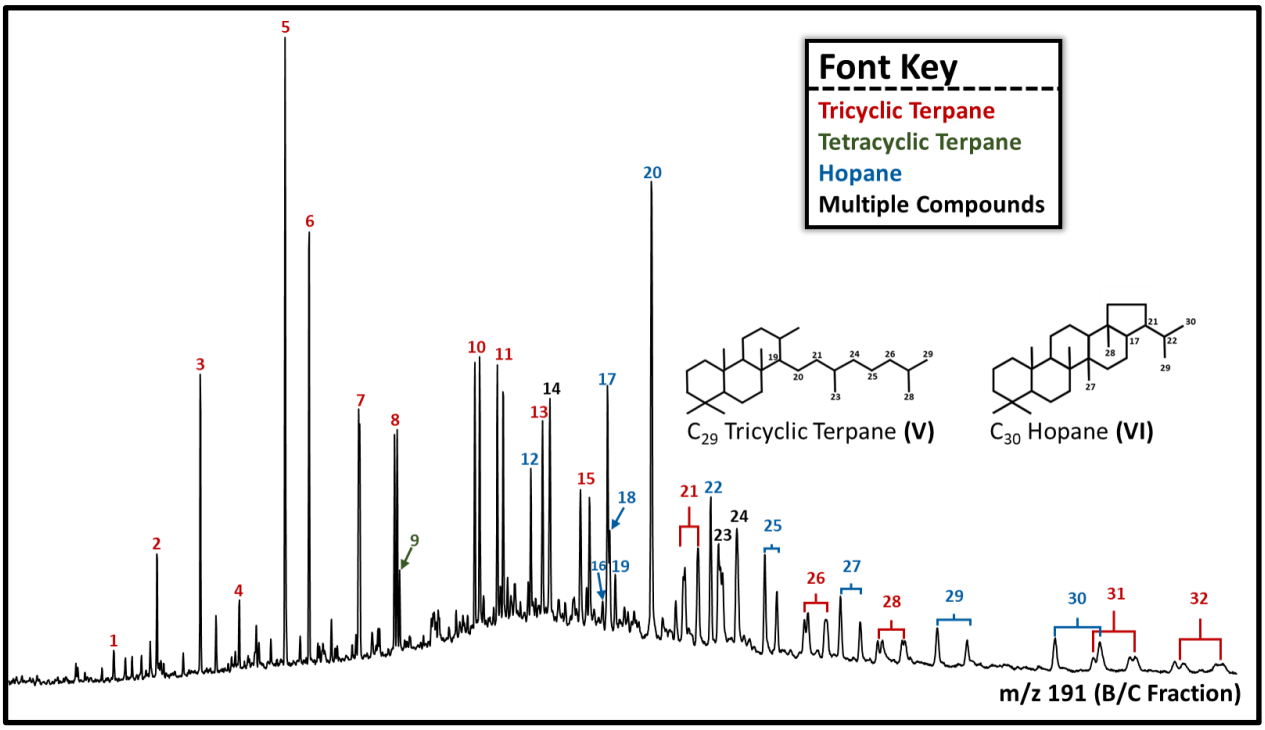

Figure 33. Detailed m/z 191 fragmentogram of a black oil B/C fraction. Labeled peaks are identified in Table 6.

Peak N°	Compound Name
1	C_{19} Tricyclic terpane
2	C_{20} Tricyclic terpane
3	C_{21} Tricyclic terpane
4	C_{22} Tricyclic terpane
5	C_{23} Tricyclic terpane
6	C_{24} Tricyclic terpane
7	C_{25} Tricyclic terpane (22S+22R)
8	C_{26} Tricyclic terpane (22S+22R)
9	C_{24} Tetracyclic terpane
10	C_{28} Tricyclic terpane (22S+22R)
11	C_{29} Tricyclic terpane (22S+22R)
12	18α(H)-22,29,30-Trisnorhopane (Ts)
13	C_{30} Tricyclic terpane (22S)
14	C_{30} Tricyclic terpane (22R) / 17α(H)-22,29,30-Trisnorhopane (Tm)
15	C_{31} Tricyclic terpane (22S+22R)
16	17α(H),21β(H)-28,30-Bisnorhopane
17	17α(H),21β(H)-30-Norhopane
18	18β(H)-30-Norneohopane
19	15α(H)-Methyl-17α(H)-27-norhopane (diahopane)
20	17α(H),21β(H)-Hopane
21	C_{33} Tricyclic terpane (22S+22R)
22	17α(H),21β(H)-Homohopane (22S)
23	C_{34} Tricyclic terpane (22S) / 17α(H),21β(H)-Homohopane (22R)
24	C_{34} Tricyclic terpane (22R) / Gammacerane
25	17α(H),21β(H)-Bishomohopane (22S+22R)
26	C_{35} Tricyclic terpane (22S+22R)
27	17α(H),21β(H)-Trishomohopane (22S+22R)
28	C_{36} Tricyclic terpane (22S+22R)
29	17α(H),21β(H)-Tetrakishomohopane (22S+22R)
30	17α(H),21β(H)-Pentakishomohopane (22S+22R)
31	C_{38} Tricyclic terpane (22S+22R)
32	C_{39} Tricyclic terpane (22S+22R)

Table 6. Identification of numbered terpane peaks as illustrated in Figure 33. Peak identification based on comparison to Lillis et al. (1999).

The tricyclic/(tricyclic+pentacyclic) terpanes maturity parameter, or 3R/(3R+5R) terpanes where R is ring count, shows a modest correlation with TVD in STACK and poor correlation in SCOOP (Figure 34). Similar to the diasteranes/steranes and TA[I]/TA[I+II] maturity parameters, the 3R/(3R+5R) terpanes ratio reaches the end of its dynamic range at approximately 10,000-11,000 ft in STACK beyond which no additional information is gained. The variable oils maturities in Dewey County which includes the flower-shaped zone are not observed in the 3R/(3R+5R) terpane ratio, possibly because the high- and low maturity oils have both reached equilibrium. The STACK East trends slightly above STACK West at any given depth and could result from differences in geothermal gradients, structural uplift, or other factors controlling thermal maturity. The SCOOP oils again plot below the main trend for STACK oils, but by a smaller margin (~1,000 ft TVD difference) than is observed in other maturity parameters in this chapter.

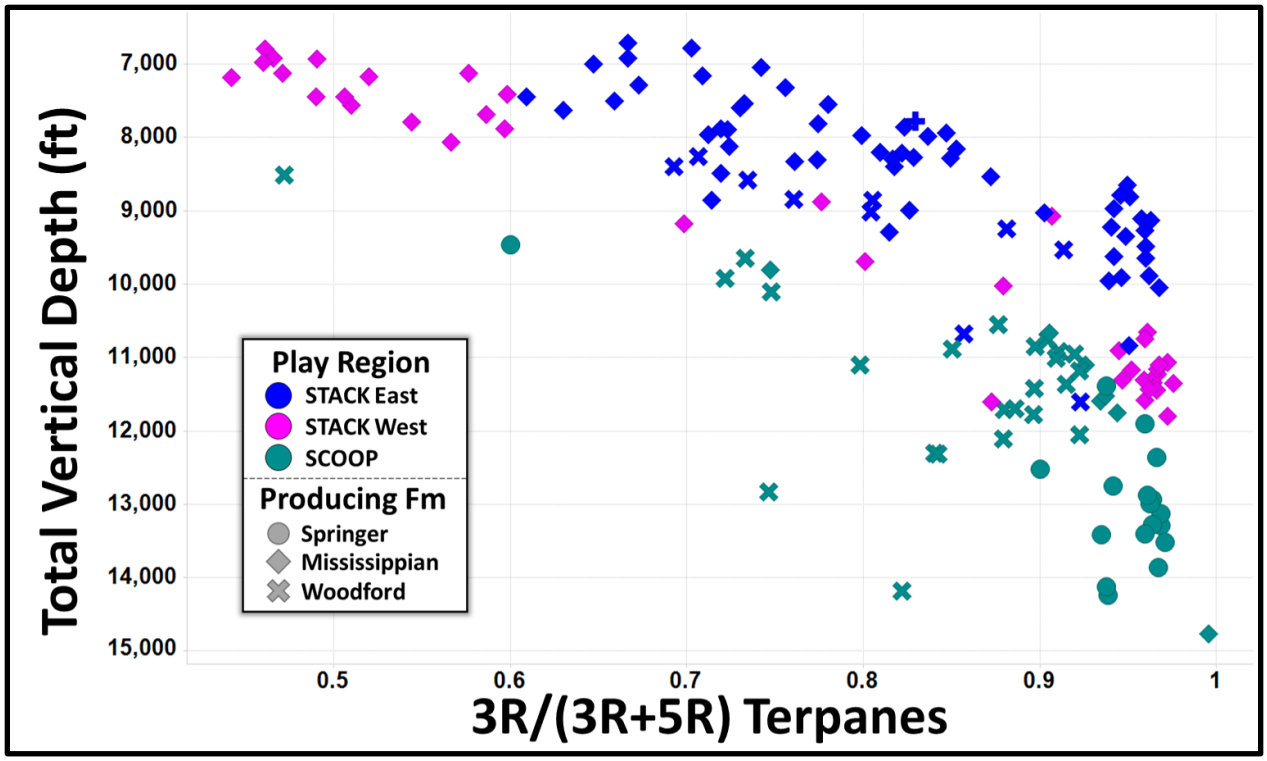

Figure 34. Ratio of all C_{19}-C_{39} tricyclic terpanes (3R) over C_{19}-C_{39} tricyclic terpanes plus C_{27}-C_{35} hopanes (5R) versus TVD. In STACK, the ratio increases with depth until it reaches equilibrium around 9,000 ft. In SCOOP, the ratio increases with depth until reaching equilibrium around 12,000 ft.

Light Hydrocarbon Maturity Parameters

Light hydrocarbons (C_4-C_9 compounds) are a major component of most petroleum liquids and composed of straight, branched, cyclic, and aromatic hydrocarbons. In general, light hydrocarbons are believed to form from the catagenic breakdown of larger molecular precursors and can contain significant information about the thermal maturity of its source (Philippi, 1975; Leythaeuser et al., 1979; Hunt, 1984; Mango, 1997). Although some isomers may have direct biological precursors (i.e. Philippi, 1977), light hydrocarbons are not considered biomarkers because their carbon skeletons are too small to preserve evidence of a unique biological origin. The identification of the light hydrocarbons used in the Thompson and Mango parameters are shown in Figure 35 and Table 7 (Walters and Hellyer 1998). This section describes two families of light hydrocarbon maturity parameters referred to as Thompson Parameters and Mango Parameters after their respective authors and which primarily utilize isomers of heptane (Table 8).

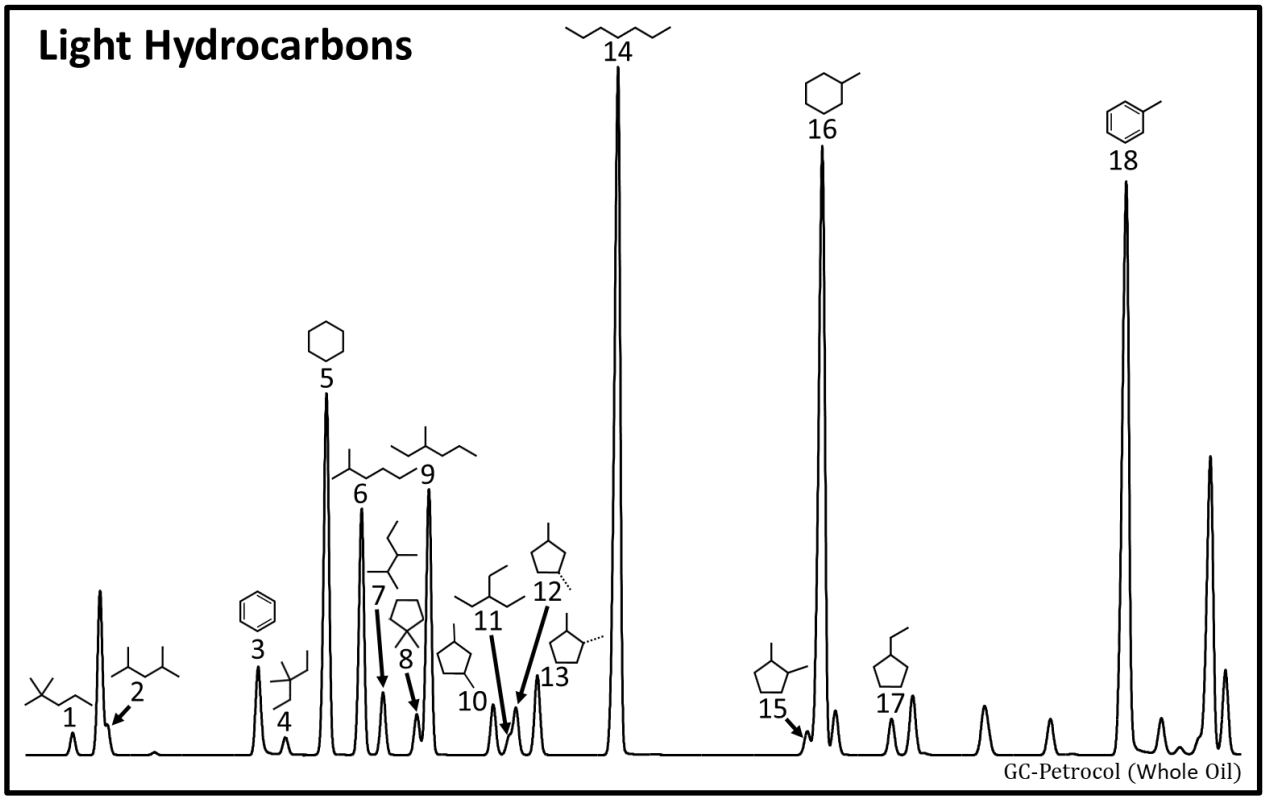

Figure 35. Light hydrocarbon peaks labeled based on comparison to Walters and Hellyer (1998).

Peak N°	Compound Name	Abbreviation
1	2,2-Dimethylpentane	2,2-DMP
2	2,4-Dimethylpentane	2,4-DMP
3	Benzene	Benz
4	3,3-Dimethylpentane	3,3-DMP
5	Cyclohexane	CC_6
6	2-Methylhexane	2-MH
7	2,3-Dimethylpentane	2,3-DMP
8	1,1-Dimethylcyclopentane	1,1-DMCP
9	3-Methylhexane	3-MH
10	cis-1,3-Dimethylcyclopentane	1*c*3-DMCP
11	3-Ethylpentane	3-EP
12	trans-1,3-Dimethylcyclopentane	1*t*3-DMCP
13	trans-1,2-Dimethylcyclopentane	1*t*2-DMCP
14	*n*-Heptane	*n*-C_7
15	cis-1,2-Dimethylcyclopentane	1*c*2-DMCP
16	Methylcyclohexane	MCH
17A	Ethylcyclopentane	ECP
17B	2,5-Dimethylcyclohexane	2,5-DMCH
18	Toluene	Tol

Table 7. Identification of numbered light hydrocarbon peaks as illustrated in Figure 35. Peak identification based on comparison to Walters and Hellyer (1998).

Key	Play Region	TVD	Isoheptane Ratio[1]	Heptane Ratio[2]	Normality[3]	Paraffinicity[4]	2-/3-methylhexane[5]	Expulsion Temperature[6]
1	STACK West	7,130	1.0	23	3.7	0.82	0.78	112
2	STACK West	6,791	1.1	23	3.6	0.87	0.79	120
3	STACK West	7,179	0.9	23	3.9	0.84	0.75	107
4	STACK West	6,917	0.9	24	3.9	0.94	0.77	116
5	STACK West	6,980	1.0	24	3.6	0.93	0.79	111
6	STACK West	7,132	0.7	21	3.7	0.88	0.71	112
7	STACK West	6,934	0.8	21	3.6	0.85	0.72	115
8	STACK West	7,444	0.8	24	3.9	0.97	0.71	111
9	STACK West	7,690	1.3	23	3.4	0.79	0.82	118
10	STACK West	8,068	1.3	24	3.6	0.81	0.82	118
11	STACK West	7,563	1.2	22	3.3	0.79	0.79	121
12	STACK West	7,443	1.2	23	3.4	0.85	0.81	107
13	STACK West	7,887	1.4	23	3.2	0.78	0.82	121
14	STACK West	7,792	1.2	23	3.4	0.85	0.80	118
15	STACK West	7,412	1.1	25	3.6	1.00	0.77	117
16	STACK West	7,172	0.9	22	3.6	0.89	0.71	117
17	STACK West	9,068	2.3	32	3.9	1.20	0.93	123
18	STACK West	11,096	1.5	26	3.9	0.90	0.83	120
19	STACK West	10,024	1.7	27	4.3	0.86	0.79	116
20	STACK West	11,173	1.3	28	4.1	1.05	0.84	119
21	STACK West	11,729	1.5	27	3.5	1.02	0.86	121
22	STACK West	11,799	1.5	29	3.9	1.09	0.86	118
23	STACK West	13,107	1.4	29	4.0	1.10	0.86	118
24	STACK West	13,047	2.0	30	3.7	1.03	0.95	121
25	STACK West	11,303	2.1	29	3.7	1.04	0.85	119
26	STACK West	10,909	1.2	27	3.9	1.05	0.75	114
27	STACK West	9,687	1.4	24	3.5	0.89	0.78	119
28	STACK West	9,171	1.2	24	3.3	0.97	0.80	116
29	STACK West	8,883	1.2	23	3.3	0.85	0.77	116
30	STACK West	11,344	1.0	26	3.8	1.08	0.75	110
31	STACK West	11,440	1.1	26	3.8	1.22	0.74	115
32	STACK West	10,743	1.2	25	3.6	0.98	0.76	115
33	STACK West	11,583	1.6	26	3.5	0.95	0.83	120
34	STACK West	11,162	1.8	25	2.9	0.95	0.84	123
35	STACK West	11,609	1.9	29	3.4	1.23	0.87	121
36	STACK West	12,693	10.9	35	2.3	2.00	1.05	132
37	STACK West	11,311	2.7	28	3.1	1.06	0.91	123
38	STACK West	11,229	3.7	31	2.9	1.22	0.97	127
39	STACK West	11,353	3.2	30	2.9	1.26	0.94	127
40	STACK West	10,655	2.1	28	3.1	1.13	0.87	123
41	STACK West	11,693	3.6	30	2.8	1.23	0.96	129
42	STACK West	11,435	3.6	30	2.9	1.21	0.95	126
43	STACK West	11,065	3.4	29	2.8	1.16	0.94	127
44	STACK West	11,487	5.8	31	2.4	1.42	1.02	131
45	STACK West	14,085	10.8	28	2.0	1.08	0.98	129
46	STACK West	11,227	4.2	31	2.8	1.20	0.95	127
47	STACK East	12,523	6.8	31	2.2	1.28	1.01	131
48	STACK East	12,208	5.8	32	2.2	1.42	1.01	131
49	STACK East	12,298	4.3	31	2.6	1.22	0.97	131
50	STACK East	8,968	2.0	28	3.2	1.13	0.87	123
51	STACK East	11,605	3.1	33	3.0	1.51	0.92	128
52	STACK East	11,439	3.0	28	2.6	1.04	0.93	129
53	STACK East	10,045	1.8	28	3.3	1.14	0.84	121
54	STACK East	9,892	1.7	27	3.1	1.17	0.85	124
55	STACK East	9,112	1.2	27	3.6	1.14	0.77	116
56	STACK East	10,573	3.0	32	3.0	1.31	0.91	129
57	STACK East	9,135	1.3	26	3.3	1.06	0.81	125
58	STACK East	9,267	1.3	26	3.3	1.07	0.81	121
59	STACK East	8,652	1.1	26	3.8	0.97	0.74	116

Key	Play Region	TVD	Isoheptane Ratio[1]	Heptane Ratio[2]	Normality[3]	Paraffinicity[4]	2-/3-methylhexane[5]	Expulsion Temperature[6]
60	STACK East	10,677	3.2	33	3.0	1.45	0.90	125
61	STACK East	8,207	2.2	29	3.2	1.10	0.87	123
62	STACK East	9,489	1.7	26	2.9	1.04	0.85	125
63	STACK East	9,642	1.9	27	2.9	1.04	0.87	125
64	STACK East	8,213	1.5	29	3.8	1.23	0.83	117
65	STACK East	9,343	1.2	24	3.0	0.99	0.78	124
66	STACK East	8,120	1.2	26	3.4	1.13	0.79	126
67	STACK East	8,787	1.2	25	3.3	0.98	0.78	121
68	STACK East	7,783	1.8	31	3.4	1.39	0.88	122
69	STACK East	8,297	1.1	24	3.3	1.01	0.78	122
70	STACK East	8,813	1.0	24	3.6	0.89	0.76	120
71	STACK East	11,932	7.3	35	2.4	1.94	0.92	128
72	STACK East	7,814	1.3	26	3.8	1.11	0.72	117
73	STACK East	10,785	3.2	33	3.1	1.70	0.86	117
74	STACK East	9,915	1.0	24	3.3	0.93	0.78	121
75	STACK East	8,282	0.9	23	3.6	1.00	0.70	115
76	STACK East	8,307	1.4	27	3.2	1.19	0.83	120
77	STACK East	9,626	1.4	26	3.2	1.00	0.83	122
78	STACK East	10,842	1.5	25	3.0	0.97	0.84	128
79	STACK East	8,275	1.1	27	3.8	1.03	0.74	119
80	STACK East	7,897	0.7	27	4.5	1.44	0.67	113
81	STACK East	8,540	1.0	24	3.4	0.96	0.74	119
82	STACK East	9,217	1.3	26	3.4	1.09	0.79	123
83	STACK East	8,161	1.1	25	3.3	1.07	0.78	117
84	STACK East	9,960	2.1	29	3.1	1.11	0.88	123
85	STACK East	7,984	0.9	25	3.6	0.99	0.74	118
86	STACK East	8,402	0.9	24	3.5	1.01	0.70	119
87	STACK East	7,552	0.8	22	3.5	0.96	0.69	111
88	STACK East	8,857	1.2	28	3.8	1.20	0.73	119
89	STACK East	7,945	0.9	24	3.5	0.98	0.78	121
90	STACK East	7,630	0.6	18	3.7	0.81	0.64	101
91	STACK East	7,862	1.0	25	3.5	1.02	0.76	114
92	STACK East	7,970	0.9	24	3.5	1.02	0.71	120
93	STACK East	7,500	0.6	22	3.8	0.96	0.67	109
94	STACK East	9,291	1.0	25	3.4	1.10	0.74	122
95	STACK East	9,033	1.3	28	3.3	1.23	0.80	121
96	STACK East	8,991	1.2	27	3.4	1.15	0.78	119
97	STACK East	8,848	1.0	26	3.6	1.18	0.71	115
98	STACK East	8,334	0.9	24	3.4	1.07	0.73	118
99	STACK East	8,586	1.0	26	3.5	1.22	0.72	121
100	STACK East	7,452	0.8	22	3.7	0.99	0.66	108
101	STACK East	7,601	0.6	23	3.8	1.06	0.66	111
102	STACK East	7,325	0.8	24	3.6	0.98	0.73	118
103	STACK East	8,258	0.9	24	3.2	1.24	0.72	124
104	STACK East	8,484	0.7	23	3.4	1.10	0.72	118
105	STACK East	7,887	0.7	23	3.6	1.12	0.67	118
106	STACK East	8,861	0.7	21	3.5	1.01	0.66	120
107	STACK East	7,965	0.8	23	3.5	1.11	0.67	110
108	STACK East	9,249	1.4	30	3.5	1.48	0.76	118
109	STACK East	9,017	1.3	30	3.6	1.53	0.74	120
110	STACK East	9,532	2.3	34	3.4	1.61	0.82	125
111	STACK East	8,392	0.9	26	3.7	1.24	0.70	119
112	STACK East	7,533	0.8	25	3.7	1.18	0.71	117
113	STACK East	7,292	0.7	24	3.7	1.23	0.66	112
114	STACK East	7,162	0.9	26	3.6	1.19	0.74	117
115	STACK East	6,714	0.8	27	4.0	1.39	0.68	113
116	STACK East	7,048	0.8	25	3.6	1.14	0.72	119
117	STACK East	6,779	0.8	26	3.8	1.35	0.66	106
118	STACK East	7,004	0.8	25	3.7	1.19	0.71	118

Key	Play Region	TVD	Isoheptane Ratio[1]	Heptane Ratio[2]	Normality[3]	Paraffinicity[4]	2-/3-methylhexane[5]	Expulsion Temperature[6]
119	STACK East	6,921	0.8	27	3.7	1.38	0.71	114
120	SCOOP	10,105	1.5	34	3.7	2.23	0.68	114
121	SCOOP	14,171	11.2	31	2.0	1.60	0.93	128
122	SCOOP	14,504	8.9	33	2.3	1.65	0.89	127
123	SCOOP	14,150	6.8	30	2.2	1.29	0.92	129
124	SCOOP	11,387	1.0	20	2.6	0.74	0.77	123
125	SCOOP	11,901	1.4	23	2.6	0.89	0.80	122
126	SCOOP	10,950	1.9	33	3.4	1.90	0.72	121
127	SCOOP	10,555	2.0	34	3.4	1.98	0.73	120
128	SCOOP	10,844	2.2	32	3.1	1.74	0.77	122
129	SCOOP	10,762	2.2	33	3.2	1.87	0.76	123
130	SCOOP	11,363	4.4	35	3.1	1.84	0.78	122
131	SCOOP	11,591	2.0	32	3.1	1.65	0.78	122
132	SCOOP	12,989	1.1	21	2.2	0.79	0.93	123
133	SCOOP	11,179	2.2	33	3.2	1.84	0.76	119
134	SCOOP	12,939	1.7	23	2.4	0.83	0.86	127
135	SCOOP	10,671	1.8	32	3.3	1.87	0.73	120
136	SCOOP	10,922	2.0	34	3.4	2.03	0.72	120
137	SCOOP	10,881	2.0	34	3.6	1.97	0.72	119
138	SCOOP	11,421	2.2	34	3.4	2.06	0.73	119
139	SCOOP	12,317	2.7	35	3.3	1.98	0.78	121
140	SCOOP	12,303	2.9	35	3.3	2.12	0.77	122
141	SCOOP	11,698	2.3	35	3.4	2.16	0.73	121
142	SCOOP	11,777	2.4	35	3.3	2.12	0.73	120
143	SCOOP	11,706	2.3	35	3.4	2.20	0.72	121
144	SCOOP	11,004	1.8	33	3.6	2.09	0.68	118
145	SCOOP	11,104	1.6	32	3.5	1.81	0.70	120
146	SCOOP	11,522	1.8	32	3.3	1.80	0.74	119
147	SCOOP	11,755	1.7	31	3.3	1.57	0.77	120
148	SCOOP	12,112	2.4	35	3.3	2.03	0.74	121
149	SCOOP	9,642	2.4	36	3.5	2.14	0.75	118
150	SCOOP	14,766	4.5	34	2.8	1.71	0.89	127
151	SCOOP	12,832	3.6	39	3.8	2.00	0.80	121
152	SCOOP	11,100	2.4	37	3.6	2.35	0.73	120
153	SCOOP	12,053	4.2	39	3.3	2.49	0.80	123
154	SCOOP	9,812	2.0	33	3.5	1.79	0.75	121
155	SCOOP	9,460	0.5	17	2.8	1.01	0.57	103
156	SCOOP	12,753	1.0	18	2.4	0.65	0.77	122
157	SCOOP	13,412	2.1	18	2.8	0.39	0.90	125
158	SCOOP	14,125	2.2	17	2.5	0.38	0.90	125
159	SCOOP	9,920	1.7	35	3.9	2.20	0.67	117
160	SCOOP	13,284	1.3	19	2.1	0.62	0.89	126
161	SCOOP	12,359	1.7	23	2.4	0.87	0.82	124
162	SCOOP	13,398	1.5	21	2.2	0.67	0.90	128
163	SCOOP	15,760	5.2	18	1.4	0.47	1.04	133
164	SCOOP	14,235	2.2	22	2.1	0.76	0.97	132
165	SCOOP	13,521	1.4	21	2.4	0.73	0.89	125
166	SCOOP	13,130	1.1	21	2.6	0.73	0.80	127
167	SCOOP	13,860	1.7	21	2.2	0.70	0.94	131
168	SCOOP	12,874	1.0	20	2.7	0.75	0.77	122
169	SCOOP	8,507	0.9	30	3.9	2.06	0.61	111
170	SCOOP	13,274	1.2	21	2.7	0.76	0.80	124
171	SCOOP	12,517	0.8	20	3.0	0.74	0.70	122
172	SCOOP	14,183	5.0	34	2.9	1.42	0.91	127

Table 8. Light hydrocarbon ratios tested as maturity parameters in this study. (1) (2-MH+3-MH)/(1*c*3-DMCP+1*t*3-DMCP+1*t*2-DMCP); (2) 100**n*-C_7/(CC_6+2-MH+2,3-DMP+1,1-DMCP+3-MH+1*c*3-DMCP+3-EP+1*t*3-DMCP+1*t*2-DMCP+*n*-C_7+1*c*2-DMCP+MCH); (3) *n*-C_7/2-MH; (4) *n*-C_7/MCH; (5) 2-MH/3-MH; (6) 140+15(ln[2,4-DMP/2,3-DMP]).

Thompson Parameters

Thompson (1979 and 1983) proposed two empirical indices of paraffinicity based on ratios of C_6-C_7 hydrocarbons as indicators of thermal maturity, later known as the isoheptane and heptane ratios, which are also strongly affected by source, kerogen type, and biodegradation. The isoheptane ratio is defined as the peak area ratio of the sum of 2-MH and 3-MH to the sum of 1*c*3-DMCP, 1*t*3-DMCP, and 1*t*2-DMCP and generally increases exponentially from 0.1 to 10 during maturation (Thompson, 1979). The heptane ratio is defined as the percentage of *n*-C_7 to the sum of all other compounds eluting CC_6 through MCH (CC_6, 2-MH, 2,3-DMP, 1,1-DMCP, 3-MH, 1*c*3-DMCP, 3-EP, 1*t*3-DMCP, 1*t2*-DMCP, *n*-C_7, 1*c*2-DMCP, and MCH) and has been shown to increase with maturity such that values of 18 to 22, 22 to 30, and >30 have been called normal, mature, and supermature, respectively (Thompson, 1983).

Two additional ratios proposed by (Thompson, 1983) which change systematically with maturity are designated normality (R) and paraffinicity (F). Normality (R) is defined as the peak area ratio of *n*-C_7 to 2-MH and is an approximation of paraffin branching which can increase with maturity and biodegradation. Furthermore, in a two phase solution, branched alkanes more readily partitions into the gas phase than *n*-C_7, so increased normality can sometimes be an indicator of migrational fractionation (Thompson, 1987). Paraffinicity (F) is the ratio of *n*-C_7 to MCH and has been used to determine the extent of biodegradation and maturity (Thompson, 1987).

The four Thompson maturity parameters discussed above are shown in Figure 36 and indicate a general increase with depth except for normality which shows a decrease. The isoheptane ratio is plotted in semi-log and is the only ratio which exhibits a good correlation coefficient in STACK East (R^2=0.76) and, to a lesser extent, STACK West (R^2=0.47). By comparison, the heptane ratio and paraffinicity show little or no correlation with depth and have

significant scatter, most notably between Woodford and Mississippian oils which cluster separately from Springer oils. Similar to other maturity parameters, SCOOP oils again plot below STACK on a parallel trend suggesting that the SCOOP Play Region is a colder portion of the Anadarko Basin or have undergone less structural uplift than STACK. The variable oil maturities previously identified in in Dewey and Woodward counties, which includes the flower-shaped zone, is also observed in the Thompson parameters, especially in the isoheptane ratio.

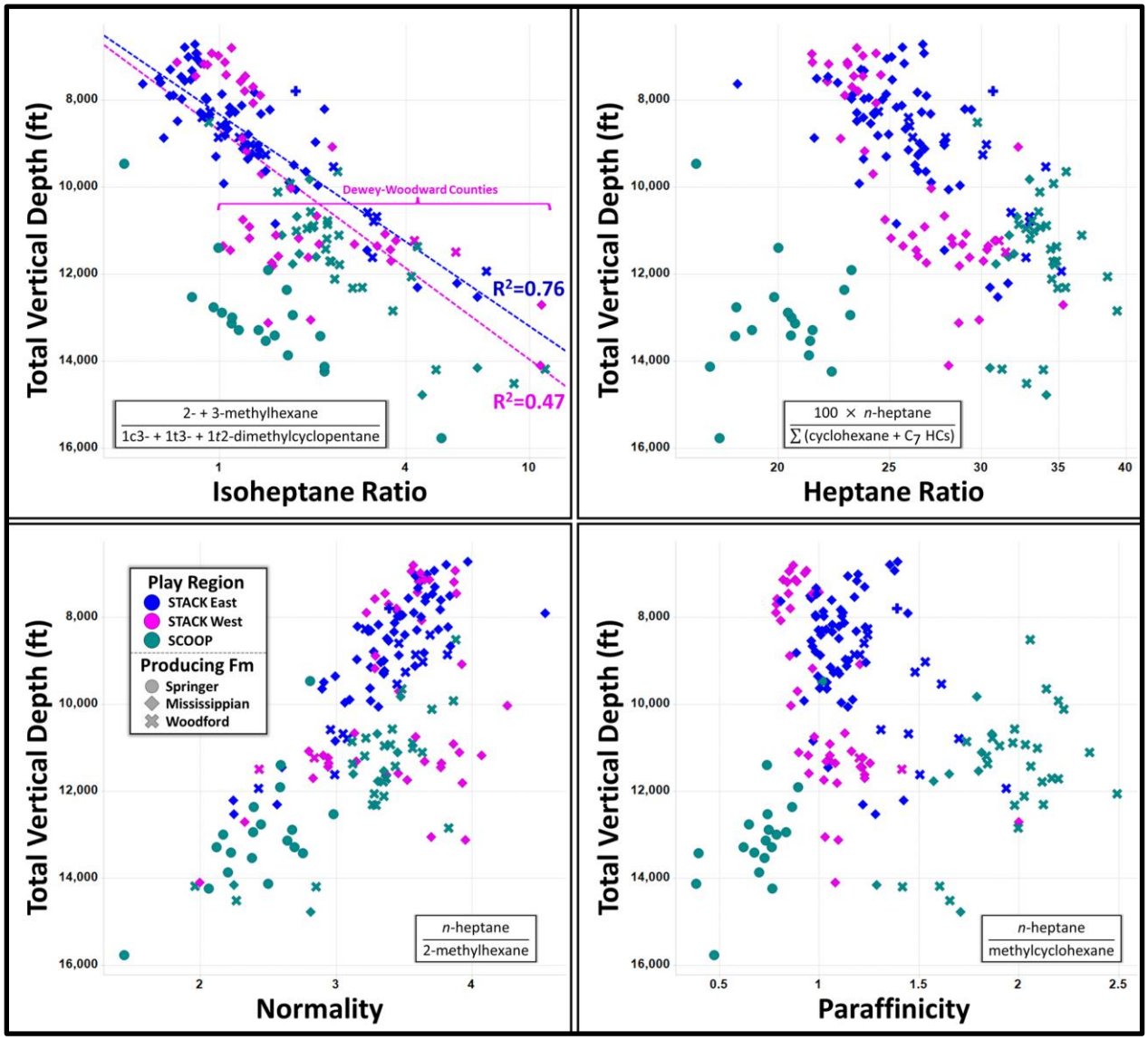

Figure 36. Maturity parameters for the isoheptane ratio, heptane ratio, normality, and paraffinicity versus depth based on Thompson (1979 and 1983). The isoheptane ratio plotted in semi-log displays the best correlation with depth, while the heptane ratio and paraffinicity show little correlation. The previously identified flower-shaped zone in STACK West of variable oil maturities at ~11,000 ft can also be observed, especially in the isoheptane ratio. HC=hydrocarbons.

Mango Parameters

Soon after the isoheptane and heptane ratios were defined, Koblava et al. (1980) noted that the ratio 2-MH/3-MH exhibited a strong relationship with temperature and proposed the ratio as a thermal maturity parameter. Mango (1987) observed a strong invariance between the ratio of the sum of 2-MH and 2,3-DMP to the sum of 3-MH and 2,3-DMP and proposed a kinetic model of isoheptane proportionality in steady-state equilibrium rather than specific biological origin. Based on Mango's model, 2,3-DMP and 2,4-DMP are daughter products of 2-MH formed catalytically through a cyclopropyl intermediate. The steady-state ratio of 2,4-/2,3-DMP is therefore a function of temperature, and the maximum temperature of burial (expulsion temperature) was calibrated empirically by Equation 9 (BeMent et al., 1995; Mango, 1997).

$$\text{Temperature}\,(^{\circ}\text{C}) = 140 + 15(\ln[\text{2,4-DMP}/\text{2,3-DMP}]) \qquad \text{Equation 9}$$

The ratios of 2-MH/3-MH and expulsion temperature are provided in Figure 37 and show good correlation with depth, especially in and SCOOP (R^2=0.79 and 0.73, respectively). Similar to other maturity trends, SCOOP oils form a parallel relationship several thousand feet below the STACK trends. STACK West oils shows a very poor correlation with depth and the wide variability in maturities can be observed in the flower-shaped zone at ~11,000 ft.

Overall, the Mango parameters exhibit better correlations with TVD with less data scatter than the Thompson parameters possibly indicative of more effective maturity parameters. Notably, the heptane ratio and paraffinicity have distinct and disparate clusters between oils produced from Woodford and Mississippian reservoirs and those produced from Springer reservoirs that will be explored more fully in Chapter V.

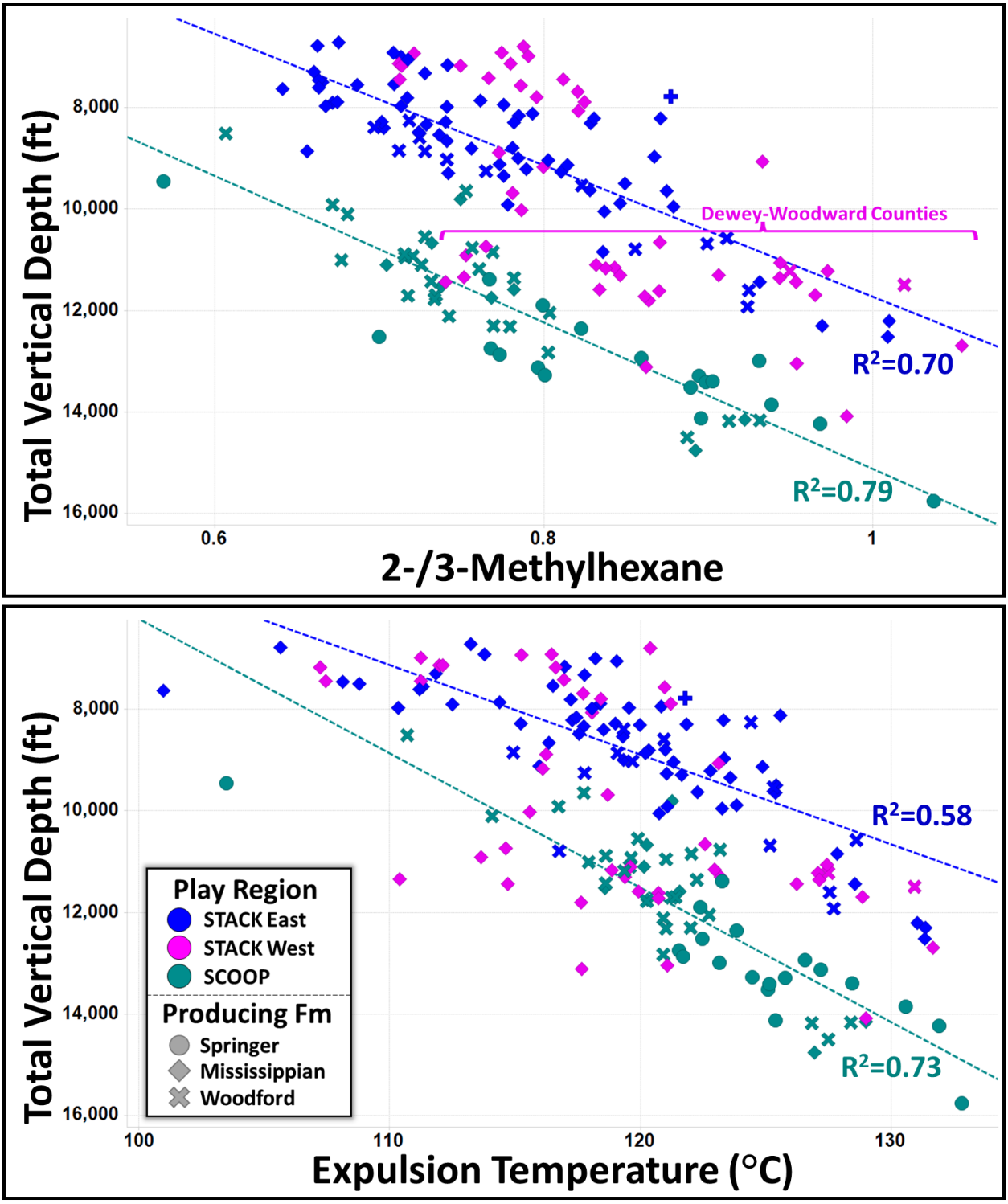

Figure 37. Maturity parameters for Mango parameters 2-/3-methylhexane (upper) and expulsion temperature (lower) versus depth based on Mango (1997). Good correlations are observed in STACK East and SCOOP, but STACK West shows significant scatter especially in the previously identified flower-shaped zone at ~11,000 ft.

Aromatic Maturity Parameters

The aromatic ratio and concentration data used in this section are summarized in Table 9.

Methylphenanthrene Index (MPI-1)

Radke (1988) developed the methylphenanthrene index (MPI-1) based on the observation that isomers of methylphenanthrene (**VII**) shift towards more thermally stable configurations with increasing thermal stress. The MPI-1 has been calibrated against vitrinite reflectance in Type III source rocks to provide a vitrinite reflectance equivalent value (Rc%) given by Equation 10:

$$\mathrm{Rc\%} = 0.825\frac{[\text{2-MP} + \text{3-MP}]}{[\text{P} + \text{1-MP} + \text{9-MP}]} + 0.44 \qquad \text{Equation 10}$$

The MPI-1 relies on the shift in the methylphenanthrene (**VII**) distribution towards the thermodynamically favorable β-Type Isomers (Figure 38) with increasing thermal stress and gives weight to the presumed parent compound (phenanthrene), thus compensating for facies-dependent variations in the degree of phenanthrene alkylation (Radke et al., 1982; Radke, 1988). No separate calibration of Ro% to Rc% for Anadarko Basin source rocks was performed for this dataset.

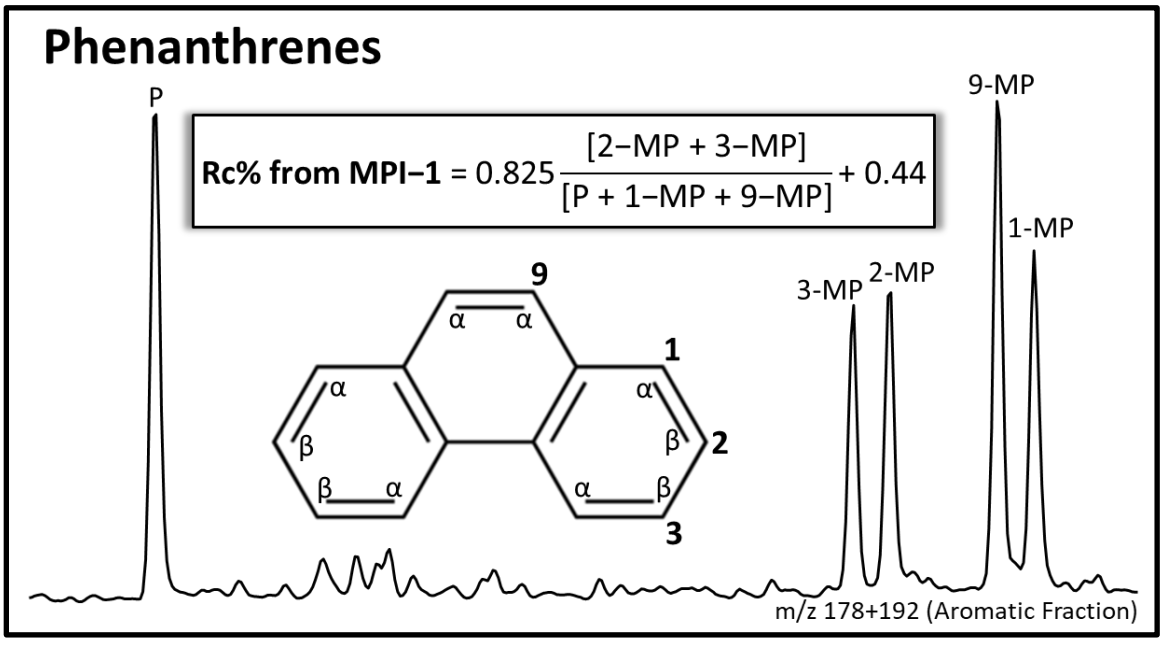

Figure 38. Peak identification for phenanthrene (P) and the methylphenanthrene isomers (x-MP) from the m/z 178+192 fragmentogram. Peak identification based on Radke et al. (1982).

Key	Play	TVD	Rc% (from MPI-1)[1]	MDR[2]	4-+1-MDBT ppm (WO)[3]
1	STACK West	7130	0.81	0.83	514
2	STACK West	6791	0.80	0.82	499
3	STACK West	7179	0.81	0.81	579
4	STACK West	6917	0.82	0.82	408
5	STACK West	6980	0.81	0.82	407
6	STACK West	7132	0.81	0.84	272
7	STACK West	6934	0.79	0.79	471
8	STACK West	7444	0.78	0.82	431
9	STACK West	7690	0.80	0.85	462
10	STACK West	8068	0.83	0.84	461
11	STACK West	7563	0.79	0.83	460
12	STACK West	7443	0.82	0.82	382
13	STACK West	7887	0.80	0.84	593
14	STACK West	7792	0.82	0.85	423
15	STACK West	7412	0.80	0.86	291
16	STACK West	7172	0.78	0.79	433
17	STACK West	9068	0.91	0.95	357
18	STACK West	11096	1.05	0.98	9
19	STACK West	10024	0.91	0.94	221
20	STACK West	11173	1.01	0.98	118
21	STACK West	11729	1.05	0.99	46
22	STACK West	11799	1.32	0.98	90
23	STACK West	13107	1.41	0.98	68
24	STACK West	13047	1.18	0.98	41
25	STACK West	11303	1.01	0.94	280
26	STACK West	10909	0.96	0.95	810
27	STACK West	9687	0.83	0.91	856
28	STACK West	9171	0.83	0.88	1364
29	STACK West	8883	0.83	0.90	1342
30	STACK West	11344	1.00	0.97	305
31	STACK West	11440	0.97	0.99	131
32	STACK West	10743	0.98	0.97	271
33	STACK West	11583	1.01	0.99	139
34	STACK West	11162	0.99	0.99	258
35	STACK West	11609	1.02	0.98	31
36	STACK West	12693	1.43	0.97	70
37	STACK West	11311	0.86	0.96	58
38	STACK West	11229	0.92	0.97	75
39	STACK West	11353	0.96	0.97	119
40	STACK West	10655	0.87	0.97	161
41	STACK West	11693	0.95	0.97	28
42	STACK West	11435	0.98	0.97	42
43	STACK West	11065	0.90	0.97	134
44	STACK West	11487	1.32	0.96	14
45	STACK West	14085	1.28	0.99	10
46	STACK West	11227	1.33	0.96	40
47	STACK East	12523	1.11	0.98	2
48	STACK East	12208	1.03	0.86	3
49	STACK East	12298	1.12	0.92	4
50	STACK East	8968	0.89	0.96	62
51	STACK East	11605	1.03	0.99	3
52	STACK East	11439	1.03	0.98	3
53	STACK East	10045	0.96	0.99	21
54	STACK East	9892	0.89	0.98	40
55	STACK East	9112	0.90	0.98	81
56	STACK East	10573	1.09	0.98	5
57	STACK East	9135	0.93	0.98	39
58	STACK East	9267	0.94	0.98	42
59	STACK East	8652	0.91	0.97	67

Key	Play	TVD	Rc% (from MPI-1)[1]	MDR[2]	4-+1-MDBT ppm (WO)[3]
60	STACK East	10677	1.05	0.97	3
61	STACK East	8207	0.84	0.91	182
62	STACK East	9489	0.98	0.96	17
63	STACK East	9642	0.98	0.98	15
64	STACK East	8213	0.83	0.94	186
65	STACK East	9343	0.94	0.97	27
66	STACK East	8120	0.83	0.92	257
67	STACK East	8787	0.87	0.97	28
68	STACK East	7783	0.82	0.94	131
69	STACK East	8297	0.84	0.96	66
70	STACK East	8813	0.88	0.97	37
71	STACK East	11932	1.21	0.97	0
72	STACK East	7814	0.79	0.88	317
73	STACK East	10785	1.12	0.91	3
74	STACK East	9915	0.90	0.95	35
75	STACK East	8282	0.81	0.96	98
76	STACK East	8307	0.79	0.93	179
77	STACK East	9626	0.99	0.97	15
78	STACK East	10842	0.97	0.98	12
79	STACK East	8275	0.84	0.95	58
80	STACK East	7897	0.84	0.90	426
81	STACK East	8540	0.85	0.93	39
82	STACK East	9217	0.89	0.95	23
83	STACK East	8161	0.85	0.95	52
84	STACK East	9960	1.03	0.98	124
85	STACK East	7984	0.86	0.95	63
86	STACK East	8402	0.87	0.91	43
87	STACK East	7552	0.83	0.95	118
88	STACK East	8857	0.87	0.93	46
89	STACK East	7945	0.85	0.95	64
90	STACK East	7630	0.78	0.91	422
91	STACK East	7862	0.85	0.92	70
92	STACK East	7970	0.83	0.92	39
93	STACK East	7500	0.76	0.89	243
94	STACK East	9291	0.85	0.93	37
95	STACK East	9033	0.87	0.94	28
96	STACK East	8991	0.89	0.93	48
97	STACK East	8848	0.85	0.90	33
98	STACK East	8334	0.85	0.91	42
99	STACK East	8586	0.84	0.91	37
100	STACK East	7452	0.76	0.88	276
101	STACK East	7601	0.78	0.94	206
102	STACK East	7325	0.83	0.92	144
103	STACK East	8258	0.83	0.89	53
104	STACK East	8484	0.86	0.90	45
105	STACK East	7887	0.81	0.89	73
106	STACK East	8861	0.83	0.88	50
107	STACK East	7965	0.82	0.87	76
108	STACK East	9249	0.85	0.94	83
109	STACK East	9017	0.86	0.92	49
110	STACK East	9532	0.92	0.94	56
111	STACK East	8392	0.83	0.86	51
112	STACK East	7533	0.80	0.87	188
113	STACK East	7292	0.79	0.92	161
114	STACK East	7162	0.82	0.87	172
115	STACK East	6714	0.77	0.89	202
116	STACK East	7048	0.80	0.89	183
117	STACK East	6779	0.76	0.90	130
118	STACK East	7004	0.82	0.83	311

Key	Play	TVD	Rc% (from MPI-1)[1]	MDR[2]	4-+1-MDBT ppm (WO)[3]
119	STACK East	6921	0.79	0.82	195
120	SCOOP	10105	0.74	0.88	55
121	SCOOP	14171	1.11	0.97	1
122	SCOOP	14504	1.13	0.98	2
123	SCOOP	14150	1.05	0.97	2
124	SCOOP	11387	0.84	0.92	66
125	SCOOP	11901	0.92	0.94	52
126	SCOOP	10950	0.81	0.97	63
127	SCOOP	10555	0.80	0.92	73
128	SCOOP	10844	0.84	0.95	49
129	SCOOP	10762	0.84	0.94	54
130	SCOOP	11363	0.88	0.96	36
131	SCOOP	11591	0.85	0.96	45
132	SCOOP	12989	0.90	0.96	33
133	SCOOP	11179	0.88	0.95	42
134	SCOOP	12939	0.96	0.97	20
135	SCOOP	10671	0.80	0.94	73
136	SCOOP	10922	0.80	0.95	60
137	SCOOP	10881	0.85	0.94	71
138	SCOOP	11421	0.81	0.96	44
139	SCOOP	12317	0.89	0.95	23
140	SCOOP	12303	0.91	0.96	21
141	SCOOP	11698	0.85	0.96	34
142	SCOOP	11777	0.89	0.97	11
143	SCOOP	11706	0.86	0.96	33
144	SCOOP	11004	0.81	0.94	61
145	SCOOP	11104	0.81	0.94	63
146	SCOOP	11522	0.86	0.96	39
147	SCOOP	11755	0.86	0.96	40
148	SCOOP	12112	0.88	0.96	29
149	SCOOP	9642	0.82	0.91	78
150	SCOOP	14766	0.99	0.97	4
151	SCOOP	12832	0.91	0.97	15
152	SCOOP	11100	0.82	0.93	101
153	SCOOP	12053	0.94	0.97	17
154	SCOOP	9812	0.83	0.92	133
155	SCOOP	9460	0.84	0.65	58
156	SCOOP	12753	0.87	0.95	22
157	SCOOP	13412	0.92	0.93	20
158	SCOOP	14125	0.94	0.94	25
159	SCOOP	9920	0.81	0.90	148
160	SCOOP	13284	0.92	0.92	13
161	SCOOP	12359	0.92	0.97	41
162	SCOOP	13398	0.96	0.95	12
163	SCOOP	15760	1.10	0.99	11
164	SCOOP	14235	1.00	0.98	3
165	SCOOP	13521	0.89	0.97	10
166	SCOOP	13130	0.92	0.97	14
167	SCOOP	13860	1.02	0.95	9
168	SCOOP	12874	0.93	0.96	26
169	SCOOP	8507	0.84	0.75	177
170	SCOOP	13274	0.94	0.97	18
171	SCOOP	12517	0.87	0.92	27
172	SCOOP	14183	0.91	0.97	13

Table 9. Aromatic ratios tested as maturity parameters in this study. (1) 0.825 x (2-+3-methylphenanthrene)/ (1-+9-methylphenanthrene+phenanthrene) + 0.44; (2) 4-methyldibenzothiophene/(4-+1-methyldibenzothiophene); (3) 4-+1-methyldibenzothiophene in ppm of whole oil without a relative response factor.

Values of Rc% from MPI-1 are provided in Figure 39 showing a range of 0.74-1.43%. There is an excellent correlation between Rc% and TVD in both STACK East and SCOOP with correlation coefficients of 0.84 and 0.71, respectively, and may indicate that Rc% calculated from MPI-1 may be one of the most effective maturity parameters in this dataset. STACK West values cluster tightly together but form a non-linear trend with TVD, and the flower-shaped zone of variable oil maturities in STACK West at ~11,000 can also be observed with values ranging from ~0.85-1.3 Rc%. Oils from all three producing reservoirs in SCOOP cluster together in a single trend approximately ~3,000 ft below the main trend in STACK East. From Rc% alone it remains uncertain if the separation of trendlines between STACK and SCOOP is the result of structural uplift in STACK or a cooler portion of the Anadarko Basin in SCOOP.

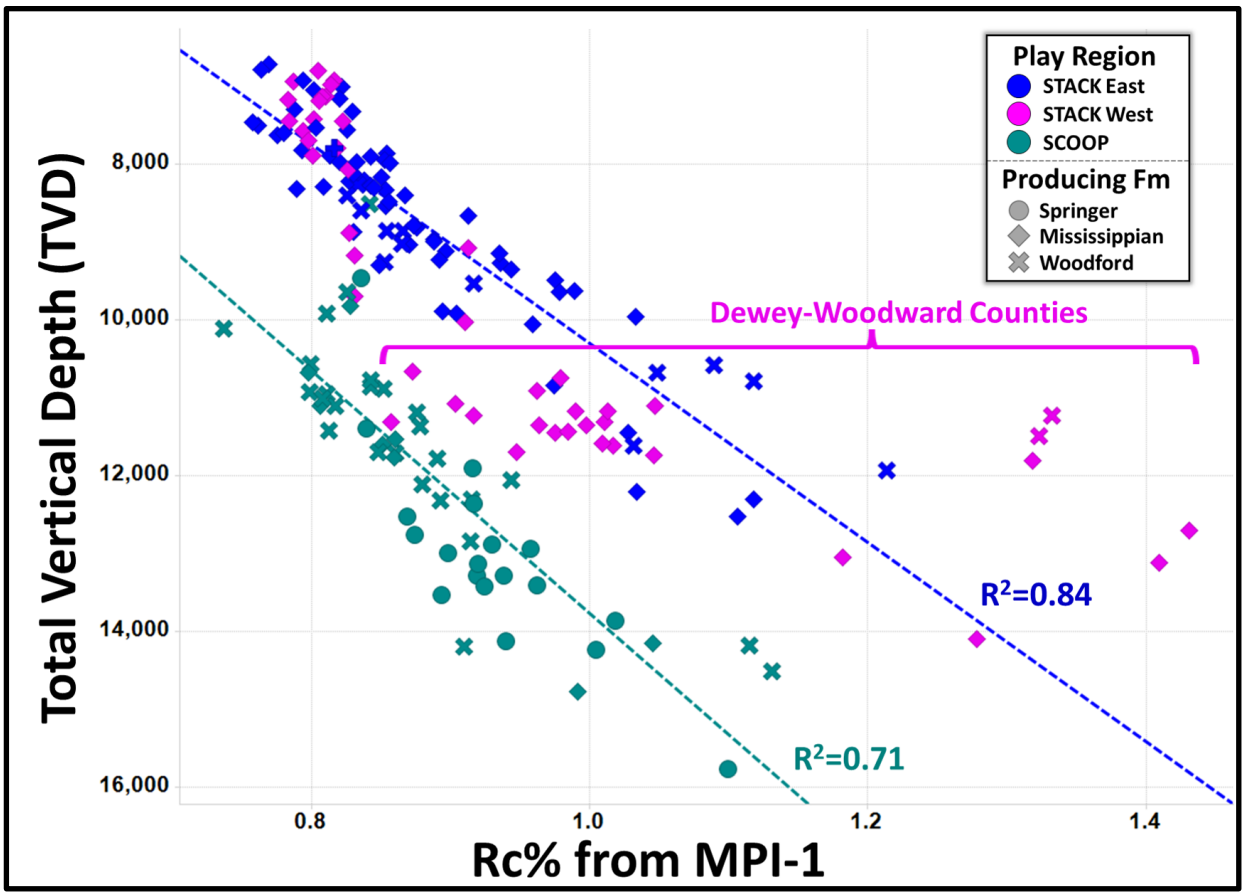

Figure 39. Vitrinite reflectance equivalent (Rc%) values from the methylphenanthrene index (MPI-1) versus TVD.

Methyldibenzothiophene Ratio (MDR)

Aromatic sulfur compounds, including benzo- and dibenzothiophene compounds and their alkyl homologues, elute with the aromatic fraction during column fractionation. In a dataset of oils from the Western Canada Basin, Radke et al. (1982) measured variations in the concentration of individual methyldibenzothiophene (**VIII**) isomers with depth and thermal stress. Of the four methyldibenzothiophene isomers (Figure 40), 1-methyldibenzothiophene (1-MDBT) is the least stable while 4-methyldibenzothiophene (4-MDBT) is the most stable. The ratio of 4-MDBT to the sum of 1-MDBT and 4-MDBT was proposed as the methyldibenzothiophene ratio (MDR) (Radke et al., 1986). The MDR could be directly related to vitrinite reflectance for Type III kerogen, but significantly different trends were observed for Type I and Type II kerogens. There is some evidence that the MDR-Ro% trends for different kerogen types converge beyond Ro>0.8% (Radke et al., 1986; Radke, 1988), but a separate calibration was not performed for this dataset.

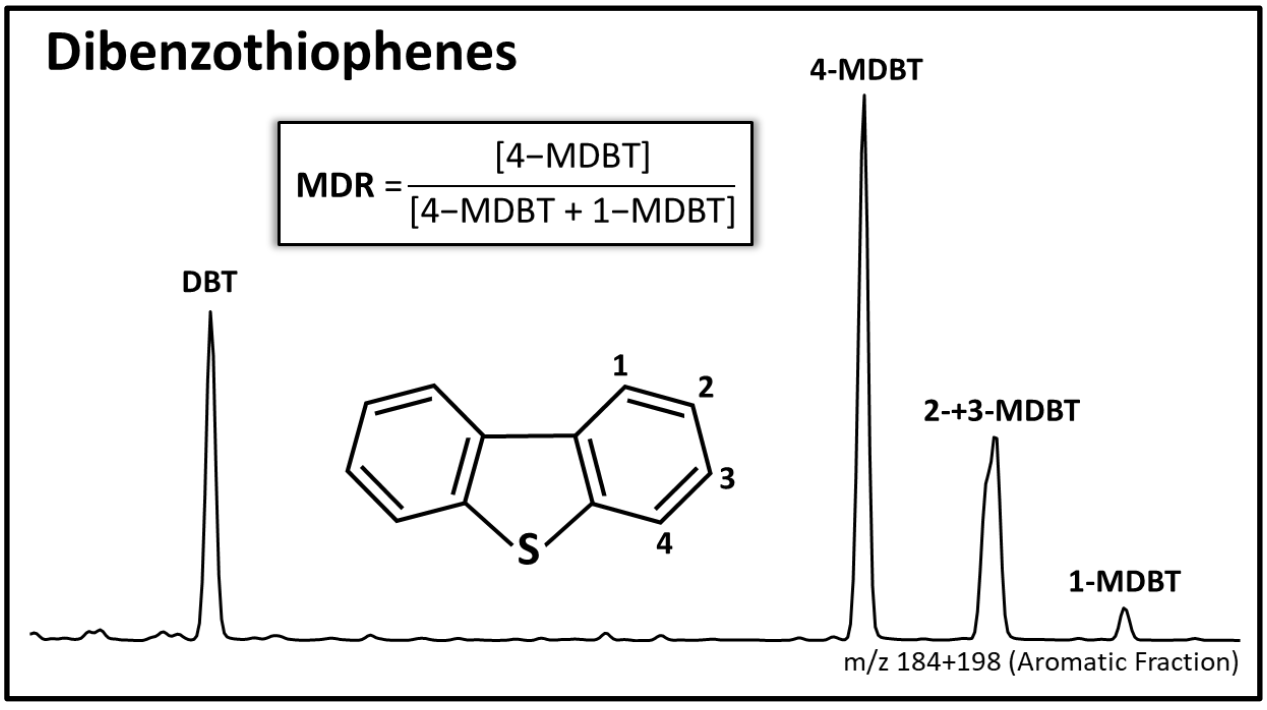

Figure 40. Peak identification for dibenzothiophene (DBT) and the four methyldibenzothiophenes isomers (x-MDBT). Peak identification based on Radke et al. (1982) and Fang et al. (2016).

The MDR for all study oils is shown in Figure 41a. Of the three Play Regions, only STACK West exhibits a good correlation with increased TVD. One possibility is that STACK West contains notably higher concentrations of 4- and 1-MDBT compared to the other Play Regions and may contribute to higher signal-to-noise ratio and lower scatter compared to STACK East and SCOOP (Figure 41b). The MDR for STACK East and SCOOP oils generally increase with TVD but with notable scatter. SCOOP oils continue to plot below the trends in STACK which continues to reinforce that it may be a cooler portion of the basin or has undergone less structural uplift. Curiously, the flower-shaped zone that is observed in most maturity parameters described in this chapter is not observed, but the MDR may reach unity (MDR=1) at depths as shallow as 7,000 ft in some datasets (Radke et al., 1986; Radke, 1988). In fact, there are several STACK oils in this dataset with near unity values by 9,000 ft TVD.

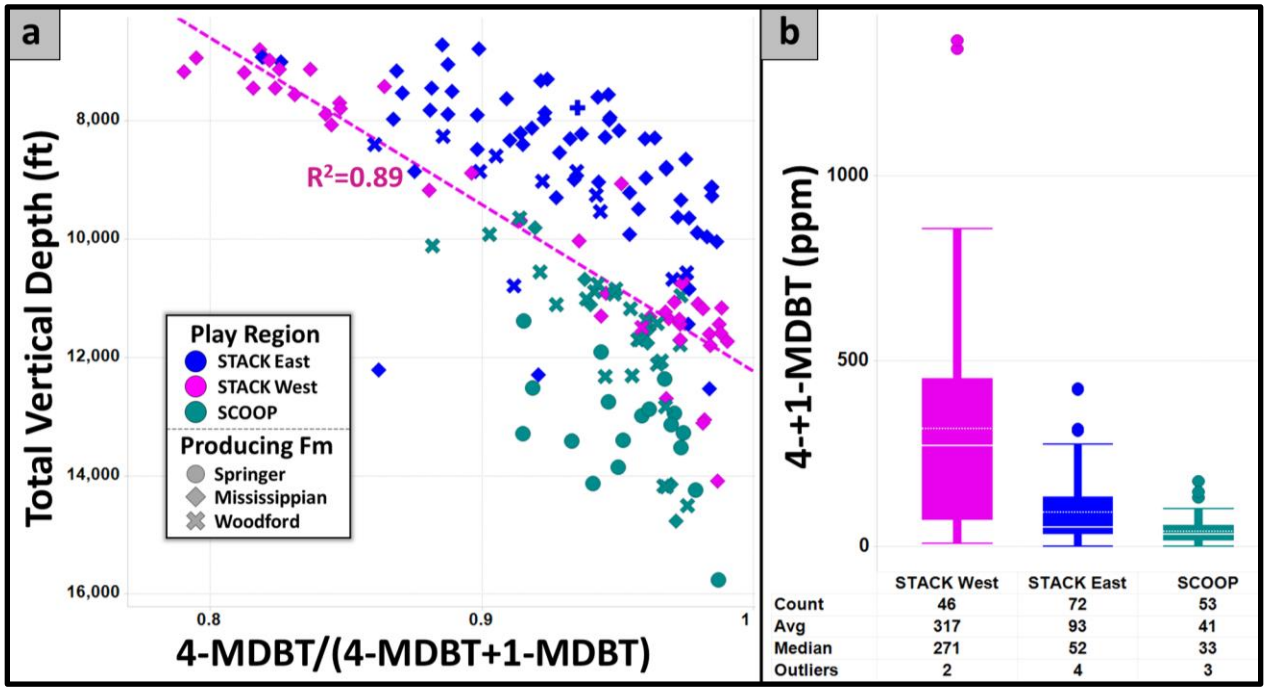

Figure 41. a) The MDR maturity parameter for this dataset whereby only STACK West shows a good correlation versus TVD. b) STACK West oils are enriched in 4- and 1-methyldibenzothiophene compared to STACK East and SCOOP and may contribute the higher signal-to-noise and less scatter of the MDR thermal maturity parameter.

Principal Component Model

Sixteen metrics have been presented which describe the thermal stress of the STACK/SCOOP. Taken individually, each parameter tells an incomplete story of thermal maturity across the study area because chemical reactions may not proceed at the same rate or chemical ratios may not be dynamic over the same range of maturities. No attempt has been made to interpret the efficacy of any individual parameter based on its own merits; instead, a consensus between maturity parameters can be quantified through statistical methods. Principal component analysis (PCA) is a statistical workflow which attempts to reduce a multidimensional data matrix (i.e. sixteen maturity parameters) to its first two principal components which can be plotted within an ellipsoid where each maturity parameter is represented by a single vector projection (Legendre and Legendre, 2012). Parallel vectors show either positive or negative correlation depending on the direction of the arrow, and orthogonal vectors have little or no agreement correlation.

Four PCA vector profiles are shown on Figure 42 for each Play Region and the entire dataset in aggregate. Within each individual Play Region, the efficacy of maturity parameters is determined by its correlation with TVD in order to reflect the local geothermal gradient and increasing thermal stress with depth. In STACK East, there is only one significant principal component (PC) axis which accounts 55.7% of the variation in the dataset, and the maturity parameters CII, expulsion temperature °C, and Rc% exhibit the best correlation with TVD. In STACK West, there is one significant PC axis which accounts for 60.0% of the variation in the dataset, and the maturity parameters CII, 3R/(3R+5R) terpanes, Rc%, and MDR exhibit the best correlation with TVD. In SCOOP, there are three significant PC axes accounting for 44.2%, 16.2%, and 11.0% of the variation in the data, and the maturity parameters 2-/3-methylhexane, expulsion temperature °C, and Rc% exhibited the best correlation with TVD.

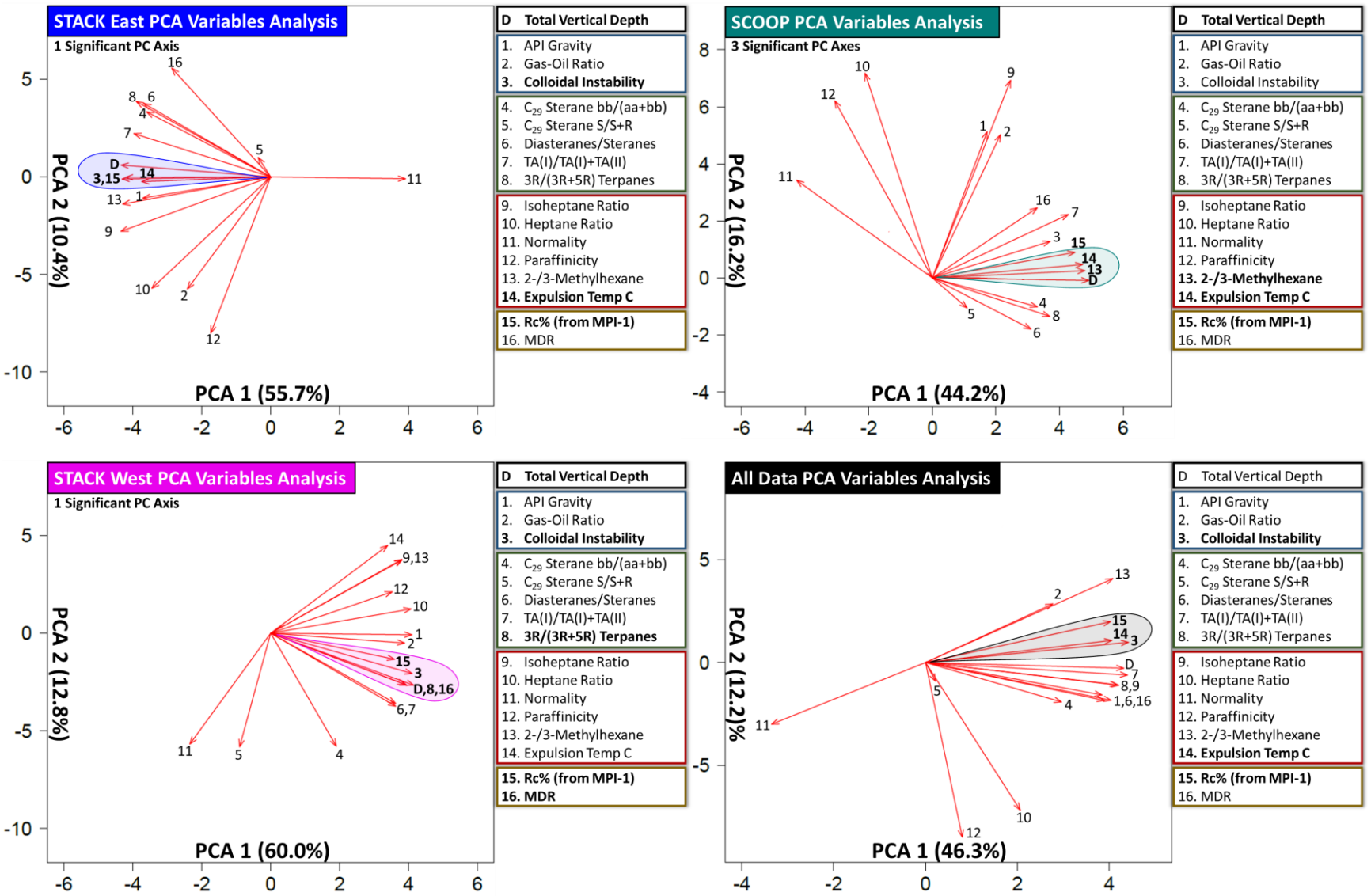

Figure 42. Principal component analysis (PCA) model for each Play Region correlating maturity parameters to TVD where good correlations are circled and bold. All Play Regions are then aggregated into a single PCA model (bottom right) to determine consensus between the most successful maturity parameters without consideration of TVD. The most successful maturity parameters in this dataset were colloidal instability, expulsion temperature, and Rc% (from MPI-1).

The three Play Regions are not expected to share a common geothermal gradient or burial history. As a result, the PCA model for the aggregate dataset seeks consensus between the most successful individual parameters from each Play Region without consideration of TVD as a whole. Only Rc% (from MPI-1) exhibited a high degree of correlation across all three Play Regions, and the aggregate PCA model indicates colloidal instability index and expulsion temperature °C exhibited good correlation with Rc% (from MPI-1) and are also good maturity parameters. For the remainder of this study, Rc% will be the principal index to measure the thermal maturity of oils.

Thermal Maturity Maps

Several maturity parameters have been discussed in this chapter which cover bulk physical characteristics, biomarkers, light hydrocarbons, and aromatics. Many parameters correlate well with TVD while others had little or no correlation, low precision due to significant scatter, a dynamic range smaller than the variability in the dataset, or were only effective in certain Play Regions. Not all areas of the basin are expected to have the same geothermal gradients or have regular increase in thermal stress with increased depth, but in unconventional reservoirs where the reorganization of oils by buoyancy is limited by permeability, TVD can provide an initial qualitative assessment of each maturity parameter. As discussed above, many trends have a strong covariance and add confidence that they are effective maturity parameters and not strongly affected by local changes in organic facies.

Thermal maturity maps of Rc% (from MPI-1) and Expulsion Temperature (°C) are shown on Figure 43 and Figure 44, respectively, accompanied with Woodford Shale Ro% contour lines from Cardott (2012). Although Rc% (from MPI-1) is the most precise metric of oil maturity in this dataset, it may fail to capture the potential effects of subsurface mixing between high maturity oils

relatively depleted in alkyl aromatic compounds which comprise the Rc% parameter and lower maturity fluids comparably enriched in alkyl aromatics. The Expulsion Temperature (°C) parameter, however, is calculated from a ratio of light hydrocarbons and exhibits a strong anomaly in the flower-shaped zone in eastern Dewey County. Moreover, the flower-shaped zone is not a vitrinite reflectance anomaly in the Woodford Shale which further supports the hypothesis of extensive subsurface mixing between high- and low-maturity oils in the brittle Osage Fm.

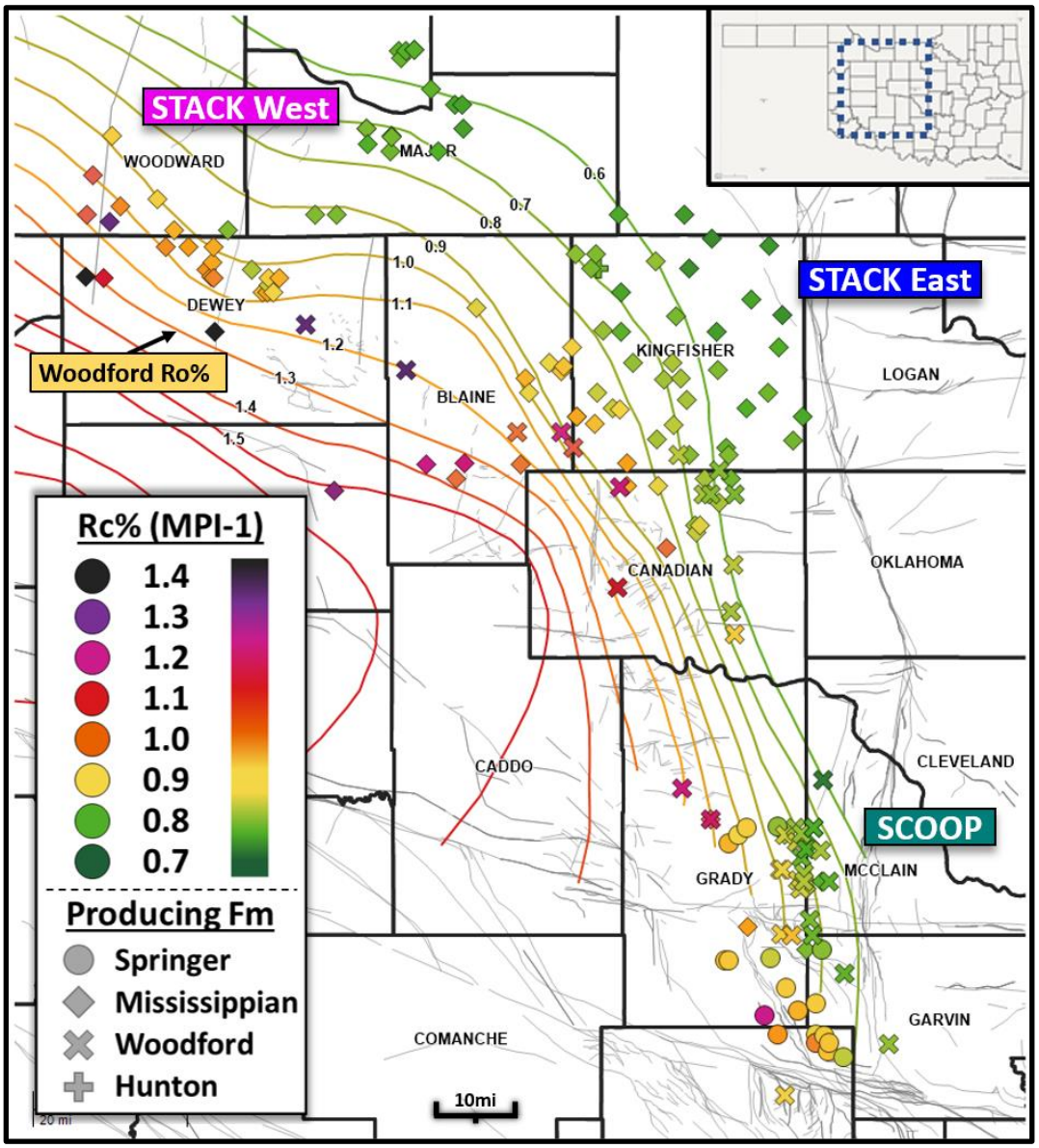

Figure 43. Map of Rc% (from MPI-1) which was found to be the most successful maturity parameter in this dataset and is the principal maturity parameter used in the remainder of this study.

Six additional thermal maturity maps are shown in Figure 45, Figure 46, and Figure 47 with maturity values of the colloidal instability index, 3R/(3R+5R) terpanes, triaromatic steroids TA[I]/TA[I+II], isoheptane ratio, 2-MH/3-MH, and MDR. The maturity anomaly associated with the flower-shaped zone is again best resolved in the light hydrocarbon maturity parameters because high maturity oils are relatively enriched in these compounds relative to lower maturity oils.

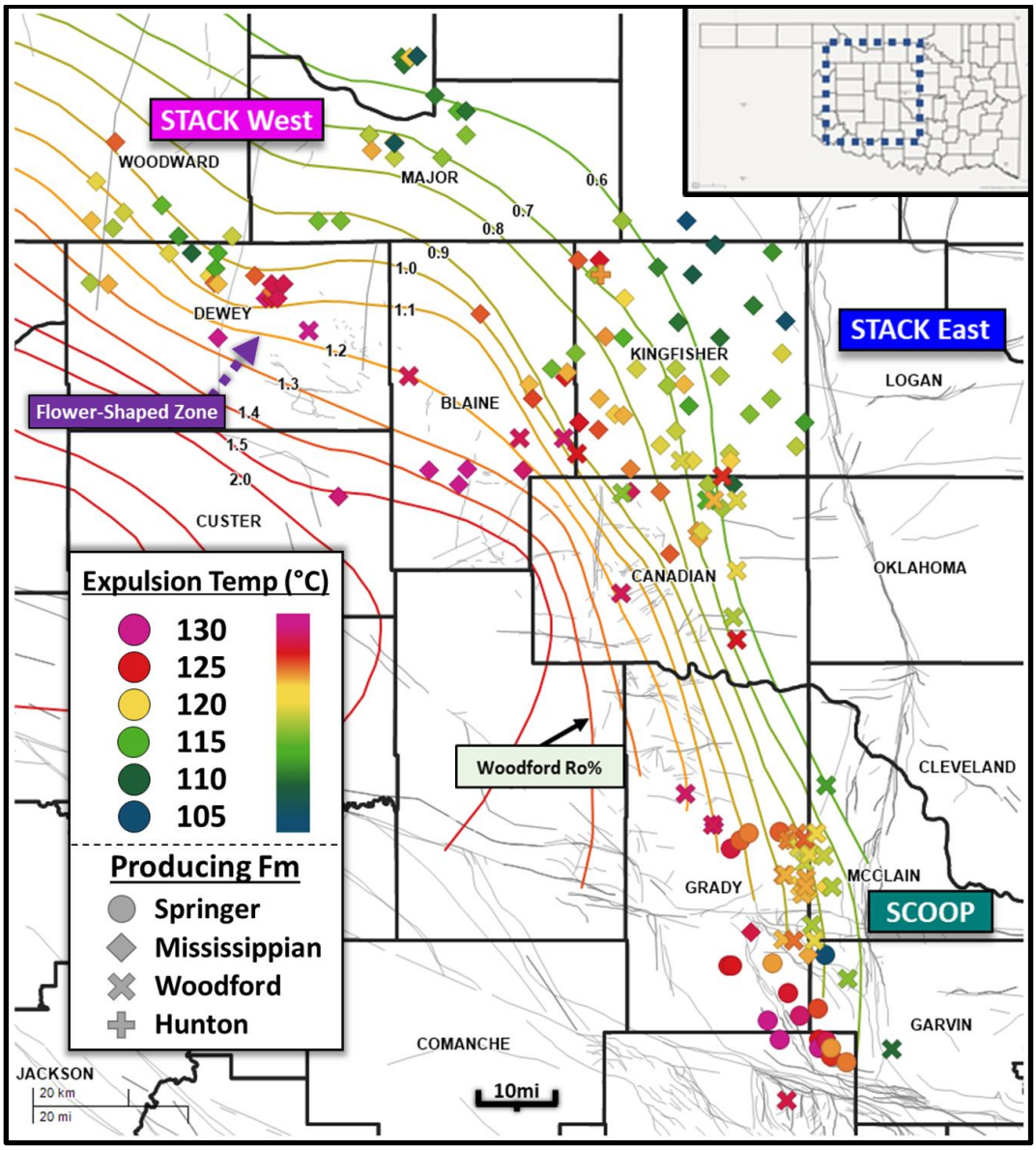

Figure 44. The Expulsion Temperature (°C) maturity parameter makes apparent the effects of high maturity fluids invading the flower-shaped zone in eastern Dewey County compared to similar TVD reservoirs in Woodward and western Dewey counties.

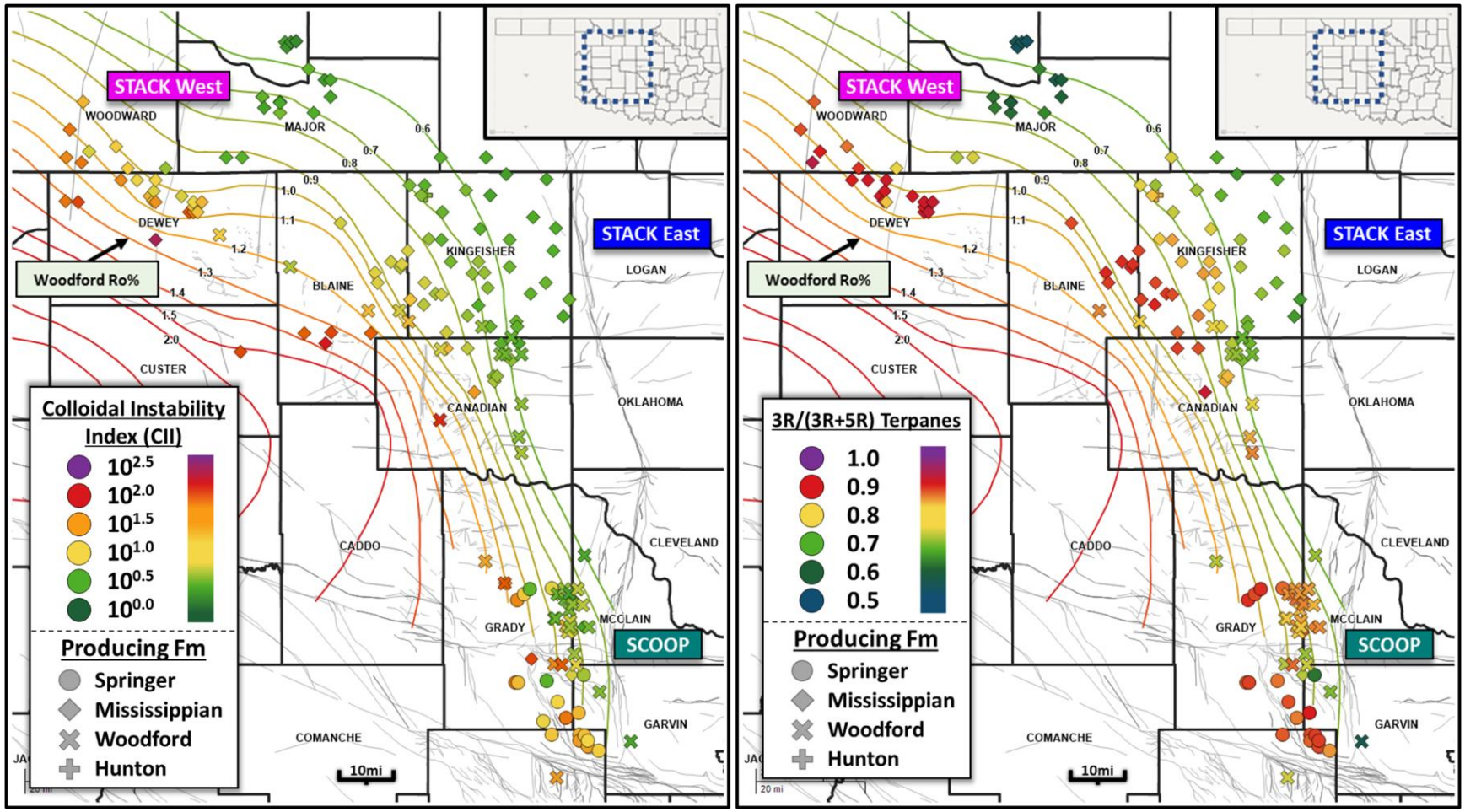

Figure 45. Maps of the colloidal instability index (CII) and tricyclic terpanes/tricyclic terpanes plus hopanes, or 3R/(3R+5R) terpanes, maturity parameters which exhibit good correlation with TVD and other maturity parameters in PCA. The thermal maturity anomaly in eastern Dewey County is not readily apparent in these maturity parameters.

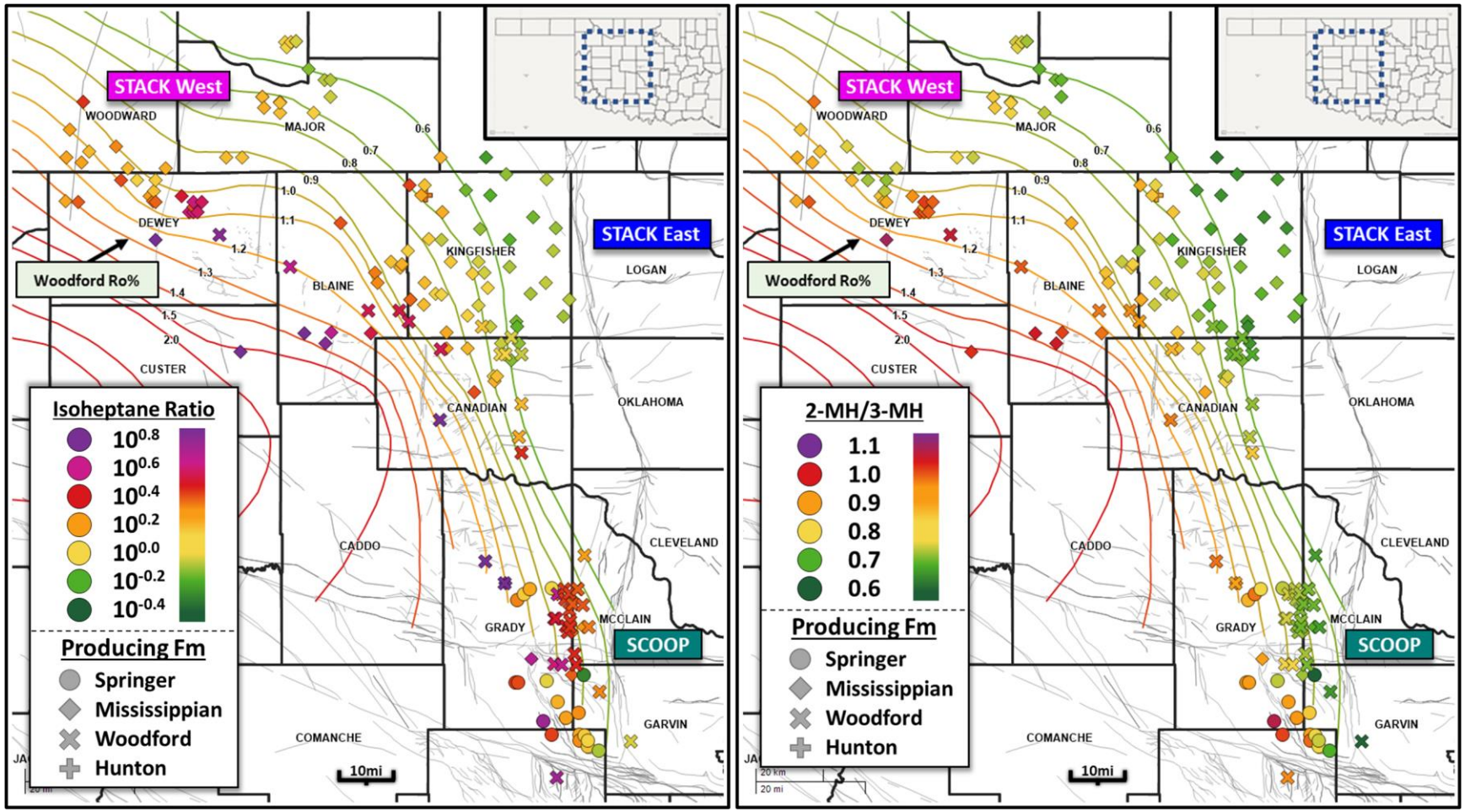

Figure 46. Maps of the isoheptane ratio and 2-MH/3-MH light hydrocarbon maturity parameters which exhibit good correlation with TVD and with other maturity parameters in PCA. Both the Isoheptane Ratio and 2-MH/3-MH maturity parameters highlight the flower-shaped zone thermal maturity anomaly previously identified in eastern Dewey County.

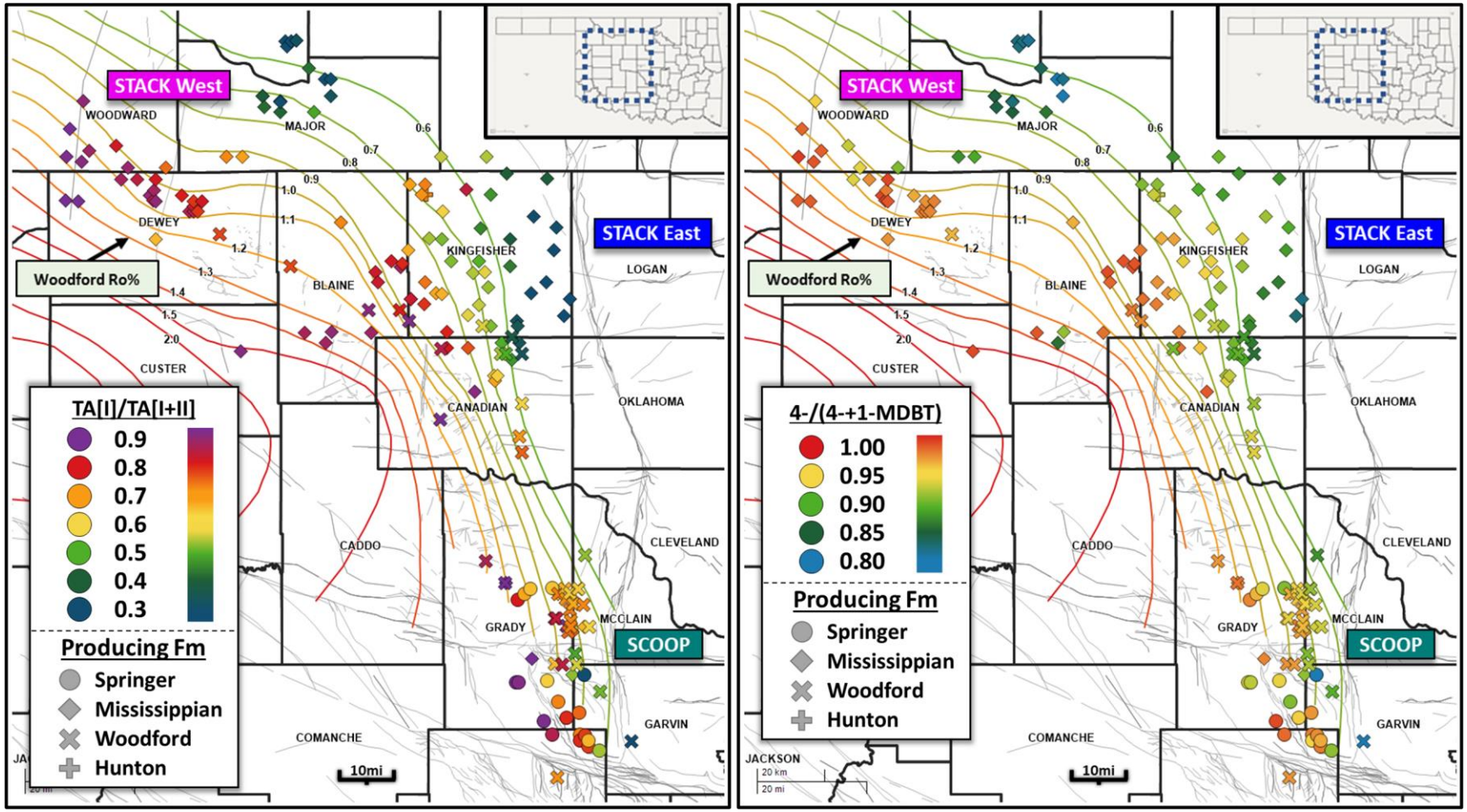

Figure 47. Maps of TA[I]/TA[I+II] and 4-/(4-+1-MDBT), also known as MDR, which have limited correlation with depth and other parameters in PCA.

Maturity and Oil Composition

The thermal maturity parameters discussed in this chapter rely on several time-temperature transformation reactions, including stereochemical reactions around a chiral center which leave the main structure unchanged, kinetic steady-state rearrangement of compounds sometimes through unstable intermediaries (i.e. cyclopropane), and the thermal degradation of compounds. With increased maturity, many compound classes will experience a substantial decrease in concentration as they undergo dilution from non-specific compounds generated from kerogen (e.g. *n*-alkanes) or undergo cracking at very high maturities (van Graas, 1990). Other compounds, like tricyclic terpanes and hopanes, are released from kerogen at different maturities (Philp et al., 2021).

The effect of maturity on oil composition has been well-studied in controlled heating and pyrolysis experiments (Aquino Neto et al., 1983; Lewan, 1985; Lewan et al., 1986; Eglinton et al., 1988; Peters et al., 1990), but is challenged in real world examples, often conventional petroleum systems, which might contain oils from different organic facies, maturities, or charging events within a single well-mixed reservoir. In contrast, unconventional reservoirs with very low permeability are expected to be poorly mixed with respect to multiple charge events, so oils produced from a single well could possibly reflect the oil composition from a single source and charge event (England et al., 1987; England and Mackenzie, 1989; Leythaeuser and Rückheim, 1989; Philp et al., 2021). In theory, produced oils from tight unconventional reservoirs could provide the opportunity to observe compositional changes in oil generated from single charge events with increasing maturity. An example of changing terpane (m/z 191) fingerprint and terpane concentration is shown in Figure 48 across a four well transect in southern Kingfisher County with depths and thermal maturity ranging from 7,000ft-11,000 ft and Rc=0.79%-1.04%, respectively.

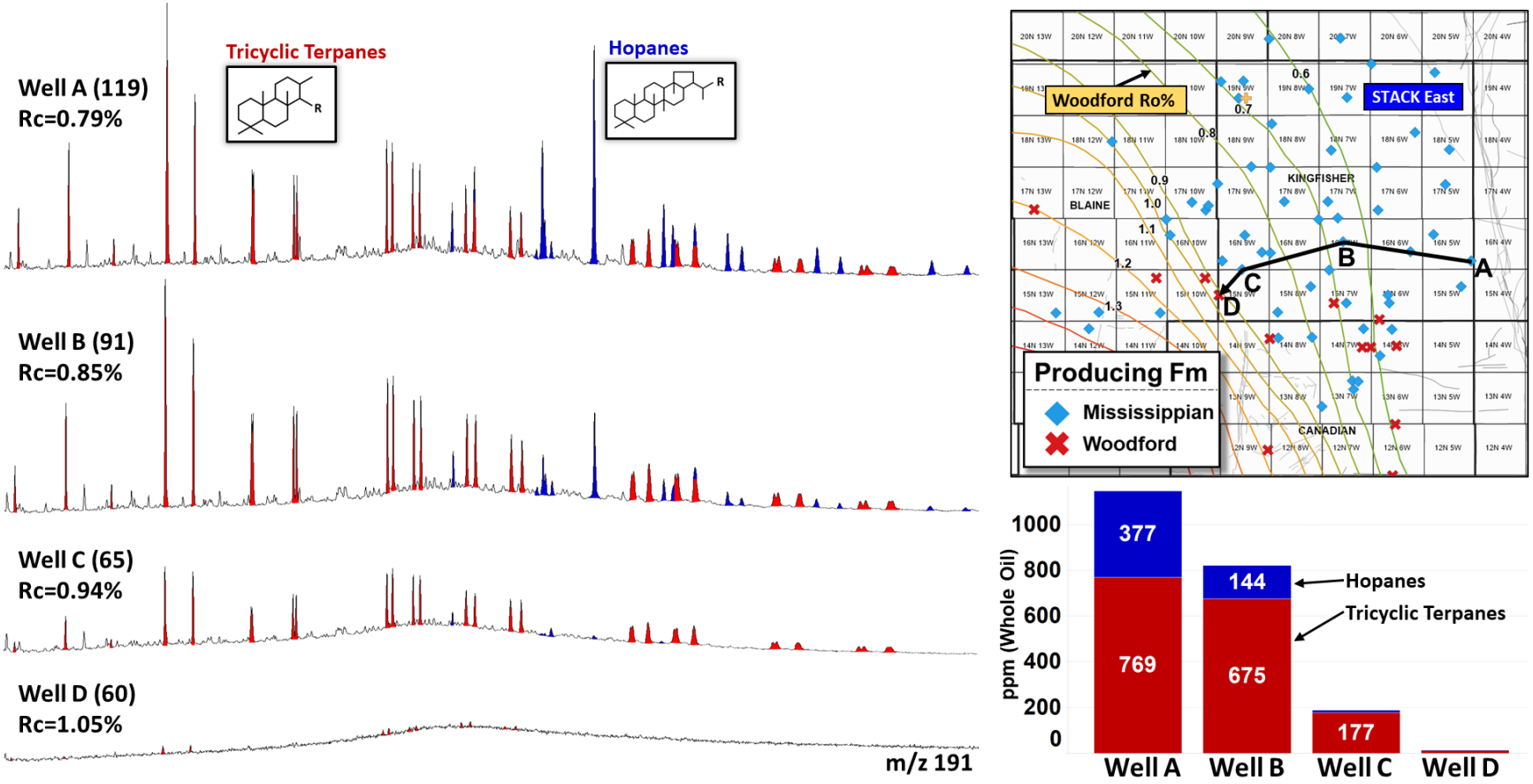

Figure 48. A transect of wells in Kingfisher Country showing changes in the m/z 191 terpane fingerprint with increasing Rc%. Oils produced from wells labeled A-D also have the associated numerical key in parenthesis and which corresponds to concentration data in Table 10. Hopanes are generated at lower maturities and almost completely absent by Rc=0.94%, while tricyclic terpanes are generated at higher maturities and are present until Rc=1.05%. The absolute concentration of hopanes and tricyclic terpanes in ppm of whole oil is provided in the adjoining bar graph (bottom right).

In this example, approximately half of the concentration of hopanes is lost between Well A (Rc=0.79%) and Well B (Rc=0.85%), and hopanes are almost completely absent by Well C (Rc%=0.94). There is almost no decrease in tricyclic terpane concentration between Well A and Well B, but approximately half of the tricyclic terpane concentration is lost by Well C and are essentially absent by Well D (Rc%=1.04). This exemplifies why caution should be used when determining organic facies to differentiate maturity- and source-related compositional changes in oils produced across a broad range of maturities and where sufficient core is not available.

The aggregate concentrations of biomarker classes bicyclic sesquiterpanes (**XI**), tricyclic terpanes (**V**), steranes (**I**), hopanes (**VI**), triaromatic steroids (**II** and **III**), phenanthrene (**VII**), and dibenzothiophene (**VIII**) are shown in Table 10 along with Rc% maturity. The change in concentration of the saturate biomarkers with Rc% is shown in Figure 49, and the concentration of aromatic compounds is shown in Figure 50. Each compound class exhibits an exponential decrease in concentration with increasing thermal stress which resembles a first order kinetic relationship. A line can be fit to the concentration of each compound class in semi-log space hereby called the rate decline exponent. The rate decline exponent represents the negative slope of a best fit line where the y-axis is given in $\log_{10}$(ppm), and the x-axis is given by Rc%. All rate decline exponents in this study are negative, so for clarity a "larger" rate decline exponent refers to the absolute value of a more negative slope indicating the concentration of a particular compound class declines more rapidly with increased maturity. For example, a rate decline exponent of -5 would consequently be termed larger than -3. For saturate biomarkers, the rate decline exponents is observed to be larger corresponding to the number of carbon rings comprising its structure. In this case, the rate decline exponents -0.64, -3.88, -4.34, and -9.06 correspond to sesquiterpanes, tricyclic terpanes, steranes, and hopanes, respectively.

Key	Play	Rc%	Sesquiterpanes[1]	Tricyclic Terpanes[2]	Steranes[3]	Hopanes[4]	Triaromatic Steroids[5]	Phenanthrene[6]	Dibenzothiophene[7]
1	STACK West	0.81	396	1127	2136	1194	654	556	259
2	STACK West	0.80	491	1093	1968	1197	720	522	271
3	STACK West	0.81	401	1021	1921	1210	485	682	331
4	STACK West	0.82	429	941	1626	1010	630	510	228
5	STACK West	0.81	385	1110	2007	1215	738	535	250
6	STACK West	0.81	282	623	1020	447	245	562	102
7	STACK West	0.79	377	823	1544	809	421	541	206
8	STACK West	0.78	271	662	1241	655	359	551	184
9	STACK West	0.80	311	757	1267	515	276	599	171
10	STACK West	0.83	301	796	1335	589	274	610	178
11	STACK West	0.79	471	1087	1913	993	380	491	183
12	STACK West	0.82	330	900	1648	837	366	518	164
13	STACK West	0.80	396	967	1668	629	250	545	222
14	STACK West	0.82	356	873	1564	704	250	524	150
15	STACK West	0.80	307	574	1052	374	161	500	91
16	STACK West	0.78	337	885	1570	784	326	514	175
17	STACK West	0.91	407	398	825	41	25	55	39
18	STACK West	1.05	202	101	202	3	5	60	0
19	STACK West	0.91	262	118	219	16	10	36	103
20	STACK West	1.01	256	101	151	5	14	97	29
21	STACK West	1.05	149	ND	25	ND	3	107	11
22	STACK West	1.32	196	14	38	ND	6	186	33
23	STACK West	1.41	159	ND	ND	ND	ND	48	46
24	STACK West	1.18	102	ND	2	ND	1	129	9
25	STACK West	1.01	181	36	81	2	5	129	150
26	STACK West	0.96	455	146	279	9	28	546	370
27	STACK West	0.83	595	595	1013	146	128	829	169
28	STACK West	0.83	827	852	1739	361	196	1039	319
29	STACK West	0.83	977	1197	2107	340	225	1054	280
30	STACK West	1.00	416	302	380	11	25	436	88
31	STACK West	0.97	218	228	240	8	19	284	16
32	STACK West	0.98	433	275	447	12	22	449	53
33	STACK West	1.01	260	69	100	3	11	348	31
34	STACK West	0.99	385	196	262	7	25	308	24
35	STACK West	1.02	532	44	78	6	4	129	13
36	STACK West	1.43	66	ND	ND	ND	ND	65	72
37	STACK West	0.86	111	70	111	3	5	92	17
38	STACK West	0.92	139	50	67	2	5	99	28
39	STACK West	0.96	231	76	112	2	9	20	35
40	STACK West	0.87	327	111	140	4	13	189	51
41	STACK West	0.95	72	ND	10	ND	1	51	16
42	STACK West	0.98	72	15	21	1	2	61	13
43	STACK West	0.90	230	80	148	2	10	121	45
44	STACK West	1.32	190	ND	15	53	ND	12	6
45	STACK West	1.28	ND	ND	ND	ND	ND	125	6
46	STACK West	1.33	ND	ND	ND	ND	3	58	19
47	STACK East	1.11	ND	ND	ND	ND	1	52	2
48	STACK East	1.03	ND	ND	ND	ND	2	73	4
49	STACK East	1.12	119	ND	ND	ND	2	77	4
50	STACK East	0.89	288	142	144	9	18	233	20
51	STACK East	1.03	154	35	33	3	4	75	3
52	STACK East	1.03	125	ND	ND	ND	3	98	4
53	STACK East	0.96	212	190	139	6	121	93	4
54	STACK East	0.89	314	228	179	9	19	162	7
55	STACK East	0.90	228	247	221	11	28	197	10
56	STACK East	1.09	429	ND	70	ND	5	99	3
57	STACK East	0.93	186	183	126	7	275	142	7
58	STACK East	0.94	188	239	173	10	23	165	7
59	STACK East	0.91	325	427	255	23	48	237	10

Key	Play	Rc%	Sesquiterpanes[1]	Tricyclic Terpanes[2]	Steranes[3]	Hopanes[4]	Triaromatic Steroids[5]	Phenanthrene[6]	Dibenzothiophene[7]
60	STACK East	1.05	80	11	11	2	38	63	2
61	STACK East	0.84	226	372	484	87	63	427	44
62	STACK East	0.98	143	116	78	5	157	88	6
63	STACK East	0.98	139	106	80	4	144	93	5
64	STACK East	0.83	290	426	483	92	73	444	29
65	STACK East	0.94	151	177	132	10	25	141	7
66	STACK East	0.83	255	248	438	93	66	510	60
67	STACK East	0.87	176	243	143	14	231	123	7
68	STACK East	0.82	210	253	301	52	50	328	24
69	STACK East	0.84	294	461	448	103	62	168	8
70	STACK East	0.88	322	434	221	22	44	175	9
71	STACK East	1.21	134	ND	ND	ND	1	26	1
72	STACK East	0.79	315	386	477	112	100	329	136
73	STACK East	1.12	77	ND	11	ND	3	58	3
74	STACK East	0.90	258	475	197	27	43	165	7
75	STACK East	0.81	296	786	673	140	125	300	12
76	STACK East	0.79	262	589	656	170	105	443	24
77	STACK East	0.99	236	151	91	9	14	97	5
78	STACK East	0.97	210	116	75	6	11	76	4
79	STACK East	0.84	232	338	304	70	61	185	12
80	STACK East	0.84	166	258	486	97	135	999	62
81	STACK East	0.85	248	432	263	63	50	184	11
82	STACK East	0.89	173	201	131	13	267	126	7
83	STACK East	0.85	262	510	347	88	59	211	9
84	STACK East	1.03	128	35	44	2	10	294	11
85	STACK East	0.86	213	479	301	94	80	208	8
86	STACK East	0.87	190	437	289	98	675	167	10
87	STACK East	0.83	150	667	714	187	155	358	16
88	STACK East	0.87	247	381	297	92	47	213	11
89	STACK East	0.85	276	559	380	101	66	247	11
90	STACK East	0.78	601	1233	1229	714	246	1180	96
91	STACK East	0.85	197	675	415	144	69	283	13
92	STACK East	0.83	232	467	272	117	61	168	9
93	STACK East	0.76	364	866	1222	440	236	561	41
94	STACK East	0.85	232	237	227	54	41	172	10
95	STACK East	0.87	142	156	125	17	226	122	7
96	STACK East	0.89	110	273	244	58	40	198	11
97	STACK East	0.85	214	324	304	101	44	123	7
98	STACK East	0.85	232	371	278	116	69	205	12
99	STACK East	0.84	212	287	233	103	59	156	9
100	STACK East	0.76	477	847	1297	530	286	684	58
101	STACK East	0.78	456	1207	1258	442	279	610	24
102	STACK East	0.83	344	821	576	262	165	480	24
103	STACK East	0.83	244	431	343	177	106	197	13
104	STACK East	0.86	189	351	306	136	80	513	12
105	STACK East	0.81	208	675	437	261	186	276	17
106	STACK East	0.83	287	639	455	254	155	203	13
107	STACK East	0.82	199	681	570	273	186	283	19
108	STACK East	0.85	226	193	157	26	39	352	23
109	STACK East	0.86	113	237	193	58	42	203	11
110	STACK East	0.92	103	124	132	12	38	102	11
111	STACK East	0.83	196	363	310	160	128	123	9
112	STACK East	0.80	420	807	621	291	275	507	46
113	STACK East	0.79	197	970	1221	467	332	554	27
114	STACK East	0.82	311	875	834	354	330	419	40
115	STACK East	0.77	348	702	745	346	218	508	41
116	STACK East	0.80	358	887	723	306	283	498	42
117	STACK East	0.76	287	832	752	348	256	357	24
118	STACK East	0.82	328	989	926	529	530	704	101

Key	Play	Rc%	Sesquiterpanes[1]	Tricyclic Terpanes[2]	Steranes[3]	Hopanes[4]	Triaromatic Steroids[5]	Phenanthrene[6]	Dibenzothiophene[7]
119	STACK East	0.79	315	769	739	377	369	378	57
120	SCOOP	0.74	131	145	168	48	20	101	13
121	SCOOP	1.11	ND	ND	ND	ND	ND	18	1
122	SCOOP	1.13	25	ND	ND	ND	1	46	2
123	SCOOP	1.05	35	ND	ND	ND	1	60	3
124	SCOOP	0.84	434	449	177	30	42	213	12
125	SCOOP	0.92	237	271	109	11	22	112	10
126	SCOOP	0.81	101	80	104	7	27	125	12
127	SCOOP	0.80	100	78	104	11	27	125	9
128	SCOOP	0.84	101	89	86	10	22	121	9
129	SCOOP	0.84	85	73	77	8	24	115	10
130	SCOOP	0.88	99	68	74	6	16	110	9
131	SCOOP	0.85	107	92	95	6	21	127	10
132	SCOOP	0.90	548	447	109	17	19	145	12
133	SCOOP	0.88	86	70	83	6	18	108	9
134	SCOOP	0.96	298	90	38	3	7	96	8
135	SCOOP	0.80	106	92	111	10	32	130	13
136	SCOOP	0.80	81	68	69	7	21	124	11
137	SCOOP	0.85	68	91	94	16	22	157	14
138	SCOOP	0.81	74	52	62	6	14	107	8
139	SCOOP	0.89	71	18	35	3	8	104	8
140	SCOOP	0.91	61	13	26	2	7	91	7
141	SCOOP	0.85	83	39	60	5	13	97	8
142	SCOOP	0.89	76	46	62	5	6	81	0
143	SCOOP	0.86	65	40	56	5	13	92	8
144	SCOOP	0.81	91	86	102	9	26	120	11
145	SCOOP	0.81	109	140	126	11	29	125	12
146	SCOOP	0.86	101	102	78	7	20	119	10
147	SCOOP	0.86	145	112	95	7	21	144	10
148	SCOOP	0.88	90	41	54	6	12	113	9
149	SCOOP	0.82	75	111	96	40	30	141	15
150	SCOOP	0.99	57	ND	3	ND	1	56	3
151	SCOOP	0.91	48	35	24	12	5	53	3
152	SCOOP	0.82	55	95	93	24	29	174	16
153	SCOOP	0.94	33	10	9	1	2	49	2
154	SCOOP	0.83	108	225	206	76	54	246	25
155	SCOOP	0.84	133	1418	681	933	291	115	25
156	SCOOP	0.87	322	417	158	26	27	111	8
157	SCOOP	0.92	245	24	16	2	1	228	16
158	SCOOP	0.94	276	44	21	3	2	282	21
159	SCOOP	0.81	105	162	215	62	49	183	31
160	SCOOP	0.92	295	235	96	8	10	79	8
161	SCOOP	0.92	315	165	64	6	12	127	12
162	SCOOP	0.96	391	191	55	8	7	96	8
163	SCOOP	1.10	107	ND	ND	ND	ND	162	6
164	SCOOP	1.00	235	29	14	2	1	39	1
165	SCOOP	0.89	289	237	68	7	8	64	5
166	SCOOP	0.92	344	426	105	14	11	77	1
167	SCOOP	1.02	430	153	40	5	6	87	8
168	SCOOP	0.93	376	512	117	21	20	117	4
169	SCOOP	0.84	133	366	763	393	433	136	94
170	SCOOP	0.94	338	386	97	15	12	97	1
171	SCOOP	0.87	432	850	232	94	37	103	5
172	SCOOP	0.91	82	5	8	1	ND	12	5

Table 10. Concentration of several biomarker classes by maturity as defined by Rc%. (1) ∑(BS-1 through BS-8) as defined in Figure 69; (2) ∑(C_{19}-$_{39}$ tricyclic terpanes); (3) ∑(m/z 217) over range of C_{27-30} steranes; (4) ∑(C_{27-35} hopanes); (5) ∑(C_{20-28} triaromatic steroids); (6) phenanthrene; (7) dibenzothiophene.

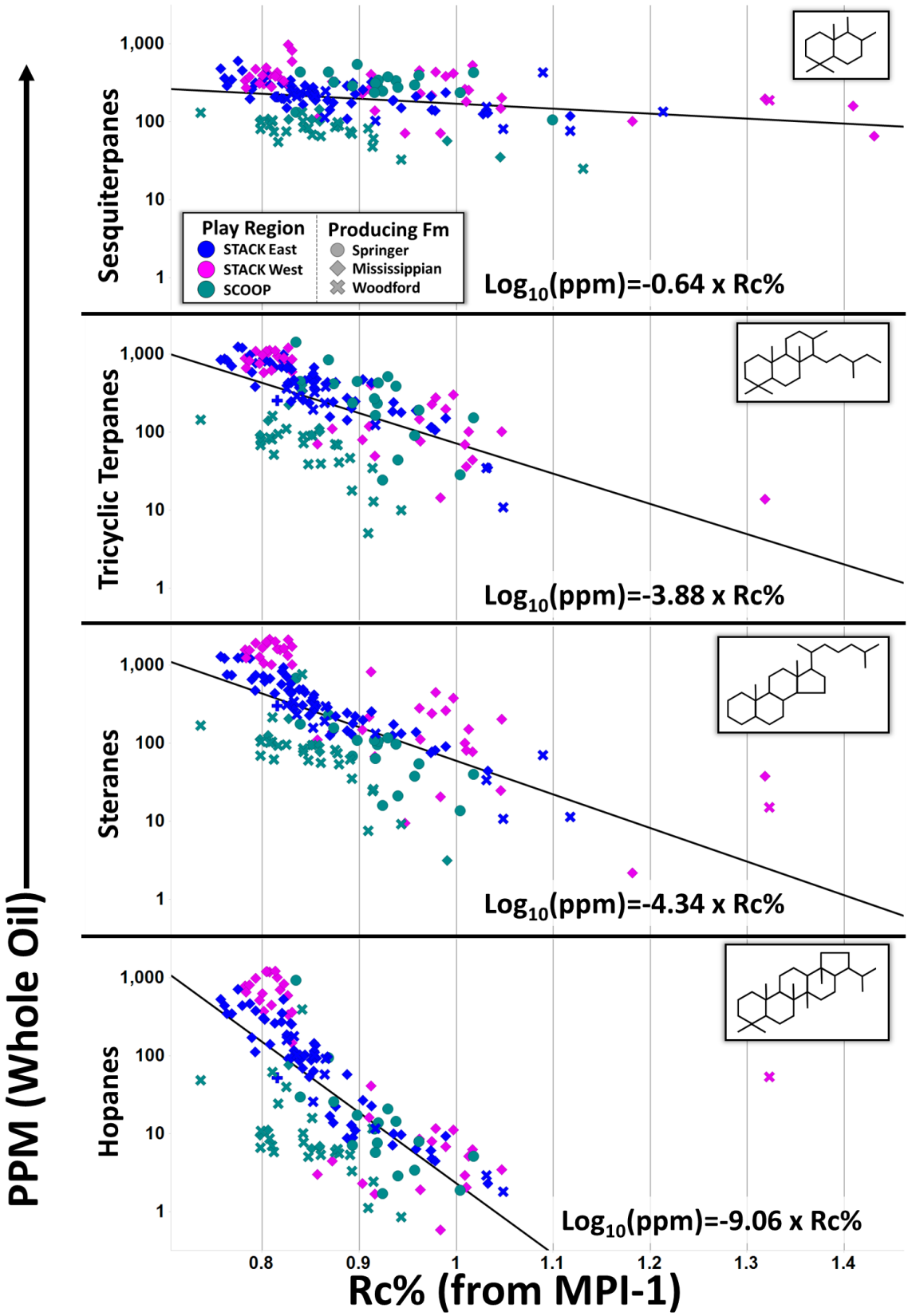

Figure 49. Rate decline exponent calculations for bicyclic sesquiterpanes, tricyclic terpanes, steranes, and hopanes.

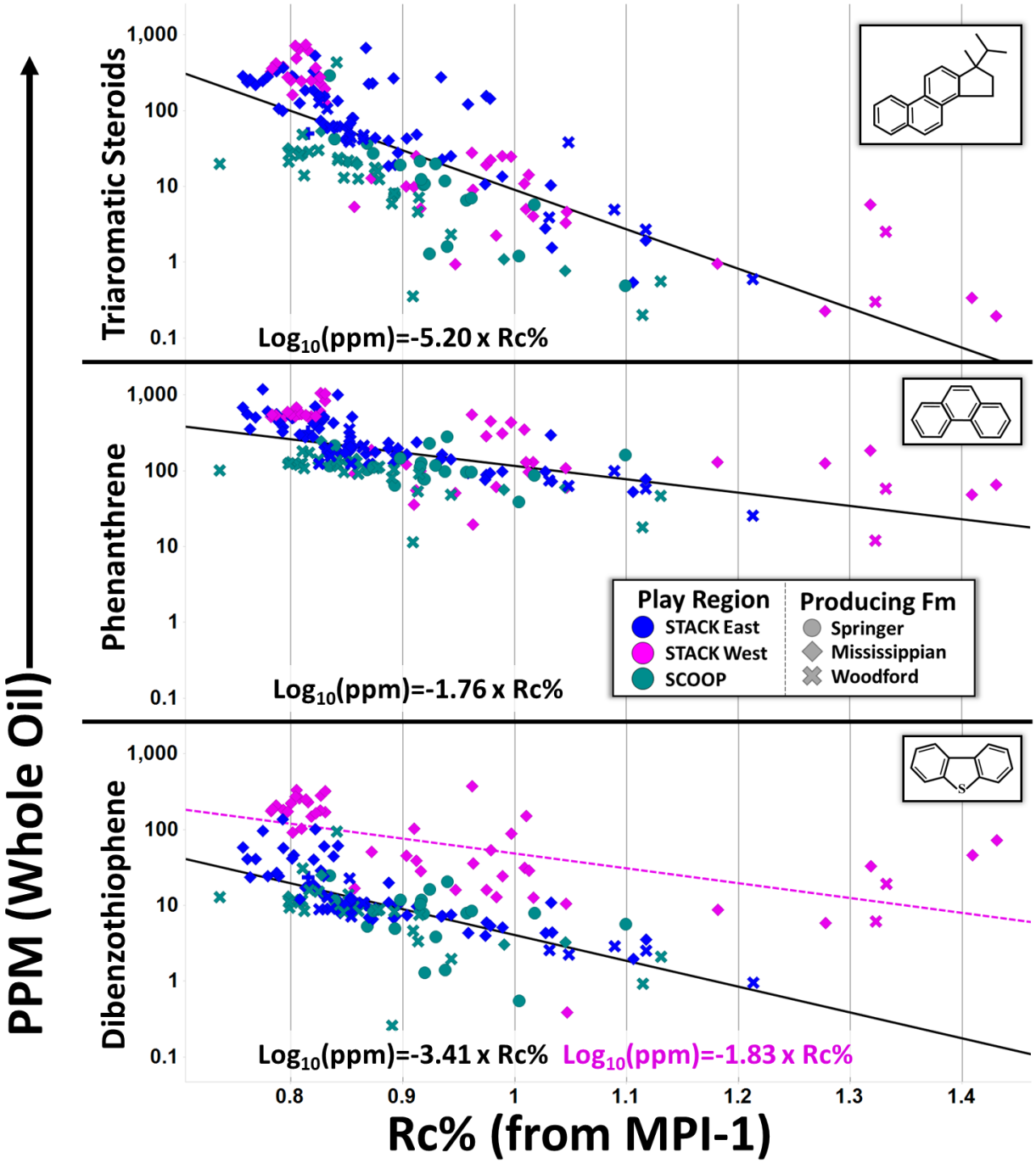

Figure 50. Rate decline exponent calculations for triaromatic steranes TA[I+II], phenanthrene, and dibenzothiophene. The dibenzothiophene in STACK West strongly deviates from the aggregate trend observed for STACK East and SCOOP and expresses a rate decline exponent approximately half.

In the aromatic fraction, triaromatic steroid hydrocarbons (**II** and **III**) have a rate decline exponent of -4.43, almost equal to the rate decline exponent of saturate steranes at -4.48. Phenanthrenes (**VII**) are polycyclic aromatic hydrocarbons composed of three fused benzene rings that are formed either during diagenesis or incomplete combustion reactions during forest fires at the time of deposition (Marynowski and Filipiak, 2007; Marynowski et al., 2014). Phenanthrenes and its methyl homologues exhibit a small rate decline exponent of -0.9. Dibenzothiophenes (**VIII**) are non-polar organosulfur compounds consisting of two benzene rings fused to a central thiophene ring. The main STACK East and SCOOP trend shows a rapid decrease in thiophenes with increasing maturity with a decline rate exponent of -3.98. Curiously, STACK West oils exhibit a much shallower DBT rate decline exponent of -1.39. This result is unexpected because similar compounds might be expected to exhibit equivalent rate decline exponents given equivalent catalyzing agents, kerogen type, and maturity. Some possible explanation, for example, could be novel generation of dibenzothiophene as a byproduct of thermochemical sulfate reduction or continued catagenesis in the presence of free sulfur (Orr, 1974, 1977; Sinninghe Damsté and de Leeuw, 1990). These and other possible explanations are explored more fully in Chapter VI.

Summary of Findings

This study surveyed sixteen thermal maturity parameters ranging from physical characteristics (e.g. API gravity, GOR, colloidal instability index), light hydrocarbons (e.g. Thompson parameters, Mango parameters), aliphatic biomarkers (e.g. C_{29} sterane S/(S+R)), and non-biomarker aromatics (e.g. methylphenanthrene index). It was discovered that by modeling each parameter for covariance with reservoir depth using principal component analysis (PCA), the major principal component axes would best describe thermal maturity independent of extant factors like organic source, reservoir lithology, or pressure. Modeling maturity in this way benefits

from added confidence by seeking an unbiased consensus between several parameters across several biomarker classes and maturity metrics while discounting parameters which may be heavily affected by source input. Based on this workflow, the colloidal instability index (CII), expulsion temperature, and the methylphenanthrene index (MPI-1) most successfully described the thermal maturity of STACK and SCOOP oils, and MPI-1 was selected as the representative measure of thermal maturity for this study. Additionally, SCOOP oils exhibited similar thermal maturities to STACK oils in reservoirs several thousand feet shallower which could result from regional uplifting in STACK or that SCOOP is a cooler portion of the basin.

Critically, the quantitative MPI-1 maturity model allowed for monitoring the concentration of source-related compounds with increasing thermal stress. It was discovered that the concentrations of compound families decreased exponentially with increased Rc% forming a linear fit in semi-log space. The slope of line was termed the rate decline exponent and was observed to become more negative with increasing ring count and molecular complexity. The novel calculations of rate decline exponents will serve as an independent variable when determining the relationship between oils of similar organic facies from different thermal regimes.

Finally, while this workflow successfully modeled thermal maturity in the STACK and SCOOP, it relied on several assumptions regarding limited oil migration, a small variety of source depositional environments, and a regular geothermal gradient common in foreland basins. Due to the nature of Anadarko Basin and what is known about the STACK/SCOOP unconventional resource play, these conditions were met; however, the workflow described in this chapter may not be appropriate for small datasets, basins with irregular geothermal gradients, areas of active geothermal activity, or datasets representing vastly different depositional environments.

V. Organic Facies Determination

Previous Geochemical Studies of Source Rocks in STACK and SCOOP

It is widely believed that the principal source rock for the Devonian-Mississippian STACK and SCOOP play is the Woodford Shale with the exception of production from the Springer Group which may be sourced by a combination of organic-rich intervals in the Caney Shale and Springer Group (Goddard) shales (Pearson, 2016; Pearson and Philp, 2019; Symcox and Philp, 2019a and b; Abrams and Thomas, 2020). Although there is some evidence of a unique Mississippian biomarker signature found in extracts and some oils (Wang and Philp, 1997, 2019; Kim and Philp, 2001; Atwah, 2015; Atwah et al., 2019, 2020), it is still uncertain if thin, sparse organic-rich shales reported in Mississippian strata can meaningfully contribute to reservoir self-sourcing.

Moreover, the Woodford Shale is comprised of varied depositional environments across the Anadarko basin which results in significant regional and vertical heterogeneity in the chemical composition and thickness of its constituent members (Miceli Romero and Philp, 2012). For example, paleogeographic studies show drastically reduced accommodation space in STACK West during Woodford time due to local highs in Hunton topography and proximity to the basin margin (Hester et al., 1990; Zhang and Slatt, 2019). This led to nondeposition of the transgressive Lower Woodford member and a thinner Middle and Upper Woodford deposited in shallower water depths and restricted marine circulation (Logsdon and Brown, 1967; Higley et al., 2014). As a result, oil/oil and oil/source-correlation efforts should be cautious when comparing oils to some unambiguous, universal Woodford Shale geochemical signature. The following sections review the published literature related to the geochemistry of the Woodford and Goddard-Caney shales.

Woodford Shale as a Source Rock

Anoxic sea floor conditions during Woodford deposition prohibited most benthic life but, in turn, facilitated excellent preservation of pelagic organic matter, commonly observed between 1-14% TOC by weight of primarily Type II kerogen (Burruss and Hatch, 1989; Cardott, 2012). The Woodford Shale is often divided into Upper, Middle, and Lower members based on well-log signatures, palynomorphs, geochemical proxies, and lithofacies associations (Sullivan, 1985; Hester et al., 1990; Lambert, 1993; Miceli Romero and Philp, 2012). The Lower Woodford was deposited during the initial phase of the Kaskaskia transgression and can contain evidence of oxidized or reworked organic matter within a shallow oxygenated water such as Type IV kerogen, siliceous logs, rip up clasts, and glauconite (Lambert, 1993; Slatt et al., 2012). The Middle Woodford was deposited during the period of maximum flooding and therefore is the most widespread member and generally contains the highest TOC (Hester et al., 1990; Lambert, 1993). The Upper Woodford was deposited during the highstand systems tract when sea level had begun to fall and contains a higher proportion of terrestrial derived and oxidized (Type III and IV) organic matter compared to the Middle Woodford (Lambert, 1993).

In the 1988 Anadarko Basin Symposium, Burruss and Hatch (1989) described the organic geochemistry of 104 crude oils and 190 source rock organic extracts from the greater Anadarko Basin. Of the three source rocks identified, only the Woodford Shale consistently contained >2% TOC by weight and extracted organic matter characteristic of oil-generating formations, including GC chromatograms with regularly decreasing abundance of *n*-alkanes with increasing carbon number and little or no odd-carbon predominance. They concluded that essentially all oils produced from Silurian through Mississippian reservoirs were sourced from the Woodford Shale.

In a separate oil-source correlation study of 30 oils and 10 cores, Jones and Philp (1990) found that the Woodford Shale sourced 85% of the Ordovician- through Pennsylvanian-aged reservoirs in the Paul's Valley of Oklahoma (in SCOOP). Of the samples analyzed, the most successful biomarker parameters which distinguished Woodford-sourced oils from other organic source were higher C_{30} sterane ratio (C_{30}/C_{29}-sterane=0.17±0.06), lower C_{24} tetracyclic ratio (C_{24}TET/C_{26}TT=0.48±0.08), lower C_{35}-homohopane ratio (C_{35}/C_{34}-homohopane=0.89±0.09), and elevated extended tricyclic terpane ratio ([$C_{28\text{-}30}$TT]/[T_s+T_m]=2.33±0.21) (Jones and Philp, 1990).

In a study of the immature Wyche-1 Woodford core in Pontotoc County of south-central Oklahoma just outside of the Anadarko Basin, Miceli Romero and Philp (2012) found primarily Type II kerogen deposited in mixed marine environment with both marine and terrigenous organic input with some degree of elevated salinity and water column stratification. The Lower and Upper Woodford members were deposited under dysoxic to suboxic conditions (Pr/Ph=1.94±0.32) with periodic episodes of photic zone anoxia (inferred from aryl isoprenoid ratio, AIR=2.73±0.32). By contrast, the Middle Woodford appears to have been influenced by more persistent dysoxia (Pr/Ph=1.50±0.19), increased water column stratification and salinity (higher gammacerane indices), and persistent photic zone anoxia with periodic water column euxinia (AIR=1.06±0.41). Connock (2015) found that the maximum flooding surface within the Wyche-1 core Middle Woodford interval contained elevated concentrations of acid catalyzed rearranged compounds like diasterenes, diahopanes, and neohop-13(18)-enes interpreted as low rates of deposition rather than the abundance of clays (Sinninghe Damsté et al., 2014). However, the low maturity of the core was responsible for undersaturated compounds. Karsts and eroded valleys in the underlying Hunton formed paleo-lows insulated from upwelling currents which formed a strong chemocline with periodic photic zone euxinia (Connock, 2015; Connock et al., 2018; Zhang and Slatt, 2019).

Caney-Goddard Shales as Source Rocks

In their survey of source rocks in the Anadarko Basin, Burruss and Hatch (1989 and 1992) observed that Pennsylvanian-sourced oils are geochemically distinct from Woodford-sourced oils. They observed that Pennsylvanian-type oils were found primarily in central and southern Oklahoma often observed with MCH>*n*-C_7, elevated $\delta^{13}C$, and abundant *n*-alkanes above *n*-C_{15} (Burruss and Hatch, 1989, 1992). One hypothesis this study explores is that these oils are sourced from the Caney or Goddard shales of the Mississippian-Pennsylvanian.

The Goddard Shale is the basal unit of the Chesterian-Morrowan Springer Group sandstones and ranges in thickness from a few hundred up to 2,000 ft thick (Hemish and Andrews, 2001). In a geochemical survey of oils and source rocks in the Anadarko Basin, Wang and Philp (1997) found that the black shales within the Upper Mississippian Springer Group of the southern Anadarko Basin were deposited in shallow marine, shoreline, and deltaic environments and contain primarily Type III, gas prone kerogen. They argued that the Goddard Shale most closely resembles the gas-prone Morrow Fm in the northern Anadarko Basin (Wang and Philp, 1997).

As rates of oil production from the Springer Group sandstones was rising in SCOOP, Pearson (2016) performed a geochemical study on new cores of the Goddard Shale to compare with oils produced from the Springer Group sandstones. Similar to the findings in this study, core plugs and sidewall core from SCOOP exhibited relatively low thermal maturities for their depth. The core plugs from Grady County from depths 12,945-13,045 ft measured Rc% (from Tmax) of 0.89±0.04%, and sidewall cores in Stephens County from depths 13,040-13,104 ft measured Rc% of 0.94±0.06%. Both Goddard Shale extracts and Springer Group oils were dominated by tricyclic terpanes, but at least one Goddard Shale extract contained aryl isoprenoids which were absent in the Springer Group oils. Moreover, Goddard extracts did not necessarily match Springer-produced

oils. For example, Goddard extract Pr/Ph=1.1±0.2 compared to Springer oils 1.4±0.1 and Pr/*n*-C_{17} of 0.6±0.1 compared to 1.0±0.1. Although she concluded the Goddard Shale is the likely source for oils in the Springer Group sands, there remains substantial uncertainty around maturity, depth, and source potential and whether the Goddard Shale is capable of generating liquid hydrocarbons.

An alternative source rock to the Goddard Shale is the Chesterian-aged Caney Shale found primarily in the SCOOP area. The Caney Shale represents the deep-water organic-rich facies deposits distal to the dominant sedimentary inputs to the north of the basin and is composed of a series of mudrocks, limestones, and siltstones, as well as bituminous shales containing between 1-9% TOC of dominantly Type II kerogen and age equivalent to the Barnett Shale of Texas and the Fayetteville Shale of Arkansas (Cardott, 2017). The Caney interval is highly argillaceous and shows strong development of organic-rich mudrocks towards the south approaching the Ardmore Basin (Miller and Cullen, 2018). Unfortunately, commercial production from the Caney Shale in the Anadarko Basin is challenged due to its high clay content and ductile rock matrix.

Outline for Determining Organic Facies

Biologic ecosystem, depositional environment, and diagenetic history can each result in variations in the character of preserved organic matter destined for hydrocarbon generation (Philp et al., 1976; Tissot and Welte, 1984; Hunt, 1996). For the purposes of this study, an organic facies is defined as a mappable rock unit distinguishable by the character of its organic matter without regard to the inorganic aspects of the sediment (Jones, 1984, 1987). In this regard, organic facies are not only limited to differences between organic rich sedimentary layers, but also lateral or vertical changes in organic matter within a continuous stratigraphic interval. Organic facies can also be inferred from the oils they generate because their geochemical patterns are inherited from

their respective source rocks. This study attempts to identify and define the organic facies within the Devonian-Mississippian petroleum system of the Anadarko Basin by analyzing a large dataset of produced oils spanning the entire oil window. Inferences made about source rocks directly from produced oils inherently carries uncertainty about migration, comingled sources, migrational fractionation, reservoir overprinting, and all other secondary reservoir processes. However, the STACK/SCOOP petroleum system is mostly comprised of tight unconventional reservoirs in which oils are captured close to their source. Most oils in this study are produced from organic lean, low permeability Mississippian reservoirs which severely reduces the risk that migration, oil mixing, and organic overprinting affect oil composition. Finally, source-specific analyses are normalized its thermal maturity to ensure to organic facies determinations are only capturing the effects of source rock depositional and diagenetic history.

The determination of organic facies is divided into four steps. First, oil samples are differentiated broadly by geography (Play Region) and producing formation, shown in Figure 51. At this stage, Play Regions and producing formation are merely interpretation guidelines and, critically, are not presumptive of organic facies. Second, geochemical metrics are analyzed to determine if separate clustering is observed potentially forming homologous sets of oils, or oils that may be related to a common organic facies at different thermal maturities. Many metrics, especially those that rely on polycyclic biomarkers, are normalized to thermal maturity to ensure covariance is source related rather than thermal stress. Third, geochemical metrics which form homologous sets of oils are plotted in map view to determine if they form mappable regions with discrete transitions therein qualifying as an organic facies. Finally, organic facies are interpreted within the context of depositional environment, biologic ecosystem, and burial/diagenetic history.

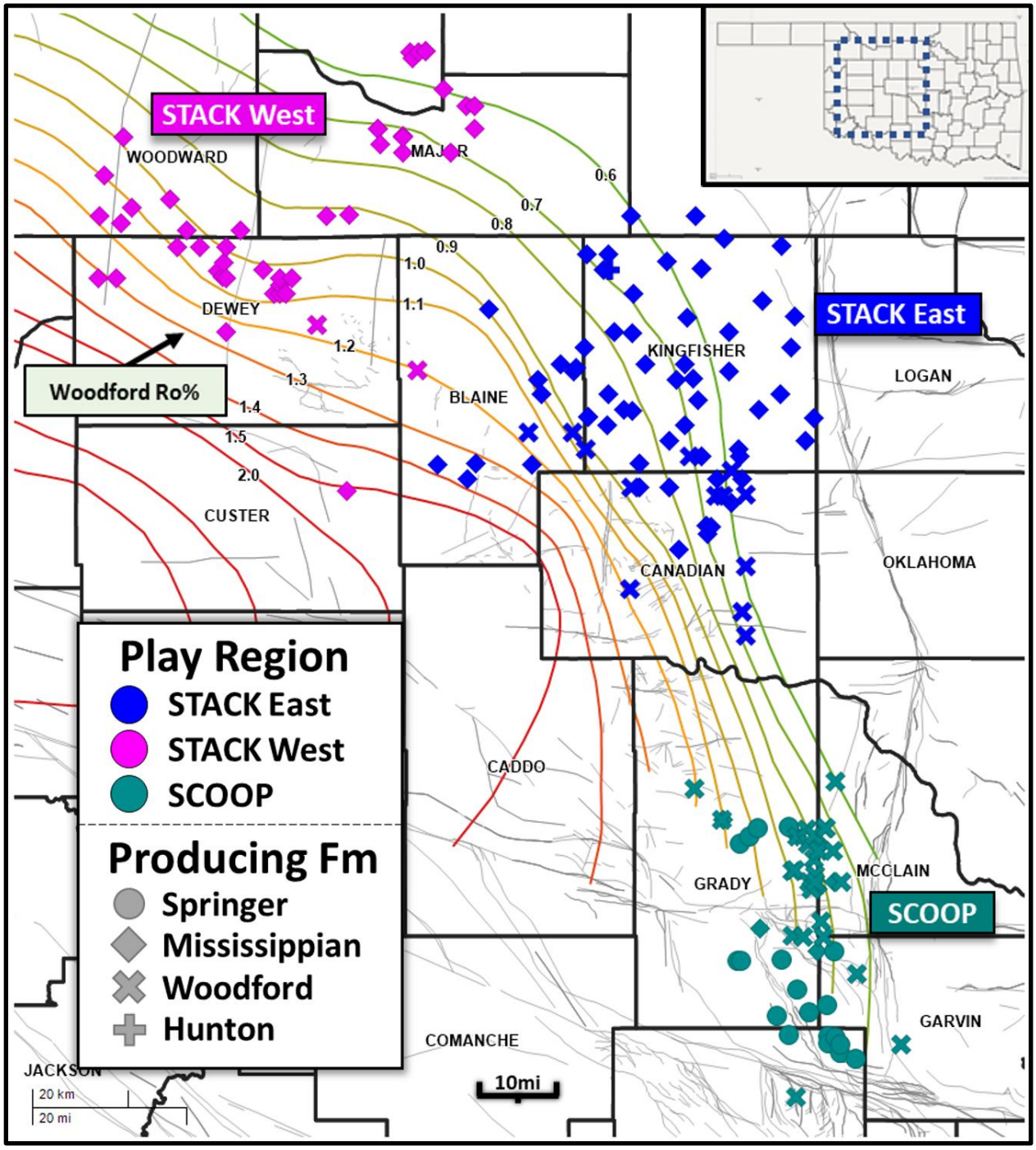

Figure 51. Map of oil samples by Play Region and producing reservoir which will serve as preliminary guides for determining organic facies.

Characteristics of the STACK Petroleum System

Light Hydrocarbons

The distribution of light hydrocarbons have been used extensively in oil-oil and oil-source correlation and has been linked to organic matter type, migration, biodegradation, water washing, and secondary processes like sulfate reduction (Thompson, 1979, 1983, 1987 and 1988; Hunt, 1984; Mango, 1987 and 1990b; Halpern, 1995; Jarvie, 2001). Relative percentage abundances of light hydrocarbons are provided in Table 11. Representative light hydrocarbon fingerprints are provided in Figure 52 showing differences in major constituents *n*-C_7, MCH, and Tol between select Play Regions and producing reservoirs. Mississippian-produced oils generally show similar amounts of *n*-C_7 and MCH, while Woodford oils contains higher *n*-C_7 than MCH. STACK West oils are significantly enriched in Tol compared to all other Play Regions.

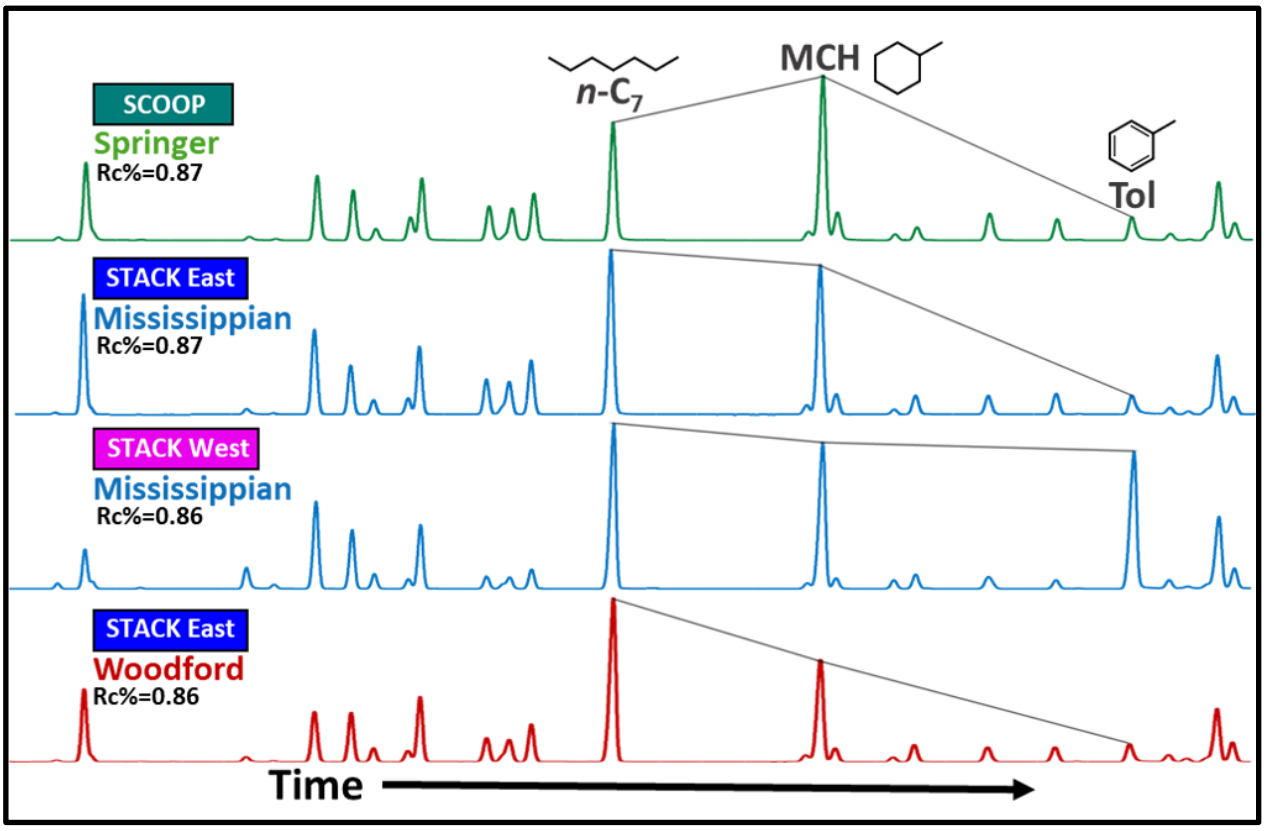

Figure 52. Typical light hydrocarbon fingerprint of oils from Springer (green), Mississippian (blue), and Woodford (red) reservoirs. Peaks for *n*-C_7 (*n*-heptane), MCH (methylcyclohexane), and Tol (Toluene) are highlighted.

		P_1	$N_1{}^6$		$N_1{}^5$			P_2		$N_2{}^5$			P_3				
Key	Play Region	*n*-C_7	MCH	Tol	ECP	1*t*2-DMCP	1*c*2-DMCP	2-MH	3-MH	1,1-DMCP	1*c*3-DMCP	1*t*3-DMCP	2,3-DMP	2,4-DMP	2,2-DMP	3,3-DMP	3-EP
1	STACK West	22.5%	27.5%	15.2%	0.8%	6.5%	1.2%	6.2%	7.9%	1.6%	3.5%	3.6%	2.1%	0.3%	0.3%	0.3%	0.5%
2	STACK West	23.3%	26.8%	13.7%	0.8%	6.5%	1.2%	6.5%	8.3%	1.7%	3.6%	3.5%	2.2%	0.6%	0.4%	0.3%	0.6%
3	STACK West	23.2%	27.6%	12.6%	0.8%	7.3%	1.4%	6.0%	8.0%	1.6%	4.0%	3.9%	2.3%	0.3%	0.3%	0.2%	0.5%
4	STACK West	24.0%	25.7%	13.6%	0.8%	7.1%	1.3%	6.2%	8.0%	1.7%	3.9%	4.0%	2.3%	0.5%	0.3%	0.2%	0.4%
5	STACK West	23.9%	25.7%	12.9%	0.8%	7.1%	1.3%	6.6%	8.3%	1.7%	4.0%	4.0%	2.4%	0.3%	0.3%	0.2%	0.4%
6	STACK West	22.2%	25.2%	9.8%	0.8%	9.6%	1.6%	6.0%	8.5%	1.8%	5.2%	5.1%	2.7%	0.4%	0.2%	0.2%	0.6%
7	STACK West	22.3%	26.3%	10.4%	0.8%	8.5%	1.5%	6.3%	8.7%	1.7%	4.6%	4.6%	2.8%	0.5%	0.3%	0.2%	0.5%
8	STACK West	23.9%	24.8%	10.8%	0.9%	8.3%	1.4%	6.2%	8.6%	1.8%	4.5%	4.7%	2.8%	0.4%	0.2%	0.2%	0.4%
9	STACK West	23.2%	29.5%	12.7%	0.9%	5.5%	1.2%	6.9%	8.4%	1.6%	3.2%	3.2%	2.1%	0.5%	0.4%	0.4%	0.5%
10	STACK West	23.2%	28.7%	16.0%	0.9%	5.1%	1.1%	6.4%	7.8%	1.4%	3.0%	3.0%	1.9%	0.4%	0.4%	0.3%	0.4%
11	STACK West	22.6%	28.6%	11.9%	0.9%	6.2%	1.2%	6.9%	8.7%	1.7%	3.6%	3.5%	2.3%	0.6%	0.4%	0.3%	0.6%
12	STACK West	23.9%	28.3%	11.1%	0.9%	6.1%	1.2%	7.1%	8.8%	1.7%	3.6%	3.5%	2.2%	0.3%	0.4%	0.3%	0.6%
13	STACK West	22.7%	28.9%	13.8%	0.9%	5.3%	1.1%	7.0%	8.5%	1.6%	3.1%	3.1%	2.1%	0.6%	0.5%	0.4%	0.4%
14	STACK West	24.1%	28.2%	11.0%	0.9%	6.1%	1.2%	7.0%	8.8%	1.6%	3.5%	3.4%	2.4%	0.6%	0.4%	0.4%	0.6%
15	STACK West	25.6%	25.6%	8.5%	0.9%	7.3%	1.3%	7.1%	9.3%	1.8%	4.1%	4.2%	2.7%	0.6%	0.3%	0.3%	0.5%
16	STACK West	23.4%	26.3%	9.1%	0.8%	8.3%	1.5%	6.5%	9.1%	1.7%	4.5%	4.7%	2.8%	0.6%	0.3%	0.2%	0.5%
17	STACK West	30.7%	25.5%	13.3%	1.0%	3.1%	0.9%	7.8%	8.4%	1.3%	2.0%	1.9%	1.9%	0.6%	0.6%	0.4%	0.5%
18	STACK West	25.0%	27.8%	16.2%	1.0%	4.1%	1.0%	6.4%	7.7%	1.9%	2.6%	2.5%	2.0%	0.5%	0.5%	0.4%	0.4%
19	STACK West	25.9%	30.1%	15.1%	1.2%	3.7%	1.0%	6.1%	7.7%	1.3%	2.2%	2.2%	2.0%	0.4%	0.3%	0.3%	0.4%
20	STACK West	26.6%	25.3%	14.1%	1.1%	5.1%	1.1%	6.5%	7.8%	2.1%	3.2%	3.2%	2.2%	0.5%	0.4%	0.3%	0.4%
21	STACK West	26.0%	25.5%	13.0%	1.0%	4.7%	0.9%	7.4%	8.6%	2.4%	3.0%	3.1%	2.4%	0.7%	0.5%	0.4%	0.4%
22	STACK West	27.7%	25.4%	13.3%	1.1%	4.5%	0.9%	7.1%	8.2%	2.2%	2.9%	2.9%	2.3%	0.5%	0.5%	0.3%	0.4%
23	STACK West	27.7%	25.3%	13.3%	1.1%	4.6%	0.9%	7.0%	8.1%	2.2%	2.9%	3.1%	2.3%	0.5%	0.4%	0.3%	0.4%
24	STACK West	25.9%	25.1%	19.9%	1.4%	3.3%	1.0%	7.0%	7.3%	1.7%	2.0%	2.0%	1.7%	0.5%	0.5%	0.4%	0.3%
25	STACK West	26.5%	25.6%	17.1%	1.3%	3.5%	0.8%	7.3%	8.6%	1.4%	2.0%	2.1%	2.1%	0.5%	0.4%	0.4%	0.4%
26	STACK West	25.1%	23.9%	15.7%	1.1%	5.6%	1.1%	6.5%	8.6%	1.9%	3.2%	3.3%	2.5%	0.4%	0.3%	0.2%	0.4%
27	STACK West	22.9%	25.7%	17.5%	1.0%	5.0%	1.0%	6.6%	8.5%	1.5%	3.1%	3.0%	2.5%	0.6%	0.5%	0.3%	0.4%
28	STACK West	23.4%	24.2%	14.6%	0.9%	6.3%	1.2%	7.1%	8.9%	1.7%	3.5%	3.3%	2.9%	0.6%	0.4%	0.3%	0.5%
29	STACK West	23.1%	27.0%	11.9%	0.9%	6.3%	1.1%	7.0%	9.1%	1.6%	3.7%	3.6%	2.8%	0.6%	0.4%	0.3%	0.5%
30	STACK West	25.6%	23.7%	10.9%	1.0%	7.1%	1.3%	6.8%	9.0%	2.2%	4.1%	4.1%	2.8%	0.4%	0.4%	0.3%	0.5%
31	STACK West	26.9%	22.1%	9.3%	0.9%	7.4%	1.2%	7.1%	9.7%	2.2%	4.2%	3.9%	3.2%	0.6%	0.3%	0.3%	0.6%
32	STACK West	23.9%	24.5%	15.1%	1.0%	5.9%	1.2%	6.7%	8.7%	2.1%	3.4%	3.6%	2.6%	0.5%	0.4%	0.3%	0.4%
33	STACK West	24.2%	25.5%	16.6%	1.2%	4.4%	1.1%	7.0%	8.4%	1.9%	2.8%	2.7%	2.3%	0.6%	0.5%	0.4%	0.5%
34	STACK West	24.0%	25.4%	13.5%	1.1%	4.5%	1.0%	8.3%	9.8%	1.6%	2.7%	2.8%	2.9%	0.9%	0.6%	0.4%	0.4%
35	STACK West	26.6%	21.7%	17.6%	1.2%	3.8%	0.9%	7.9%	9.1%	1.8%	2.4%	2.5%	2.3%	0.6%	0.6%	0.5%	0.4%
36	STACK West	26.1%	13.0%	24.6%	3.5%	1.0%	1.6%	11.2%	10.6%	0.5%	0.5%	0.5%	2.2%	1.3%	1.3%	1.3%	0.7%
37	STACK West	24.2%	22.9%	23.2%	1.2%	2.6%	0.8%	7.7%	8.5%	1.3%	1.6%	1.6%	2.0%	0.7%	0.6%	0.6%	0.5%
38	STACK West	25.3%	20.7%	23.6%	1.6%	2.1%	0.9%	8.6%	8.8%	1.1%	1.3%	1.3%	1.9%	0.8%	0.8%	0.7%	0.6%
39	STACK West	26.9%	21.4%	18.5%	1.5%	2.6%	1.0%	9.1%	9.7%	1.2%	1.6%	1.6%	2.1%	0.9%	0.8%	0.6%	0.5%
40	STACK West	27.3%	24.2%	12.1%	1.1%	4.0%	0.9%	8.7%	10.0%	1.8%	2.6%	2.5%	2.4%	0.8%	0.6%	0.4%	0.5%

		P_1	N_1^6		N_1^5			P_2		N_2^5			P_3				
Key	Play Region	*n*-C_7	MCH	Tol	ECP	1*t*2-DMCP	1*c*2-DMCP	2-MH	3-MH	1,1-DMCP	1*c*3-DMCP	1*t*3-DMCP	2,3-DMP	2,4-DMP	2,2-DMP	3,3-DMP	3-EP
41	STACK West	26.0%	21.2%	20.5%	1.5%	2.3%	0.9%	9.2%	9.5%	1.1%	1.4%	1.5%	2.0%	1.0%	0.8%	0.7%	0.4%
42	STACK West	22.1%	18.3%	20.3%	14.0%	1.9%	0.8%	7.5%	7.9%	0.9%	1.2%	1.2%	1.6%	0.7%	0.7%	0.6%	0.4%
43	STACK West	24.8%	21.3%	21.9%	1.5%	2.4%	0.9%	8.8%	9.4%	1.2%	1.4%	1.5%	2.1%	0.9%	0.8%	0.7%	0.5%
44	STACK West	26.0%	18.4%	21.3%	1.8%	1.7%	0.9%	10.7%	10.5%	0.9%	1.0%	1.0%	2.1%	1.1%	1.0%	0.9%	0.6%
45	STACK West	23.5%	21.8%	16.2%	3.5%	1.1%	2.0%	11.8%	12.0%	0.5%	0.6%	0.5%	2.4%	1.2%	1.1%	1.2%	0.9%
46	STACK West	27.2%	22.6%	18.1%	1.4%	2.1%	0.8%	9.6%	10.1%	0.9%	1.3%	1.2%	1.9%	0.8%	0.7%	0.7%	0.6%
47	STACK East	27.3%	21.3%	13.7%	2.1%	1.6%	1.2%	12.2%	12.0%	0.8%	1.0%	1.0%	2.0%	1.1%	1.1%	0.8%	0.7%
48	STACK East	28.4%	20.0%	12.4%	1.9%	1.9%	1.1%	12.7%	12.6%	0.8%	1.2%	1.2%	2.2%	1.2%	1.0%	0.6%	0.7%
49	STACK East	28.5%	23.4%	11.3%	1.6%	2.3%	1.0%	11.1%	11.5%	1.2%	1.4%	1.5%	2.0%	1.1%	0.9%	0.6%	0.6%
50	STACK East	27.3%	24.1%	12.3%	1.1%	4.1%	0.9%	8.6%	10.0%	1.8%	2.6%	2.4%	2.3%	0.8%	0.7%	0.4%	0.6%
51	STACK East	33.4%	22.2%	4.2%	1.3%	3.2%	0.9%	11.2%	12.1%	1.5%	2.1%	2.2%	2.7%	1.2%	0.7%	0.4%	0.6%
52	STACK East	27.2%	26.1%	8.8%	1.4%	3.2%	1.0%	10.5%	11.3%	1.7%	2.1%	2.0%	2.1%	1.0%	0.7%	0.5%	0.5%
53	STACK East	28.5%	24.9%	8.1%	1.1%	4.7%	1.0%	8.6%	10.3%	2.2%	3.1%	3.0%	2.5%	0.7%	0.5%	0.3%	0.5%
54	STACK East	27.7%	23.7%	8.1%	1.0%	4.9%	1.1%	8.9%	10.6%	2.3%	3.4%	3.3%	2.5%	0.9%	0.7%	0.3%	0.7%
55	STACK East	27.7%	24.4%	6.5%	1.0%	6.5%	1.2%	7.7%	10.0%	2.5%	4.2%	4.2%	2.4%	0.5%	0.4%	0.2%	0.5%
56	STACK East	30.9%	23.6%	8.7%	1.3%	3.1%	0.3%	10.4%	11.4%	1.4%	2.1%	2.1%	2.2%	1.0%	0.7%	0.4%	0.5%
57	STACK East	27.0%	25.5%	6.0%	1.0%	6.0%	1.2%	8.3%	10.2%	2.5%	4.0%	3.8%	2.4%	0.9%	0.4%	0.3%	0.6%
58	STACK East	27.2%	25.4%	6.9%	1.0%	5.8%	1.2%	8.1%	10.0%	2.5%	3.9%	3.8%	2.2%	0.6%	0.4%	0.3%	0.5%
59	STACK East	26.4%	27.3%	6.1%	1.0%	6.5%	1.4%	6.9%	9.3%	2.5%	4.2%	4.4%	2.2%	0.5%	0.3%	0.5%	0.4%
60	STACK East	32.4%	22.4%	7.5%	1.4%	3.1%	0.9%	10.6%	11.8%	1.4%	1.9%	2.0%	2.3%	0.9%	0.6%	0.4%	0.6%
61	STACK East	28.2%	25.7%	9.9%	1.3%	3.9%	1.0%	8.9%	10.3%	1.5%	2.4%	2.5%	2.2%	0.7%	0.5%	0.5%	0.5%
62	STACK East	26.7%	25.7%	7.5%	0.8%	4.9%	1.2%	9.2%	10.8%	2.1%	3.4%	3.2%	2.2%	0.8%	0.5%	0.3%	0.5%
63	STACK East	27.4%	26.4%	5.9%	1.7%	4.6%	1.1%	9.5%	10.8%	2.0%	3.1%	3.0%	2.2%	0.8%	0.5%	0.4%	0.6%
64	STACK East	29.3%	23.8%	10.6%	0.9%	5.3%	1.0%	7.7%	9.2%	1.7%	3.2%	3.2%	2.3%	0.5%	0.4%	0.3%	0.5%
65	STACK East	25.3%	25.5%	4.9%	0.9%	6.5%	1.2%	8.5%	10.9%	2.8%	4.6%	4.5%	2.3%	0.8%	0.4%	0.3%	0.6%
66	STACK East	26.2%	23.3%	10.0%	0.9%	5.6%	1.0%	7.6%	9.6%	1.8%	3.4%	5.6%	2.6%	1.0%	0.4%	0.3%	0.6%
67	STACK East	26.3%	26.8%	4.8%	1.0%	6.4%	1.3%	8.0%	10.3%	2.5%	4.4%	4.0%	2.2%	0.6%	0.4%	0.2%	0.7%
68	STACK East	30.5%	22.0%	9.3%	1.0%	5.0%	1.0%	9.0%	10.3%	1.5%	3.0%	3.0%	2.4%	0.7%	0.5%	0.3%	0.6%
69	STACK East	25.5%	25.2%	5.3%	0.9%	7.4%	1.3%	7.8%	10.0%	2.5%	4.6%	4.5%	2.5%	0.8%	0.4%	0.5%	0.5%
70	STACK East	25.8%	29.1%	4.4%	1.0%	6.9%	1.4%	7.1%	9.3%	2.4%	4.5%	4.4%	2.1%	0.6%	0.3%	0.3%	0.5%
71	STACK East	33.7%	17.4%	6.5%	1.6%	1.8%	0.8%	13.9%	15.0%	0.7%	1.2%	1.1%	2.8%	1.2%	0.7%	0.5%	1.1%
72	STACK East	26.3%	23.7%	12.0%	0.9%	5.9%	1.1%	7.0%	9.7%	1.8%	3.3%	3.6%	3.1%	0.7%	0.3%	0.2%	0.2%
73	STACK East	34.0%	20.0%	6.7%	1.2%	3.1%	0.7%	11.0%	12.9%	1.2%	2.2%	2.3%	2.5%	0.5%	0.5%	0.4%	0.8%
74	STACK East	24.9%	26.9%	5.3%	0.9%	7.1%	1.2%	7.6%	9.8%	2.8%	4.7%	5.0%	2.1%	0.6%	0.4%	0.4%	0.2%
75	STACK East	24.7%	24.8%	5.3%	1.0%	8.9%	1.7%	6.9%	9.8%	2.4%	5.3%	5.1%	2.6%	0.5%	0.3%	0.2%	0.7%
76	STACK East	27.6%	23.3%	7.4%	1.0%	6.3%	1.3%	8.5%	10.3%	1.9%	3.7%	3.7%	2.7%	0.7%	0.5%	0.4%	0.5%
77	STACK East	27.2%	27.1%	5.9%	1.0%	5.4%	1.2%	8.4%	10.1%	2.4%	3.8%	3.9%	2.0%	0.6%	0.4%	0.3%	0.4%
78	STACK East	26.7%	27.5%	4.1%	1.0%	5.3%	1.1%	8.9%	10.7%	2.7%	3.8%	3.8%	2.0%	0.9%	0.4%	0.5%	0.5%
79	STACK East	27.4%	26.5%	5.3%	1.1%	6.7%	1.5%	7.3%	9.9%	2.2%	4.2%	4.3%	2.1%	0.5%	0.3%	0.3%	0.4%
80	STACK East	27.2%	18.8%	8.7%	0.7%	10.8%	1.8%	6.0%	8.9%	1.6%	5.6%	5.1%	3.0%	0.5%	0.2%	0.1%	1.0%

		P_1	$N_1{}^6$		$N_1{}^5$			P_2		$N_2{}^5$			P_3				
Key	Play Region	*n*-C_7	MCH	Tol	ECP	1*t*2-DMCP	1*c*2-DMCP	2-MH	3-MH	1,1-DMCP	1*c*3-DMCP	1*t*3-DMCP	2,3-DMP	2,4-DMP	2,2-DMP	3,3-DMP	3-EP
81	STACK East	25.3%	26.4%	5.2%	0.9%	7.1%	1.4%	7.5%	10.2%	2.4%	4.9%	4.8%	2.2%	0.5%	0.3%	0.3%	0.7%
82	STACK East	27.8%	25.4%	4.7%	0.9%	6.4%	1.2%	8.3%	10.5%	2.5%	4.4%	4.0%	2.2%	0.7%	0.4%	0.2%	0.6%
83	STACK East	26.7%	25.1%	4.1%	1.0%	7.4%	1.3%	8.1%	10.3%	2.4%	4.6%	4.9%	2.4%	0.5%	0.4%	0.4%	0.3%
84	STACK East	29.1%	26.2%	6.8%	1.1%	4.0%	1.0%	9.5%	10.8%	1.9%	2.8%	2.9%	2.0%	0.7%	0.5%	0.3%	0.5%
85	STACK East	25.8%	26.2%	4.2%	1.0%	8.4%	1.6%	7.1%	9.6%	2.3%	4.9%	5.0%	2.2%	0.5%	0.3%	0.3%	0.5%
86	STACK East	25.5%	25.3%	3.6%	0.9%	8.6%	1.6%	7.3%	10.3%	2.5%	5.5%	5.0%	2.2%	0.5%	0.3%	0.2%	0.8%
87	STACK East	23.1%	24.1%	7.3%	0.8%	9.7%	1.7%	6.5%	9.5%	2.2%	5.5%	5.6%	2.7%	0.4%	0.3%	0.2%	0.4%
88	STACK East	29.7%	24.6%	2.7%	0.9%	7.2%	1.5%	7.8%	10.7%	2.3%	4.4%	4.4%	2.3%	0.6%	0.3%	0.4%	0.5%
89	STACK East	25.7%	26.2%	3.4%	0.9%	8.4%	1.6%	7.4%	9.5%	2.4%	5.2%	5.1%	2.3%	0.6%	0.4%	0.4%	0.5%
90	STACK East	17.6%	21.8%	18.1%	0.6%	10.4%	1.6%	4.8%	7.5%	2.3%	5.7%	5.6%	2.8%	0.2%	0.2%	0.1%	0.6%
91	STACK East	26.1%	25.6%	5.2%	0.9%	7.7%	1.4%	7.6%	9.9%	2.3%	4.8%	4.6%	2.1%	0.4%	0.4%	0.2%	0.8%
92	STACK East	25.6%	25.0%	2.6%	0.8%	8.8%	1.6%	7.4%	10.4%	2.7%	5.5%	5.4%	2.2%	0.6%	0.3%	0.3%	0.6%
93	STACK East	22.4%	23.5%	8.1%	0.7%	11.0%	1.9%	5.8%	8.8%	1.9%	5.9%	6.1%	2.8%	0.3%	0.2%	0.1%	0.4%
94	STACK East	26.5%	24.1%	2.6%	0.8%	8.1%	1.4%	7.9%	10.7%	2.9%	5.4%	5.6%	2.3%	0.7%	0.3%	0.3%	0.5%
95	STACK East	29.2%	23.7%	4.0%	0.9%	6.4%	1.2%	8.8%	10.9%	2.4%	4.4%	4.0%	2.3%	0.7%	0.4%	0.2%	0.5%
96	STACK East	27.8%	24.2%	4.5%	0.9%	6.7%	1.3%	8.3%	10.6%	2.6%	4.6%	4.4%	2.3%	0.6%	0.4%	0.2%	0.7%
97	STACK East	27.8%	23.6%	2.2%	0.9%	8.4%	1.5%	7.8%	10.9%	2.5%	5.1%	5.4%	2.4%	0.5%	0.3%	0.4%	0.5%
98	STACK East	25.5%	24.0%	3.8%	0.9%	8.8%	1.5%	7.5%	10.2%	2.8%	5.6%	5.6%	2.3%	0.5%	0.3%	0.3%	0.5%
99	STACK East	27.8%	22.7%	2.1%	0.8%	8.6%	1.5%	8.0%	11.1%	2.5%	5.2%	5.2%	2.5%	0.7%	0.3%	0.4%	0.5%
100	STACK East	23.1%	23.4%	8.6%	0.8%	10.1%	1.8%	6.2%	9.4%	1.8%	5.3%	5.2%	2.9%	0.4%	0.2%	0.1%	0.7%
101	STACK East	23.5%	22.1%	5.9%	0.8%	11.7%	2.0%	6.2%	9.4%	2.0%	6.3%	6.2%	2.6%	0.4%	0.2%	0.1%	0.5%
102	STACK East	24.8%	25.3%	4.7%	0.9%	9.2%	1.7%	6.9%	9.5%	2.3%	5.4%	5.5%	2.3%	0.5%	0.3%	0.2%	0.5%
103	STACK East	26.3%	21.2%	2.2%	0.8%	9.5%	1.6%	8.2%	11.4%	2.6%	5.7%	5.8%	2.6%	0.9%	0.3%	0.4%	0.6%
104	STACK East	24.7%	22.4%	3.3%	0.8%	8.1%	1.5%	7.3%	10.1%	2.6%	10.4%	5.3%	2.1%	0.5%	0.3%	0.2%	0.5%
105	STACK East	24.3%	21.7%	3.8%	0.7%	11.3%	2.1%	6.8%	10.1%	2.5%	6.5%	6.0%	2.3%	0.5%	0.2%	0.2%	0.9%
106	STACK East	23.1%	23.0%	1.9%	0.8%	11.9%	2.2%	6.7%	10.2%	2.6%	6.8%	6.8%	2.3%	0.6%	0.2%	0.3%	0.6%
107	STACK East	24.6%	22.1%	3.1%	0.8%	10.9%	2.0%	7.1%	10.6%	2.5%	6.4%	6.1%	2.4%	0.3%	0.2%	0.1%	0.8%
108	STACK East	31.1%	21.0%	4.6%	0.9%	6.5%	1.3%	8.8%	11.6%	2.0%	4.2%	3.9%	2.5%	0.6%	0.3%	0.2%	0.7%
109	STACK East	31.2%	20.3%	3.8%	0.9%	7.2%	1.3%	8.6%	11.6%	1.9%	4.4%	4.3%	2.4%	0.6%	0.4%	0.2%	0.7%
110	STACK East	33.7%	20.9%	6.2%	1.2%	4.1%	1.0%	9.8%	11.9%	1.3%	2.6%	2.5%	2.3%	0.9%	0.6%	0.3%	0.7%
111	STACK East	27.3%	21.9%	3.6%	0.8%	9.2%	1.8%	7.4%	10.6%	2.3%	5.5%	5.6%	2.3%	0.6%	0.3%	0.3%	0.6%
112	STACK East	26.5%	22.5%	3.2%	0.8%	10.2%	1.9%	7.2%	10.2%	2.2%	5.6%	5.7%	2.4%	0.5%	0.3%	0.2%	0.5%
113	STACK East	24.6%	20.0%	5.8%	0.8%	11.6%	2.0%	6.6%	10.0%	1.8%	6.3%	5.9%	2.9%	0.4%	0.2%	0.3%	0.7%
114	STACK East	26.6%	22.4%	5.3%	0.9%	9.5%	1.7%	7.3%	9.9%	2.0%	5.3%	5.0%	2.3%	0.5%	0.3%	0.2%	0.7%
115	STACK East	27.9%	20.1%	5.0%	0.8%	10.3%	1.8%	7.0%	10.4%	1.5%	5.4%	5.3%	2.8%	0.5%	0.3%	0.2%	0.7%
116	STACK East	26.1%	22.8%	4.2%	0.8%	9.7%	1.8%	7.3%	10.2%	2.0%	5.5%	5.5%	2.4%	0.6%	0.3%	0.2%	0.6%
117	STACK East	26.9%	19.9%	3.7%	0.8%	11.1%	2.1%	7.1%	10.7%	1.8%	6.0%	5.9%	2.7%	0.3%	0.3%	0.2%	0.7%
118	STACK East	26.0%	21.7%	4.9%	0.9%	10.5%	1.9%	7.1%	9.9%	1.8%	5.5%	5.4%	2.5%	0.6%	0.3%	0.2%	0.8%
119	STACK East	27.6%	20.0%	4.5%	0.9%	10.5%	1.9%	7.4%	10.5%	1.7%	5.4%	5.3%	2.5%	0.4%	0.4%	0.2%	0.8%
120	SCOOP	34.1%	15.3%	4.8%	0.9%	6.9%	1.4%	9.2%	13.5%	1.1%	4.0%	3.9%	2.9%	0.5%	0.3%	0.2%	0.9%

		P_1	N_1^6		N_1^5			P_2		N_2^5			P_3				
Key	Play Region	*n*-C_7	MCH	Tol	ECP	1*t*2-DMCP	1*c*2-DMCP	2-MH	3-MH	1,1-DMCP	1*c*3-DMCP	1*t*3-DMCP	2,3-DMP	2,4-DMP	2,2-DMP	3,3-DMP	3-EP
121	SCOOP	28.5%	17.8%	9.4%	2.2%	1.3%	0.9%	14.5%	15.6%	0.5%	0.8%	0.6%	3.5%	1.6%	0.8%	0.8%	1.4%
122	SCOOP	30.4%	18.4%	9.3%	1.8%	1.5%	0.8%	13.4%	15.1%	0.6%	0.9%	0.8%	3.1%	1.4%	0.7%	0.6%	1.3%
123	SCOOP	28.0%	21.8%	10.6%	1.8%	1.7%	0.9%	12.5%	13.6%	0.7%	1.1%	1.0%	2.6%	1.3%	0.7%	0.7%	1.0%
124	SCOOP	20.8%	28.2%	3.8%	1.0%	7.8%	1.5%	8.0%	10.5%	3.7%	5.5%	5.4%	2.0%	0.7%	0.4%	0.2%	0.4%
125	SCOOP	23.2%	26.0%	7.1%	1.2%	5.9%	1.2%	9.0%	11.2%	2.7%	4.1%	4.0%	2.3%	0.7%	0.5%	0.3%	0.6%
126	SCOOP	33.7%	17.7%	3.1%	1.1%	5.6%	1.2%	10.0%	14.0%	1.4%	3.4%	3.5%	2.9%	0.8%	0.3%	0.3%	0.8%
127	SCOOP	34.4%	17.4%	3.6%	1.0%	5.7%	1.2%	10.1%	13.8%	1.2%	3.3%	3.2%	2.8%	0.7%	0.3%	0.3%	1.1%
128	SCOOP	33.3%	19.1%	2.9%	1.1%	5.0%	1.1%	10.7%	13.9%	1.4%	3.1%	2.9%	2.9%	0.9%	0.4%	0.4%	1.0%
129	SCOOP	34.1%	18.2%	3.2%	1.1%	5.0%	1.1%	10.6%	14.0%	1.4%	3.1%	2.9%	2.8%	0.9%	0.4%	0.3%	1.0%
130	SCOOP	35.4%	19.2%	4.4%	1.1%	0.1%	1.0%	11.3%	14.5%	1.5%	3.0%	2.9%	2.9%	0.9%	0.4%	0.3%	1.0%
131	SCOOP	32.6%	19.7%	3.6%	1.1%	5.0%	1.1%	10.4%	13.3%	1.7%	3.3%	3.3%	2.7%	0.8%	0.4%	0.3%	0.8%
132	SCOOP	20.7%	26.3%	4.8%	1.1%	7.3%	1.4%	9.6%	10.3%	3.6%	5.6%	5.1%	2.2%	0.7%	0.5%	0.3%	0.6%
133	SCOOP	33.9%	18.4%	3.7%	1.0%	4.8%	1.1%	10.6%	13.9%	1.4%	3.1%	3.1%	2.8%	0.7%	0.3%	0.3%	0.8%
134	SCOOP	23.5%	28.2%	5.4%	1.2%	5.2%	1.1%	9.8%	11.4%	2.7%	3.6%	3.6%	2.2%	0.9%	0.6%	0.3%	0.3%
135	SCOOP	33.2%	17.8%	2.9%	1.0%	6.0%	1.2%	10.1%	13.7%	1.5%	3.7%	3.7%	2.9%	0.8%	0.3%	0.3%	1.0%
136	SCOOP	34.8%	17.1%	2.7%	1.0%	5.4%	1.2%	10.2%	14.2%	1.3%	3.3%	3.5%	2.9%	0.8%	0.3%	0.3%	0.8%
137	SCOOP	35.0%	17.8%	3.7%	1.0%	5.4%	1.1%	9.8%	13.7%	1.2%	3.2%	3.1%	2.8%	0.7%	0.3%	0.3%	1.0%
138	SCOOP	35.0%	17.0%	4.6%	0.9%	4.9%	1.2%	10.2%	13.9%	1.2%	3.0%	3.0%	2.8%	0.7%	0.3%	0.2%	0.9%
139	SCOOP	35.5%	17.9%	4.6%	1.0%	4.0%	0.9%	10.8%	13.8%	1.2%	2.6%	2.6%	2.8%	0.8%	0.3%	0.2%	1.0%
140	SCOOP	36.2%	17.1%	4.1%	1.0%	3.8%	0.9%	11.1%	14.4%	1.2%	2.5%	2.5%	2.8%	0.9%	0.3%	0.2%	1.1%
141	SCOOP	35.8%	16.6%	3.1%	0.9%	5.2%	1.1%	10.6%	14.5%	1.1%	2.9%	2.9%	2.8%	0.8%	0.3%	0.3%	1.0%
142	SCOOP	35.4%	16.7%	4.4%	0.9%	4.6%	1.0%	10.6%	14.4%	1.2%	2.9%	2.8%	2.9%	0.8%	0.3%	0.3%	1.0%
143	SCOOP	35.5%	16.2%	3.4%	0.9%	4.9%	1.1%	10.6%	14.7%	1.2%	3.0%	3.1%	3.0%	0.9%	0.3%	0.3%	0.9%
144	SCOOP	34.1%	16.3%	4.0%	0.9%	6.2%	1.3%	9.6%	14.1%	1.3%	3.6%	3.6%	2.9%	0.7%	0.3%	0.3%	1.1%
145	SCOOP	32.7%	18.0%	3.4%	0.9%	6.4%	1.3%	9.5%	13.4%	1.5%	3.9%	4.1%	2.7%	0.7%	0.3%	0.3%	0.8%
146	SCOOP	33.2%	18.4%	3.9%	0.9%	5.6%	1.1%	9.9%	13.4%	1.6%	3.6%	3.7%	2.7%	0.6%	0.3%	0.3%	0.7%
147	SCOOP	32.0%	20.4%	3.7%	0.9%	5.6%	1.1%	9.7%	12.6%	1.9%	3.7%	3.7%	2.6%	0.7%	0.3%	0.3%	0.8%
148	SCOOP	35.3%	17.4%	3.7%	1.0%	4.6%	1.0%	10.5%	14.2%	1.3%	2.9%	3.0%	2.8%	0.8%	0.3%	0.3%	0.8%
149	SCOOP	36.2%	16.9%	4.4%	0.9%	4.9%	1.1%	10.4%	13.8%	1.1%	2.7%	2.6%	2.9%	0.7%	0.3%	0.3%	0.9%
150	SCOOP	33.5%	19.6%	7.2%	1.3%	2.5%	0.8%	11.9%	13.4%	1.0%	1.6%	1.5%	2.7%	1.1%	0.6%	0.4%	0.9%
151	SCOOP	38.3%	19.2%	6.3%	1.4%	2.9%	0.9%	10.0%	12.4%	0.8%	1.6%	1.7%	2.4%	0.7%	0.3%	0.3%	0.9%
152	SCOOP	37.2%	15.8%	4.7%	0.9%	4.9%	1.0%	10.2%	14.1%	0.9%	2.7%	2.5%	2.9%	0.7%	0.3%	0.3%	1.1%
153	SCOOP	38.5%	15.4%	5.2%	1.1%	3.0%	0.8%	11.7%	14.6%	0.7%	1.7%	1.6%	2.8%	0.9%	0.4%	0.3%	1.3%
154	SCOOP	33.5%	18.7%	5.5%	0.9%	5.3%	1.1%	9.6%	12.9%	1.4%	3.1%	3.1%	2.6%	0.8%	0.3%	0.3%	0.8%
155	SCOOP	17.6%	17.4%	1.7%	0.9%	16.1%	2.9%	6.3%	11.0%	3.6%	9.6%	9.3%	2.3%	0.2%	0.2%	0.2%	0.8%
156	SCOOP	19.1%	29.6%	4.5%	1.0%	7.7%	1.6%	7.8%	10.2%	3.8%	5.7%	5.5%	1.9%	0.5%	0.4%	0.3%	0.4%
157	SCOOP	14.2%	36.1%	27.0%	1.7%	2.3%	1.1%	5.2%	5.8%	0.9%	1.4%	1.5%	1.2%	0.5%	0.4%	0.3%	0.3%
158	SCOOP	13.8%	36.1%	26.3%	1.6%	2.4%	1.1%	5.5%	6.2%	1.0%	1.5%	1.5%	1.3%	0.5%	0.5%	0.4%	0.3%
159	SCOOP	35.1%	16.0%	5.2%	0.8%	6.6%	1.3%	9.1%	13.6%	0.9%	3.3%	3.5%	2.8%	0.6%	0.2%	0.2%	0.8%
160	SCOOP	19.3%	31.0%	6.7%	1.2%	6.0%	1.2%	9.1%	10.2%	3.2%	4.2%	4.2%	1.8%	0.7%	0.6%	0.3%	0.3%

		P_1	N_1^6		N_1^5			P_2		N_2^5			P_3				
Key	Play Region	*n*-C_7	MCH	Tol	ECP	1*t*2-DMCP	1*c*2-DMCP	2-MH	3-MH	1,1-DMCP	1*c*3-DMCP	1*t*3-DMCP	2,3-DMP	2,4-DMP	2,2-DMP	3,3-DMP	3-EP
161	SCOOP	23.2%	26.9%	5.6%	1.2%	5.4%	1.1%	9.7%	11.8%	2.9%	3.8%	3.8%	2.4%	0.8%	0.5%	0.3%	0.5%
162	SCOOP	20.7%	30.7%	6.3%	1.3%	5.5%	1.2%	9.3%	10.3%	3.0%	3.8%	3.7%	1.9%	0.9%	0.7%	0.3%	0.4%
163	SCOOP	12.1%	25.5%	33.2%	2.7%	1.4%	1.2%	8.4%	8.1%	0.6%	0.9%	0.9%	1.7%	1.1%	0.9%	0.7%	0.5%
164	SCOOP	21.6%	28.3%	9.2%	1.5%	4.1%	1.0%	10.5%	10.9%	2.2%	2.8%	2.9%	2.0%	1.2%	0.9%	0.5%	0.4%
165	SCOOP	21.5%	29.6%	6.4%	1.2%	5.7%	1.2%	9.0%	10.2%	3.1%	4.0%	4.0%	2.0%	0.7%	0.6%	0.4%	0.4%
166	SCOOP	21.4%	29.2%	4.6%	1.0%	7.0%	1.2%	8.1%	10.2%	3.3%	4.8%	4.9%	2.0%	0.8%	0.5%	0.3%	0.6%
167	SCOOP	21.3%	30.6%	6.5%	1.3%	5.0%	1.2%	9.7%	10.3%	2.7%	3.5%	3.5%	1.9%	1.0%	0.7%	0.4%	0.4%
168	SCOOP	20.6%	27.6%	6.8%	1.0%	7.2%	1.4%	7.7%	10.0%	3.6%	5.1%	5.0%	2.2%	0.6%	0.5%	0.3%	0.4%
169	SCOOP	29.9%	14.6%	4.9%	0.9%	11.2%	2.2%	7.7%	12.7%	0.8%	5.6%	5.3%	2.6%	0.4%	0.2%	0.1%	1.0%
170	SCOOP	21.8%	28.7%	6.2%	1.0%	6.5%	1.3%	8.1%	10.1%	3.2%	4.7%	4.6%	1.9%	0.7%	0.5%	0.3%	0.4%
171	SCOOP	20.6%	27.8%	4.5%	0.9%	8.7%	1.6%	6.9%	9.9%	3.9%	6.0%	5.9%	1.9%	0.6%	0.4%	0.2%	0.3%
172	SCOOP	31.0%	21.9%	10.7%	2.0%	2.1%	1.0%	10.9%	11.9%	0.8%	1.3%	1.2%	2.4%	1.0%	0.5%	0.4%	0.9%

Table 11. Light hydrocarbon isomers of heptane used in this chapter as a percentage of their sum. Compound identification shown previously in Figure 35 and Table 7. Groupings with labels “P” and “N” at top of table refer to light hydrocarbons which share a common parent or formation mechanism within the hydrocarbon kinetic scheme as described in Figure 55 and in the adjoining text.

The relative abundance of *n*-C_7, MCH, and Tol as a percentage of their sum is plotted as a ternary diagram in Figure 53. Woodford-produced oils contain slightly more *n*-C_7 than Mississippian-produced oils but cluster primarily by Play Region. Oils in STACK West are notably enriched in Tol compared to SCOOP and STACK East, sometimes quantified by the parameter "aromaticity" and defined in this study as the peak area ratio of Tol to the sum of *n*-C_7 and MCH. Aromaticity in this study was modified from B-Aromaticity (Tol/*n*-C_7) defined in Thompson (1983). In map view, a NE-SW trending transition from low (<0.10) to high (>0.20) aromaticity is observed in central Blaine and northwestern Kingfisher counties (Figure 54).

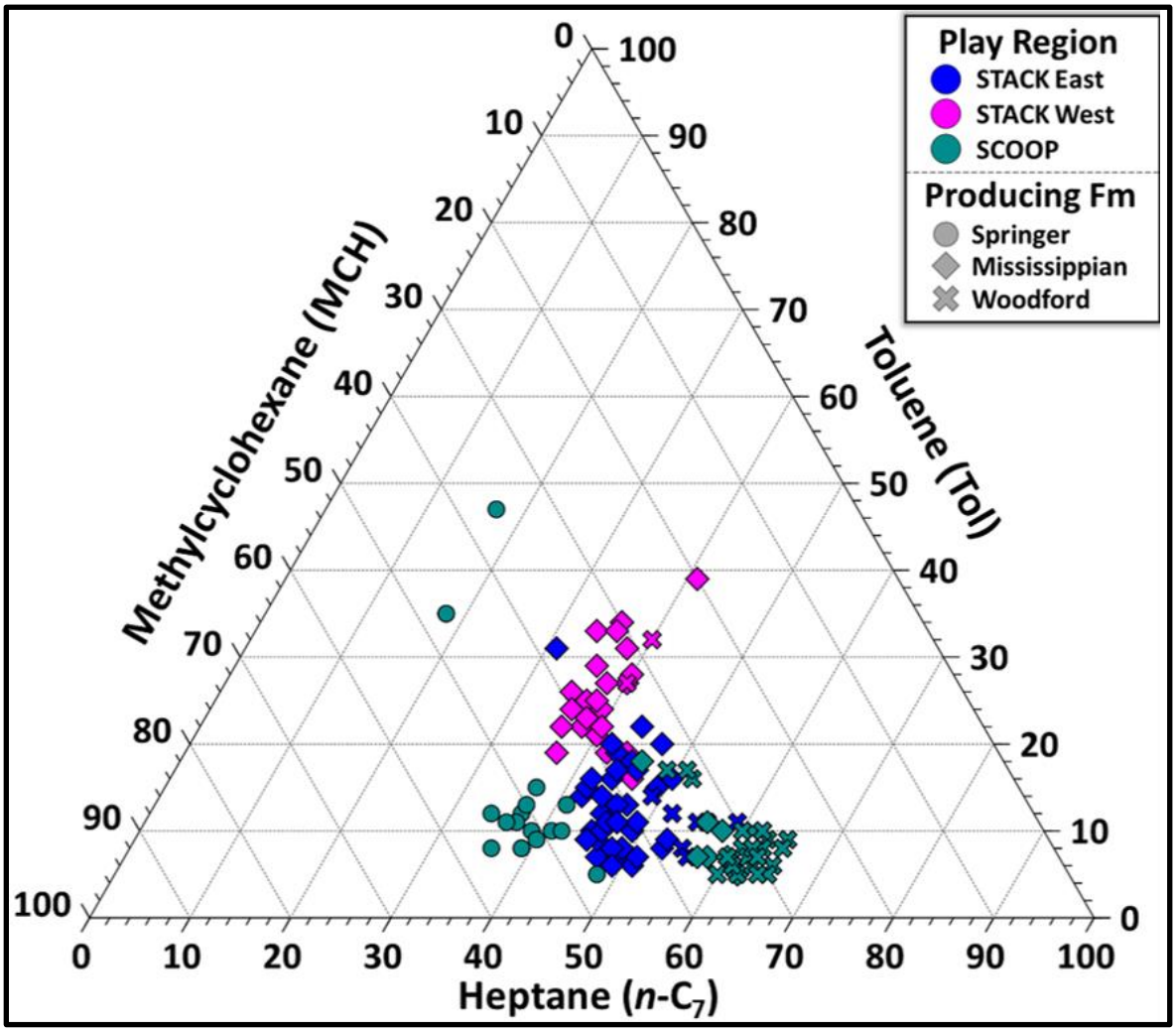

Figure 53. Ternary diagram showing the percent abundances of *n*-C_7, MCH, Tol as a percentage of the sum of the three. STACK West oils are comparably enriched in Tol while SCOOP has two distinct clusters separating Springer production from Mississippian/Woodford production based on the relative abundances of *n*-C_7 and MCH.

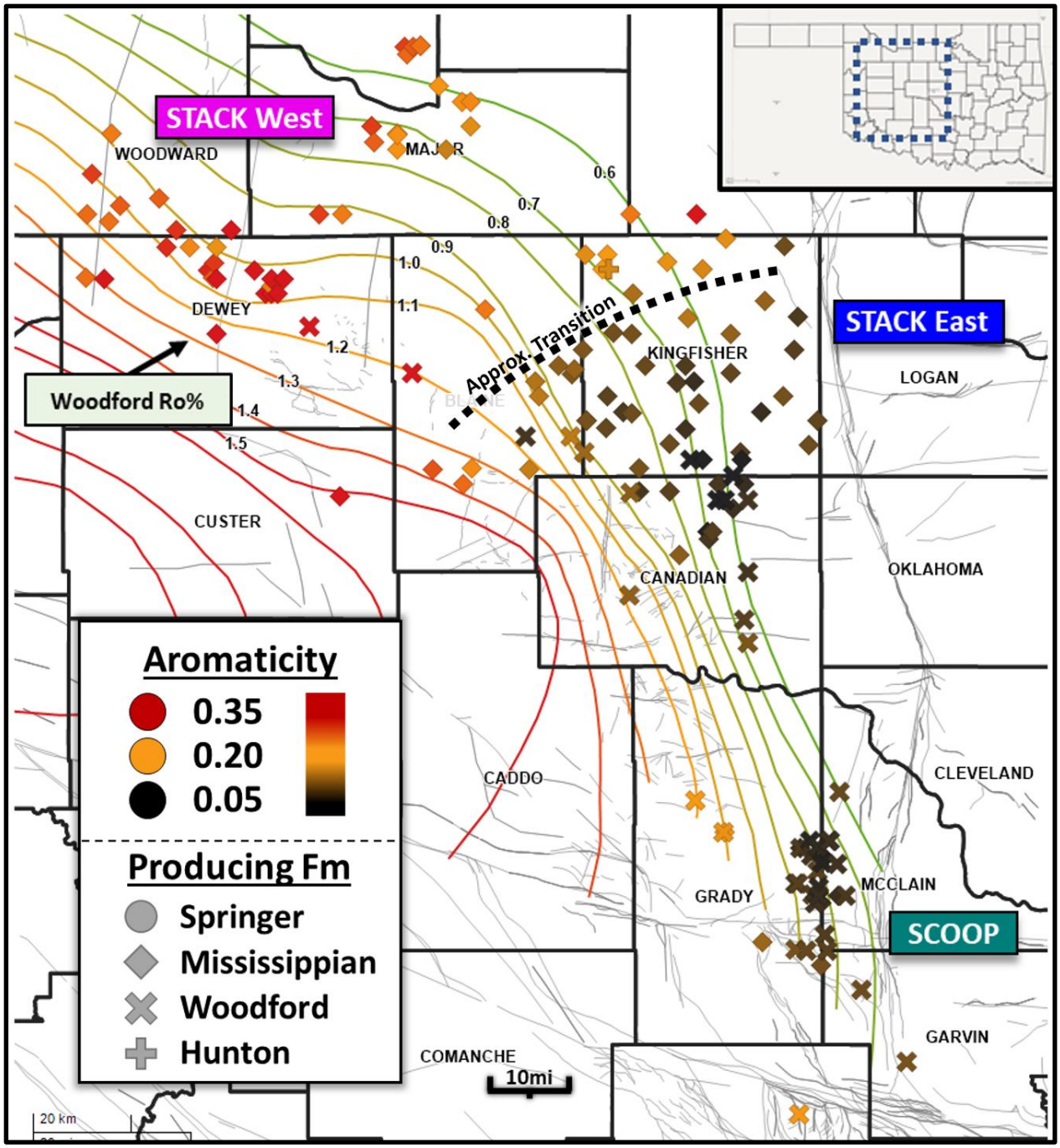

Figure 54. Map of aromaticity values across STACK and SCOOP. STACK West oils contain elevated aromaticity compared to the other Play Regions with the approximate transition occurring in central Blaine and northwest Kingfisher counties. Aromaticity=Tol/(*n*-C_7+MCH) which is modified from B-Aromaticity (Thompson, 1983).

Generally, oils with high aromaticity values have been associated with Type III organic matter rich in cellulose and lignin (Connan and Cassou, 1980; Tissot and Welte, 1984). However, free sulfur radicals (e.g., HS^-, HS_x) present during diagenesis and catagenesis have been shown to facilitate the dehydrogenation (oxidation) of saturate hydrocarbons which can form Tol and other alkyl-benzenes through the cyclization and aromatization of *n*-alkanes (Orr, 1974; Sinninghe Damsté et al., 1991, 1993). In the Williston Basin, oils generated from the sulfur-rich Madison Group have much higher aromaticity values (0.60±0.08, n=38) compared to oils produced from the Bakken marine shale (0.14±0.01, n=19) despite no evidence of terrigenous organic matter input (Jarvie, 2001). By contrast, low aromaticity can be indicative of post-generative processes like water washing, migrational fractionation, seal leakage, or long distance migration (Leythaeuser et al., 1983; Thompson, 1988; Halpern, 1995; Jarvie, 2001). Woodford-sourced oils in Kansas and on the Cherokee Platform often lack observable Tol peaks as a result of long-distance migration out of the Anadarko Basin (Burruss and Hatch, 1989; Atwah et al., 2019; Tamborello, 2020).

Light hydrocarbons can also be grouped by the kinetic mechanisms governing their formation. Mango (1990a) observed that several light hydrocarbon groups are always observed in proportional amounts similar to what is observed in steady-state kinetic equilibriums between parent-daughter pairs. If light hydrocarbons are formed in steady-state, then the ratio of reactants to products will be controlled by temperature, pressure, and the presence of catalyzing agents (Mango, 1992, 1994, 1997). The ratio between parent-daughter pairs would remain proportional for source-related oils, but possibly different from oils from a different source. For these purposes, "source-related" refers to oils generated and expelled from the same source rock with similar structural kerogens at different stages of maturity. The kinetic scheme for isomers of heptane organized by ring closure during intermediate steps of formation is shown in Figure 55.

Light hydrocarbons are rarely preserved in source rock extracts, but the kinetic controls on light hydrocarbons can still facilitate oil/oil correlation (e.g. ten Haven, 1996; Obermajer et al., 2000; Jarvie, 2001). For example, an oil enriched in methylhexanes would indicate a kinetic preference for three-ring closures since the skeletal isomerization to branched isomers proceeds through three-carbon ring intermediates (i.e. cyclopropane; Mango, 1987). Steady-state reactions occur in both directions, so the concentration of each parent-daughter pair is controlled both by their respective rate of formation but also the rate of conversion to other intermediaries or products.

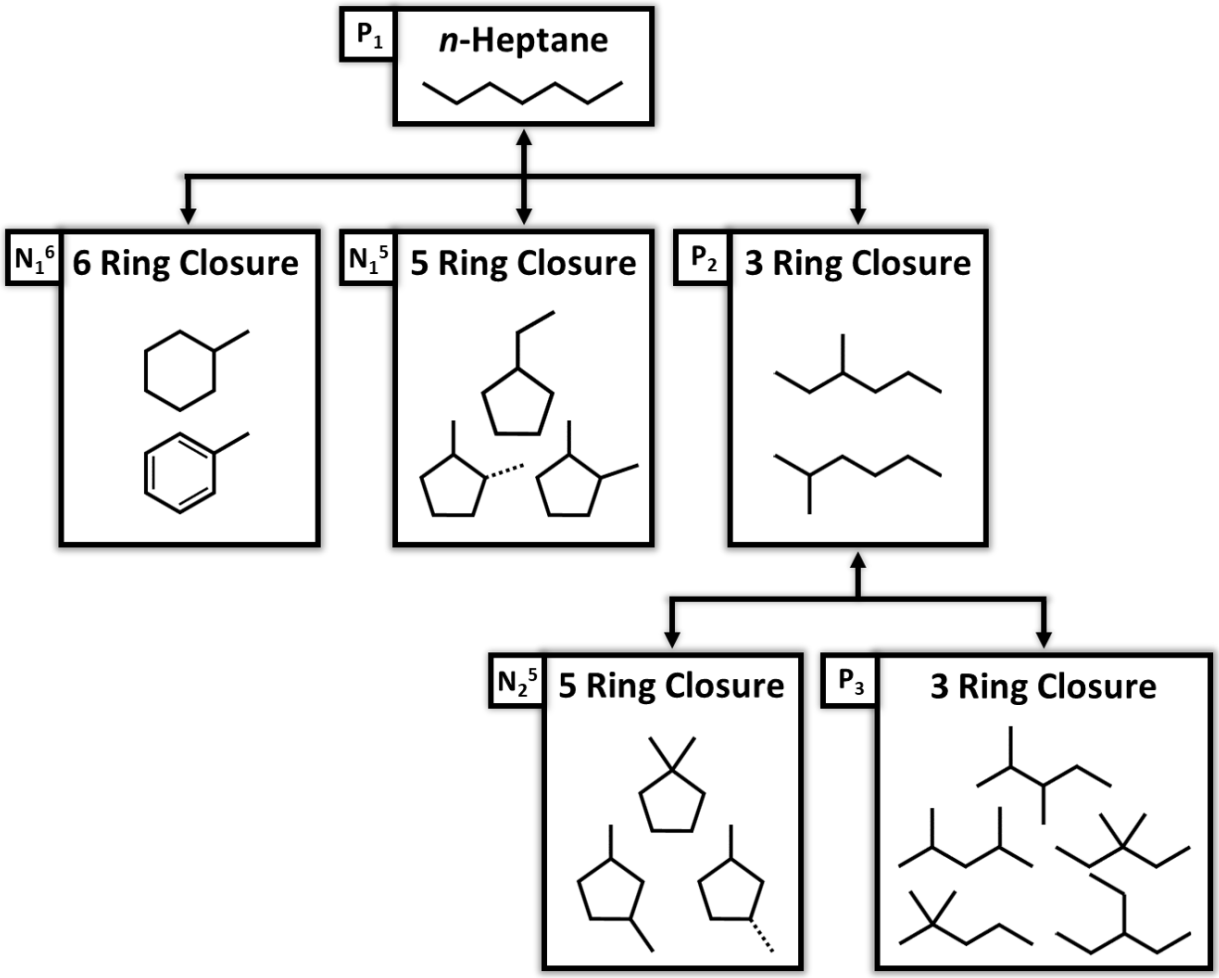

Figure 55. A schematic representation of the light hydrocarbon kinetic model at C_7 by the number of carbon ring in the intermediate structure. The connecting lines represent two-way reactions controlled by steady state catalysis rather than thermolysis. At steady state, the abundance of each grouping is controlled by temperature, pressure, and catalyzing agents. Groups "P" indicate parent compounds or are formed by opening three-ring closure. Group "N" are cyclic compounds where the superscript gives the believed number of carbons in ring closure of the intermediary product. Recreated and modified from Mango, 1994.

The most striking examples of Mango's kinetic scheme (see Figure 55) relates 2-MH and 3-MH and their 2,3-DMP and 2,4-DMP daughter products in along 3-ring closure/opening pathway ($P_2 \rightarrow P_3$), known as K_1, which remains constant near unity in Equation 11 (Mango, 1987):

$$K_1 = \frac{(2\text{–methylhexane}) + (2,3\text{–dimethylpentane})}{(3\text{–methylhexane}) + (2,4\text{–dimethylpentane})} \cong 1 \qquad \text{Equation 11}$$

The Mango K_1 crossplot formed by plotting the numerator against the denominator for all STACK data (Figure 56) shows strong invariance around unity. STACK West oils tend to plot slightly above unity while STACK East oils tend to plot below suggesting that K_1 may be an effective parameter in this dataset for successfully differentiating oils derived from different organic facies. In some cases, sets of oils with K_1 values above unity have been associated with catalytic conditions conducive to thermochemical sulfate reduction (TSR) and the production of H_2S gas (ten Haven, 1996; Peters and Fowler, 2002).

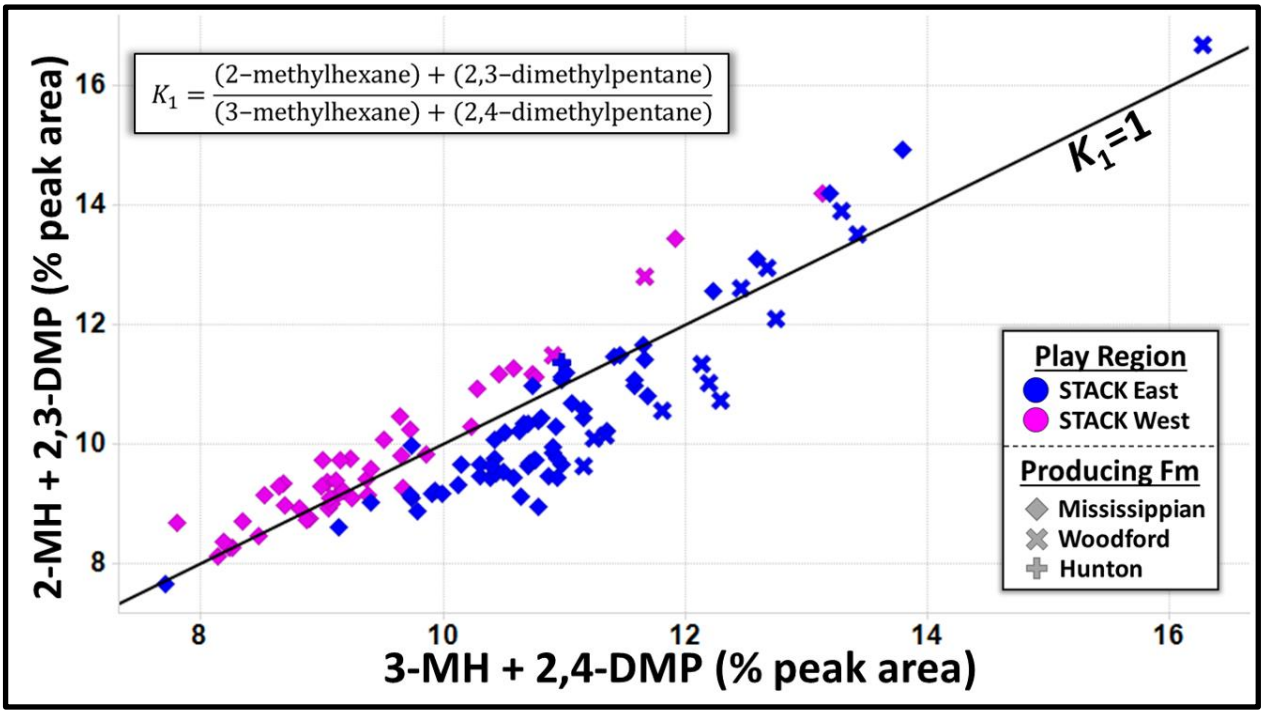

Figure 56. Mango K_1 crossplot showing general invariance in isoheptanes. STACK West generally plots above the line K_1=1 and STACK East generally plot below. The term K_1 may be effective for oil-oil correlation in this dataset.

Mango (1990a) predicted a second term K_2 which would theoretically remain constant between source-related oils. In steady-state, the ratio of rate constants from a common parent is proportional to the ratio of their products, so if the rate constants for forming rings of the same carbon number are proportional then the ratio of their respective products would share the same proportionality. If true, then of K_2 should reflect the catalytic activity in a source rock and can be calculated whereby the methylhexanes in P_2, the dimethylpentanes in P_3, and the dimethylcyclopentanes in N_2^5 are dependent variables as shown in Equation 12:

$$K_2 = \frac{P_3}{P_2 + N_2^5} \qquad \text{Equation 12}$$

The plot of K_2 for all STACK oils is shown in Figure 57 showing two clusters of STACK oils by Play Region. Interestingly, proportionality in K_2 is not observed, possibly because of catalyzing substrates from other geologic materials like clays, metals, and sulfides; however, the ratio does appear effective for differentiating between STACK East and West oils.

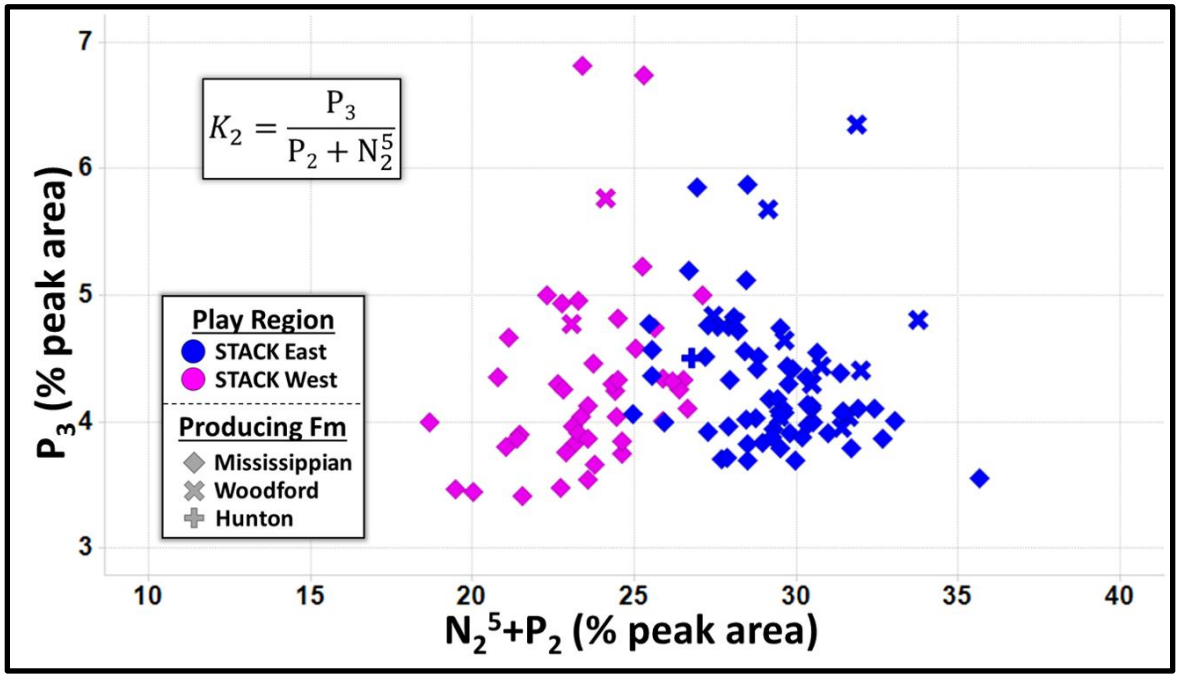

Figure 57. Crossplot derivation of the kinetic constant K_2 shows two clusters of STACK oils primarily along the X-axis representing $N_2^5+P_2$ as a percentage of light hydrocarbon peak area. The theorized invariance of K_2 is not observed. P_3=2,3-DMP+2,4-DMP+3,3-DMP+3-EP; N_2^5=1,1-DMCP+1*c*3-DMCP+1*t*3-DMCP; P_2=2-MH+3-MH.

Alternatively, it is possible to derive a selectivity ratio between daughter products sourced from a common parent as long as their respective rate constants are free to change independently with reaction conditions. Mango (1990a) proposed a "Ring Preference" ratio defined as P_2 over (P_3/N_2^5) to measure the carbon number preference of the rings formed by intermediary compounds as parent methylhexanes (P_2) compounds react to form three-ring (P_3) and five-ring (N_2^5) daughter products. Ring Preference has proven useful to discriminate between homologous sets of oils (e.g. ten Haven, 1996; Obermajer et al., 2000; Huang et al., 2014). Parent-daughter selectivity for methylhexanes (P_2) for all STACK oils is shown in Figure 58 and shows two trends which cluster according to Play Region and show no separation by producing reservoir. In general, oils from STACK West exhibit a preference for the three-ring closure daughter product pathway (P_3) compared to STACK East. Based on these findings, the measure of P_2 daughter selectivity may be an effective correlation parameter for discerning homologous sets of oil in STACK.

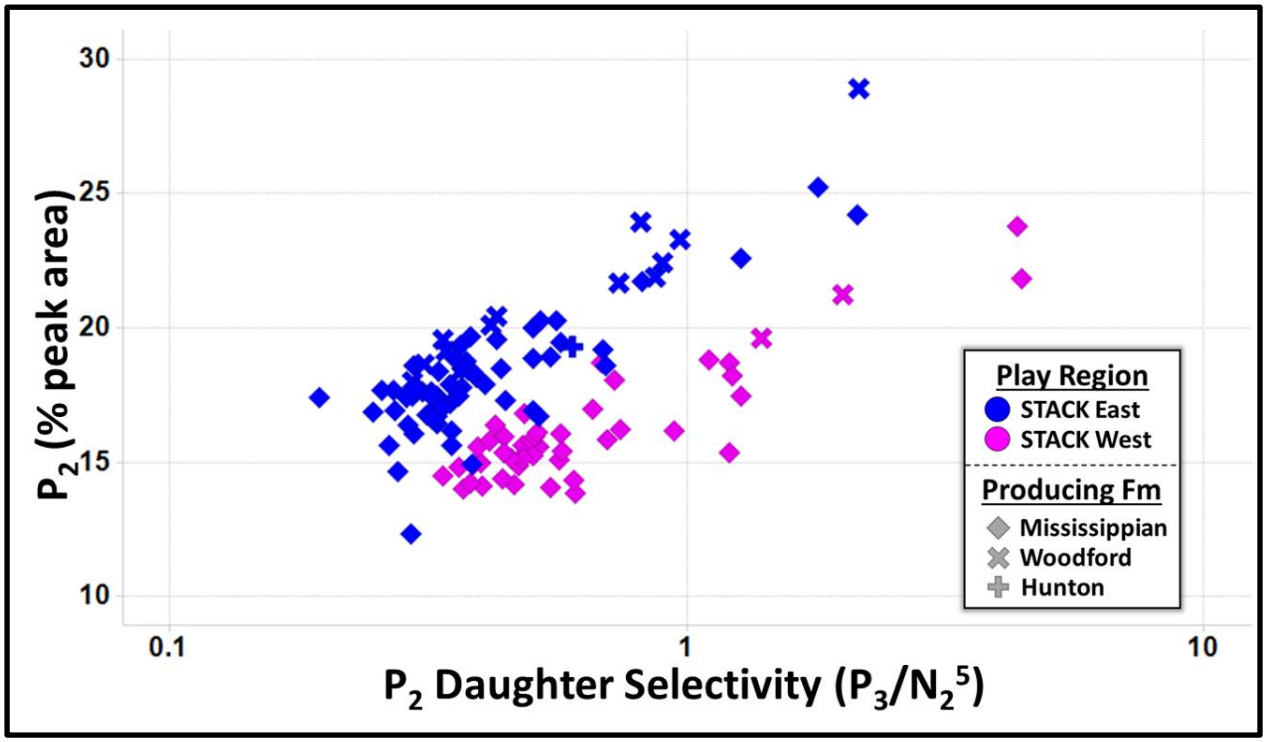

Figure 58. Parent-daughter selectivity for 2-MH and 3-MH (P_2) based on kinetic scheme in Figure 55. STACK West shows a preference for branched isoalkanes in P_3, while STACK East exhibits a preference for cyclopentanes in N_2^5. P_2=2-MH+3-MH; P_3=2,3-DMP+2,4-DMP+3,3-DMP+3-EP; N_2^5=1,1-DMCP+1*c*3-DMCP+1*t*3-DMCP.

The kinetic model can be summarized more broadly by summing each of the 3-ring, 5-ring, and 6-ring closure reaction products into a single ternary diagram (Figure 59). Again, STACK oils appear to cluster separately based primarily on Play Region. STACK West oils have a higher fractional abundance of 6-ring closure compounds due to its elevated toluene concentration in exchange for lower fractional abundance of 5-ring closure compounds. Interestingly, all STACK oils have approximately equal 3-ring closure compounds except Woodford-produced oils generally have higher amounts compared to Mississippian-produced oils across both Play Regions.

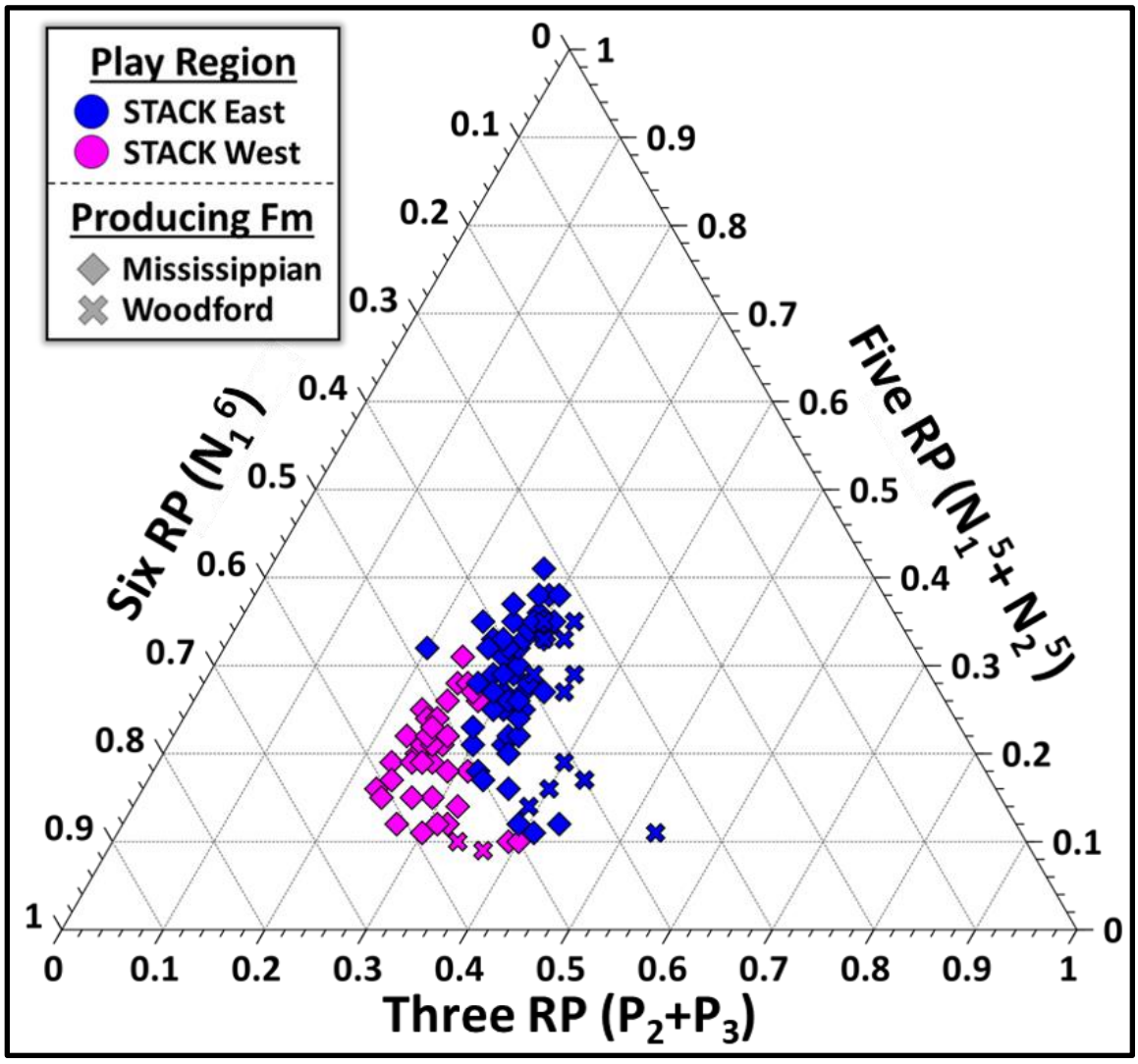

Figure 59. Ternary diagram showing the fractional abundance of ring preference (RP) products for all STACK oils. Oils in STACK West generally exhibit higher Six RP compared to STACK East oils, likely driven by higher abundances of Tol. Six RP=MCH+Tol; Five RP=ECP+1*t*2-DMCP+1*c*2-DMCP+1,1-DMCP+1*c*3-DMCP+1*t*3-DMCP; Three RP=2-MH+3-MH+2,3-DMP+2,4-DMP+2,2-DMP+3,3-DMP+3-EP.

In summary, light hydrocarbon ratios in STACK appear to form clusters representative of two separate homologous sets of oils distinguished primarily by Play Region. STACK West oils are substantially enriched in toluene compared to STACK East oils by up to a factor of five, and a map of aromaticity shows the transition between low- and high-aromaticity oils occurs in central Blaine and northwestern Kingfisher counties. The transition to higher toluene concentration in STACK West oils may correspond to the presence of non-mineral sulfur which could act as a catalyst for dehydrogenation reactions resulting in cyclization and aromatization of paraffins. If true, the enrichment of Tol in STACK West may reflect changing sedimentation or depositional environments between the two Play Regions, especially in the amount of sedimentary iron which is a sulfur sink during early diagenesis. This possibility will be explored more fully in Chapter VI.

STACK oils also form separate clusters in source-parameters derived from the kinetics of light hydrocarbon formation. The catalytic processes which govern carbocyclic ring-closure in steady state are strongly affected by the presence of metals, its oxidation state, and the structures of the surrounding ligands. Given the mineral complexity of many unconventional petroleum systems, it is reasonable to anticipate catalytic activity from a number of transition metals in sedimentary rocks, including Ni, V, Ti, Fe, Mo, Cr, and Co. Therefore the kinetic scheme which dictates the composition of light hydrocarbons is likely an indicator of lithology. Kerogen structure could also play a key role in controlling the light hydrocarbon formation by imposing enzyme-like kinetic preferences on them, thereby directing the flow of reaction along a specific carbocyclic pathway. Whichever explanation is true, the relative abundance of light hydrocarbons in STACK oils are probably controlled by source-specific variables linked directly to depositional environment and organic matter type. Light hydrocarbons will be an important variable when determining the organic facies in STACK at the end of this section.

Steranes

Sterols are essential components of the cell membranes of all eukaryotic life and have been studied extensively in microalgae, yeasts, fungi, protozoans, and microheterotrophs (Mackenzie et al., 1982; Volkman, 1986, 2003). There are four main families of 4-desmethyl sterols containing between C_{27}-C_{30} carbon skeletons depending on the length of the side chain at the C-24 position (Figure 60).

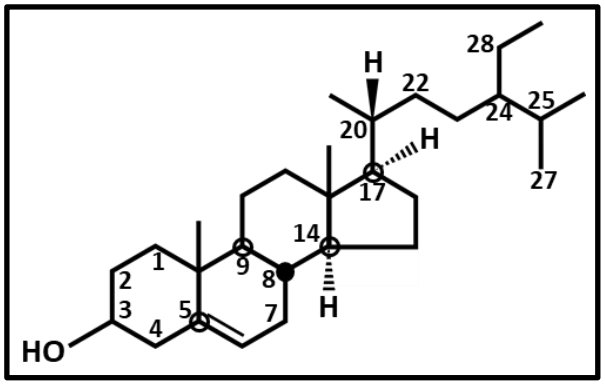

Figure 60. Generalized carbon skeleton of a C_{29} sterol. Additional methyl groups can be found at positions C-4, C-14, and C-23. Methyl, ethyl, or propyl groups occur at position C24 (denoted by R). Double bonds may be found at C-5, C-7, C-8, C-8(14), C-22, C-24, C-24(28), and C-25(27). From Volkman (2003).

The remarkable diversity in microalgal classes, genera, and species combined with the long evolutionary history of most microalgae has resulted in an equally diverse sterol distribution in the biosphere (Huang and Meinschein, 1979; Seifert and Moldowan, 1981; Raederstorff and Rohmer, 1984; Summons and Capon, 1991; Dahl et al., 1992; Volkman et al., 1994; Volkman, 2003).

While sterols are ubiquitous among eukaryotes, it can be difficult to assign any particular sterol to a single group of organisms because identical hydrocarbon skeletons may be synthesized by phylogenetically diverse taxa. In modern biomass, sterols can exhibit taxonomically specific patterns of unsaturation and functional groups, but the diagenetic transformation of sterols into steranes causes many of these identifying features to be lost. It is generally believed that C_{27} and C_{28} sterols are derived mainly from algae, while C_{29} sterols are more typically associated with land plants (Huang and Meinschein, 1979; Philp, 1985; Volkman, 1986), but there are numerous exceptions to this rule including several microorganisms which produce multiple types of sterols (i.e. Volkman, 2003). Intuitively, the prominence of C_{29} sterols in pre-Silurian oils would suggest

other sources have existed long before higher plant life evolved (Grantham and Wakefield, 1988). In fact, one of the two main classes of green algae, Prasinophyceae, is a major constituent of marine phytoplankton and produces abundant C_{29} sterols (Volkman, 1986; Volkman et al., 1994), and at least one study of modern coastal waters concludes that most present-day C_{29} sterol is actually of marine origin (Pearson and Eglinton, 2000). Given the vast diversity of microorganisms in modern and ancient oceans, sterol data should be interpreted as a unique fingerprint of benthic and pelagic life within oceanic ecosystems and cautiously applied as a deterministic measure of depositional environment, lithology, or the metabolic processes of its living inhabitants.

Huang and Meinschein (1979) observed that the relative abundances of C_{27}-C_{29} sterols could act as a biodiversity fingerprint for ancient ecosystems, and hypothesized that the distribution of C_{27}-C_{29} steranes might mirror their sterol precursors because the diagenetic changes are mostly limited to the hydrogenation of double bonds and defunctionalization of the hydroxyl group at C-3. Mackenzie et al. (1983) argued that the relative abundance of C_{27}-C_{29} steranes when measured by high resolution GC-MS would greatly improve efforts to determine organic matter type and source rocks. Moldowan et al. (1985) advanced this hypothesis by developing a ternary diagram populated by the relative abundance of 5α(H),14α(H),17α(H) 20R C_{27}-C_{29} steranes with interpreted zones for various depositional environments, but there is significant overlap between the designated zones which limit its applicability.

The recreation of the ternary diagram containing the relative abundance of $C_{27\text{-}29}$ regular steranes is illustrated in Figure 61 using sterane data in Table 12. Similar to many previously reviewed light hydrocarbon parameters, sample oils in STACK cluster primarily by Play Region, and producing reservoir is not a determinative factor in regular sterane distribution suggesting oils in Woodford and Mississippian reservoirs may share a common source.

Key	Play Region	Rc%	%C_{27} Sterane[1]	%C_{28} Sterane[2]	%C_{29} Sterane[3]	C_{30} Sterane Index[4]	Diasteranes/Total Steranes[5]
1	STACK West	0.81	0.29	0.19	0.52	0.03	0.41
2	STACK West	0.80	0.30	0.18	0.52	0.03	0.40
3	STACK West	0.81	0.29	0.19	0.53	0.03	0.49
4	STACK West	0.82	0.23	0.21	0.57	0.04	0.44
5	STACK West	0.81	0.29	0.19	0.52	0.03	0.43
6	STACK West	0.81	0.32	0.18	0.50	0.06	0.49
7	STACK West	0.79	0.22	0.22	0.56	0.04	0.37
8	STACK West	0.78	0.32	0.18	0.50	0.04	0.46
9	STACK West	0.80	0.26	0.21	0.53	0.04	0.45
10	STACK West	0.83	0.31	0.21	0.48	0.04	0.39
11	STACK West	0.79	0.24	0.20	0.55	0.04	0.39
12	STACK West	0.82	0.30	0.20	0.50	0.03	0.42
13	STACK West	0.80	0.30	0.19	0.52	0.03	0.40
14	STACK West	0.82	0.30	0.20	0.50	0.04	0.42
15	STACK West	0.80	0.32	0.19	0.49	0.05	0.45
16	STACK West	0.78	0.34	0.18	0.47	0.04	0.35
17	STACK West	0.91	0.28	0.19	0.53	0.03	0.50
18	STACK West	1.05	0.28	0.19	0.53	0.04	0.63
19	STACK West	0.91	0.31	0.18	0.51	0.04	0.47
20	STACK West	1.01	0.38	0.19	0.43	0.05	1.00
21	STACK West	1.05	0.44	0.15	0.40	0.04	0.87
22	STACK West	1.32	0.38	0.15	0.47	0.13	0.99
23	STACK West	1.41	NA	NA	NA	NA	NA
24	STACK West	1.18	NA	NA	NA	NA	0.99
25	STACK West	1.01	0.40	0.16	0.44	0.07	0.88
26	STACK West	0.96	0.41	0.16	0.43	0.09	0.95
27	STACK West	0.83	0.25	0.21	0.54	0.03	0.50
28	STACK West	0.83	0.25	0.19	0.55	0.05	0.46
29	STACK West	0.83	0.26	0.20	0.54	0.04	0.41
30	STACK West	1.00	0.35	0.19	0.46	0.04	0.79
31	STACK West	0.97	0.33	0.23	0.44	0.06	0.84
32	STACK West	0.98	0.29	0.23	0.48	0.05	0.62
33	STACK West	1.01	0.42	0.19	0.39	0.06	0.94
34	STACK West	0.99	0.35	0.19	0.46	0.05	0.99
35	STACK West	1.02	0.38	0.22	0.40	0.11	0.99
36	STACK West	1.43	NA	NA	NA	NA	NA
37	STACK West	0.86	0.29	0.23	0.49	0.04	0.62
38	STACK West	0.92	0.32	0.22	0.46	0.05	0.74
39	STACK West	0.96	0.39	0.13	0.48	0.04	0.86
40	STACK West	0.87	0.38	0.18	0.44	0.05	0.78
41	STACK West	0.95	0.43	0.12	0.45	0.08	0.55
42	STACK West	0.98	0.32	0.11	0.57	0.04	0.99
43	STACK West	0.90	0.38	0.15	0.47	0.06	0.77
44	STACK West	1.32	0.43	0.25	0.32	0.03	0.63
45	STACK West	1.28	NA	NA	NA	NA	NA
46	STACK West	1.33	0.35	0.18	0.47	0.10	0.83
47	STACK East	1.11	NA	NA	NA	NA	NA
48	STACK East	1.03	NA	NA	NA	NA	NA
49	STACK East	1.12	NA	NA	NA	NA	NA
50	STACK East	0.89	0.29	0.22	0.49	0.05	0.66
51	STACK East	1.03	0.54	0.14	0.32	0.06	0.98
52	STACK East	1.03	NA	NA	NA	NA	NA
53	STACK East	0.96	0.39	0.19	0.43	0.08	0.99
54	STACK East	0.89	0.35	0.22	0.43	0.10	0.99
55	STACK East	0.90	0.35	0.21	0.44	0.05	0.99
56	STACK East	1.09	0.68	0.24	0.08	0.10	0.89
57	STACK East	0.93	0.37	0.15	0.48	0.11	0.99
58	STACK East	0.94	0.34	0.22	0.44	0.09	0.99
59	STACK East	0.91	0.35	0.25	0.40	0.07	0.86
60	STACK East	1.05	NA	NA	NA	NA	0.99
61	STACK East	0.84	0.28	0.23	0.50	0.05	0.62
62	STACK East	0.98	0.42	0.24	0.34	0.09	0.99
63	STACK East	0.98	0.40	0.20	0.40	0.12	0.99
64	STACK East	0.83	0.31	0.21	0.48	0.04	0.71

Key	Play Region	Rc%	%C_{27} Sterane[1]	%C_{28} Sterane[2]	%C_{29} Sterane[3]	C_{30} Sterane Index[4]	Diasteranes/Total Steranes[5]
65	STACK East	0.94	0.36	0.26	0.38	0.11	0.99
66	STACK East	0.83	0.28	0.21	0.51	0.04	0.53
67	STACK East	0.87	0.35	0.21	0.44	0.09	0.99
68	STACK East	0.82	0.31	0.20	0.49	0.05	0.74
69	STACK East	0.84	0.32	0.23	0.45	0.06	0.68
70	STACK East	0.88	0.36	0.23	0.41	0.08	0.99
71	STACK East	1.21	NA	NA	NA	NA	NA
72	STACK East	0.79	0.32	0.22	0.46	0.05	0.63
73	STACK East	1.12	NA	NA	NA	NA	0.86
74	STACK East	0.90	0.36	0.25	0.39	0.09	0.79
75	STACK East	0.81	0.32	0.28	0.41	0.06	0.68
76	STACK East	0.79	0.27	0.24	0.48	0.05	0.66
77	STACK East	0.99	0.43	0.22	0.34	0.10	0.91
78	STACK East	0.97	0.54	0.17	0.29	0.10	0.84
79	STACK East	0.84	0.35	0.23	0.42	0.06	0.57
80	STACK East	0.84	0.33	0.20	0.47	0.04	0.58
81	STACK East	0.85	0.37	0.29	0.34	0.08	0.74
82	STACK East	0.89	0.35	0.19	0.46	0.12	0.92
83	STACK East	0.85	0.35	0.26	0.39	0.08	0.60
84	STACK East	1.03	0.31	0.24	0.46	0.09	0.94
85	STACK East	0.86	0.39	0.28	0.33	0.07	0.89
86	STACK East	0.87	0.28	0.26	0.46	0.07	0.78
87	STACK East	0.83	0.32	0.27	0.41	0.05	0.69
88	STACK East	0.87	0.31	0.25	0.44	0.06	0.75
89	STACK East	0.85	0.35	0.27	0.38	0.08	0.62
90	STACK East	0.78	0.34	0.23	0.43	0.06	0.39
91	STACK East	0.85	0.29	0.28	0.43	0.07	0.66
92	STACK East	0.83	0.36	0.24	0.40	0.09	0.71
93	STACK East	0.76	0.31	0.23	0.46	0.05	0.53
94	STACK East	0.85	0.32	0.24	0.43	0.07	0.99
95	STACK East	0.87	0.29	0.18	0.53	0.09	0.90
96	STACK East	0.89	0.30	0.24	0.46	0.08	0.80
97	STACK East	0.85	0.28	0.23	0.49	0.07	0.71
98	STACK East	0.85	0.33	0.21	0.47	0.09	0.74
99	STACK East	0.84	0.32	0.20	0.48	0.09	0.74
100	STACK East	0.76	0.29	0.21	0.49	0.06	0.35
101	STACK East	0.78	0.30	0.23	0.47	0.06	0.44
102	STACK East	0.83	0.30	0.22	0.48	0.07	0.65
103	STACK East	0.83	0.33	0.25	0.42	0.07	0.68
104	STACK East	0.86	0.36	0.23	0.41	0.08	0.72
105	STACK East	0.81	0.33	0.27	0.40	0.07	0.63
106	STACK East	0.83	0.35	0.22	0.44	0.07	0.69
107	STACK East	0.82	0.33	0.24	0.42	0.09	0.58
108	STACK East	0.85	0.25	0.22	0.53	0.09	0.79
109	STACK East	0.86	0.37	0.23	0.40	0.13	0.87
110	STACK East	0.92	0.30	0.19	0.52	0.08	0.76
111	STACK East	0.83	0.36	0.20	0.44	0.06	0.61
112	STACK East	0.80	0.31	0.25	0.45	0.06	0.55
113	STACK East	0.79	0.28	0.25	0.47	0.05	0.47
114	STACK East	0.82	0.31	0.24	0.44	0.07	0.43
115	STACK East	0.77	0.27	0.23	0.50	0.05	0.54
116	STACK East	0.80	0.30	0.24	0.46	0.07	0.56
117	STACK East	0.76	0.30	0.25	0.45	0.06	0.51
118	STACK East	0.82	0.30	0.20	0.49	0.07	0.55
119	STACK East	0.79	0.34	0.23	0.43	0.07	0.45
120	SCOOP	0.74	0.27	0.22	0.50	0.04	0.57
121	SCOOP	1.11	NA	NA	NA	NA	NA
122	SCOOP	1.13	NA	NA	NA	NA	NA
123	SCOOP	1.05	NA	NA	NA	NA	NA
124	SCOOP	0.84	0.38	0.25	0.37	0.10	0.69
125	SCOOP	0.92	0.44	0.24	0.32	0.10	0.81
126	SCOOP	0.81	0.33	0.15	0.52	0.14	0.92
127	SCOOP	0.80	0.37	0.22	0.42	0.08	0.70
128	SCOOP	0.84	0.34	0.24	0.42	0.13	0.98

Key	Play Region	Rc%	%C_{27} Sterane[1]	%C_{28} Sterane[2]	%C_{29} Sterane[3]	C_{30} Sterane Index[4]	Diasteranes/Total Steranes[5]
129	SCOOP	0.84	0.38	0.25	0.37	0.03	0.81
130	SCOOP	0.88	0.42	0.19	0.39	0.09	0.72
131	SCOOP	0.85	0.28	0.19	0.53	0.09	0.87
132	SCOOP	0.90	0.47	0.24	0.29	0.11	0.83
133	SCOOP	0.88	0.39	0.16	0.46	0.06	0.75
134	SCOOP	0.96	0.60	0.19	0.21	0.18	0.99
135	SCOOP	0.80	0.36	0.23	0.41	0.09	0.74
136	SCOOP	0.80	0.37	0.28	0.35	0.10	0.81
137	SCOOP	0.85	0.38	0.20	0.42	0.09	0.77
138	SCOOP	0.81	0.44	0.25	0.31	0.11	0.67
139	SCOOP	0.89	0.43	0.36	0.21	0.03	0.66
140	SCOOP	0.91	0.44	0.31	0.25	0.03	0.68
141	SCOOP	0.85	0.47	0.26	0.27	0.11	0.71
142	SCOOP	0.89	0.42	0.33	0.25	0.09	0.82
143	SCOOP	0.86	0.40	0.28	0.32	0.15	0.83
144	SCOOP	0.81	0.37	0.20	0.43	0.11	0.73
145	SCOOP	0.81	0.33	0.28	0.39	0.09	0.73
146	SCOOP	0.86	0.31	0.29	0.40	0.12	0.99
147	SCOOP	0.86	0.42	0.21	0.36	0.19	0.99
148	SCOOP	0.88	0.38	0.31	0.31	0.19	0.65
149	SCOOP	0.82	0.31	0.22	0.47	0.05	0.66
150	SCOOP	0.99	NA	NA	NA	NA	1.00
151	SCOOP	0.91	0.43	0.24	0.33	0.10	0.82
152	SCOOP	0.82	0.33	0.21	0.46	0.05	0.79
153	SCOOP	0.94	0.56	0.18	0.26	0.10	0.82
154	SCOOP	0.83	0.29	0.27	0.44	0.06	0.86
155	SCOOP	0.84	0.40	0.25	0.36	0.10	0.59
156	SCOOP	0.87	0.49	0.18	0.34	0.12	0.99
157	SCOOP	0.92	0.54	0.14	0.32	0.11	0.78
158	SCOOP	0.94	NA	NA	NA	NA	0.90
159	SCOOP	0.81	0.31	0.15	0.54	0.06	0.48
160	SCOOP	0.92	0.46	0.16	0.38	0.15	0.93
161	SCOOP	0.92	0.47	0.20	0.33	0.13	0.82
162	SCOOP	0.96	0.33	0.27	0.40	0.15	0.82
163	SCOOP	1.10	NA	NA	NA	NA	NA
164	SCOOP	1.00	NA	NA	NA	NA	0.64
165	SCOOP	0.89	0.48	0.17	0.35	0.09	0.99
166	SCOOP	0.92	0.46	0.29	0.26	0.08	0.99
167	SCOOP	1.02	NA	NA	NA	NA	0.83
168	SCOOP	0.93	0.45	0.22	0.33	0.10	0.94
169	SCOOP	0.84	0.33	0.22	0.45	0.06	0.46
170	SCOOP	0.94	0.46	0.40	0.14	0.08	0.99
171	SCOOP	0.87	0.37	0.31	0.32	0.15	0.88
172	SCOOP	0.91	0.38	0.23	0.39	0.04	0.35

Table 12. Sterane parameters used in this section for STACK and SCOOP oils. (1) $C_{27}/C_{27\text{-}29}$ steranes each of 5α(H),14α(H),17α(H),20R isomers; (2) $C_{28}/C_{27\text{-}29}$ steranes each of 5α(H),14α(H),17α(H),20R isomers; (3) $C_{29}/C_{27\text{-}29}$ sterane each of 5α(H),14α(H),17α(H),20R isomers; (4) $C_{30}/C_{27\text{-}30}$ steranes each of 5α(H),14α(H),17α(H),20R isomers; (5) [m/z 259]/[m/z 217] over the range of C_{27}-C_{30} steranes.

Thermal maturity, however, also influences the relative abundance of regular steranes because higher carbon number steranes have been shown to decrease more rapidly with increasing maturity (Moldowan et al., 1989; Dzou et al., 1995). To account for this, the abundances of C_{27-29} regular steranes can be normalized to maturity as shown in Figure 62. When normalized for thermal maturity, STACK West oils are comparatively enriched in C_{29} steranes by approximately 5-15% while proportionally depleted in C_{28} steranes. Both Play Regions have similar amounts of C_{27} steranes. Furthermore, STACK West oils have the highest absolute concentrations of steranes at all levels of maturity which could indicate greater levels of eukaryotic productivity.

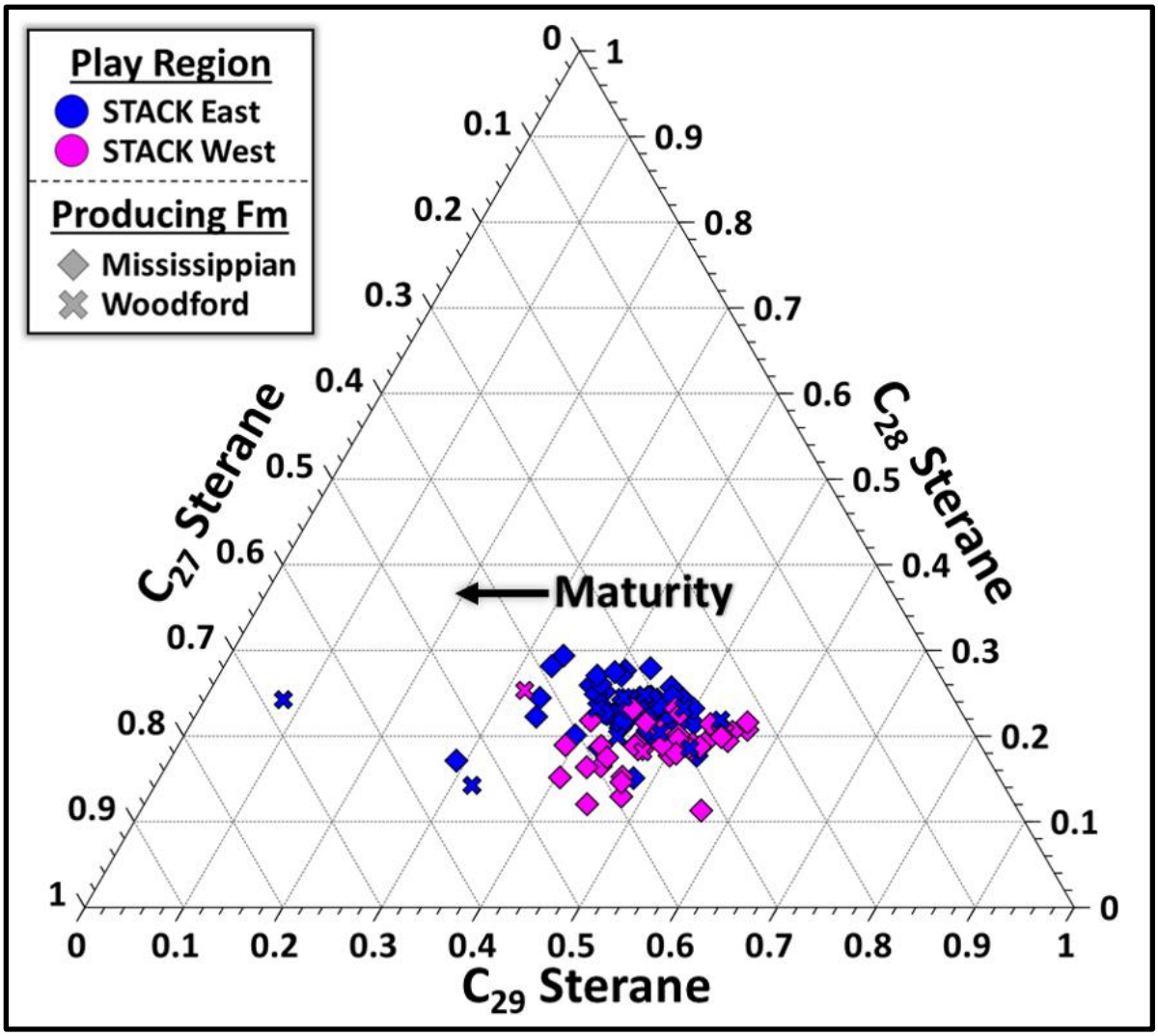

Figure 61. Ternary diagram showing the relative abundance of C_{27}-C_{29}5α(H),14α(H),17α(H) 20R steranes in STACK oils as a fraction of their sum. STACK West samples are characterized by slightly higher amounts of the C_{29} sterane.

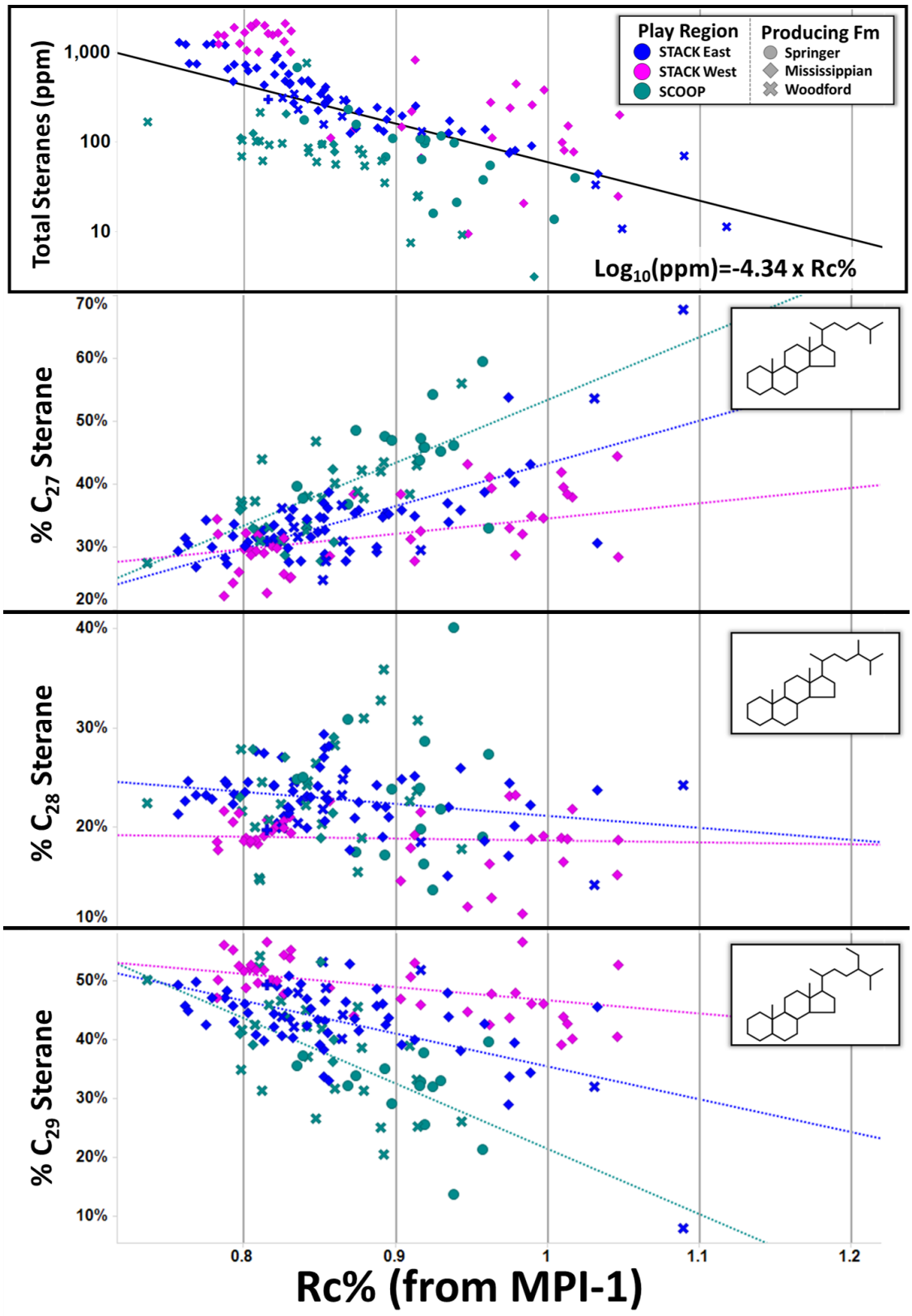

Figure 62. Upper: absolute concentration of regular steranes versus Rc%. The solid black line shows the rate decline exponent of -4.34. Lower: Relative abundance of C_{27}-C_{29} 5α(H),14α(H),17α(H),20R steranes by Play Region.

Another source-specific sterane parameter is the C_{30} Sterane Index, defined by Moldowan et al. (1985) as the ratio $C_{30}/(C_{27}\text{-}C_{30})$ regular steranes using the 5α(H),14α(H),17α(H),20R epimer at each C number to calculate the ratio and shown for STACK oils in Figure 63. Once again, two trends emerge in STACK oils primarily by Play Region and not producing reservoir. The C_{30} sterane has the carbon skeleton 24-*n*-propylcholestanes, which originate from 24-*n*-propylcholesterols primarily synthesized by golden Chrysophyte algae of the order Sarcinochrysidales, with trace amounts also reported in some green Chlorophyte algae species, and is considered a strong indicator of marine input (Raederstorff and Rohmer, 1984; Peters et al., 1986; Moldowan et al., 1990; Volkman et al., 1994). Empirical studies worldwide have shown that oils sourced from restricted saline or hypersaline lagoonal conditions show lower C_{30} Sterane Index values than those from open marine conditions (Moldowan et al., 1989). Even accounting for maturity, C_{30} Steranes Index values for STACK West oils are generally less than half than those in STACK East which may suggest an organic source deposited in a less open marine environment such as a restricted marine basin or even lagoonal environment. Based on these findings, the C_{30} Steranes Index could be useful to differentiate between organic facies in STACK.

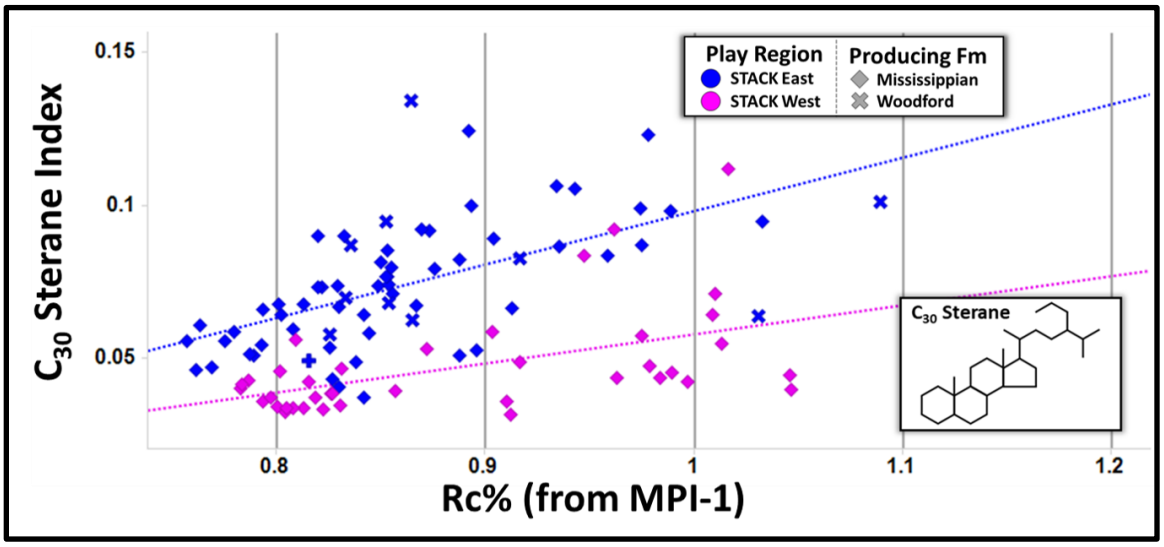

Figure 63. The C_{30} Sterane Index ($C_{30}/C_{27\text{-}30}$ 5α(H),14α(H),17α(H),20R steranes) for all STACK oils. STACK West samples have consistently lower values at maturities and could indicate a restricted marine depositional environment.

Finally, the ratio of diasteranes/steranes, also considered as a maturity parameter in Chapter IV, has been used to distinguish oils generated from carbonate versus clastic source rocks. Diasteranes (**II**) are believed to form as the result of catalytic rearrangement of sterenes during diagenesis in the presence of active acid sites on certain clays, such as montmorillonite or illite (Rubinstein et al., 1975; Sieskind et al., 1979). In fact, only a small amount of clay is necessary to catalyze the rearrangement into diasteranes, and the diasterane/sterane ratio more closely correlates to the amount of clay relative to TOC rather than clay content alone (Requejo et al., 1997; van Kaam-Peters et al., 1998). Moreover, high diasterane/sterane ratios have been reported in organic lean carbonate rocks, clay poor limestones, and bituminous evaporites (e.g. Clark and Philp, 1989), probably because the rearrangement of sterenes into diasterenes is actually facilitated by acidic (low pH) and oxic (high Eh) conditions which reactive clays can imitate (Berner et al., 1970; Moldowan et al., 1986). The diasterane/sterane ratios in STACK show significant covariance with maturity (Figure 64). Nevertheless, STACK West has comparably lower values which may indicate that the source rock for those oils may have been starved for clay-rich sediments or have restricted access to open marine conditions compared to STACK East.

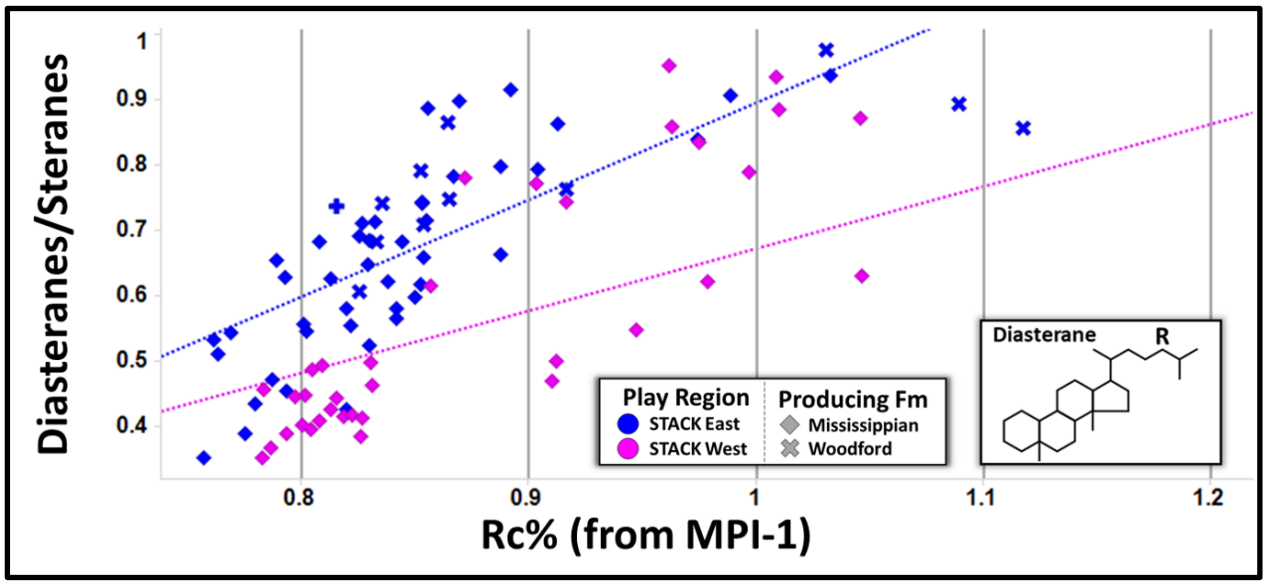

Figure 64. Plot of the ratio diasteranes/steranes, defined as m/z 259 over m/z 217 over the range $C_{27\text{-}30}$ steranes.

This study also observed the sterane fingerprint from two Woodford Shale core intervals in STACK West from Major (ABCDS 1-6) and Blaine (KC 1-36) counties and one core interval in STACK East from Kingfisher County (John 1H-5X). The summary of these findings is shown in Table 13 and Figure 65. The C_{27} and C_{29} steranes are the dominant regular sterane similar to the oils observed in this study. Furthermore, the Woodford in STACK West contains slightly higher $\%C_{29}$ sterane (40% ± 2%, n=8) compared to the STACK East (33% ± 1%, n=3) which agrees with higher C_{29} sterane abundances in STACK West oils. There are also slightly lower C_{30} sterane index values in STACK West (0.04 ± 0.01, n=8) compared to STACK East (0.07 ± 0.03, n=3) which agrees with the pattern observed between STACK oils that STACK West was deposited in a more restricted marine environment with more abundant golden Chrysophyte algae. Finally, the diasteranes/total steranes values are lower in STACK West (0.46 ± 0.05, n=8) compared to STACK East (0.54 ± 0.06, n=3) which again mirrors the pattern observed between STACK oils. No statistically significant differences are observed between the Upper-, Middle-, and Lower Woodford intervals from the limited available core. There are substantial similarities between STACK oils and Woodford Shale extracts, and it is reasonable to suspect the Woodford Shale has sourced some or all oils in the STACK Play.

Core	Depth	Formation	Play Region	Rc%	$\%C_{27}$ Sterane[1]	$\%C_{28}$ Sterane[2]	$\%C_{29}$ Sterane[3]	C_{30} Sterane Index[4]	Dia/Total Steranes[5]
ABCDS 1-6	8098	Upper Woodford	STACK West	0.79	35%	21%	44%	0.04	0.43
ABCDS 1-6	8099	Upper Woodford	STACK West	0.79	38%	19%	43%	0.05	0.41
ABCDS 1-6	8110	Middle Woodford	STACK West	0.79	40%	20%	40%	0.03	0.44
ABCDS 1-6	8121	Middle Woodford	STACK West	0.81	43%	18%	39%	0.04	0.45
KC 1-36	8538.5	Upper Woodford	STACK West	0.82	41%	23%	37%	0.05	0.48
KC 1-36	8543.5	Upper Woodford	STACK West	0.84	39%	25%	36%	0.04	0.57
KC 1-36	8557	Lower Woodford	STACK West	0.83	41%	19%	40%	0.06	0.46
KC 1-36	8566.5	Lower Woodford	STACK West	0.82	40%	22%	38%	0.05	0.42
John 1H-5X	9165	Upper Woodford	STACK East	0.89	42%	25%	33%	0.05	0.50
John 1H-5X	9180	Middle Woodford	STACK East	0.87	40%	26%	34%	0.10	0.61
John 1H-5X	9202	Lower Woodford	STACK East	0.92	46%	21%	33%	0.06	0.50

Table 13. Sterane parameters used for Woodford Shale Extracts in STACK. (1) $C_{27}/C_{27\text{-}29}$ sterane each of 5α,14α,17α(H),20R stereoisomerization; (2) $C_{28}/C_{27\text{-}29}$ sterane each of 5α,14α,17α(H),20R stereoisomerization; (3) $C_{29}/C_{27\text{-}29}$ sterane each of 5α,14α,17α(H),20R stereoisomerization; (4) $C_{30}/C_{27\text{-}30}$ sterane each of 5α,14α,17α(H),20R stereoisomerization; (5) [m/z 259]/[m/z 217] over the range of C_{27}-C_{30} steranes.

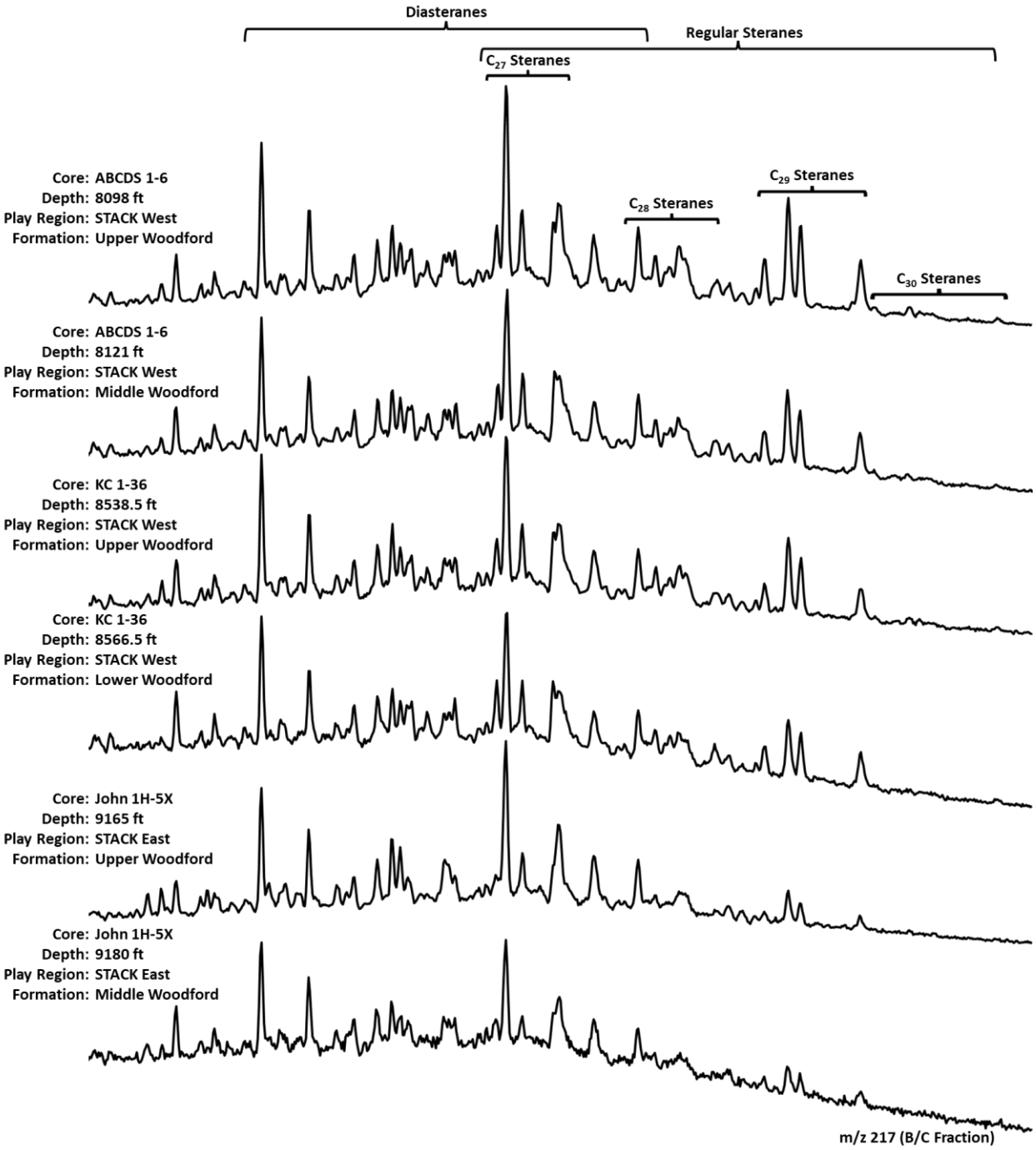

Figure 65. Example m/z 217 mass chromatograms taken from six Woodford Shale core extracts from across STACK. The Woodford Shale in STACK West contain higher amounts of C_{29} regular sterane compared to C_{27} and C_{28} regular steranes. The Woodford Shale in STACK West also contains fewer diasteranes and slightly higher C_{30} sterane index. There is significant co-elution between regular steranes and some diasteranes (see Figure 28).

Acyclic Terpanes

Terpenoids are a broad class of compounds ubiquitous to nearly all forms of life that are biosynthesized by the polymerization and, in some cases, cyclization of appropriately functionalized isoprene (methylbutadiene) subunits (Eglinton and Calvin, 1967; Whitehead, 1973; Bendoraitis, 1974; Philp et al., 1976; Simoneit, 1977). Terpenoids are often characterized by the number of isoprene subunits they contain whereby monoterpanes (C_{10}), sesquiterpanes (C_{15}), diterpanes (C_{20}), sesterterpanes (C_{25}), and triterpanes (C_{30}) containing two to six isoprene subunits, respectively (Figure 66). The most common isoprene linkage is head-to-tail, but there are numerous examples of tail-to-tail (e.g. squalene), head-to-head (e.g. bisphytane), and irregular linkages (e.g. botryococcane). Unlike other biopolymers, such as proteins and polysaccharides, the terpenoid carbon skeleton is relatively stable in the rock record because it is comprised of covalent carbon-carbon bonds that are not as readily degraded (Tissot et al., 1974). During diagenesis, functionalized terpenoids are converted through a complex series of chemical changes into more stable saturated terpane biomarkers preserved in the geological record.

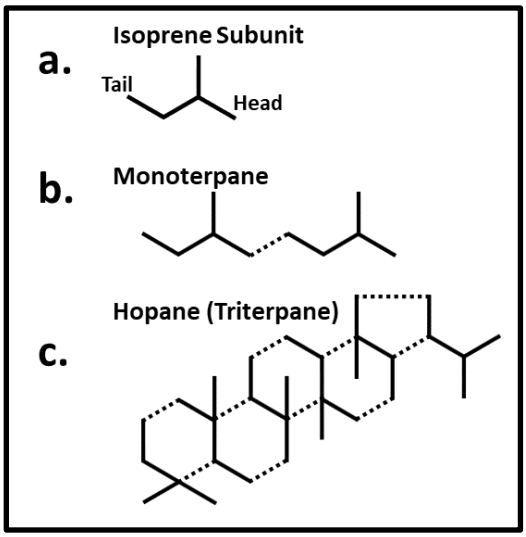

Figure 66. Simplified scheme of terpane structures. a) carbon skeleton of basic isoprene subunit; b) monoterpane skeleton showing head-to-tail linkage; c) carbon skeleton of hopane, a common polycyclic terpane, and its isoprene subunits.

Most acyclic terpanes (isoprenoids) containing twenty or fewer carbon atoms are derived from the ester bound phytol side chain of chlorophyll-*a* ubiquitous in photosynthetic marine life and higher plants (Volkman and Maxwell, 1986); however, chlorophyll-*b*, chlorophyll-*c*, chlorophyll-*d*, and bacteriochlorophyll-*a* contribute small amounts of phytol in certain marine

environments (Gillan and Johns, 1980; Rontani and Volkman, 2003). The cleavage of the phytol side chain results in the formation of the saturate terpanes pristane (**IX**; 2,6,10,14-tetramethylpentadecane) and phytane (**X**; 2,6,10,14-tetramethylhexadecane) depending on the redox conditions of the source-rock (Didyk et al., 1978). Shanmugam (1985) proposed a log-log crossplot with axes consisting of the peak area ratios of pristane/*n*-C_{17} and phytane/*n*-C_{18} with designated zones used to approximate redox, maturity, biodegradation, and depositional environment of a source rock. The recreation of this crossplot is shown in Figure 67 showing that the source rock(s) for STACK oils were deposited under reducing conditions of a marine or transitional shallow marine environment. Even accounting for thermal maturity, STACK East oils are slightly enriched in isoprenoids relative to *n*-alkanes plotting more to the upper right compared to STACK West oils. No evidence of biodegradation has been reported in STACK oils.

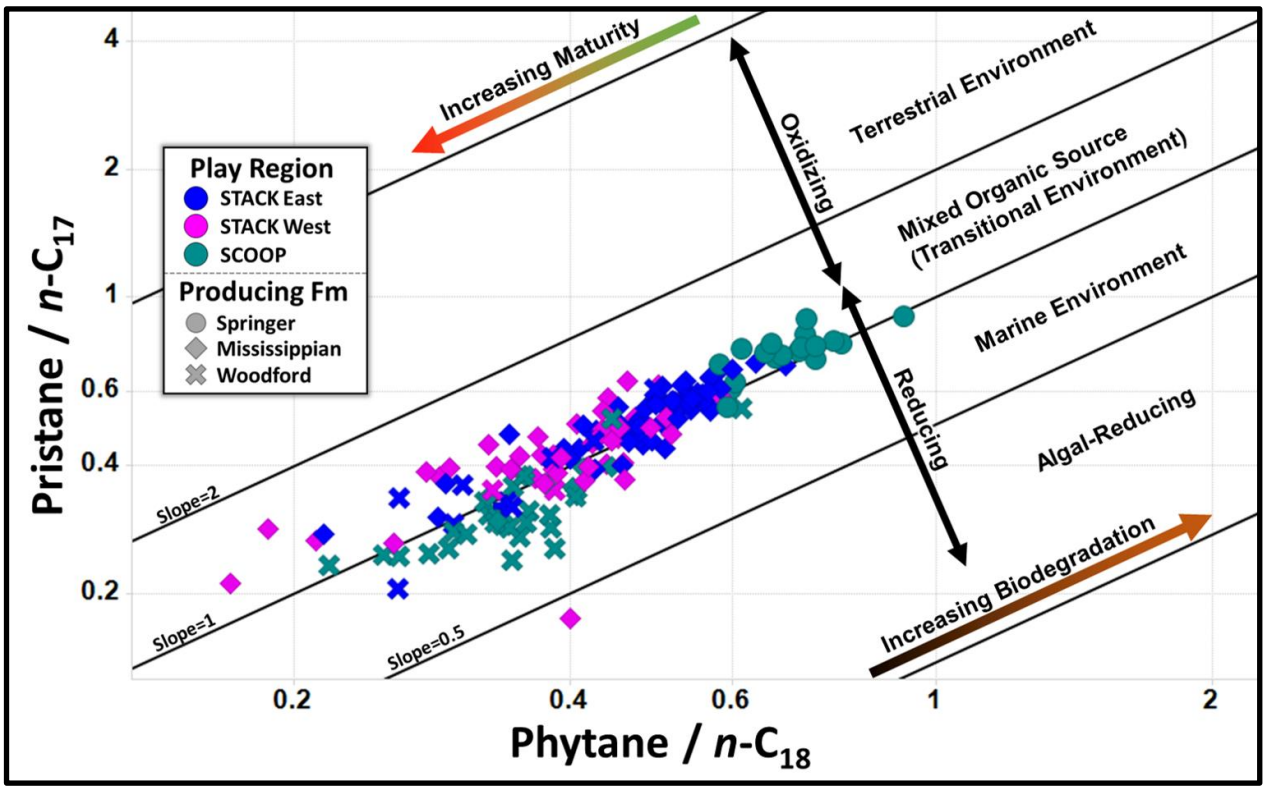

Figure 67. Crossplot of pristane/*n*-C_{17} against phytane/*n*-C_{18} for all oils in this study showing a predominantly marine or transitional marine depositional environment. STACK East oils have slightly higher values for both axes compared to STACK West. SCOOP oils form two clusters discussed in the next section. Plot adapted from Shanmugam (1985).

Hughes et al. (1995) proposed a cross plot of pristane/phytane (Pr/Ph) versus DBT/P, delineated certain predetermined zones corresponding to the lithology and redox conditions that could be expected in certain depositional environments. Normally, the ratio of dibenzothiophene (**VIII**; DBT) to phenanthrene (**VII**; P) is a powerful predictor of source rock depositional environment because organosulfur compounds are often formed in the absence of iron derived primarily from terrigenous sediments (Berner, 1984; Raiswell and Berner, 1985). The re-creation of this crossplot shows most oils in this study plot in Zone 3 (Marine Shale) or Zone 2 (Marine/Lacustrine) corresponding to Pr/Ph between 0.8-1.8 and DBT/P<1 (Figure 68). Curiously, the values for DBT/P are significantly higher and more scattered in STACK West (0.43±0.14, n=46) compared to STACK East (0.06±0.01, n=73) and SCOOP (0.09±0.03, n=53), and some STACK West oils even plot outside of the lithologic zones with DBT/P values between 1-3.

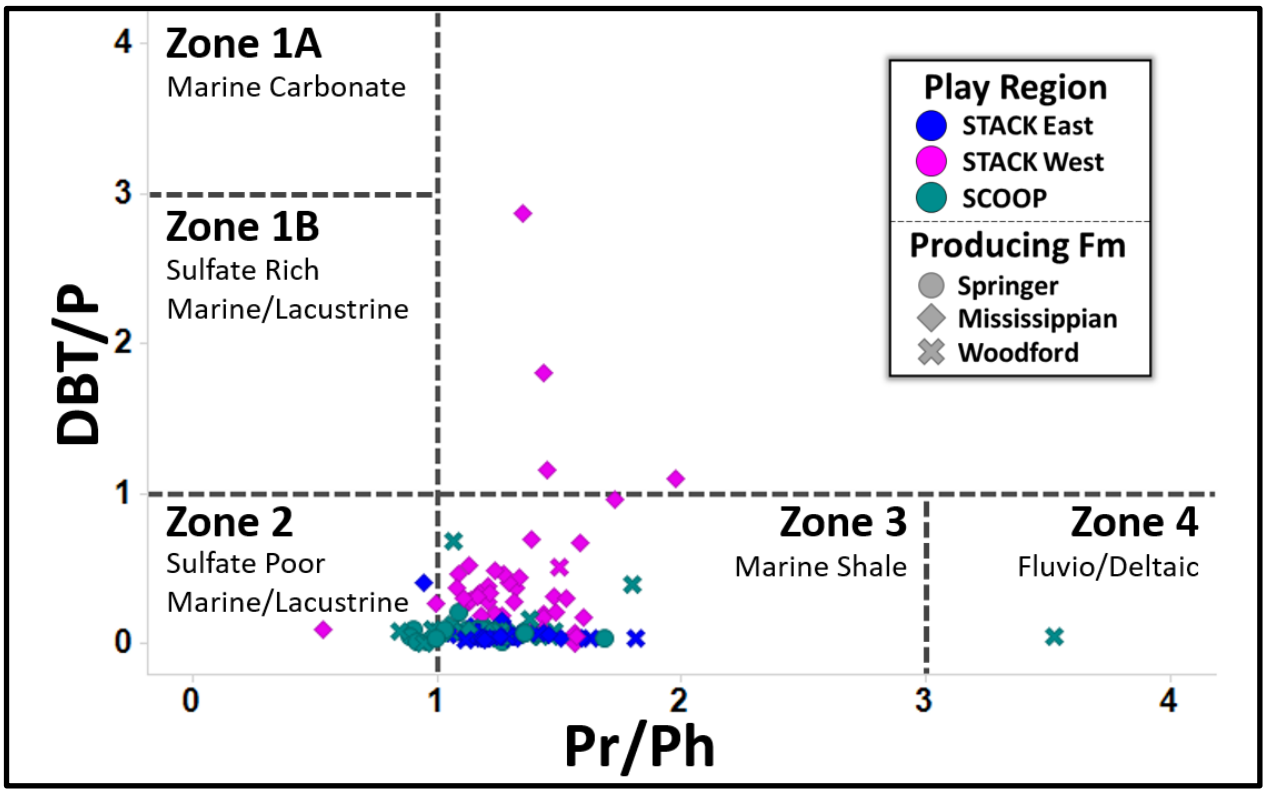

Figure 68. Crossplot of DBT/P and Pr/Ph used to determine depositional environments (Hughes et al. 1995). A small number of STACK West samples are elevated in DBT/P despite originating from a marine shale.

Sesquiterpanes

Sesquiterpanes are a family of bicyclic polymethyl-substituted decalins comprised of three isoprene subunits and are ubiquitous components of crude oils, coals, and ancient sediments (Bendoraitis, 1974; Philp et al., 1981). The most common sesquiterpanes in petroleum have the drimane (**XI**) skeleton and contain between 14 and 16 carbons and yield a notable m/z 123 mass fragment in GC-MS analysis due to the formation of a C_9H_{15} fragment ion. While some sesquiterpanes are associated with higher plants, most notably 4β(H)-eudesmane (**XII**; Alexander et al., 1983), most sesquiterpanes are present across all depositional environments and geologic times suggesting they are also synthesized by algae and/or bacteria which are universal in the sedimentary record (Alexander et al., 1984). Although there is little evidence that they provide high degrees of biological specificity in the geologic record, sesquiterpanes are generally resistant to biodegradation (Dimmler et al., 1984; Wang et al., 2005), thermal degradation (Figure 49; Alexander et al., 1984), and evaporative weathering (Yang et al., 2009) and are therefore compelling candidates for oil-source and oil-oil correlation across a broad maturity spectrum.

A series of eight C_{14}-C_{16} bicyclic sesquiterpanes (BS-1 through BS-8) were identified in this dataset from the m/z 123 partial mass chromatograms of the B/C fractions (Figure 69). Oils from STACK East, STACK West, and SCOOP Woodford were found to have similar sesquiterpane signatures, with drimane (**XI**; BS-5) and homodrimane (**XI**; BS-8) often dominant constituents. This reflects a common sesquiterpane signature found in many oils globally. Like rearranged steranes (**II**; diasteranes), rearranged drimanes (BS-3 and BS-4) are believed to result primarily from acid catalyzed rearrangement in the presence of clays during diagenesis, but other mechanisms related to low pH and high Eh may also contribute to their formation (Alexander et al., 1984). The relative abundances of 8β(H)-drimane (BS-5) and 8β(H)-homodrimane (BS-8) in

oils and sediments are strongly maturity dependent (Noble et al., 1987). It has been hypothesized that some sesquiterpanes could result from C-ring cleavage in tricyclic or pentacyclic terpanes, and therefore the ratio of certain sesquiterpanes may reflect the catalytic nature of the mineral matrix related to depositional environment (Weston et al., 1989). However, C-ring cleavage requires both the breaking of two C-C bonds and the subsequent rearrangement of methyl groups on the B ring and therefore is unlikely to be a major contributor to sesquiterpane generation or formation.

Peak	Compound Name	Formula
BS-1	C_{14} sesquiterpane	$C_{14}H_{26}$
BS-2	C_{14} sesquiterpane	$C_{14}H_{26}$
BS-3	Rearranged drimane	$C_{15}H_{28}$
BS-4	Rearranged drimane	$C_{15}H_{28}$
BS-5	8β(H)-drimane	$C_{15}H_{28}$
BS-6	C_{15} sesquiterpane	$C_{15}H_{28}$
BS-7	C_{16} sesquiterpane	$C_{16}H_{30}$
BS-8	8β(H)-homodrimane	$C_{16}H_{30}$

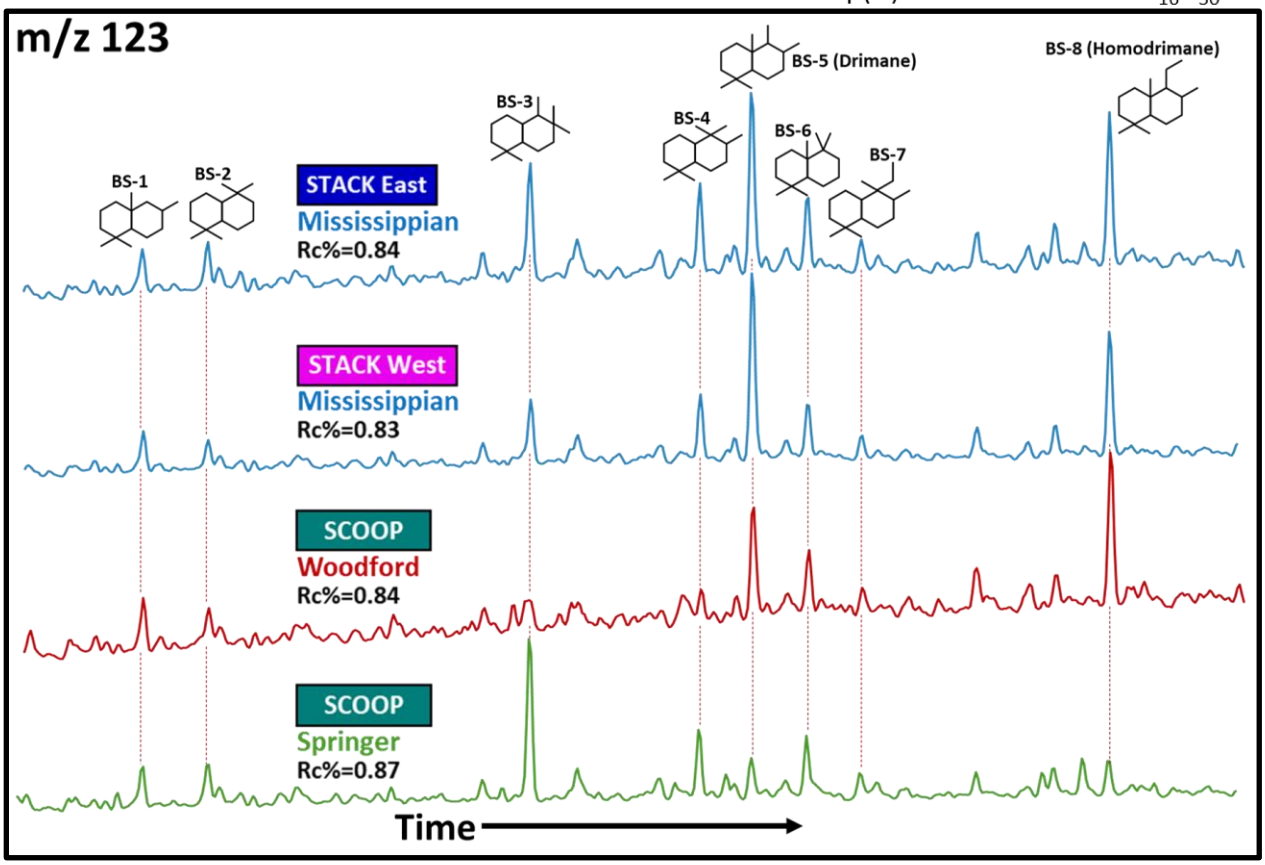

Figure 69. Typical bicyclic sesquiterpane (BS) signature for STACK and SCOOP oils by producing formation. Peaks BS-1 through BS-8 and structures were identified from literature review (Philp et al., 1981; Alexander et al., 1983, 1984; Noble et al., 1987; Weston et al., 1989; Oung and Philp, 1994; Wang et al., 2005; Yang et al., 2009).

Three sesquiterpanes were selected as axial components of a ternary diagram to determine a sesquiterpane fingerprint, shown in Figure 70, including a rearranged drimane (BS-4), drimane (**XI**; BS-5), and a third sesquiterpane (BS-6) from data in Table 14. The axes of the ternary diagram (e.g. %BS-4=BS-4/[BS-4+BS-5+BS-6]) are plotted individually in Figure 71 versus maturity. Oils from STACK West are generally enriched in 8β(H)-drimane (BS-5) at the expense of other two sesquiterpanes, most notably the rearranged drimane (BS-4), when compared to STACK East. The source of the relative enrichment of drimane in STACK West remains uncertain, but previous studies indicate it could be related to increased input of terrigenous or higher plant organic material

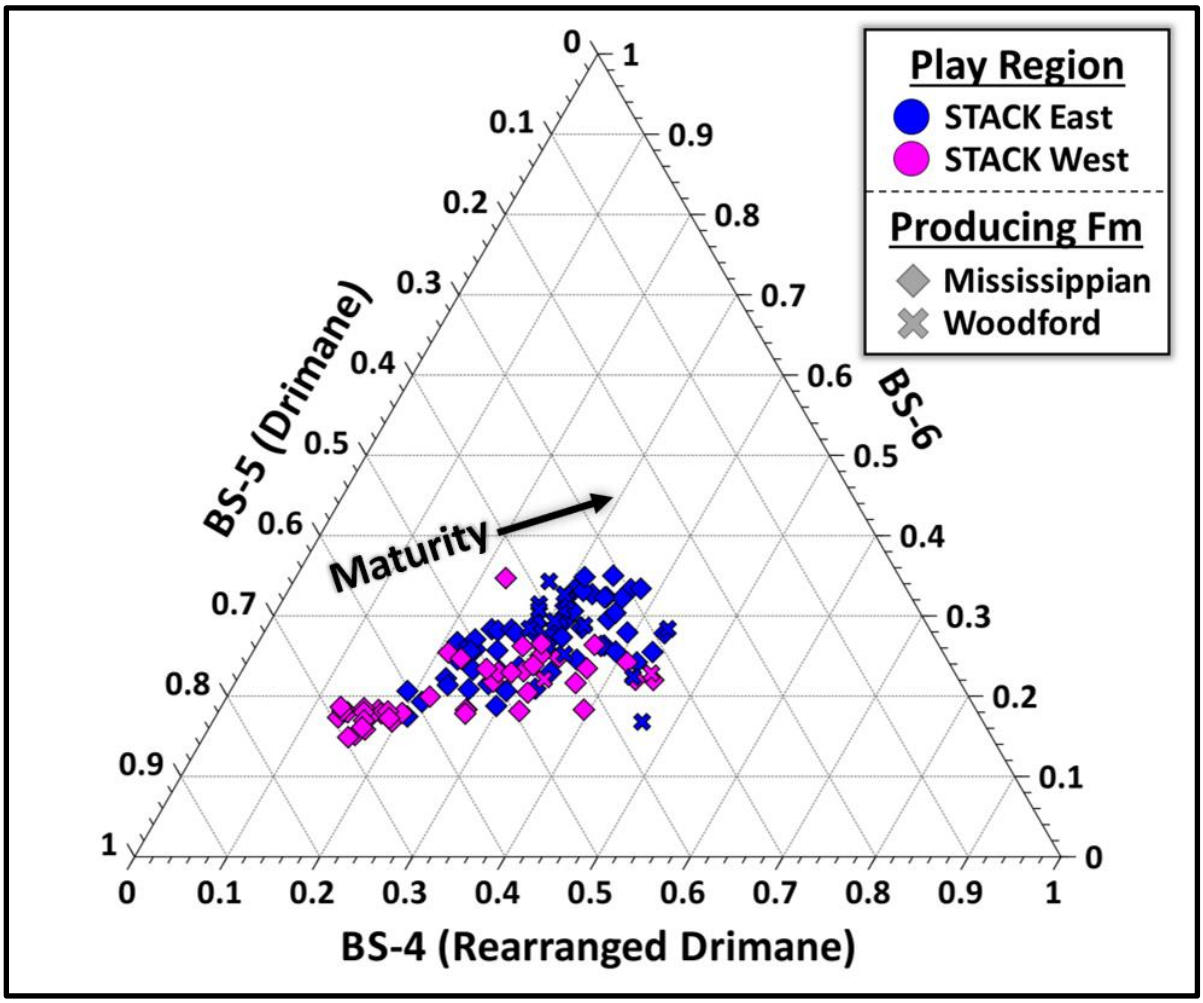

Figure 70. Ternary diagram of three closely eluting C_{15} sesquiterpanes include a rearranged drimane (BS-4), drimane (BS-5), and a third sesquiterpane (BS-6) as a fraction of the sum of the three. STACK East samples have higher relative abundances of rearranged drimane BS-4 compared to STACK West. This mirrors the higher abundances of rearranged diasteranes (**II**) also observed in STACK East and could indicate a higher abundance of acid clay sites.

(e.g. Philp et al., 1981; Weston et al., 1989). This hypothesis is supported by the lower C_{30} Sterane Index also observed in STACK West oils. Similarly, the low concentrations of rearranged drimanes in STACK West relative to STACK East is significant because it mirrors the similarly low diasterane/sterane ratios observed in those same oils, both of which are indicative of acid catalyzed rearrangement processes during diagenesis (Alexander et al., 1984).

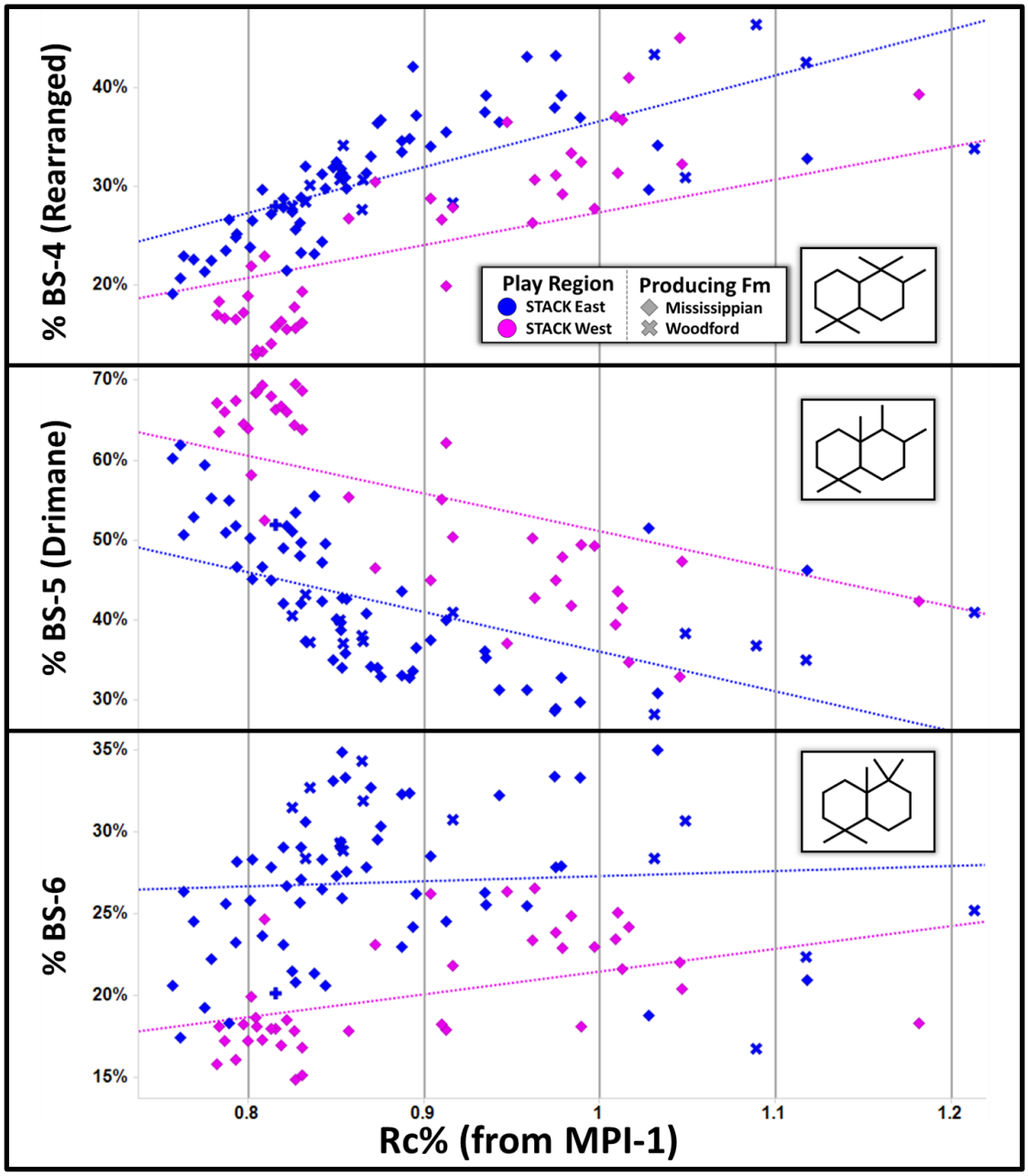

Figure 71. Individual axes of the ternary diagram shown in Figure 70 and normalized to maturity. Lines of best fit are provided as a visual aid to guide interpretation and not meant to suggest a strong relationship with maturity.

Key	Play Region	%BS-4	%BS-5	%BS-6
1	STACK West	13.3%	69.4%	17.3%
2	STACK West	12.9%	68.4%	18.7%
3	STACK West	13.4%	68.5%	18.2%
4	STACK West	15.7%	66.3%	18.0%
5	STACK West	14.0%	68.0%	18.0%
6	STACK West	22.9%	52.4%	24.7%
7	STACK West	16.6%	66.1%	17.3%
8	STACK West	18.3%	63.6%	18.1%
9	STACK West	17.2%	64.5%	18.3%
10	STACK West	17.7%	64.4%	17.9%
11	STACK West	16.5%	67.4%	16.1%
12	STACK West	15.5%	66.0%	18.5%
13	STACK West	18.8%	63.9%	17.3%
14	STACK West	16.3%	66.8%	17.0%
15	STACK West	21.9%	58.2%	19.9%
16	STACK West	16.9%	67.2%	15.9%
17	STACK West	19.9%	62.2%	17.9%
18	STACK West	32.2%	47.3%	20.5%
19	STACK West	26.6%	55.1%	18.3%
20	STACK West	36.8%	41.6%	21.6%
21	STACK West	45.0%	33.0%	22.0%
22	STACK West	43.0%	34.9%	22.0%
23	STACK West	22.7%	42.6%	34.7%
24	STACK West	39.3%	42.3%	18.3%
25	STACK West	31.3%	43.6%	25.1%
26	STACK West	26.3%	50.3%	23.4%
27	STACK West	19.4%	63.8%	16.8%
28	STACK West	16.2%	68.6%	15.2%
29	STACK West	15.6%	69.5%	14.9%
30	STACK West	27.8%	49.2%	23.0%
31	STACK West	31.1%	45.0%	23.9%
32	STACK West	29.2%	47.9%	22.9%
33	STACK West	37.1%	39.4%	23.5%
34	STACK West	32.5%	49.4%	18.1%
35	STACK West	41.0%	34.7%	24.2%
36	STACK West	21.2%	53.4%	25.4%
37	STACK West	26.8%	55.4%	17.8%
38	STACK West	27.8%	50.4%	21.8%
39	STACK West	30.6%	42.8%	26.5%
40	STACK West	30.4%	46.5%	23.1%
41	STACK West	36.5%	37.1%	26.4%
42	STACK West	33.4%	41.7%	24.9%
43	STACK West	28.8%	45.0%	26.2%
44	STACK West	44.3%	32.8%	22.9%
45	STACK West	NA	NA	NA
46	STACK West	33.2%	44.8%	22.1%
47	STACK East	NA	NA	NA
48	STACK East	NA	NA	NA
49	STACK East	32.8%	46.3%	20.9%
50	STACK East	33.4%	43.6%	23.0%
51	STACK East	43.4%	28.2%	28.4%
52	STACK East	29.6%	51.6%	18.8%
53	STACK East	43.2%	31.3%	25.5%
54	STACK East	42.1%	33.7%	24.2%
55	STACK East	37.2%	36.5%	26.3%
56	STACK East	46.4%	36.8%	16.8%
57	STACK East	37.5%	36.1%	26.3%
58	STACK East	39.2%	35.3%	25.6%
59	STACK East	35.5%	40.0%	24.6%
60	STACK East	30.9%	38.4%	30.7%
61	STACK East	23.1%	55.5%	21.4%
62	STACK East	43.3%	28.9%	27.8%
63	STACK East	39.2%	32.8%	27.9%
64	STACK East	25.6%	53.5%	20.9%

Key	Play Region	%BS-4	%BS-5	%BS-6
65	STACK East	36.5%	31.3%	32.2%
66	STACK East	23.2%	49.7%	27.1%
67	STACK East	36.3%	34.1%	29.6%
68	STACK East	28.0%	51.9%	20.2%
69	STACK East	29.8%	49.6%	20.7%
70	STACK East	36.7%	32.9%	30.4%
71	STACK East	33.8%	41.0%	25.2%
72	STACK East	24.9%	51.8%	23.3%
73	STACK East	42.6%	35.0%	22.4%
74	STACK East	34.0%	37.5%	28.5%
75	STACK East	29.7%	46.7%	23.7%
76	STACK East	26.6%	55.0%	18.3%
77	STACK East	36.9%	29.8%	33.3%
78	STACK East	37.9%	28.7%	33.4%
79	STACK East	31.2%	42.3%	26.5%
80	STACK East	24.4%	47.3%	28.3%
81	STACK East	31.8%	38.8%	29.4%
82	STACK East	34.8%	32.9%	32.4%
83	STACK East	32.5%	40.2%	27.3%
84	STACK East	34.2%	30.8%	35.0%
85	STACK East	29.7%	42.7%	27.6%
86	STACK East	31.3%	40.9%	27.8%
87	STACK East	27.4%	51.1%	21.5%
88	STACK East	30.7%	37.4%	31.9%
89	STACK East	31.2%	39.8%	29.0%
90	STACK East	21.4%	59.3%	19.3%
91	STACK East	31.3%	42.7%	26.0%
92	STACK East	32.0%	37.4%	30.6%
93	STACK East	20.7%	61.8%	17.5%
94	STACK East	31.9%	35.0%	33.1%
95	STACK East	33.0%	34.2%	32.7%
96	STACK East	34.6%	33.1%	32.3%
97	STACK East	34.1%	37.0%	28.8%
98	STACK East	31.2%	34.0%	34.8%
99	STACK East	30.1%	37.3%	32.7%
100	STACK East	19.1%	60.2%	20.6%
101	STACK East	22.5%	55.3%	22.2%
102	STACK East	26.3%	48.0%	25.7%
103	STACK East	28.4%	43.2%	28.4%
104	STACK East	30.9%	35.8%	33.3%
105	STACK East	27.2%	44.9%	27.8%
106	STACK East	28.9%	42.1%	29.1%
107	STACK East	28.8%	42.1%	29.1%
108	STACK East	30.6%	40.0%	29.3%
109	STACK East	27.6%	38.1%	34.3%
110	STACK East	28.3%	41.0%	30.8%
111	STACK East	27.9%	40.6%	31.5%
112	STACK East	26.5%	45.2%	28.3%
113	STACK East	23.5%	50.9%	25.6%
114	STACK East	27.9%	49.0%	23.1%
115	STACK East	22.6%	52.9%	24.6%
116	STACK East	23.9%	50.3%	25.8%
117	STACK East	22.9%	50.7%	26.3%
118	STACK East	21.5%	51.8%	26.7%
119	STACK East	25.1%	46.7%	28.2%
120	SCOOP	22.4%	47.9%	29.7%
121	SCOOP	NA	NA	NA
122	SCOOP	14.8%	54.6%	30.6%
123	SCOOP	20.2%	47.2%	32.7%
124	SCOOP	38.1%	29.4%	32.5%
125	SCOOP	40.0%	29.6%	30.4%
126	SCOOP	26.1%	40.9%	33.1%
127	SCOOP	27.8%	40.3%	31.9%
128	SCOOP	29.6%	39.0%	31.4%

Key	Play Region	%BS-4	%BS-5	%BS-6
129	SCOOP	26.8%	38.3%	34.9%
130	SCOOP	28.8%	36.6%	34.6%
131	SCOOP	33.8%	31.6%	34.6%
132	SCOOP	41.5%	24.0%	34.5%
133	SCOOP	26.9%	34.2%	38.9%
134	SCOOP	40.8%	24.7%	34.5%
135	SCOOP	29.0%	37.8%	33.2%
136	SCOOP	26.6%	37.8%	35.6%
137	SCOOP	23.5%	44.1%	32.5%
138	SCOOP	27.5%	35.8%	36.7%
139	SCOOP	32.5%	32.9%	34.6%
140	SCOOP	26.9%	39.2%	33.9%
141	SCOOP	25.9%	39.0%	35.1%
142	SCOOP	26.9%	36.3%	36.8%
143	SCOOP	26.1%	38.6%	35.3%
144	SCOOP	26.1%	42.5%	31.5%
145	SCOOP	28.0%	37.9%	34.1%
146	SCOOP	28.2%	36.7%	35.1%
147	SCOOP	28.7%	35.8%	35.5%
148	SCOOP	28.1%	36.2%	35.7%
149	SCOOP	23.7%	45.6%	30.7%
150	SCOOP	28.9%	37.3%	33.8%

Key	Play Region	%BS-4	%BS-5	%BS-6
151	SCOOP	30.5%	36.5%	33.0%
152	SCOOP	24.5%	43.8%	31.7%
153	SCOOP	24.4%	39.7%	35.9%
154	SCOOP	24.3%	43.9%	31.8%
155	SCOOP	25.2%	37.8%	37.0%
156	SCOOP	35.9%	26.8%	37.3%
157	SCOOP	39.2%	34.1%	26.7%
158	SCOOP	37.5%	29.2%	33.3%
159	SCOOP	19.9%	52.2%	27.9%
160	SCOOP	44.1%	26.0%	29.9%
161	SCOOP	41.5%	26.0%	32.5%
162	SCOOP	43.5%	29.2%	27.3%
163	SCOOP	26.7%	51.8%	21.5%
164	SCOOP	36.9%	36.5%	26.6%
165	SCOOP	42.7%	25.8%	31.5%
166	SCOOP	44.6%	21.1%	34.2%
167	SCOOP	46.9%	25.6%	27.5%
168	SCOOP	42.3%	25.0%	32.7%
169	SCOOP	12.9%	57.9%	29.2%
170	SCOOP	45.0%	18.8%	36.2%
171	SCOOP	39.4%	26.3%	34.3%
172	SCOOP	35.5%	35.7%	28.8%

Table 14. Relative abundance of three sesquiterpanes from STACK oils labeled BS-4 (rearranged drimane), BS-5 (drimane), and BS-6 as a percentage of the peak area sum of the three (see Figure 69). Several high maturity oils had no discernible sesquiterpane peaks and have values marked NA (not available).

The sesquiterpane fingerprint for the three Woodford Shale cores in STACK are summarized in Figure 72 and Table 15. The %BS-4 (rearranged drimane) in Woodford extracts ranges from 22% to 32%, well within the range of values observed in STACK oils. In STACK West, the %BS-4 is higher in the Upper Woodford (27%±1%, n=4) compared to the Lower and Middle Woodford (23%±1%, n=4) which may indicate higher amounts of acid clay sites or a more oxidizing diagenetic environment in the Upper Woodford. The Lower and Middle Woodford more closely resembled values observed in STACK West oils. Core extracts from STACK West also had more abundant %BS-6 (34%±2%, n=8) than observed in the oils. In STACK East, the one Upper Woodford extract also had a higher %BS-4 value (32%) compared to the Lower and Middle Woodford (26%-29%) as was observed in STACK West. In general, STACK West contained lower amounts of the rearranged drimane compared to STACK East which mirrored the pattern observed between STACK oils.

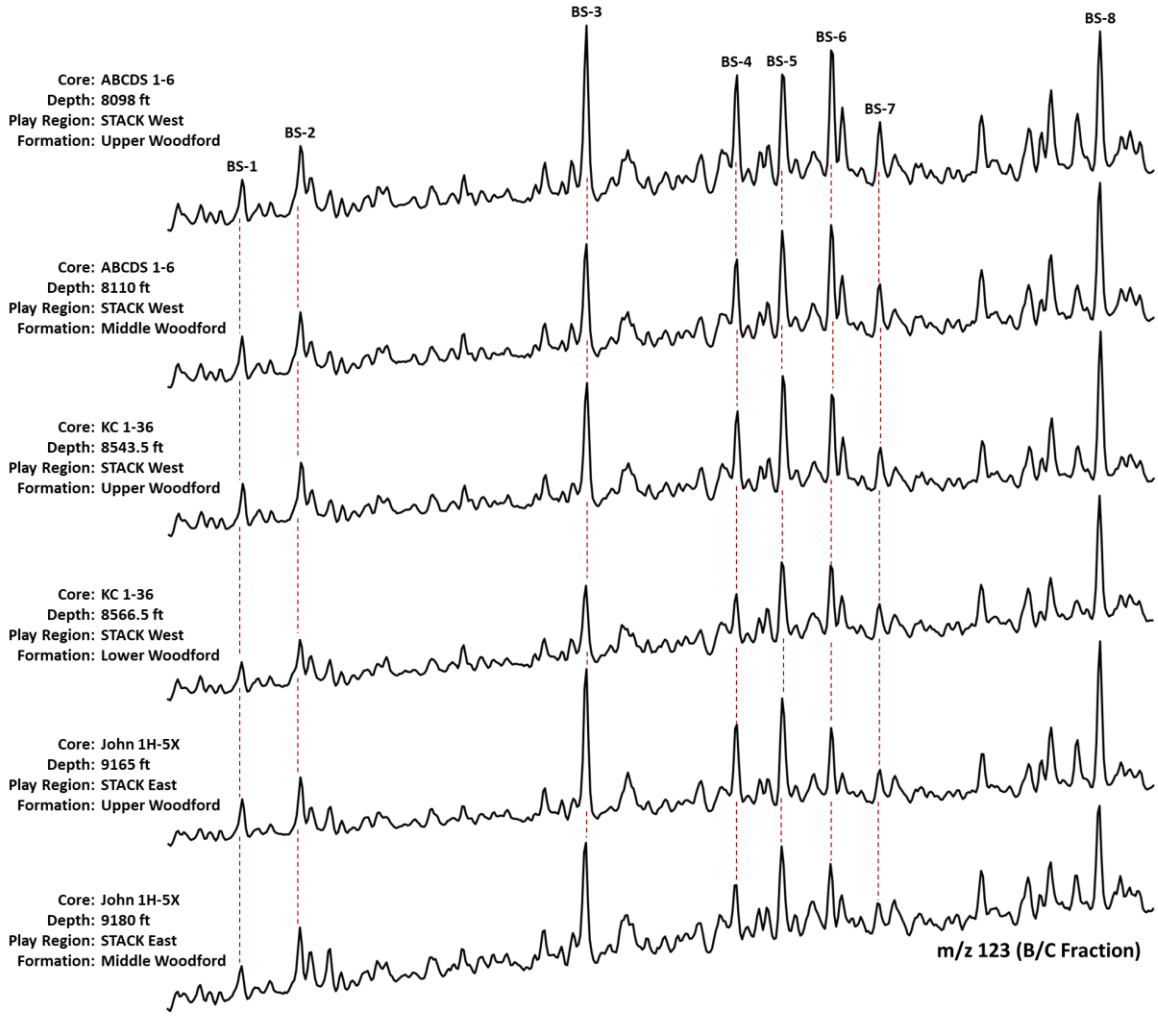

Figure 72. Bicyclic sesquiterpane (BS) signature for six Woodford Shale extracts from STACK. Peaks BS-1 through BS-8 correspond to the peaks and structures identified in Figure 69. The Woodford Shale in STACK West has a higher relative abundance of BS-4 relative to BS-5 and BS-6 compared to the Woodford Shale in STACK East.

Core	Depth	Formation	Play Region	%BS-4	%BS-5	%BS-6
ABCDS 1-6	8098	Upper Woodford	STACK West	28%	36%	36%
ABCDS 1-6	8099	Upper Woodford	STACK West	29%	34%	37%
ABCDS 1-6	8110	Middle Woodford	STACK West	24%	39%	36%
ABCDS 1-6	8121	Middle Woodford	STACK West	24%	40%	36%
KC 1-36	8538.5	Upper Woodford	STACK East	26%	40%	34%
KC 1-36	8543.5	Upper Woodford	STACK East	26%	45%	29%
KC 1-36	8557	Lower Woodford	STACK East	22%	44%	33%
KC 1-36	8566.5	Lower Woodford	STACK East	22%	45%	33%
John 1H-5X	9165	Upper Woodford	STACK East	32%	44%	24%
John 1H-5X	9180	Middle Woodford	STACK East	29%	44%	27%
John 1H-5X	9202	Lower Woodford	STACK East	26%	47%	27%

Table 15. Relative abundance of three sesquiterpanes from Woodford Shale core extracts in STACK labeled BS-4 (rearranged drimane), BS-5 (drimane), and BS-6 as a percentage of the peak area sum of the three (see Figure 69).

Tricyclic Terpanes

Some of the most widely studied biomarkers are the polycyclic triterpenoids, which include the tricyclic terpanes (**V**; cheilanthanes), tetracyclic terpanes (**XIII**), and pentacyclic terpanes (**VI**; hopanes). Polycyclic terpenoids in the geologic record are the diagenetic product of polycyclic terpenoids such as tricyclohexaprenol, diplopterol, isoarborinol, or bacteriohopanetetrol which are synthesized via cyclization of squalene-type (C_{30}) isoprenoidal substrates in microorganisms (Rohmer et al., 1979; Ourisson et al., 1982). Much like steroids in eukaryotic organisms, polycyclic terpenoids comprise the amphipathic lipid bilayer found in the cell membranes of prokaryotic organisms by regulating the osmotic pressure across the cell membrane (Ourisson et al., 1984, 1987).

Cheilanthanes are tricyclic terpanes (**V**; TT) abundant in many sediments and oils and form a homologous series ranging from C_{19} to at least C_{54} depending on the length of the isoprenoid side chain at the C-14 position (Moldowan et al., 1983; De Grande et al., 1993). Cheilanthanes of C_{30} or less are thought to be derived primarily from the tricyclohexaprenol substrate common in many microorganisms and with rarer higher homologues (C_{31}+) forming from tricyclooctaprenol or larger precursors (Ourisson et al., 1982; Aquino Neto et al., 1983; Azevedo et al., 1998). The origin of cheilanthanes in the geologic record is still uncertain, especially those C_{30}+, but there is some evidence they are associated with *Tasmanites*, a primitive algae of the taxonomic class Chlorophyceae (Simoneit et al., 1990; Aquino Neto et al., 1992; Azevedo et al., 1992). While tricyclic terpanes have been found to be abundant in *Tasmanites* rich rocks, some data, including stable carbon isotope (Revill et al., 1994), suggest they may also be biosynthesized by certain species of algae, bacteria, and higher plant life as well (Philp et al., 1981).

Identities of the tricyclic and tetracyclic terpanes from C_{19}-C_{39} for a Mississippian-produced oil in STACK West are shown in Figure 73 and show a dominant C_{23} tricyclic terpane common in marine source rocks. Tricyclics above C_{28}TT are defined as the extended tricyclic terpanes, and tricyclics starting at C_{25}TT contain S and R peaks due to possible chiral centers starting at C-22, C-27, and every five carbons thereafter. Hopanes also share a m/z 191 mass fragment and are often abundant in low maturity oils (Rc<0.9%). The concentration of tricyclic and tetracyclic terpanes are provided in Table 16, and the percentage abundance of the C_{19} through C_{31}TTs measured from peak areas for all STACK oils is shown in Figure 74. The most striking difference between the two Play Regions is the relative enrichment of C_{19} and C_{20}TT in nearly all STACK West oils. Both Play Regions share a most abundant C_{23} peak, but oils in STACK West generally have a lower percentage of extended tricyclic terpanes compared to STACK East.

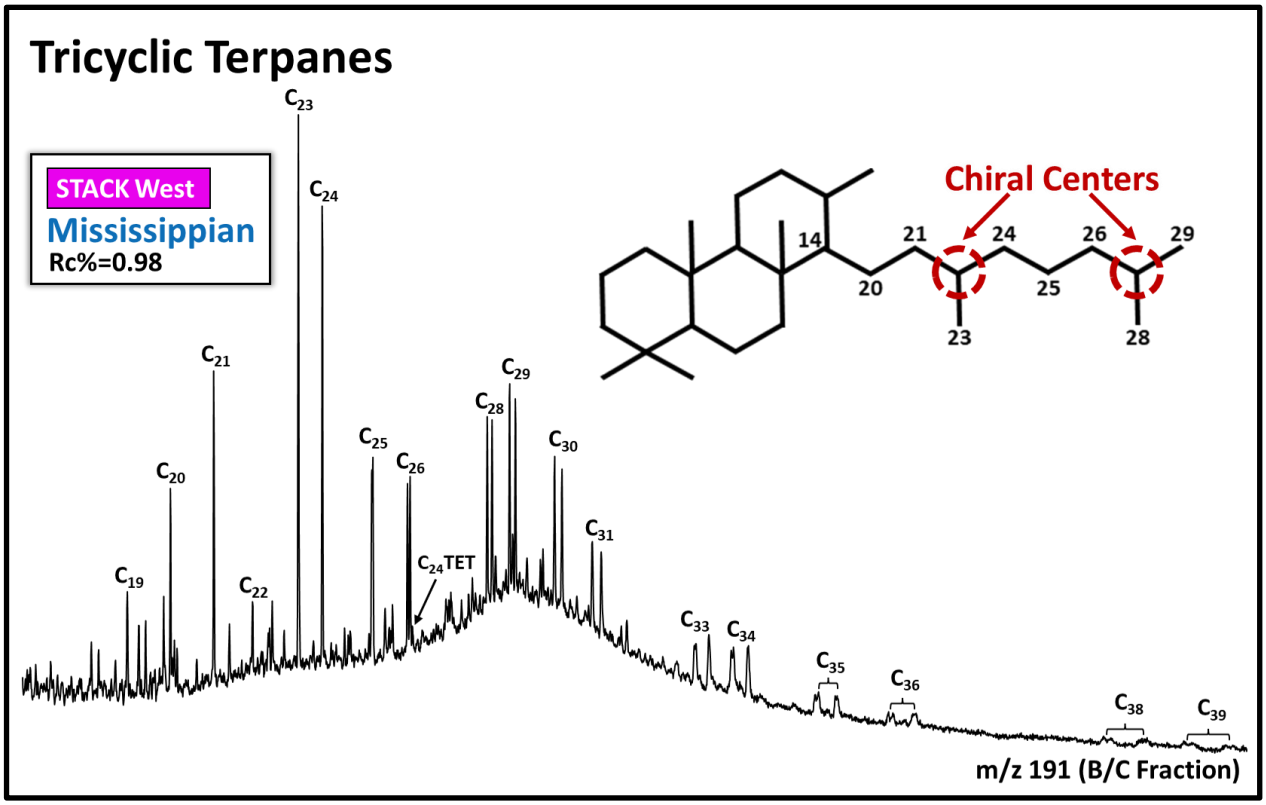

Figure 73. Identification of the tricyclic and tetracyclic terpane series between C_{19}-C_{39}. Chiral centers at C-22, C-27, and every five carbons thereafter form S and R couplets in C_{25}TT and higher homologues. Pentacyclic terpanes (hopanes) also share a dominant m/z 191 fraction in low maturity oils (Rc<0.9%).

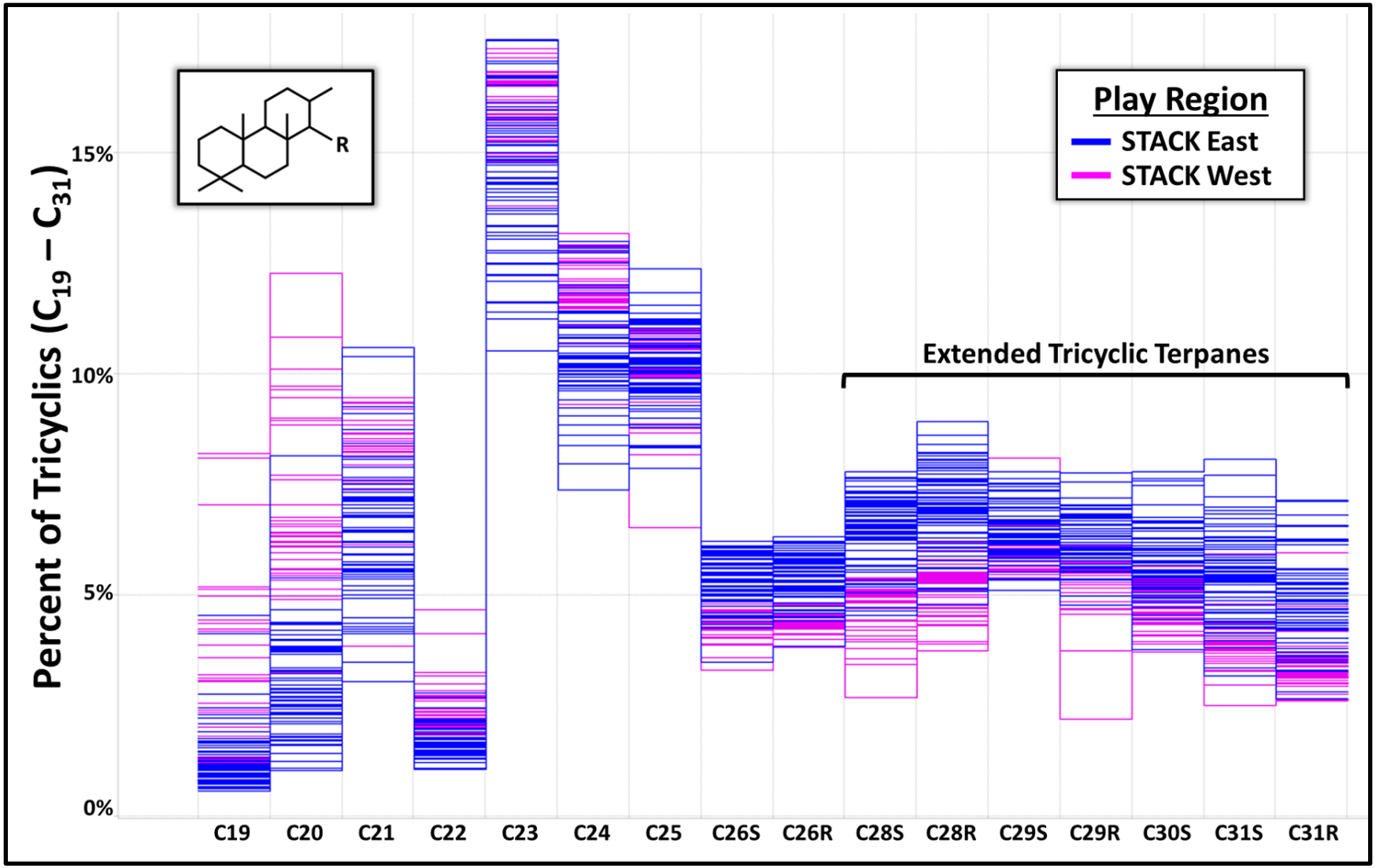

Figure 74. Abundance of the C_{19} through C_{31} tricyclic terpanes for all STACK oils relative to total tricyclic terpanes as determined from peak areas.

Key	Play Region	$C_{19}TT$	$C_{20}TT$	$C_{21}TT$	$C_{22}TT$	$C_{23}TT$	$C_{24}TT$	$C_{25}TT$	$C_{26}TT(S)$	$C_{26}TT(R)$	$C_{28}TT(S)$	$C_{28}TT(R)$	$C_{29}TT(S)$	$C_{29}TT(R)$	$C_{30}TT(S)$	$C_{31}TT(S)$	$C_{31}TT(R)$	$C_{33}TT+$	$C_{24}TET$
1	STACK West	12.8	65.3	83.4	20.9	165.9	117.7	107.6	44.7	42.2	47.0	47.7	58.4	58.2	56.4	37.2	33.7	340.7	36.9
2	STACK West	13.6	68.8	88.0	23.0	171.0	120.1	110.8	45.8	43.4	49.3	53.7	60.1	53.2	50.7	38.3	29.8	327.8	38.3
3	STACK West	12.3	62.2	82.7	20.5	161.9	113.8	105.4	43.4	41.8	49.0	52.4	57.4	55.3	42.1	37.8	29.6	303.2	36.1
4	STACK West	11.5	56.8	76.5	19.2	148.7	104.6	97.2	41.2	38.2	48.1	48.0	51.8	50.5	40.0	35.5	28.2	305.3	31.7
5	STACK West	12.8	64.4	85.1	21.1	167.7	117.1	110.2	45.5	43.9	51.5	54.2	59.0	59.1	46.2	39.0	31.9	421.9	39.5
6	STACK West	8.7	33.9	61.2	12.9	109.3	80.5	75.6	30.9	29.5	39.0	42.9	40.4	41.2	36.4	27.5	22.3	229.2	14.5
7	STACK West	9.9	45.7	66.7	16.1	127.5	91.3	85.2	36.3	33.9	37.9	41.5	48.4	48.1	42.6	29.9	26.5	297.0	27.6
8	STACK West	8.4	36.5	54.7	13.9	106.9	75.5	72.3	30.1	30.0	32.2	36.3	41.4	42.0	34.5	28.4	20.6	205.9	23.1
9	STACK West	9.8	41.4	60.5	15.1	118.8	85.6	79.4	34.6	33.9	38.0	40.8	45.0	42.7	39.4	29.2	28.5	243.8	21.3
10	STACK West	9.0	39.5	57.5	14.9	113.1	83.2	77.5	33.3	33.3	36.7	41.2	46.3	44.9	36.3	32.2	26.6	283.4	21.6
11	STACK West	12.2	66.4	86.5	22.0	174.4	123.3	112.3	46.2	45.3	51.9	56.0	62.7	62.2	53.2	39.6	35.6	378.1	37.6
12	STACK West	11.9	59.7	84.9	19.8	156.0	115.8	105.5	44.5	42.1	54.5	58.9	60.3	58.2	48.8	35.3	25.4	284.9	32.1
13	STACK West	11.9	55.7	73.5	19.8	150.9	108.9	100.4	41.2	41.0	43.9	43.3	53.5	52.5	48.9	33.5	32.5	367.0	32.5
14	STACK West	12.0	56.1	82.4	21.5	158.8	116.9	105.2	43.7	42.8	47.4	47.8	53.3	50.6	46.0	31.0	28.5	322.2	31.9
15	STACK West	8.5	34.1	56.3	14.3	108.7	83.2	74.5	31.9	30.4	33.5	36.3	40.0	36.7	29.3	27.4	22.5	238.6	18.3
16	STACK West	10.8	52.1	77.2	19.1	148.3	111.1	102.6	41.0	41.4	49.5	51.5	55.1	55.3	49.8	40.7	29.7	316.1	32.5
17	STACK West	12.9	45.6	42.1	13.6	82.5	60.9	51.5	20.4	20.2	21.3	25.0	29.1	26.2	21.9	17.8	16.0	110.7	9.1
18	STACK West	7.4	18.8	14.2	6.1	29.7	20.1	17.1	8.2	8.7	8.5	9.2	11.4	10.3	9.1	7.5	6.9	56.0	0.9
19	STACK West	6.2	14.9	17.8	4.4	32.0	25.5	20.0	7.9	7.4	8.3	8.5	10.8	9.4	8.9	6.5	5.4	57.6	3.5
20	STACK West	6.3	7.7	11.9	3.4	22.1	17.4	14.4	6.4	6.4	6.7	6.8	9.7	7.6	6.9	5.8	5.3	47.2	0.7
21	STACK West	0.0	0.0	0.0	0.0	0.0	0.0	0.0	0.0	0.0	0.0	0.0	0.0	0.0	0.0	0.0	0.0	0.0	0.0
22	STACK West	0.0	0.0	0.0	0.0	0.0	0.0	0.0	0.0	0.0	0.0	0.0	0.0	0.0	0.0	0.0	0.0	0.0	0.0
23	STACK West	0.0	0.0	0.0	0.0	0.0	0.0	0.0	0.0	0.0	0.0	0.0	0.0	0.0	0.0	0.0	0.0	0.0	0.0
24	STACK West	0.0	0.0	0.0	0.0	0.0	0.0	0.0	0.0	0.0	0.0	0.0	0.0	0.0	0.0	0.0	0.0	0.0	0.0
25	STACK West	6.2	7.8	6.6	2.8	13.1	9.3	7.7	3.4	4.2	3.0	3.4	5.0	4.2	3.3	3.7	3.8	11.5	0.6
26	STACK West	12.5	23.9	23.5	5.3	39.9	29.9	21.9	9.7	10.9	10.0	11.3	14.7	12.0	11.2	7.4	8.2	49.2	2.7
27	STACK West	12.2	37.7	56.9	14.8	104.7	77.9	64.6	26.6	26.9	28.7	30.5	35.8	33.3	25.0	19.3	16.0	206.3	14.5
28	STACK West	19.7	69.0	92.4	23.0	178.4	129.9	113.8	46.6	46.2	48.7	52.5	56.5	54.6	40.6	33.7	28.5	72.2	31.4
29	STACK West	22.7	96.4	118.7	30.7	220.1	159.0	134.1	53.3	52.1	55.7	57.6	68.2	61.4	52.9	42.4	43.7	357.3	33.8
30	STACK West	15.4	31.0	43.2	11.1	76.6	64.5	50.0	21.0	22.0	24.9	26.7	30.8	27.9	23.0	17.2	15.6	155.7	1.9
31	STACK West	9.1	16.0	28.7	6.9	57.0	49.3	40.3	18.9	19.0	22.2	22.1	22.9	21.7	19.5	15.3	12.4	146.9	2.2
32	STACK West	11.9	18.9	31.3	8.2	56.5	46.3	38.5	16.3	17.1	20.5	21.0	24.1	24.1	18.5	14.5	13.6	110.7	2.7
33	STACK West	6.5	8.3	12.6	3.5	24.3	18.1	14.4	6.6	6.7	7.6	8.1	9.3	8.4	7.3	6.3	5.2	30.4	0.6
34	STACK West	8.4	18.0	23.1	7.8	46.3	32.1	27.4	12.7	12.8	12.2	13.0	15.3	12.9	13.8	10.1	9.6	75.5	1.0
35	STACK West	12.1	4.9	9.1	2.9	20.6	13.9	14.6	5.4	7.1	4.0	5.8	12.1	8.3	9.3	7.2	8.9	0.0	1.4
36	STACK West	0.0	0.0	0.0	0.0	0.0	0.0	0.0	0.0	0.0	0.0	0.0	0.0	0.0	0.0	0.0	0.0	0.0	0.0
37	STACK West	4.9	13.9	17.0	5.6	35.5	26.6	22.3	9.5	9.6	10.5	10.8	11.4	9.9	9.6	7.5	6.6	60.6	2.4
38	STACK West	9.3	24.1	19.7	5.2	36.2	26.9	21.6	9.5	10.1	7.9	8.3	14.6	8.3	8.6	5.5	6.7	42.8	1.2
39	STACK West	7.3	12.4	10.5	3.7	21.5	15.6	11.5	6.1	5.4	5.7	6.0	9.4	6.4	7.2	6.1	5.9	57.2	0.3
40	STACK West	8.0	15.8	17.1	5.9	35.1	26.3	21.6	9.1	9.5	9.6	10.4	13.8	13.6	11.5	9.1	8.3	79.2	0.9
41	STACK West	0.0	0.0	0.0	0.0	0.0	0.0	0.0	0.0	0.0	0.0	0.0	0.0	0.0	0.0	0.0	0.0	0.0	0.0
42	STACK West	2.3	6.3	2.4	1.2	6.3	5.1	4.7	2.3	2.2	2.4	3.2	2.9	1.9	2.8	3.0	1.5	7.8	0.8
43	STACK West	8.0	15.8	10.7	4.3	23.1	15.6	13.7	5.6	6.7	6.2	6.7	9.1	7.9	7.9	7.5	7.4	34.9	0.4
44	STACK West	0.0	0.0	0.0	0.0	0.0	0.0	0.0	0.0	0.0	0.0	0.0	0.0	0.0	0.0	0.0	0.0	0.0	0.0
45	STACK West	0.0	0.0	0.0	0.0	0.0	0.0	0.0	0.0	0.0	0.0	0.0	0.0	0.0	0.0	0.0	0.0	0.0	0.0

Key	Play Region	$C_{19}TT$	$C_{20}TT$	$C_{21}TT$	$C_{22}TT$	$C_{23}TT$	$C_{24}TT$	$C_{25}TT$	$C_{26}TT(S)$	$C_{26}TT(R)$	$C_{28}TT(S)$	$C_{28}TT(R)$	$C_{29}TT(S)$	$C_{29}TT(R)$	$C_{30}TT(S)$	$C_{31}TT(S)$	$C_{31}TT(R)$	$C_{33}TT+$	$C_{24}TET$
46	STACK West	0.0	0.0	0.0	0.0	0.0	0.0	0.0	0.0	0.0	0.0	0.0	0.0	0.0	0.0	0.0	0.0	0.0	0.0
47	STACK East	0.0	0.0	0.0	0.0	0.0	0.0	0.0	0.0	0.0	0.0	0.0	0.0	0.0	0.0	0.0	0.0	0.0	0.0
48	STACK East	0.0	0.0	0.0	0.0	0.0	0.0	0.0	0.0	0.0	0.0	0.0	0.0	0.0	0.0	0.0	0.0	0.0	0.0
49	STACK East	0.0	0.0	0.0	0.0	0.0	0.0	0.0	0.0	0.0	0.0	0.0	0.0	0.0	0.0	0.0	0.0	0.0	0.0
50	STACK East	5.1	9.8	17.6	5.4	33.5	29.6	26.6	11.7	11.7	12.9	13.8	17.7	16.2	13.3	11.0	10.4	107.0	2.0
51	STACK East	2.6	1.9	2.6	1.2	6.7	5.7	6.1	2.6	2.7	3.2	3.5	4.1	3.3	4.3	3.8	3.6	26.5	0.1
52	STACK East	0.0	0.0	0.0	0.0	0.0	0.0	0.0	0.0	0.0	0.0	0.0	0.0	0.0	0.0	0.0	0.0	0.0	0.0
53	STACK East	3.1	3.6	8.5	3.3	22.8	20.4	19.1	10.0	10.4	13.2	15.1	15.5	14.0	15.2	12.8	12.5	137.1	0.6
54	STACK East	4.6	5.4	13.1	3.8	31.2	25.6	24.0	12.9	12.7	15.9	16.3	18.0	17.1	17.2	13.7	13.1	165.3	0.4
55	STACK East	4.6	8.0	19.4	4.7	37.8	29.8	28.1	14.7	16.6	18.4	19.7	19.9	20.2	16.9	15.4	13.8	160.3	2.6
56	STACK East	0.0	0.0	0.0	0.0	0.0	0.0	0.0	0.0	0.0	0.0	0.0	0.0	0.0	0.0	0.0	0.0	0.0	0.0
57	STACK East	3.2	3.5	10.8	3.1	24.3	19.3	18.8	11.1	10.6	12.9	14.9	14.6	13.5	13.1	12.5	12.3	131.3	0.6
58	STACK East	3.8	5.9	13.5	3.5	34.2	28.7	26.4	15.1	14.9	18.0	19.4	20.6	21.3	18.2	16.1	14.4	156.2	1.1
59	STACK East	4.6	9.2	24.4	5.2	53.3	43.3	41.2	21.8	21.6	25.2	26.7	28.0	26.9	25.8	22.9	20.2	233.6	2.0
60	STACK East	0.8	0.9	1.3	0.6	2.3	1.5	1.7	0.7	0.8	1.1	1.8	1.5	1.4	1.5	1.3	1.1	0.0	0.6
61	STACK East	5.8	19.0	35.6	8.9	69.2	58.1	50.9	23.0	23.0	26.2	28.2	30.2	24.8	23.8	20.3	17.6	210.3	10.2
62	STACK East	2.5	1.4	4.9	1.5	17.1	12.5	12.7	8.2	8.9	10.4	10.4	10.5	10.1	9.1	10.8	10.0	99.2	0.5
63	STACK East	3.2	1.4	6.7	1.9	14.8	11.0	11.0	6.5	7.2	8.4	10.7	9.9	9.1	10.2	10.6	9.0	94.3	0.7
64	STACK East	8.4	19.9	40.4	9.5	74.3	59.3	53.9	25.2	26.7	26.2	29.4	30.9	29.5	26.1	22.9	18.1	206.0	11.4
65	STACK East	3.1	3.9	12.1	3.8	33.8	26.6	25.3	16.8	17.2	21.1	22.3	18.1	18.8	17.9	18.9	16.9	63.4	0.9
66	STACK East	7.2	14.5	33.1	6.8	54.8	40.6	34.0	14.0	13.8	14.1	14.8	16.7	16.7	11.7	10.5	8.7	119.0	7.7
67	STACK East	3.2	4.6	15.5	2.8	36.5	26.2	26.4	14.9	15.4	19.2	22.0	19.0	17.2	16.1	17.2	16.9	148.1	1.0
68	STACK East	6.1	18.6	36.2	8.0	67.4	54.8	44.5	18.9	19.4	24.4	24.1	27.3	24.3	21.7	18.3	15.9	151.4	7.9
69	STACK East	6.4	17.2	35.6	8.4	76.2	58.2	54.8	27.2	26.7	32.2	32.2	34.5	33.7	29.9	26.6	23.6	251.0	7.0
70	STACK East	3.8	7.2	22.9	4.9	53.5	40.4	37.6	23.8	24.0	29.7	30.8	27.5	27.5	24.1	25.2	22.2	227.9	1.6
71	STACK East	0.0	0.0	0.0	0.0	0.0	0.0	0.0	0.0	0.0	0.0	0.0	0.0	0.0	0.0	0.0	0.0	0.0	0.0
72	STACK East	6.4	17.7	30.3	8.6	61.3	51.6	47.8	17.2	18.2	18.7	20.5	27.3	25.5	22.3	17.1	13.1	163.7	9.9
73	STACK East	0.0	0.0	0.0	0.0	0.0	0.0	0.0	0.0	0.0	0.0	0.0	0.0	0.0	0.0	0.0	0.0	0.0	0.0
74	STACK East	4.5	8.9	28.1	6.7	71.2	52.6	50.8	31.0	30.6	38.0	39.0	34.1	34.1	31.3	30.0	29.0	309.5	1.8
75	STACK East	5.7	20.3	46.2	10.4	99.1	75.2	75.8	35.8	34.9	47.3	49.2	47.0	46.8	44.5	37.8	31.9	465.4	6.7
76	STACK East	7.2	23.8	47.0	11.4	94.0	74.0	72.5	31.8	32.7	37.9	36.4	43.5	39.1	37.6	34.0	28.0	338.5	10.1
77	STACK East	2.6	1.7	6.5	1.9	18.0	14.1	13.7	9.3	9.8	11.8	13.4	11.9	10.3	10.4	10.7	9.7	101.4	0.8
78	STACK East	2.4	1.7	6.0	2.2	16.4	12.2	11.8	8.3	8.7	11.0	11.6	10.1	9.8	9.5	10.2	9.3	84.7	0.2
79	STACK East	3.4	8.6	23.7	4.8	49.0	36.5	34.2	18.0	18.3	21.3	22.8	19.9	19.2	18.2	17.8	15.1	165.5	3.7
80	STACK East	8.6	16.8	40.5	9.5	68.4	50.2	44.3	17.6	18.0	18.3	20.1	21.5	18.6	14.7	12.3	10.3	132.9	9.9
81	STACK East	4.4	9.6	26.1	6.6	66.6	46.9	45.2	28.1	28.4	32.0	35.7	29.0	27.4	25.4	25.6	24.4	233.6	3.8
82	STACK East	2.7	3.4	9.7	4.2	29.5	21.8	20.9	14.7	14.7	17.3	19.8	15.7	15.9	14.6	15.9	15.5	128.1	1.3
83	STACK East	4.2	14.1	34.7	8.1	82.9	60.1	60.6	33.5	34.5	41.6	41.4	37.6	35.8	35.8	34.3	28.6	322.0	5.5
84	STACK East	1.2	3.5	1.3	0.6	4.6	3.4	3.4	2.0	2.4	2.6	3.3	2.9	2.9	2.6	3.0	3.1	17.6	0.5
85	STACK East	4.7	13.1	31.2	7.1	69.5	49.9	51.1	25.9	26.2	32.8	33.6	31.1	29.2	28.9	26.2	21.7	265.8	5.1
86	STACK East	3.3	12.7	25.9	6.1	72.5	45.9	45.0	26.1	26.6	32.9	35.3	28.9	28.3	25.4	29.1	23.5	247.0	3.4
87	STACK East	5.6	23.8	51.0	11.5	106.6	81.1	82.0	36.1	36.1	44.8	44.6	43.8	42.2	38.1	32.7	29.8	320.2	9.3
88	STACK East	5.0	9.4	23.2	6.5	57.9	42.1	39.2	22.1	22.3	28.0	29.2	26.2	27.3	22.5	22.9	20.7	190.8	3.2
89	STACK East	4.8	16.9	39.8	9.6	95.4	66.6	68.3	36.4	36.1	44.2	44.9	41.1	37.9	36.7	34.0	30.1	338.3	5.6
90	STACK East	20.9	54.8	132.6	28.4	205.2	183.6	177.0	61.7	64.1	72.2	73.2	92.7	86.9	75.7	54.6	47.0	629.3	42.9

Key	Play Region	C_{19}TT	C_{20}TT	C_{21}TT	C_{22}TT	C_{23}TT	C_{24}TT	C_{25}TT	C_{26}TT(S)	C_{26}TT(R)	C_{28}TT(S)	C_{28}TT(R)	C_{29}TT(S)	C_{29}TT(R)	C_{30}TT(S)	C_{31}TT(S)	C_{31}TT(R)	C_{33}TT+	C_{24}TET
91	STACK East	5.2	20.2	48.2	11.2	117.4	81.7	83.1	44.7	45.0	61.9	57.6	48.7	50.9	53.0	44.8	39.4	396.0	7.8
92	STACK East	3.9	9.2	28.2	7.1	73.2	49.5	48.9	29.4	29.5	35.8	37.8	30.5	30.1	28.4	28.7	25.0	252.1	3.8
93	STACK East	9.1	35.3	73.5	16.4	129.9	95.9	93.9	40.8	40.4	46.8	50.9	51.6	47.0	43.6	36.0	30.4	356.1	18.5
94	STACK East	3.3	4.8	14.0	3.7	35.6	25.9	24.4	15.6	15.4	17.9	20.7	17.2	15.7	15.6	15.6	13.5	130.8	2.4
95	STACK East	3.0	3.4	10.4	3.4	26.8	20.1	19.3	12.2	12.8	14.9	16.6	14.0	14.0	13.1	13.8	11.7	120.9	1.2
96	STACK East	3.9	6.1	19.0	5.4	46.3	34.6	34.3	21.1	20.5	24.8	27.8	25.0	26.8	21.0	21.4	16.6	190.1	2.5
97	STACK East	3.1	7.5	18.5	4.9	47.6	34.4	31.6	19.2	19.4	23.4	24.3	20.8	20.4	19.9	18.4	16.4	183.3	3.4
98	STACK East	3.8	6.4	18.7	5.5	50.9	34.7	36.2	21.6	21.7	25.8	28.0	22.9	21.8	20.7	21.8	18.5	171.8	3.3
99	STACK East	4.0	7.4	18.7	4.6	46.2	30.0	30.8	17.2	17.4	20.4	20.1	18.7	17.4	16.7	17.2	14.0	145.5	3.4
100	STACK East	10.3	44.4	75.0	17.8	137.7	98.4	91.6	37.9	38.5	42.7	47.6	42.0	41.1	36.4	34.2	29.1	351.1	23.1
101	STACK East	10.3	41.9	89.4	20.2	176.2	125.4	127.6	55.2	56.3	65.8	72.5	74.1	73.5	58.5	46.0	40.9	600.5	19.2
102	STACK East	6.4	25.4	60.4	14.3	128.6	85.5	84.2	43.3	43.3	51.1	56.4	48.1	48.4	46.3	39.8	34.5	403.8	10.0
103	STACK East	4.0	14.0	32.0	7.9	78.9	50.7	50.8	28.3	28.6	35.6	35.5	31.1	27.6	26.8	27.2	19.4	246.3	6.1
104	STACK East	3.6	6.8	22.0	5.7	57.2	37.7	40.1	23.5	24.1	29.8	32.8	25.4	23.7	22.7	24.5	21.1	189.9	3.3
105	STACK East	4.5	24.7	53.0	12.5	124.5	75.8	76.8	41.3	41.6	50.0	54.9	40.2	42.4	36.2	39.8	34.8	335.1	7.7
106	STACK East	4.2	18.0	42.7	9.3	104.8	62.6	63.5	35.2	35.0	43.1	44.3	37.6	34.6	30.9	33.9	27.8	311.2	6.1
107	STACK East	3.9	16.8	42.3	9.5	105.4	65.4	69.7	39.9	39.6	49.4	50.8	40.7	42.6	38.7	43.1	37.8	332.5	8.6
108	STACK East	3.2	5.5	15.1	3.8	33.6	24.0	22.2	12.8	12.6	13.9	15.0	13.3	14.1	10.9	11.2	9.3	124.4	3.1
109	STACK East	4.6	4.8	16.5	4.3	42.6	30.9	30.2	16.6	17.6	20.8	23.5	19.7	17.7	16.6	18.5	13.0	148.6	3.7
110	STACK East	3.2	4.8	12.3	3.7	25.3	19.3	17.4	10.0	10.6	12.1	12.4	11.2	10.3	10.4	10.0	8.5	91.9	1.9
111	STACK East	3.1	9.5	26.6	6.4	64.6	40.6	42.2	24.1	24.0	29.3	30.2	24.1	24.2	22.1	22.1	20.2	193.9	4.8
112	STACK East	8.0	25.7	56.1	13.0	127.2	78.8	81.2	40.7	40.6	51.9	56.7	50.4	50.0	37.2	37.5	33.0	405.2	9.3
113	STACK East	6.7	27.6	64.8	15.4	136.9	96.2	104.0	47.5	48.2	57.9	59.7	57.4	58.8	54.9	51.3	43.0	509.1	18.2
114	STACK East	6.6	31.9	64.9	13.5	143.4	92.6	95.6	45.4	44.6	53.7	57.7	48.6	45.7	41.7	37.0	34.3	492.7	11.8
115	STACK East	8.8	25.5	54.9	14.4	108.6	75.7	75.9	34.7	34.5	37.3	42.0	39.6	39.5	35.1	26.8	23.4	339.3	15.4
116	STACK East	6.8	29.1	64.4	14.1	139.6	92.3	96.1	44.4	44.7	56.6	59.7	50.6	50.2	43.9	40.5	36.9	482.0	10.9
117	STACK East	6.5	23.0	55.3	13.9	120.3	80.7	83.8	40.3	40.1	46.5	50.0	44.7	45.4	37.8	33.1	32.7	454.1	11.8
118	STACK East	6.9	34.0	64.3	14.4	151.6	90.2	94.6	46.1	46.4	58.3	62.7	51.4	49.9	40.4	44.1	35.8	460.4	14.5
119	STACK East	6.8	27.7	54.4	12.6	125.6	74.8	78.4	38.2	38.9	47.3	48.4	43.7	43.5	35.4	31.2	28.8	414.1	12.2
120	SCOOP	2.7	6.1	12.8	3.2	27.0	18.8	17.6	9.2	9.6	9.4	9.6	12.5	13.5	8.4	7.4	7.0	56.7	3.6
121	SCOOP	0.0	0.0	0.0	0.0	0.0	0.0	0.0	0.0	0.0	0.0	0.0	0.0	0.0	0.0	0.0	0.0	0.0	0.0
122	SCOOP	0.0	0.0	0.0	0.0	0.0	0.0	0.0	0.0	0.0	0.0	0.0	0.0	0.0	0.0	0.0	0.0	0.0	0.0
123	SCOOP	0.0	0.0	0.0	0.0	0.0	0.0	0.0	0.0	0.0	0.0	0.0	0.0	0.0	0.0	0.0	0.0	0.0	0.0
124	SCOOP	4.7	5.0	19.7	8.7	52.3	45.9	43.7	30.2	30.9	41.1	44.7	38.2	37.8	35.3	31.4	28.8	301.8	2.3
125	SCOOP	2.5	3.0	10.8	2.6	29.9	30.9	29.8	17.6	18.0	21.2	21.6	26.4	26.2	20.5	17.0	16.9	143.4	0.6
126	SCOOP	1.6	1.7	4.6	2.2	12.7	10.2	8.9	5.6	6.1	7.3	7.2	6.3	6.1	6.1	6.7	6.5	29.1	0.8
127	SCOOP	2.2	3.6	5.5	2.8	12.1	9.4	8.4	4.5	4.4	6.5	6.6	5.5	5.0	5.6	6.1	4.4	20.8	0.8
128	SCOOP	2.3	1.5	4.8	1.4	12.2	8.7	8.0	6.6	6.1	6.7	7.3	6.4	5.8	6.4	6.6	6.5	43.8	1.0
129	SCOOP	1.7	1.1	4.9	1.4	11.7	7.7	8.0	4.9	5.0	6.1	7.0	5.9	6.1	5.6	5.5	5.0	32.6	0.9
130	SCOOP	1.6	1.0	3.5	0.2	9.8	6.8	6.6	5.0	5.3	5.6	5.8	5.1	4.9	5.6	6.4	4.8	40.0	0.4
131	SCOOP	1.8	1.2	4.7	1.9	10.8	6.9	6.7	4.7	5.3	6.2	7.2	6.4	6.0	5.2	6.3	6.4	64.7	0.5
132	SCOOP	3.0	3.0	11.8	7.8	37.3	32.9	33.6	24.7	25.8	35.1	38.0	36.2	36.7	31.6	32.0	30.7	339.6	1.6
133	SCOOP	2.1	1.6	4.5	2.3	10.4	6.8	7.3	5.0	5.5	6.8	7.4	5.7	6.6	5.5	6.8	6.6	34.2	1.0
134	SCOOP	3.4	6.3	3.6	2.5	10.4	8.6	9.0	7.6	8.1	9.9	10.2	9.4	9.2	10.0	10.7	7.4	50.1	0.2
135	SCOOP	1.7	2.0	6.2	1.7	13.2	9.7	9.9	7.2	7.2	7.5	8.5	6.6	6.5	5.5	7.2	6.4	40.6	1.1

Key	Play Region	$C_{19}TT$	$C_{20}TT$	$C_{21}TT$	$C_{22}TT$	$C_{23}TT$	$C_{24}TT$	$C_{25}TT$	$C_{26}TT(S)$	$C_{26}TT(R)$	$C_{28}TT(S)$	$C_{28}TT(R)$	$C_{29}TT(S)$	$C_{29}TT(R)$	$C_{30}TT(S)$	$C_{31}TT(S)$	$C_{31}TT(R)$	$C_{33}TT+$	$C_{24}TET$
136	SCOOP	1.5	1.0	3.6	1.8	11.1	7.2	6.6	4.7	4.8	5.1	5.7	5.6	5.1	4.2	5.4	5.4	32.7	0.4
137	SCOOP	1.7	2.1	5.0	1.3	11.7	9.1	8.8	5.9	5.8	6.7	7.8	6.8	7.7	5.6	5.7	5.1	46.7	0.8
138	SCOOP	1.2	1.4	3.1	1.0	6.7	4.8	5.0	3.1	3.0	3.6	3.6	3.9	3.7	3.0	3.6	3.5	21.4	0.8
139	SCOOP	0.8	0.7	1.5	0.7	3.8	2.6	2.9	1.8	2.0	1.5	2.2	1.3	1.7	1.4	2.5	1.5	0.0	0.6
140	SCOOP	0.9	1.0	1.2	0.3	2.6	1.9	1.8	0.9	1.2	0.9	1.4	1.6	1.6	1.0	1.4	0.8	0.0	0.7
141	SCOOP	1.5	1.5	2.6	0.8	7.2	4.6	5.1	3.4	3.5	3.6	4.3	3.6	3.8	3.8	3.0	2.9	7.9	0.5
142	SCOOP	1.7	2.2	2.1	2.2	6.8	4.7	6.0	3.3	4.0	4.1	5.0	3.3	4.4	3.4	3.8	3.5	15.8	0.6
143	SCOOP	1.0	1.0	2.5	1.3	6.5	4.9	4.0	3.4	3.3	4.4	3.9	3.0	3.5	3.3	3.9	3.9	14.1	0.3
144	SCOOP	1.8	2.4	6.3	2.4	14.3	10.1	10.2	5.8	5.8	7.6	7.8	6.0	6.2	7.1	6.7	5.2	43.1	1.1
145	SCOOP	1.8	4.1	6.3	1.6	17.2	11.8	12.7	8.7	9.2	10.8	11.1	10.0	9.8	9.3	10.1	7.9	84.5	1.7
146	SCOOP	1.7	1.9	6.2	2.0	15.2	9.2	9.7	7.2	7.8	8.9	10.6	7.8	7.8	6.9	8.3	6.8	72.2	1.7
147	SCOOP	2.3	1.7	7.1	1.8	14.0	10.5	9.0	7.2	7.5	7.3	8.8	7.6	7.4	6.1	7.9	7.2	73.3	1.5
148	SCOOP	1.7	1.2	2.2	1.4	6.1	4.7	4.4	4.3	3.5	4.3	4.1	3.8	3.5	2.8	4.0	3.2	18.3	0.5
149	SCOOP	3.0	6.3	12.4	4.1	28.9	19.8	18.8	10.9	11.1	12.7	14.5	11.8	12.2	10.4	11.4	8.6	72.3	2.7
150	SCOOP	0.0	0.0	0.0	0.0	0.0	0.0	0.0	0.0	0.0	0.0	0.0	0.0	0.0	0.0	0.0	0.0	0.0	0.0
151	SCOOP	2.8	3.0	5.8	2.0	14.9	11.3	10.3	6.8	7.0	8.4	9.4	7.8	7.1	6.6	6.5	6.1	47.3	0.9
152	SCOOP	3.2	4.3	9.0	3.3	21.2	15.5	14.4	9.0	9.0	10.7	9.9	8.6	7.3	8.7	8.3	6.8	59.3	2.2
153	SCOOP	1.5	3.0	2.6	1.7	4.6	3.8	2.8	1.7	1.9	1.8	1.6	1.5	1.3	2.0	1.4	0.9	6.4	0.7
154	SCOOP	2.9	7.7	16.6	4.8	40.1	28.9	27.7	16.7	16.6	19.3	21.4	16.7	17.1	14.8	14.0	12.4	112.4	3.5
155	SCOOP	5.8	23.9	68.5	19.2	247.2	146.0	171.0	94.1	95.2	143.5	149.9	104.4	98.1	104.2	95.7	85.6	998.6	18.8
156	SCOOP	2.3	2.2	9.3	2.4	29.9	26.1	26.4	20.9	22.1	33.1	36.5	31.8	30.3	28.3	29.9	28.6	282.9	1.7
157	SCOOP	2.0	1.5	2.7	1.6	5.3	4.7	3.7	3.3	3.1	3.0	3.5	3.3	3.3	3.1	3.5	2.2	5.2	0.5
158	SCOOP	1.9	1.5	2.2	0.6	6.5	4.9	4.4	3.0	3.6	3.2	3.9	4.2	3.6	3.9	3.7	3.1	25.2	0.9
159	SCOOP	3.2	7.9	13.4	3.7	29.1	20.0	19.0	10.1	10.2	12.1	12.4	11.3	10.4	9.4	9.3	7.2	68.4	3.1
160	SCOOP	1.6	1.4	4.7	1.6	14.6	11.7	13.3	10.2	11.7	15.4	17.9	17.8	18.9	16.8	17.6	16.6	198.7	1.0
161	SCOOP	1.8	5.8	7.0	3.7	20.5	20.2	18.9	12.6	12.6	13.7	13.8	17.0	17.7	14.5	12.1	11.8	101.2	0.5
162	SCOOP	1.3	1.4	3.0	2.5	10.5	8.4	10.3	7.0	8.7	10.3	13.0	16.9	16.6	13.1	15.2	15.0	214.2	0.7
163	SCOOP	0.0	0.0	0.0	0.0	0.0	0.0	0.0	0.0	0.0	0.0	0.0	0.0	0.0	0.0	0.0	0.0	0.0	0.0
164	SCOOP	1.3	2.0	2.4	1.3	5.2	4.2	4.0	2.2	3.1	3.2	4.6	4.4	3.4	4.3	3.8	4.0	24.3	0.4
165	SCOOP	1.3	1.0	4.5	3.0	12.5	9.3	11.9	9.1	10.3	16.4	18.1	18.9	18.3	17.4	17.8	17.6	221.6	0.2
166	SCOOP	2.6	3.5	7.8	3.8	23.4	22.2	22.9	18.5	20.2	28.4	32.2	32.5	30.8	29.0	29.8	28.1	344.9	1.2
167	SCOOP	1.6	1.0	2.7	2.2	6.6	6.3	7.0	4.8	6.3	7.9	9.6	14.3	12.4	8.9	11.1	10.0	155.9	0.2
168	SCOOP	2.6	4.8	11.5	4.7	36.2	34.3	36.2	25.4	25.8	39.8	43.0	39.8	39.1	35.6	33.7	33.4	341.8	0.7
169	SCOOP	2.9	12.6	26.8	7.1	65.2	34.1	40.6	19.8	18.8	21.6	24.1	18.6	19.3	15.3	17.5	14.4	128.8	8.7
170	SCOOP	3.7	3.4	8.9	3.5	23.4	23.2	23.2	19.2	20.3	29.6	31.3	31.7	31.6	30.7	29.1	28.0	310.6	0.4
171	SCOOP	3.1	6.0	22.0	5.2	69.1	61.8	62.6	41.4	42.7	63.4	68.4	62.0	57.9	54.1	52.6	46.4	577.7	1.6
172	SCOOP	0.7	1.3	1.5	0.8	2.5	2.0	1.5	1.0	1.1	1.3	1.7	1.3	1.0	1.7	1.4	1.0	0.0	0.3

Table 16. The concentration in ppm of each member of the tricyclic terpane homologue series ranging from $C_{19}TT$ through $C_{39}TT$ and the C_{24} tetracyclic terpane ($C_{24}TET$). The extended tricyclic terpanes $C_{33}TT$ through $C_{39}TT$ are grouped into a single column $C_{33}TT+$.

While the exact origin of tricyclic terpanes remains ambiguous, some tricyclic terpanes have been shown empirically to correlate well with depositional environment. For example, RQ-mode factor analysis of global oil databases found that the C_{19}, C_{20}, C_{24}, and C_{25} TT were useful for differentiating oils from paralic and deltaic sources (Zumberge, 1987), and elevated C_{20}/C_{23} ratios have been correlated to relative sea level drop and marine regression in the phosphatic Galembo member in the La Luna formation of the Magdelena Basin, Colombia (Rangel et al., 2000). By plotting the tricyclic terpane ratios C_{22}/C_{21} versus C_{24}/C_{23}, Zumberge et al. (2007) were able to successfully differentiate oils generated from carbonate and siliciclastic source rocks. A re-creation of this cross plot is shown in Figure 75 and demonstrates that all STACK oils cluster tightly in the zone attributed to siliciclastic source rock lithology. This is important because while there appears to be at least two geochemically distinct organic facies in STACK, both appear to broadly share a common siliciclastic source rock lithology.

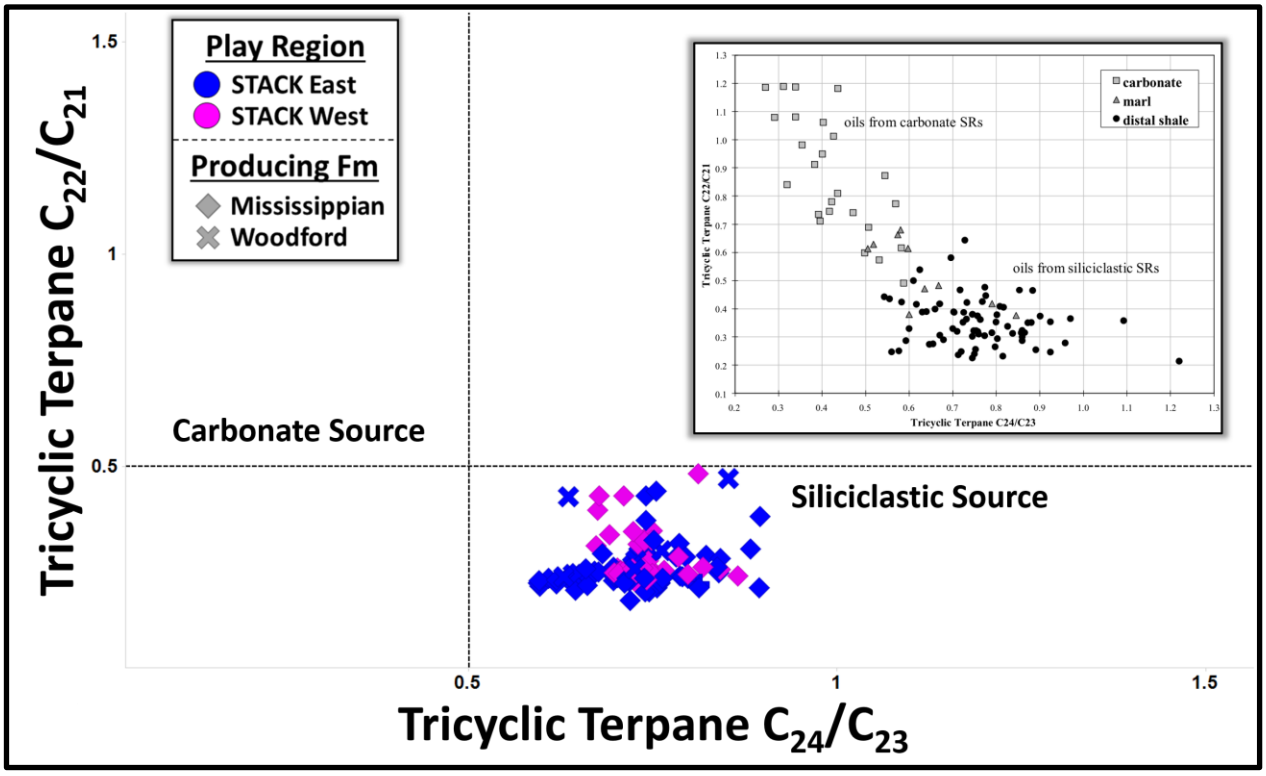

Figure 75. Crossplot of the C_{22}/C_{21} TT versus C_{24}/C_{23} TT showing all STACK oils plot in the zone attributed to siliciclastic source material. Original plot from Zumberge et al., (2007).

In heating experiments of immature bitumen, Aquino Neto et al. (1983) observed an overall shift towards smaller tricyclic terpanes with increased maturity, especially C_{19}-C_{21}TTs, and hypothesized that some tricyclic terpanes may result from thermal cleavage of the isoprenoidal side chain attached to the tricyclic ring structure. In a study of tar sands, Ekweozor (1984) compared the biomarker fingerprints of maltenes to the solvent extracts of chemically degraded asphaltenes and observed that tricyclic terpanes were found in the asphaltene fraction at the near complete exclusion of hopanes, and vice versa. It was speculated that asphaltene material possess openings of specific dimensions that are capable of including or excluding non-asphaltene material depending on molecular size and structure; therefore, both the capture and subsequent release of asphaltene-bound material would relate to the size, arrangement, and stability of chemical bonds affording molecular porosity to the asphaltenes. In outcrop, Kruge et al. (1990) observed a shift in the m/z 191 fingerprint from cheilanthane-dominated to hopane-dominated in extracts moving farther from a known mature source rock (~1.1% Ro) and speculated that tricyclic terpanes are progressively released at higher maturities by cracking polar compounds. A more detailed summary of tricyclic terpane enrichment in oils and extracts can be reviewed in Philp et al. (2021).

If the release of tricyclic terpanes relative to hopanes reflects the chemical nature of its asphaltenes and, by extension, its organic facies, so too might the relative release of different members of the tricyclic terpane homologue series. To test this hypothesis, the individual rate decline exponents for each of C_{19}-C_{31}TT is plotted in Figure 76 and shows different trends in each Play Region. The smaller (less negative) rate decline exponent for C_{19}-C_{21} TT likely reflects novel generation of these compounds by cleavage of the isoprenoidal side chain as predicted by Aquino Neto et al. (1983). STACK East oils show large rate decline exponents for smaller cheilanthanes (-5.54) which gets smaller with increasing carbon number (-3.42), meaning the efficiency of

generating these compounds with maturity depends on the length of the isoprenoidal chain at C-14. Smaller cheilanthanes are released more efficiently at lower maturities and are rapidly depleted with increased maturity. STACK West, however, shows almost no preference for generating smaller cheilanthanes and show similar rate decline exponents across the entire series.

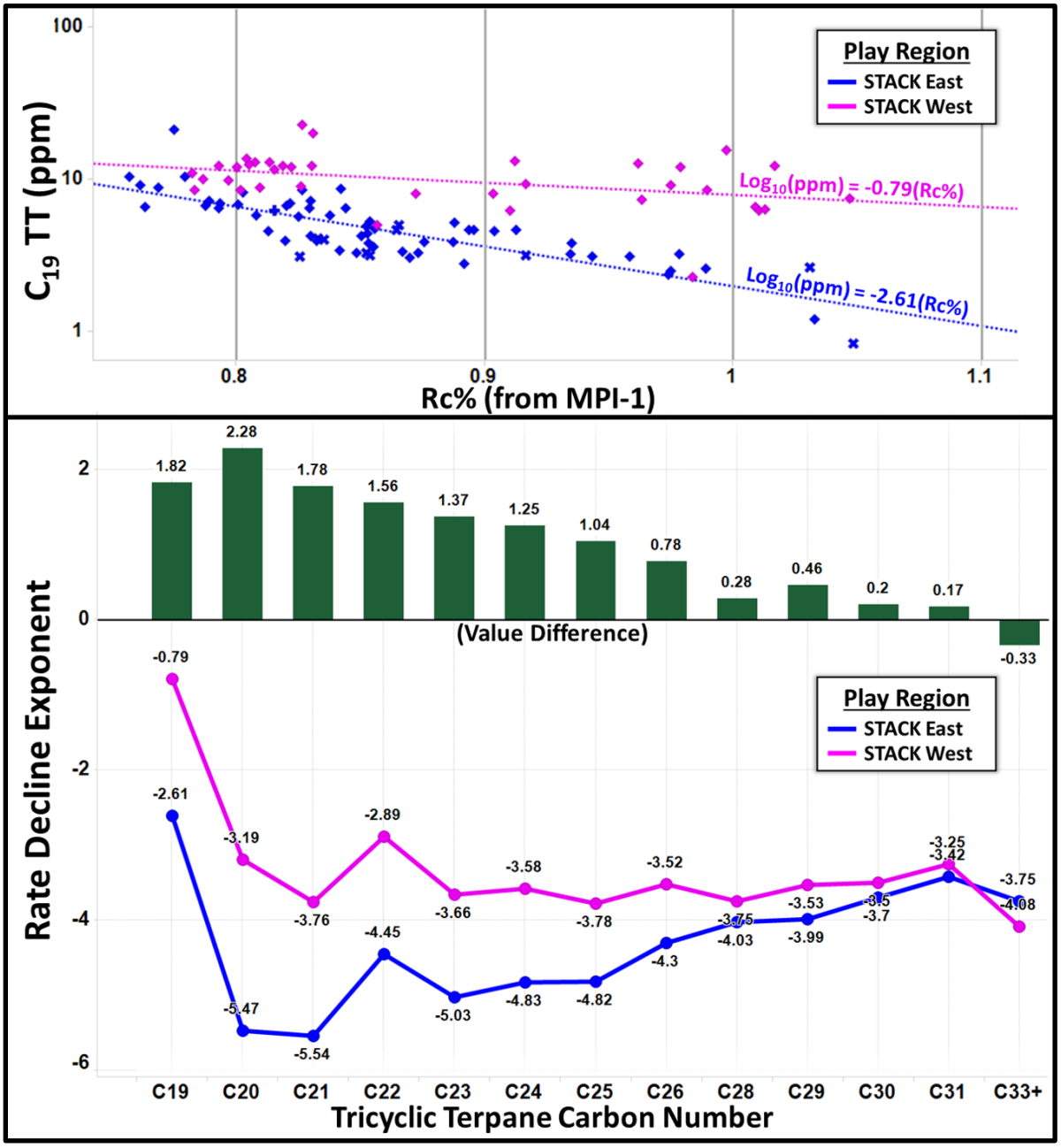

Figure 76. Upper: Example rate decline exponent calculation for the C_{19} tricyclic terpane (STACK West=-0.79; STACK East=-2.61). Lower: Combination plot showing rate decline exponents for the tricyclic terpane series in STACK Play Regions (lines) as well as the difference in values between STACK East and STACK West (bars).

The exact mechanism governing the preferential generation of some cheilanthanes over others is still unclear, but it is here hypothesized to result from the chemical nature, molecular porosity, and bond stability of macromolecules like kerogen, bitumen, or asphaltene material inherited from its organic facies. It is promising that the differences in rate decline exponents between Play Regions mirror the distinct clustering observed in numerous other source parameters reviewed in this chapter, most notably the light hydrocarbons. One explanation is that the macromolecule material in STACK West could contains a higher proportion of labile bonds as part of the molecular pore geometry, such as ether and thioether bonds, which are more easily degraded resulting in the more efficient release of the occluded components like tricyclic terpanes. By comparison, STACK East may contain pores bounded by unreactive bonds that are less easily degraded and retain their trapped material until higher stages of thermal cracking.

C_{24} Tetracyclic Terpane

The C_{24} tetracyclic terpane (**XIII**; C_{24}TET) has been linked to source rocks deposited in shallow marine shelves of semi-closed oceanic basins with limited access to upwelling nutrients (Zumberge et al., 2007), epicontinental carbonate or evaporite settings (Palacas, 1988; Clark and Philp, 1989), and oxic and/or terrigenous deposition (Philp and Gilbert, 1986). Although its origin remain largely inconclusive, C_{24}TET is thought to form through cleavage of the E-ring in precursor hopanoids by oxidation or microbial attack (Trendel et al., 1982; Aquino Neto et al., 1983), but isotopic evidence suggests it could be independently synthesized (Grice, 2001).

The abundance of C_{24}TET is often measured by a variety of common ratios, including C_{24}TET/C_{26}TT, C_{24}TET/C_{23}TT, and C_{24}TET/hopane; however, these ratios contain compounds of different ring counts in the numerator and denominator which may exacerbate the effect of

maturity on the ratio (see Figure 49). Additional care should be taken when selecting ratios to measure C_{24}TET such that the values reflect differences in organic facies rather than maturity. To account for this, two plots containing the concentration of C_{24}TET and the ratio of C_{24}TET/C_{26}TT (S) are plotted against maturity in semi-log space and shown in Figure 77. When normalized to maturity, oils in STACK West exhibit both higher concentrations of C_{24}TET and higher values for C_{24}TET/C_{26}TT (S) compared to STACK East. Unfortunately, the strong correlation both of these ratios show with maturity limits makes it difficult to utilize in map view without a transformation to somehow normalize for maturity. However, while this ratio may not provide a deterministic way to observe changes in organic facies in map view, it may provide valuable insight into the nature of organic facies that have otherwise been determined.

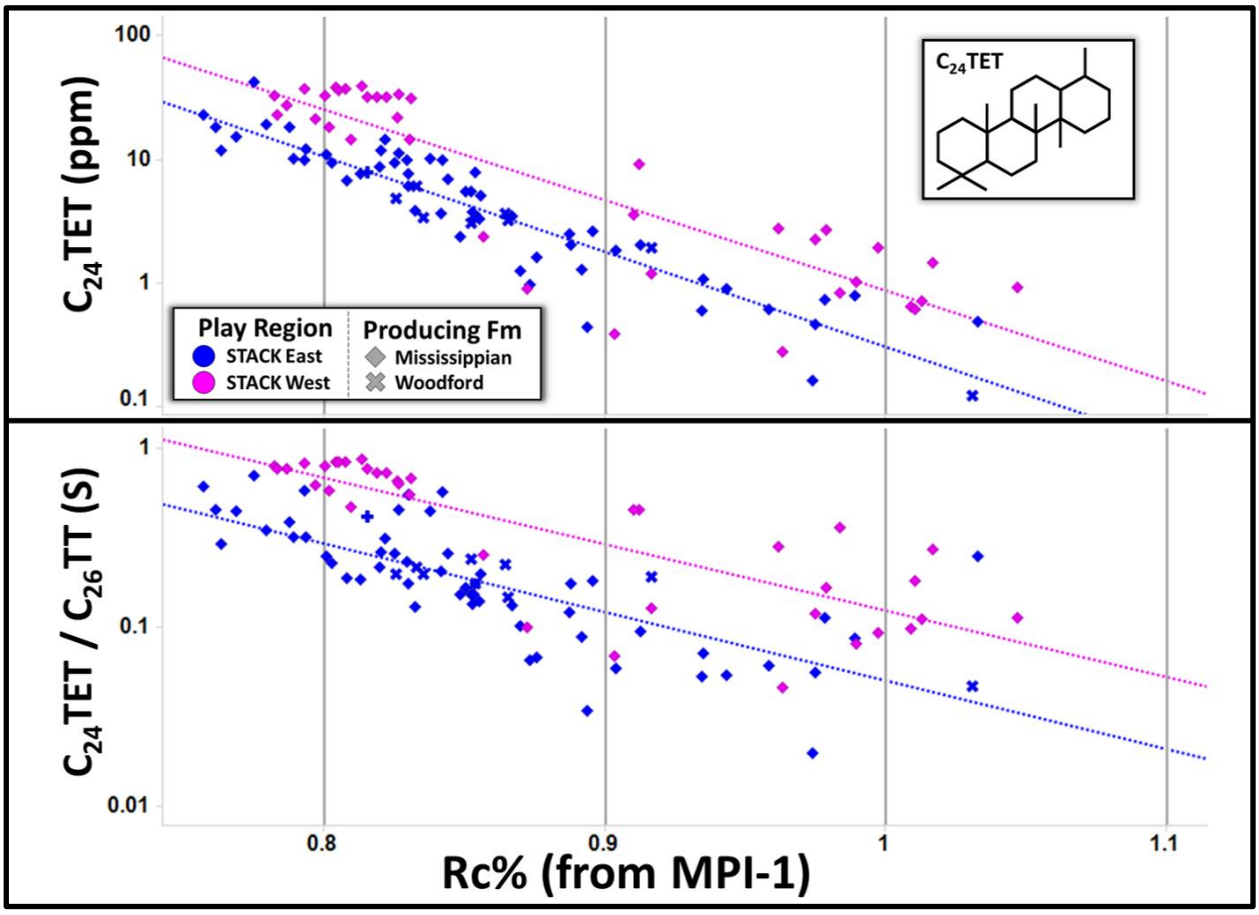

Figure 77. Two semi-log cross plots showing both enrichment of C_{24}TET in STACK West samples both in terms of absolute concentrate (upper) and relative to a nearby eluting tricyclic terpane (lower).

Hopanes

Hopanes are pentacyclic triterpanes most often associated with lipid cell membranes found in aerobic prokaryotic bacteria (Rohmer et al., 1979). The C_{30} hopane derivatives are formed from the direct cyclization of squalene into diploptene and/or diplopterol; however, in the C_{35} hopane derivatives, the C_{30} hopane skeleton (**VI**) is linked at C-30 to a C_5 *n*-alkyl polysubstituted chain, the most common of which are the bacteriohopane-tetrol and -amino-triol (Rohmer et al., 1979; Ourisson et al., 1982, 1984, and 1987). Examples of the m/z 191 mass chromatograms in Figure 78 show that in oils of similar maturities, STACK West oils have more pronounced peaks for the 17α(H),21β(H)-30-norhopane ($C_{29}H$) and C_{31}-C_{35} homohopanes ($C_{31\text{-}35}H$) compared to STACK East. Oils and extracts from organic-rich carbonates and evaporates have been observed containing unusually high amounts of $C_{29}H$ (Zumberge, 1984; Connan et al., 1986; Price et al., 1987), and Riva et al. (1989) proposed that the ratio $C_{29}H/C_{30}H$ may relate a source rocks "carbonaticity," or to depositional conditions more favorable for anoxic carbonate or marl deposition.

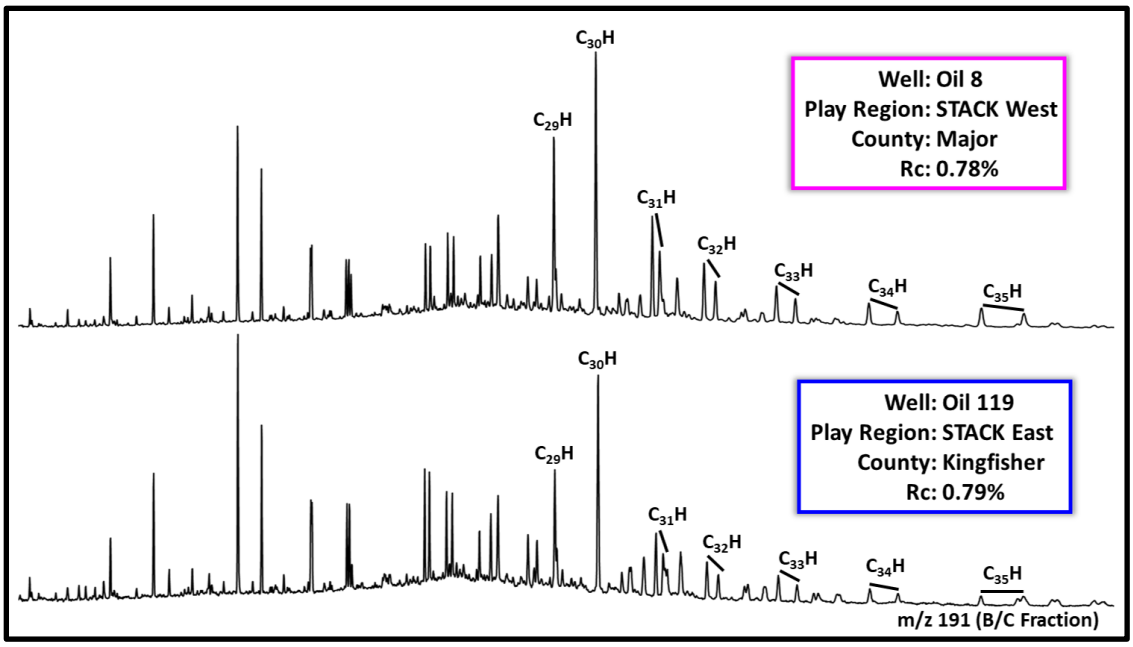

Figure 78. Examples of m/z 191 mass chromatograms from two oils in STACK West and STACK East of similar maturity. Peaks for C_{29} 17α(H),21β(H)-30-norhopane ($C_{29}H$), C_{30} 17α(H),21β(H)-hopane ($C_{30}H$), and the C_{31} through C_{35} 17α(H),21β(H)-homohopanes ($C_{31}H$ through $C_{35}H$, respectively) are shown. STACK West oils have more $C_{29}H$ and C_{31}-$C_{35}H$ relative to $C_{30}H$ which may indicate a more carbonate-style or reducing depositional environment.

The C_{31}-C_{35} homohopanes are thought to be derived from the C_{35} bacteriohopanepolyols found in bacteria, such as bacteriohopanetetrol, and often exhibit a regular decrease in peak height with increasing carbon number in clastic source rocks (Peters and Moldowan, 1991). The ratio of hopanoids derived from C_{35} precursors over hopanoids derived from C_{30} precursors, sometimes taking the form $C_{31}H/C_{30}H$, has been used to differentiate between carbonate (high values), marine (medium values), and lacustrine (low values) depositional environments (Peters et al., 2005b). In this study, a positive correlation was observed when the peak area ratio of $C_{29}H/C_{30}H$ was plotted against the peak area ratio of $C_{31\text{-}35}H/C_{30}H$ indicating that both parameters are likely responding to changes in depositional environment (Figure 79). STACK West oils generally plot with higher values for both parameters than STACK East oils. When $C_{31\text{-}35}H/C_{30}H$ is plotted in map view (Figure 80), a transition zone can be observed that mirrors the transition zone between low- and high-aromaticity observed in Figure 54. The oils in STACK West are likely sourced from a more restricted marine or carbonate-style source rock.

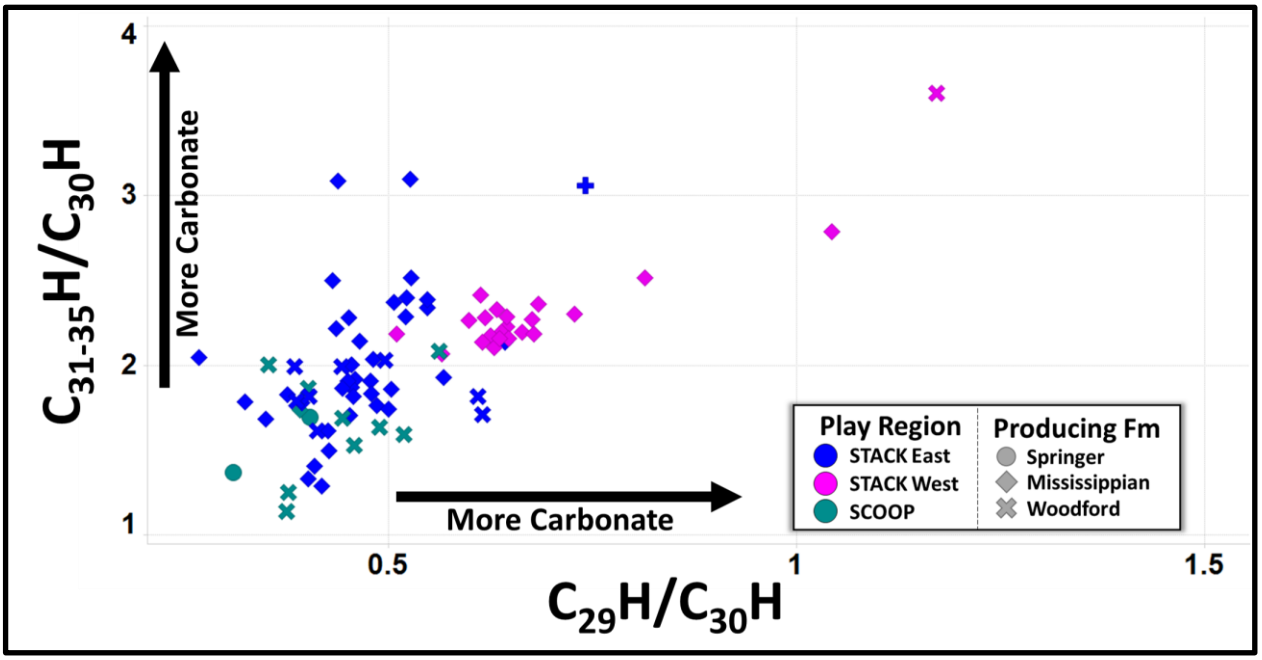

Figure 79. Crossplot of the ratios $C_{29}H/C_{30}H$ versus $C_{31\text{-}35}H/C_{30}H$. Higher values in both ratios have been linked to depositional environment. Oils from the STACK West Play Region have higher values indicating a restricted marine or carbonate-style conditions when the source rock was deposited. Data in Table 17.

Key	Play Region	Hopanes ppm[1]	$C_{31-35}/C_{30}H$[2]	$C_{29}/C_{30}H$[3]	$C_{31}HHI$[4]	$C_{32}HHI$[4]	$C_{33}HHI$[4]	$C_{34}HHI$[4]	$C_{35}HHI$[4]
1	STACK West	1194.1	2.2	0.64	38%	23%	17%	11%	11%
2	STACK West	1196.6	2.11	0.63	39%	24%	17%	10%	9%
3	STACK West	1209.9	2.18	0.63	38%	24%	18%	11%	10%
4	STACK West	1010.4	2.14	0.62	38%	24%	17%	11%	9%
5	STACK West	1215.2	2.18	0.68	38%	24%	18%	11%	9%
6	STACK West	446.7	2.18	0.51	30%	22%	17%	15%	16%
7	STACK West	809.5	2.27	0.6	35%	23%	16%	13%	12%
8	STACK West	655.5	2.41	0.61	35%	24%	17%	12%	13%
9	STACK West	515.3	2.19	0.66	37%	25%	18%	11%	10%
10	STACK West	589.2	2.28	0.62	38%	23%	18%	12%	10%
11	STACK West	992.9	2.16	0.65	38%	23%	18%	12%	10%
12	STACK West	836.9	2.29	0.64	38%	23%	17%	10%	11%
13	STACK West	629.1	2.16	0.64	37%	25%	18%	11%	10%
14	STACK West	703.6	2.27	0.68	38%	23%	17%	11%	11%
15	STACK West	374.2	2.07	0.57	37%	22%	17%	12%	11%
16	STACK West	784.3	2.33	0.63	35%	23%	17%	12%	14%
17	STACK West	48.2	2.79	1.04	43%	19%	17%	13%	9%
18	STACK West	3.4	NA	NA	NA	NA	NA	NA	NA
19	STACK West	16.2	2.51	0.81	37%	22%	19%	11%	11%
20	STACK West	5.1	NA	NA	NA	NA	NA	NA	NA
21	STACK West	0	NA	NA	NA	NA	NA	NA	NA
22	STACK West	0	NA	NA	NA	NA	NA	NA	NA
23	STACK West	0	NA	NA	NA	NA	NA	NA	NA
24	STACK West	0	NA	NA	NA	NA	NA	NA	NA
25	STACK West	2.1	NA	NA	NA	NA	NA	NA	NA
26	STACK West	8.5	NA	NA	NA	NA	NA	NA	NA
27	STACK West	145.8	2.23	0.64	36%	24%	18%	14%	9%
28	STACK West	360.8	2.36	0.68	37%	24%	18%	12%	10%
29	STACK West	339.5	2.3	0.73	34%	20%	18%	15%	12%
30	STACK West	11.3	NA	NA	NA	NA	NA	NA	NA
31	STACK West	8	NA	NA	NA	NA	NA	NA	NA
32	STACK West	11.7	NA	NA	NA	NA	NA	NA	NA
33	STACK West	2.9	NA	NA	NA	NA	NA	NA	NA
34	STACK West	6.8	NA	NA	NA	NA	NA	NA	NA
35	STACK West	6.3	NA	NA	NA	NA	NA	NA	NA
36	STACK West	0	NA	NA	NA	NA	NA	NA	NA
37	STACK West	3	NA	NA	NA	NA	NA	NA	NA
38	STACK West	1.7	NA	NA	NA	NA	NA	NA	NA
39	STACK West	1.9	NA	NA	NA	NA	NA	NA	NA
40	STACK West	4.5	NA	NA	NA	NA	NA	NA	NA
41	STACK West	0	NA	NA	NA	NA	NA	NA	NA
42	STACK West	0.6	NA	NA	NA	NA	NA	NA	NA
43	STACK West	2.3	NA	NA	NA	NA	NA	NA	NA
44	STACK West	53.4	3.61	1.17	31%	19%	17%	15%	19%
45	STACK West	0	NA	NA	NA	NA	NA	NA	NA
46	STACK West	0	NA	NA	NA	NA	NA	NA	NA
47	STACK East	0	NA	NA	NA	NA	NA	NA	NA
48	STACK East	0	NA	NA	NA	NA	NA	NA	NA
49	STACK East	0	NA	NA	NA	NA	NA	NA	NA
50	STACK East	8.8	NA	NA	NA	NA	NA	NA	NA
51	STACK East	2.9	NA	NA	NA	NA	NA	NA	NA
52	STACK East	0	NA	NA	NA	NA	NA	NA	NA
53	STACK East	6.4	NA	NA	NA	NA	NA	NA	NA
54	STACK East	9	NA	NA	NA	NA	NA	NA	NA
55	STACK East	11	NA	NA	NA	NA	NA	NA	NA
56	STACK East	0	NA	NA	NA	NA	NA	NA	NA
57	STACK East	7.1	NA	NA	NA	NA	NA	NA	NA
58	STACK East	10	NA	NA	NA	NA	NA	NA	NA
59	STACK East	22.7	NA	NA	NA	NA	NA	NA	NA
60	STACK East	1.8	NA	NA	NA	NA	NA	NA	NA
61	STACK East	87	1.93	0.57	33%	20%	19%	16%	11%
62	STACK East	4.8	NA	NA	NA	NA	NA	NA	NA
63	STACK East	4.5	NA	NA	NA	NA	NA	NA	NA
64	STACK East	92.2	2.14	0.64	36%	22%	19%	14%	9%

Key	Play Region	Hopanes ppm[1]	$C_{31-35}/C_{30}H$[2]	$C_{29}/C_{30}H$[3]	$C_{31}HHI$[4]	$C_{32}HHI$[4]	$C_{33}HHI$[4]	$C_{34}HHI$[4]	$C_{35}HHI$[4]
65	STACK East	9.7	NA	NA	NA	NA	NA	NA	NA
66	STACK East	92.9	2.28	0.45	33%	23%	16%	15%	12%
67	STACK East	13.9	NA	NA	NA	NA	NA	NA	NA
68	STACK East	51.9	3.06	0.74	30%	22%	19%	13%	15%
69	STACK East	103	2.34	0.55	34%	21%	19%	14%	11%
70	STACK East	22.5	NA	NA	NA	NA	NA	NA	NA
71	STACK East	0	NA	NA	NA	NA	NA	NA	NA
72	STACK East	112.3	3.1	0.53	31%	22%	18%	16%	12%
73	STACK East	0	NA	NA	NA	NA	NA	NA	NA
74	STACK East	27.1	NA	NA	NA	NA	NA	NA	NA
75	STACK East	139.7	2.5	0.43	35%	21%	17%	14%	13%
76	STACK East	170.4	2.39	0.55	31%	19%	19%	19%	12%
77	STACK East	9.4	NA	NA	NA	NA	NA	NA	NA
78	STACK East	6.1	NA	NA	NA	NA	NA	NA	NA
79	STACK East	69.7	2.04	0.48	33%	23%	21%	15%	8%
80	STACK East	97.3	2.37	0.51	31%	22%	18%	14%	14%
81	STACK East	63.4	1.87	0.46	34%	25%	18%	15%	8%
82	STACK East	12.8	NA	NA	NA	NA	NA	NA	NA
83	STACK East	88	2	0.46	32%	25%	21%	13%	9%
84	STACK East	2.3	NA	NA	NA	NA	NA	NA	NA
85	STACK East	93.6	1.91	0.48	30%	23%	20%	14%	12%
86	STACK East	97.5	1.7	0.45	36%	25%	20%	12%	8%
87	STACK East	187	1.91	0.45	35%	24%	19%	13%	9%
88	STACK East	91.6	1.99	0.44	34%	25%	22%	13%	7%
89	STACK East	100.9	1.61	0.43	36%	23%	20%	12%	9%
90	STACK East	713.7	3.09	0.44	22%	20%	15%	18%	26%
91	STACK East	144	1.33	0.4	35%	26%	19%	12%	9%
92	STACK East	117.3	1.78	0.39	36%	24%	20%	11%	10%
93	STACK East	440.1	2.52	0.53	30%	23%	17%	14%	16%
94	STACK East	53.9	1.83	0.38	31%	26%	23%	13%	7%
95	STACK East	16.9	NA	NA	NA	NA	NA	NA	NA
96	STACK East	55.2	2.05	0.27	29%	24%	23%	14%	10%
97	STACK East	101.2	1.99	0.39	34%	24%	20%	11%	10%
98	STACK East	116	1.79	0.32	32%	26%	20%	12%	10%
99	STACK East	103.5	1.79	0.39	34%	25%	20%	13%	8%
100	STACK East	530.3	2.4	0.52	30%	23%	17%	14%	17%
101	STACK East	441.6	2.22	0.44	34%	24%	19%	12%	11%
102	STACK East	262.5	1.92	0.46	36%	24%	19%	12%	9%
103	STACK East	177.4	1.61	0.41	36%	26%	20%	11%	7%
104	STACK East	136	1.68	0.35	32%	25%	20%	14%	9%
105	STACK East	261.2	1.29	0.42	39%	25%	20%	10%	6%
106	STACK East	254.1	1.5	0.43	38%	24%	20%	12%	6%
107	STACK East	264.3	1.4	0.41	37%	25%	20%	11%	7%
108	STACK East	29.8	1.71	0.62	41%	25%	19%	12%	3%
109	STACK East	57.7	2.03	0.5	33%	26%	20%	12%	9%
110	STACK East	15.5	1.81	0.61	36%	19%	21%	15%	9%
111	STACK East	159.8	1.82	0.4	38%	24%	19%	12%	7%
112	STACK East	291	1.86	0.5	35%	25%	19%	12%	8%
113	STACK East	467.4	2.14	0.47	34%	24%	18%	12%	13%
114	STACK East	354	1.83	0.48	35%	25%	20%	12%	8%
115	STACK East	345.7	2.29	0.52	31%	23%	17%	14%	14%
116	STACK East	305.7	1.82	0.46	34%	24%	19%	13%	10%
117	STACK East	348.1	1.86	0.44	31%	24%	20%	14%	11%
118	STACK East	529.3	1.76	0.49	36%	23%	20%	13%	8%
119	STACK East	376.8	1.74	0.5	36%	24%	20%	12%	8%
120	SCOOP	48.4	1.59	0.52	35%	26%	21%	11%	6%
121	SCOOP	0	NA	NA	NA	NA	NA	NA	NA
122	SCOOP	0	NA	NA	NA	NA	NA	NA	NA
123	SCOOP	0	NA	NA	NA	NA	NA	NA	NA
124	SCOOP	29.8	NA	NA	NA	NA	NA	NA	NA
125	SCOOP	11.5	NA	NA	NA	NA	NA	NA	NA
126	SCOOP	7	NA	NA	NA	NA	NA	NA	NA
127	SCOOP	13.1	1.63	0.49	NA	NA	NA	NA	NA
128	SCOOP	9.4	1.25	0.38	NA	NA	NA	NA	NA

Key	Play Region	Hopanes ppm[1]	$C_{31-35}/C_{30}H^2$	$C_{29}/C_{30}H^3$	$C_{31}HHI^4$	$C_{32}HHI^4$	$C_{33}HHI^4$	$C_{34}HHI^4$	$C_{35}HHI^4$
129	SCOOP	7.7	NA	NA	NA	NA	NA	NA	NA
130	SCOOP	6.3	NA	NA	NA	NA	NA	NA	NA
131	SCOOP	6.5	NA	NA	NA	NA	NA	NA	NA
132	SCOOP	17.3	NA	NA	NA	NA	NA	NA	NA
133	SCOOP	5.9	NA	NA	NA	NA	NA	NA	NA
134	SCOOP	3.4	NA	NA	NA	NA	NA	NA	NA
135	SCOOP	9.6	NA	NA	NA	NA	NA	NA	NA
136	SCOOP	6.7	NA	NA	NA	NA	NA	NA	NA
137	SCOOP	15.9	1.86	0.4	36%	24%	20%	11%	8%
138	SCOOP	5.9	NA	NA	NA	NA	NA	NA	NA
139	SCOOP	3.3	NA	NA	NA	NA	NA	NA	NA
140	SCOOP	2.4	NA	NA	NA	NA	NA	NA	NA
141	SCOOP	5	NA	NA	NA	NA	NA	NA	NA
142	SCOOP	5.4	NA	NA	NA	NA	NA	NA	NA
143	SCOOP	5.4	NA	NA	NA	NA	NA	NA	NA
144	SCOOP	8.6	NA	NA	NA	NA	NA	NA	NA
145	SCOOP	11.3	NA	NA	NA	NA	NA	NA	NA
146	SCOOP	6.9	NA	NA	NA	NA	NA	NA	NA
147	SCOOP	6.6	NA	NA	NA	NA	NA	NA	NA
148	SCOOP	5.6	NA	NA	NA	NA	NA	NA	NA
149	SCOOP	39.9	1.69	0.44	39%	23%	21%	11%	6%
150	SCOOP	0	NA	NA	NA	NA	NA	NA	NA
151	SCOOP	11.7	2	0.35	26%	23%	29%	14%	8%
152	SCOOP	24.2	1.14	0.38	33%	28%	20%	14%	5%
153	SCOOP	0.8	NA	NA	NA	NA	NA	NA	NA
154	SCOOP	76	1.73	0.39	35%	23%	20%	14%	8%
155	SCOOP	933.1	1.69	0.4	31%	21%	32%	10%	7%
156	SCOOP	25.9	NA	NA	NA	NA	NA	NA	NA
157	SCOOP	1.7	NA	NA	NA	NA	NA	NA	NA
158	SCOOP	2.9	NA	NA	NA	NA	NA	NA	NA
159	SCOOP	62.1	1.53	0.46	35%	26%	18%	13%	9%
160	SCOOP	7.6	NA	NA	NA	NA	NA	NA	NA
161	SCOOP	5.8	NA	NA	NA	NA	NA	NA	NA
162	SCOOP	8	NA	NA	NA	NA	NA	NA	NA
163	SCOOP	0	NA	NA	NA	NA	NA	NA	NA
164	SCOOP	1.9	NA	NA	NA	NA	NA	NA	NA
165	SCOOP	7.2	NA	NA	NA	NA	NA	NA	NA
166	SCOOP	13.9	NA	NA	NA	NA	NA	NA	NA
167	SCOOP	5.1	NA	NA	NA	NA	NA	NA	NA
168	SCOOP	20.9	NA	NA	NA	NA	NA	NA	NA
169	SCOOP	392.8	2.09	0.56	39%	23%	19%	12%	6%
170	SCOOP	14.5	NA	NA	NA	NA	NA	NA	NA
171	SCOOP	94.5	1.37	0.31	36%	20%	26%	11%	6%
172	SCOOP	1.1	NA	NA	NA	NA	NA	NA	NA

Table 17. Select hopane values for oils in this study. (1) concentration of all hopanes in ppm of the whole oil; (2) (17α(H),21β(H)-homohopane (22S+22R) + 17α(H),21β(H)-bishomohopane (22S+22R) + 17α(H),21β(H)-trishomohopane (22S+22R) + 17α(H),21β(H)-tetrakishomohopane (22S+22R) + 17α(H),21β(H)-pentakishomohopane (22S+22R))/17α(H),21β(H)-hopane; (3) 17α(H),21β(H)-30-norhopane/17α(H), 21β(H)-hopane. Samples marked NA indicate where one or both ratios were not available due to insufficient signal to noise. (3) Abundance of each C_{31}-C_{35} homohopane (S+R) as a percentage of the sum of all homohopanes (C_{31}-C_{35}).

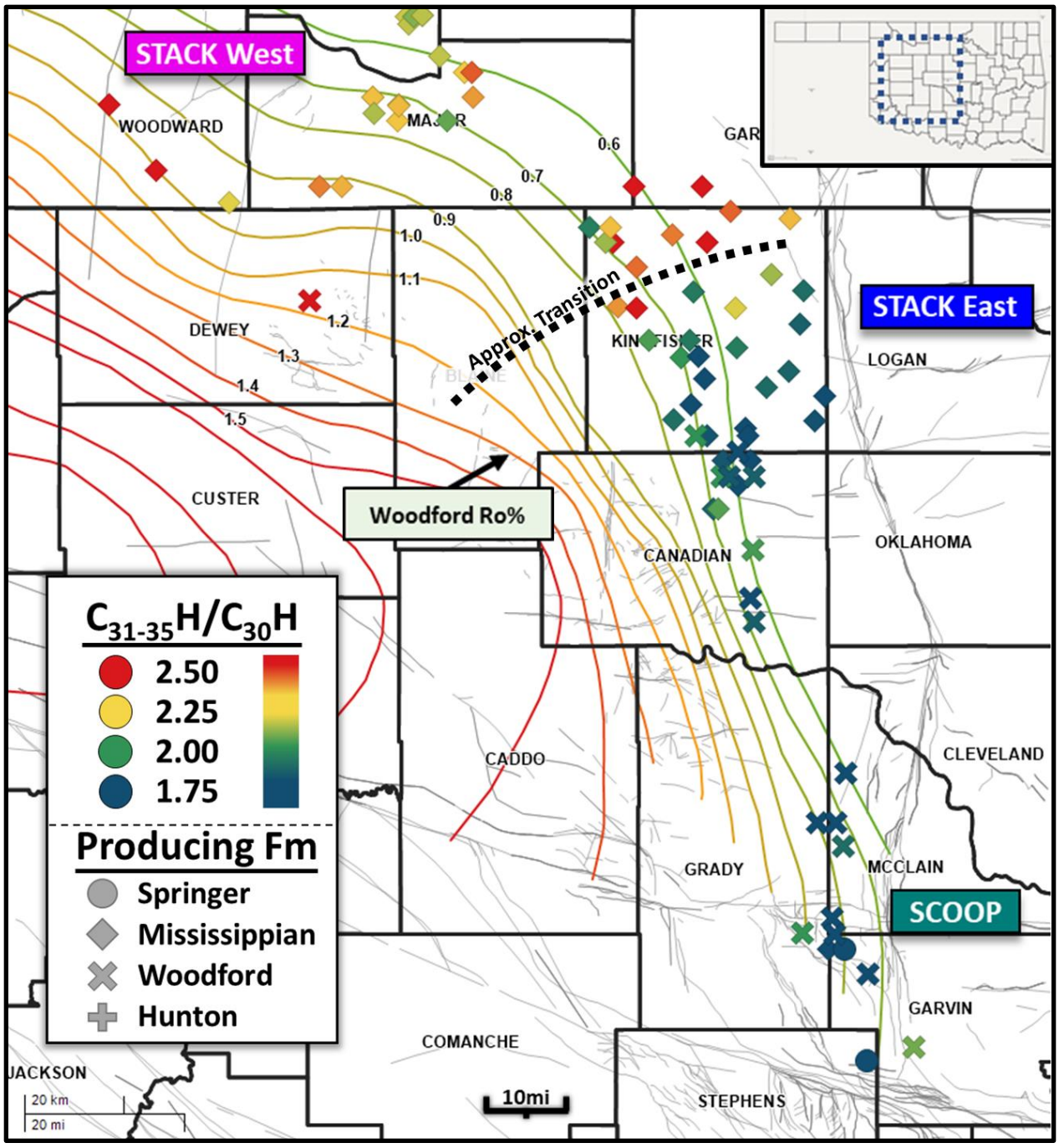

Figure 80. Map of the ratio of homohopanes ($C_{31\text{-}35}H/C_{30}H$) as expressed in Table 17. The transition between low values observed in STACK East and SCOOP mirrors the transition observed in aromaticity (Tol/MCH+*n*-C_7) values as shown in Figure 54. The STACK West side of the transition zone has higher values indicative of more reducing (low Eh) marine conditions during deposition and early diagenesis.

The homohopanes indices from each Play Region show elevated C_{35}/C_{34} homohopanes across all of STACK West and some oils in STACK East, indicating a highly anoxic or reducing depositional and diagenetic environment (Figure 81). This supports other findings that suggest a transition from restricted- to semi-open marine occurs between STACK East and STACK West.

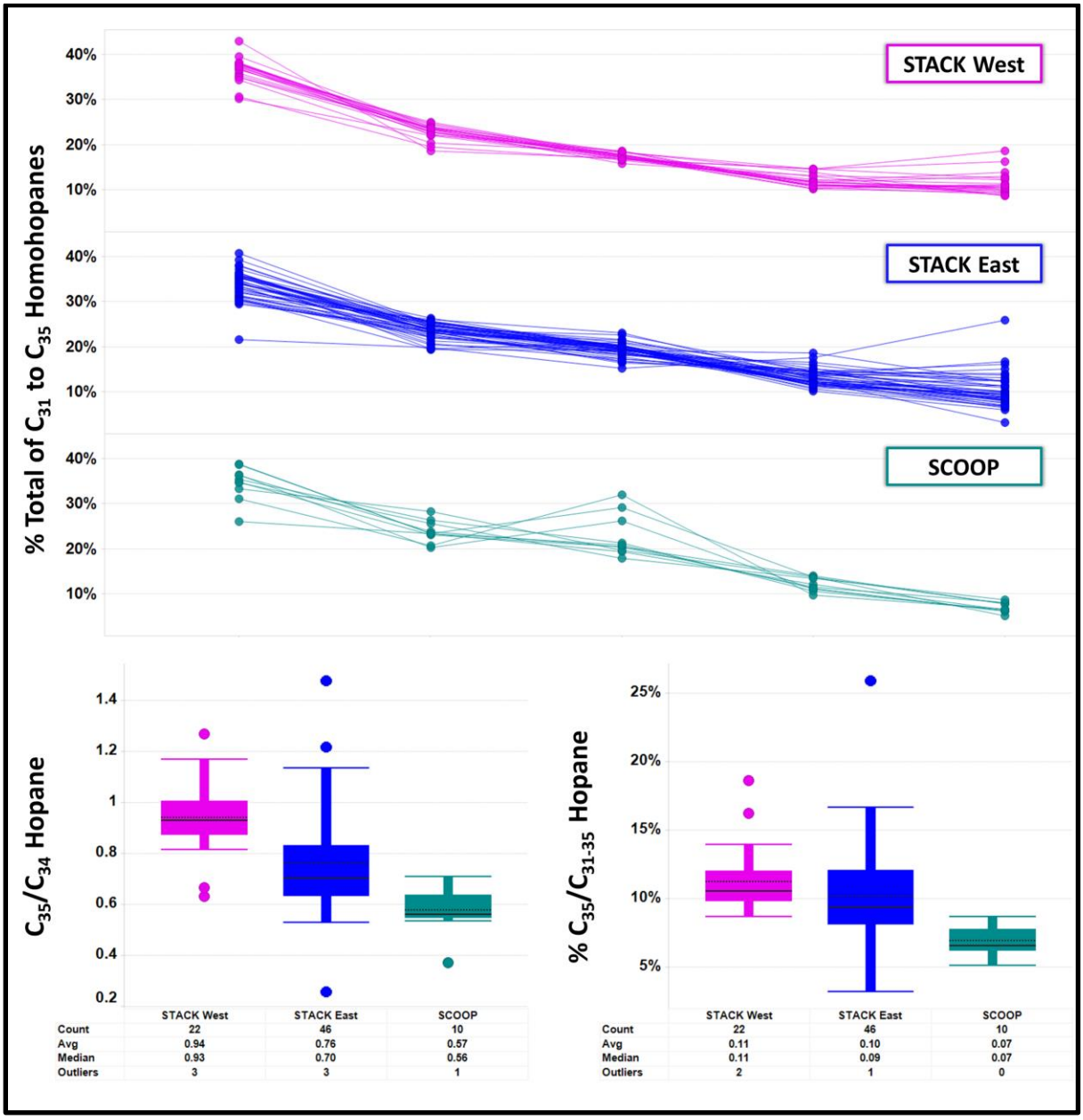

Figure 81. Homohopane distributions for each of the three Play Regions from data in Table 17. In general, STACK West exhibits a higher abundance of C_{35}/C_{34} homohopanes indicative of more reducing environments. STACK East shows a wide range of values indicative of the previously indicated transition zone which appears to occur in northern Kingfisher and central Blaine counties. Some SCOOP samples contain anomalous C_{33} homohopanes abundances.

The terpane fingerprint (m/z 191) taken from the extracts from three Woodford Shale cores in Kingfisher, Blaine, and Major counties are summarized in Table 18 and Figure 82. In all samples, the $C_{24}TT/C_{23}TT$ was between 0.58-0.73 which matches closely the ratios observed in all STACK oils and reflects values commonly observed in siliciclastic source rocks. The ratio $C_{24}TET/C_{26}TT(S)$ was higher in STACK West (0.35±0.11, n=8) compared to STACK East (0.19±0.10, n=8) which mirrors the relationship observed between STACK Oils. Furthermore, a significant difference was also observed in $C_{24}TET/C_{26}TT(S)$ between STACK West core extracts in the Upper Woodford (0.45±0.07, n=4) compared to Lower/Middle Woodford (0.25±0.02, n=4).

The Woodford Shale extracts generally show less abundant hopanoids and extended tricyclic terpanes compared to the C_{19}-C_{26} tricyclic terpanes. Extended tricyclic terpanes above C_{33} were observed in all samples, but in small amounts in the John 1H-5X core. Curiously, the Woodford Shale extracts exhibit large hopanoid peaks for 18α(H)-22,29,30-trisnorhopane (Ts) and 15α(H)-methyl-17α(H)-27-norhopane ($C_{30}DH$) which are not observed in produced oils in STACK. The abundances of these unexpected peaks is larger in the Upper Woodford than in the Lower/Middle Woodford.

Core	Depth	Formation	Play Region	$C_{24}TT/C_{23}TT$[1]	$C_{24}TET/C_{26}TT(S)$[2]	$Ts/C_{30}H$[3]	$C_{30}DH/C_{30}H$[4]	$C_{31-35}H/C_{30}H$[5]
ABCDS 1-6	8098	Upper Woodford	STACK West	0.63	0.50	1.1	1.0	2.3
ABCDS 1-6	8099	Upper Woodford	STACK West	0.60	0.52	1.0	0.8	1.6
ABCDS 1-6	8110	Middle Woodford	STACK West	0.66	0.27	1.1	1.1	2.1
ABCDS 1-6	8121	Middle Woodford	STACK West	0.64	0.22	1.2	1.3	2.8
KC 1-36	8538.5	Upper Woodford	STACK East	0.61	0.38	1.4	1.4	2.1
KC 1-36	8543.5	Upper Woodford	STACK East	0.58	0.38	1.1	1.0	1.8
KC 1-36	8557	Lower Woodford	STACK East	0.71	0.25	1.6	2.1	1.3
KC 1-36	8566.5	Lower Woodford	STACK East	0.73	0.27	0.9	0.7	0.7
John 1H-5X	9165	Upper Woodford	STACK East	0.59	0.23	4.1	4.0	1.4
John 1H-5X	9180	Middle Woodford	STACK East	0.64	0.09	1.9	2.9	0.5
John 1H-5X	9202	Lower Woodford	STACK East	0.60	0.25	0.8	0.8	0.2

Table 18. Selected ratios from the m/z 191 chromatograms of Woodford Shale extracts taken from three cores in STACK. (1) C_{24} tricyclic terpane/C_{23} tricyclic terpane; (2) C_{24} tetracyclic terpane/C_{26} tricyclic terpane (S); (3) 18α(H)-22,29,30-trisnorhopane/17α(H),21β(H)-hopane; (4) 5α(H)-methyl-17α(H)-27-norhopane/17α(H),21β(H)-hopane; (5) (17α(H),21β(H)-homohopane(22S+22R) + 17α(H),21β(H)-bishomohopane (22S+22R) + 17α(H),21β(H)-trishomohopane (22S+22R) + 17α(H),21β(H)-tetrakishomohopane (22S+22R) + 17α(H),21β(H)-pentakishomohopane (22S+22R))/17α(H),21β(H)-hopane.

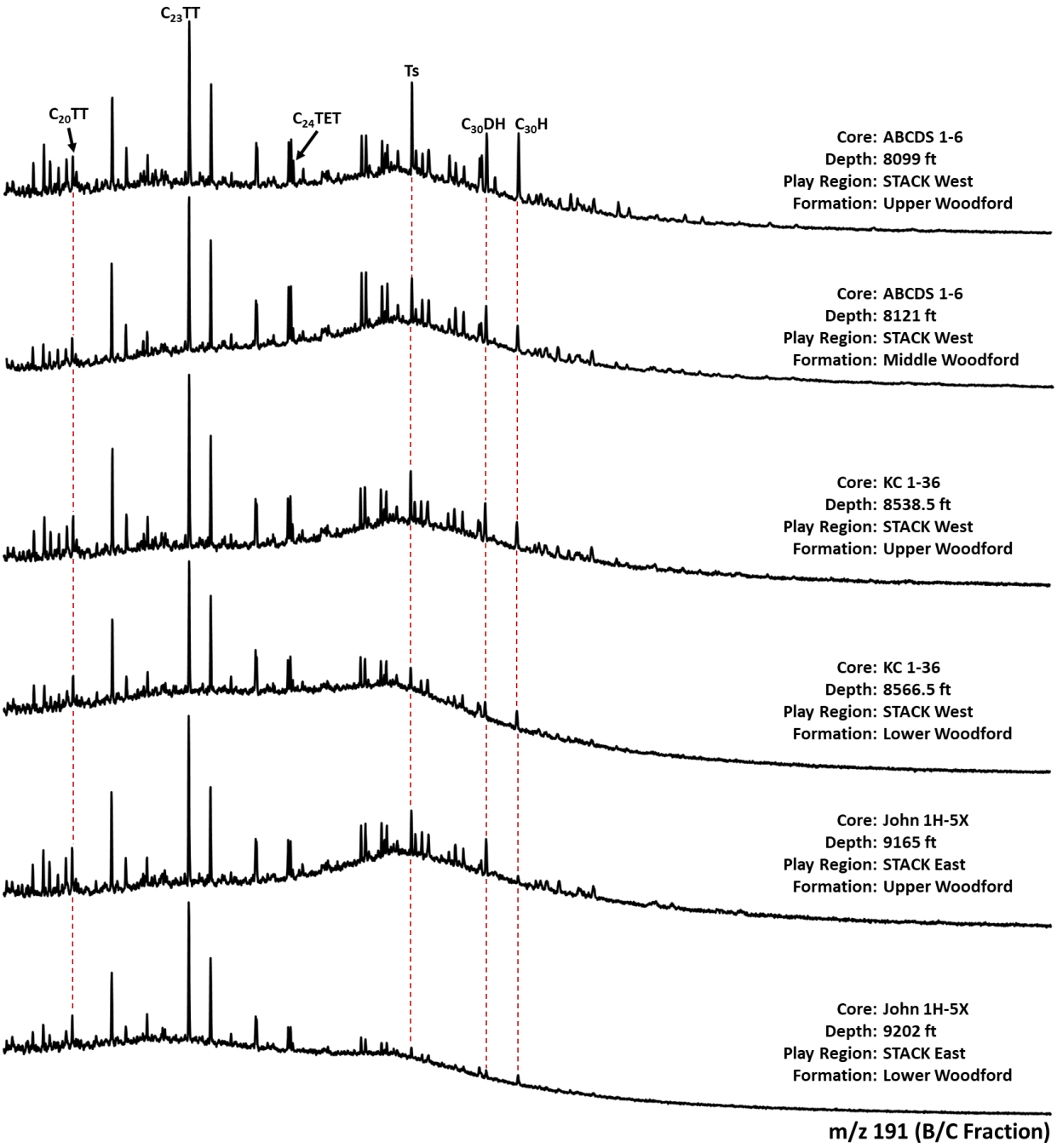

Figure 82. Example m/z 191 mass chromatograms taken from Woodford Shale core extracts from three cores in STACK. The Woodford Shale in STACK West contains higher C_{24}TET/C_{26}TT(S) values than STACK East, but also higher values in the Upper Woodford than in the Lower/Middle Woodford. Large Ts and C_{30}DH peaks observed in the Woodford core extracts were not observed in any STACK oils, but are more pronounced in the Upper Woodford than the Lower/Middle Woodford.

Mapping Organic Facies in STACK

An organic facies has been defined as a mappable rock unit, distinguishable by the character of its organic matter without regard to the inorganic aspects of the sediment (Jones, 1984, 1987). Where the spatial resolution of rock core is limited, it may be possible to approximate the distribution and nature of organic facies from the oils they generate if there is reasonable confidence that the oils are captured near their organic source. This is accomplished by first determining source-related sets of oils, defined as oils generated and expelled from the same organic facies at different stages of maturity. Plotting the geochemical parameters in map view may provide sufficient spatial resolution to appropriately map the approximate transitions between two or more organic facies.

This chapter reviews several geochemical parameters, including light hydrocarbons, steranes, acyclic terpanes, sesquiterpanes, tricyclic terpanes, tetracyclic terpanes, and hopanes in order to determine which parameters most successfully formed two or more clusters which may indicate the presence of separate organic facies. Two geochemical maps have been shown already which illustrate a potential geochemical transition zone occurring in central Blaine and northwest Kingfisher counties based on light hydrocarbon aromaticity (Figure 54) and extended hopanes (Figure 80). Six additional maps illustrating several additional geochemical parameters in this study which successfully formed two or more clusters are provided in Figure 83, Figure 84, and Figure 85 with an overlay showing the approximate transition for that parameter. Geochemical maps only provide a single dimension in the value axis, therefore in several cases only a single axis of a multi-axial plot, such as crossplots or ternary diagram, could be selected. Furthermore, parameters which covaried strongly with maturity, such as the $C_{24}TET/C_{26}(S)$, were not considered even if they formed two or more trend lines when plotted against maturity.

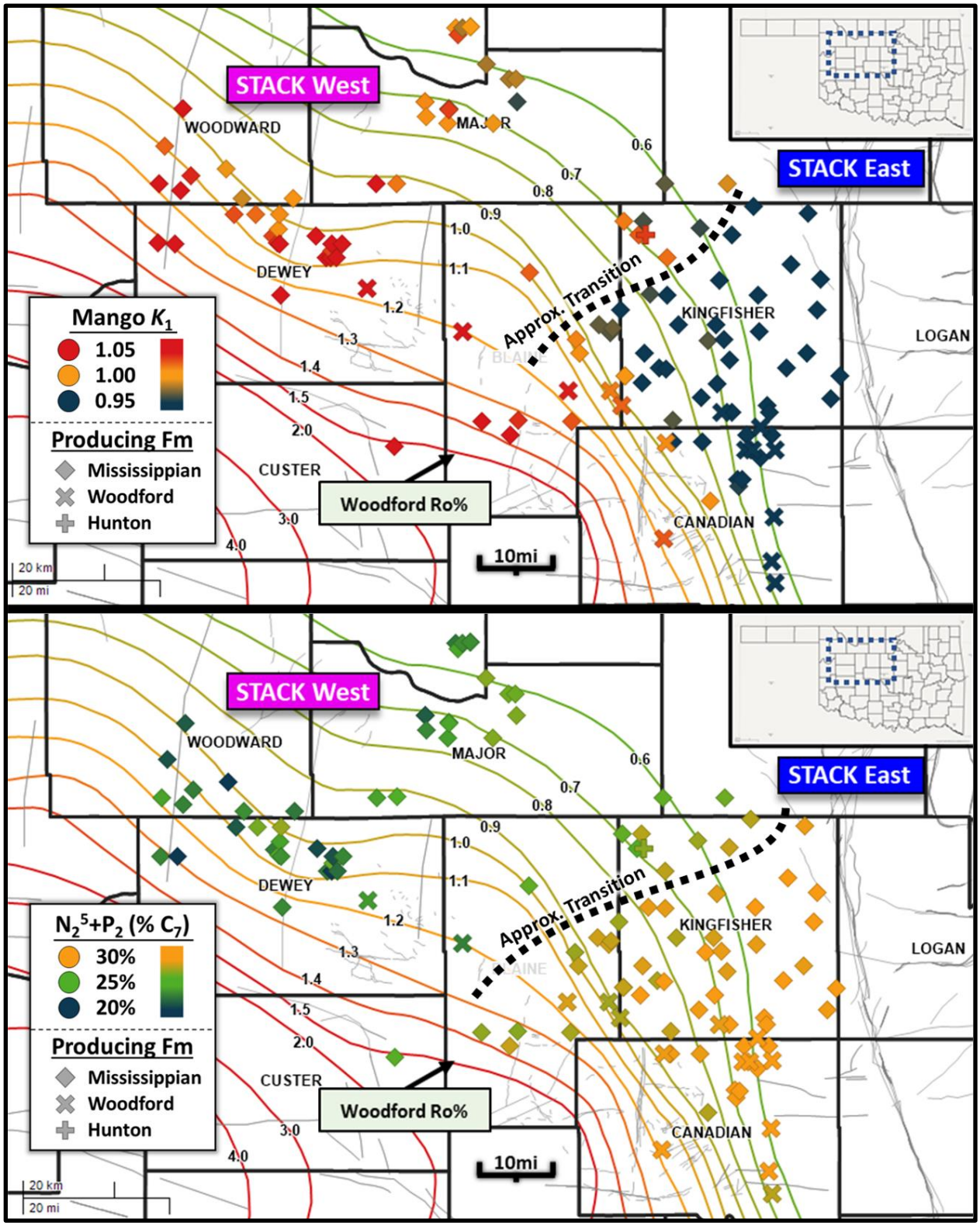

Figure 83. Maps showing the values for Mango's K_1 and $N_2^5+P_2$ (denominator in K_2) for all STACK oils showing slightly different transition zones across northern Kingfisher and central Blaine counties.

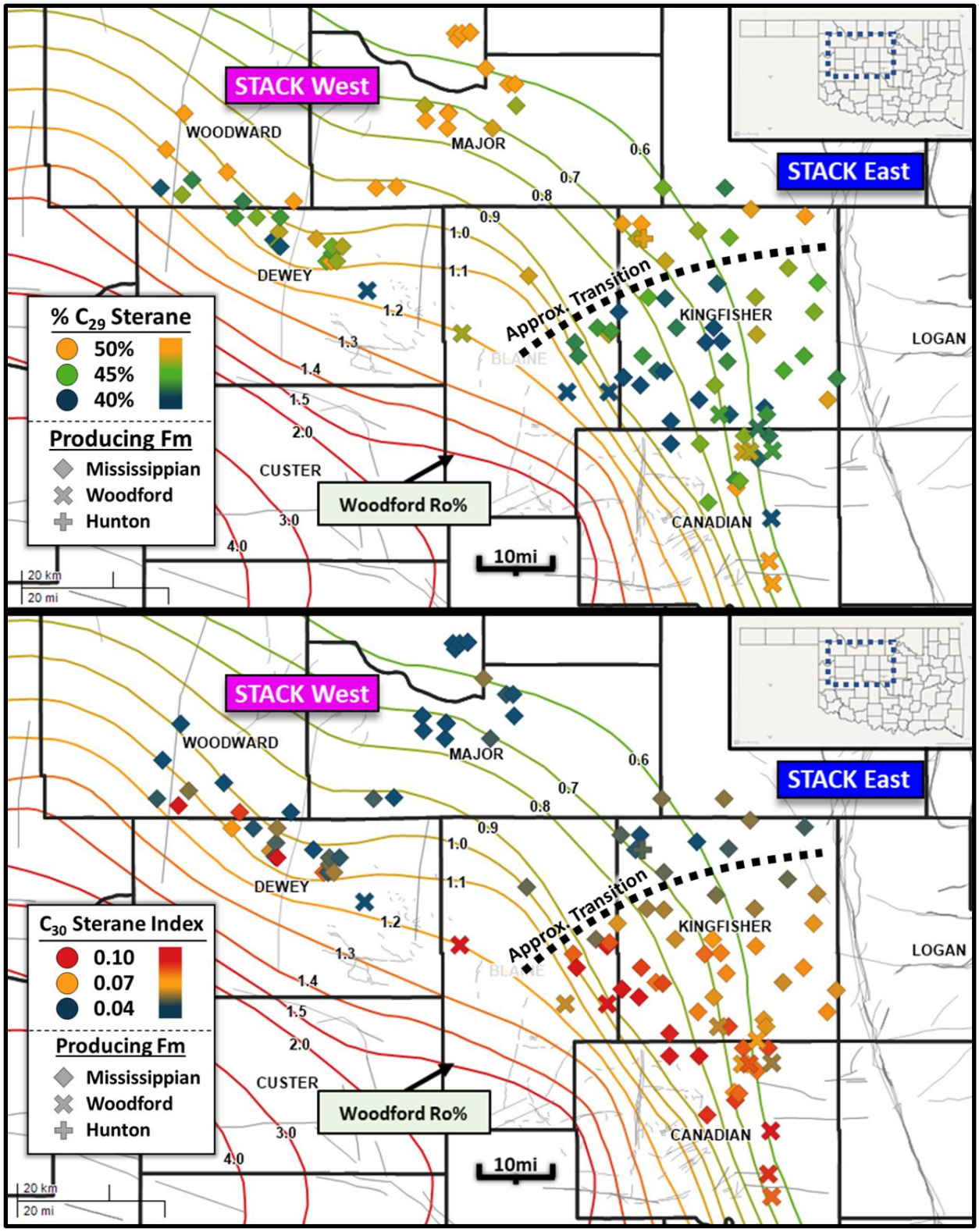

Figure 84. Maps showing values of %C_{29} Sterane ($C_{29}/C_{27\text{-}29}$ Sterane) and the C_{30} Sterane Index ($C_{30}/C_{27\text{-}30}$ Sterane) for all STACK oils showing mirroring transition zones across northern Kingfisher and central Blaine counties.

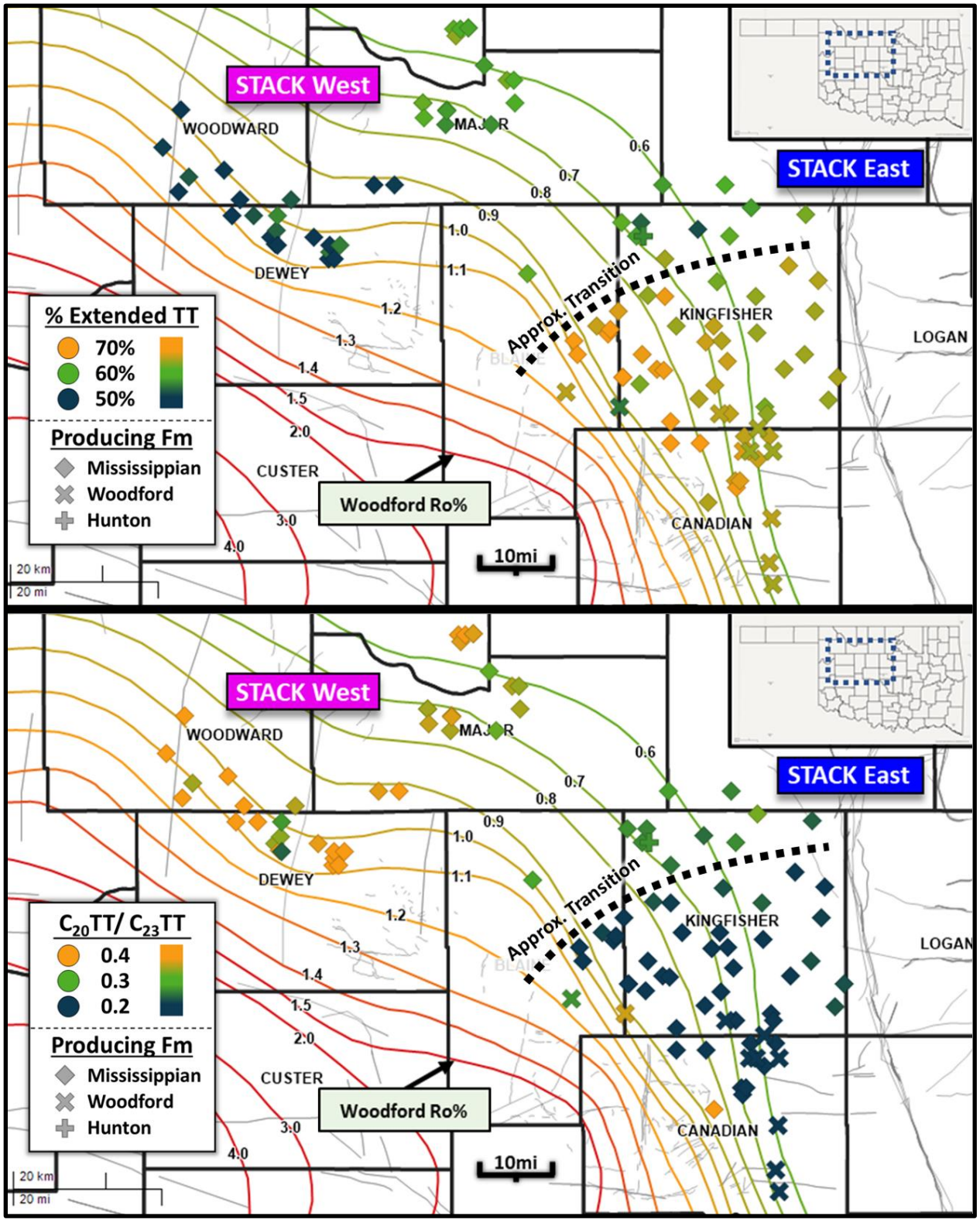

Figure 85. Maps showing values of %Extended Tricyclic Terpanes ($C_{28\text{-}39}TT/C_{19\text{-}39}TT$) and $C_{20}TT/C_{23}TT$ for all STACK oils showing mirroring transition zones across northern Kingfisher and central Blaine counties.

Based on the maps in Figure 54, Figure 80, Figure 83, Figure 84, and Figure 85, there is a striking southwest-northeast trending transition zone in central Blaine and northwestern Kingfisher counties which separate two source-related sets of oils which are geochemically distinct and internally consistent. Notably, oils from Woodford and Mississippian reservoirs in STACK are geochemically identical within a Play Region suggesting produced oils from these reservoirs share a common source, likely the Woodford Shale (Burruss and Hatch, 1989). This is especially clear in Canadian and southern Kingfisher counties where Woodford and Mississippian production in close proximity show almost no geochemical differences. Any contribution from secondary source(s) is volumetrically too small to impress an observable difference in geochemical character. Moreover, tight unconventional reservoir rocks with low permeabilities are unlikely to be well-mixed with respect to different charge events (England et al., 1987; Leythaeuser and Rückheim, 1989), so it is reasonable that each sample in this study is representative of only one organic facies at one moment in its thermal history.

Based on the transition between geochemically distinct source-related sets of oils, two organic facies are proposed which are hereafter referred to as STACK 1 ("West Facies") and STACK 2 ("East Facies") and shown in Figure 86. The organic facies transition is approximated based on changes in geochemical character of oils, but the transition also closely follows the Meramec isopach and its depositional pinchout mapped by Price (2020). While it may be tempting to argue that the transition between sets of source-related oils results from contribution from a separate Mississippian organic source or overprint of autochthonous Mississippian organic matter, a more likely explanation is that the ecological and depositional controls during Woodford times first affected sediment input, access to upwelling nutrients, oceanic circulation, and paleoecology and would later control the extent and growth of Osage carbonate platform millions of years later.

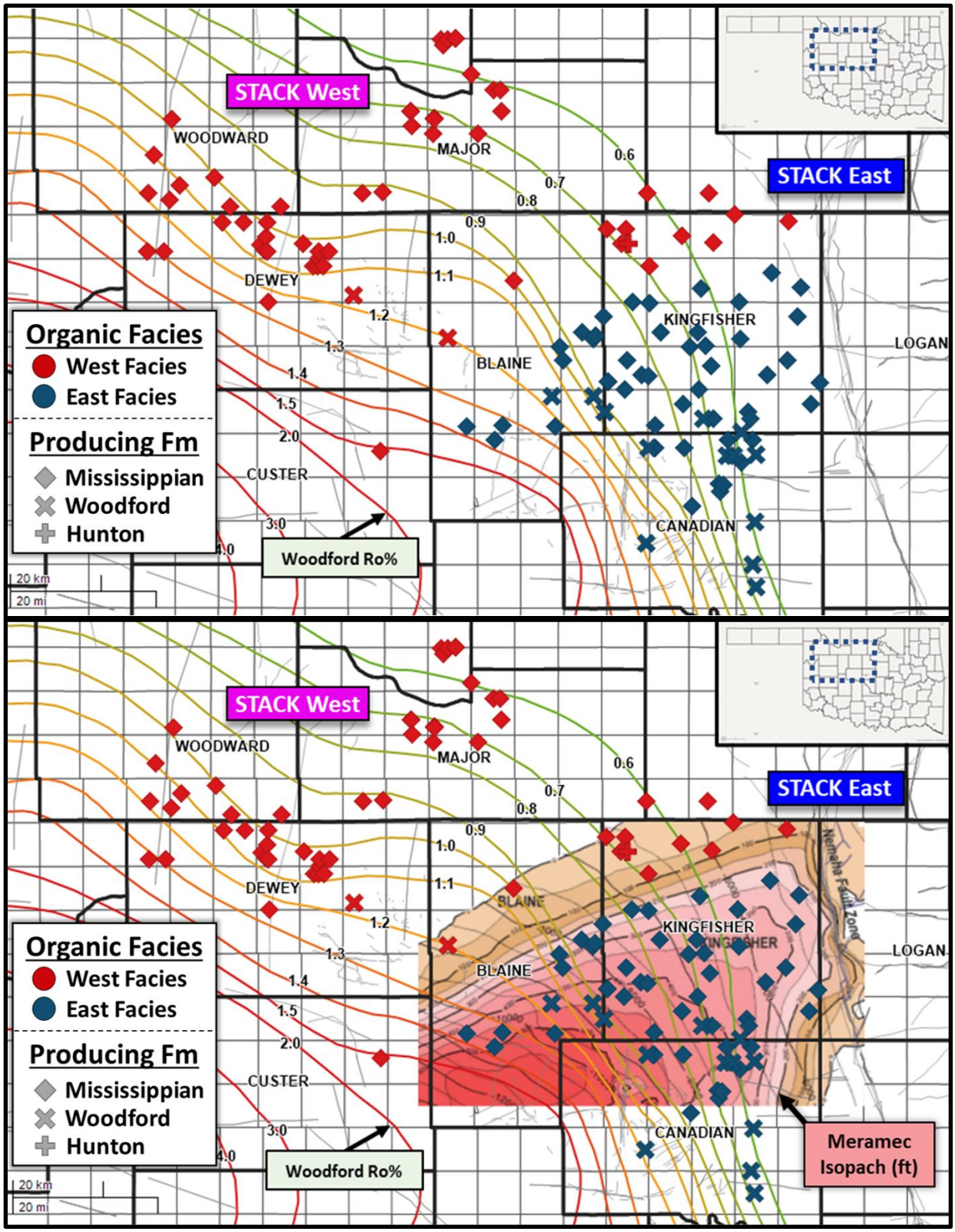

Figure 86. Upper: Delineation of two organic facies based on Figure 54, Figure 80, Figure 83, Figure 84, and Figure 85. Lower: The transition corresponds with the thinning edge of Osage Platform and clinoformal deposition of the Meramec. Isopach from (Price, 2020)

The range of geochemical parameters for 58 oils found to be sourced from the West Facies and 61 oils sourced from the East Facies organic facies are shown as box and whisker plots in Figure 87 colored red and blue, respectively. In aggregate, oil samples from both organic facies are approximately the same median maturity (0.84% Rc vs. 0.86% Rc), but West Facies samples represent a wider range of maturities. Whole oil carbon isotopes show that oils sourced from West Facies is on average isotopically heavier, but unfortunately the overall sampling is incomplete (69 isotope samples vs. 119 total STACK oils) and biased towards deeper, more mature samples (see Figure 22). The remaining parameters are source-related and organized into three groupings which cover redox/lithology, light hydrocarbons, and other biomarkers.

In the summary of redox/lithology parameters, oils from both organic facies contain Pr/Ph values which plot comfortably between 1-1.5, indicative of marine deposition, but oils sourced from the West Facies exhibit a wider range. West Facies oils have lower % diasteranes, mirrored by a similarly lower amount of rearranged sesquiterpanes (see Figure 71), which could indicate either fewer clays with active acid sites or a shift towards a more basic (high pH) or reducing (low Eh) diagenetic condition. These findings are supported by the higher $C_{29}H/C_{30}H$ ratio in the West Facies (median 0.63) versus East Facies (0.44) which is consistent with a more restricted marine environment with some carbonate or evaporite type depositional systems. These restricted environments may have been affected by differences in sediment supply, salinity, water temperature, alkalinity, water stratification, or ecosystem (Zumberge, 1984; Connan et al., 1986; Price et al., 1987). This is also supported by higher $C_{24}TET/C_{26}TT$ values in the West Facies oils (median 0.45) compared to East Facies (median 0.17) oils indicating that its source rock was deposited in a more restricted marine environment such as a shallow shelf or semi-closed oceanic basin with limited upwelling currents and nutrients (Zumberge et al., 2007).

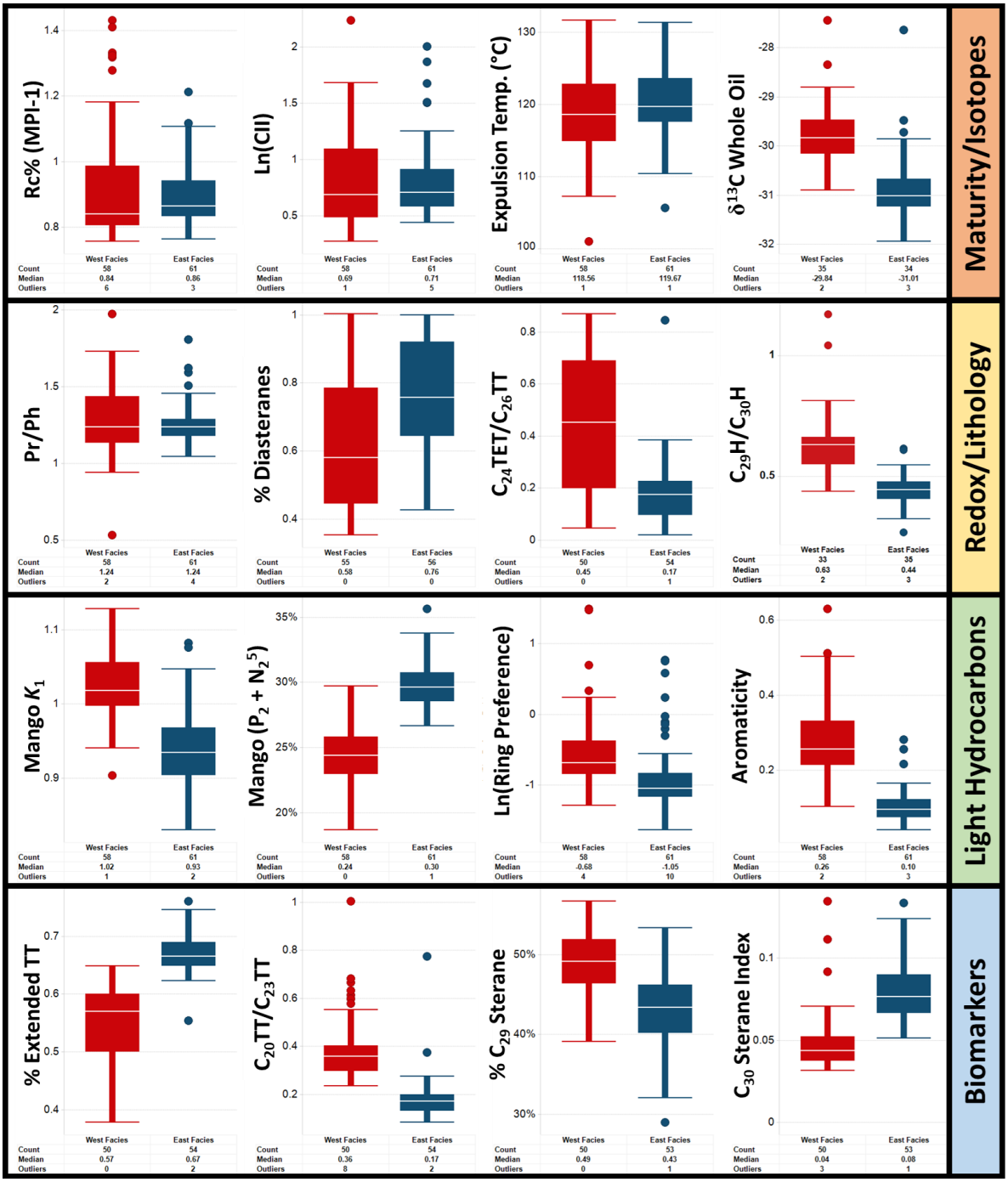

Figure 87. Box and whisker plots detailing the geochemical parameters for two organic facies identified in Figure 86 and organized by Maturity/Isotopes, Redox/Lithology, Light Hydrocarbons, and Biomarkers. The West Facies (red) has 58 oil samples primarily in the STACK West Play Region while the East Facies (blue) has 61 oil samples. By comparison, the West Facies samples have a wider range of thermal maturities containing both the highest- and lowest-maturity oils. The West Facies have lower % Diasteranes, higher $C_{24}TET/C_{26}TT$, and higher $C_{29}H/C_{30}H$ indicative of a restricted marine environment with limited access to nutrient rich upwelling currents and low input of terrestrial sediments. Light hydrocarbons ratios based on kinetic equilibrium show differences in catalytic activity between the source rocks containing the two organic facies. The West Facies also contains a different tricyclic terpane fingerprint with lower % extended TT and higher amounts of $C_{20}TT/C_{23}TT$. Finally, the West Facies has higher $\%C_{29}$ sterane and lower C_{30} Sterane Index, indicating a more restricted marine and coastal waters with abundant green algae.

The light hydrocarbon parameters in Figure 87 show clear separation between the two proposed organic facies. The three parameters derived from Mango's light hydrocarbon model (K_1, the denominator of K_2, and Ring Preference) show a striking dissimilarity in kinetic equilibrium variables within their respective source rocks. Critically, the West Facies has K_1 values consistently above 1 which has been associated with sulfate reduction reactions (ten Haven, 1996; Peters and Fowler, 2002) and could support a depositional environment with low amounts of terrestrially derived sedimentary iron (Dinur et al., 1980). Additionally, West Facies oils are strongly enriched in toluene compared to East Facies oils, often by a factor of 3-5, which is reflected in the elevated light hydrocarbon aromaticity value. The elevated aromaticity and K_1 values generally greater than 1 in the West Facies are both indicators of increased free and/or organic sulfur compounds present during diagenesis and is explored more fully in Chapter VI.

Oils generated from the two proposed organic facies also show two geochemically distinct tricyclic terpane and sterane biomarker signatures. Oils sourced from the West Facies have comparatively lower amounts of extended (>C_{28}) relative to regular tricyclic terpanes and higher amounts of the smaller tricyclic terpanes, C_{19}TT and C_{20}TT, relative to C_{23}TT. The difference in tricyclic terpane signatures between the East Facies and West Facies oils can be related to the calculated rate decline exponents of individual tricyclic terpanes. With increasing maturity, the East Facies appears to preferentially release shorter chain tricyclic terpanes which are progressively depleted in later generated oils. The rate of depletion, given by the rate decline exponent, appears to decrease systematically with increased length of the isoprenoidal chain. It is hypothesized that this may relate to the molecular composition, bond stability, or molecular porosity found in macromolecules like kerogen, bitumen, or asphaltenes which have been shown to be capable of occluding compounds like tricyclic terpanes at the time of generation. In the West

Facies, short- and long-chained tricyclic terpanes share a constant rate decline. In the working hypothesis, the West Facies may be explained by a higher proportion of weak or labile bonds in the macromolecular structure which are more easily degraded resulting in the more efficient release of the occluded components.

Finally, the West Facies oils have comparatively higher C_{29} steranes and lower C_{30} sterane index than the East Facies, interpreted as evidence of more restricted marine deposition with a coastal algal ecosystem dominated by green algae like Prasinophyceae and sparse golden Chrysophyte algae. Oils produced from the previously identified flower-shaped zone in eastern Dewey County are higher maturity than adjacent production in western Dewey Woodward counties with comparable reservoir TVD, but otherwise the high maturity oils are geochemically indistinguishable from other similarly mature Stack 1 ("West Facies") facies derived oils. The incursion of higher maturity fluids along the major faults in the flower-shaped zone supports the hypothesis that oils generated deeper in the basin may have migrated into shallower reservoirs and mixed with locally generated oils, a possibility that will be explored more fully in Chapter VI.

In summary, the producing reservoir (Woodford, Osage, Meramec, or Chester) appears to have little or no control on the geochemical character of the produced oil itself, suggesting a common organic source for each of these reservoirs. As a result, all STACK oils in this dataset are interpreted as being sourced from two chemically distinct organic facies in Woodford Shale, and contributions from Mississippian organic matter is believed to be geochemically negligible. The West Facies was deposited in a restricted marine environment with limited access to upwelling nutrients and starved of terrestrial sediment. Extracts from the Lower and Middle Woodford, which contains the maximum flooding surface and are often the most organic-rich members of the Woodford Shale, are geochemically the most similar to oils produced in STACK.

Characteristics of the SCOOP Petroleum System

The South Central Oklahoma Oil Province (SCOOP) is a structurally and stratigraphically complex play primarily in Grady, McClain, Garvin, and Stephens counties, with production from Upper Devonian through Lower Pennsylvanian reservoirs. A stratigraphic type log is provided in Figure 88. This study contains 53 oil samples from the three producing reservoirs: the 26 Woodford Shale samples, 8 Mississippian Sycamore and Meramec formations samples, and 19 Springer Group sandstones samples as shown in Figure 89.

The Springer Group is separated from the Woodford-Mississippian by the argillaceous Caney Shale which often contains TOC between 1-9 wt% (Cardott, 2017). This section will attempt to determine if the Springer and Mississippian group reservoirs are charged by one or more organic facies and if the Woodford or Caney/Goddard shales are responsible for charging the Springer and/or Mississippian reservoirs. The SCOOP Play Region is smaller than STACK and not broken up into separate Play Regions, so geochemical plots in this section will be colored by producing reservoir. Additionally, it was shown in Chapter IV that oils in SCOOP have lower thermal maturities for any given depth compared to STACK oils and also have lower concentrations of most observed biomarkers.

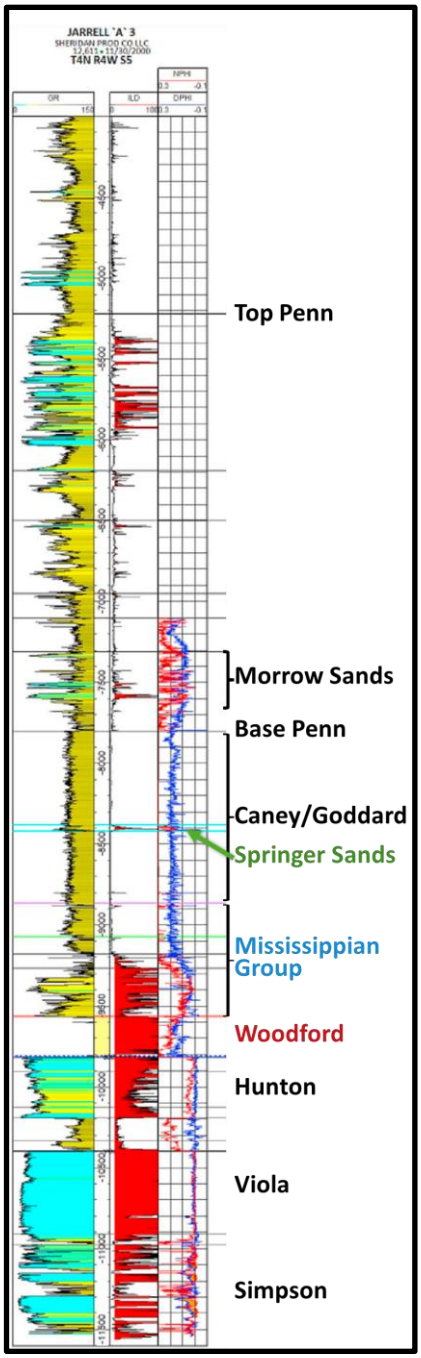

Figure 88. Stratigraphic type well log from SCOOP. This study includes oils produced from the Springer Group, Mississippian Group, and Woodford Shale denoted in green, blue, and red , respectively. Modified from Abrams and Thomas (2020).

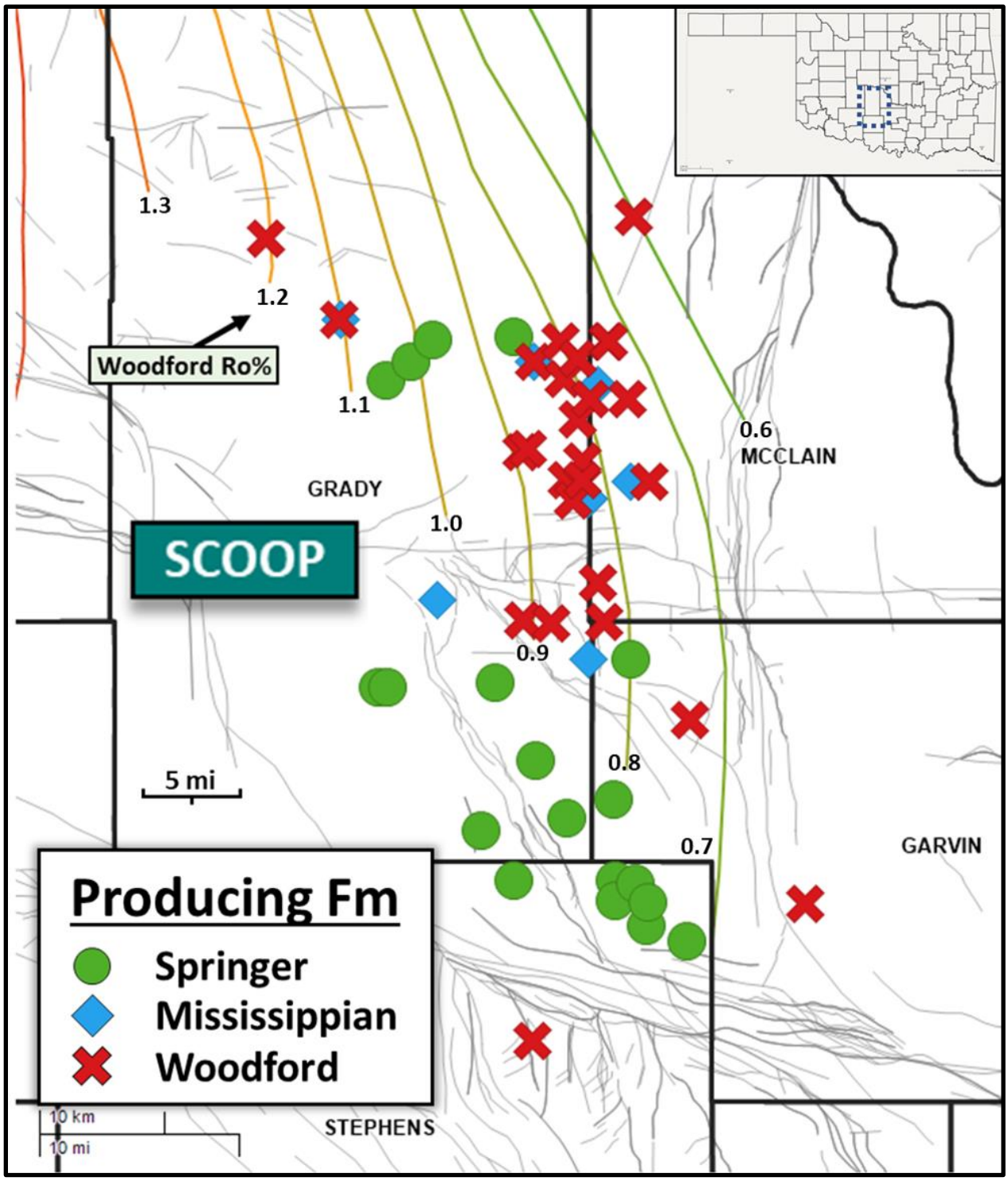

Figure 89. Map of SCOOP oil samples in this dataset by producing formation. The SCOOP dataset includes a total of 53 oils from Woodford (26), Mississippian (8), and Springer (19) reservoirs.

Studies of Oklahoma source rocks by Burruss and Hatch (1989 and 1992) have previously reported geochemical characteristics common in Pennsylvanian-sourced oils which distinguish them from Woodford-sourced oils, including MCH more abundant than *n*-C_7, isotopically enriched carbon, and abundant alkanes greater than *n*-C_{15}. To compare to these findings, typical whole oil GC chromatograms from the three producing reservoirs in SCOOP are provided in Figure 90 and show a strong resemblance between Woodford- and Mississippian-produced oils that is distinct from Springer-produced oils. The Caney-Springer formations straddles the Mississippian-Pennsylvanian boundary and produces oils in this dataset with abundant *n*-alkanes between *n*-C_{10} and *n*-C_{22}, *n*-C_7 in lower abundance relative to MCH, and abundant isoprenoids compared to *n*-alkanes which closely resemble the chemical signature attributed to Pennsylvanian-type oils. In contrast, Woodford- and Mississippian-produced oils are rich in light hydrocarbons below *n*-C_{10}, abundant *n*-C_7 relative to MCH, and low abundance of isoprenoids compared to *n*-alkanes.

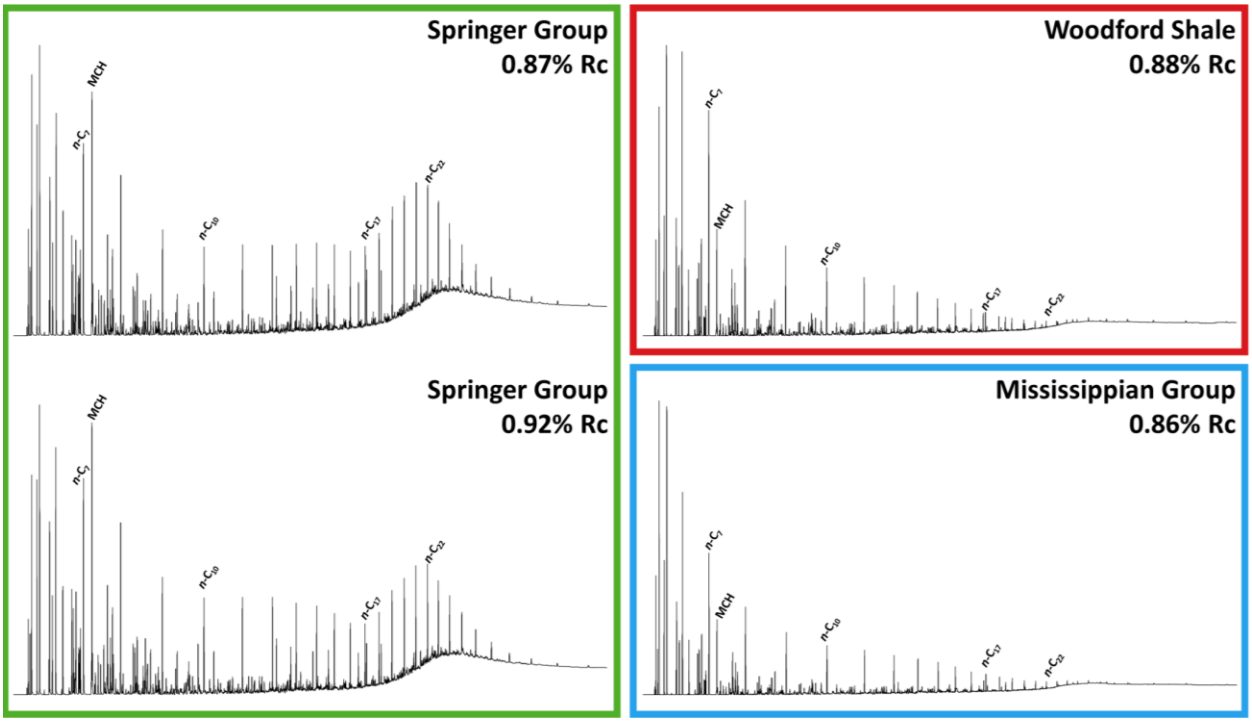

Figure 90. Characteristic whole oil GC fingerprint for the three SCOOP reservoirs. Springer-produced oils have a distinct and different character than Woodford- and Mississippian-produced oils at the same level of thermal maturity.

Light Hydrocarbons

The SCOOP whole oil GC chromatograms show Woodford- and Mississippian-produced oils differ from Springer-produced oils by the abundance of *n*-C_7 relative to MCH (see also Figure 53). In Chapter IV, the heptane ratio developed by Thompson (1979, 1983) was introduced both as a potential maturity and/or source parameter, but was found to have little or no relationship to maturity in SCOOP oils (Figure 36). The heptane ratio, defined as 100**n*-C_7/(CC_6+2-MH+2,3-DMP+1,1-DMCP+3-MH+1*c*3-DMCP+3-EP+1*t*3-DMCP+1*t*2-DMCP+*n*-C_7+1*c*2-DMCP+MCH), is shown in Figure 91 for all SCOOP oils where Woodford- and Mississippian- oils cluster separately from Springer-produced oils at all Rc%. The heptane ratio for Woodford- and Mississippian- produced oils (33.7±0.7, n=34) is approximately 50% larger than for Springer-produced oils (20.3±0.9, n=19) which reflects the less abundant *n*-C_7 observed in Springer-produced oils. Higher heptane ratio has been empirically linked to more aliphatic kerogen and lower heptane ratio to more aromatic kerogen (Thompson, 1983), so one explanation for higher values in Woodford/Mississippian oils is that they may be sourced from a more aliphatic source.

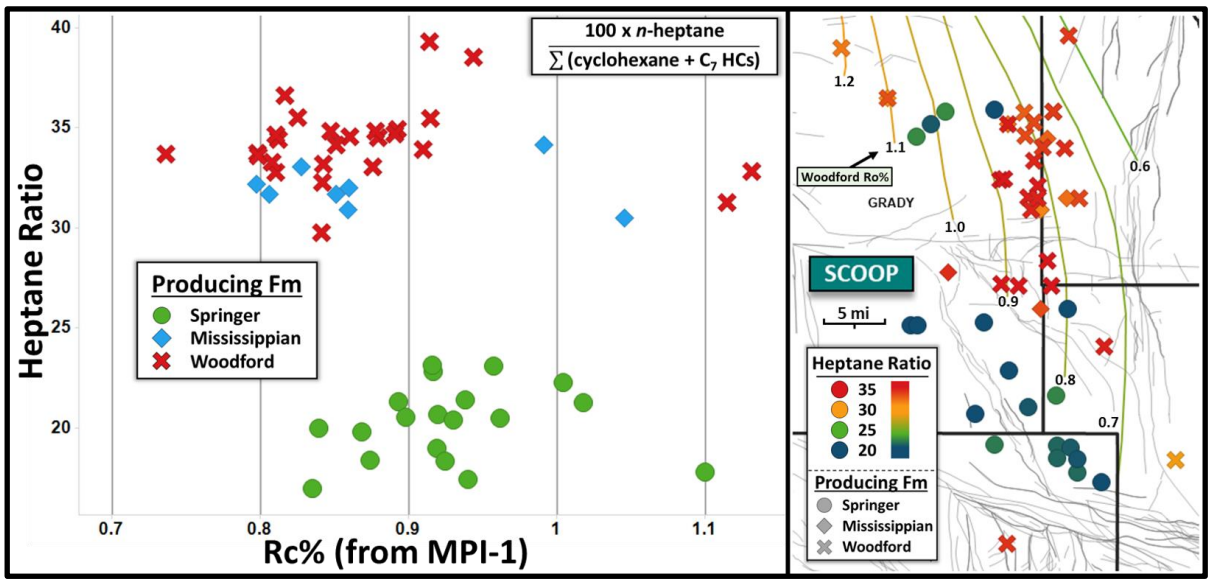

Figure 91. The heptane ratio versus maturity forms separate trends for Woodford/Mississippian- and Springer-produced oils. Samples in map view and colored by heptane ratio values. Heptane ratio=100**n*-C_7/(CC_6+2-MH+2,3-DMP+1,1-DMCP+3-MH+1*c*3-DMCP+3-EP+1*t*3-DMCP+1*t*2-DMCP+*n*-C_7+1*c*2-DMCP+MCH).

The isoheptane ratio, defined as (2-MH+3-MH)/(1*c*3-DMCP+1*t*3-DMCP+1*t*2-DMCP), generally increases exponentially with maturity (see Figure 36) but is often observed with different trends depending on the aliphatic or aromatic content of its source kerogen (Thompson, 1979, 1983). The isoheptane ratio values for SCOOP oils are shown in Figure 92 and indicate two parallel trends for Woodford/Mississippian and Springer oils with increasing maturity. The separate trends for Woodford/Mississippian and Springer oils supports the hypothesis that the Springer Group may be charged by a less aliphatic non-Woodford source, most likely the Caney or Goddard shales. One or both of these shales may also act as barriers to migration between the Woodford-Mississippian and the Springer Group reservoirs forming two separate petroleum systems.

The kinetic model proposed by Mango (1994) (see Figure 55) argues that light hydrocarbons exist in steady state equilibrium between parent-daughter pairs with intermediate compounds containing three-, five-, or six-carbon rings. The constants which define the kinetic equilibrium for each reaction is controlled by temperature, pressure, and the presence of catalysts. A ternary diagram which shows the fractional abundance of three-, five-, and six-ring preference

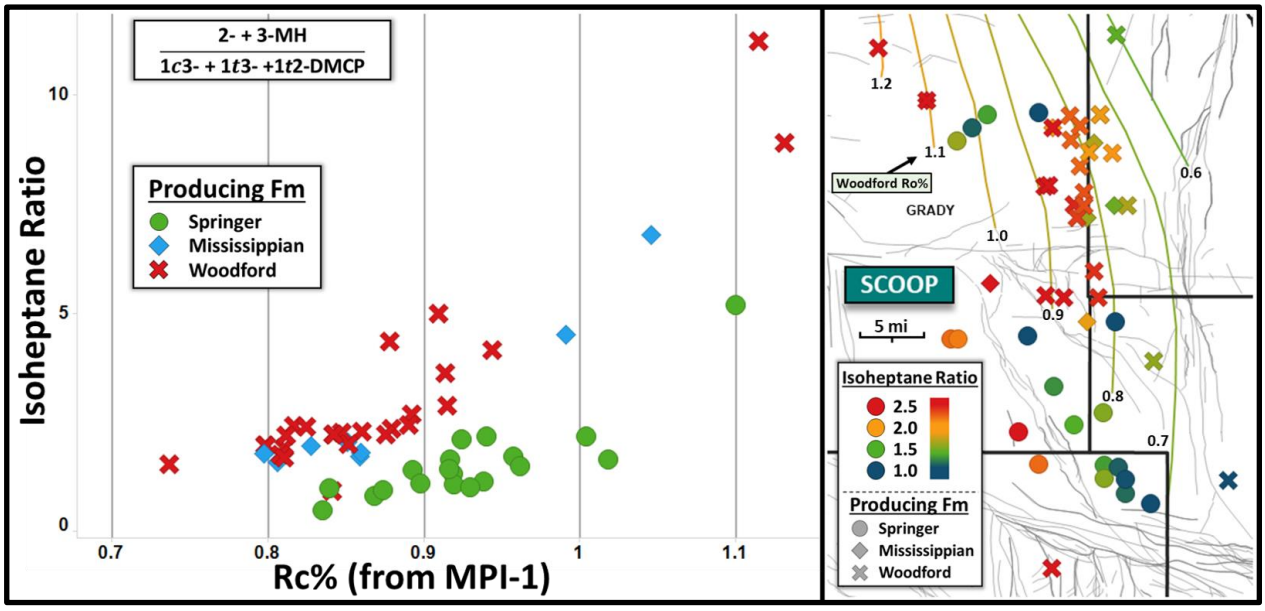

Figure 92. The isoheptane ratio shows separation betweenWoodford/Mississippian and Springer oils. Samples in map view and colored by isoheptane ratio values. Isoheptane ratio= (2-MH+3-MH)/(1*c*3-DMCP+1*t*3-DMCP+1*t*2-DMCP)

(RP) compounds based on Mango's kinetic model for SCOOP oils is provided in Figure 93 with data from Table 11. Once again, the Woodford- and Mississippian-produced oils cluster separately from Springer-produced oil. The different clustering is primarily due to a substantial increase in Six RP (N_1^6) in Springer oils resulting from higher abundances of methylcyclohexane. Similar to STACK, Woodford oils contain slightly higher Three RP (P_2 + P_3) values compared to Mississippian oils. Since carboxylic ring-closure in steady state is affected by the presence of metals, oxidation states, and structure of its surrounding ligands, the separate clustering between Springer and Woodford/Mississippian is likely an indicator of lithologic differences in the source.

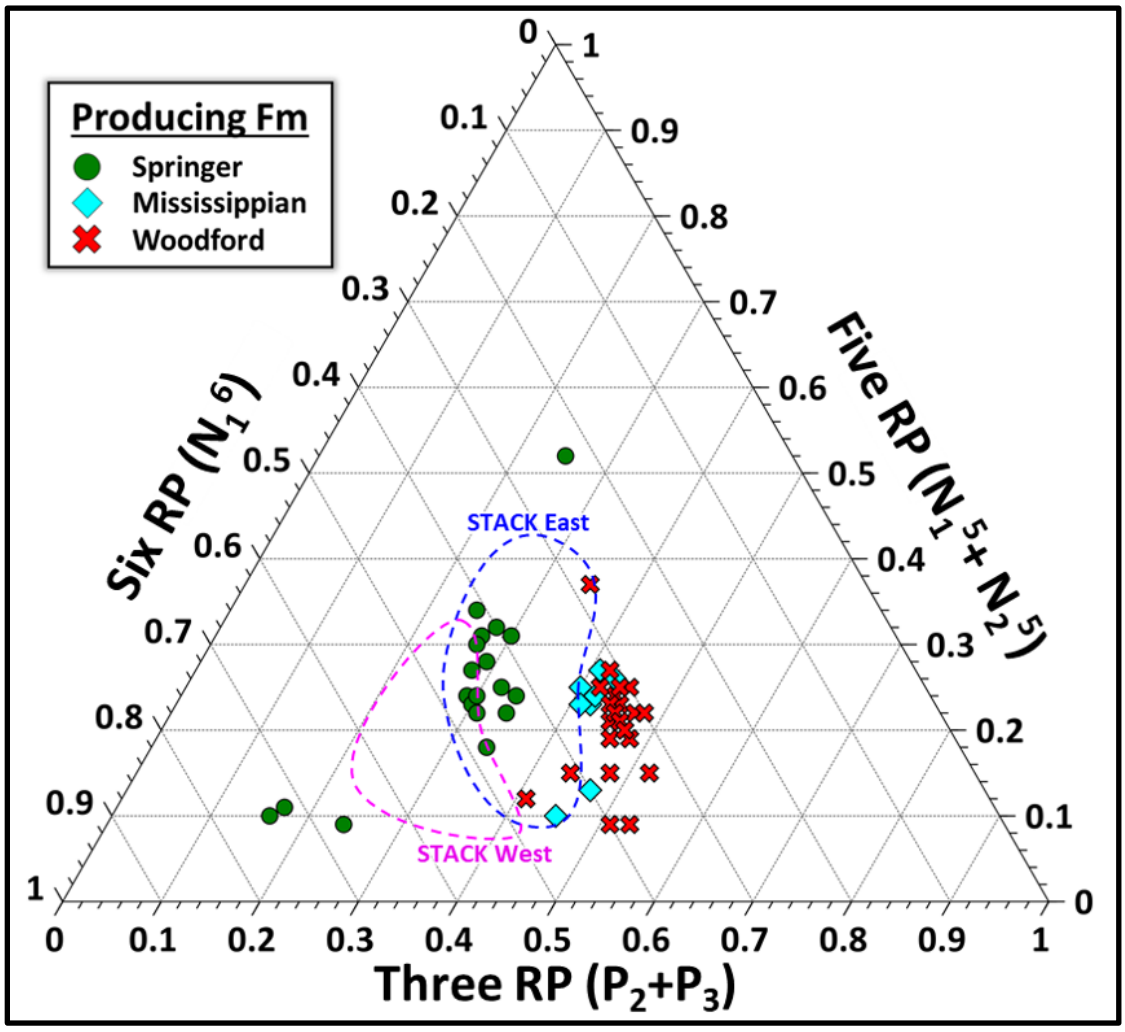

Figure 93. Ternary diagram showing the fractional abundance of three-, five, and six-ring preference (RP) compounds based on Mango's kinetic model. Six RP=MCH+Tol; Five RP=ECP+1*t*2-DMCP+1*c*2-DMCP+1,1-DMCP+1*c*3-DMCP+1*t*3-DMCP; Three RP=2-MH+3-MH+2,3-DMP+2,4-DMP+2,2-DMP+3,3-DMP+3-EP.

Sterane Biomarkers

Steranes (**I**) are biomarkers derived from sterols, ubiquitous in eukaryotic life, and were reviewed in detail previously in this chapter for STACK. Unfortunately, sterane data in SCOOP oils are limited by low signal to noise ratios in GC-MS. Nonetheless, the classic ternary diagram showing the fractional abundances of the C_{27}, C_{28}, and C_{29} regular steranes is provided in Figure 94 and shows significant data scatter. In general, Springer oils have slightly higher abundances of C_{27} sterane and lower abundance of C_{29} sterane compared to Woodford and Mississippian oils.

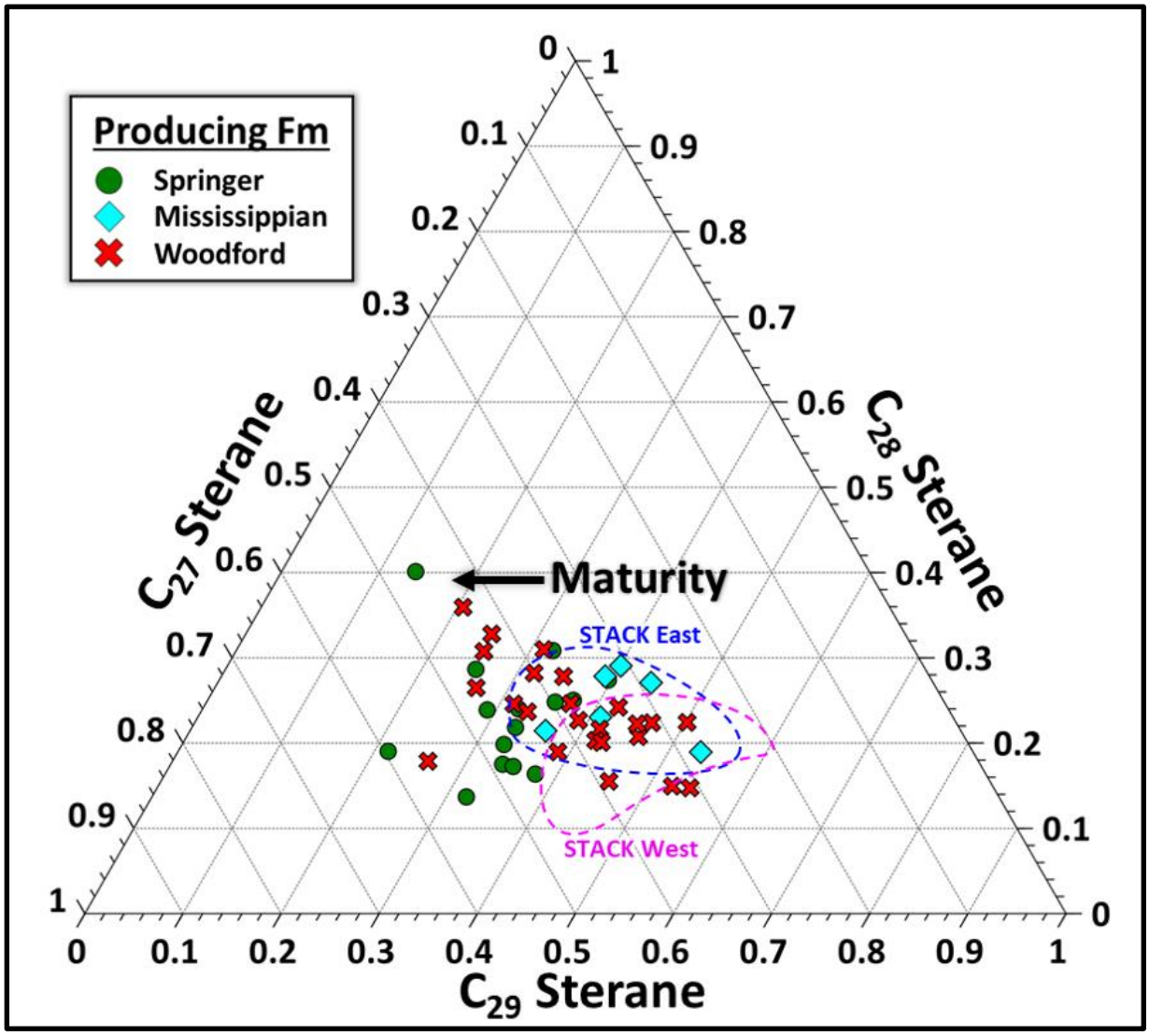

Figure 94. Ternary diagram of the C_{27}-C_{29} 5α(H),14α(H),17α(H) 20R steranes in SCOOP oils as a fraction of their sum. STACK data clusters are outlined.

The two additional sterane parameters used to characterize organic source facies in STACK were the ratios of the C_{30} Sterane Index and diasteranes/total steranes, shown in Figure 95, which are thought to reflect marine organic matter input and the presence of active acid sites on certain clay minerals, respectively (Rubinstein et al., 1975; Sieskind et al., 1979; Moldowan et al., 1985). Despite significant scatter, the C_{30} Sterane Index is higher in Springer oils (0.12±0.01, n=15) compared to Woodford/Mississippian oils (0.08±0.02, n=30), suggesting a more open marine source with more abundant golden Chrysophyte algae. Additionally, the ratio diasteranes/total steranes is also higher in Springer oils (0.86±0.06, n=18) than Woodford/Mississippian oils (0.75±0.05, n=31) suggesting a more argillaceous source.

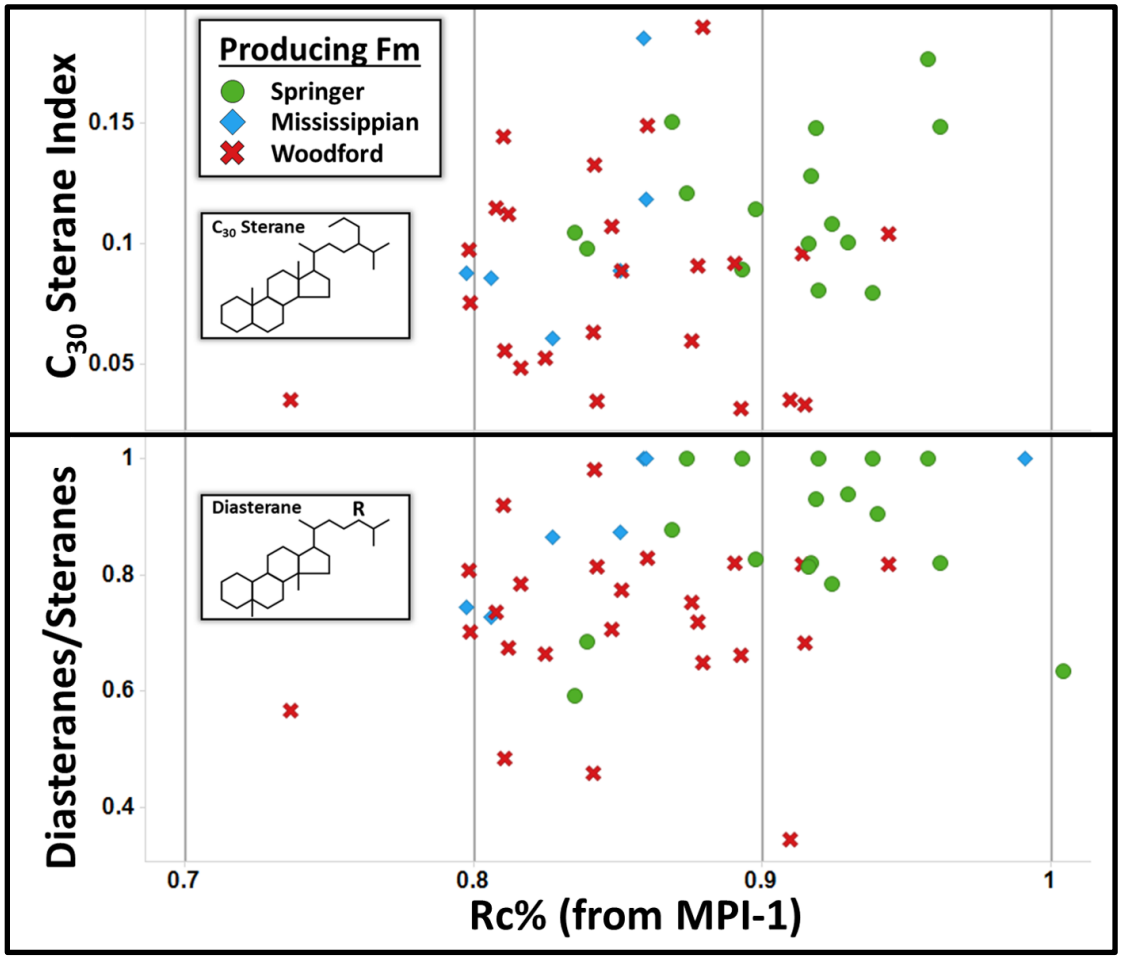

Figure 95. Two plots generated from the distribution of steranes in SCOOP oils. The C_{30} Sterane Index=C_{30}/(C_{27}-C_{30}) steranes each of the 5α,14α,17α(H),20R isomers; diasteranes/total steranes=[m/z 259]/[m/z 217] over the range of C_{27}-C_{30} steranes

Terpenoid Biomarkers

Earlier in this chapter, the crossplot comprising the ratios pristane (**X**; Pr) to *n*-C_{17} and phytane (**XI**; Ph) to *n*-C_{18} was shown for both STACK and SCOOP oils and overlain with common interpretations for depositional redox, thermal maturity, and biodegradation (see Figure 67). All SCOOP oils plotted as sourced from a transitional or marine depositional environment, and this interpretation was also supported by the same finding in the crossplot of Pr/Ph versus DBT/P (see Figure 68). The Pr/*n*-C_{17} ratio is substantially higher in Springer-produced oils (0.73±0.04, n=19) compared to Woodford- and Mississippian-produced oils (0.32±0.02, n=34), and there is no observable change in the ratio Pr/*n*-C_{17} with maturity (Figure 96). The findings agree with the overall observations of whole oil GC chromatograms in Figure 90 that Springer oils have higher abundances of isoprenoids relative to *n*-alkanes compared to Woodford and Mississippian oils. Although higher Pr/*n*-C_{17} ratios in some oils could result from the preferential biodegradation of alkanes relative to isoprenoids (Connan, 1984), there is no evidence of biodegradation in any SCOOP oils and instead the difference is believed to be source-related.

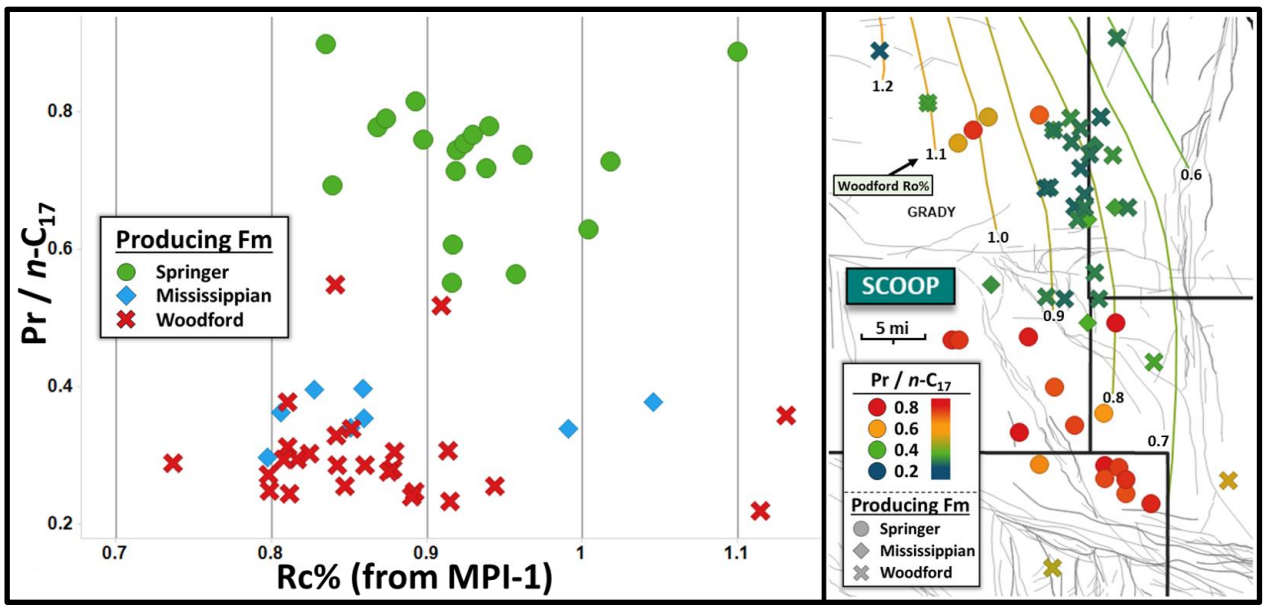

Figure 96. Ratio of Pr/*n*-C_{17} normalized to maturity show separate clusters for Woodford/Mississippian- and Springer-produced oils. Samples are plotted in map view and colored by Pr/*n*-C_{17} values.

Source related groups of SCOOP oils might also be distinguished by the absolute concentrations of polycyclic biomarkers. The concentrations three polycyclic terpenoid classes, bicyclic sesquiterpanes (**XI**), tricyclic terpanes (**V**), and hopanes (**VI**), for SCOOP oils are provided in Figure 97. Springer-produced oils have higher concentrations for each of the three terpenoid biomarkers compared to Woodford- and Mississippian-produced oils.

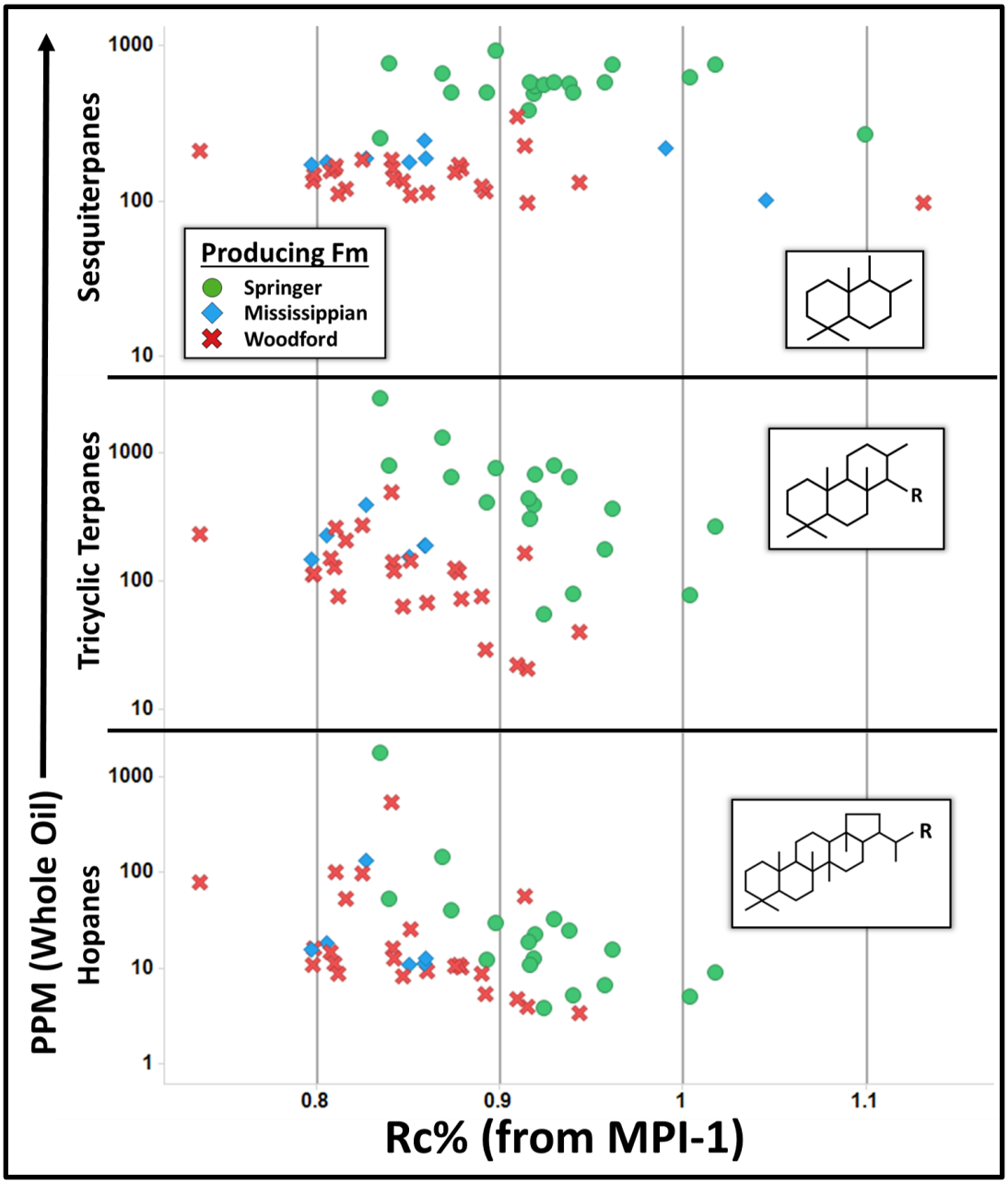

Figure 97. Concentration of sesquiterpanes, tricyclic terpanes, and hopanes in ppm (whole oil) for all SCOOP oils. Springer oils have higher concentrations than Woodford and Mississippian oils when normalized to maturity.

This study identified eight sesquiterpanes, shown previously in Figure 69, three of which were selected for a source-specific ternary diagram (Table 14) shown for STACK oils in Figure 70 and re-created for SCOOP oils in Figure 98. Springer oils cluster separately and have higher amounts of the rearranged drimane (BS-4) compared to Woodford and Mississippian oils. Like diasteranes, the formation of rearranged drimanes is believed to be catalyzed by the presence of active acid sites like clay surfaces. The sesquiterpane data in SCOOP continues to support the hypothesis that the Springer Group was charged more argillaceous non-Woodford source.

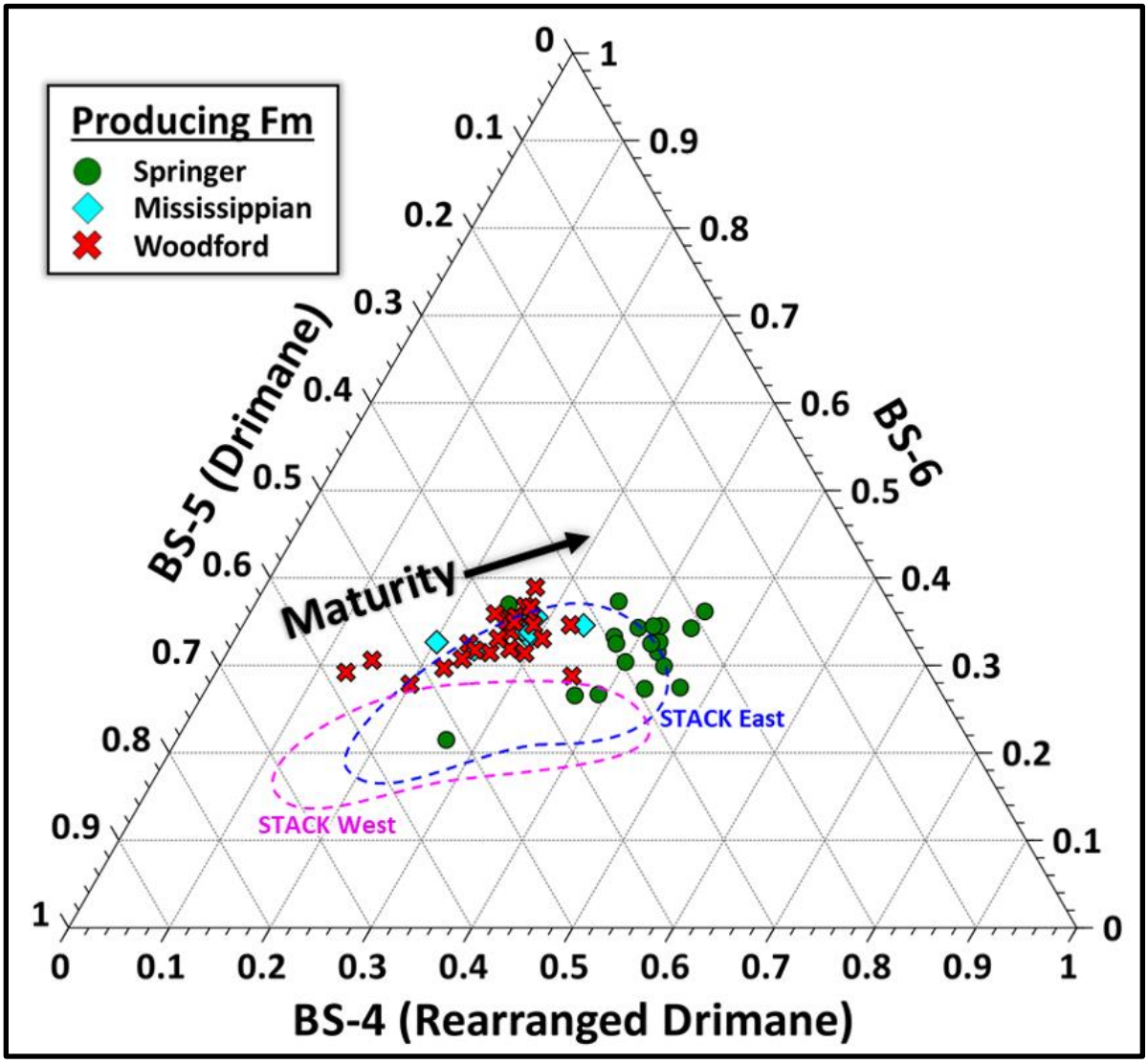

Figure 98. Ternary diagram of three closely eluting C_{15} sesquiterpanes include a rearranged drimane (BS-4), drimane (BS-5), and a third sesquiterpane (BS-6) as a fraction of the sum of the three. Springer-produced oils plot separately from Woodford- and Mississippian-produced oils which cluster together.

Cheilanthanes, or tricyclic terpanes (**V**; TT), were used earlier in this chapter to determine that all STACK oils analyzed were generated from a siliciclastic source rock. By plotting the tricyclic terpane ratios C_{22}/C_{21} as a function of C_{24}/C_{23}, Zumberge et al. (2007) created expected zones for oils generated from carbonate and siliciclastic source rocks. A re-creation of this cross plot is provided in Figure 99 and shows significant data scatter, but all SCOOP oils plot inside or near the expected range of values for oils generated from siliciclastic source rocks. Springer oils have higher C_{24}TT/C_{23}TT values compared to Woodford and Mississippian oils.

A summary of terpane fingerprints from Springer, Woodford and Mississippian oils is shown in Figure 100, and the relative abundance of the C_{19}TT through C_{31}TT is shown in Figure 101. Springer oils have more abundant extended tricyclic terpanes (C_{28}-C_{31}) relative to regular tricyclic terpanes (C_{19}-C_{26}) compared to Woodford and Mississippian oils. Notably, some extended tricyclics (e.g. C29TT(S)) in Springer oils are more abundant than the C_{23} and C_{24} tricyclic terpanes which are usually the most abundant tricyclic terpanes in oils sourced from marine source rocks.

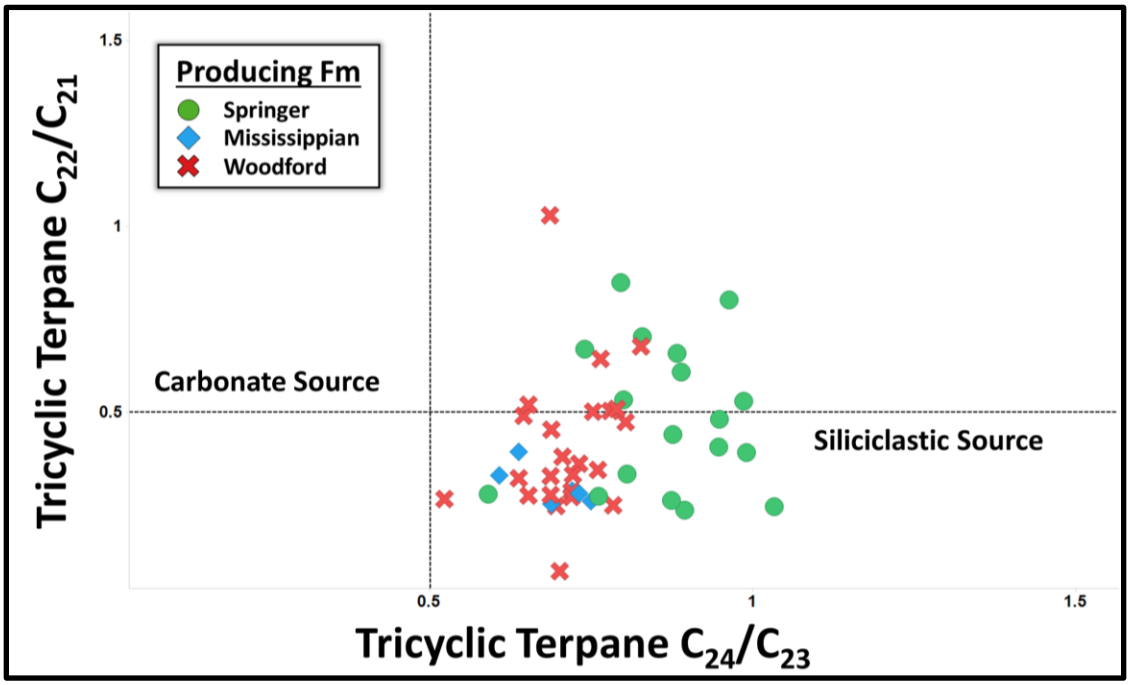

Figure 99. Crossplot of the C_{22}/C_{21} TT as a function of C_{24}/C_{23} TT showing all STACK oils plot in the zone attributed to siliciclastic source material. Original plot from Zumberge et al., (2007).

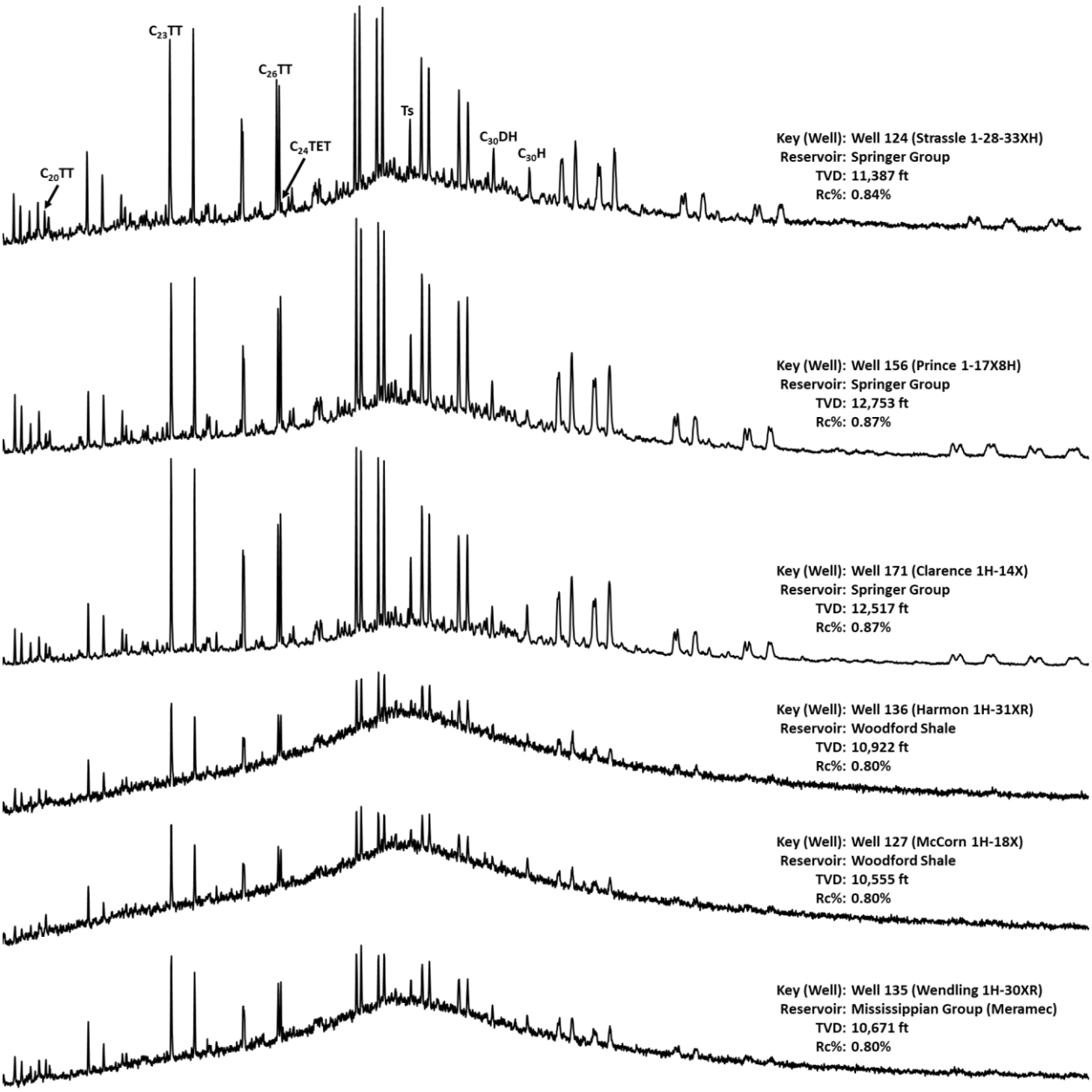

Figure 100. Terpane fingerprints taken from the m/z 191 chromatogram from six oils produced from SCOOP reservoirs—three from Springer Group, two from the Woodford Shale, and one from the Mississippian Group. All oils are between 0.80-0.87% Rc and were produced from between 10,555-12,753 ft TVD. Oils from all three reservoirs show a dominance of tricyclic terpanes over hopanes, but Springer Group oils show dominant extended tricyclic terpanes between C_{28}TT up through C_{39}TT compared to Woodford and Mississippian oils. Springer Group oils also contain near equal abundances of C_{23}TT and C_{24}TT where the C_{23}TT is dominant in Woodford and Mississippian oils in both STACK and SCOOP. The C_{24}TET peak is small in all oil SCOOP oils, suggesting a more open marine depositional environment. Finally, a C_{30}DH is observed in Springer Group oils which is not readily observed in Mississippian and Woodford oils.

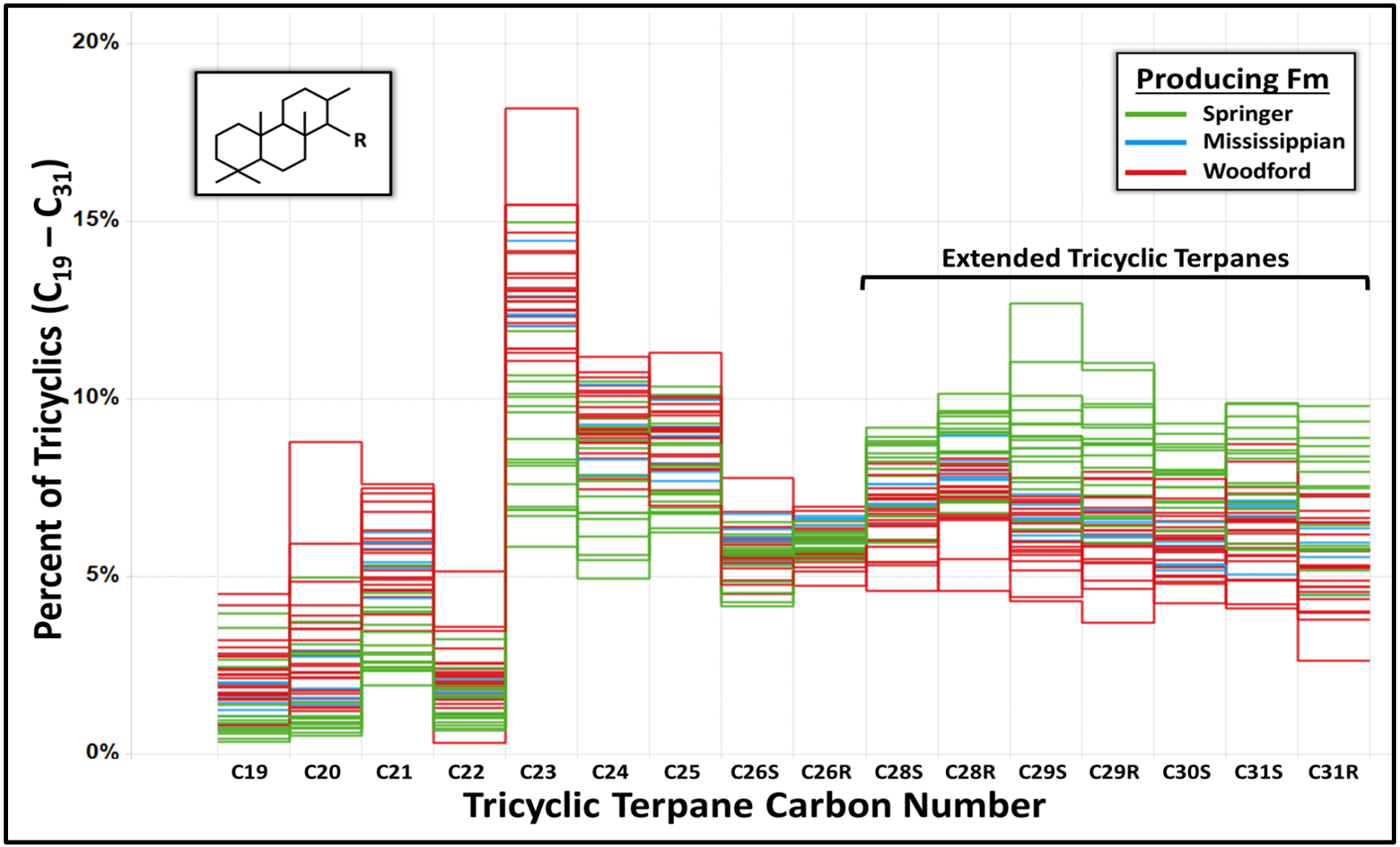

Figure 101. Abundance of the C_{19} through C_{31} tricyclic terpanes for all SCOOP oils relative to total tricyclic terpanes as determined from peak areas.

Earlier in this chapter, it was demonstrated that the nature of chemical bonds and molecular porosity in asphaltenes may affect the release of tricyclic terpane homologues into the maltene fraction with maturity, and that the efficiency of this process may be related to organic facies. This hypothesis was tested in SCOOP by calculating the rate decline exponents for each tricyclic terpane carbon number for Springer oils as well as combined Woodford and Mississippian oils as shown in Figure 102. Woodford and Mississippian oils exhibit a trend which closely mirrors the Woodford-sourced oils in STACK, but Springer oils show larger rate decline exponents at all carbon numbers and form a second trend well below the three Woodford-sourced trends. This phenomenon needs to be studied more closely, but it is hypothesized that organic sources may be successfully differentiated based on the preferential release of terpanes during catagenesis.

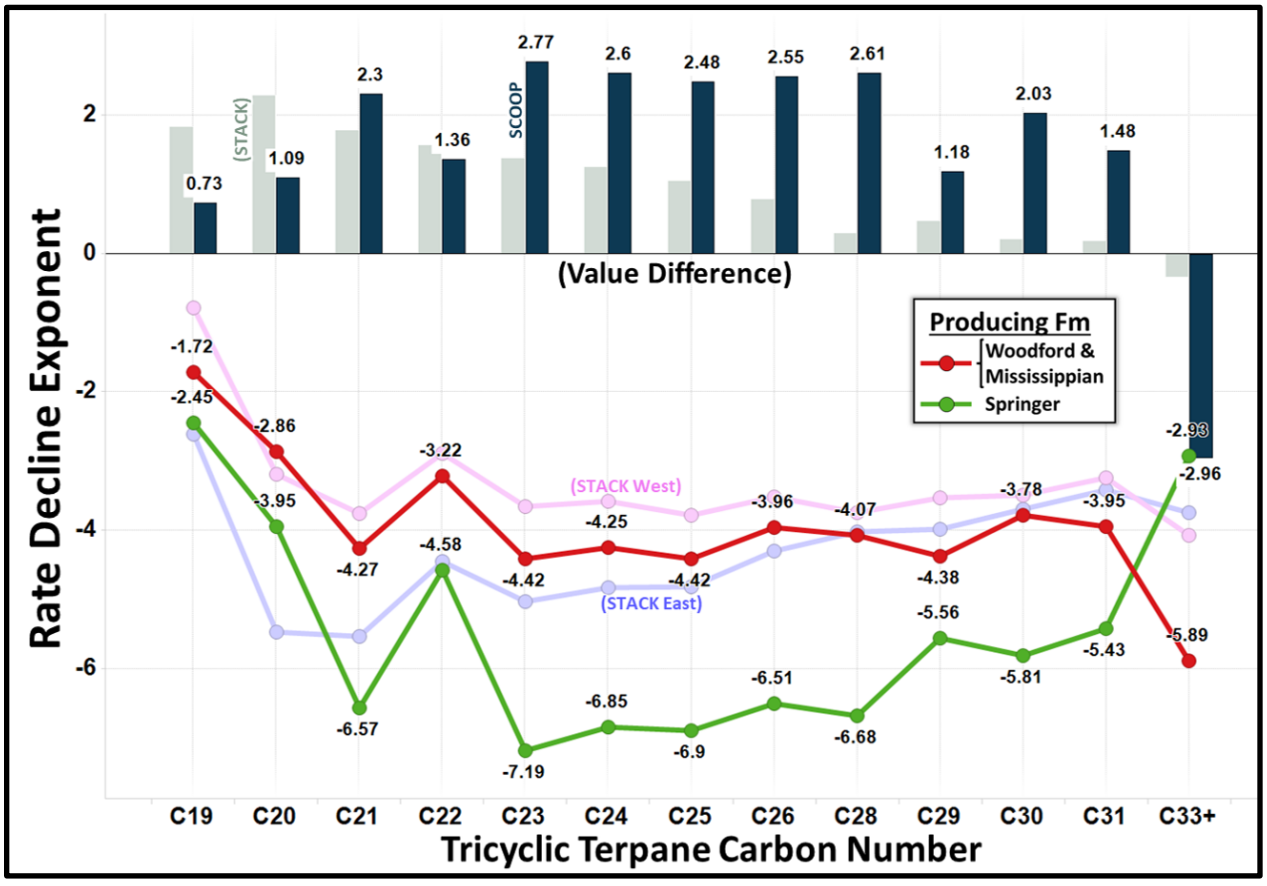

Figure 102. Combination plot showing rate decline exponents for the tricyclic terpane series in SCOOP (lines) as well as the difference in values between Woodford/Mississippian and Springer Group oils (bars).

C_{24} Tetracyclic Terpane

The C_{24} tetracyclic terpane (**XIII**; C_{24}TET) has been linked to source rocks deposited in shallow or restricted marine environments with limited access to upwelling nutrients (Zumberge et al., 2007), epicontinental carbonate or evaporite settings (Palacas, 1988; Clark and Philp, 1989), and in some cases high levels of terrigenous input (Philp and Gilbert, 1986). The C_{24}TET/C_{26}TT(S) ratio for SCOOP oils is provided in Figure 103 and shows higher values in Woodford/Mississippian-produced oils (0.22±0.05, n=30) compared to Springer-produced oils (0.09±0.04, n=18). The low values observed in all SCOOP oils are characteristic of source rocks deposited in a reducing or anoxic marine depositional environment, and the very low values in Springer oils suggests its source contained a more open marine environment compared to the source for Woodford and Mississippian oils. This finding agrees with the higher C_{30} sterane index values in Springer-produced oils compared to Woodford- and Mississippian-produced oils which is a strong indicator of marine input known to source primarily from golden Chrysophyte algae.

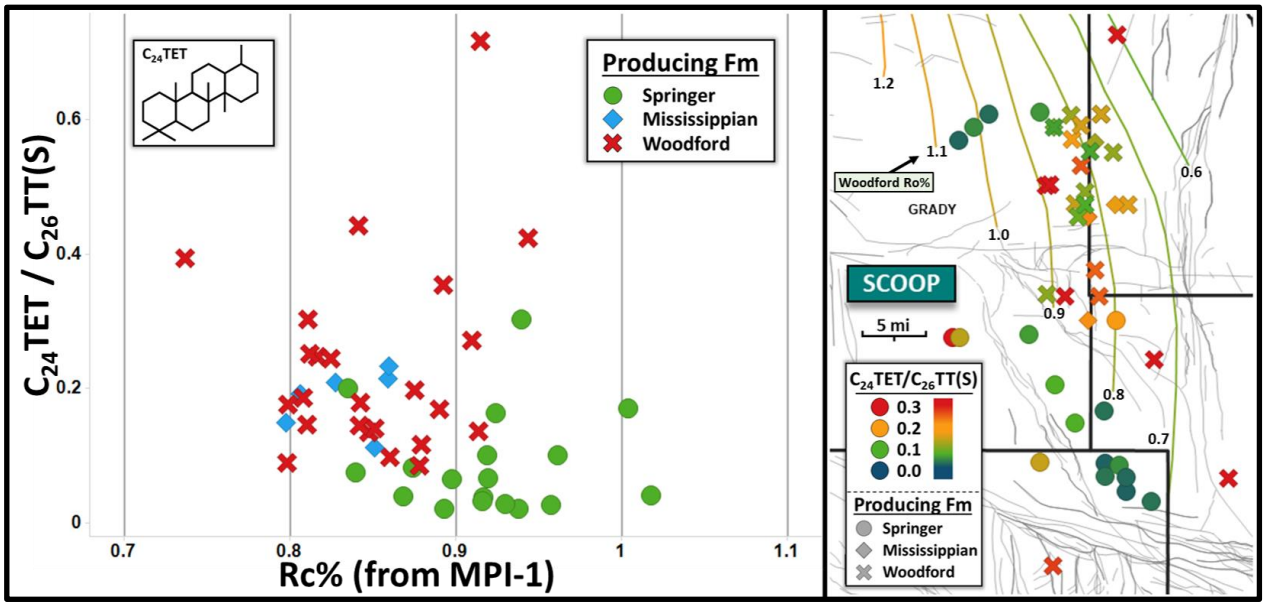

Figure 103. Ratio of C_{24}TET/C_{26}TT(S) normalized to maturity show slightly higher values for Woodford/ Mississippian-produced oils than Springer-produced oils. Mapped sample are colored by C_{24}TET/C_{26}TT(S) values.

Summary of SCOOP Geochemistry

Oils produced from SCOOP were found to belong to one of two source related families of oils partitioned entirely by producing reservoir. One family contained all oils produced from Woodford and Mississippian Group reservoirs, including the Sycamore and Meramec formations, and the second set contained all oils produced from the Springer Group reservoirs. The most notable characteristics of Woodford- and Mississippian-produced oils in SCOOP are the unimodal distribution of *n*-alkanes, heptane ratio value <30, *n*-C_7>MCH, three-RP C_7 compounds ≥40% (see Figure 93), C_{30} sterane index between 0.06-0.11, Pr/*n*-C_{17}<0.4, rearranged drimane BS-4/∑(BS-4 through BS-6) <0.30, sesquiterpane concentrations <200ppm of whole oil, $C_{26\text{-}39}$TT (extended)/total TT <60%, and C_{24}TET/C_{26}TT(S) between 0.14-0.25. No significant geochemical differences were observed between Woodford- and Mississippian-produced oils, and as such the oils are interpreted as sharing a single organic facies with no volumetrically significant contribution from secondary sources. The source for these oils was deposited in an argillaceous, transitional- or open-marine environment containing high abundances of well-preserved aliphatic organic matter and is therefore interpreted as the Woodford Shale.

By contrast, the Springer Group of oils is characterized by bimodal distribution of *n*-alkanes with abundant *n*-C_{15} through *n*-C_{22} after which there is a steep decline in the abundance of higher carbon number *n*-alkanes, Heptane Ratio value <25, *n*-C_7<MCH, three-RP C_7 compounds ≤30% of light hydrocarbons, C_{30} Sterane Index between 0.10-0.14, Pr/*n*-C_{17}>0.7, rearranged drimane BS-4/∑(BS-4 through BS-6)>0.35, sesquiterpane concentration <100ppm of whole oil, extended/total tricyclic terpanes>70%, C_{24}TET/C_{26}TT(S) between 0.0.-0.10. The source for Springer oils was deposited in a very clay rich, argillaceous shale deposited in an open marine environment with aliphatic organic matter, most likely the Caney or Goddard Shales.

This Study in Relation to Previous Geochemical Findings

This study has reviewed the geochemistry of 3 cores and 172 oils produced from thirteen counties across the STACK and SCOOP plays of the Anadarko Basin, Oklahoma. Based on the geochemical fingerprints, four families of source related oils have been identified which each correspond to an organic facies (Figure 104). A summary of each organic facies is provided in Table 19 detailing its producing reservoirs as well as interpretations of source formation, lithology, depositional environment, and notable geochemical characteristics. The range of geochemical values are presented as first- and third-quartile range within each homologue set. Three homologue sets of oils correspond to the three interpreted organic facies within the Woodford Shale which range from restricted, transitional, and transitional/open marine depositional environments. All oils produced from Springer Group reservoirs belong to a single homologue set of oils originating from an organic facies from a non-Woodford marine source. Without additional core it is unclear if Springer oils are sourced from the Goddard or Caney shales.

This study has found no evidence to support a contribution of volumetrically significant Mississippian-sourced oil into Mississippian reservoirs. Critically, no source-specific geochemical differences were observed between oils produced from Woodford (41 samples) and Mississippian (111 samples) reservoirs in close proximity. Instead, this study concludes that all Woodford- and Mississippian-produced oils are sourced from three organic facies in the Woodford Shale which correspond to regional differences in accommodation space, ocean circulation, sediment supply, biomass, and organic preservation across a single depositional system. Moreover, the transitions between different portions of the depositional system might successfully be mapped by the oils generated nearby since tight unconventional oils are thought to be generated, trapped, and produced very near their organic source (Meckel and Thomasson, 2005).

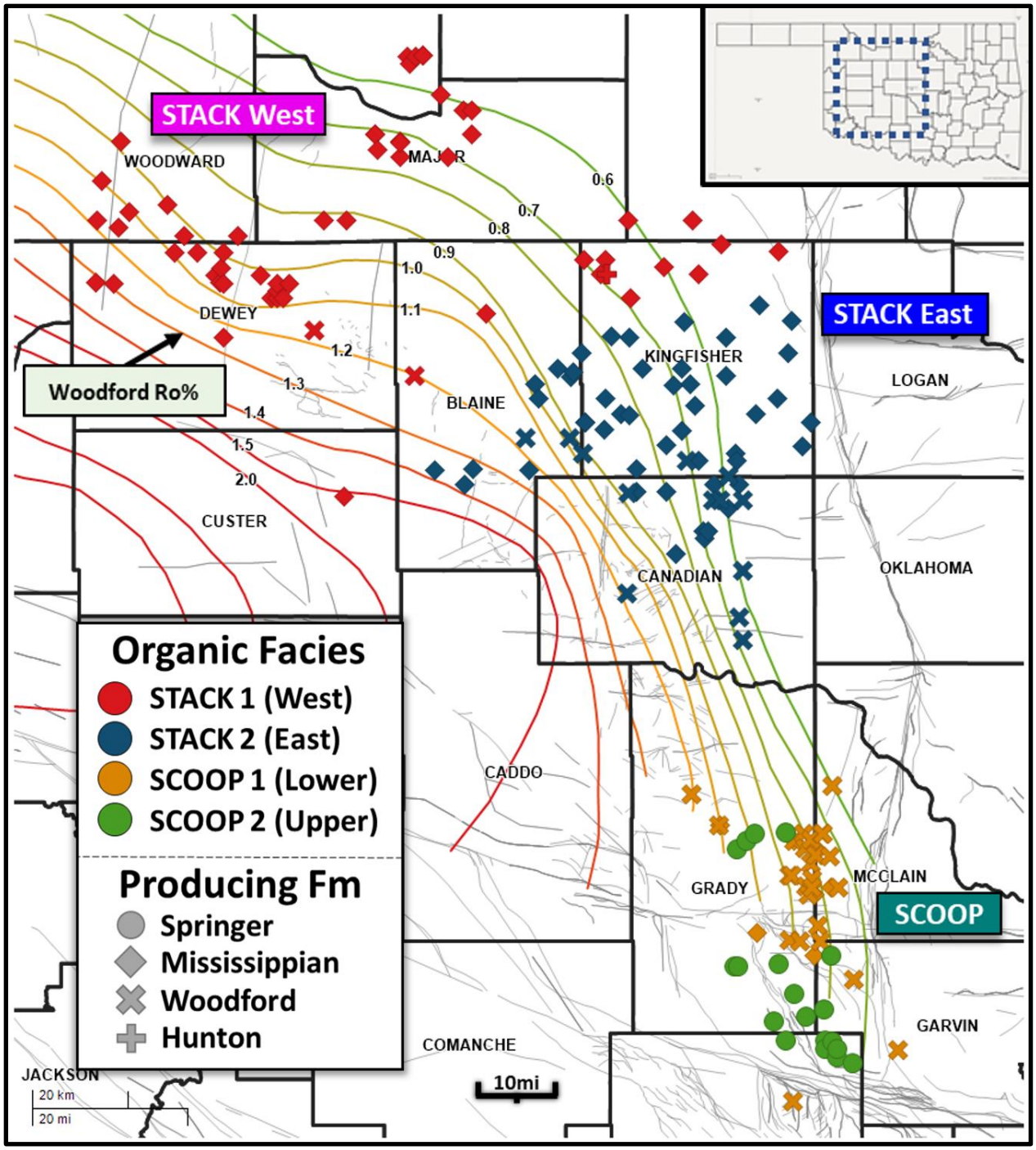

Figure 104. Map of STACK and SCOOP showing oils generated from each of the four identified organic facies.

	STACK 1 (West)	STACK 2 (East)	SCOOP 1 (Lower)	SCOOP 2 (Upper)
Producing Reservoirs	**Woodford, Mississippian**	**Woodford, Mississippian**	**Woodford, Mississippian**	**Springer Group**
Source Fm	**Woodford Shale**	**Woodford Shale**	**Woodford Shale**	**Caney or Goddard Shale**
Source Lithology	**V. Clay Poor or Calcareous Shale**	**Clay Rich Shale**	**Clay Rich Shale**	**V. Clay Rich Shale**
Dep. Environment	**Restricted Marine**	**Transitional Marine**	**Transitional/Open Marine**	**Open Marine**
Number of Samples	58	61	34	19
n-Alkane Distribution	Unimodal Distribution	Unimodal Distribution	Unimodal Distribution	Bimodal Distribution
[1]Aromaticity	0.21-0.33	0.08-0.12	0.07-0.10	0.10-0.14
n-C_7/MCH	0.9-1.2	1.0-1.2	1.8-2.1	0.7-0.8
[2]Heptane Ratio	23-29	24-28	32-35	19-21
[3]Mango K_1	1.00-1.06	0.90-0.97	0.88-0.93	0.92-1.02
[4]N_2+P_2 (% of Light HC)	0.23-0.26	0.29-0.31	0.31-0.32	0.30-0.32
[5]% Three-RP	25% to 30%	29% to 34%	43% to 47%	26% to 31%
[6]% Six-RP	48% to 55%	36% to 44%	32% to 35%	42% to 47%
Pr/Ph	1.1-1.4	1.2-1.3	1.1-1.4	1.0-1.3
Pr/*n*-C_{17}	0.39-0.49	0.46-0.58	0.27-0.35	0.70-0.78
DBT/P	0.09-0.40	0.04-0.06	0.08-0.09	0.04-0.09
[7]C_{29}/$C_{27\text{-}29}$ Sterane	0.46-0.52	0.40-0.46	0.32-0.45	0.31-0.35
[8]C_{30} Sterane Index	<0.05	0.07-0.09	0.06-0.11	0.10-0.14
[9]Diasteranes/Total Steranes	0.44-0.79	0.64-0.92	0.68-0.82	0.82-0.98
[10]BS-4/(BS-4 through BS-6)	0.18-0.31	0.29-0.36	0.24-0.29	0.38-0.43
Sesquiterpane ppm	210-400	150-280	70-100	260-380
C_{20}TT/C_{23}TT	0.30-0.40	0.10-0.20	0.14-0.23	0.10-0.22
[11]% Extended TT	50% to 60%	65% to 69%	59% to 67%	72% to 85%
$C_{23\text{-}31}$TT Rate Decline Exp.	-3.3 to -3.8	-3.4 to -5.0	-3.8 to -4.4	-5.4 to -7.2
C_{24}TET/C_{26}TT(S)	0.20-0.69	0.10-0.23	0.14-0.25	0.03-0.10
C_{35}/C_{34} Homohopane (S+R)	0.85-1.07	0.59-0.81	0.54-0.62	0.58-0.64

Table 19. Summary of the four identified organic facies indicating the producing reservoirs, source formation, source lithology, interpreted depositional environment, and some notable geochemical characteristics described in this chapter. Geochemical parameters are given as a range between first- and third-quartile values, meaning at least half of the oils sourced from that organic facies fall within the presented range.

[1]Aromaticity=Tol/(MCH+*n*-C_7)
[2]Heptane Ratio=100**n*-C_7/(CC_6+2-MH+2,3-DMP+1,1-DMCP+3-MH+1*c*3-DMCP+3-EP+1*t*3-DMCP+1*t*2-DMCP+*n*-C_7+1*c*2-DMCP+MCH)
[3]Mango K_1=(2-MH+2,3-DMP)/(3-MH+2,4=DMP)
[4]N_2+P_2 (% of Light HC)=1,1-DMCP+1*c*3-DMCP+1*t*3-DMCP+2-MH+3-MH
[5]%Three-RP=(2-MH+3-MH+2,3-DMP+2,4-DMP+2,2-DMP+3,3-DMP+3-EP)/(2-MH+3-MH+2,3-DMP+2,4-DMP+2,2-DMP+3,3-DMP+3-EP+ECP+1*t*2-DMCP+1*c*2-DMCP+1,1-DMCP+1*c*3-DMCP+1*t*3-DMCP+MCH+Tol)
[6]%Six-RP=(MCH+Tol)/(2-MH+3-MH+2,3-DMP+2,4-DMP+2,2-DMP+3,3-DMP+3-EP+ECP+1*t*2-DMCP+1*c*2-DMCP+1,1-DMCP+1*c*3-DMCP+1*t*3-DMCP+MCH+Tol)
[7]C_{29}/$C_{27\text{-}29}$ Sterane=C_{29}/$C_{27\text{-}29}$ sterane each of 5α(H),14α(H),17α(H),20R stereoisomerization
[8]C_{30} Sterane Index=C_{30}/$C_{27\text{-}30}$ steranes each of 5α,14α,17α(H),20R stereoisomerization
[9]Diasteranes/Total Steranes=[m/z 259]/[m/z 217] over the range of C_{27}-C_{30} steranes
[10]BS-4/(BS4 through BS-6)=BS-4/(BS-4+BS-5+BS-6)
[11]%Extended Tricyclic Terpanes=$C_{28\text{-}39}$TT/$C_{19\text{-}39}$TT

Recent studies have proposed a separate Mississippian source independent of the Woodford Shale in STACK based on the biomarker signature of some Mississippian-produced oils and core extracts (Atwah et al., 2019 and 2021). But the limestones, siltstones, and cherts that comprise most of the Mississippian Group in STACK are organic lean and have weight percent TOC generally much less than 1%. For example, of the 15 extracts sampled from the Osage Fm. in Blaine County by Kim and Philp (2001), only two had at least 0.5% TOC by weight. In this study, core intervals were selected to represent the most organic rich intervals, yet Mississippian samples averaged only 0.29% ± 0.09% TOC by weight (n=110) and only seven depths had a TOC greater than 1% (Figure 105; Table 20). In fact, an organic lean Mississippian interval agrees with numerous ichnologic studies which have reported trace fossils indicative of a diverse seafloor community (e.g. *Planolites*, *Teichichnus*, *Zoophycos*, *Chondrites*, *Phycosiphon*, and *Cruiziana*) as well as the fossil remains of numerous benthic organisms (e.g. crinoids, brachiopods, bryozoans, sponges), all of which are evidence of a well-oxygenated seafloor with low organic preservation (Harris, 1975; Johnson, 1989; Kim and Philp, 2001; Bynum and Wethington, 2020; Price, 2020).

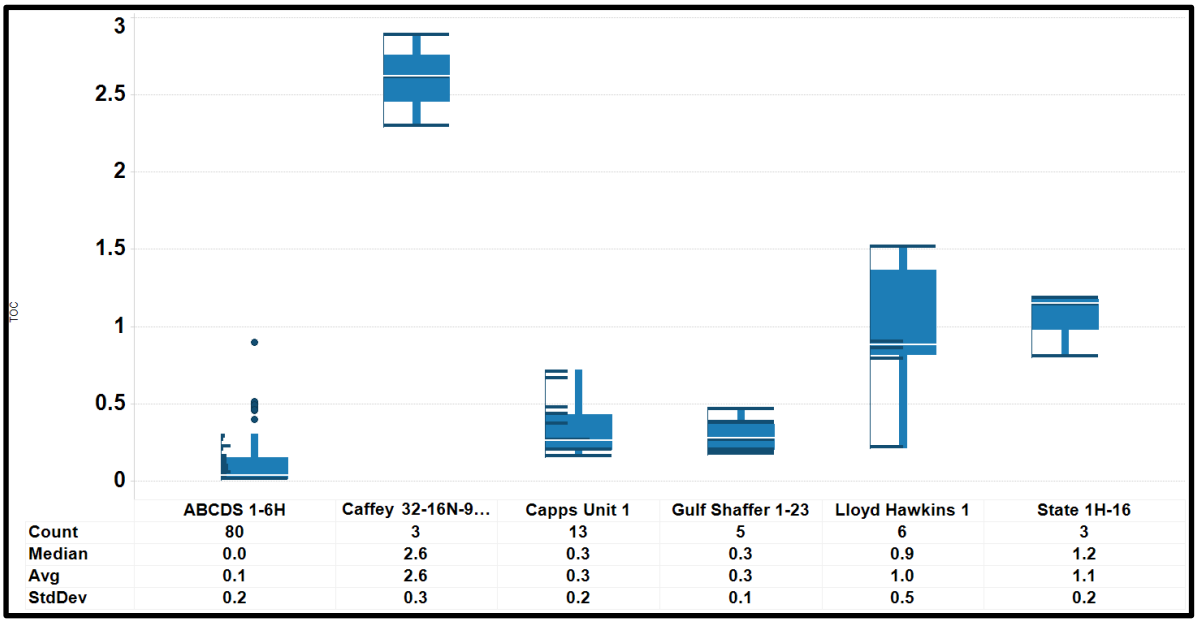

	ABCDS 1-6H	Caffey 32-16N-9...	Capps Unit 1	Gulf Shaffer 1-23	Lloyd Hawkins 1	State 1H-16
Count	80	3	13	5	6	3
Median	0.0	2.6	0.3	0.3	0.9	1.2
Avg	0.1	2.6	0.3	0.3	1.0	1.1
StdDev	0.2	0.3	0.2	0.1	0.5	0.2

Figure 105. LECO TOC measurements taken from 110 core depths across six Mississippian Group cores in STACK based on data in Table 20. Mississippian strata average a TOC of only 0.29% by weight in STACK.

Core Sample	Depth	TOC
ABCDS 1-6H	7390	0.22
ABCDS 1-6H	7392	0.23
ABCDS 1-6H	7396	0.23
ABCDS 1-6H	7398	0.30
ABCDS 1-6H	7400	0.50
ABCDS 1-6H	7404	0.52
ABCDS 1-6H	7406	0.48
ABCDS 1-6H	7408	0.49
ABCDS 1-6H	7410	0.13
ABCDS 1-6H	7412	0.90
ABCDS 1-6H	7414	0.01
ABCDS 1-6H	7416	0.05
ABCDS 1-6H	7418	0.01
ABCDS 1-6H	7420	0.01
ABCDS 1-6H	7422.25	0.10
ABCDS 1-6H	7424	0.13
ABCDS 1-6H	7426.15	0.01
ABCDS 1-6H	7428	0.16
ABCDS 1-6H	7430.4	0.07
ABCDS 1-6H	7432	0.01
ABCDS 1-6H	7434	0.06
ABCDS 1-6H	7436	0.09
ABCDS 1-6H	7438.3	0.08
ABCDS 1-6H	7440	0.01
ABCDS 1-6H	7442.15	0.01
ABCDS 1-6H	7444	0.04
ABCDS 1-6H	7446.6	0.11
ABCDS 1-6H	7448	0.01
ABCDS 1-6H	7450	0.01
ABCDS 1-6H	7452	0.08
ABCDS 1-6H	7454.15	0.01
ABCDS 1-6H	7456	0.01
ABCDS 1-6H	7458	0.01
ABCDS 1-6H	7460	0.01
ABCDS 1-6H	7462	0.01
ABCDS 1-6H	7464	0.01
ABCDS 1-6H	7466.25	0.01
ABCDS 1-6H	7468	0.01
ABCDS 1-6H	7470	0.01
ABCDS 1-6H	7472	0.03
ABCDS 1-6H	7474	0.07
ABCDS 1-6H	7476	0.01
ABCDS 1-6H	7478	0.01
ABCDS 1-6H	7480	0.01
ABCDS 1-6H	7482.25	0.01
ABCDS 1-6H	7484	0.01
ABCDS 1-6H	7486	0.01
ABCDS 1-6H	7488	0.08
ABCDS 1-6H	7490	0.01
ABCDS 1-6H	7492	0.08
ABCDS 1-6H	7494.65	0.03
ABCDS 1-6H	7496	0.12
ABCDS 1-6H	7498	0.01
ABCDS 1-6H	7500	0.01
ABCDS 1-6H	7502.15	0.01
ABCDS 1-6H	7504	0.17
ABCDS 1-6H	7506.05	0.16
ABCDS 1-6H	7508	0.23
ABCDS 1-6H	7510	0.13
ABCDS 1-6H	7512	0.14
ABCDS 1-6H	7514.05	0.02
ABCDS 1-6H	7516	0.01
ABCDS 1-6H	7518	0.01
ABCDS 1-6H	7520	0.01
ABCDS 1-6H	7522.2	0.01
ABCDS 1-6H	7524	0.01
ABCDS 1-6H	7526	0.10
ABCDS 1-6H	7528	0.46
ABCDS 1-6H	7530	0.26
ABCDS 1-6H	7532	0.46
ABCDS 1-6H	7534	0.20
ABCDS 1-6H	7536	0.06
ABCDS 1-6H	7538.65	0.30
ABCDS 1-6H	7540	0.15
ABCDS 1-6H	7542.1	0.40
ABCDS 1-6H	7544	0.23
ABCDS 1-6H	7546.55	0.01
ABCDS 1-6H	7548	0.01
ABCDS 1-6H	7550.3	0.01
ABCDS 1-6H	8069.35	0.01
Caffey 32-16N-9W 1H	9617.1	2.90
Caffey 32-16N-9W 1H	9669.1	2.29
Caffey 32-16N-9W 1H	9863.7	2.62
Capps Unit 1	8722	0.27
Capps Unit 1	8724	0.17
Capps Unit 1	8857	0.38
Capps Unit 1	8862	0.67
Capps Unit 1	8869	0.72
Capps Unit 1	8873	0.47
Capps Unit 1	8877	0.43
Capps Unit 1	8880	0.15
Capps Unit 1	8888	0.20
Capps Unit 1	8892	0.21
Capps Unit 1	8897	0.21
Capps Unit 1	8903	0.26
Capps Unit 1	8904	0.16
Gulf Shaffer 1-23	9667.5	0.17
Gulf Shaffer 1-23	9681.1	0.20
Gulf Shaffer 1-23	9703	0.28
Gulf Shaffer 1-23	9798.9	0.48
Gulf Shaffer 1-23	9848	0.37
Lloyd Hawkins 1	7741.2	1.52
Lloyd Hawkins 1	7757.8	0.85
Lloyd Hawkins 1	7908.8	0.80
Lloyd Hawkins 1	7918.8	0.21
Lloyd Hawkins 1	7939.6	0.91
Lloyd Hawkins 1	7959.3	1.53
State 1H-16	7938	1.20
State 1H-16	7953	0.80
State 1H-16	8110.5	1.15

Table 20. TOC measurements by depth across the six Mississippian cores analyzed in this study.

An increase in carbonate-type biomarkers in Mississippian extracts and oils has been proposed as evidence of a Mississippian source, including elevated C_{27}/C_{29} regular steranes, elevated 28,30-bisnorhopane/hopane, certain light hydrocarbon ratios, and extended tricyclic terpanes beyond C_{31} (Atwah et al., 2019 and 2021). Each of these will be addressed in the following paragraphs. These studies fail to capture the broad heterogeneity which can be observed between the most restricted and open-marine portions of the Woodford seaway as well as the spatial and geochemical heterogeneity of the three Woodford constituent members. More importantly, however, is the extent to which those geochemical metrics can be affected by maturity. For example, the depletion of C_{29} regular sterane to its C_{27-28} homologues in response to increased thermal maturity is well-documented both in the published literature (e.g. Moldowan et al., 1989; Dzou et al., 1995; Yi et al., 2020) and confirmed by this study (Figure 62).

Indeed, 28,30-bisnorhopane (**XIV**) concentrations above 25 ppm are common in oils generated from Type IIS source rocks and some anoxic, high-sulfur facies (Seifert et al., 1978; Grantham et al., 1980; Rullkötter et al., 1982; Philp, 1983; Volkman et al., 1983), but the abundant evidence of benthic life in the Mississippian indicates a well-oxygenated seafloor and would seem to preclude the possibility of euxinic or high-sulfur facies. In fact, demethylated hopanes like 28,30-bisnorhopane are not generated from kerogen but rather stored as free hydrocarbons in sediments (Noble et al., 1985; Isaksen et al., 1998). The concentration of 28,30-bisnorhopane in oils is instead usually controlled by dilution by other hydrocarbons which can be a function of maturity (Gransch and Posthuma, 1974; Grantham et al., 1980), and in this study the concentration of 28,30-bisnorhopane is inversely related to maturity for all homologue sets of oils and the highest concentration is only 11ppm (Figure 106). Therefore, the small variability observed in 28,30-bisnorhopane is not a likely indicator of a prolific Mississippian source.

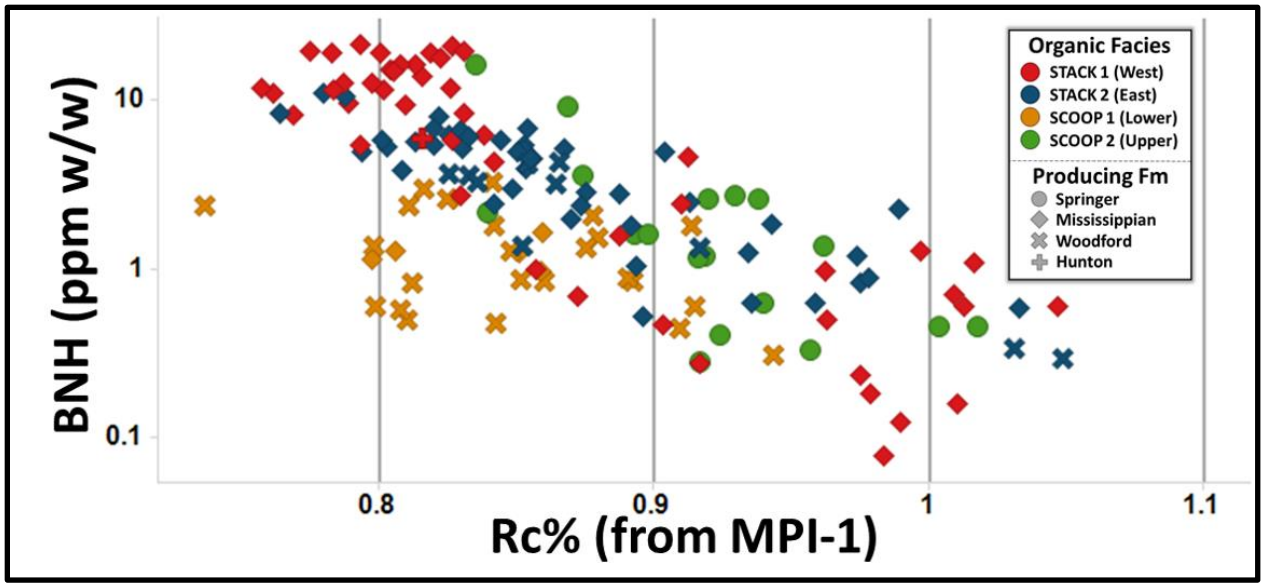

Figure 106. Concentration of 28,30-bisnorhopane (BNH) by organic facies and producing reservoir. The highest concentration in this study is 11 ppm.

Changes in light hydrocarbon fingerprint has also been invoked to differentiate between Woodford- and potential Mississippian-sources (Atwah et al., 2019). The study utilized a light hydrocarbon analysis developed by Halpern (1995) to correlate oils to each other using a pair of star diagrams (multivariate plots in polar coordinates) populated with ratios of C_7 isomers by leveraging their respective differences in boiling point, solubility, and susceptibility to bacterial attack. Although each representative region analyzed by Atwah et al. (2019) exhibited a unique geochemical signature which differed from the other two, only one region compared oils produced from both Woodford and Mississippian reservoirs and showed no differences in light hydrocarbon signatures. The study also showed that oils produced outside of the basin on the Anadarko Shelf and Nemaha Ridge show depletion in phenol, toluene, and cresols—strong indicators of long-distance migration out of the Anadarko or Arkoma basins, respectively, rather than a local organic source (Price, 1976). This conclusion is supported by numerous publications which argue that a large amount of oil migrated out of the Anadarko Basin and traveled as far north as the Cambridge Arch in southwestern Nebraska (Walters, 1958; Burruss and Hatch, 1989; Tamborello, 2020).

Finally, extended tricyclic terpanes above C_{31}TT have been observed in several extracts of Mississippian core and, in some cases, have been invoked as evidence of a unique Mississippian organic facies (Wang and Philp, 1997, 2019; Kim and Philp, 2001; Atwah, 2015; Wang, 2016; Atwah et al., 2019, 2020, 2021; Symcox and Philp, 2019a; Abrams and Thomas, 2020). Although their origin remains unknown, tricyclic terpanes above C_{31}TT are actually not unique to oils or extracts of the Mississippian Group. In fact, extended tricyclic terpanes were found in all analyzed Woodford-produced oils as well as most rock extracts, with examples shown in Figure 107. This study has shown that the occlusion and subsequent release of tricyclic terpanes might directly relate to the size, arrangement, and stability of chemical bonds affording molecular porosity to macromolecular structures—characteristics inherited from organic facies—and might also be intimately related to natural deasphaltene processes during generation, expulsion, and migration.

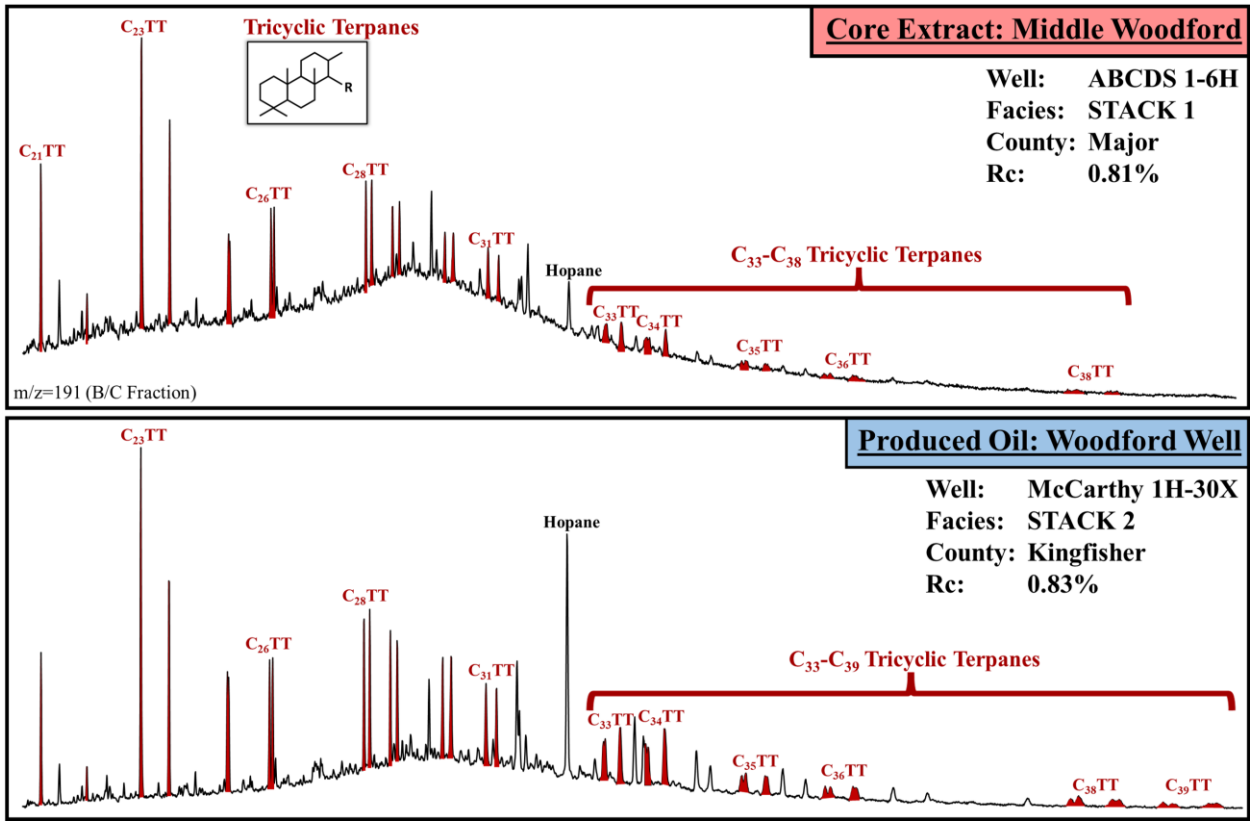

Figure 107. Tricyclic terpane fingerprints of Woodford Shale rock extract (upper) and Woodford-producing oil (lower) showing that extended tricyclic terpanes above C_{31}TT are present in both samples.

Summary of Findings

An organic facies is defined as "a mappable rock unit distinguishable by the character of its organic matter without regard to the inorganic aspects of the sediment" (Jones, 1984). To meet this standard, a homologous set of oils must first be identified by a preponderance of source-specific parameters which consistently cluster separately. When plotted in map view, those same source-specific parameters must form a cogent trend distinguishable from other homologous sets. Numerous source-specific parameters were surveyed to determine their efficacy at forming two or more data clusters. By normalizing source-related parameters to their maturity, oils across the maturity spectrum could be compared on organic source alone. Some source-specific parameters strongly affected by maturity (e.g. $C_{24}TET/C_{26}TT$) formed strong trendlines when normalized to Rc% which reinforced homologous sets but were not plotted in map view.

Oils from two organic facies were identified in STACK with the transition occurring in northwestern Kingfisher and central Blaine counties. The source for the STACK 1 (West) organic facies was deposited in a restricted marine environment comprising a semi-closed oceanic basin with limited access to upwelling nutrients or an epicontinental shelf with low accommodation space approaching the Cimarron Arch. In contrast, the source for the STACK 2 (East) organic facies (which comprise the core of STACK drilling activity) was deposited in a transitional or open marine environment. Despite the organic facies boundary corresponding with the leading edge of the Osage carbonate platform, no difference was observed between Woodford- and Mississippian-produced oils in STACK indicating that they originate from a common Woodford source. This further establishes that the sediment starved, restricted marine conditions which cultivated the growth of a carbonate platform during the Osagean had persisted in some capacity at least as far back as the time of Woodford deposition during the Late Devonian.

Oils from two organic facies were identified in SCOOP which were observed exclusively in different producing reservoirs. The source for the SCOOP 1 (Lower) organic facies was deposited in a clay rich deep or open marine environment. Oils comprising the SCOOP 1 organic facies were only produced from Woodford and Mississippian reservoirs and were sourced from the Woodford Shale. The source for the SCOOP 2 (Upper) organic facies was deposited in a clay rich transitional marine environment. Oils comprising the SCOOP 2 organic facies were only produced from Springer reservoirs and were generated by a non-Woodford source, likely the Goddard or Caney shales. SCOOP 2 oils share many characteristics to the Pennsylvanian-type oils first described by Burruss and Hatch (1989), notably being enriched in methylcyclohexane and regular isoprenoids relative to *n*-alkanes in whole oil GC chromatograms. SCOOP oils, especially Woodford-type, had low biomarker concentrations compared to STACK oils, an observation also made by Jones and Philp (1990), and could result from the high-pressure low-temperature regime in SCOOP counties.

VI. Secondary Processes

Elevated Sulfur Trend in STACK West

The STACK 1 (West) organic facies is identified as a region of geochemically similar Woodford Shale deposited in a restricted marine depositional environment with limited access to upwelling nutrients and starved of terrestrial sediment. The notable increase in light hydrocarbon aromaticity and dibenzothiophene (**VIII**; DBT) in oils from this organofacies has thus far remained unresolved (Figure 108). In Chapter V, the presence of free sulfur radicals (e.g., HS^-, HS_x) during diagenesis was cited as a possible catalyst in the formation of DBT and Tol through the dehydrogenation and cyclization of paraffins. This section will explore three possible mechanisms by which sulfur might be incorporated into a petroleum system, including high sulfur kerogen, bacterial sulfate reduction, and thermochemical sulfate reduction.

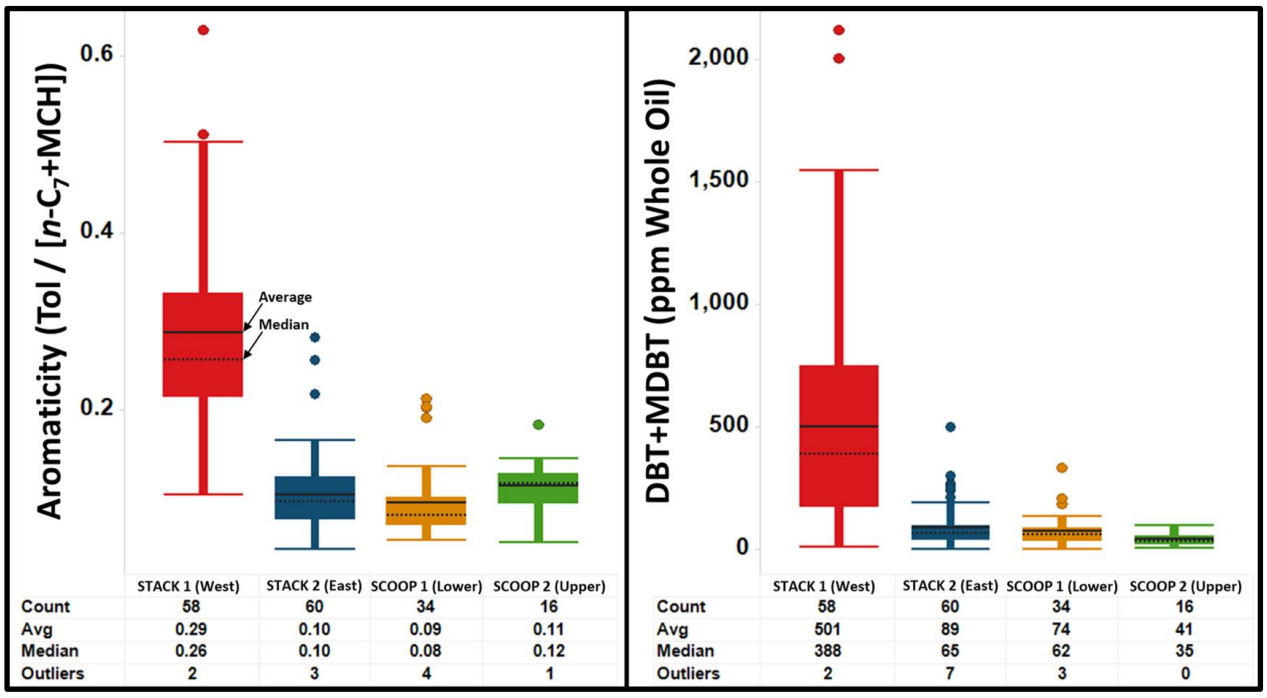

	STACK 1 (West)	STACK 2 (East)	SCOOP 1 (Lower)	SCOOP 2 (Upper)
Count	58	60	34	16
Avg	0.29	0.10	0.09	0.11
Median	0.26	0.10	0.08	0.12
Outliers	2	3	4	1

	STACK 1 (West)	STACK 2 (East)	SCOOP 1 (Lower)	SCOOP 2 (Upper)
Count	58	60	34	16
Avg	501	89	74	41
Median	388	65	62	35
Outliers	2	7	3	0

Figure 108. Box and whisker plots of aromaticity and DBT showing notable increases in oils generated from the STACK 1 (West) organic facies. DBT concentration includes both DBT and its methyl isomers (MDBT).

Hypothesis 1: Elevated Sulfur in Kerogen

Marine organic matter is mostly composed of proteins, carbohydrates, and lipids (Forsman and Hunt, 1958; Abelson, 1963). Although a small fraction organic of sulfur originates from amino acids found in proteins, most kerogen-bound sulfur originates from early diagenetic reactions between recently deposited organic matter and aqueous sulfide species (S^{2-}), such as hydrogen sulfide (H_2S) and polysulfides, produced by respiratory sulfate reduction by organisms like *Desulfovibrio desulfuricans*, a species of microaerophilic anaerobe (Davis and Yarbrough, 1966; Demaison and Moore, 1980; Francois, 1987). Under normal marine conditions, iron and organic matter both act as a sink for free sulfide, but iron competes more successfully to form hydrotroilite, troilite, and eventually pyrite (Berner, 1984; Raiswell and Berner, 1985). Most iron deposited in marine systems is carried by clastic sediments during continental erosion, so organosulfur compounds formed during diagenesis often occurs in non-clastic depositional environments like carbonates, siliceous oozes, and evaporites, and high-sulfur kerogens are found in basins where biologic production of reduced sulfur exceeds the input of sedimentary iron (Dinur et al., 1980).

The STACK 1 (West) organic facies is interpreted as being deposited under restricted marine conditions with limited access to upwelling nutrients and starved of terrestrial sediment because it contained lower amounts of rearranged steranes and sesquiterpanes compared to the STACK 2 (East) organic facies. Could this lead to increased sulfur incorporated into the STACK 1 (West) organic facies? To test this, a crossplot showing the weight percent sulfur and iron oxide (Fe_2O_3) from the ABCDS 1-6 core in Major County is provided in Figure 109. A line labeled "Ideal Pyrite Trend" indicates the theoretical ratio whereby iron and sulfur are balanced in the formation of pyrite (FeS_2) with none left over. The slope can be easily calculated by dividing the molecular weight of S_2 (64.2 amu) by the molecular weight of Fe_2O_3 (159.8 amu), and the resulting

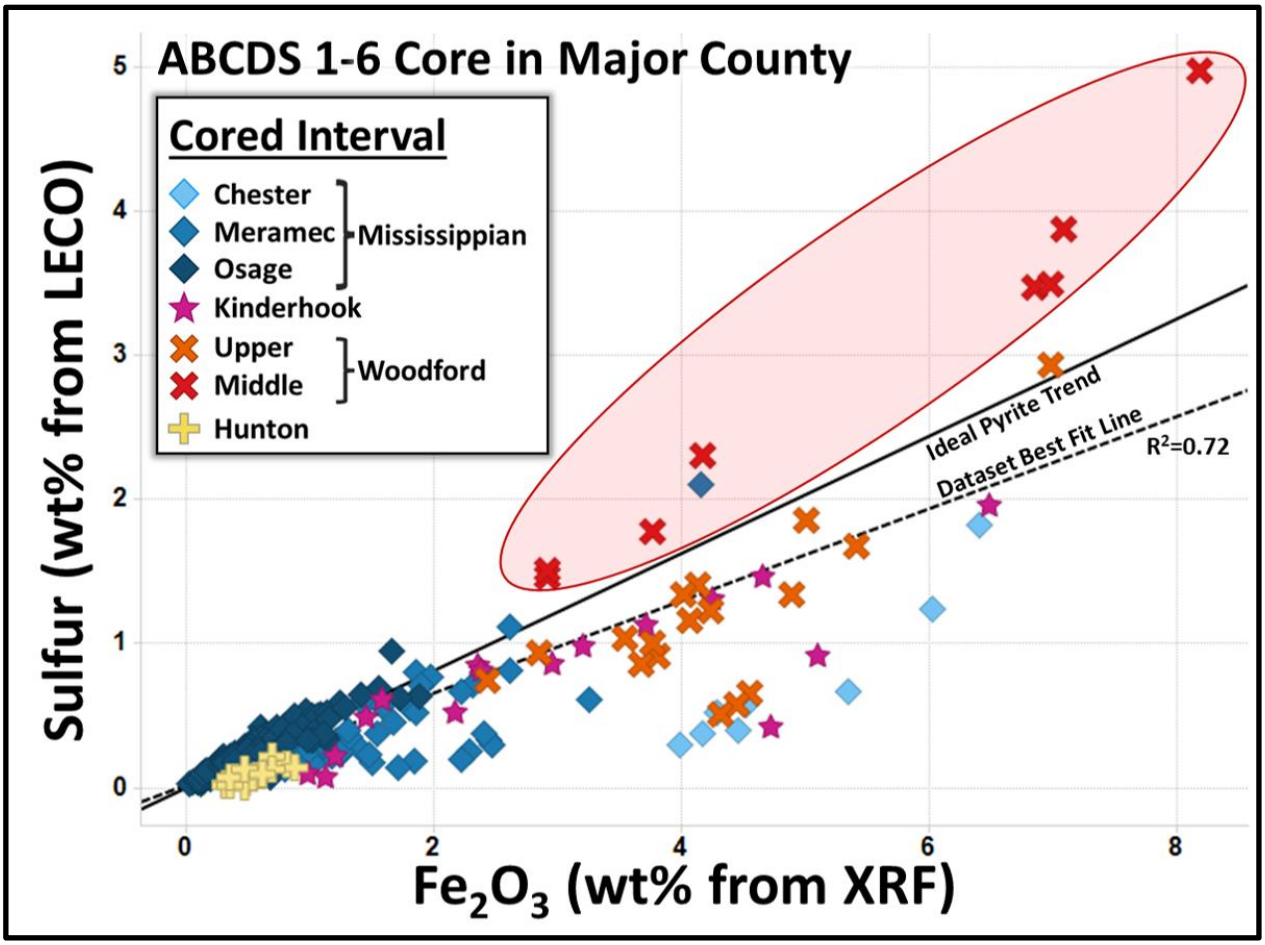

Figure 109. Crossplot of weight percent sulfur (from LECO) and Fe_2O_3 oxide (from XRF) of the ABCDS 1-6 core in Major County (map on Figure 110). The Ideal Pyrite Trend is a theoretical ratio whereby all iron and sulfur were sequestered in pyrite with none remaining. The Middle Woodford contains more sulfur than can be accounted for by pyrite mineralization based on the amount of iron in the sample. Data generated by Weatherford Labs (Table 21).

function takes the slope intercept form [S%]=0.402*[Fe_2O_3%]. Collectively, the eight Middle Woodford samples plot above the Ideal Pyrite Line by between 0.27-1.69 wt% sulfur (average 0.71%±0.47%) indicating sulfur in excess of what can be accounted for by common sulfide minerals. The Middle Woodford also contains the highest TOC values in the ABCDS 1-6 core (Table 22) having an average wt% TOC of 4.3%±0.4% (n=7) compared to the Upper Woodford containing 2.5%±1.1% (n=13). The Lower Woodford was not present. Elemental assays were not performed to determine sulfur content of the kerogen, but it is certainly possible that excess sulfur was incorporated into the organic matter of the Middle Woodford in the ABCDS 1-6 core.

Depth	Formation	Fe_2O_3[1]	Sulfur[2]	EGR[3]
7390	Chester	4.5	0.4	68.0
7392	Chester	4.0	0.3	65.5
7394.1	Chester	4.2	0.4	69.7
7396	Chester	4.3	0.5	70.4
7398	Chester	4.5	0.6	67.3
7402.3	Chester	6.0	1.2	84.2
7404	Chester	5.4	0.7	80.6
7406	Chester	6.4	1.8	83.6
7410	Meramec	1.7	0.5	53.8
7412	Meramec	3.3	0.6	81.9
7414	Meramec	1.4	0.3	49.3
7416	Meramec	2.3	0.3	58.2
7418	Meramec	2.5	0.3	57.9
7420	Meramec	2.2	0.2	58.4
7422.25	Meramec	1.8	0.2	54.4
7424	Meramec	1.7	0.1	57.6
7426.15	Meramec	2.5	0.3	65.1
7428	Meramec	1.5	0.2	53.4
7430.4	Meramec	1.1	0.2	45.9
7432	Meramec	0.8	0.1	52.4
7434	Meramec	1.1	0.3	58.5
7436	Meramec	0.9	0.2	52.2
7438.3	Meramec	0.7	0.2	49.7
7440	Meramec	0.6	0.2	35.7
7442.15	Meramec	0.9	0.2	50.5
7444	Meramec	1.3	0.3	42.7
7446.6	Meramec	0.9	0.4	53.4
7448	Meramec	0.4	0.1	47.1
7450	Meramec	0.5	0.2	64.8
7452	Meramec	0.9	0.3	41.6
7454.15	Meramec	0.4	0.1	29.2
7456	Meramec	1.2	0.2	59.3
7458	Meramec	0.8	0.2	46.3
7460	Meramec	2.4	0.4	82.6
7462	Meramec	1.2	0.2	48.5
7464	Meramec	0.9	0.2	42.1
7466.25	Meramec	4.2	2.1	65.2
7468	Meramec	1.4	0.6	47.6
7470	Meramec	1.5	0.4	55.1
7472	Meramec	0.8	0.2	42.8
7474	Meramec	1.3	0.3	47.9
7476	Meramec	1.5	0.2	57.1
7478	Meramec	0.7	0.1	55.9
7480	Meramec	0.3	0.1	28.6
7482.25	Meramec	0.7	0.2	41.4
7484	Meramec	0.2	0.1	26.7
7486	Meramec	1.0	0.2	43.3
7488	Meramec	0.9	0.2	51.3
7490	Meramec	1.9	0.8	58.8
7492	Meramec	1.8	0.6	60.9
7494.65	Meramec	1.9	0.5	57.4
7496	Meramec	1.1	0.3	46.3
7498	Meramec	1.3	0.4	44.9
7500	Meramec	1.1	0.3	41.4
7502.15	Meramec	1.0	0.3	50.6
7504	Meramec	2.3	0.7	68.2
7506.05	Meramec	2.2	0.7	69.3
7508	Meramec	2.6	0.8	76.6
7510	Meramec	2.4	0.8	77.8
7512	Meramec	1.9	0.6	76.8
7514.05	Meramec	1.3	0.4	71.9
7516	Meramec	0.8	0.2	59.5
7518	Meramec	0.8	0.3	54.8
7520	Meramec	0.8	0.4	78.7
7522.2	Meramec	0.7	0.3	46.2
7524	Meramec	0.6	0.2	43.2
7526	Meramec	1.4	0.6	50.7
7528	Meramec	1.6	0.6	52.1
7530	Meramec	2.0	0.8	54.2

Depth	Formation	Fe_2O_3[1]	Sulfur[2]	EGR[3]
7532	Meramec	2.6	1.1	62.1
7534	Meramec	1.9	0.7	56.9
7536	Meramec	0.5	0.2	134.5
7538.65	Meramec	1.1	0.4	89.8
7540	Meramec	0.6	0.2	63.8
7542.1	Meramec	1.3	0.6	94.0
7544	Osage	0.4	0.1	62.4
7546.55	Osage	0.3	0.1	29.7
7548	Osage	0.3	0.1	27.6
7550.3	Osage	0.2	0.1	25.0
7552	Osage	0.1	0.0	28.1
7554.25	Osage	0.3	0.1	40.0
7556	Osage	1.1	0.3	101.1
7558.85	Osage	0.1	0.0	26.8
7560	Osage	0.2	0.1	29.4
7562.25	Osage	0.1	0.0	23.7
7564	Osage	0.4	0.2	39.5
7566.05	Osage	0.1	0.1	23.9
7568	Osage	0.5	0.2	58.1
7570.65	Osage	0.4	0.1	40.1
7572	Osage	0.1	0.1	30.6
7574	Osage	0.3	0.2	24.9
7576	Osage	0.1	0.0	33.2
7578.15	Osage	0.7	0.1	41.7
7580	Osage	0.4	0.2	65.5
7582.25	Osage	0.2	0.1	35.8
7584	Osage	0.0	0.0	4.2
7586.6	Osage	0.4	0.2	33.5
7588	Osage	0.4	0.1	30.8
7590.15	Osage	0.5	0.2	41.4
7592	Osage	0.5	0.2	38.5
7594.15	Osage	0.2	0.1	26.6
7596	Osage	0.3	0.1	31.0
7598	Osage	0.2	0.1	27.5
7600	Osage	0.6	0.3	43.7
7602	Osage	0.3	0.2	34.8
7604	Osage	0.3	0.1	37.6
7606.8	Osage	0.3	0.1	39.5
7608	Osage	0.2	0.1	34.8
7610	Osage	0.3	0.1	37.3
7612	Osage	0.3	0.1	33.4
7614.75	Osage	0.3	0.1	40.1
7616	Osage	0.2	0.1	30.8
7618.1	Osage	0.2	0.1	28.4
7620	Osage	0.2	0.1	40.4
7622.1	Osage	0.1	0.1	29.9
7624	Osage	0.1	0.0	30.8
7626.3	Osage	0.1	0.0	33.7
7628	Osage	0.1	0.1	33.9
7630.45	Osage	0.2	0.1	29.4
7632	Osage	0.6	0.4	23.6
7634	Osage	0.1	0.0	26.7
7636	Osage	0.1	0.1	27.6
7638.55	Osage	0.3	0.1	37.4
7640	Osage	0.4	0.2	42.5
7642	Osage	0.2	0.1	27.4
7644	Osage	0.2	0.1	22.6
7646.45	Osage	0.4	0.2	28.5
7648	Osage	0.4	0.2	29.6
7650.5	Osage	0.4	0.2	28.1
7652	Osage	0.3	0.1	24.2
7654.8	Osage	0.3	0.2	24.1
7656	Osage	0.6	0.2	34.2
7658.35	Osage	0.4	0.1	26.2
7660	Osage	0.4	0.2	27.3
7662.05	Osage	0.4	0.2	30.3
7664	Osage	0.4	0.1	31.1
7666.15	Osage	0.6	0.2	36.9
7668	Osage	1.6	0.7	73.3

Depth	Formation	Fe_2O_3[1]	Sulfur[2]	EGR[3]
7670.15	Osage	0.6	0.2	37.6
7672	Osage	0.5	0.2	30.4
7674.95	Osage	0.6	0.3	36.7
7676	Osage	0.4	0.1	29.3
7678.4	Osage	0.4	0.2	28.7
7680	Osage	0.5	0.2	33.9
7682.5	Osage	0.4	0.2	28.3
7684	Osage	1.0	0.4	46.2
7686.45	Osage	0.5	0.2	25.8
7688	Osage	1.4	0.6	60.6
7690.7	Osage	0.5	0.2	28.9
7692	Osage	0.9	0.4	39.2
7694	Osage	0.7	0.3	37.1
7696	Osage	0.6	0.3	35.8
7698.8	Osage	0.5	0.3	28.3
7700	Osage	0.5	0.2	26.2
7702	Osage	0.4	0.1	26.2
7704	Osage	0.5	0.2	32.6
7706.1	Osage	0.4	0.2	28.7
7708	Osage	0.5	0.2	27.6
7710.2	Osage	1.1	0.5	45.3
7712	Osage	0.5	0.2	32.4
7714.2	Osage	0.7	0.3	43.6
7716	Osage	0.4	0.2	40.5
7718.05	Osage	0.3	0.1	32.8
7720	Osage	0.1	0.1	29.9
7722.9	Osage	0.1	0.1	5.7
7724	Osage	0.1	0.1	32.0
7726	Osage	0.4	0.2	51.1
7728	Osage	0.6	0.3	62.3
7730.1	Osage	0.3	0.1	42.3
7732	Osage	0.2	0.1	30.9
7734.35	Osage	0.1	0.1	24.1
7736	Osage	0.3	0.2	26.0
7738.5	Osage	0.1	0.1	32.3
7740	Osage	0.3	0.1	52.7
7742.25	Osage	0.1	0.0	24.9
7744	Osage	0.4	0.2	53.6
7746.3	Osage	0.2	0.1	41.3
7748	Osage	0.1	0.1	29.9
7750.8	Osage	0.1	0.1	26.2
7752	Osage	0.8	0.4	86.2
7754.1	Osage	0.1	0.1	22.6
7756	Osage	0.2	0.1	26.6
7758.55	Osage	0.1	0.1	22.5
7760	Osage	0.2	0.1	26.6
7762	Osage	0.1	0.1	26.0
7764	Osage	0.1	0.1	22.9
7766.3	Osage	0.2	0.1	29.0
7768	Osage	0.3	0.2	37.6
7770.05	Osage	1.0	0.5	50.7
7772	Osage	0.4	0.2	28.3
7774.15	Osage	0.3	0.1	26.0
7776	Osage	0.3	0.2	30.5
7778.5	Osage	0.2	0.1	24.2
7780	Osage	0.4	0.2	27.8
7782.1	Osage	0.3	0.2	21.7
7851.5	Osage	0.1	0.1	26.1
7853.15	Osage	0.2	0.1	31.5
7855.5	Osage	0.5	0.3	40.9
7857.5	Osage	0.7	0.4	45.4
7859.5	Osage	0.5	0.3	41.7
7861.15	Osage	0.5	0.3	39.5
7863.5	Osage	0.6	0.3	40.2
7865.5	Osage	0.5	0.3	36.8
7867.5	Osage	0.9	0.5	44.3
7869.35	Osage	0.4	0.2	31.9
7871.5	Osage	1.7	0.9	67.1
7873.05	Osage	0.4	0.2	31.6

Depth	Formation	Fe_2O_3[1]	Sulfur[2]	EGR[3]
7875.5	Osage	0.7	0.4	36.4
7877.3	Osage	0.3	0.2	26.4
7879.5	Osage	0.4	0.2	28.3
7881.3	Osage	0.4	0.2	25.4
7883.5	Osage	0.4	0.2	26.9
7885.3	Osage	0.3	0.2	24.6
7887.5	Osage	0.3	0.2	25.0
7889.55	Osage	0.3	0.2	23.8
7891.5	Osage	0.4	0.2	27.6
7893.2	Osage	0.3	0.2	26.0
7895.5	Osage	0.6	0.3	34.4
7897.75	Osage	0.2	0.1	24.0
7899.5	Osage	0.6	0.3	33.9
7901.75	Osage	0.5	0.3	34.8
7903.5	Osage	0.7	0.4	35.1
7905.7	Osage	0.3	0.2	25.8
7907.5	Osage	0.7	0.4	34.0
7909.2	Osage	0.4	0.2	27.9
7911.5	Osage	0.3	0.2	25.8
7913.7	Osage	0.6	0.3	36.1
7915.5	Osage	0.7	0.4	35.4
7917.65	Osage	0.3	0.2	26.6
7919.5	Osage	0.5	0.3	30.7
7921.75	Osage	0.3	0.2	29.2
7923.5	Osage	0.4	0.2	27.1
7925.85	Osage	0.4	0.2	27.7
7927.5	Osage	0.5	0.3	29.6
7929.65	Osage	0.4	0.2	27.8
7931.5	Osage	0.6	0.3	30.8
7933.5	Osage	0.5	0.3	30.8
7935.5	Osage	0.5	0.3	30.0
7937.7	Osage	0.5	0.2	30.3
7939.5	Osage	0.4	0.2	27.7
7941.65	Osage	0.5	0.3	31.8
7943.52	Osage	0.6	0.3	37.0
7945.7	Osage	0.5	0.3	31.5
7947.5	Osage	0.4	0.2	27.6
7949.75	Osage	0.3	0.2	27.2
7951.5	Osage	0.3	0.1	32.7
7953.55	Osage	0.3	0.2	27.9
7955.5	Osage	0.5	0.2	39.1
7957.85	Osage	1.1	0.4	69.1
7959.5	Osage	1.9	0.6	107.2
7961.45	Osage	0.4	0.2	31.0
7963.5	Osage	0.5	0.3	27.3
7965.3	Osage	0.4	0.2	29.2
7967.5	Osage	0.3	0.2	28.2
7969.6	Osage	0.8	0.4	34.4
7971.5	Osage	0.7	0.3	34.2
7973.5	Osage	0.5	0.3	42.5
7975.5	Osage	0.3	0.2	27.3
7977.5	Osage	0.5	0.3	34.5
7979.5	Osage	1.0	0.5	45.1
7981.65	Osage	0.4	0.2	27.2
7983.5	Osage	0.6	0.3	28.9
7985.55	Osage	1.1	0.5	46.2
7987.5	Osage	1.2	0.6	46.5
7989.5	Osage	0.5	0.2	26.9
7991.5	Osage	0.8	0.4	32.0
7993.45	Osage	0.4	0.2	28.3
7995.5	Osage	0.6	0.3	33.5
7997.5	Osage	0.4	0.2	32.8
7999.5	Osage	1.0	0.4	47.0
8001.55	Osage	0.4	0.2	28.1
8003.5	Osage	0.8	0.3	37.4
8005.35	Osage	0.6	0.3	29.7
8007.5	Osage	1.1	0.5	35.7
8009.5	Osage	0.5	0.3	27.5
8011.5	Osage	0.9	0.4	40.9

Depth	Formation	Fe_2O_3[1]	Sulfur[2]	EGR[3]
8013.5	Osage	1.0	0.4	40.8
8015.5	Osage	1.3	0.6	43.5
8017.15	Osage	0.9	0.4	41.2
8019.5	Osage	0.5	0.2	30.5
8021.5	Osage	0.4	0.2	28.3
8023.5	Osage	1.2	0.5	41.3
8025.55	Osage	0.6	0.2	28.6
8027.5	Osage	0.7	0.2	30.7
8029.55	Osage	1.0	0.3	33.4
8031.5	Osage	1.1	0.4	34.0
8033.45	Osage	1.7	0.6	46.7
8035.5	Osage	0.8	0.3	32.2
8037.5	Osage	1.0	0.3	32.5
8039.5	Kinderhook	1.6	0.6	39.3
8041.4	Kinderhook	2.4	0.9	47.8
8043.5	Kinderhook	2.4	0.8	50.9
8045.55	Kinderhook	3.2	1.0	63.2
8047.5	Kinderhook	3.0	0.9	57.3
8049.4	Kinderhook	3.7	1.1	68.4
8051.5	Kinderhook	4.3	1.3	68.3
8053.5	Kinderhook	4.7	1.5	77.9
8055.5	Kinderhook	5.1	0.9	91.5
8057.5	Kinderhook	6.5	2.0	86.4
8059.5	Kinderhook	4.7	0.4	83.8
8061.5	Kinderhook	1.2	0.2	34.3
8063.5	Kinderhook	2.2	0.5	45.7
8065.7	Kinderhook	1.5	0.5	25.9
8067.5	Kinderhook	1.0	0.1	25.4
8069.35	Kinderhook	1.1	0.1	27.4
8071.5	Upper Woodford	5.4	1.7	232.0
8073.4	Upper Woodford	4.9	1.3	285.3
8075.5	Upper Woodford	4.6	0.7	104.5
8077.5	Upper Woodford	4.4	0.6	88.1
8079.55	Upper Woodford	4.3	0.5	106.5
8081.4	Upper Woodford	7.0	2.9	103.6
8083.5	Upper Woodford	4.2	1.2	176.8
8085.3	Upper Woodford	4.1	1.2	170.0
8087.5	Upper Woodford	3.8	0.9	157.0
8089.55	Upper Woodford	3.7	0.9	133.0
8091.5	Upper Woodford	3.8	1.0	211.1
8093.4	Upper Woodford	5.0	1.9	135.2
8097.75	Upper Woodford	2.4	0.8	104.8
8099.5	Upper Woodford	3.5	1.0	232.3
8101.3	Upper Woodford	4.1	1.4	92.5
8103.5	Upper Woodford	4.0	1.3	93.3
8105.5	Upper Woodford	2.9	0.9	213.6
8107.5	Middle Woodford	3.8	1.8	351.7
8109.4	Middle Woodford	2.9	1.5	262.1
8111.5	Middle Woodford	2.9	1.5	264.1
8113.5	Middle Woodford	4.2	2.3	391.1
8117.4	Middle Woodford	8.2	5.0	269.9
8119.5	Middle Woodford	7.1	3.9	286.2
8121.45	Middle Woodford	6.9	3.5	333.6
8123.5	Middle Woodford	7.0	3.5	372.0
8125.5	Hunton	0.3	0.0	28.9
8127.5	Hunton	0.4	0.1	30.5
8129.6	Hunton	0.3	0.0	28.5
8131.5	Hunton	0.5	0.0	25.4
8133.85	Hunton	0.5	0.0	25.3
8135.5	Hunton	0.4	0.0	28.6
8137.85	Hunton	0.6	0.1	28.6
8139.5	Hunton	0.5	0.1	30.2
8141.65	Hunton	0.8	0.2	42.9
8143.5	Hunton	0.9	0.1	44.0
8145.5	Hunton	0.6	0.1	32.3
8147.5	Hunton	0.4	0.1	27.1
8149.5	Hunton	0.5	0.1	35.2
8151.5	Hunton	0.7	0.2	38.9
8153.5	Hunton	0.7	0.1	34.4
8155.5	Hunton	0.6	0.1	34.5

Table 21. Elemental data from the ABCDS 1-6 core in Major County by core depth and formation. Data was generated by Weatherford Labs. (1) Weight percent of Fe_2O_3 as measured by x-ray fluorescence. (2) Weight percent elemental sulfur as measured by LECO analysis. (3) Estimated Gamma Ray (EGR) measured from elemental composition of uranium, thorium, and potassium in the sample.

Core Depth	Formation	TOC
8071.5	Upper Woodford	2.8
8075.5	Upper Woodford	0.9
8077.5	Upper Woodford	0.5
8079.55	Upper Woodford	0.5
8083.5	Upper Woodford	2.3
8085.3	Upper Woodford	1.9
8087.5	Upper Woodford	2.1
8091.5	Upper Woodford	2.8
8093.4	Upper Woodford	2.3
8095.5	Upper Woodford	7.6
8099.5	Upper Woodford	5.3
8101.3	Upper Woodford	2.1
8103.5	Upper Woodford	1.3
8107.5	Middle Woodford	4.0
8109.4	Middle Woodford	4.0
8111.5	Middle Woodford	5.2
8115.5	Middle Woodford	4.8
8117.4	Middle Woodford	4.0
8119.5	Middle Woodford	4.2
8123.5	Middle Woodford	4.0

Table 22. Total organic carbon (TOC) data from the ABCDS 1-6 core in Major County by core depth and formation. TOC data was generated from LECO by Weatherford Labs.

Another key observation is that at least sixteen deep wells drilled in STACK West have encountered H_2S with fourteen containing critically high concentrations above 20 ppm (Eucker and Ashby, 2020), and H_2S has even been measured as high as 900 ppm in some wells (Tapstone, personal communication). A map of townships with at least one incident of H_2S gas is provided in Figure 110. Most incidences occurred in wells producing from the volatile oil and wet gas window (1.0-1.3 Ro%) near the flower-shaped zone in the Woodward, Dewey, Ellis tricounty region with the shallowest occurring at 9,242 ft. Cracking sulfur compounds in high sulfur petroleum can form small amounts of H_2S gas (Le Tran et al., 1974; Orr, 1977; Machel et al., 1995), but STACK 1 (West) oils consistently contain low sulfur <0.2 wt% (Tapstone, personal communication), and therefore cracking organosulfur compounds is unlikely to source the H_2S gas in STACK West.

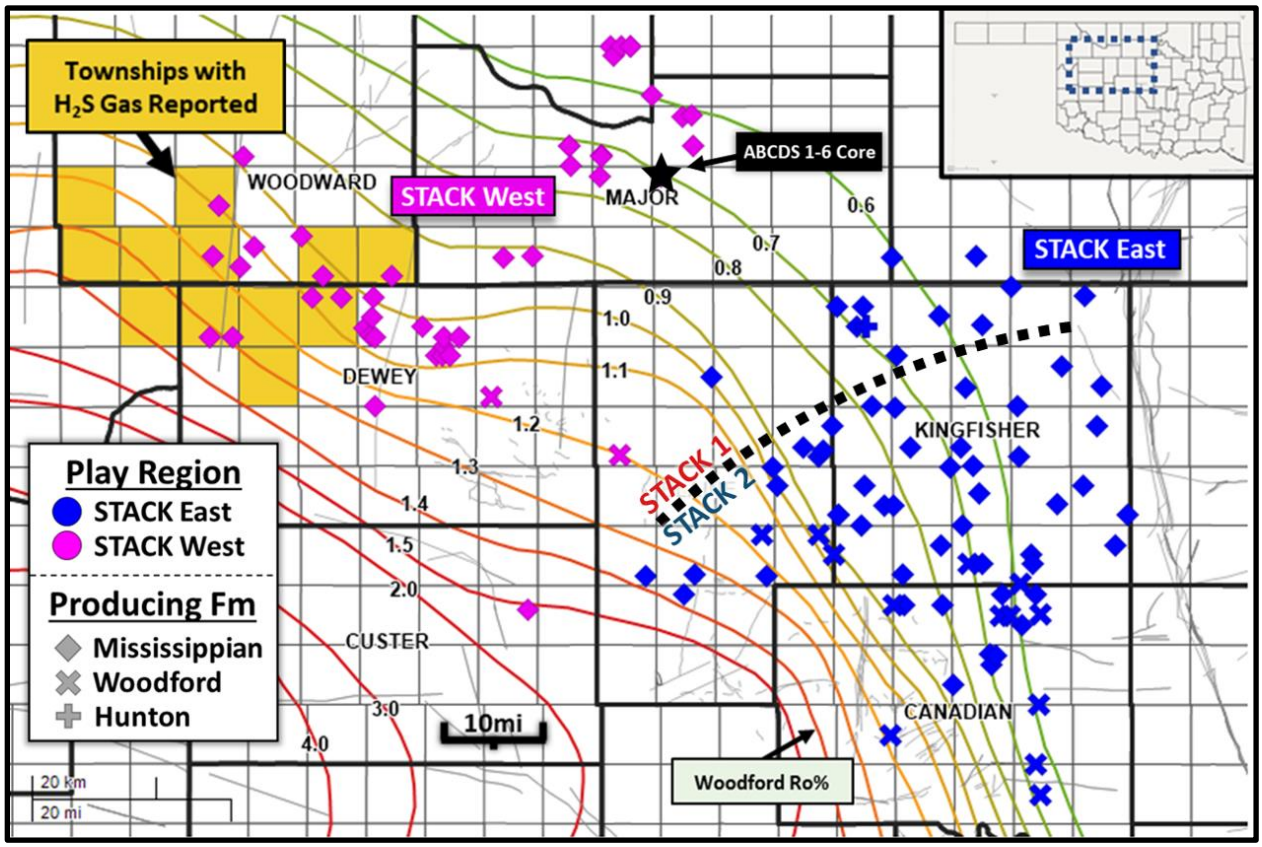

Figure 110. Map of STACK showing townships with reported incidents of H_2S gas. Most incidences occurred in deep wells producing from the volatile oil and wet gas window (1.0-1.3 Ro%) in the Woodward, Dewey, Ellis tricounty region with the shallowest instance occurring at 9,242 ft.

Hypothesis 2: Bacterial Sulfate Reduction Reactions

Most H_2S gas is formed by the reduction of inorganic sulfate by either bacterial respiration or thermochemical reactions occurring in two mutually exclusive thermal regimes, illustrated in Figure 111. Bacterial sulfate reduction (BSR) is a process of dissimilatory sulfate reduction at low-temperatures (<80°C) by anaerobic microbial respiration utilizing dissolved sulfate and hydrocarbons as electron acceptors and donors, respectively (Davis and Yarbrough, 1966). Initiating BSR requires a viable population of sulfate reducing bacteria which are highly sensitive to formation water salinity, organic substrate, reservoir temperature, and even the concentration of H_2S which is toxic to sulfate reducing bacteria in high concentrations necessitating its removal from sites of active sulfate reduction for BSR to continue (Orr, 1977). Moreover, BSR ceases above 60-80°C, which corresponds to a vitrinite reflectance values of about 0.6 and depths of less than 6,000 ft in normal geothermal gradients (Machel, 2001). Based on these factors, H_2S gas production in STACK West occurs at higher temperatures and in amounts in excess of what is expected from BSR and is not considered a viable source of the H_2S observed in STACK West.

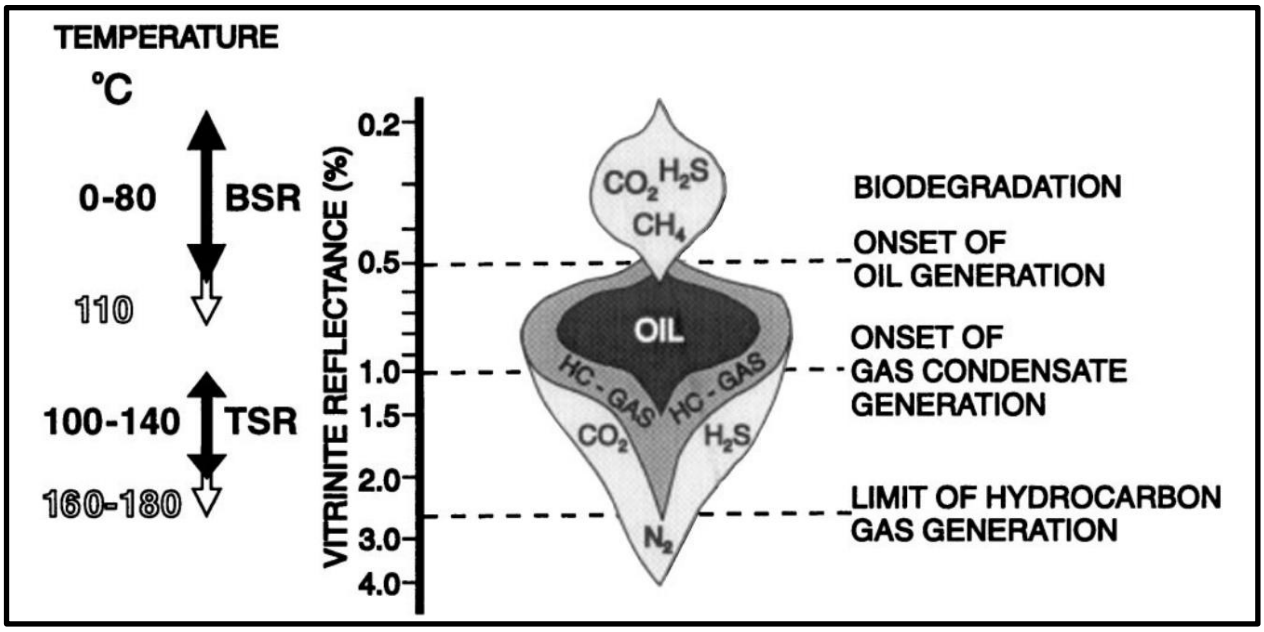

Figure 111. Kerogen generation products with increasing maturation. Small amounts of H_2S gas can be formed by BSR at low maturities (<0.5 Ro%). Most H_2S is formed by TSR between 1.0 and 2.0 Ro%. From (Machel, 2001).

Hypothesis 3: Thermochemical Sulfate Reduction Reactions

Above the BSR temperature threshold, sulfur can be incorporated into organic matter in contact with sedimentary anhydrite or gypsum by a process called thermochemical sulfate reduction (TSR). The temperature required for the onset of TSR is controversial, but most studies have suggested that TSR minimum temperatures range between 100-140°C depending on the hydrocarbons present in the reservoir, corresponding to 1.0-2.0 Ro%, with higher temperatures (between 160-180°C) required to initiate TSR for methane (Krouse et al., 1988; Goldhaber and Orr, 1995; Machel et al., 1995; Worden et al., 1995; Machel, 2001). A simplified TSR net reaction scheme is provided in Equation 13 (Orr, 1974):

$$SO_4^{2-} + 3\ H_2S \leftrightarrow 4\ S^0 + 2\ H_2O + 2\ OH^- \quad (1)$$
$$4\ S^0 + 1.33\ (CH_2) + 2.66\ H_2O \rightarrow 4\ H_2S + 1.33\ CO_2 \quad (2)$$
$$SO_4^{2-} + 1.33\ (CH_2) + 0.66\ H_2O \rightarrow H_2S + 1.33\ CO_2 + 2\ OH^- \quad (3)$$

Equation 13

In the above equation, H_2S is both a reactant and product and must be present at the onset of TSR to form intermediate oxidation state sulfur species like polysulfides, thiosulfates, or elemental sulfur. The intermediate reduced sulfur species (S^o) can then react with hydrocarbons to form organic acids which in turn may undergo decarboxylation reactions to yield H_2S and CO_2 (Toland et al., 1958; Toland, 1960; Orr, 1977; Goldhaber and Orr, 1995; Zhang et al., 2008). Intermediate sulfur species can also facilitate other reactions such as dehydrogenation (oxidation) or even become incorporated into the formation of new organosulfur compounds. The formation of S^o species, therefore, offers a mechanism for the conversion of saturate hydrocarbons to naphthenic acids, aromatic hydrocarbons, and inorganic and organic sulfur compounds. High concentrations of H_2S gas in some deep STACK West wells all but confirms the influence of TSR in the deep basin. Additional circumstantial evidence that supports this hypothesis is discussed below.

First, Mango (1987 and 1990b) argues light hydrocarbon speciation is controlled by steady-state isomerization involving metal catalysts which control preferential ring openings of cyclopropane intermediaries to form isoheptanes. The value K_1, defined as the area sum ratio of 2-MH and 2,3-DMP over 3-MH and 2,4-DMP, remains proportional such that the value $K_1 \cong 1$. Contaminants like H_2S, even at low levels, can substantially reduce the level of catalytic activity in a source rock from transition metals (Mango, 1992). As a result, TSR-affected oils have been observed to have higher values of K_1 and plot above the line $K_1 \cong 1$ (ten Haven, 1996; Peters and Fowler, 2002). The plot expressing K_1 for all Woodford-sourced organofacies shows that STACK 1 organofacies oils generally plot above $K_1=1$ while STACK 2 and SCOOP 1 organofacies oils plot almost exclusively below $K_1=1$ except some of the highest maturity samples (Figure 112). However, there are more oils generated from the STACK 1 organofacies which plot above $K_1=1$ than are produced from the known areas of H_2S production, so higher K_1 values may be related to depositional/diagenetic conditions associated with TSR but not TSR reactions directly.

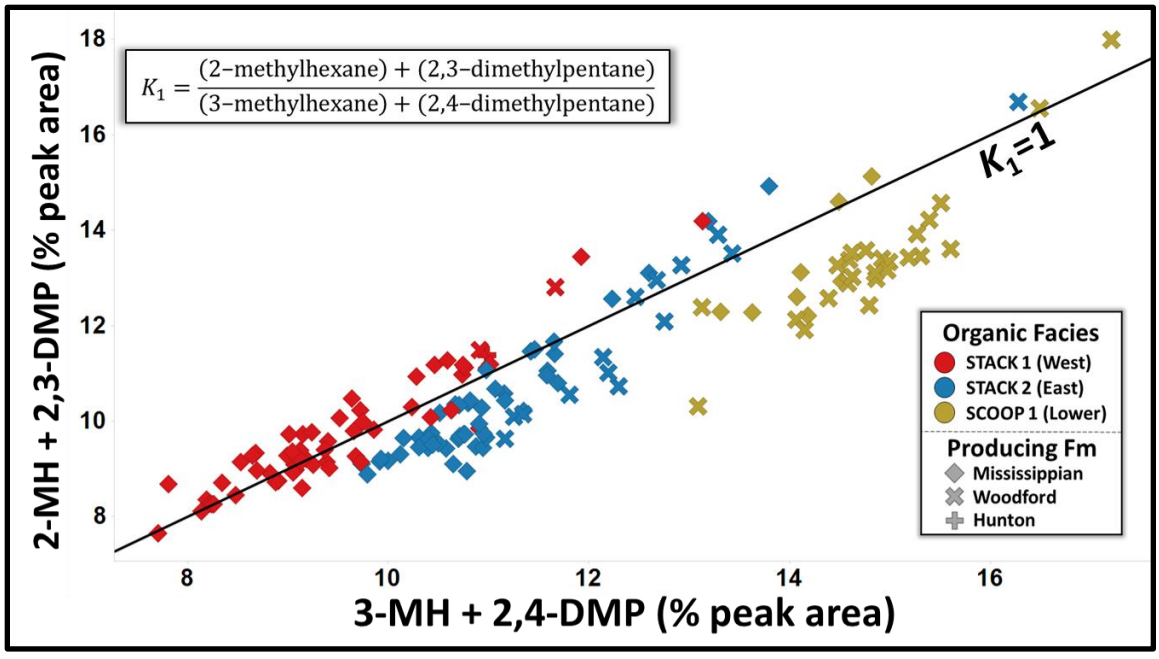

Figure 112. Mango K_1 plot for oils sourced from each Woodford organofacies (after Figure 56). STACK 1 (West) oils consistently plot above unity which is characteristic in TSR-affected oils (ten Haven, 1996; Peters and Fowler, 2002).

Second, several oils near the reported incidences of H_2S gas and the flower-shaped zone (see Figure 20) have anomalously high values for DBT/P. During maturation, the ratio DBT/P is expected to decrease because the rate decline exponent of DBT (-3.41) in the numerator is larger than phenanthrene (-1.76) in the denominator (see Figure 50). However, TSR can greatly increase the ratio DBT/P in oils because aromatic sulfur compounds (i.e. DBT) are formed alongside H_2S during sulfate reduction (Equation 13). A cross plot of DBT and phenanthrene concentration in log-log space shows a linear main trend corresponding to oils with similar DBT/P ratios at different stages of maturity (Figure 113). Several oils (marked red) contain DBT concentrations far in excess of what is expected from similarly sourced oils, even within samples sourced from the same STACK 1 (West) organofacies. The highlighted oils may contain significantly elevated DBT as the result post-generative TSR reactions.

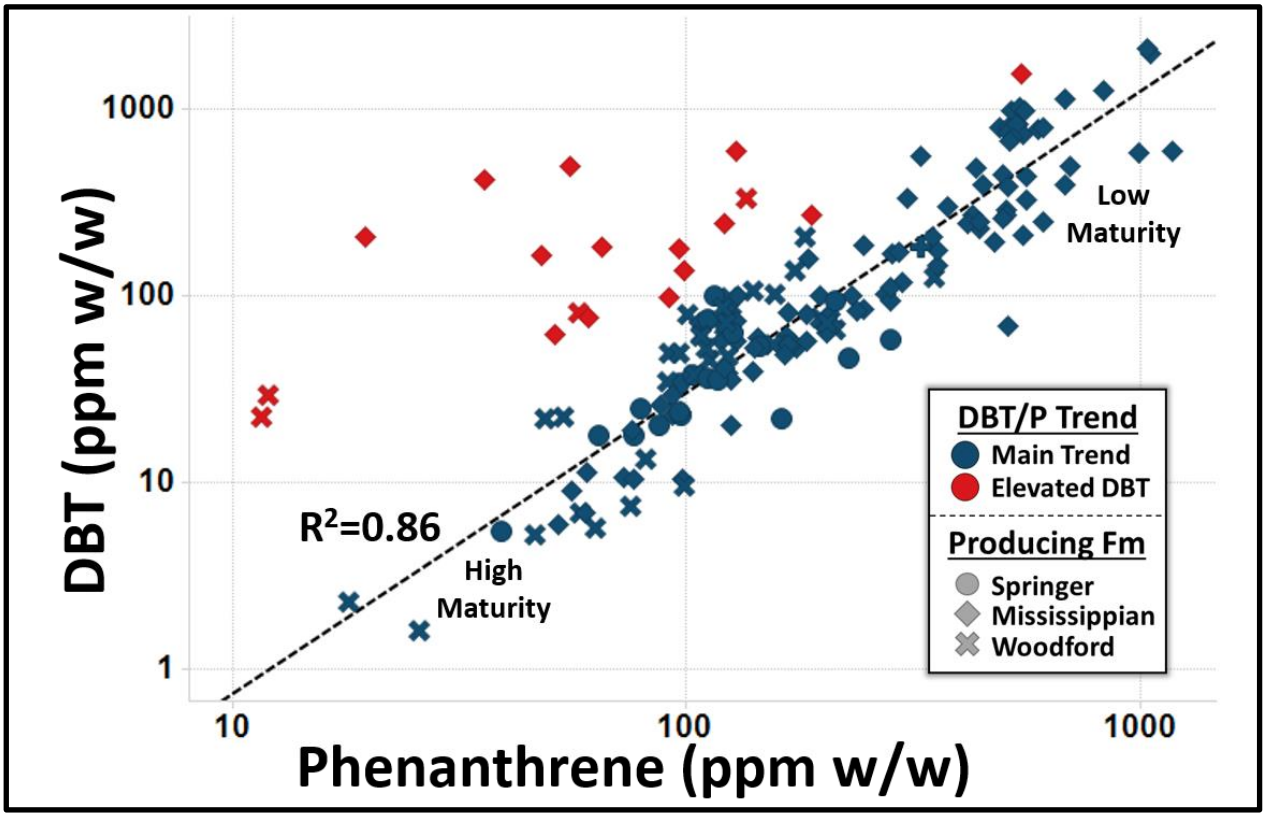

Figure 113. Log-log plot of DBT and phenanthrene concentration (see Table 10). Most samples follow the main trend corresponding to changing DBT/P values with maturity. Samples which deviate from this trend are highlighted red.

Third, the oils produced in the heavily faulted area associated with H_2S and the flower-shaped zone in STACK West show evidence of mixing with high maturity condensates which could have entrained H_2S formed deeper in the basin. Dahl et al. (1999) observed that the concentration of thermally resistant methyldiamantanes (MDA; **XV**) are only found enriched in highly mature oils that have undergone severe thermal cracking where most biomarkers are absent. Using the concentration of the C_{29} 5α(H),14α(H),17α(H),20R sterane as a reference for the degree of cracking, Dahl et al. (1999) argues that an oil which contains both abundant steranes and MDA isomers must therefore be a mixture of highly-mature cracked oils with low-maturity uncracked oils. Figure 114 below shows example low- and high-maturity unmixed oils, and a potentially mixed oil which contains both. MDA and C_{29} sterane data for all oils in Table 23.

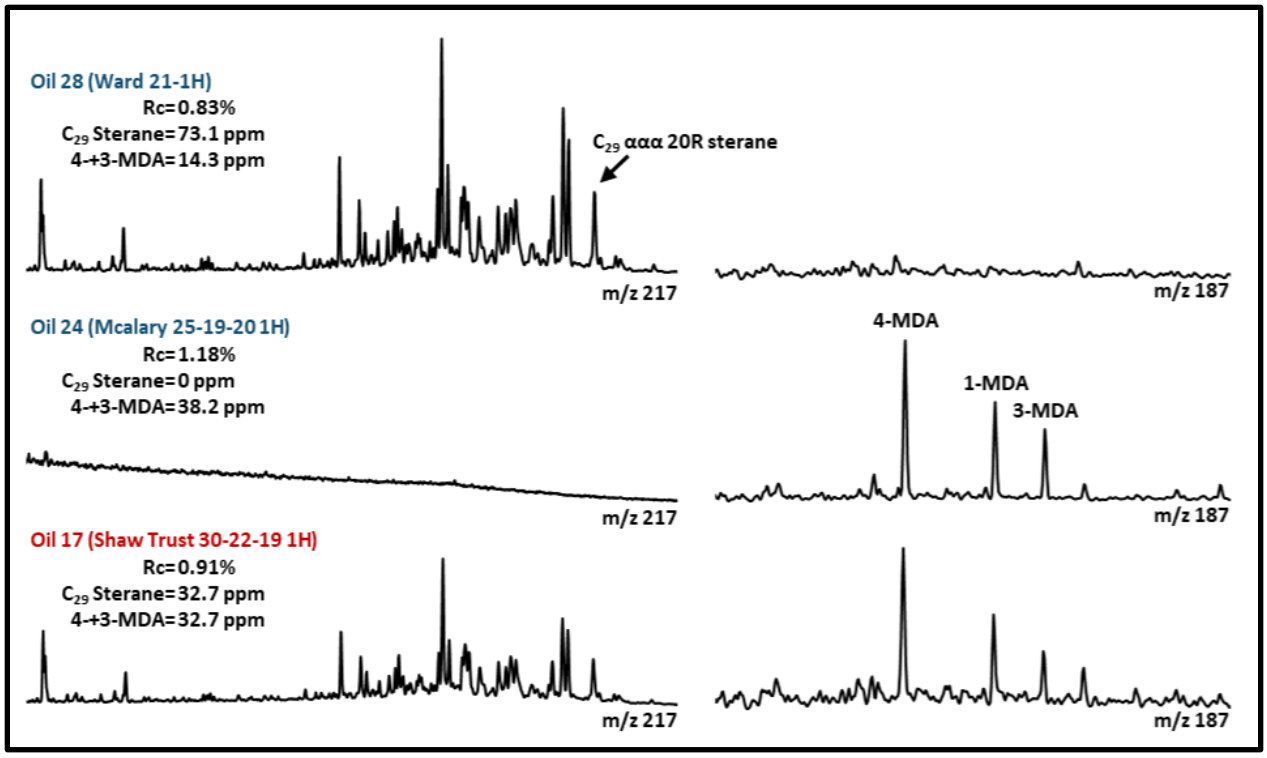

Figure 114. Partial fragmentograms monitoring the C_{29} 5α(H),14α(H),17α(H),20R sterane in m/z 217 and the 4-, 1-, and 3-methyldiamantanes (x-MDA) in m/z 187 which are abundant in oils in mutually exclusive maturity ranges. In unmixed oils (blue), the low-maturity oil (Ward 21-1H) contains abundant steranes but low methyldiamantanes, and the high-maturity cracked oil (Mcalary 25-19-20 1H) contains abundant methyldiamantanes and no steranes. The mixed oil (Shaw Trust 30-22-19 1H) contains abundant steranes and methyldiamantanes indicating a likely mixture of low- and high-maturity oils. Methyldiamantane picks based off comparison to Grice et al. (2000).

Key	Play	C_{29} Sterane	4-+3-MDA
1	STACK West	104.7	13.8
2	STACK West	109.1	14.7
3	STACK West	106.5	14.3
4	STACK West	93.8	14.2
5	STACK West	110.8	13.4
6	STACK West	50.0	11.3
7	STACK West	79.4	14.5
8	STACK West	64.3	10.6
9	STACK West	59.5	13.0
10	STACK West	61.1	12.7
11	STACK West	101.8	16.2
12	STACK West	91.8	15.6
13	STACK West	85.1	15.5
14	STACK West	88.3	15.1
15	STACK West	50.7	13.2
16	STACK West	86.0	13.1
17	STACK West	32.7	32.7
18	STACK West	10.1	30.7
19	STACK West	12.2	35.2
20	STACK West	4.7	16.5
21	STACK West	0.9	24.7
22	STACK West	1.0	19.3
23	STACK West	0.0	66.0
24	STACK West	0.0	38.2
25	STACK West	2.7	32.9
26	STACK West	8.9	27.5
27	STACK West	44.8	20.6
28	STACK West	73.1	14.3
29	STACK West	91.2	16.1
30	STACK West	15.6	24.8
31	STACK West	10.2	11.5
32	STACK West	21.7	13.8
33	STACK West	2.8	19.7
34	STACK West	5.9	8.6
35	STACK West	1.5	91.7
36	STACK West	0.0	101.1
37	STACK West	12.0	16.1
38	STACK West	7.8	27.7
39	STACK West	3.3	13.4
40	STACK West	5.9	22.0
41	STACK West	0.5	22.1
42	STACK West	1.0	15.7
43	STACK West	4.6	16.3
44	STACK West	5.4	139.5
45	STACK West	0.0	176.0
46	STACK West	0	22.2
47	STACK East	0.0	35.6
48	STACK East	0.0	17.1
49	STACK East	0.0	16.6
50	STACK East	8.1	13.3
51	STACK East	0.6	9.7
52	STACK East	0.0	11.8

Key	Play	C_{29} Sterane	4-+3-MDA
53	STACK East	2.7	6.2
54	STACK East	3.3	7.5
55	STACK East	4.7	6.9
56	STACK East	1.5	29.1
57	STACK East	2.7	5.7
58	STACK East	4.3	6.3
59	STACK East	7.3	8.1
60	STACK East	0.0	4.6
61	STACK East	26.5	8.9
62	STACK East	1.1	5.3
63	STACK East	1.1	6.8
64	STACK East	25.2	10.7
65	STACK East	2.2	5.9
66	STACK East	21.4	8.5
67	STACK East	3.2	5.6
68	STACK East	21.4	7.5
69	STACK East	20.7	7.6
70	STACK East	4.6	7.0
71	STACK East	0.0	30.9
72	STACK East	16.5	9.2
73	STACK East	0.0	6.1
74	STACK East	6.5	8.2
75	STACK East	27.3	8.7
76	STACK East	34.4	9.6
77	STACK East	1.1	5.9
78	STACK East	1.3	6.3
79	STACK East	8.5	6.9
80	STACK East	26.0	8.6
81	STACK East	7.2	6.1
82	STACK East	3.9	5.4
83	STACK East	13.5	7.9
84	STACK East	0.7	5.6
85	STACK East	7.9	7.5
86	STACK East	10.3	5.6
87	STACK East	29.8	5.6
88	STACK East	11.4	7.4
89	STACK East	15.6	7.8
90	STACK East	73.4	14.9
91	STACK East	17.9	8.1
92	STACK East	9.1	6.6
93	STACK East	59.5	11.5
94	STACK East	6.0	5.4
95	STACK East	4.7	6.3
96	STACK East	9.2	5.1
97	STACK East	9.6	6.8
98	STACK East	7.1	5.9
99	STACK East	8.0	6.3
100	STACK East	63.6	14.1
101	STACK East	56.2	13.2
102	STACK East	26.1	8.2
103	STACK East	14.8	7.1
104	STACK East	8.7	7.7

Key	Play	C_{29} Sterane	4-+3-MDA
105	STACK East	17.6	7.1
106	STACK East	18.0	7.0
107	STACK East	18.1	7.1
108	STACK East	6.9	7.6
109	STACK East	7.4	6.7
110	STACK East	5.2	7.3
111	STACK East	12.6	7.4
112	STACK East	30.3	10.0
113	STACK East	53.4	6.9
114	STACK East	44.2	9.3
115	STACK East	39.0	10.5
116	STACK East	38.2	11.9
117	STACK East	33.2	9.4
118	STACK East	53.9	8.9
119	STACK East	44.0	10.9
120	SCOOP	8.0	7.7
121	SCOOP	0.0	18.5
122.	SCOOP	0.0	12.4
123	SCOOP	0.0	11.2
124	SCOOP	4.8	8.3
125	SCOOP	2.1	4.2
126	SCOOP	2.5	6.5
127	SCOOP	2.4	6.1
128	SCOOP	1.3	6.2
129	SCOOP	1.9	5.5
130	SCOOP	1.6	6.4
131	SCOOP	1.3	5.2
132	SCOOP	2.0	6.2
133	SCOOP	1.9	5.7
134	SCOOP	0.6	6.1
135	SCOOP	2.1	7.9
136	SCOOP	2.0	6.9
137	SCOOP	2.2	5.6
138	SCOOP	0.9	6.1

Key	Play	C_{29} Sterane	4-+3-MDA
139	SCOOP	0.6	4.3
140	SCOOP	0.5	3.8
141	SCOOP	1.2	7.6
142	SCOOP	1.3	5.4
143	SCOOP	0.7	5.8
144	SCOOP	2.8	9.8
145	SCOOP	2.6	7.1
146	SCOOP	2.4	7.3
147	SCOOP	2.2	7.3
148	SCOOP	1.6	8.5
149	SCOOP	5.2	7.7
150	SCOOP	0.0	7.0
151	SCOOP	1.8	6.0
152	SCOOP	4.0	5.4
153	SCOOP	0.7	6.5
154	SCOOP	7.7	7.0
155	SCOOP	34.2	3.7
156	SCOOP	2.2	3.7
157	SCOOP	0.4	14.1
158	SCOOP	0.0	14.4
159	SCOOP	8.0	6.8
160	SCOOP	1.2	4.4
161	SCOOP	1.2	6.2
162	SCOOP	0.9	6.4
163	SCOOP	0.0	44.3
164	SCOOP	0.0	8.2
165	SCOOP	0.8	4.0
166	SCOOP	1.2	4.0
167	SCOOP	0.0	7.1
168	SCOOP	2.0	4.4
169	SCOOP	38.1	8.5
170	SCOOP	1.2	3.3
171	SCOOP	5.7	3.9
172	SCOOP	0.5	8.8

Table 23. Concentration in ppm of the C_{29} 5α(H),14α(H),17α(H),20R sterane and the sum of 4- and 3-methyldiamantae (MDA) isomers in all sample oils. Relative response factor of 0.27 was used to calculate absolute concentration methyldiamantanes from the deuterated sterane internal standard (see Figure 17).

The Dahl crossplot of C_{29} ααα 20R sterane versus the sum of 4- and 3-MDA shows several oils (marked in red) in the zone indicating a mixture of mature cracked oils with low-maturity uncracked oils (Figure 115). Two maps in Figure 116 show that the zone of oil mixing and the zone of high DBT oils (see Figure 113) both occur in a thin northwest-southeast trending corridor in Woodward, Dewey, and Blaine counties near occurrences of H_2S gas. The minimum temperature required to initiate TSR is between 100-140°C, equivalent to 1.0-2.0 Ro%, but the H_2S in STACK West has only been reported in a thin band of townships containing Woodford Shale between 0.9-1.3 Ro% near the minimum required temperature to initiate TSR. It is very possible that TSR could occur at hotter temperatures deeper in the basin and DBT rich oils could migrate updip along major faults mapped in Dewey County and be associated with production in the brittle Osage carbonates and the flower-shaped zone.

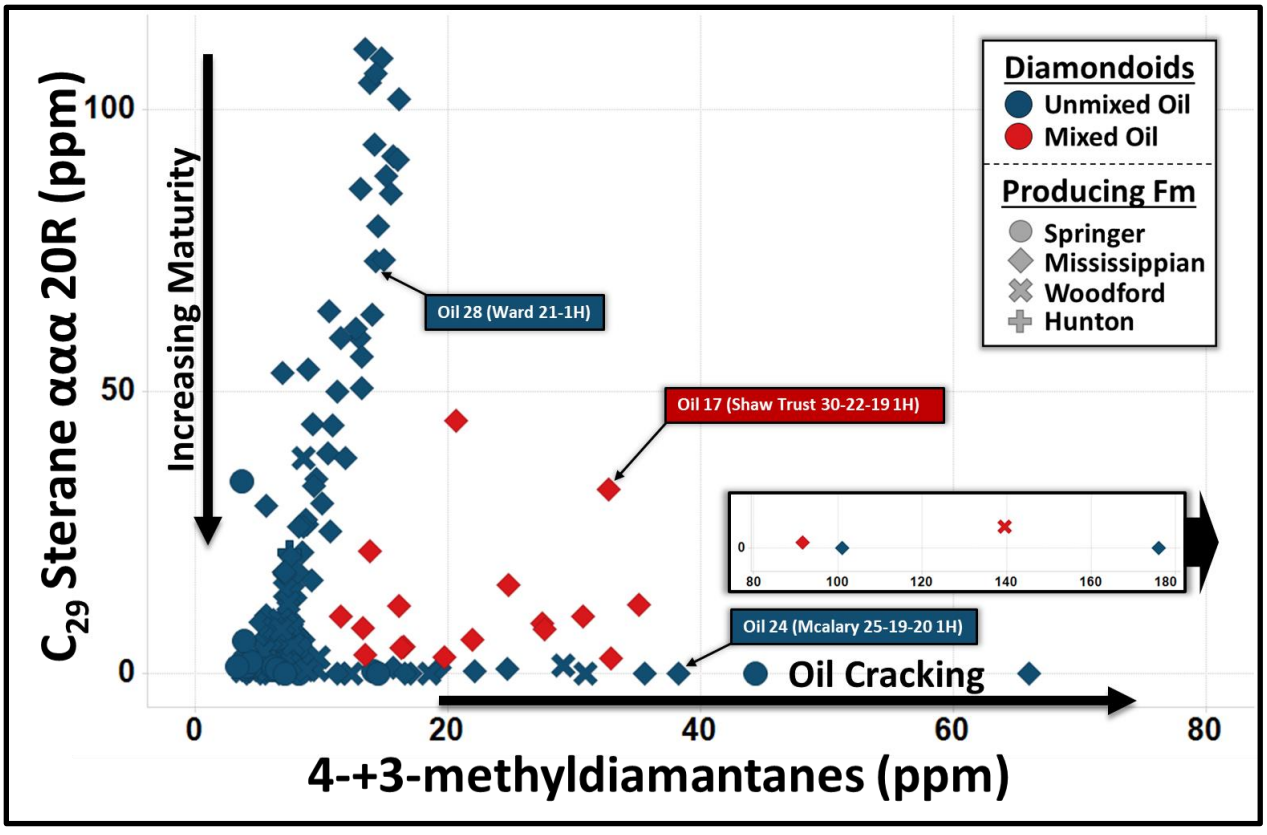

Figure 115. Crossplot of the concentration of C_{29} 5α(H),14α(H),17α(H),20R sterane versus the sum of 4- and 3-methyldiamantane to determine mixing of low- and high-maturity oils. Based on Dahl et al. (1999).

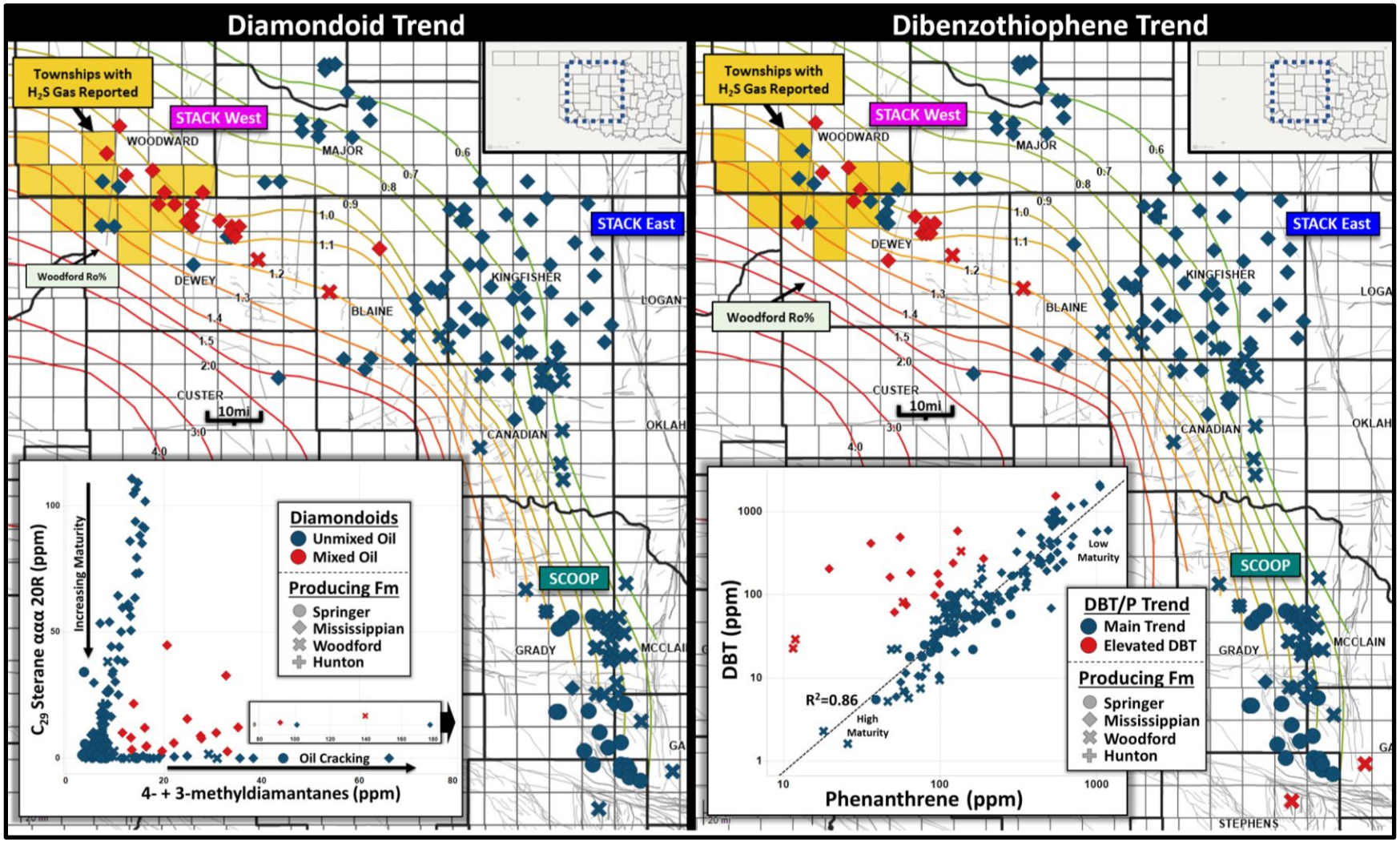

Figure 116. Composite maps showing oils which indicate oil mixing between low- and high-maturity oils using MDA (see Figure 115), and oils which contain elevated DBT above which can be accounted for by changes in thermal maturity (see Figure 113). Both the mixed oils and the high DBT oils occur near the flower-shaped zone and where H_2S is observed in STACK West. There is not exact agreement between these two trends, but they both occur in similar portions of STACK West.

Although they both occur in the same areas in STACK West near the flower-shaped zone and H_2S occurrences, there is not an exact agreement between the oils which are enriched in DBT and the oils containing a mixture of low- and high maturity oils, possibly because of lithologic controls on TSR or migration pathways in the Osage. For example, if TSR reactants are rate limited by the reservoir lithology (i.e. anhydrite deposits adjoining hydrocarbon bearing facies), then it is possible that TSR would be lithology dependent and may occur erratically in map view with heterogeneous sulfate deposits. In this case, the degree of sulfate reduction could be mapped as a lithologic phenomenon and referenced when predicting drilling hazards and reservoir fluid characteristics. To date, there are no known occurrences of anhydrite deposits in the Woodford Shale; however, the Osagean Miss "Chat" is a major drilling target in STACK West which contains evidence of extensive subaerial exposure, periodic hypersaline events, and even reports of micro-vugular anhydrite in Woodward and Harper (STACK West) counties (Eucker and Ashby, 2020).

Without TSR, the main controls on the concentration of aromatic sulfur compounds in oils are its source-rock depositional environment (Hughes et al., 1995) and thermal maturity (Ho et al., 1974). A map of DBT/P values for studied oils is shown in Figure 117. In STACK West at depths too shallow for TSR reactions, elevated DBT/P may be sourced from elevated organosulfur compounds in the Middle Woodford in STACK West (see Figure 109). This is comparable to the Woodford-sourced oils produced from the Hugoton Embayment, Kansas containing DBT/P values between 0.05-0.50 (Tamborello, 2020). This also aligns with low maturity extracts of the Woodford Shale (Rc=0.59%) in the Arbuckle Uplift in Pottawatomie County with DBT/P of 0.75±0.15 (n=9) and 1.14±0.14 (n=3) in the Lower and Middle Woodford, respectively (Villalba, 2016). The higher DBT/P values in the Arbuckle Uplift is expected not only because DBT/P decreases with increased maturity, but also because an increase in DBT/P is observed upon exiting

the basin towards the Arbuckle Uplift. This is evident by the two extrabasinal Woodford-produced oils in this study in Garvin and Stephens counties which contain DBT/P values of 0.69 and 0.40, respectively, compared to all other SCOOP 1 (Lower) organic facies Woodford-producing oils which average DBT/P=0.08±0.01 (n=24). In the Dewey, Woodward, Ellis tricounty region, high DBT/P are likely the result of TSR reactions occurring in situ (at the lowest range of TSR temperatures) or deeper in the basin and migrating updip to mix with locally generated oils.

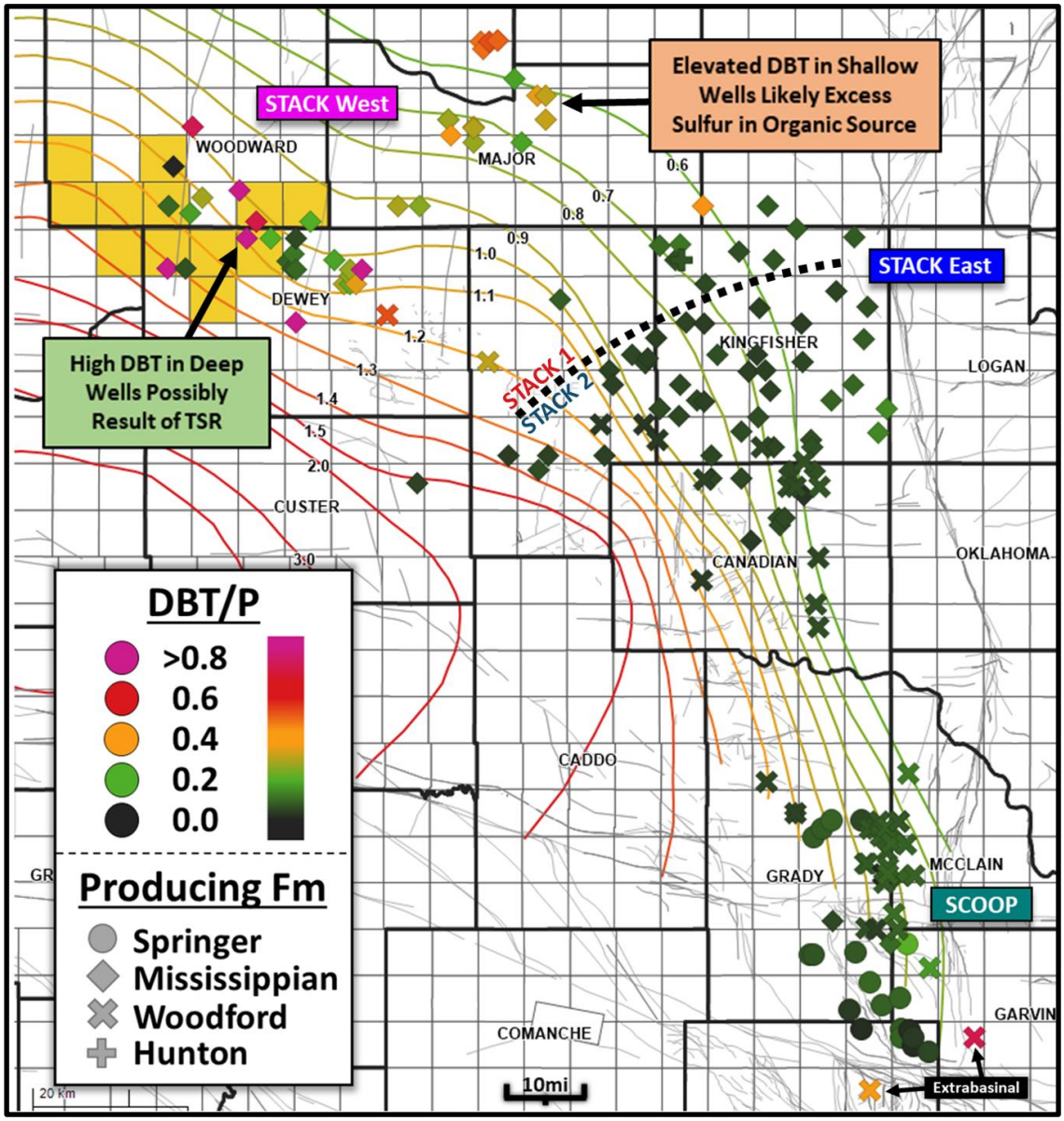

Figure 117. Map of DBT/P values in this study. Elevated DBT/P in shallow reservoirs likely the result of elevated organosulfur in organic source. Elevated DBT/P in deep wells possibly the result of TSR reactions.

Finally, the occurrence of TSR can be observed by compound specific isotope analysis (CSIA) of the gasoline range hydrocarbons. Claypool and Mancini (1989) noted that oils affected by TSR had more positive whole oil $\delta^{13}C$ by 2-3‰ and suggested that isotopically lighter carbon is more readily oxidized during TSR. Rooney (1995) used CSIA of the gasoline fraction to measure isotopic shifts in light isotopic between different speciation. Compounds with fewer carbons also show larger shifts in $\delta^{13}C$ because a the addition of a single ^{13}C a larger fractional change in the overall in the mass of the compound. She observed larger shifts in $\delta^{13}C$ from branched and *n*-alkanes (up to 22‰) and smaller shifts from cyclic and monoaromatic species (3-6‰). In summary, a notable increase in $\delta^{13}C$ of branched and *n*-alkane hydrocarbons in the gasoline range (C_2-C_8) compared to minimal increase in $\delta^{13}C$ for cyclic and monoaromatic hydrocarbons is an isotopic indicator of TSR reactions in crude oil (Machel, 2001).

This study performed CSIA on fourteen samples spanning all three Play Regions with the majority of samples taken from STACK West (Figure 118). The CSIA $\delta^{13}C$ values for branched, cyclic, and monoaromatic gasoline range hydrocarbons (C_4-C_7) is provided in Table 24 and for *n*-alkanes in Table 25. Two line plots of the CSIA data show more positive $\delta^{13}C$ values in STACK West especially over the gasoline range *n*-alkanes which show a positive isotope excursion of between 2-10‰, far more than the 2-3‰ expected from thermal maturity alone (Figure 119). Furthermore, STACK West samples also show a positive $\delta^{13}C$ trend in the gasoline-range branched compounds, marked in red, of approximately 4-6‰ compared to cyclic and monoaromatic compounds over the same range. In fact, almost no isotopic shift is observed in cyclic and monoaromatic across any of the Play Regions which may indicate that the isotopic effects of maturity are small compared to TSR oxidation of hydrocarbons. This evidence supports the hypothesis that some or all STACK West oils have been affected by TSR reactions.

Furthermore, the whole oil GC chromatograms for several of the oils analyzed by CSIA show notable depletion in *n*-alkanes below *n*-C_{15} (Figure 120). This observation supports the hypothesis that TSR reactions may have oxidized significant portions of the *n*-alkane fraction of oils and caused an overall isotopic shift observed in CSIA. While the GC signature observed in many STACK West oils could certainly be the result of TSR, the depletion of light end components can also result from other subsurface processes like migrational fractionation and seal leakage. Additional analyses could further support the hypothesis of substantial influence of TSR on some STACK West oils, including isotopic analyses of mineral and aqueous sulfate species and compared with the $\delta^{34}S$ from local H_2S production.

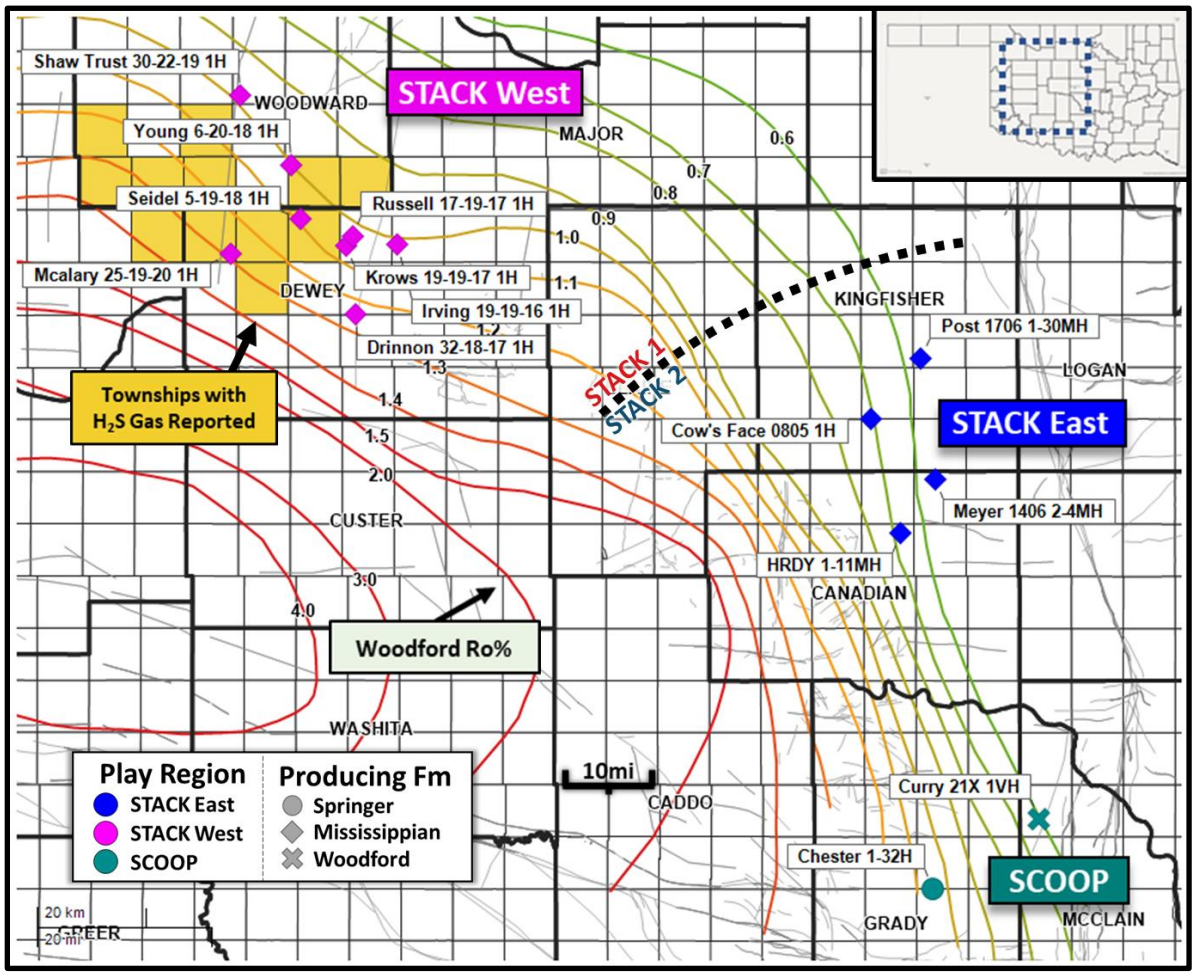

Figure 118. A map of oil samples where CSIA $\delta^{13}C$ analysis was performed in this study.

Key	Oil Name	*i*-C4	*i*-C5	2-MP	3-MP	MCP	BENZ	CC_6	2-MH	2,3-DMP	3-MH	*c*-1,3-DMCP	*t*-1,3-DMCP	*t*-1,2-DMCP	MCH	TOL
17	Shaw Trust 30-22-19 1H	-31.0	-30.2	-30.1	-30.0	-27.9	-26.4	-29.1	-30.5	-30.1	-30.1	-26.6	-27.4	-27.0	-29.2	-28.4
19	Young 6-20-18 1H	-31.4	-29.4	-29.5	-28.8	-27.9	-29.4	-29.3	-30.1	-29.3	-29.1	-26.9	-26.9	-27.0	-29.6	-30.2
24	Mcalary 25-19-20 1H	-29.8	-28.5	-27.8	-28.0	-26.9	-27.3	-29.6	-29.1	-26.8	-27.9	-26.7	-26.3	-26.5	-29.6	-28.1
25	Seidel 5-19-18 1H	-31.1	-28.8	-28.7	-28.6	-27.3	-27.1	-29.3	-29.8	-28.9	-28.7	-26.0	-26.3	-26.5	-29.6	-28.1
32	Russell 17-19-17 1H	-31.5	-30.1	-30.1	-29.5	-27.7	-29.1	-30.0	-30.7	-29.1	-30.4	-27.1	-27.1	-26.5	-30.0	-29.9
33	Krows 19-19-17 1H	-30.7	-29.7	-29.8	-29.5	-27.8	-28.6	-29.8	-30.5	-29.5	-29.3	-26.8	-26.8	-26.7	-29.5	-29.2
36	Drinnon 32-18-17 1H	-24.3	-23.8	-24.3	-24.1		-21.5	-23.6	-24.8	-24.8	-27.7				-25.5	-23.5
37	Irving 19-19-16 1H	-29.5	-28.1	-28.2	-28.1	-27.3	-26.7	-29.3	-29.0	-27.4	-27.9	-26.4	-26.5	-26.3	-29.9	-28.0
86	Cow's Face 0805 1H	-35.9	-32.1	-32.5	-31.4	-28.8	-31.2	-31.5	-33.1	-32.0	-31.8	-28.0	-27.6	-27.1	-30.6	-31.8
96	HRDY 1-11MH	-34.9	-31.9	-32.1	-31.0	-28.3	-31.1	-32.4	-31.8	-30.5	-31.5	-27.1	-27.3	-26.5	-30.2	-31.7
102	Post 1706 1-30MH	-34.3	-31.8	-32.1	-30.7	-29.0	-32.0	-31.3	-32.3	-31.4	-30.7	-27.9	-27.7	-27.3	-30.4	-32.0
107	Meyer 1406 2-4MH	-36.0	-32.0	-32.9	-31.2	-28.9	-32.4	-31.9	-33.3	-32.2	-31.6	-27.9	-27.7	-26.8	-30.9	-32.8
120	Curry 21X 1VH	-34.4	-31.6	-31.4	-31.1	-26.9	-30.9	-30.4	-32.2	-30.5	-31.1	-25.7	-26.5	-24.3	-29.2	-31.0
134	Chester 1-32H	-34.1	-31.8	-31.3	-31.2	-27.5		-28.3	-32.1	-31.7	-31.4	-25.3	-25.9	-25.4	-28.4	-28.5

Table 24. Compound specific $\delta^{13}C$ of branched and cyclic compounds taken from the gasoline fraction of 14 oils in this study.

Key	Oil Name	DBT/P	*n*-C_4	*n*-C_5	*n*-C_6	*n*-C_7	*n*-C_8	*n*-C_9	*n*-C_{10}	*n*-C_{11}	*n*-C_{12}	*n*-C_{13}	*n*-C_{14}	*n*-C_{15}	*n*-C_{16}
17	Shaw Trust 30-22-19 1H	0.70	-30.0	-29.4	-29.4	-29.3	-29.4	-29.7	-29.4	-29.8	-30.7	-30.2	-30.1	-30.0	-30.4
19	Young 6-20-18 1H	2.87	-29.8	-29.5	-29.9	-30.3	-30.3	-30.6	-30.3	-30.4	-30.2	-30.7	-30.7	-30.7	-31.0
24	Mcalary 25-19-20 1H	0.07	-27.6	-28.1	-29.0	-29.6	-29.8	-30.2	-30.0	-30.3	-30.7	-31.0	-30.6	-30.6	-30.5
25	Seidel 5-19-18 1H	1.16	-28.8	-28.9	-29.6	-29.7	-29.9	-30.4	-30.3	-30.5	-30.5	-30.3	-30.4	-30.6	-30.8
32	Russell 17-19-17 1H	0.12	-30.2	-30.4	-31.1	-31.4	-31.1	-31.2	-31.1	-31.1	-30.6	-30.3	-31.0	-30.4	-30.6
33	Krows 19-19-17 1H	0.09	-29.2	-30.0	-30.8	-31.1	-30.7	-30.9	-30.8	-30.8	-31.2	-30.9	-31.1	-31.4	-31.3
36	Drinnon 32-18-17 1H	1.10	-21.8	-22.3	-23.8	-24.9	-25.6	-26.3	-26.8	-27.0	-27.6	-27.7	-27.8	-28.0	-28.2
37	Irving 19-19-16 1H	0.18	-27.2	-27.5	-28.4	-29.2	-29.0	-29.3	-29.2	-29.6	-30.2	-30.5	-30.7	-30.6	-30.6
86	Cow's Face 0805 1H	0.06	-33.2	-33.1	-33.5	-33.2	-32.6	-33.2	-32.7	-32.3	-32.9	-32.6	-32.5	-32.3	-32.5
96	HRDY 1-11MH	0.06	-33.1	-32.5	-32.6	-32.5	-31.9	-32.2	-31.8	-32.1	-32.2	-31.9	-32.3	-32.3	-32.3
102	Post 1706 1-30MH	0.05	-32.6	-32.5	-33.0	-33.0	-32.1	-32.5	-32.3	-32.3	-32.0	-31.6	-31.5	-31.9	-32.2
107	Meyer 1406 2-4MH	0.07	-34.0	-33.6	-34.0	-33.8	-32.9	-33.4	-32.7	-33.2	-32.7	-32.5	-32.9	-32.7	-33.3
120	Curry 21X 1VH	0.13	-34.1	-33.1	-32.7	-31.8	-31.4	-31.6	-31.0	-31.0	-31.2	-30.7	-30.9	-31.1	-31.1
134	Chester 1-32H	0.08	-33.4	-32.4	-32.4	-32.3	-31.5	-32.0	-31.6	-31.4	-31.5	-31.5	-31.1	-31.3	-31.5

Table 25. Compound specific $\delta^{13}C$ of *n*-alkane compounds taken from 14 oils in this study. The ratio DBT/P is also provided.

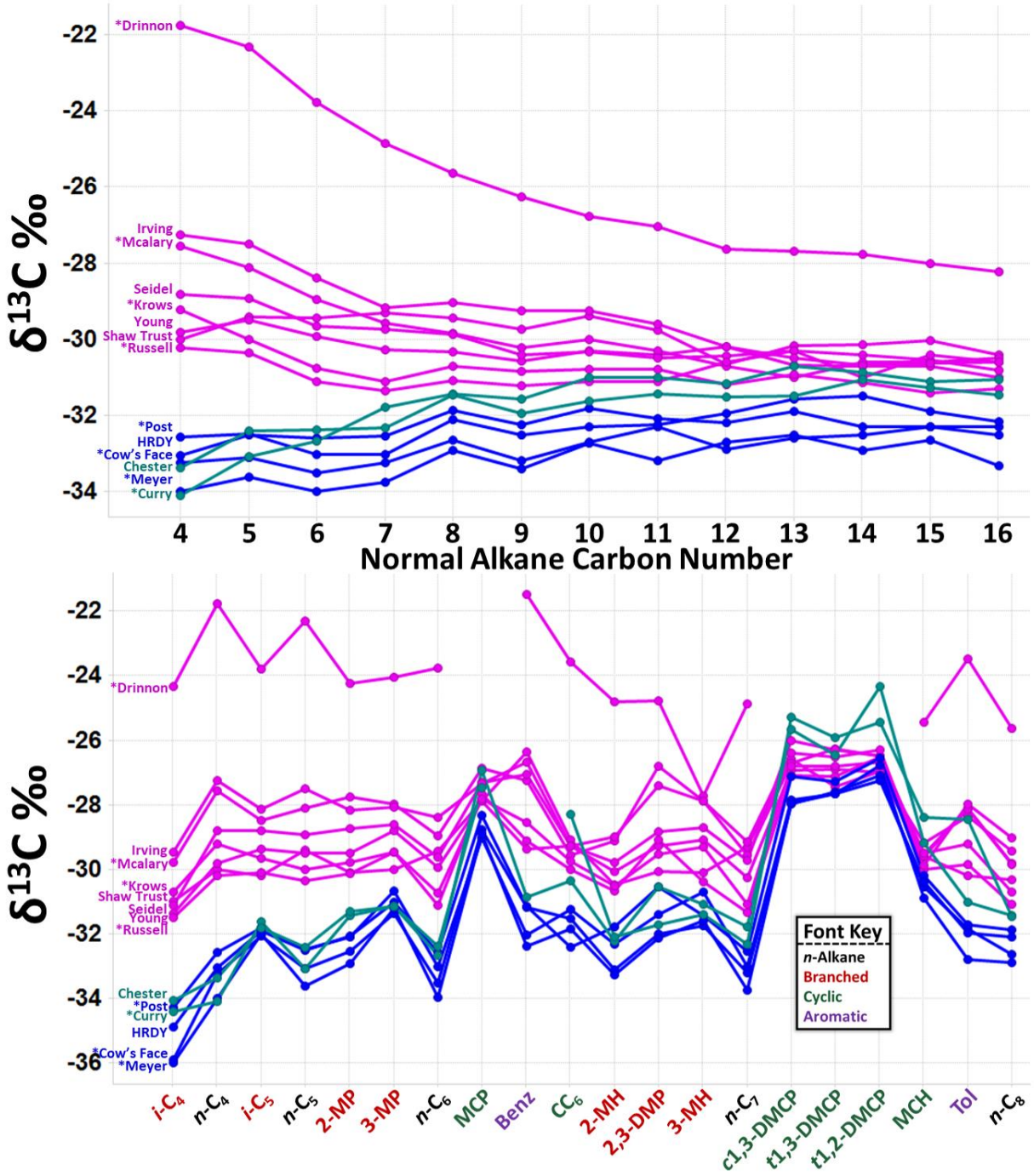

Figure 119. (Upper) CSIA of gasoline and diesel range *n*-alkanes. STACK West samples show significant isotope excursion in the gasoline range *n*-alkanes and branched compounds. (Lower) CSIA of all gasoline range light hydrocarbons (C_4-C_8). Little or no isotope excursion is observed in the cyclic and monoaromatic compounds over the same range. Samples marked * have GC traces shown in Figure 120. Hydrocarbon abbreviations provided in Table 7 with the addition of i-C_4 (isobutane), i-C_5 (isopentane), 2-MP (2-methylpentane), 3-MP (3-methylpentane), and MCP (methylcyclopentane).

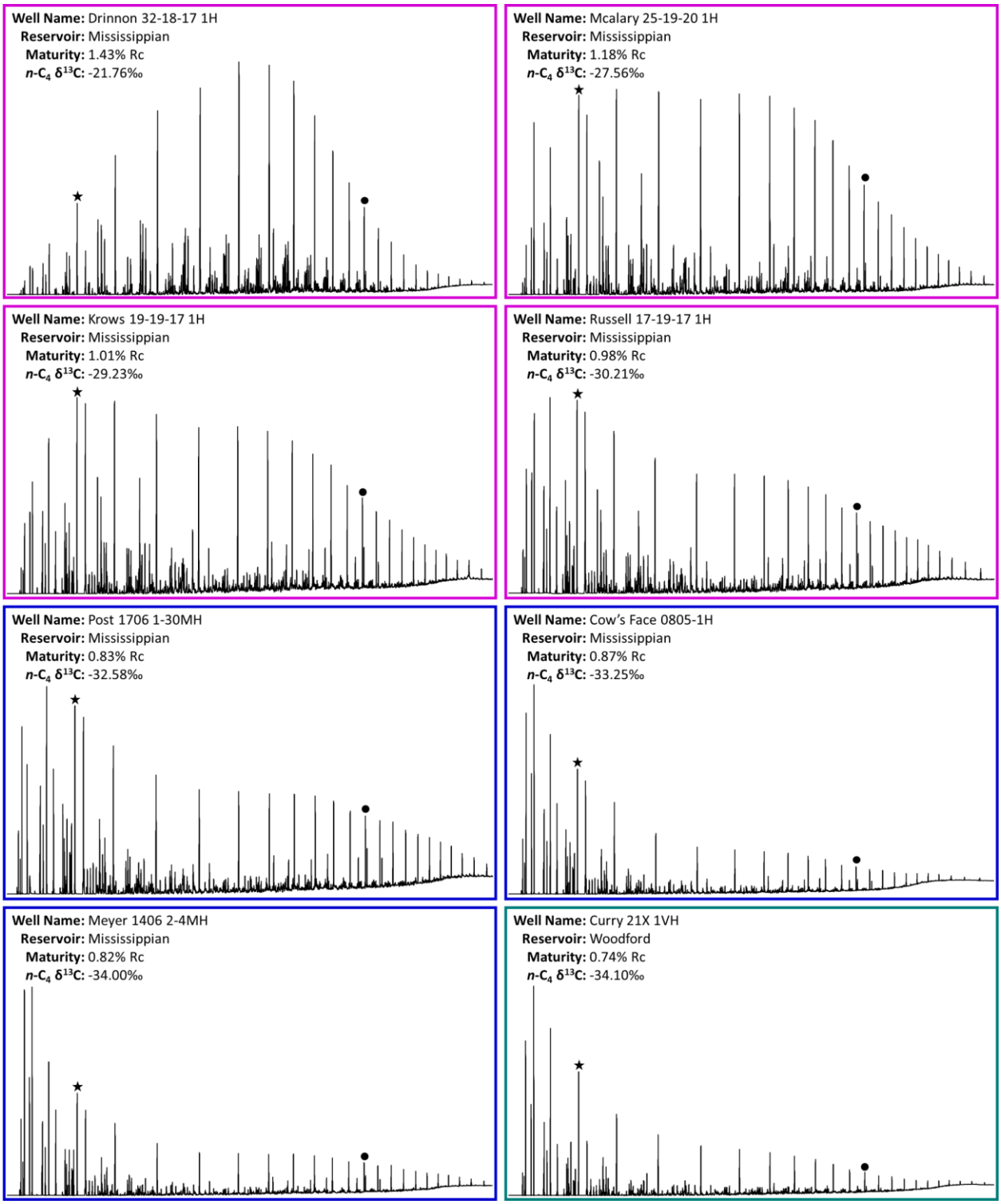

Figure 120. Whole oil GC trace for eight oils depicted in Figure 119. STACK West oils with elevated CSIA $\delta^{13}C$ show a corresponding depletion in *n*-alkanes below *n*-C_{15}. Peaks corresponding to *n*-C_7 and *n*-C_{18} are marked with a star and circle, respectively.

Predicting Overpressure

This section describes an unproven hypothesis that pristine oils exhibit a predictable relationship between geochemical maturity and some physical characteristics like gas-oil-ratio in unconventional plays. If true, then identifying oils that deviate from that trend could be predictive of subsurface processes or properties which deplete or enrich an oil reservoir of solution gas.

The geochemical relationship between vitrinite reflectance and reservoir fluid class (black oil, volatile oil, wet gas, and dry gas) for Type II kerogens has been well established (Tissot and Welte, 1984; Hunt, 1996; McCarthy et al., 2011; Cardott, 2012; Peters et al., 2012; Philp, 2014; Hackley and Cardott, 2016; Hackley, 2017). Likewise, production and phase behavior of reservoir fluids with respect to Initial Producing Gas-Oil Ratio (IP GOR) has been well-documented by reservoir and production engineers (e.g. Clark, 1960; Moses, 1986; McCain, 1990). A summary of the geochemical and production definitions for each reservoir fluid class is provided in Table 26, although exact cutoffs are not universally agreed on.

In theory, a pristine hydrocarbon fluid (neither enriched nor depleted in gas) might exhibit a predictable relationship between its thermal maturity (Rc%) and its IP GOR. A semi-log plot of IP GOR and Rc% for all STACK samples is shown in Figure 121. Two production-maturity trends emerged, colored in orange and grey, which closely correspond to the boundary of normal- and

Reservoir Fluid	Production (IP GOR)	Geochemistry
Black Oil	<2,000 scf/STB	<0.9 Ro%
Volatile Oil	2,000-10,000 scf/STB	0.9-1.1 Ro%
Wet Gas	10,000-100,000 scf/STB	1.1-1.3 Ro%
Dry Gas	>100,000 scf/STB	>1.3 Ro%

Table 26. Reservoir fluid defined by production and geochemistry. Scf/STB=standard cubic ft per stock tank barrel.

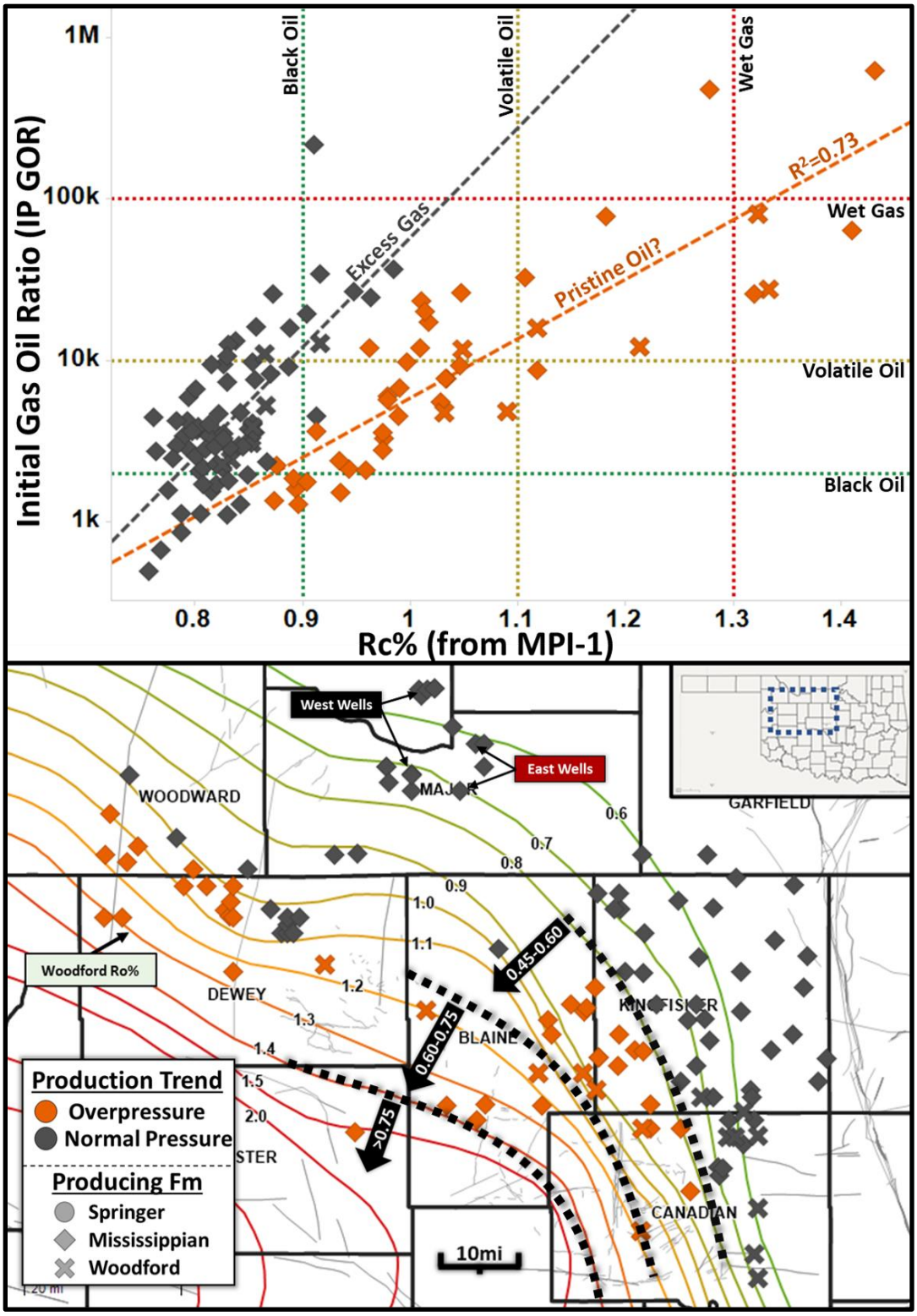

Figure 121. Upper: Crossplot of IP GOR and Rc% showing two distinct production trends. Lower: Map of STACK colored by production trends overlain with STACK pressure gradients (black arrows) in psi/ft. The production-maturity trends mirror reservoir overpressure (>0.45psi/ft). Pressure gradient zones from Cullen (2017). Data found in Table 3 and Table 9. "East Wells" and "West Wells" refer to wellhead gas isotope samples (see text; Figure 122).

overpressure reservoirs (<0.45 psi/ft) in STACK. In areas of over-pressure, a strong relationship (R^2=0.73) is observed between IP GOR and Rc%, and the over-pressured oil trend (orange) overlays the intersection of expected values of IP GOR and Rc% as defined in Table 26. It is proposed here that the strong relationship between Rc% and IP GOR in overpressure areas comprises near pristine oils trapped in a "closed-system" reservoir.

Oils produced from normal- and under-pressured reservoirs have thermal maturities that correspond with peak oil generation from source rocks (0.75-0.95% Rc). To be clear, Rc% (from MPI-1) and vitrinite reflectance (Ro%) rely on different chemical reactions and may not always agree, but limited data in this study suggests they closely agree. For example, mean vitrinite reflectance measurements of the Woodford Shale in the ABCDS 1-6 core was Ro=0.74%±0.03% (n=21), while MPI-1 from extracts measured Rc=0.79%±0.01% (n=4). Some production in Kingfisher and Garfield counties is from reservoirs above under-mature Woodford (<0.6% Ro). Curiously, normal- and under-mature oils exhibit significantly higher IP GOR at any given Rc% compared to over-pressured reservoirs—up to an order of magnitude—and plot well above the predicted IP GOR for any Rc%. It is critical to remember that Rc% is an independent measurement of thermal stress undergone by an oil and not affected by enrichment or depletion of gas. If over-pressured oils are interpreted as pristine, then normal- and under-pressured oils have IP GOR almost an order of magnitude higher than expected. What might cause this extra gas production?

One possibility is that the reservoir was inundated with gas either before or after the primary oil charge. At least one recent study has argued that a charge of very mature dry gas has mixed with locally generated hydrocarbons in some STACK Woodford and Mississippian reservoirs based on the enrichment of methane ^{13}C relative to its coproduced natural gas liquids (Kornacki and Dahl, 2016). Gas component maturity plots can help determine if deep methane has

migrated and mixed with oil in shallow reservoirs. Stahl and Carey (1975) derived an empirical relationship between the carbon isotopic composition of methane, ethane, and propane and the maturity (Ro%) of its organic source material and proposed a combination of individual gas component carbon isotopes as a tool for recognizing gas mixing. Berner and Faber (1988) refined the empirical gas-maturity model from a large dataset of sapropelic organic sources and derived a mathematical model to quantify gas mixing. Around the same time, Chung et al. (1988) showed that the carbon isotopes of co-genetically formed gasses (C_1-C_5) will form parallel relationships, usually as a straight line, when plotted against 1/*n* where *n* is the carbon number.

Data from four wellhead gas isotopes, labeled East Wells and West Wells in Figure 121, were made available to this study taken from two sides of a structural graben in Major and Woods counties (Fairway Resources, Personal Communication). Two gas maturity-mixing plots based on the work of Chung et al. (1988) and Berner and Faber (1988) are shown in Figure 122. The East Wells were drilled into a thickened Mississippian interval inside the graben while the West Wells

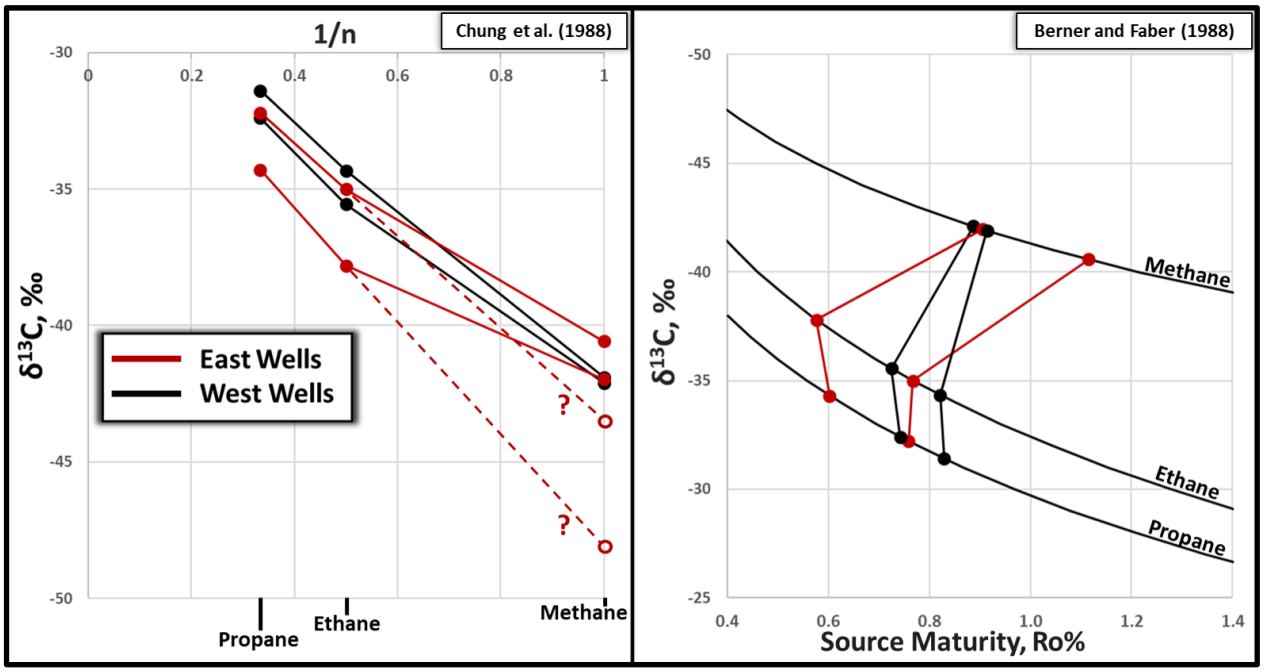

Figure 122. Two gas maturity plots for four STACK West wells showing possibly more mature (isotopically heavier) methane compared to ethane and propane. Well locations shown in Figure 121. Data generated by GeoMark Research.

were drilled outside of the graben. The two East Wells drilled inside the graben show an apparent bend towards isotopically heavy methane not observed in the West Wells. It is important to realize that this is a small dataset and uncalibrated to the STACK, but this relationship may explain the origin of excess gas observed in normal- and under-mature oils compared to overpressured oils.

While still in its infancy, the excess gas model in Figure 121 provides another means of predicting the edge of the internal capillary sealing of continuous unconventional reservoirs from two variables independent of pressure. This could aid in unconventional exploration efforts where pressure data can be unavailable or prohibitively expensive to obtain. Legacy drill stem tests are rarely performed in unconventional reservoirs because the low permeability of the reservoir requires the test to remain open for extended periods and can threaten the integrity of the hole, and more modern diagnostic fracture injection tests (DFIT) are expensive or difficult to obtain. This model is capable of using publicly available production data in combination with routine geochemical maturity measurements to possibly predict reservoir pressure regime.

Spatial Heterogeneity in Oil Charge and Accumulation

Spatial heterogeneity in bulk or molecular composition of oil in conventional reservoirs due to processes like gravity segregation, biodegradation, and water washing have been studied at least since the 1970s (Bailey et al., 1973; Milner et al., 1977; Connan, 1984; Tissot and Welte, 1984). This prompted interest in other forms of compositional heterogeneity in reservoirs, most notably the result of low rates of in-reservoir mixing of successive petroleum charges and accumulation in conventional reservoirs (England et al., 1987; England and Mackenzie, 1989; Leythaeuser and Rückheim, 1989; England, 2007). The question remains whether oil accumulation models designed for conventional reservoirs can be adapted to unconventional reservoirs to better

understand the production heterogeneity in modern resource plays. This section attempts to describe and explain the geochemical heterogeneity observed in extracts from several STACK Mississippian cores within the context of an extremely low permeability petroleum system.

During the rise of unconventional resource plays near the turn of the 21st century, Meckel and Thomasson (2005) coined the term "pervasive tight" resource play, which described a regional coupling of a thermally mature source rock adjacent to a "Tight Gas Sands" or "Shale" reservoirs containing micro- or nano-Darcy permeability (see Figure 123). They argue that these petroleum systems differ from conventional systems primarily in the principal forces governing migration across pore throats. In conventional systems, petroleum moves along "fluid potential gradients," or the sum of forces comprising excess water pressure from lithologic compaction/dewatering, fluid buoyancy forces, and capillary forces (England et al., 1987; England and Mackenzie, 1989). At sufficiently low permeabilities, the fluid potential gradient is too low to overcome pore-entry capillary pressure and the rock instead acts as a barrier to flow. Bulk or molecular heterogeneity of oil in conventional reservoirs, they argue, is the result of incomplete in-reservoir mixing of individual oil charging episodes by convection or diffusion.

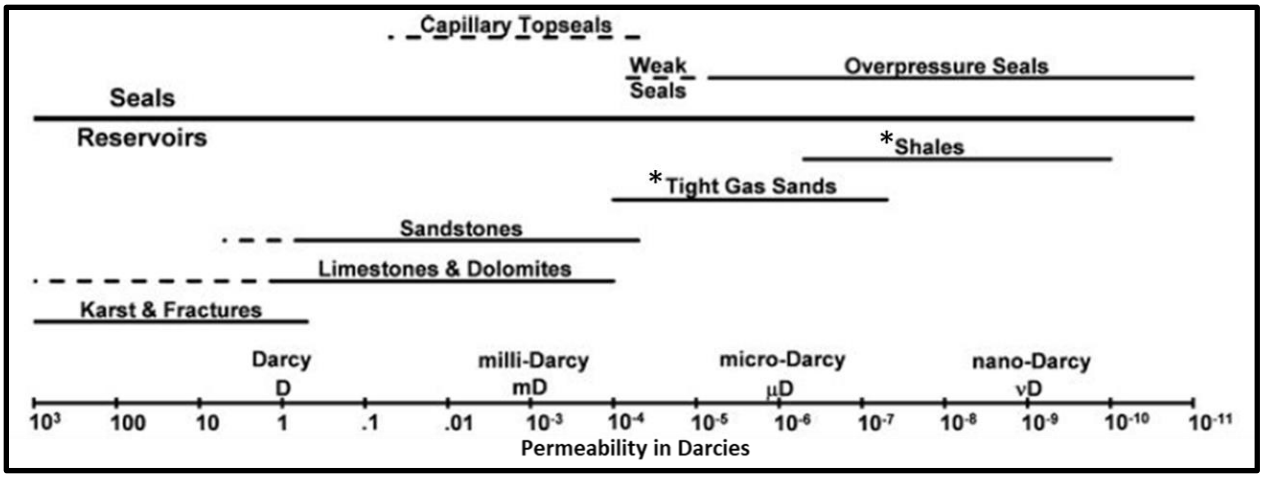

Figure 123. A comparison of the permeabilities between conventional and unconventional reservoir (marked by *). Note that tight sands and shales reservoirs are more similar to seals than they are to conventional sand and carbonate reservoirs. From Dembick (2016).

In one notable case study, Leythaeuser and Rückheim (1989) analyzed the bulk and molecular heterogeneity of a conventional oil field by comparing solvent extracts of core samples taken from impregnated reservoir sands (described as "extracted oils") to oil produced from drill stem tests (DST). They observed pronounced geochemical differences between high- and low-porosity zones over short distances even within the same vertical cored profile. Extracted oil from high porosity zones was more mature and resembled the producible oil captured from DST, and extracted oil from low porosity zones was less mature than the DST oil (Figure 124). They argued that early hydrocarbon charge(s) carrying a low-maturity chemical signature originally accumulated in the high-porosity/high-permeability sand intervals since their pore-entry capillary

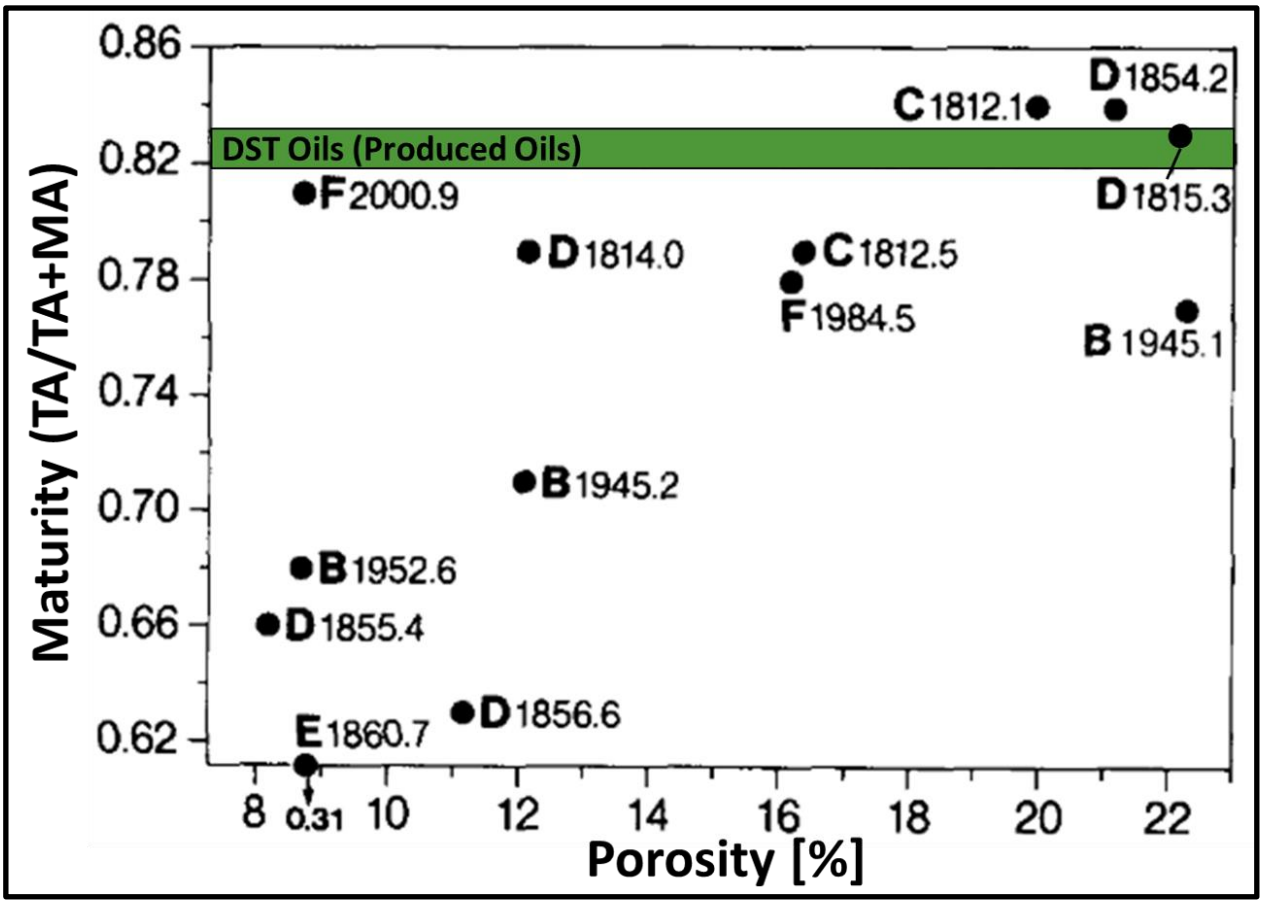

Figure 124. The heterogeneity in a conventional oil field shows a positive relationship between porosity and extracted oil maturity in core. High porosity intervals closely resemble DST produced oils. Modified from Leythaeuser and Rückheim (1989).

pressures are the lowest. Continued burial resulted in the arrival of more, and progressively higher maturity, oil in the entrapment area increasing the height of the oil column and the buoyancy pressure. In the higher porosity zones, the early-accumulated lower-maturity oil was displaced by the higher-maturity oil, forcing the former into progressively lower-porosity intervals. The geochemical differences between higher and lower porosity zones is a real world example of the inefficient mixing of different petroleum charges predicted by England et al. (1987).

The question remains if the spatial heterogeneity models designed for conventional petroleum migration can be applied to pervasive tight reservoirs. To start, Meckel and Thomasson (2005) outlines four criteria which differentiate pervasive tight reservoirs: 1) low porosity generally between 6-9% and permeability between 0.001-0.1 millidarcies (conventional porosity range 10-25% and permeability 10-1,000 millidarcies); 2) close proximity to a mature source rock which provides overpressuring sufficient to overcome high capillary entry pressures; 3) near irreducible water saturation (Sw_{irr}) due to super-charging and dewatering by the nearby over-pressured source rock; and 4) an inverted oil column (water above oil above gas) with no down-dip water contact. The STACK meets each of the criteria of a pervasive tight petroleum system. For example, the Meramec production in the core of STACK has an average effective porosity 0.5-5.8%, permeability 0.05-4.75 millidarcies, and a 30-50% water saturation (Fritz, 2017; Eucker and Ashby, 2020). The high capillary pressure in STACK maintains an inverted oil column even with large oil column height, and as a result the height of the oil column in STACK East is at least ~5,800 ft just from oils in this study alone (deepest oil: 12,523 ft; shallowest oil: 6,714 ft).

This study analyzed solvent extracts ("extracted oils") from seven oil impregnated Mississippian cores for geochemical heterogeneity. Porosity and permeability at sample depths were not made available, but because the reservoirs are known to be at or near Sw_{irr}, it is proposed

here that the amount of extractable organic matter per gram of rock (EOM µg/g) might serve as a relative approximation for original oil in place (OOIP) and, by extension, sample porosity. Unfortunately, due to the age of the cores and prolonged exposure to open air, parameters for light hydrocarbons, colloidal instability index, and even alkyl-aromatics were found unreliable or absent to determine the maturity of the extracted oil. Instead, an approximate maturity was derived from the preferential expulsion of tricyclic terpanes (**V**) and hopanes (**VI**) at different stages of maturity (Figure 48; Aquino Neto et al., 1983; Kruge et al., 1990; Philp et al., 2021). Higher percent hopanes corresponds to lower thermal maturity and vice versa. In several cores, an alternating pattern of thermal maturity with depth is observed. For example in the Caffey 32-16N-9W 1H Meramec core (Figure 125), depths 9,617 ft and 9,863 contain low-maturity (high % hopanes) extracted oil and corresponds to a low-porosity (low EOM µg/g) interval, while the middle sample depth 9,669 ft contains high-maturity extracted oil which corresponds to a high-porosity interval.

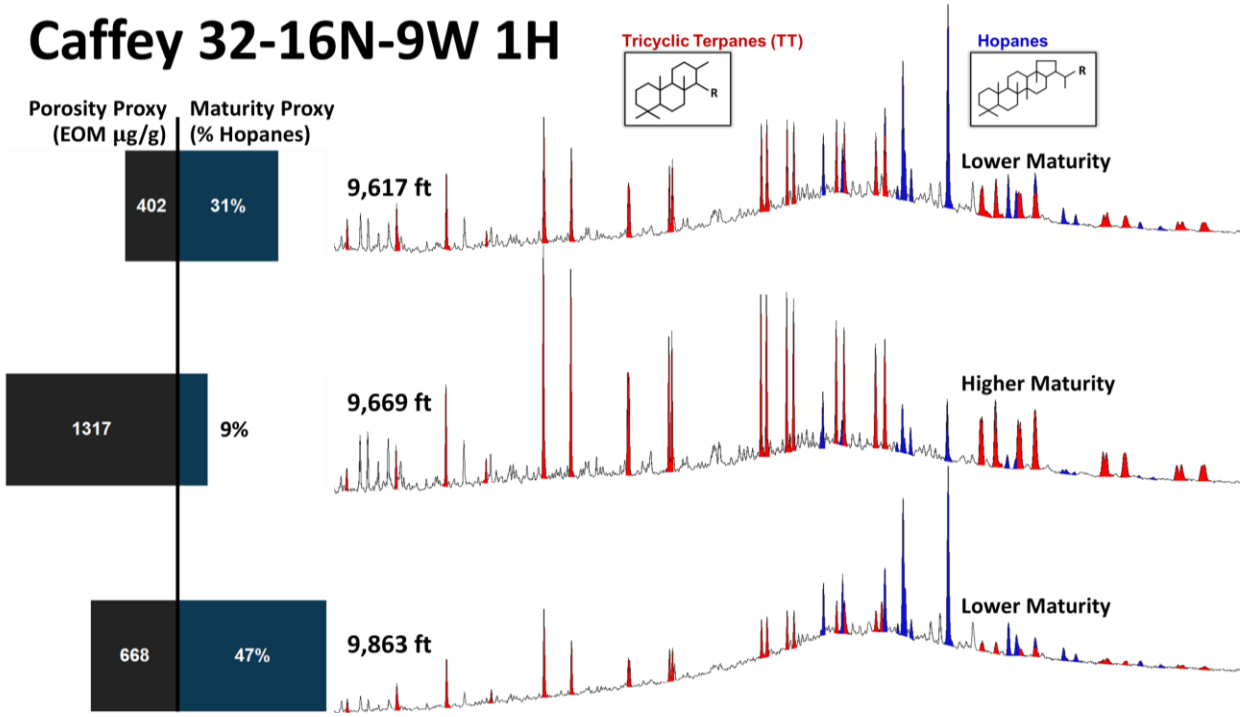

Figure 125. Terpane fingerprint of three core depths of the Caffey 32-16N-9W 1H core in STACK East with accompanying EOM (µg/g) and percent hopanes (hopanes/hopanes+tricyclic terpanes) values. There is an inverse relationship between EOM and percent hopanes over a cored interval of 246 ft.

Additionally, the extracted oil from Caffey 32-16N-92 1H core depth 9,669 ft also more closely resembles the maturity of nearby producing Meramec oil wells in a nine-township area in this dataset, shown in Figure 126. If reproducible, this observation may demonstrate that distinct beds containing high EOM are responsible for the largest stimulated rock volume drained by horizontal drilling and hydraulic fracturing. Furthermore, it highlights the geochemical character of oil most likely to be stored in the most producible (and therefore most porous/permeable) Meramec intervals. In the case of the Caffey 32-16N-92 1H core, the most mature oils are stored in the most producible rock volume of the Meramec reservoir, while lower maturity oils are not significant contributors to oil production when drilled. This mirrors the findings from conventional reservoirs predicted by England et al. (1987) and observed by Leythaeuser and Rückheim (1989).

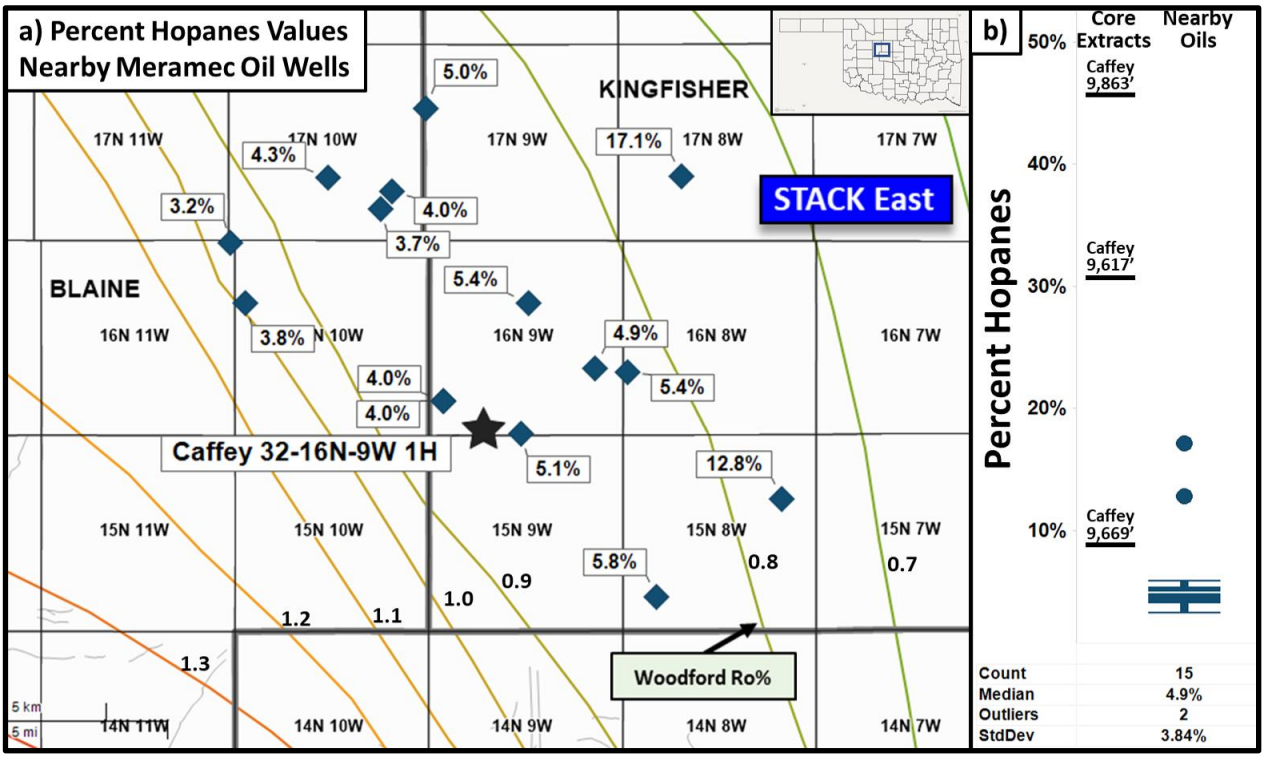

Figure 126. a) Map showing location of the Caffey 32-16N-9W 1H core (black star). Offsetting wells in a nine-township region around the cored well are labeled by percent hopanes (hopanes/hopanes+tricyclic terpanes); b) Calculated percent hopanes of the three Caffey core depths in addition to the values for offsetting oils. The terpane signature of Caffey depth 9,669' has the highest producibility, as measured by EOM, and most resembles nearby produced oils.

The positive relationship between porosity and maturity observed in the Caffey 32-16N-92 1H core is repeatable in other STACK East cores, as shown in Figure 127. Five extracts from the nearby Gulf Shaffer 1-23 in Blaine County show four high-porosity intervals across the 180 ft sampling depth. Higher sampling resolution in the Capps Unit 1 shows a gradual transition in maturity between 8,873-8,904 (6% to 24% hopanes) but an immediate increase in porosity between 8,873-8,877 ft (355 to 1,127 µg/g EOM).

Further work is needed to prove the oil migration/accumulation model in pervasive tight reservoirs, including higher resolution sampling combined with real measurements of porosity and permeability. If proven, this analysis could provide a cheap an effective way to predict porosity and permeability in very tight reservoirs where that data is often prohibitively expensive, unreliable, or difficult to obtain. Other maturity proxies could also be predictive of porosity and

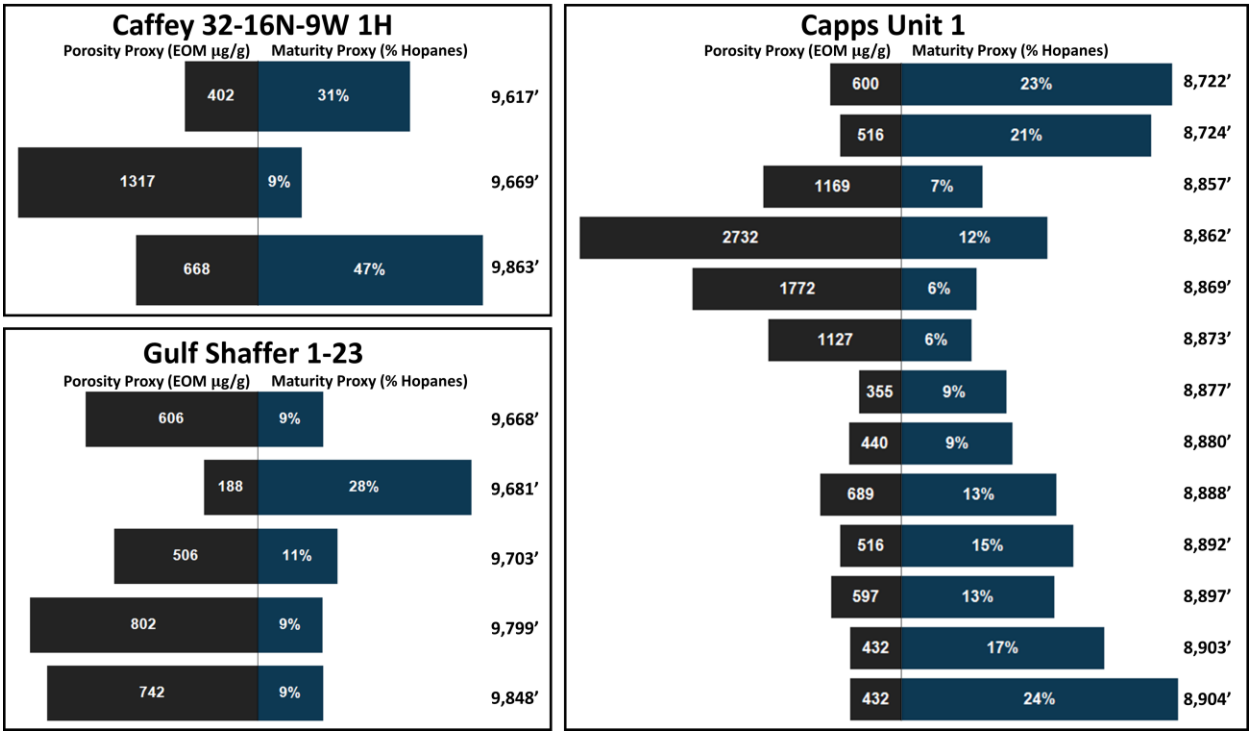

Figure 127. Notable geochemical heterogeneity is observed in STACK solvent extracts. Three cores exhibit positive relationship between porosity and maturity proxies in core depths. In this model, percent hopanes is used to approximate the thermal maturity of the extracted oil at depth and EOM is used to approximate porosity. Porous beds (high EOM) correspond to higher maturity oils (low percent hopanes) and closely resemble offset oil production.

permeability while drilling, possibly taken from drill cuttings during horizontal drilling to better stay in the highest quality reservoir intervals. Further work will also delineate when the model does not work, which is equally important. For example, although each of the seven Mississippian cores analyzed exhibited significant geochemical heterogeneity, the positive relationship between porosity and maturity proxies was only observed in the three wells taken from overpressured Mississippian reservoirs, as shown in Figure 128. This seems to indicate that overpressuring is a prerequisite to overcome the significant capillary pressures necessary to displace the early charge of low-maturity oils from high-porosity intervals into low-porosity intervals.

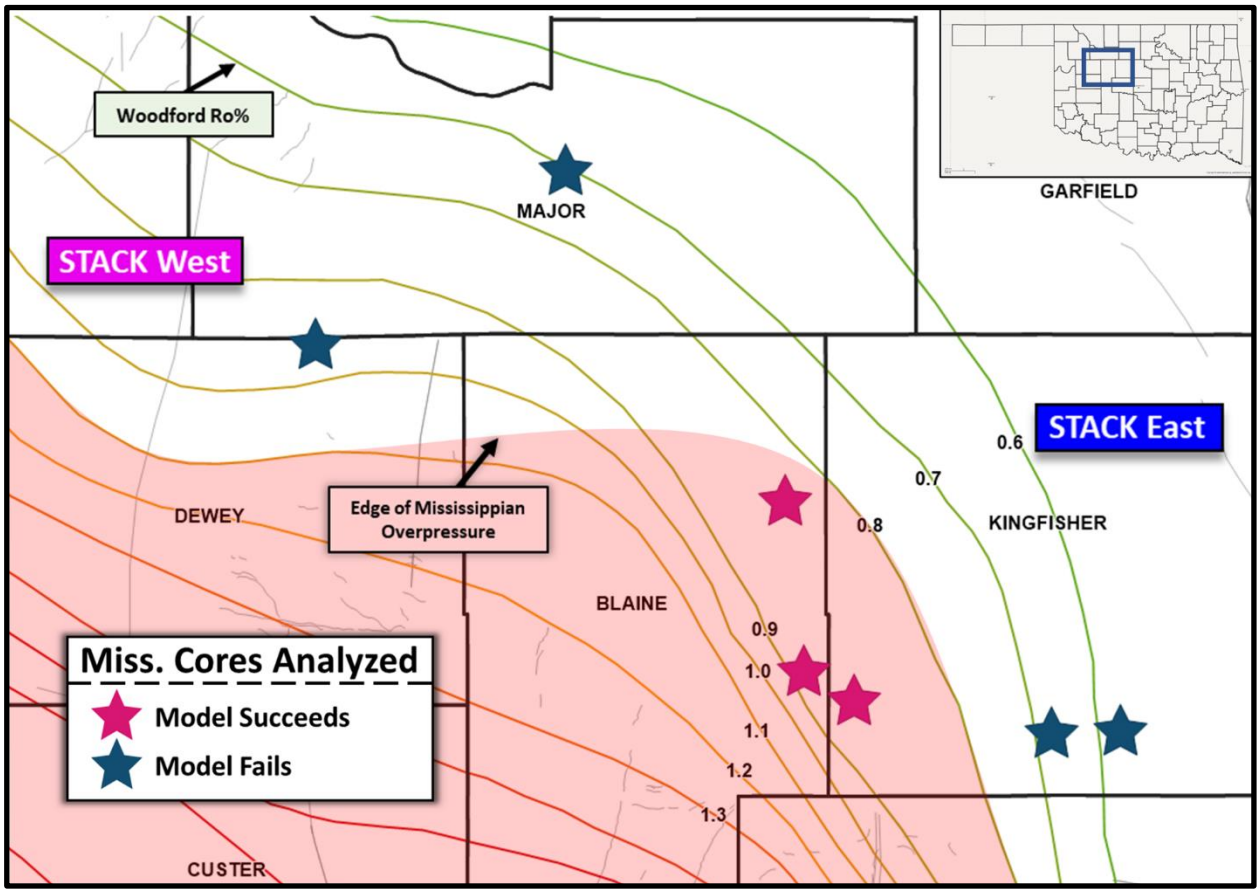

Figure 128. While all analyzed cores show significant spatial geochemical heterogeneity, the positive relationship between porosity and maturity proxies (EOM and % hopanes) was only observed in areas of reservoir overpressure. No relationship between EOM and % hopanes was observed in under- or normally pressured reservoirs.

Summary of Findings

Three secondary reservoir processes were identified in this study. First, substantial enrichment of toluene and dibenzothiophene (DBT) was observed in STACK West oils (DBT=166±74 ppm) compared to STACK East (DBT=17±4 ppm) and SCOOP (DBT=16±5 ppm) and may be the result of elevated sulfur in STACK West. In shallow STACK West reservoirs, increased DBT and toluene may result from reactions with organosulfur compounds believed to be observed in the TOC-rich Middle Woodford. In the volatile oil window, high DBT/P values are associated with H_2S production as well as migration and mixing from methyldiamantane rich fluids produced deeper in the basin before migrating up major fractures in the Osage Limestone and mixing with lower-maturity locally generated oils. While DBT enrichment alone could be attributed to restricted depositional environments with low terrigenous input (low iron), the presence of high concentration H_2S gas (<20 ppm) reported in Woodward, Dewey, and Ellis counties suggests the presence of thermochemical sulfate reduction (TSR) reactions.

Second, two trends were observed when gas-oil-ratio (GOR) was crossplotted against Rc% which corresponded to areas of reservoir overpressure. Oils from overpressured reservoirs formed a highly correlative trend between Rc% and GOR which mirrors the expected physical properties for pristine oils at various stages of maturity—black oil, volatile oil, and wet gas. Oils from under- and normally pressured reservoirs contained GOR up to an order of magnitude higher than comparably mature oils from overpressured reservoirs. Gas data from four wells in Major County shows methane consistently isotopically enriched in ^{13}C compared to ethane and propane from the same well. While still in its infancy, this exciting hypothesis could supplement an exploration strategy by replacing expensive DFIT or downhole pressure tests with a simple fluid extraction which measures both GOR and thermal maturity to predict overpressure.

Finally, spatial heterogeneity in bulk or molecular composition observed in Mississippian cores is the result of incomplete mixing of increasingly mature petroleum charges (e.g. Leythaeuser and Rückheim, 1989). In areas of overpressure, a positive relationship was observed between proxies used to estimate porosity and maturity in solvent extracted oils. Offset oil production closely resembles extracted oils from high porosity intervals. Measuring porosity and permeability in tight unconventional reservoirs is often expensive and unreliable; however, the observed relationship may help estimate porosity by simply measuring fluid maturity. Using this workflow, explorationists may improve well efficiency by rapidly predicting the most porous and permeable intervals.

VII. Conclusions

- Oil maturity can be modeled independently of organic source using principal component analysis for unconventional resource plays within normally heated basins.
- Three Woodford Shale organic facies were identified which sourced oil to all Woodford and Mississippian Group reservoirs in STACK/SCOOP. A separate Caney/Goddard shale organic facies is present in SCOOP which sourced oil to the Springer Group, and which closely resembles Pennsylvanian-type oil.
- High concentration H_2S gas produced in STACK West is likely the result of thermochemical sulfate reduction (TSR) reactions deeper in the basin. TSR-affected fluids migrated updip and mixed with locally generated oils.
- Under- and normally pressured reservoirs exhibit gas-oil-ratios up to an order of magnitude higher than overpressured reservoirs at the same thermal maturity.
- Cored intervals from overpressured reservoirs exhibit spatial geochemical heterogeneities resulting from incomplete mixing of petroleum charges derived from source rocks at progressively increasing maturity stages and could be leveraged to model paragenesis, porosity, permeability, and pressure.

References

Abbott, G.D., Maxwell, J.R., 1988. Kinetics of the aromatisation of rearranged ring-C monoaromatic steroid hydrocarbons. Organic Geochemistry 13, 881–885.

Abelson, P.H., 1963. Organic Geochemistry and the Formation of Petroleum, in: 6th World Petroleum Congress Proceedings, Sec 1. pp. 397–407.

Abrams, M.A., Thomas, D., 2020. Geochemical evaluation of oil and gas samples from the Upper Devonian and Mississippian reservoirs Southern Anadarko Basin Oklahoma and its implication for the Woodford Shale unconventional play. Marine and Petroleum Geology 112, 1–17.

Alexander, R., Kagi, R., Noble, R.A., 1983. Identification of the Bicyclic Sesquiterpenes Drimane and Eudesmane in Petroleum. Journal of the Chemical Society, Chemical Communications 226–228.

Alexander, R., Kagi, R.I., Noble, R.A., Volkman, J.K., 1984. Identification of some bicyclic alkanes in petroleum. Organic Geochemistry 6, 63–70.

Anders, D.E., Robinson, W.E., 1971. Cycloalkane constituents of the bitumen from Green River Shale. Geochimica et Cosmochimica Acta 35, 661–678.

Andrusevich, V.E., Engel, M.H., Zumberge, J.E., 2000. Effects of paleolatitude on the stable carbon isotope composition of crude oils. Geology 28, 847–850.

Andrusevich, V.E., Engel, M.H., Zumberge, J.E., Brothers, L.A., 1998. Secular, episodic changes in stable carbon isotope composition of crude oils. Chemical Geology 152, 59–72.

Aquino Neto, F.R., Trendel, J.M., Restle, A., Connan, J., Albrecht, P.A., 1983. Occurrence and formation of tricyclic and tetracyclic terpanes in sediments and petroleums, in: Bjorøy, M. (Ed.), Advances in Organic Geochemistry 1981. Wiley, 1983, pp. 659–667.

Aquino Neto, F.R., Triguis, J., Azevedo, D.A., Rodriques, R., Simoneit, B.R.T., 1992. Organic geochemistry of geographically unrelated tasmanites. Organic Geochemistry 18, 791–803.

Asomaning, S., Watkinson, A.P., 2000. Petroleum stability and heteroatom species effects in fouling of heat exchangers by asphaltenes. Heat Transfer Engineering 21, 10–16.

Atwah, I., 2015. Organic Geochemistry and Crude Oil Source Rock Correlation of the Devonian-Mississippian Petroleum Systems of Northern Oklahoma. Bachelor Thesis, Oklahoma State University, Stillwater, Oklahoma.

Atwah, I., Mohammadi, S., Moldowan, J.M., Dahl, J., 2021. Episodic hydrocarbon charge in tight Mississippian reservoirs of Central Oklahoma, USA: Insights from oil inclusion geochemistry. Marine and Petroleum Geology 123, 1–16.

Atwah, I., Puckette, J., Becker, M., Moldowan, J.M., 2020. Source-rock reservoirs geochemistry of Devonian-Mississippian mudrocks in central Oklahoma. AAPG Bulletin 104, 657–680.

Atwah, I., Sweet, S., Pantano, J., Knap, A., 2019. Light Hydrocarbon Geochemistry: Insight into Mississippian Crude Oil Sources from the Anadarko Basin, Oklahoma, USA. Geofluids 2019,

15.

Azevedo, D.A., Aquino Neto, F.R., Simoneit, B.R.T., Pinto, A.C., 1992. Novel series of tricyclic aromatic terpanes characterized in Tasmanian tasmanite. Organic Geochemistry 18, 9–16.

Azevedo, D.A., Neto, F.R.A., Simoneit, B.R.T., 1998. Extended ketones of the tricyclic terpane series in a Tasmanian tasmanite bitumen. Organic Geochemistry 28, 289–295.

Bailey, N.J.L., Jobson, A.M., Rogers, M.A., 1973. Bacterial degradation of crude oil: Comparison of field and experimental data. Chemical Geology 11, 203–221.

Beach, F., Peakman, T.M., Abbott, G.D., Sleeman, R., Maxwell, J.R., 1989. Laboratory thermal alteration of triaromatic steroid hydrocarbons. Organic Geochemistry 14, 109–111.

Beaumont, C., 1981. Foreland Basins. Geophysical Journal of the Royal Astronomical Society 65, 291–329.

BeMent, W.O., Levey, R.A., Mango, F.D., 1995. The temperature of oil generation as defined with C7 chemistry maturity parameter (2,4-DMP/2,3-DMP ratio), in: Grimalt, J.O., Dorronsoro, C. (Eds.), Organic Geochemistry: Developments and Applications to Energy, Climate, Environment and Human History. AIGOA, Donostia-San Sebastian, Spain, pp. 505–507.

Bendoraitis, J.G., 1974. Hydrocarbon of biogenic origin in petroleum-aromatic triterpenes and bicyclic sesquiterpenes, in: Tissot, B., Beiner, F. (Eds.), Advances in Organic Geochemistry. Paris, pp. 209–224.

Berner, R.A., 1984. Sedimentary pyrite formation: An update. Geochimica et Cosmochimica Acta 48, 605–615.

Berner, R.A., Scott, M.R., Thomlinson, C., 1970. Carbonate alkalinity in the pore waters of anoxic marine sediments. American Society of Limnology and Oceanography 14, 544–549.

Berner, U., Faber, E., 1988. Maturity related mixing model for methane, ethane and propane, based on carbon isotopes. Organic Geochemistry 13, 67–72.

Brassell, S.C., Eglinton, G., Maxwell, J.R., Philp, R.P., 1978. Natural background of alkanes in the aquatic environment, in: Hutzinger, O., van Lelyveld, I.H., Zoeteman, B.C.J. (Eds.), Aquatic Pollutants. Pergamon Press, Oxford; New York, pp. 69–86.

Bray, E.E., Evans, E.D., 1961. Distribution of n-paraffins as a clue to recognition of source beds. Geochimica et Cosmochimica Acta 22, 2–15.

Budzikiewicz, H., Wilson, J.M., Djerassi, C., 1963. Mass Spectrometry in Structural and Stereochemical Problems. XXXII. Pentacyclic Terpanes. Journal of the American Chemical Society 85, 3688–3699.

Bunker, B., Witzke, B., Watney, W., Ludvigson, G., 1988. Phanerozoic history of the midcontinent, United States, in: Sloss, L. (Ed.), Sedimentary Cover—North American Craton: The Geology of North America, v. D-2. Geological Society of America, pp. 243–260.

Burruss, R.C., Hatch, J.R., 1989. Geochemistry of Oils and Hydrocarbon Source Rocks, Greater Anadarko Basin: Evidence for Multiple Sources of Oils and Long-Distance Oil Migration, in: Johnson, K.S. (Ed.), Anadarko Basin Symposium, 1988. Oklahoma Geological Survey Circular 90, Norman, Oklahoma, pp. 53–64.

Burruss, R.C., Hatch, J.R., 1992. Geochemistry of Pennsylvanian Crude Oils and Source Rocks in the Greater Anadarko Basin, Oklahoma Texas, Kansas, Colorado, and Nebraska: An Update, in: Johnson, K.S., Cardott, B.J. (Eds.), Source Rocks in the Southern Midcontinent, 1990 Symposium. Oklahoma Geologic Survey Circular 93, Norman, Oklahoma, p. 197.

Bynum, J., Wethington, C., 2020. Mississippian (Lower Carboniferous) Facies Heterogeneity and Distribution within the Mixed Carbonate and Siliciclastic Reservoirs of the Midcontinent STACK play, Oklahoma, USA, in: Unconventional Resources Technology Conference 2020. SPE/AAPG/SEG, Austin, pp. 1–19.

Cardott, B.J., 2012. Thermal maturity of Woodford Shale gas and oil plays, Oklahoma, USA. International Journal of Coal Geology 103, 109–119.

Cardott, B.J., 2017. Oklahoma Shale Resource Plays. Oklahoma Geology Notes 76, 21–30.

Carter, L.S., Kelley, S. a, Blackwell, D.D., Naeser, N.D., 1998. Heat Flow and Thermal History of the Anadarko Basin, Oklahoma. AAPG Bulletin 82, 291–316.

Chung, H.M., Brand, S.W., Grizzle, P.L., 1981. Carbon isotope geochemistry of Paleozoic oils from Big Horn Basin. Geochimica et Cosmochimica Acta 45, 1803–1815.

Chung, H.M., Gormly, J.R., Squires, R.M., 1988. Origin of gaseous hydrocarbons in subsurface environments: Theoretical considerations of carbon isotope distribution. Chemical Geology 71, 97–104.

Clark, J.P., Philp, R.P., 1989. Geochemical characterization of evaporite and carbonate depositional environments and correlation of associated crude oils in the Black Creek Basin, Alberta. Bulletin of Canadian Petroleum Geology 37, 401–416.

Clark, N.J., 1960. Elements of Petroleum Reservoirs (Henry L. Doherty series). Society of Petroleum Engineers, Dallas, Texas.

Cole, T., 1989. A surface to subsurface study of the Sycamore Limestone (Mississippian) along the north flank of the Arbuckle Anticline. Shale Shaker Digest XII 39, 205–221.

Conant, L.C., Swanson, V.E., 1961. Chattanooga Shale and related rocks of Central Tennessee and nearby areas. USGS Professional Paper 357, 91.

Connan, J., 1974. Time-Temperature Relation in Oil Genesis. AAPG Bulletin 58, 2516–2521.

Connan, J., 1984. Biodegradation of crude oils in reservoirs, in: Brooks, J., Welte, D.H. (Eds.), Advances in Petroleum Geochemistry. Academic Press, New York, pp. 299–335.

Connan, J., Bouroullec, J., Dessort, D., Albrecht, P.A., 1986. The microbial input in carbonate-anhydrite facies of a sabkha palaeoenvironment from Guatemala: a molecular approach, in: Leythaeuser, D., Rullkötter, J. (Eds.), Advances in Organic Geochemistry 1985. Pergamon Press, Oxford, pp. 29–50.

Connan, J., Cassou, A.M., 1980. Properties of Gases and Petroleum Liquids Derived from Terrestrial Kerogen at Various Maturation Levels. Geochimica et Cosmochimica Acta 44, 1–23.

Connock, G.T., 2015. Paleoenvironmental Interpretation of the Woodford Shale, Wyche Farm Shale Pit, Pontotoc County, Arkoma Basin, Oklahoma with Primary Focus on Water Column Structure. University of Oklahoma.

Connock, G.T., Nguyen, T.X., Philp, R.P., 2018. The development and extent of photic-zone euxinia concomitant with Woodford Shale deposition. AAPG Bulletin 102, 959–986.

Craig, H., 1957. Isotopic standards for carbon and oxygen and correction factors for mass-spectrometric analysis of carbon dioxide. Geochimica et Cosmochimica Acta 12, 133–149.

Cullen, A., 2017. Devonian-Mississippian Petroleum Systems of Southern Laurasia: What Makes the STACK-Merge-SCOOP Play in Oklahoma so Special. Search and Discovery Article #10998.

Curiale, J.A., Curtis, J.B., 2016. Organic geochemical applications to the exploration for source-rock reservoirs - A review. Journal of Unconventional Oil and Gas Resources 13, 1–31.

Curtis, D.M., Champlin, S.C., 1959. Depositional Environments of Mississippian Limestones of Oklahoma. Tulsa Geological Society Digest 27, 90–103.

Dahl, J., Moldowan, J.M., McCaffrey, M.A., Lipton, P.A., 1992. A new class of natural products revealed by 3β -alkyl steranes in petroleum. Nature 355, 154–157.

Dahl, J., Moldowan, J.M., Peters, K.E., Claypool, G.E., Rooney, M.A., Michael, G.E., Mello, M.R., Kohnen, M.L., 1999. Diamondoid hydrocarbons as indicators of natural oil cracking. Nature 399, 54–57.

Davis, J.B., Yarbrough, H.F., 1966. Anaerobic oxidation of hydrocarbons by Desulfovibrio desulfuricans. Chemical Geology 1, 137–144.

De Grande, S.M.B., Aquino Neto, F.R., Mello, M.R., 1993. Extended tricyclic terpanes in sediments and petroleums. Organic Geochemistry 20, 1039–1047.

Demaison, G.J., Moore, G.T., 1980. Anoxic environments and oil source bed genesis. American Association of Petroleum Geologists, Bulletin 64, 1179–1209.

Dembick, H.J., 2016. Petroleum - Geochemistry for Exploration and Production, Practical Petroleum Geochemistry for Exploration and Production. Candice Janco, Amsterdam, Netherlands.

Dickie, J.P., Yen, T.F., 1967. Macrostructures of the Asphaltic Fractions by Various Instrumental Methods. Analytical Chemistry 39, 1847–1852.

Didyk, B.M., Simoneit, B.R.T., Brassell, S.C., Eglinton, G., 1978. Organic geochemical indicators of palaeoenvironmental conditions of sedimentation. Nature 272, 216–222.

Dimmler, A., Cyr, T.D., Strausz, O.P., 1984. Identification of bicyclic terpenoid hydrocarbons in the saturate fraction of Athabasca oil sand bitumen. Organic Geochemistry 7, 231–238.

Dinur, D., Spiro, B., Aizenshtat, Z., 1980. The distribution and isotopic composition of sulfur in organic-rich sedimentary rocks. Chemical Geology 31, 37–51.

Dow, W.G., 1977. Kerogen Studies and Geological Interpretations. Journal of Geochemical Exploration 7, 79–99.

Dzou, L.I.P., Noble, R.A., Senftle, J.T., 1995. Maturation Effects on Absolute Biomarker Concentration in a suite of Coals and Associated Vitrinite Concentrates. Organic Geochemistry 23, 681–697.

Eglinton, G., Calvin, M., 1967. Chemical Fossils. Scientific American 216, 32–43.

Eglinton, G., Scott, P.M., Belsky, T., Burlingame, A.L., Calvin, M., 1964. Hydrocarbons of biological Origin from a One-Billion-Year-Old Sediment. Science 145, 263–264.

Eglinton, T.I., Philp, R.P., Rowland, S.J., 1988. Flash pyrolysis of artificially matured kerogens from the Kimmeridge Clay, U.K. Organic Geochemistry 12, 33–41.

Ekweozor, C.M., 1984. Tricyclic terpenoid derivatives from chemical degradation reactions of asphaltenes. Organic Geochemistry 6, 51–61.

Engel, M.H., Imbus, S.W., Zumberge, J.E., 1988. Organic geochemical correlation of Oklahoma crude oils using R- and Q-mode factor analysis. Organic Geochemistry 12, 157–170.

England, W.A., 2007. Reservoir geochemistry - A reservoir engineering perspective. Journal of Petroleum Science and Engineering 58, 344–354.

England, W.A., Mackenzie, A.S., 1989. Some aspects of the organic geochemistry of petroleum fluids. Geologische Rundschau 78, 291–303.

England, W.A., Mackenzie, A.S., Mann, D.M., Quigley, T.M., 1987. The movement and entrapment of petroleum fluids in the subsurface. Journal of the Geological Society 144, 327–347.

Espitalié, J., La Porte, J.L., Madec, M., Marquis, F., Le Plat, P., Paulet, J., Boutefeu, A., 1977. Methode rapide de caracterisation des roches meres de leur potential petrolier et de leur degre d'evolution. Revue l'Inst. Francais du Petrole 32, 23–42.

Ettensohn, F.R., Barron, L.S., 1981. Depositional Model for the Devonian-Mississippian Black-Shale Sequence of North America: A Tectono-Climatic Approach. U.S. Department of Energy Technical Report.

Eucker, W., Ashby, A.M., 2020. STACK 2020 Anadarko Basin, Oklahoma. Shale Shaker Digest 71, 146–161.

Fang, R., Wang, T.G., Li, M., Xiao, Z., Zhang, B., Huang, S., Shi, S., Wang, D., Deng, W., 2016. Dibenzothiophenes and benzo[b]naphthothiophenes: Molecular markers for tracing oil filling pathways in the carbonate reservoir of the Tarim Basin, NW China. Organic Geochemistry 91, 68–80.

Forsman, J.P., Hunt, J.M., 1958. Insoluble organic matter (kerogen) in sedimentary rocks. Geochimica et Cosmochimica Acta 15, 170–182.

Francois, R., 1987. A study of sulphur enrichment in the humic fraction of marine sediments during early diagenesis. Geochimica et Cosmochimica Acta 51, 17–27.

Fritz, R.D., 2017. Deep STACK-Exploration of hte Over-Pressured Meramec Shale in Blaine and Dewey Counties, OK. AAPG Search and Discovery Article 90296.

Fuex, A.N., 1977. The use of stable carbon isotopes in hydrocarbon exploration. Journal of Geochemical Exploration 7, 155–188.

Gillan, F.T., Johns, R.B., 1980. Input and early diagenesis of chlorophylls in a temperate intertidal sediment. Marine Chemistry 9, 243–253.

Goldhaber, M.B., Orr, W.L., 1995. Kinetic Controls on Thermochemical Sulfate Reduction as a Source of Sedimentary H2S, in: Vairavamurthy, M.A., Schoonen, M.A.A. (Eds.),

Geochemical Transformations of Sedimentary Sulfur. American Chemical Society Symposium Series 612. Washington DC, pp. 412–425.

Gransch, J.A., Posthuma, J., 1974. On the origin of sulphur in crudes, in: Tissot, B.P., Bienner, F. (Eds.), Advances in Organic Geochemistry. Editions Technip, Paris, pp. 727–830.

Grantham, P.J., Posthuma, J., de Groot, K., 1980. Variation and significance of the C27 and C28 triterpane content of a North Sea core and various North Sea crude oils. Physics and Chemistry of the Earth 12, 29–38.

Grantham, P.J., Wakefield, L.L., 1988. Variations in the sterane carbon number distributions of marine source rock derived crude oils through geological time. Organic Geochemistry 12, 61–73.

Grice, K., 2001. δ13C as an indicator of paleoenvironments: a molecular approach, in: Unkovich, M., Pate, J., McNeill, A., Gibbs, J. (Eds.), Application of Stable Isotope Techniques to Study Biological Processes and Functioning Ecosystems. Kluwer Scientific, Dordrecht, The Netherlands, pp. 247–281.

Grice, K., Alexander, R., Kagi, R.I., 2000. Diamondoid hydrocarbon ratios as indicators of biodegradation in Australian crude oils. Organic Geochemistry 31, 67–73.

Hackley, P.C., 2017. Application of Organic Petrology In High Maturity Shale Gas Systems, in: Suárez-ruiz, I., Filho, J.G.M. (Eds.), Geology: Current and Future Developments. Bentham Science Publishers, pp. 206–236.

Hackley, P.C., Cardott, B.J., 2016. Application of organic petrography in North American shale petroleum systems: A review. International Journal of Coal Geology 163, 8–51.

Halpern, H.I., 1995. Development and applications of light-hydrocarbon-based star diagrams. American Association of Petroleum Geologists Bulletin 79, 801–815.

Ham, W.E., Denison, R.E., Merritt, C.A., 1964. Basement Rocks and Structural Evolution of Southern Oklahoma. Oklahoma Geological Survey Bulletin 95 1–303.

Ham, W.E., Wilson, J.L., 1967. Paleozoic Epeirogeny and Orogeny in the Central United States. American Journal of Science 265, 332–407.

Harris, S.A., 1975. Hydrocarbon Accumulation in “Meramec-Osage” (Mississippian) Rocks, Sooner Trend, Northwest-Central Oklahoma. AAPG Bulletin 59, 633–664.

Harrison, W.E., Prater, L.M., Cheung, P.K., 1983. Geothermal Resource Assessment in Oklahoma. Oklahoma Geological Survey Special Publication 83, 1–42.

Hemish, L.A., Andrews, R.D., 2001. Stratigraphy and depositional environments of the sandstones of the Springer Formation and the Primrose Member of the Golf Course Formation in the Ardmore Basin, Oklahoma. Oklahoma. Oklahoma Geological Survy. Guidebook 32.

Henry, M.E., Hester, T.C., 1995. Southern Oklahoma Province (061), in: Gautier, D.L., Dolton, G.I., Takahashi, K.I., Varnes, K.I. (Eds.), 1995 National Assessment of United States Oil and Gas Resources - Results, Methodology, and Supporting Data. U.S. Geological Survey digital Data Series 30, pp. 1–24.

Hester, T.C., Schmoker, J.W., Sahl, H.L., 1990. Log-derived regional source-rock characteristics of the Woodford Shale, Anadarko Basin, Oklahoma. US Geological Survey Bulletin 1866 D.

Higley, D.K., 2013. 4D Petroleum System Model of the Mississippian System in the Anadarko Basin Province, Oklahoma, Kansas, Texas, and Colorado, USA. The Mountain Geologist 50, 81–98.

Higley, D.K., Cook, T.A., Pawlewicz, M.J., 2014. Petroleum Systems and Assessment of Undiscovered Oil and Gas in the Anadarko Basin Province, Colorado, Kansas, Oklahoma, and Texas — Woodford Shale Assessment Units, in: Higley, D.K. (Ed.), Petroleum Systems and Assessment of Undiscovered Oil and Gas in the Anadarko Basin Province, Colorado, Kansas, Oklahoma, and Texas - USGS Province 58. U.S. Geological Survey Digital Data Series, pp. 1–24.

Ho, T.Y., Rogers, M.A., Drushel, H. V., Koons, C.B., 1974. Evolution of Sulfur Compounds in Crude Oils. AAPG Bulletin 58, 2338–2348.

Huang, S., Wang, Z., Lv, Z., Gong, D., Yu, C., Wu, W., 2014. Geochemical identification of marine and terrigenous condensates — A case study from the Sichuan Basin, SW China. Organic Geochemistry 74, 44–58.

Huang, W., Meinschein, W.G., 1979. Sterols as ecological indicators. Geochimica et Cosmochimica Acta 43, 739–745.

Huffman, G.G., 1959. Pre-Desmoinesian Isopachous and Paleogeologic Studies in Central Mid-Continent Region. AAPG Bulletin 43, 2541–2574.

Hughes, W.B., Holba, A.G., Dzou, L.I.P., 1995. The ratios of dibenzothiophene to phenanthrene and pristane to phytane as indicators of depositional environment and lithology of petroleum source rocks. Geochimica et Cosmochimica Acta 59, 3581–3598.

Hunt, J.M., 1984. Generation and Migration of Light Hydrocarbons. American Association for the Advancement of Science 226, 1265–1270.

Hunt, J.M., 1996. Petroleum Geochemistry and Geology, 2nd ed. W.H. Freeman.

Hunt, J.M., Philp, R.P., Kvenvolden, K.A., 2002. Early developments in petroleum geochemistry. Organic Geochemistry 33, 1025–1052.

Hunt, J.M., Stewart, F., Dickey, P.A., 1954. Origin of Hydrocarbons of Uinta Basin, Utah. AAPG Bulletin 38, 1671–1698.

Hutton, J., 1788. Theory of the Earth, in: Transactions of the Royal Society of Edinburgh, Vol. I, Part II. pp. 209–304.

Isaksen, G.H., Pottorf, R.J., Jenssen, A.I., 1998. Correlation of fluid inclusions and reservoired oils to infer trap fill history in the South Viking Graben, North Sea. Petroleum Geoscience 4, 41–55.

Jarvie, D.M., 2001. Williston Basin Petroleum Systems: Inferences from Oil Geochemistry and Geology. The Mountain Geologist 38, 19–41.

Jefferies, 2016. STACK/MERGE/SCOOP [WWW Document]. URL https://www.jefferies.com/CMSFiles/Jefferies.com/files/Teach-In - STACK-SCOOP.pdf (accessed 10.10.20).

Johnson, K.S., 1989. Geologic evolution of the Anadarko Basin, in: Johnson, K.S. (Ed.), Anadarko Basin Symposium, 1988. Oklahoma Geologic Survey Circular 90, Norman, Oklahoma, pp.

3–12.

Johnson, K.S., 2008. Earth Sciences and Mineral Resources of Oklahoma. Oklahoma Geologic Survey, Norman, Oklahoma.

Johnson, K.S., Amsden, T.W., Denison, R.E., Dutton, S.P., Goldstein, A.G., Rascoe Jr., B., Sutherland, P.K., Thompson, D.M., 1988. Southern Midcontinent region, in: Sloss, L.L. (Ed.), Sedimentary Cover—North American Craton. Geological Society of America, pp. 307–359.

Johnson, K.S., Cardott, B.J., 1992. Geologic Framework and Hydrocarbon Source Rocks of Oklahoma, in: Johnson, K.S., Cardott, B.J. (Eds.), Source Rocks in the Southern Midcontinent, 1990. Oklahoma Geological Survey Circular 93, Norman, Oklahoma, pp. 21–37.

Jones, P.J., Philp, R.P., 1990. Oils and source rocks from Pauls Valley, Anadarko Basin, Oklahoma, U.S.A. Applied Geochemistry 5, 429–448.

Jones, R.W., 1984. Comparison of Carbonate and Shale Source Rocks, in: Palacas, J.G. (Ed.), Petroleum Geochemistry and Source Rock Potential of Carbonate Rocks. American Association of Petroleum Geologists, pp. 163–180.

Jones, R.W., 1987. Organic Facies, in: Brooks, J., Welte, D.H. (Eds.), Advances in Petroleum Geochemistry. Academic Press, London, pp. 1–90.

Jordan, T.E., 1981. Crustal Loading and Foreland Basin Evolution, Cretaceous, Western United States. AAPG Bulletin 65, 2506–2520.

Kim, D., Philp, R.P., 2001. Extended Tricyclic Terpanes in Mississippian Rocks from the Anadarko Basin, Oklahoma, in: Johnson, K.S. (Ed.), Oklahoma Geological Survey Circular 105. Oklahoma Geological Survey Circular 105, pp. 109–127.

Koblava, A.Z., Frik, M.G., Shnee, V.D., 1980. Geochemical information content of hydrocarbon composition of naphtha cuts from crude oils (on the example of the Kama River region). Geokhimiya 11, 1117–1133.

Kornacki, A., Dahl, J., 2016. Evidence Some Oil Accumulations in the Woodford Formation and the Meramec Formation Received an Additional Charge of Very Dry Thermal Gas. AAPG Search and Discovery Article #41879.

Krooss, B.M., Leythaeuser, D., 1997. Diffusion of methane and ethane through the reservoirs cap rock: implications for the timing and duration of catagenesis. AAPG Bulletin 81, 155–161.

Krouse, H.R., Viau, C.A., Eliuk, L.S., Ueda, A., Halas, S., 1988. Chemical and isotopic evidence of thermochemical sulphate reduction by light hydrocarbon gases in deep carbonate reservoirs. Nature 333, 415–419.

Kruge, M.A., Hubert, J.F., Akes, R.J., Meriney, P.E., 1990. Biological markers in Lower Jurassic synrift lacustrine black shales, Hartford basin, Connecticut, U.S.A. Organic Geochemistry 16, 689–701.

Lambert, M.W., 1993. Internal stratigraphy and organic facies of the Devonian- Mississippian Chattanooga (Woodford) Shale in Oklahoma and Kansas, in: Katz, B.J., Pratt, L.M. (Eds.), Source Rocks in a Sequence Stratigraphic Framework. AAPG Studies in Geology 37, pp.

163–176.

Le Tran, K., Connan, J., van der Weide, B., 1974. Problemes relatifs a la formation d'hydrocarbures et d'hydrogene sulfure dans le bassin sud-ouest Aquitain, in: Tissot, B.P., Bienner, F. (Eds.), Advances in Organic Geochemistry, 1973 (Proceedings of the 6th International Meeting on Organic Geochemistry). Editions Technip, Paris, pp. 761–789.

Legendre, P., Legendre, L., 2012. Numerical Ecology, Edition, 3. ed. Elsevier, Amsterdam.

Lewan, M.D., 1985. Evaluation of Petroleum Generation by Hydrous Pyrolysis Experimentation. Philosophical Transactions of the Royal Society of London. Series A, Mathematical and Physical Sciences 315, 123–134.

Lewan, M.D., Bjorøy, M., Dolcater, D.L., 1986. Effects of thermal maturation on steroid hydrocarbons as determined by hydrous pyrolysis of Phosphoria Retort Shale. Geochimica et Cosmochimica Acta 50, 1977–1987.

Leythaeuser, D., Rückheim, J., 1989. Heterogeneity of oil composition within a reservoir as a reflection of accumulation history. Geochimica et Cosmochimica Acta 53, 2119–2123.

Leythaeuser, D., Schaefer, R.G., Cornford, C., Weiner, B., 1979. Generation and migration of light hydrocarbons (C2-C7) in sedimentary basins. Organic Geochemistry 1, 191–204.

Leythaeuser, D., Schaefer, R.G., Poocff, H., 1983. Diffusion of Light Hydrocarbons in Subsurface Sedimentary Rocks. AAPG Bulletin 67, 889–895.

Leythaeuser, D., Schaefer, R.G., Yukler, A., 1982. Role of diffusion in primary migration of hydrocarbons. American Association of Petroleum Geologists Bulletin 66, 408–429.

Lillis, P.G., Lewan, M.D., Warden, A., Monk, S.M., King, J.D., 1999. Identification and Characterization of Oil Types and Their Source Rocks, The Oil and Gas Resource Potential of the 1002 Area, Arctic National Wildlife Refuge, Alaska, by ANWR Assessment Team, U.S. Geological Survey Open-File Report 98-34.

Lillis, P.G., Selby, D., 2013. Evaluation of the rhenium-osmium geochronometer in the Phosphoria petroleum system, Bighorn Basin of Wyoming and Montana, USA. Geochimica et Cosmochimica Acta 118, 312–330.

Logsdon, T., Brown, A.R., 1967. The Hunton Play in Oklahoma. Shale Shaker Digest 6, 63–70.

Machel, H.G., 2001. Bacterial and thermochemical sulfate reduction in diagenetic settings - old and new insights. Sedimentary Geology 140, 143–175.

Machel, H.G., Krouse, H.R., Riciputi, L.R., Cole, D.R., 1995. Devonian Nisku Sour Gas Play, Canada: A Unique Natural Laboratory for Study of Thermochemical Sulfate Reduction, in: Vairavamurthy, M.A., Schoonen, M.A.A. (Eds.), Geochemical Transformations of Sedimentary Sulfur. American Chemical Society Symposium Series 612. Washington DC, pp. 439–454.

Mackenzie, A.S., Brassell, S.C., Eglinton, G., Maxwell, J.R., 1982. Chemical fossils: the geological fate of steroids. Science (New York, N.Y.) 217, 491–504.

Mackenzie, A.S., Disko, U., Rullkötter, J., 1983. Determination of hydrocarbon distributions in oils and sediment extracts by gas chromatography-high resolution mass spectrometry. Organic Geochemistry 5, 57–63.

Mackenzie, A.S., Hoffmann, C.F., Maxwell, J.R., 1981. Molecular parameters of maturation in the Toarcian shales, Paris Basin, France-III. Changes in aromatic steroid hydrocarbons. Geochimica et Cosmochimica Acta 45, 1345–1355.

Mackenzie, A.S., Maxwell, J.R., 1981. Assessment of thermal maturation in sedimentary rocks by molecular measurements, in: Brooks, J. (Ed.), Organic Maturation Studies and Fossil Fuel Exploration. Academic Press, London, pp. 239–254.

Mango, F.D., 1987. An Invariance in the Isoheptanes of Petroleum. Science 237, 514–517.

Mango, F.D., 1990a. The origin of light hydrocarbons in petroleum: A kinetic test of the steady-state catalytic hypothesis. Geochimica et Cosmochimica Acta 54, 1315–1323.

Mango, F.D., 1990b. The origin of light cycloalkanes in petroleum. Geochimica et Cosmochimica Acta 54, 23–27.

Mango, F.D., 1992. Transition metal catalysis in the generation of petroleum and natural gas. Geochimica et Cosmochimica Acta 56, 553–555.

Mango, F.D., 1994. The origin of light hydrocarbons in petroleum: Ring preference in the closure of carbocyclic rings. Geochimica et Cosmochimica Acta 58, 895–901.

Mango, F.D., 1997. The light hydrocarbons in petroleum: A critical review. Organic Geochemistry 26, 417–440.

Martin, R.L., Winters, J.C., Williams, J.A., 1963. Composition of crude oils by gas chromatography: Geological significance of hydrocarbon distribution, in: 6th World Petroleum Congress Proceedings. World Petroleum Congress, Frankfurt am Main, pp. 231–260.

Marynowski, L., Filipiak, P., 2007. Water column euxinia and wildfire evidence during deposition of the Upper Famennian Hangenberg event horizon from the Holy Cross Mountains (central Poland). Geological Magazine 144, 569–595.

Marynowski, L., Kubik, R., Uhl, D., Simoneit, B.R.T., 2014. Molecular composition of fossil charcoal and relationship with incomplete combustion of wood. Organic Geochemistry 77, 22–31.

McCain, W.D., 1990. Properties of Petroleum Fluids, 2nd ed. PennWell Publishing Company, Tulsa, Oklahoma.

McCarthy, K., Niemann, M., Palmowski, D., Peters, K.E., Stankiewicz, A., 2011. Basic Petroleum Geochemistry for Source Rock Evaluation. Oilfield Review 23, 32–43.

McConnell, D.A., 1989. Constraints on Magnitude and Sense of Slip Across the Northern Margin of the Wichita Uplift, Southwest Oklahoma, in: Johnson, K.S. (Ed.), Anadarko Basin Symposium, 1988. Oklahoma Geologic Survey Circular 90, Norman, Oklahoma, pp. 85–96.

McIver, R.D., 1967. Composition of Kerogen-Clue To Its Role in the Origin of Petroleum, in: 7th World Petroleum Congress. World Petroleum Congress, Mexico City, pp. 25–36.

McNab, J.. G., Smith, P. V., Betts, R.L., 1952. The Evolution of Petroleum. Industrial and Engineering Chemistry 44, 2556–2563.

Meckel, L.D., Thomasson, M.R., 2005. Pervasive Tight Gas Sandstone Reservoirs : An Overview,

in: Bishop, M.G., Cumella, S.P., Robinson, J.W., Silvermen, M.R. (Eds.), Gas in Low Permeability Reservoirs of the Rocky Mountain Region. The Rocky Mountain Association of Geologists, Denver, pp. 1–14.

Miceli Romero, A., Philp, R.P., 2012. Organic geochemistry of the Woodford Shale, southeastern Oklahoma: How variable can shales be? AAPG Bulletin 96, 493–517.

Miller, J., Cullen, A., 2018. My Favorite Outcrop: Sycamore Formation I-35 South, Arbuckle Mountains, OK. The Shale Shaker 69, 87–99.

Milner, C.W.D., Rogers, M.A., Evans, C.R., 1977. Petroleum transformations in reservoirs. Journal of Geochemical Exploration 7, 101–153.

Moldowan, J.M., Fago, F.J., Lee, C.Y., Jacobson, S.R., Watt, D.S., Slougui, N.E., Jeganathan, A., Young, D.C., 1990. Sedimentary 24-n-propylcholestanes, molecular fossils diagnostic of marine algae. Science 247, 309–312.

Moldowan, J.M., Seifert, W.K., Gallegos, E.J., 1983. Identification of an extended series of tricyclic terpanes in petroleum. Geochimica et Cosmochimica Acta 47, 1531–1534.

Moldowan, J.M., Seifert, W.K., Gallegos, E.J., 1985. Relationship between petroleum composition and depositional environment of petroleum source rocks. AAPG Bulletin 69, 1255–1268.

Moldowan, J.M., Sundararaman, P., Salvatori, T., Alajbeg, A., Gjukic, B., Demaison, G.J., 1989. Source Correlation and Maturity Assessment of Select Oils and Rocks from the Central Adriatic Basin (Italy and Yugoslavia). Biomarkrs in petroleum: memorial symposium for Wolfgang K. Seifert 34, 112–121.

Moldowan, J.M., Sundararaman, P., Schoell, M., 1986. Sensitivity of biomarker properties to depositional environment and/or source input in the Lower Toarcian of SW-Germany. Organic Geochemistry 10, 915–926.

Moses, P.L., 1986. Engineering Applications of Phase Behavior of Crude Oil and Condensate Systems. Journal of Petroleum Technology 38, 715–723.

Mullins, O.C., 2011. The Asphaltenes. Annual Review of Analytical Chemistry 4, 393–418.

Noble, R.A., Alexander, R., Kagi, R.I., 1985. The occurrence of bisnorhopane, trisnorhopane and 25-norhopanes as free hydrocarbons in some Australian shales. Organic Geochemistry 8, 171–176.

Noble, R.A., Alexander, R., Kagi, R.I., 1987. Configurational isomerization in sedimentary bicyclic alkanes. Organic Geochemistry 11, 151–156.

Obermajer, M., Osadetz, K.G., Fowler, M.G., Snowdon, L.R., 2000. Light hydrocarbon (gasoline range) parameter refinement of biomarker-based oil-oil correlation studies: an example from Williston Basin. Organic Geochemistry 31, 959–976.

Oksanen, J., Blanchet, F.G., Kindt, R., Legendre, P., Minchin, P.R., O'Hara, R.B., Simpson, G.L., Solymos, P., Stevens, M.H.H., Wagner, H., 2015. Vegan: Community Ecology Package. R Package Version 2.2-1 [WWW Document]. http://CRAN.R-project.org/package=vegan.

Orr, W.L., 1974. Changes in Sulfur Content and Isotopic Ratios of Sulfur during Petroleum Maturation--Study of Big Horn Basin Paleozoic Oils. AAPG Bulletin 58, 2295–2318.

Orr, W.L., 1977. Geologic and geochemical controls on the distribution of hydrogen sulfide in natural gas, in: Campos, R., Goni, J. (Eds.), Advances in Organic Geochemistry 1975 (Proceedings of the 7th International Meeting on Organic Geochemistry). Empresa Nacional Adaro de Investigaciones Mineras, Enadisma, Madrid, pp. 571–597.

Oung, J.N., Philp, R.P., 1994. Geochemical Characteristics of Oils from Taiwan. Journal of Southeast Asian Earth Sciences 9, 193–206.

Ourisson, G., Albrecht, P.A., Rohmer, M., 1982. Predictive microbial biochemistry - from molecular fossils to procaryotic membranes. Trends in Biochemical Sciences 7, 236–239.

Ourisson, G., Albrecht, P.A., Rohmer, M., 1984. The Microbial Origin of Fossil Fuels. Scientific American 251, 44–51.

Ourisson, G., Rohmer, M., Poralla, K., 1987. Prokaryotic hopanoids and other polyterpenoid sterol surrogates. Annual Review of Microbiology 41, 301–333.

Palacas, J.G., 1988. Characteristics of Carbonate Source Rocks of Petroleum, in: Magoon, L.B. (Ed.), US Geological Survey Bulletin 1870. U.S Geological Survey, Denver, CO, pp. 20–25.

Paul, D., Skrzypek, G., Forizs, I., 2007. Normalization of measured stable isotopic compositions to isotope reference scales - a review. Rapid Communications in Mass Spectrometry 21, 3006–3014.

Pearson, A., Eglinton, T.I., 2000. An organic tracer for surface ocean radiocarbon. Paleoceanography 15, 541–550.

Pearson, C.A., 2016. Geochemical Characterization of the Upper Mississippian Goddard Formation, Springer Group, in the Anadarko Basin of Oklahoma. Master's Thesis, University of Oklahoma, Norman, Oklahoma.

Pearson, C.A., Philp, R.P., 2019. Geochemical characterization of the Upper Mississippian Goddard Formation, Noble Ranch Group, and related oils in the Anadarko Basin of Oklahoma. AAPG Bulletin 103, 2545–2571.

Pepper, A.S., Corvi, P.J., 1995. Simple kinetic models of petroleum formation. Part I: oil and gas generation from kerogen. Marine and Petroleum Geology 12, 291–319.

Pepper, A.S., Dodd, T.A., 1995. Simple kinetic models of petroleum formation. Part II: oil-gas cracking. Marine and Petroleum Geology 12, 321–340.

Peters, K. E., Curry, D.J., Kacewicz, M., 2012. An Overview of Basin and Petroleum System Modeling: Definitions and Concepts, in: Peters, Kenneth E, Curry, D.J., Kacewicz, M. (Eds.), Basin Modeling: New Horizons in Research and Applications. AAPG Hedberg Series, no. 4, pp. 1–16.

Peters, K.E., Fowler, M.G., 2002. Applications of petroleum geochemistry to exploration and reservoir management. Organic Geochemistry 33, 5–36.

Peters, K.E., Moldowan, J.M., 1991. Effects of source, thermal maturity, and biodegradation on the distribution and isomerization of homohopanes in petroleum. Organic Geochemistry 17, 47–61.

Peters, K.E., Moldowan, J.M., Schoell, M., Hempkins, W.B., 1986. Petroleum isotopic and biomarker composition related to source rock organic matter and depositional environment.

Organic Geochemistry 10, 17–27.

Peters, K.E., Moldowan, J.M., Sundararaman, P., 1990. Effects of hydrous pyrolysis on biomarker thermal maturity parameters: Monterey Phosphatic and Siliceous members. Organic Geochemistry 15, 249–265.

Peters, K.E., Walters, C.C., Moldowan, J.M., 2005a. The Biomarker Guide Vol. I, 2nd ed. Cambridge University Press, Cambridge, UK. doi:10.1017/CBO9781107415324.004

Peters, K.E., Walters, C.C., Moldowan, J.M., 2005b. The Biomarker Guide Vol. II, 2nd ed. Cambridge University Press 2005, Cambridge, UK. doi:10.1002/pssb.201000856

Pfeiffer, J., Saal, R.N.J., 1940. Asphaltic Bitumen as Colloid System. Journal of Physical Chemistry 44, 139–149.

Philippi, G.T., 1965. On the Depth, Time and Mechanism of Petroleum Generation. Geochimica et Cosmochimica Acta 29, 1021–1049.

Philippi, G.T., 1975. The deep subsurface temperature controlled origin of the gaseous and gasoline-range hydrocarbons of petroleum. Geochimica et Cosmochimica Acta 39, 1353–1373.

Philippi, G.T., 1977. Proteins as a possible source material of low molecular weight petroleum hydrocarbons. Geochimica et Cosmochimica Acta 41, 1083–1086.

Philp, R.P., 1983. Correlation of crude oils from the San Jorges Basin, Argentina. Geochimica et Cosmochimica Acta 47, 267–275.

Philp, R.P., 1985. Biological markers in fossil fuel production. Mass Spectrometry Reviews 4, 1–54.

Philp, R.P., 2014. Formation and Geochemistry of Oil and Gas, in: Holland, H.D., Turekian, K.K. (Eds.), Treatise on Geochemistry: Second Edition. Elsevier Ltd., Oxford, pp. 233–265.

Philp, R.P., Gilbert, T.D., 1986. Biomarker distributions in Australian oils predominantly derived from terrigenous source material. Organic Geochemistry 10, 73–84.

Philp, R.P., Gilbert, T.D., Friedrich, J., 1981. Bicyclic sesquiterpenoids and diterpenoids in Australian crude oils. Geochimica et Cosmochimica Acta 45, 1173–1180.

Philp, R.P., Lewis, C.A., 1987. Organic Geochemistry of Biomarkers. Annual Review of Earth and Planetary Sciences1 15, 363–395.

Philp, R.P., Maxwell, J.R., Eglinton, G., 1976. Environmental organic geochemistry of aquatic sediments. Science Progress 63, 521–545.

Philp, R.P., Symcox, C.W., Wood, M., Nguyen, T., Wang, H., Kim, D., 2021. Possible explanations for the predominance of tricyclic terpanes over pentacyclic terpanes in oils and rock extracts. Organic Geochemistry 155, 104220.

Portilla, H.A.G., 2017. Detailed Lithostratigraphic Characterization and Sequence Stratigraphy of a Complete Woodford Shale Outcrop Section in Southern Oklahoma. Master's Thesis, University of Oklahoma, Norman, Oklahoma.

Pranter, M.J., Turnini, A.M., Marfurt, K.J., Devegowda, D., 2016. Multidisciplinary characterization and modeling of Mississippian carbonate and silica-rich reservoirs, northern

Oklahoma, AAPG Mid-continent, in: AAPG Search and Discovery. Tulsa, Oklahoma.

Price, B., 2020. Depositional interpretation and sequence stratigraphic control on reservoir quality and distribution in the Meramecian Sooner trend Anadarko Basin, Canadian, and Kingfisher Counties (STACK) play, Anadarko Basin, Oklahoma, United States. AAPG Bulletin 104, 357–386.

Price, L.C., 1976. Aqueous Solubility of Petroleum As Applied To Its Origin and Primary Migration. AAPG Bulletin (American Association of Petroleum Geologists) 60, 213–244.

Price, P.L., O'Sullivan, T., Alexander, R., 1987. The nature and occurrence of oil in Seram, Idonesia, in: Proceedings of the Indonesian Petroleum Association, Sixteenth Annual Convention, Volume 1. Indonesian Petroleum Association, Jakarta, pp. 141–173.

Radke, M., 1988. Application of aromatic compounds as maturity indicators in source rocks and crude oils. Marine and Petroleum Geology 5, 224–236.

Radke, M., Welte, D.H., Willsch, H., 1982. Geochemical study on a well in the Western Canada Basin: relation of the aromatic distribution pattern to maturity of organic matter. Geochimica et Cosmochimica Acta 46, 1–10.

Radke, M., Welte, D.H., Willsch, H., 1986. Maturity parameters based on aromatic hydrocarbons: Influence of the organic matter type. Organic Geochemistry 10, 51–63.

Raederstorff, D., Rohmer, M., 1984. Sterols of the unicellular algae Nematochrysopsis roscoffensis and Chrysotila lamellosa: isolation of (24E)-24-n-propylidenecholesterol and 24-n-propylcholesterol. Phytochemistry 23, 2835–2838.

Rahman, M.W., Veach, D., Jayakumar, R., Esmaili, S., 2017. Application of Organic Geochemistry on Assessment of Fluid Behavior and Oil Migration within the Woodford Shale in the Anadarko Basin, in: Unconventional Resources Technology Conference. SPE/AAPG/SEG, Austin, pp. 1–12.

Raiswell, R., Berner, R.A., 1985. Pyrite formation in euxinic and semi-euxinic environments. American Journal of Science 285, 710–724.

Rangel, A., Parra, P., Niño, C., 2000. The La Luna formation: Chemostratigraphy and organic facies in the Middle Magdalena Basin. Organic Geochemistry 31, 1267–1284.

Rascoe, B.J., Adler, F.J., 1983. Permo-Carboniferous Hydrocarbon Accumulations, Mid-Continent, U.S.A. AAPG Bulletin 67, 979–1001.

Requejo, A.G., Hieshima, G.B., Hsu, C.S., McDonald, T.J., Sassen, R., 1997. Short-chain (C21 and C22) diasteranes in petroleum and source rocks as indicators of maturity and depositional environment. Geochimica et Cosmochimica Acta 61, 2653–2667.

Revill, A.T., Volkman, J.K., O'Leary, T., Summons, R.E., Boreham, C.J., Banks, M.R., Denwar, K., 1994. Hydrocarbon biomarkers, thermal maturity, and depositional setting to Tasmanite oil shales from Tasmania, Australia. Geochimica et Cosmochimica Acta 58, 3803–3822.

Riolo, J., Hussler, G., Albrecht, P.A., Connan, J., 1986. Distribution of aromatic steroids in geological samples: their evaluation as geochemical parameters. Organic Geochemistry 10, 981–990.

Riva, A., Riolo, B., Ocampo, R., Callot, H.J., Albrecht, P., Nali, M., 1989. Molecular parameters

in Italian carbonate oils: reconstruction of past depositional environments, in: 14th International Meeting on Organic Geochemistry, Paris, September 18-22, Abstracts, Number 335.

Robert F. Walters, 1958. Differential Entrapment of Oil and Gas in Arbuckle Dolomite of Central Kansas. AAPG Bulletin 42, 2133–2173.

Rohmer, M., Bouvier, P., Ourisson, G., 1979. Molecular Evolution of Biomembranes: Structural Equivalents and Phylogenetic Precursors of Sterols. Proceedings of the National Academy of Sciences of the United States of America 2, 847–851.

Rontani, J.-F., Volkman, J.K., 2003. Phytol degradation products as biogeochemical tracers in aquatic environments. Organic Geochemistry 34, 1–35.

Rubinstein, I., Sieskind, O., Albrecht, P.A., 1975. Rearranged sterenes in a shale: occurrence and simulated formation. Journal of the Chemical Society, Perkin Transactions 1 19, 1833–1836.

Rullkötter, J., Leythaeuser, D., Wendisch, D., 1982. Novel 23,28-bisnorlupanes in Tertiary sediments. Widespread occurrence of nuclear demethylated triterpanes. Geochimica et Cosmochimica Acta 46, 2501–2509.

Rullkötter, J., Mackenzie, A.S., Welte, D.H., Leythaeuser, D., Radke, M., 1984. Quantitative gas chromatography-mass spectrometry analysis of geological samples. Organic Geochemistry 6, 817–827.

Seifert, W.K., Moldowan, J.M., 1978. Applications of steranes, terpanes and monoaromatics to the maturation, migration, and source of crude oils. Geochimica et Cosmochimica Acta 42, 77–95.

Seifert, W.K., Moldowan, J.M., 1981. Paleoreconstruction by biological markers. Geochimica et Cosmochimica Acta 45, 783–794.

Seifert, W.K., Moldowan, J.M., Smith, G.W., Whitehead, E. V., 1978. First proof of structure of a C28-pentacyclic triterpane in petroleum. Nature 271, 436–437.

Shanmugam, G., 1985. Significance of Coniferous Rain Forests and Related Organic Matter in Generating Commercial Quantities of Oil, Gippsland Basin, Australia. AAPG Bulletin 69, 1241–1254.

Sieskind, O., Joly, G., Albrecht, P.A., 1979. Simulation of the geochemical transformations of sterols: superacid effect of clay minerals. Geochimica et Cosmochimica Acta 43, 1675–1679.

Silverman, S.R., Epstein, S., 1958. Carbon Isotopic Compositions of Petroleums and Other Sedimentary Organic Materials. AAPG Bulletin 42, 998–1012.

Simoneit, B.R.T., 1977. Diterpenoid compounds and other lipids in deep-sea sediments and their geochemical significance. Geochimica et Cosmochimica Acta 41, 463–476.

Simoneit, B.R.T., Leif, R.N., Radler de Aquino Neto, F., Almeida Azevedo, D., Pinto, A.C., Albrecht, P.A., 1990. On the presence of tricyclic terpane hydrocarbons in permian tasmanite algae. Naturwissenschaften 77, 380–383.

Sinninghe Damsté, J.S., Dalen, A.C.K.-V., Albrecht, P.A., de Leeuw, J.W., 1991. Identification of long-chain 1,2-di-n-alkylbenzenes in Amposta crude oil from the Tarragona Basin, Spanish Mediterranean: Implications for the origin and fate of alkylbenzenes. Geochimica Et

Cosmochimica Acta 55, 3677–3683.

Sinninghe Damsté, J.S., de Leeuw, J.W., 1990. Analysis, structure and geochemical significance of organically-bound sulphur in the geosphere: State of the art and future research. Advances in Organic Geochemistry 16, 1077–1101.

Sinninghe Damsté, J.S., Schouten, S., Volkman, J.K., 2014. C27-C30 neohop-13(18)-enes and their saturated and aromatic derivatives in sediments: Indicators for diagenesis and water column stratification. Geochimica et Cosmochimica Acta 133, 402–421.

Sinninghe Damsté, J.S., Xavier, F., Heras, C.D. Las, Van Bergen, P.F., de Leeuw, J.W., 1993. Characterization of Tertiary Catalan lacustrine oil shales: Discovery of extremely organic sulphur-rich Type I kerogens. Geochimica Et Cosmochimica Acta 57, 389–415.

Slatt, R.M., Buckner, N., Abousleiman, Y., Sierra, R., Philp, R.P., Miceli Romero, A., Brien, N.O., Davis, R., Wawrzyniec, T., 2012. Outcrop-behind Outcrop (Quarry): Multiscale Characterization of the Woodford Gas Shale, Oklahoma, in: Breyer, A. (Ed.), Shale Reservoirs—Giant Resources for the 21st Century: AAPG Memoir 97. pp. 382–402.

Sloss, L., 1963. Sequences in the cratonic interior of North America. Geological Society of America Bulletin 74, 93–114.

Sofer, Z., 1984. Stable Carbon Isotope Composition of Crude Oils: Application to Source Depositional Environments and Petroleum Alteration. AAPG Bulletin 68, 31–49.

Stahl, W.J., 1977. Carbon and Nitrogen Isotopes in Hydrocarbon Research and Exploration. Chemical Geology 20, 121–149.

Stahl, W.J., 1978. Source rock-crude oil correlation by isotopic type-curves. Geochimica et Cosmochimica Acta 42, 1573–1577.

Stahl, W.J., Carey, B.D., 1975. Source-rock identification by isotope analyses of natural gases from fields in the Val Verde and Delaware basins, west Texas. Chemical Geology 16, 257–267.

Sullivan, K.L., 1985. Organic facies variation of the Woodford Shale in western Oklahoma. Shale Shaker Digest XI 35, 185–198.

Summons, R.E., Capon, R.J., 1991. Identification and significance of 3β-ethyl steranes in sediments and petroleum. Geochimica et Cosmochimica Acta 55, 2391–2395.

Symcox, C.W., Philp, R.P., 2019a. Some Observations on the Geochemical Character of STACK and SCOOP Oils. Shale Shaker Digest 70, 248–260.

Symcox, C.W., Philp, R.P., 2019b. Heterogeneity of STACK/SCOOP Production in the Anadarko Basin, Oklahoma—Geochemistry of Produced Oils, in: Unconventional Resources Technology Conference. SPE/AAPG/SEG, pp. 1–14.

Tamborello, B., 2020. Potential Sources of Oil from Hugoton Embayment Reservoirs. Master's Thesis, University of Oklahoma, Norman, Oklahoma.

ten Haven, H.L., 1996. Applications and limitations of Mango's light hydrocarbon parameters in petroleum correlation studies. Organic Geochemistry 24, 957–976.

Thompson, K.F.M., 1979. Light Hydrocarbons in subsurface sediments. Geochimica et

Cosmochimica Acta 43, 657–672.

Thompson, K.F.M., 1983. Classification and thermal history of petroleum based on light hydrocarbons. Geochimica et Cosmochimica Acta 47, 303–316.

Thompson, K.F.M., 1987. Fractionated aromatic petroleums and the generation of gas-condensates. Organic Geochemistry 11, 573–590.

Thompson, K.F.M., 1988. Gas-condensate migration and oil fractionation in deltaic systems. Marine and Petroleum Geology 5, 237–246.

Tissot, B.P., Durand, B., Espitalié, J., Combaz, A., 1974. Influence of Nature and Diagenesis of Organic Matter in Formation of Petroleum. AAPG Bulletin 58, 499–506.

Tissot, B.P., Welte, D.H., 1984. Petroleum Formation and Occurrence, 2nd ed., 2nd ed. Springer. doi:10.1007/978-3-642-87813-8

Toland, W.G., 1960. Oxidation of Organic Compounds with Aqueous Sulfate. Journal of the American Chemical Society 82, 1911–1916.

Toland, W.G., Hagmann, D.L., Wilkes, J.B., Brutschy, F.J., 1958. Oxidation of Organic Compounds with Aqueous Base and Sulfur. Journal of the American Chemical Society 80, 5423–5427.

Torres-Parada, E.J., 2020. Woodford Shale Enclosed Mini-Basin Fill on the Hunton Paleo Shelf, a Depositional Model for Unconventional Resource Shales. Doctoral Dissertation, University of Oklahoma, Norman, Oklahoma.

Treibs, A., 1936. Chlorophyll and Hemin Derivatives in Organic Mineral Substances. Angewandte Chemie 49, 682–686.

Trendel, J.M., Restle, A., Connan, J., Albrecht, P., 1982. Identification of a novel series of tetracyclic terpene hydrocarbons (C24 - C27) in sediments and petroleums. Journal of the Chemical Society, Chemical Communications 304–306.

Urey, H.C., 1947. The thermodynamic properties of isotopic substances. Journal of the Chemical Society 1, 562–581.

van Graas, G., 1990. Biomarker maturity parameters for high maturities: calibration of the working range up to the oil/condensate threshold. Organic Geochemistry 16, 1025–1032.

van Kaam-Peters, H.M.E., Köster, J., van der Gaast, S.J., Dekker, M., de Leeuw, J.W., Sinninghe Damsté, J.S., 1998. The effect of clay minerals on diasterane/sterane ratios. Geochimica et Cosmochimica Acta 62, 2923–2929.

van Krevelen, D.W., 1961. Coal: Typology-Chemistry-Physics-Constitution. Elsevier Pub. Co., Amsterdam.

Villalba, D.M., 2016. Organic Geochemistry of the Woodford Shale, Cherokee Platform, OK and Its Role in a Complex Petroleum System. Master's Thesis, University of Oklahoma, Norman, Oklahoma.

Volkman, J.K., 1986. A review of sterol markers for marine and terrigenous organic matter. Organic Geochemistry 9, 83–99.

Volkman, J.K., 2003. Sterols in microorganisms. Applied Microbiology and Biotechnology 60,

495–506.

Volkman, J.K., Alexander, R., Kagi, R.I., Rullkötter, J., 1983. GC-MS characterisation of C27 and C28 triterpanes in sediments and petroleum. Geochimica et Cosmochimica Acta 47, 1033–1040.

Volkman, J.K., Barrett, S.M., Dunstan, G.A., Jeffrey, S.W., 1994. Sterol biomarkers for microalgae from the green algal class Prasinophyceae. Organic Geochemistry 21, 1211–1218.

Volkman, J.K., Maxwell, J.R., 1986. Acyclic isoprenoids as biological markers, in: Johns, R.B. (Ed.), Biological Markers in the Sedimentary Record. Elsevier, Amsterdam, pp. 1–46.

Walters, C.C., Hellyer, C.L., 1998. Multi-dimensional gas chromatographic separation of C7 hydrocarbons. Organic Geochemistry 29, 1033–1041.

Wang, H. Da, Philp, R.P., 1997. Geochemical study of potential source rocks and crude oils in the Anadarko basin, Oklahoma. AAPG Bulletin 81, 249–275.

Wang, T., 2016. An Organic Geochemical Study of Woodford Shale and Woodford-Mississippian Tight Oil from Central Oklahoma. Ph. D. Dissertation, University of Oklahoma, Norman, Oklahoma.

Wang, T., Philp, R.P., 2019. Oil families and inferred source rocks of the Woodford–Mississippian tight oil play in northcentral Oklahoma. AAPG Bulletin 103, 871–903.

Wang, Z., Yang, C., Fingas, M., Hollebone, B.P., Peng, X., Hansen, A., Christensen, J., 2005. Characterization, Weathering, and Application of Sesquiterpanes to Source Identification of Spilled Lighter Petroleum Products. Environmental Science and Technology 39, 8700–8707.

Wavrek, D.A., 1992. Characterization of Oil Types in the Ardmore and Marietta Basins, Southern Oklahoma Aulacogen, in: Oklahoma Geological Survey Circular 93. Oklahoma Geological Survey, pp. 185–195.

West, N., Alexander, R., Kagi, R.I., 1990. The use of silicalite for rapid isolation of branched and cyclic alkane fractions of petroleum. Organic Geochemistry 15, 499–501.

Weston, R.J., Philp, R.P., Sheppard, C.M., Woolhouse, A.D., 1989. Sesquiterpanes, diterpanes and other higher terpanes in oils from the Taranaki basin of New Zealand. Organic Geochemistry 14, 405–421.

Whitehead, E. V., 1973. Molecular Evidence for the Biogenesis of Petroleum and Natural Gas, in: Ingerson, E. (Ed.), Proceedings of Symposium on Hydrogeochemistry and Biogeochemistry. pp. 158–211.

Worden, R.H., Smalley, P.C., Oxtoby, N.H., 1995. Gas souring by thermochemical sulfate reduction at 140°C. American Association of Petroleum Geologists Bulletin 79, 854–863.

Yang, C., Wang, Z., Hollebone, B.P., Brown, C.E., Landriault, M., 2009. Characteristics of bicyclic sesquiterpanes in crude oils and petroleum products. Journal of Chromatography 1216, 4475–4484.

Yee, D., Johnston, G., Howard, D., Ahmed, S., 2017. STACKing it up: An economic and geological analysis of the STACK, in: Unconventional Resources Technology Conference 2017. SPE/AAPG/SEG, Austin, pp. 1–6.

Yi, C., Zhang, M., Teng, L., 2020. Maturity effects on steranes of source rocks in Lishu fault depression, Songliao Basin. Acta Geochimica 39, 561–573.

Zhang, J., Slatt, R.M., 2019. The significance of karst unconformities on overlying resource shales: Lessons learned from the Devonian Woodford Formation applied to the Permian Wolfcamp Shale. Interpretation 7, 33–43.

Zhang, T., Amrani, A., Ellis, G.S., Ma, Q., Tang, Y., 2008. Experimental investigation on thermochemical sulfate reduction by H2S initiation. Geochimica et Cosmochimica Acta 72, 3518–3530.

Zumberge, J.E., 1984. Source Rocks of the La Luna Formation (Upper Cretaceous) in the Middle Magdalena Valley, Colombia, in: Palacas, J.G. (Ed.), Petroleum Geochemistry and Source Rock Potential of Carbonate Rocks, AAPG Studies in Geology #18. AAPG, Tulsa, pp. 127–133.

Zumberge, J.E., 1987. Prediction of source rock characteristics based on terpane biomarkers in crude oils: A multivariate statistical approach. Geochimica et Cosmochimica Acta 51, 1625–1637.

Zumberge, J.E., Illich, H., Scotese, C., 2007. Biomarkers from Marine Crude Oils Reflect Modeled Climatic/Oceanographic Conditions for the Late Cretaceous, in: Farrimond, P. (Ed.), The 23rd International Meeting on Organic Chemistry. Bideford, Devon : Integrated Geochemical Interpretation, Torquay, England, pp. 555–556.

Appendix: Compound Structures

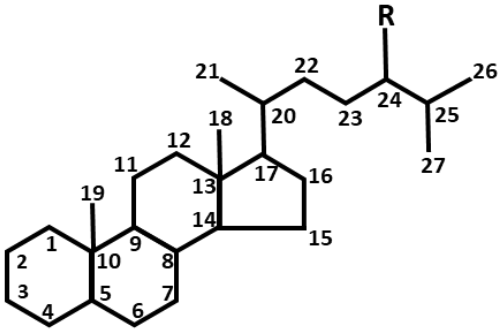

I: 24-*n*-cholestane (reg. sterane)
C_{27}: R=H
C_{28}: R=methyl
C_{29}: R=ethyl
C_{30}: R=propyl

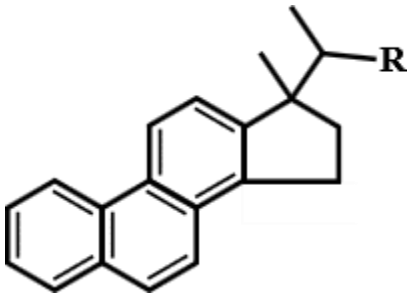

III: triaromatic steranes (TA[I])
C_{20}: R=H
C_{21}: R=methyl

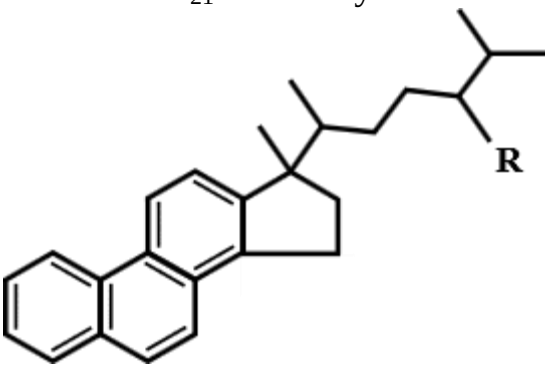

IV: triaromatic steranes (TA[II])
C_{26}: R=H
C_{27}: R=methyl
C_{28}: R=ethyl

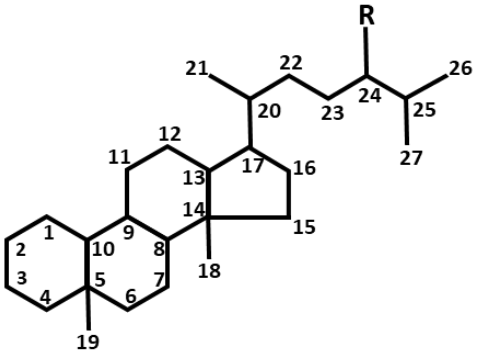

II: 24-*n*-diasterane
C_{27}: R=H
C_{28}: R=methyl
C_{29}: R=ethyl
C_{30}: R=propyl

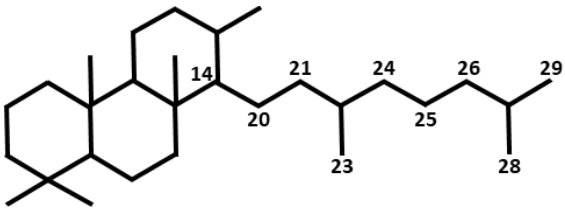

V: tricyclic terpane

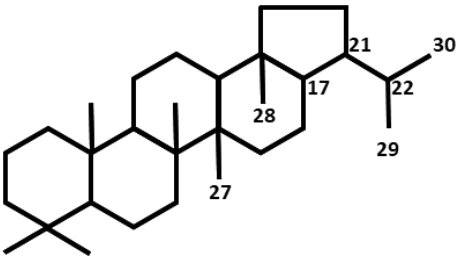

VI: C_{30} hopane

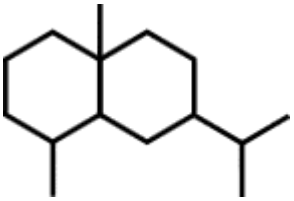

XII: eudesmane

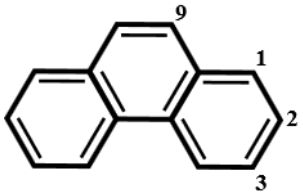

VII: phenanthrene

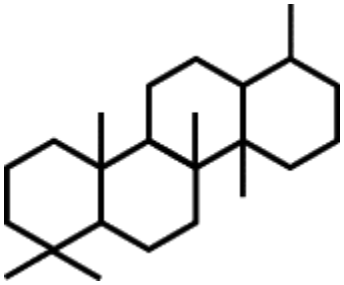

XIII: C_{24} tetracyclic terpane

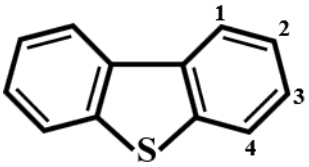

VIII: dibenzothiophene

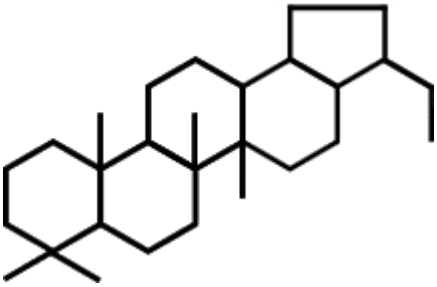

XIV:28,30-bisnorhopane



IX: pristane

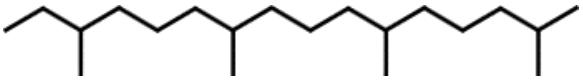

X: phytane

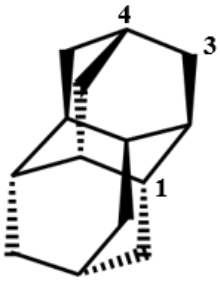

XV: diamantane

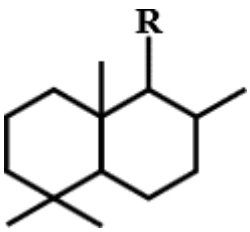

XI: (homo)drimane
C_{15}: R=methyl
C_{16}: R=ethyl